

AD-A068 980

ADVISORY GROUP FOR AEROSPACE RESEARCH AND DEVELOPMENT--ETC F/G 11/6
ADVANCED FABRICATION PROCESSES. (U)
MAR 79

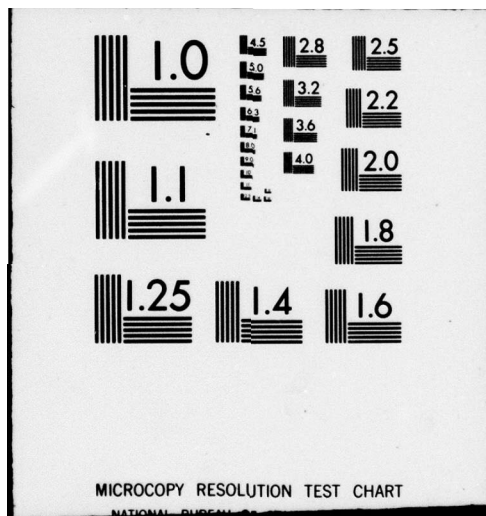
UNCLASSIFIED

AGARD-CP-256

NL

1 OF 3
AD
AO-8980





AD A 068980

DDC FILE COPY

LEVEL II

B.S. 2
AGARD-CP-256

AGARD

ADVISORY GROUP FOR AEROSPACE RESEARCH & DEVELOPMENT

7 RUE ANCELLE 92200 NEUILLY SUR SEINE FRANCE

AGARD CONFERENCE PROCEEDINGS No. 256

Advanced Fabrication Processes

DDC
RECEIVED
MAY 25 1979
D

DISTRIBUTION STATEMENT A

Approved for public release;
Distribution Unlimited

NORTH ATLANTIC TREATY ORGANIZATION



DISTRIBUTION AND AVAILABILITY
ON BACK COVER

LEVEL II

14 AGARD-CP-256
2

NORTH ATLANTIC TREATY ORGANIZATION
ADVISORY GROUP FOR AEROSPACE RESEARCH AND DEVELOPMENT
(ORGANISATION DU TRAITE DE L'ATLANTIQUE NORD)

9 Conference proceedings,

AGARD Conference Proceedings No.256

6 ADVANCED FABRICATION PROCESSES

11 Mar 79

12 262p

ACCESSION FOR	
DTIC	White Section <input checked="" type="checkbox"/>
DDC	Grey Section <input type="checkbox"/>
UNANNOUNCED	<input type="checkbox"/>
JUSTIFICATION	
BY	
DISTRIBUTION/AVAILABILITY CODES	
Dist.	AVAIL. and/or SPECIAL
A	

DDC
RECEIVED
MAY 25 1979
D

DISTRIBUTION STATEMENT A
Approved for public release;
Distribution Unlimited

Papers presented at the 47th Meeting of the AGARD Structures and Materials Panel
held in Florence, Italy on 26-28 September 1978.

400 043

JAB

THE MISSION OF AGARD

The mission of AGARD is to bring together the leading personalities of the NATO nations in the fields of science and technology relating to aerospace for the following purposes:

- Exchanging of scientific and technical information;
- Continuously stimulating advances in the aerospace sciences relevant to strengthening the common defence posture;
- Improving the co-operation among member nations in aerospace research and development;
- Providing scientific and technical advice and assistance to the North Atlantic Military Committee in the field of aerospace research and development;
- Rendering scientific and technical assistance, as requested, to other NATO bodies and to member nations in connection with research and development problems in the aerospace field;
- Providing assistance to member nations for the purpose of increasing their scientific and technical potential;
- Recommending effective ways for the member nations to use their research and development capabilities for the common benefit of the NATO community.

The highest authority within AGARD is the National Delegates Board consisting of officially appointed senior representatives from each member nation. The mission of AGARD is carried out through the Panels which are composed of experts appointed by the National Delegates, the Consultant and Exchange Programme and the Aerospace Applications Studies Programme. The results of AGARD work are reported to the member nations and the NATO Authorities through the AGARD series of publications of which this is one.

Participation in AGARD activities is by invitation only and is normally limited to citizens of the NATO nations.

The content of this publication has been reproduced directly from material supplied by AGARD or the authors.

Published March 1979

Copyright © AGARD 1979
All Rights Reserved

ISBN 92-835-0227-2



*Printed by Technical Editing and Reproduction Ltd
Harford House, 7-9 Charlotte St, London, W1P 1HD*

PREFACE

The Specialists' Meeting on "Advanced Fabrication Processes" in Florence in Fall 1978 was planned by a sub-committee of the Structures and Materials Panel under the same title. Planning started immediately after the most successful Specialists' Meeting on "Advanced Fabrication Techniques in Powder Metallurgy and their Economic Implications" in Ottawa in Spring 1976. The purpose of the Ottawa meeting was to focus not only on the technological but also on the economic achievements of powder metallurgy techniques.

The Structures and Materials Panel's interests in advanced fabrication processes stem from the increasing acquisition and maintenance costs of current aerospace systems. This has led to greatly increased emphasis, within many of the NATO nations, on means of reducing processing costs and improving the quality of manufacturers' components through improved material/process selection and control. There are emerging efforts in many of the NATO nations to bring together the design, materials and mechanics fundamentals underlying materials deformation, metal removal, joining, coating and other related processes. Similarly, new processes are emerging both within the aerospace processing community and within the more general commercial area, that offer significant opportunities for lower cost, higher quality aerospace components.

Therefore the purpose of the Specialists' Meeting was threefold. Most importantly it was to elucidate on some specific high payoff new processing concepts selected from a cross-section of NATO nations. This broad base of coverage was invaluable in and of itself but also was intended to aid in a second purpose which was hopefully to steer the Structures and Materials Panel toward selection of specific new area(s) where data and information interchange in much greater depth would be beneficial, such as was achieved in the powder metallurgy area. The third purpose was to promote a coupling of the fundamental research activities to more applied efforts. There is increasing emphasis and also much progress being made across NATO nations in research on the fundamental aspects of processing.

The meeting was attended by about one hundred participants from nearly all NATO countries, and was highlighted by the Panel Session. At this Session, based on the work presented as well as other work not presented, a significant spectrum of extremely interesting, high payoff, new processing areas was discussed. Advantages for each new area were elucidated. These areas as well as possible new ones will be the subject of Structures and Materials Panel review in Spring 1979 to determine the future course of action.

On behalf of the Structures and Materials Panel I would like to express my thanks to all authors, recorders, Session Chairmen and particularly to the Panel Session Leader, Mr Henry A. Johnson for their outstanding contributions and cooperation which were instrumental in making the meeting such a success.

GEORGE P. PETERSON
Chairman, Sub-Committee on
Advanced Fabrication Processes

CONTENTS

	Page
PREFACE by G.P.Peterson	iii
	Reference
 <u>KEYNOTE ADDRESS</u>	
BASIC TRENDS IN ADVANCED FABRICATION PROCESSES by H.H.Walther	K
 <u>SESSION I: RESEARCH AND PRODUCTION ASPECTS OF MACHINING PROCESSES</u>	
APPLIED RESEARCH ON THE MACHINABILITY OF TITANIUM AND ITS ALLOYS by W.König	1
RESIDUAL STRESSES IN GRINDING by J.Peters, R.Snoeys and M.Maris	2
EXPERIENCE D'UTILISATION DE LA COMMANDE ADAPTATIVE EN FRAISAGE par J.Y.Lhomme	3
INNOVATIVE MANUFACTURING FOR AUTOMATED DRILLING OPERATIONS by C.Micillo and J.Huber	4
 <u>SESSION II: SURFACE TREATMENTS AND PROCESSES</u>	
ION VAPOR DEPOSITED ALUMINUM COATINGS FOR IMPROVED CORROSION PROTECTION by E.R.Fannin	5
AN EVALUATION OF COATINGS FOR STEEL AND TITANIUM ALLOY FASTENERS FOR AIRCRAFT APPLICATIONS by V.C.R.McLoughlin	6
PHYSICAL VAPOUR DEPOSITION AND ION BEAM TECHNIQUES FOR SURFACE DURABILITY by J.P.Coad and N.E.W.Hartley	7
METAL BONDED CARBIDES FOR WEAR RESISTANT SURFACES by L.F.Norris, V.Silins, M.Adamovic and M.A.Clegg	8
SURFACE TREATMENTS BY HIGH POWER LASER ON NICKEL BASE SUPERALLOYS by D.Bacci and S.Tosto	9
 <u>SESSION III: FUNDAMENTAL ASPECTS OF NET SHAPE PROCESSING</u>	
PLASTICITY MODELLING by G.W.Rowe and P.Hartley	10
ASPECTS FONDAMENTAUX DE LA SUPERPLASTICITE – EXEMPLES DE REALISATION INDUSTRIELLE EN ALLIAGE DE TITANE Ti-6Al-4V par E.Budillon et J.P.Lechten	11
RAPIDLY SOLIDIFIED POWDERS, THEIR PRODUCTION, PROPERTIES, AND POTENTIAL APPLICATIONS by A.R.Cox, J.B.Moore and E.C. van Reuth	12

	Reference
HOT ISOSTATIC PROCESSING OF IN-738 TURBINE BLADES by G. Van Drunen, J. Liburdi, W. Wallace and T. Terada	13
NET-SHAPE PROCESSING OF NON-OXIDE CERAMICS by E. Gugel	14
 <u>SESSION IV: PRODUCTION ASPECTS OF NET SHAPE PROCESSING</u> 	
CONCURRENT SUPERPLASTIC FORMING/DIFFUSION BONDING OF B-1 COMPONENTS by G.W. Stacher and E.D. Weisert	15
FABRICATION OF TITANIUM AT HIGH TEMPERATURES by S.J. Swadling	16
PRODUCTION OF HIGH PURITY METAL POWDERS BY ELECTRON BEAM TECHNIQUES by H. Stephan, H. Schmitt and R. Ruthardt	17
HEAT TREATMENT OF P/M NICKEL-BASE SUPERALLOYS FOR TURBINE DISKS by P.L. Antona and A. Bennani	18
FORMING METALS BY RAPID SOLIDIFICATION by A.R.E. Singer	19
 DISCUSSION SUMMARY	 D

BASIC TRENDS IN ADVANCED FABRICATION PROCESSES

by

H.H. Walther
FIAT-Centro Ricerche
Strada Torino 50
10043 Orbassano
Italy

I accepted with pleasure the opportunity to present the keynote address to this specialists meeting of the AGARD Structures and Materials Panel. In doing so, I think it is essentially my task to give some comments on the actual and future trends of development so far as the title of the meeting, "Advanced Fabrication Processes" is concerned. These comments must of course be understood as the expression of a personal opinion on the subjects selected by the conference committee.

Could I therefore begin to recall in our minds the objectives of the meeting with the help of Tab. I. First listed there is the basic problem which all of us have to deal with; this is to look for lower cost, higher quality aerospace components. The AGARD "Structures and Materials Panel" is considered as an ideal forum to bring together material specialists, component designers and process engineers from the various NATO nations so that they could find occasions to identify new process opportunities when they discuss the emerging technological fundamentals in metals deformation, removal, joining, alloying and structural transformation. Such fundamentals have to be discussed of course in relation to the obtained material properties, the component performance and the possibilities of control during the process and during service. The panel will discuss both, the research needs and the production aspects of these items as far as the actually more important processes are concerned, such as machining, surface treatments and net shape processing; these processes in fact coincide practically with the thematics of the various sessions. As a result of the meeting, one may find highlights that could help to define current potentials and fruitful approaches for process improvements and to provide practical actions for achieving them in the various NATO nations.

Next I should shortly mention those of the technological fundamentals which have already emerged in former AGARD specialists - or working group meetings. This is done with Tab. II, where I have tried to summarise the views given in the preparatory working group meetings by G.P. Peterson, W. Bunk, G. Bollani, J.R. Lee, E. Huellec, the national representatives respectively of the U.S.A., the Fed. Rep. of Germany, Italy, the U.K. and France.

Powder metallurgy has emerged probably as the most important highlight as discussed in the Ottawa meeting of 1976.

In a first part of that meeting the various processes of centrifugal atomization for producing titanium powders were examined as well as argon and vacuum atomization processes for nickel base superalloy particles. All stages of the consolidation process (powder handling, canning techniques, consolidation, residual working, thermal treatments) were discussed in the second part. The specialists felt, that a cost saving potential of $\sim 50\%$ exists, using P.M. net shape processing instead of conventional manufacturing, and hot isostatic pressing appeared to be most promising. Areas, recommended for further R & D work are manyfold:

- The deformation process requires, besides improved canning techniques, the development of mathematical models which describe the best way of net shape achievement, the forming limits and models which would allow for Computer Aided Design (CAD).
- Joining will certainly concern the problem of powder metallurgically processed metal matrix composites besides the weldability problems of P.M. materials itself.
- New and quality improved alloys will be developed, since P.M. alloys would not be limited by constraints of being "castable" or "workable". Composition and microstructure of these alloys will be designed according to the specific mission of the component, using, instead of the conventional approach by means of a "safety factor" (which is often an ignorance factor), the components reliability and its survival probability in function of stress and time.
- As heat treatment procedures for P.M. alloys, one can certainly not use a priori the ones for conventional alloys. On the one hand it is no more necessary, because of the isotropic and homogeneous fine grain structures of P.M. alloys, to dissolve the macrosegregations; on the other hand the metallurgist may find himself faced with problems of diffused microporosities and microinclusions along the original grain boundaries. Furthermore the intermetallic phases, distributed in an extremely fine way, do certainly exhibit a different kinetic evolution process.
- Concerning performance in service, there is need of correlating materials properties with compaction parameters and microstructure, of evaluating the importance of residual stresses and of developing methods for lifetime prediction in function of the mission analysis.

- Problems of process control regard the contamination of powders, the presence of defects like micropores and inclusions and should possibly be feasible "on line" and by non destructive inspection, whilst control of material performance should face the problem of the evolution of the microstructure and of the defects.
- Development of P.M. should not lead however to a situation where the assessment of other technologies, competing in net shape processing is being neglected. Competitive technologies include hot die forging, superplastic formation, extrusion etc; they do present to a certain extent analogous R & D problems as P.M. techniques.

Machining processes, despite the increasing efforts to achieve metal removal savings through net shape processing, machining still represent a high fraction of manufacturing costs.

- Research in the field of materials removal should be concentrated very much on the development of mathematical models which relate the cutting speed with tool wear and surface finish.
- The performance of machined surfaces should then be described by studying the surface finish with the surface properties in relation to wear, friction, residual stresses etc.
- The design of surface finish, according to specific requirements in service, its integration with process optimization and automatic control of the process, is then the logical further step.

Laser metal working is a process which has very recently entered into the picture, since continuous wave high power CO_2 - lasers became commercially available.

Because of its application in cutting and drilling, the laser technique could be placed in Tab. II rather close to machining. A more logical place is however amongst the surface treatments and processes because the interaction depth between photons and matter is limited to about $10 \mu\text{m}$, the used wavelength. The state of the art in laser processing may be summarised as follows. Fully reliable laser sources are available up to a power level of a few kilowatts and more than hundred of them are already used in production. At the highest power levels now available (say 15 kw) industrial reliability of the source is expected to be reached in a very few years, just the time necessary for developing the technological fundamentals for many economically interesting high quality processes. High power laser manufacturers have already performed extremely useful process development work, in order to demonstrate laser potentialities, but much more work is still to be done by the utilizers in tailoring the so developed potential towards practical applications.

- Concerning deformation, it can be mentioned that all the various laser processes are generating very little thermal distortions. This is due to the fact that the laser energy can be used very economically just in such surface zones of a component where processing is really necessary; useless heating of other zones and of the volume of the component can in general be avoided because of the high power densities available (say 10^6 W/cm^2) and the consequently short times of processing.
- Materials removal as high speed cutting and drilling in conjunction with numerical control is promising, especially because of the fact that mechanical clamping systems become useless and the inertia free laser beam can be moved instead of the sample or the whole tool machine.
- The joining processes such as welding or coating are characterized by very thin heat affected zones.
Laser welding is comparable in speed and quality with electron beam welding but with the advantage to be executed in open air. In coating, the laser achieves a bonding between the protective surface and the substrate which is comparable with that obtained in welding.
- Surface alloying with the laser offers an enormously wide range of new possibilities, such as: using strategical elements (e.g. Cr) just at the surface where they are useful, developing new compositions not so strictly limited by thermodynamic stability considerations, controlling grain size and grain orientation and obtaining, always just at the surface, glass like structures of amorphous metals, the discussion of which could alone be subject of a complete symposium.
- Heat treatment of the surface, which in the case of the laser is essentially transformation hardening, shall be useable for precompression or hardening of dynamically stressed alloyed steel components such as shafts, levers, bearings etc.
- The evaluation of the performance of laser treated materials and components will logically require consideration of the behaviour of multilayer systems in relation to all the involved properties and the resulting mutual compatibility of those layers.
- The control of laser working processes, which present the tendency of being executed as "on line processes", will consequently be on line as well and furthermore automatic. Temperature measuring devices shall control the laser power during the process, case thicknesses of the product are thought to be measurable by magnetic, electric and acoustic devices whilst for defects in the structure (e.g. microcracks in welding) the acoustic emission might be employed.

Looking back to Tab. II, I found myself attempting to define the highlight of the listed highlights. As mathematical modelling is the subject listed most frequently, I should like to

make a comment on this. In a somewhat schematic way I would say, as shown in Tab. III, that we had a boom of computer installations in the 1960's, a period in which programming was however still restricted to a special group of mathematicians. In the 1970's then, programming became a more or less common tool of the research worker, and we had a programming boom. The widespread availability of computer and programs together makes further more sophisticated modeling of the processing and the performance of materials and components more attractive and more feasible. We should therefore expect for the 1980's a boom driven by the steadily increasing needs for compensating the cost increase of man power, energy and raw materials.

After this general remarks, I should like to comment further on two items, hot isostatic pressing (HIP) and laser metal working, which constitute two specific contributions from Italy.

Hot isostatic pressing is infact applied in the FIAT-Research Center for producing a near net shape turbine disk of ASTROLOY with a diameter of 30 cm, aiming for a cost reduction of 40% as compared to conventional processing. Fig. 1 shows the shape prior to the consolidation step by HIP. This initial shape has been defined after an intensive study of the deformation process with a series of models simulating critical parts of the disk.

This technology shows a very high potential for cost savings, provided however that high temperature properties, namely low cycle fatigue and creep and processing properties, mainly weldability, of HIP produced materials confirm the promises so far indicated.

In addition, future efforts in the field of fabrication processes shall concern:

- The development of cheaper canning systems, considering also vitreous or ceramic materials.
- New inspection criteria for testing complex preforms.
- The performance of HIP superalloys in true scale tests.
- Optimization of specific heat treatments.

On this latter item a paper will be presented in session four of this conference.

Laser processing can be proposed in a large range of power densities and interaction times, as displayed in Fig. 2. The processes now being utilized include:

- deep penetration welding
- laser cutting
- drilling of holes
- transformation hardening
- surface alloying and coating.

It is a general opinion that the feasibility of these five operations has thoroughly been demonstrated so that an increasing industrial use appears assured. Two further techniques have been proposed more recently:

- laser shockhardening, where the blast wave, that accompanies rapid surface evaporation induced by an intense laser pulse, is used to cause a work hardening effect;
- melt quenching where extremely fast quenching of a molten layer allows one to obtain not only fine grain but even amorphous solid state structures.

From the display of Fig. 2, I want to discuss three typical examples:

The first one is welding. In this case the laser could substitute in principle electron beam welding with the advantage that vacuum would no longer be required. This might compensate the actual disadvantage that laser equipments cost still ~ 20 to 30% more than comparable electron beam devices. It seems to us, that roughly 50 to 100 electron beam devices, having a power range between 5 to 10 KW, are being actually sold per year to the aeronautical industry; this compares with an actual selling rate of ~ 5 equivalent lasers. Such a situation, where advantages and disadvantages of two equivalent techniques are almost balanced, leads us to the assumption that in about 10 years the laser will do the same amount of aerospace welding as the electron beam will do at that time.

Fig. 3 indicates very concisely the field where laser (and electron beam) welding can develop its full economic potential. Shown is an experimentally confirmed calculated correlation between welding speed V and power P , indicating that as much as 50% of the dissipated heat can be used to melt the material if the speed is sufficiently high. One expects then a minimum of heat affected zones and distortions. Speed times welding width b is normalized to thermal diffusivity k (low values help for optimization), and laser power to melting temperature T_M , heat conductivity α and penetration depth t (again low values help for optimization). As an example, the lowest reported experimental point refers to $t = S = 8$ mm, $V = 0,5$ m/min and $P = 8,5$ KW. It is evident from this picture that one should preferentially use the laser at several kilowatts (say ~ 5 KW) for fast welding (say ~ 3 m/min) and for materials up to medium thicknesses (say 5 mm).

The second example is transformation hardening with the laser, as compared with the conventional induction method. A typical result is shown in Fig. 4 with the obtained martensitic structure on a

ferritic base material and the intermediate transition zone, together with the achieved hardness profile. In this field, one should not expect (as in the case of electron beam welding) a tendency to replace the conventional technique; the induction method is in fact sufficiently cheaper to prevent this. One could however expect the laser to extend transformation hardening also in zones not accessible by induction coils. Such zones could be especially the ones where fatigue cracks are generated; martensite formation would create there a state of local precompression and prevent or delay crack-generation.

As a third example, I should like to mention a problem not resolved so far by any conventional process. Fig. 5 shows a wear resistant coating of Mo, Ni and Cr - carbide on a lamellar cast iron substrate. It is seen, from the concentration and hardness profiles, that the coating is sufficiently thick and perfectly bonds to the substrate. For comparison, plasma sprayed layers have notoriously bad bondings, but a porosity which might be useful for retaining a certain quantity of lubricant. Without sacrificing the bonding, one can provide by means of the laser for a useful porosity as well. This is shown in Fig. 6 by almost spherical pores, distributed uniformly in the zone ranging from the surface to the interface with the base material. These pores have been produced by Si - particles evaporating during the laser coating process.

It would now be logical to bring a fourth example in which laser processing opportunities have stimulated engineers to redesign components, but I regret not to have one. I suppose that not many examples do yet exist but I am expecting many of them in the near future.

TABLE I

PROBLEM :

TO PRODUCE

- LOWER COST
 - HIGHER QUALITY
- AEROSPACE COMPONENTS

TO BRING TOGETHER

- MATERIALS SPECIALISTS
- COMPONENT DESIGNERS
- PROCESS ENGINEERS

IN ORDER

TO IDENTIFY PROCESS OPPORTUNITIES IN

OBJECTIVES :

- MACHINING
- SURFACE TREATMENTS
- NET SHAPE PROCESSING

TO DEFINE

- CURRENT POTENTIALS
 - FRUITFUL APPROACHES
- FOR ACHIEVING IMPROVEMENTS

TO PROMOTE PRACTICAL APPLICATIONS OF
PROCESS IMPROVEMENTS TO

- AEROSPACE HARDWARE
- WITHIN ALL THE NATO NATIONS

TABLE II - EMERGING TECHNOLOGICAL FUNDAMENTALS FOR VARIOUS ACTUALLY INTERESTING PROCESSES

FUNDAMENTALS PROCESSES	DEFORMATION	REMOVAL	JOINING	ALLOYING	HEAT TREATM.	PERFORMANCES	CONTROL
	<ul style="list-style-type: none"> - DEVEL. OF P.M. CANNING TECHNIQUES • POWDER MET. • HOT DIE FORG. • SUPERPL. FORM. • EXTRUSION 	<ul style="list-style-type: none"> - TO BE KEPT MINIMUM - FINISHING MACHINING 	<ul style="list-style-type: none"> - P.M. METAL MATRIX COMPOSITES - WELDABILITY OF P.M. - MAT. 	<ul style="list-style-type: none"> - NEW P.M. ALLOYS - DESIGN OF COMPOSITION AND MICRO-STRUCTURE ACCORDING TO MISSION 	<ul style="list-style-type: none"> - TO BE OPTIMIZED FOR ALL THE SINGLE P.M. MATERIALS - TRANSFORMATION HARDENING 	<ul style="list-style-type: none"> - CORRELATION WITH : • COMPACTION • MICRO-STRUCTURE - EFFECTS OF RES. STRESS - MISSION ANALYSIS - LIFETIME PREDICTION 	<ul style="list-style-type: none"> - CONTAMIN. - EVOLUTION OF : • MICROSTRUC. • DEFECTS - ON LINE PROCESS - DEVEL. OF N.D. I.
• MACHINING		<ul style="list-style-type: none"> - MODELLING : • CUT SPEED • TOOL WEAR • SURF. FINISH 				<ul style="list-style-type: none"> - CORRELATION WITH : • SURFACE FINISH • PROPERTIES 	<ul style="list-style-type: none"> - SURFACE FINISH BY REMOTE AUTOMATISM
<ul style="list-style-type: none"> • LASER WORKING • VAPOR DEPOS. • ION IMPLANTAT. 	<ul style="list-style-type: none"> - STRESS ANALYSIS TO AVOID DISTORSION 	<ul style="list-style-type: none"> - HIGH SPEED • CUTTING • DRILLING 	<ul style="list-style-type: none"> - PRECISION WELDING - COATINGS WITH IMPROVED BINDING 	<ul style="list-style-type: none"> - NEW ALLOYS • FINE GRAIN • GRAIN ORIENTED • AMORPHOUS 	<ul style="list-style-type: none"> - TRANSFORMATION HARDENING 	<ul style="list-style-type: none"> - MODELLING OF THE BEHAVIOUR OF MULTILAYER SYSTEMS 	<ul style="list-style-type: none"> - ON LINE PROCESS BY N.D. I.

TABLE III

1960 ' S :	COMPUTER BOOM
1970 ' S :	PROGRAMMING BOOM
1980 ' S :	MODELLING BOOM

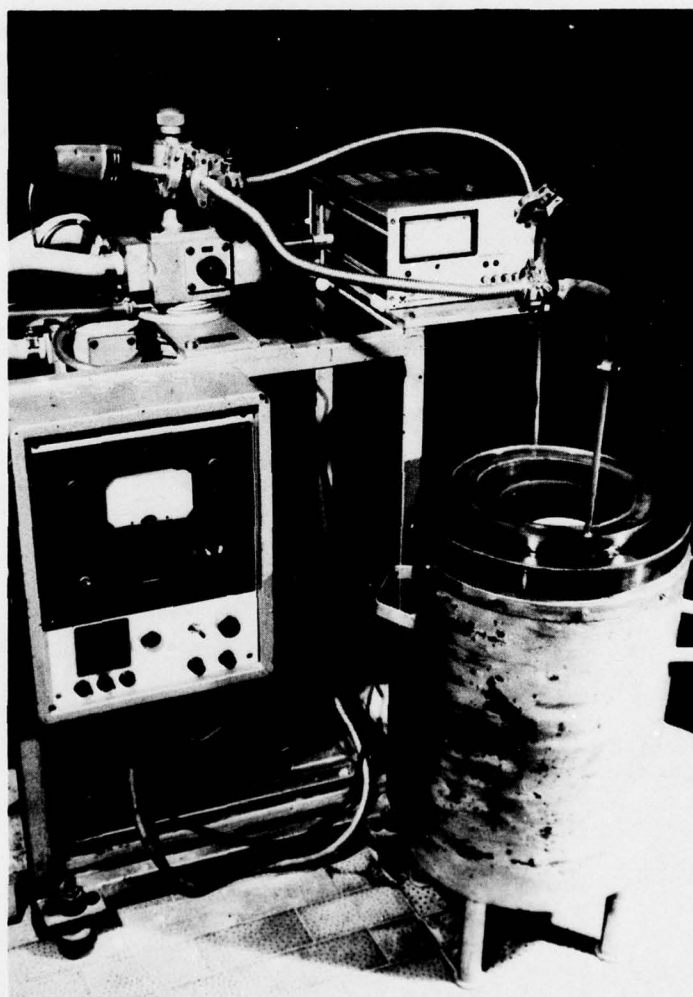


FIG. 1 — PRIOR TO CONSOLIDATION SHAPE OF A 30 cm DIAMETER ASTROLOY
TURBINE DISK

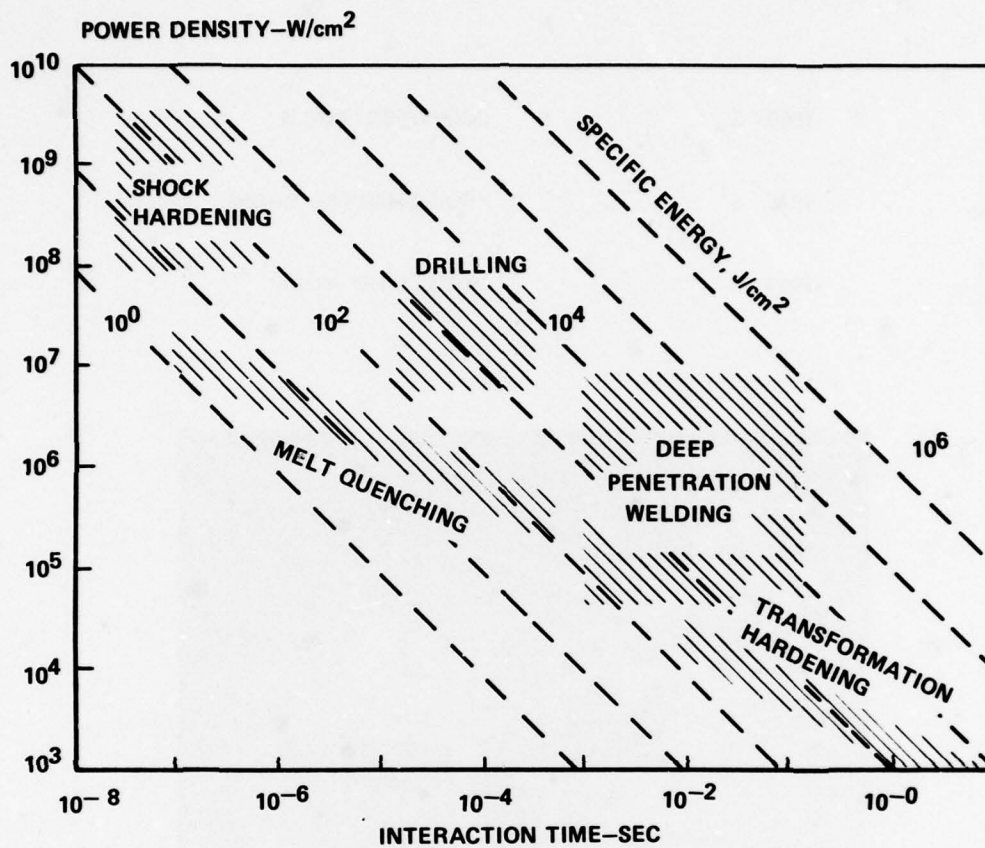
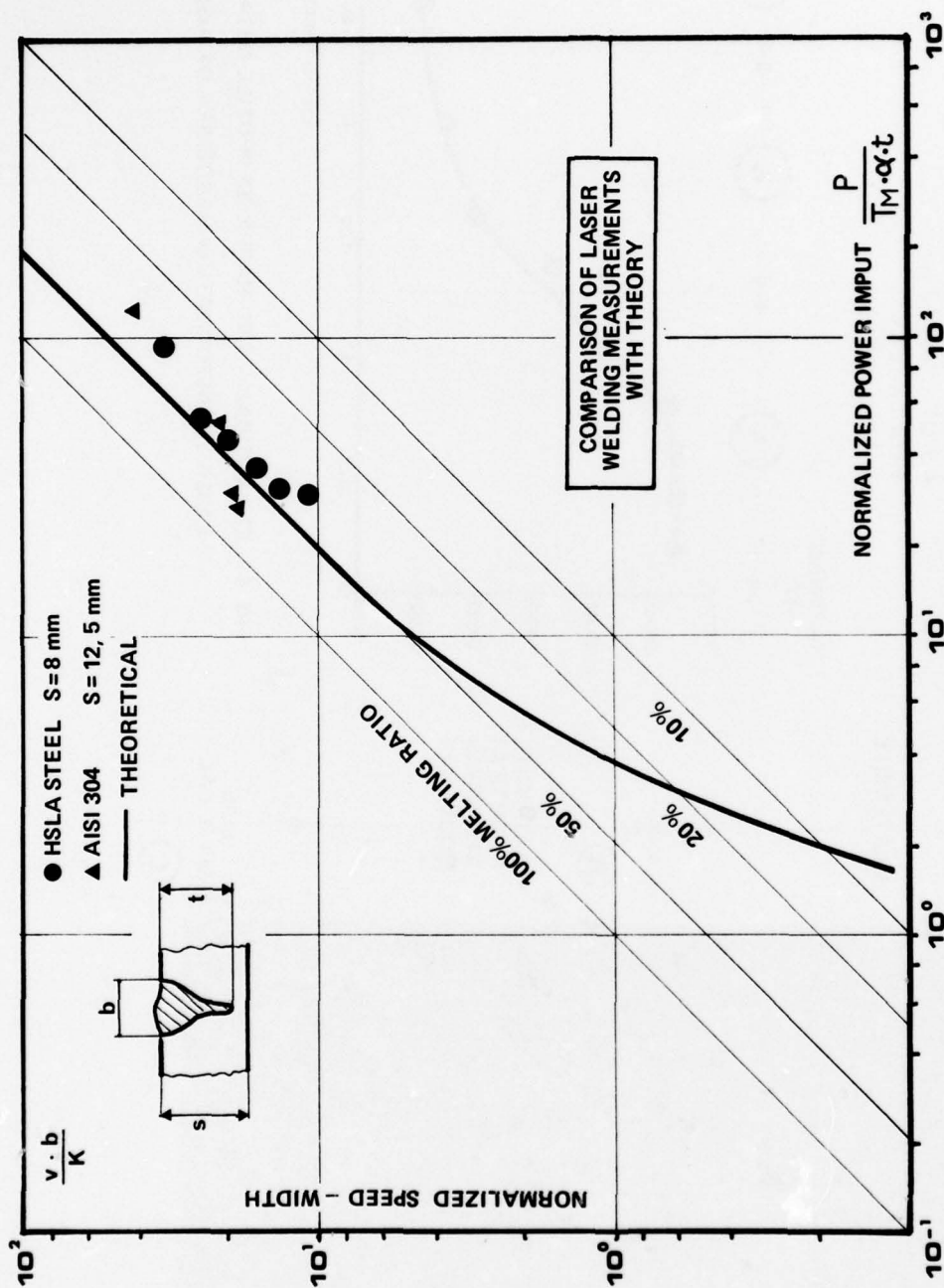


FIG. 2 - DISPLAY OF LASER PROCESSING TECHNIQUES IN FUNCTION OF POWER DENSITY AND INTERACTION TIME



LASER TRANSFORMATION HARDENING

MATERIAL : AISI 1045 STEEL

- SPOT 1,2 x 1,2 cm
- POWER 12 Kw
- SPEED 0,8 m/min

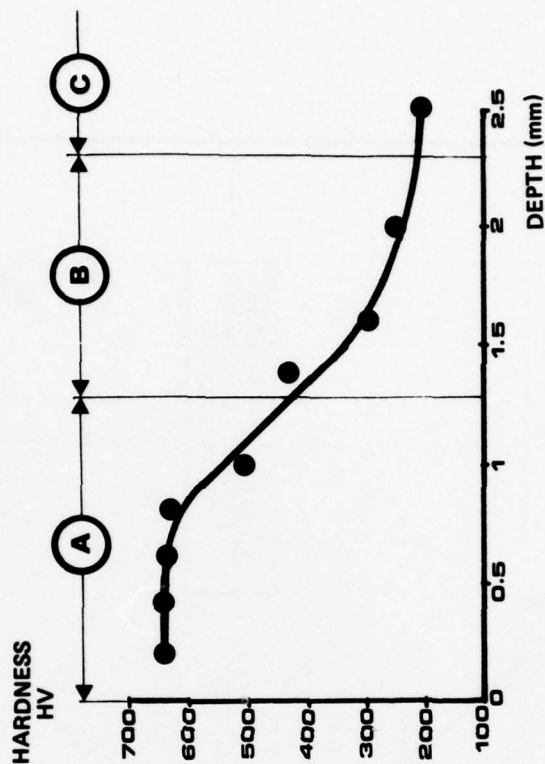
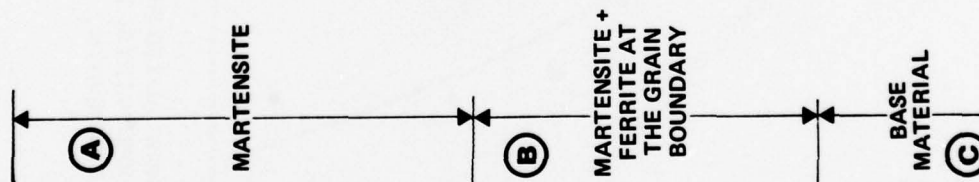
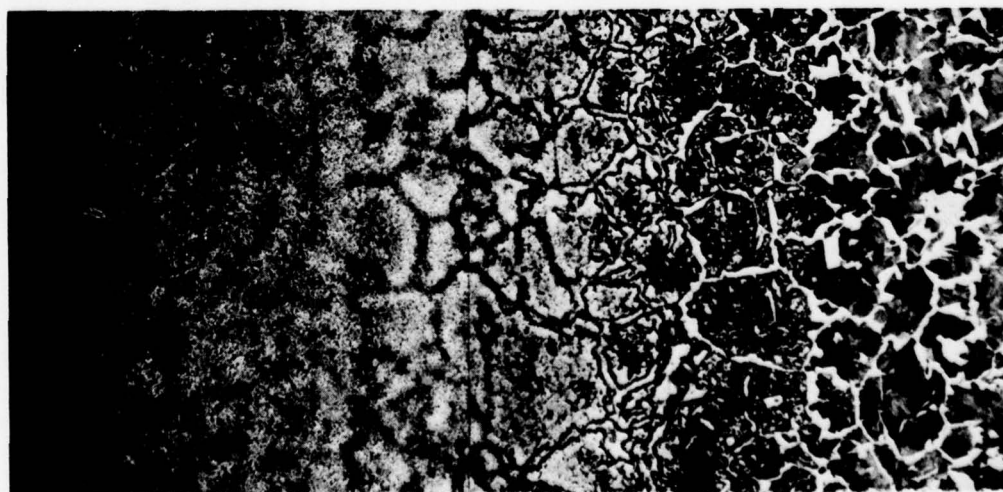


FIG. 4 - STRUCTURAL - AND HARDNESS PROFILE OBTAINED BY
LASER TRANSFORMATION HARDENING OF AISI 1045



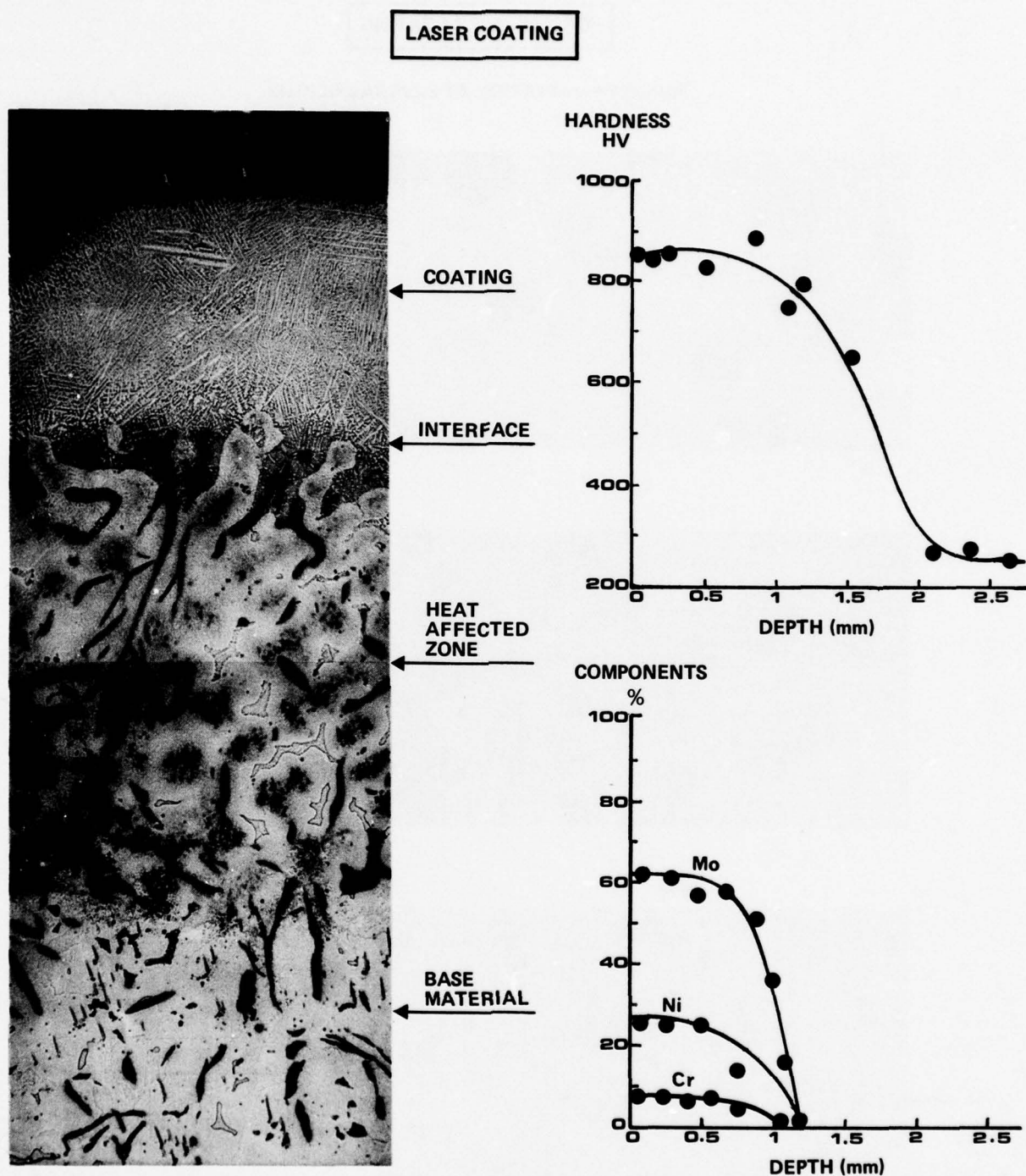
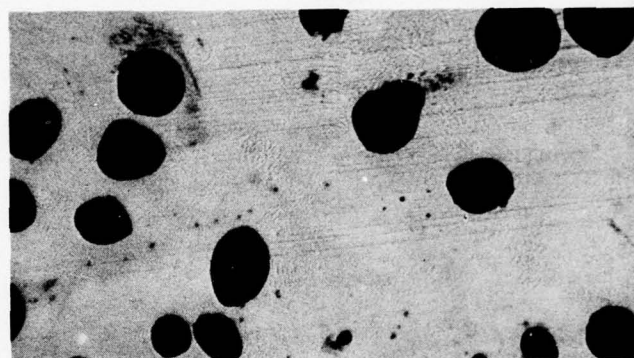
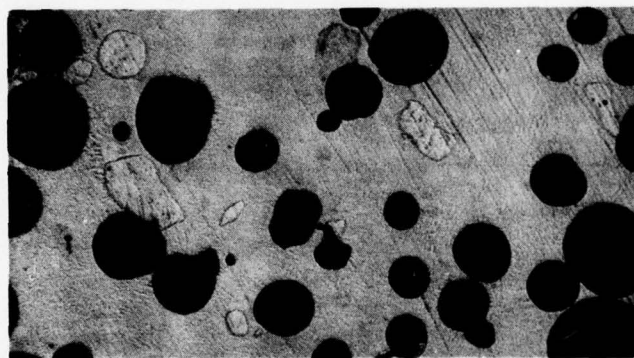
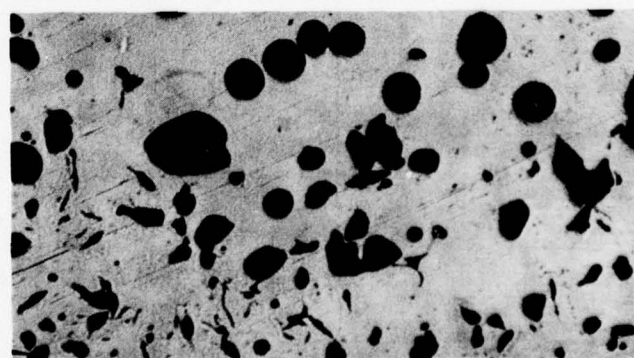


FIG. 5 — HIGH DENSITY Cr/Ni/Mo - COATING ON LAMELLAR CAST IRON
OBTAINED BY LASER PROCESSING

POROUS LASER COATING**POROSITY VARIATION AT SEVERAL DEPTHS****NEAR SURFACE****HALF DEPTH****INTERFACE**

**FIG. 6 - Cr/Ni/Mo - COATING WITH LUBRICANT RETAINING PORES ON LAMELLAR
CAST IRON OBTAINED BY LASER PROCESSING**

Applied Research on the Machinability of Titanium and its Alloys

o. Prof. Dr.-Ing. W. König
 Lehrstuhl für Technologie der Fertigungsverfahren
 Laboratorium für Werkzeugmaschinen und Betriebs-
 lehre der Rhein.-Westf. Technischen Hochschule Aachen
 Sommerfeldstraße - D-5100 Aachen - West Germany

Summary

Low thermal conductivity and high mechanical resistance at elevated temperatures are characteristic properties of titanium alloys. They cause high thermal and mechanical loads during machining. Thus, cutting materials with high toughness and good thermal conductivity shall be used. Small changes in cutting speed cause extremely high changes in tool life. To obtain maximum material removal rates the feed should be selected as high as possible. In order to reduce wear cooling is very important, especially the supply of sufficient quantities of cutting fluids. The analysis of the endmilling process results in recommendations to increase both, productivity and accuracy.

In grinding the choice of wheels is restricted by the thermal and chemical properties of the titanium. Oxidic abrasives shall not be used also not wheels with resinoid bond. Within the group of vitrified silicon carbide wheels, the wear finally is a matter of hardness. The "super-abrasives" diamond and cubic boron nitride give considerable improvements in G-ratio. In general, oil has proved to be more suitable than water based coolants.

1. Problems in the machining of titanium

Problems in the machining of titanium alloys result mainly from the following physical properties of these materials: low specific heat and thermal conductivity, constant decrease in strength with rising temperature, a small degree of rigidity as a result of the low modulus of elasticity and relatively low elongation.

In comparison with steel, the heat capacity of titanium is much reduced. The consequence is that a considerably greater part of the heat that is generated during cutting enters into the tool because it cannot be removed with the chip or flow into the workpiece being machined (fig. 1). In the case of the machining of steel the tool must absorb a maximum of half the generated heat, with the machining of titanium it is about 80 per cent. It is true that the thermal properties of various cutting materials also influence the distribution of the stream of heat, but they have no effect on the fundamentally more unfavourable conditions in the working of titanium /1/.

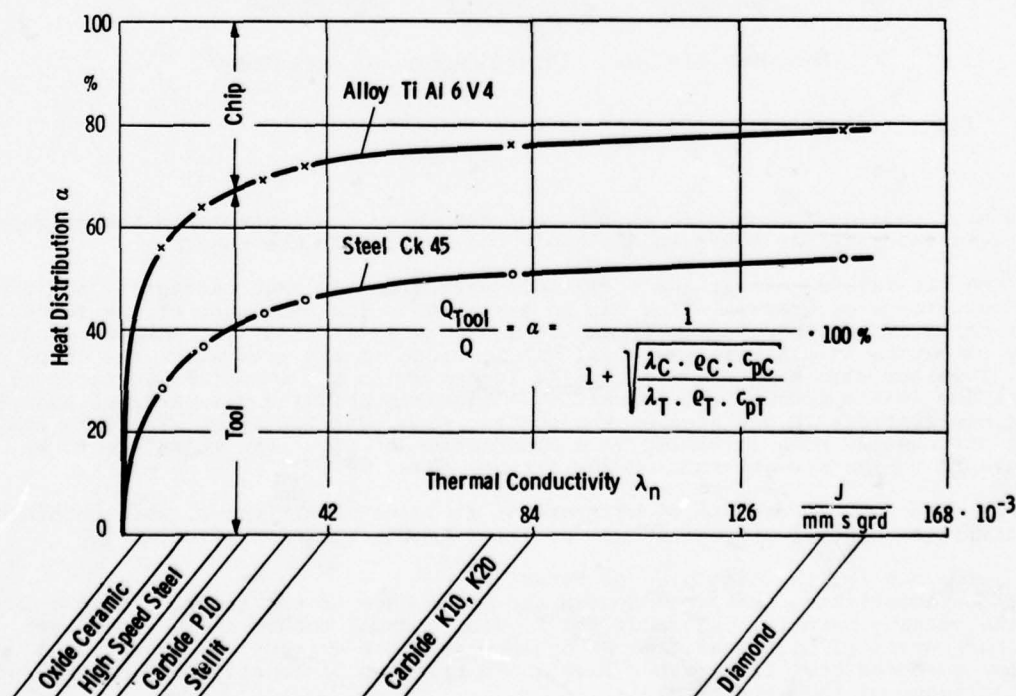


Fig. 1: Distribution of thermal load on turning tools

In addition to the high thermal load, high mechanical stresses occur in the immediate neighbourhood of the cutting edge (fig. 2). If the normal and tangential stresses in the turning of a normalised steel, a nickel-base alloy and a titanium alloy are compared, the size of the extra load on the cutting edge caused by the titanium is obvious. The stresses are three to four times as high as in the case of steel. A reason for this is to be found in the high resistance to deformation of titanium which is decreasing considerably only with temperatures above 800° to 1000° C. A further reason is the comparatively small surface of contact on the rake face of the tools /2/.

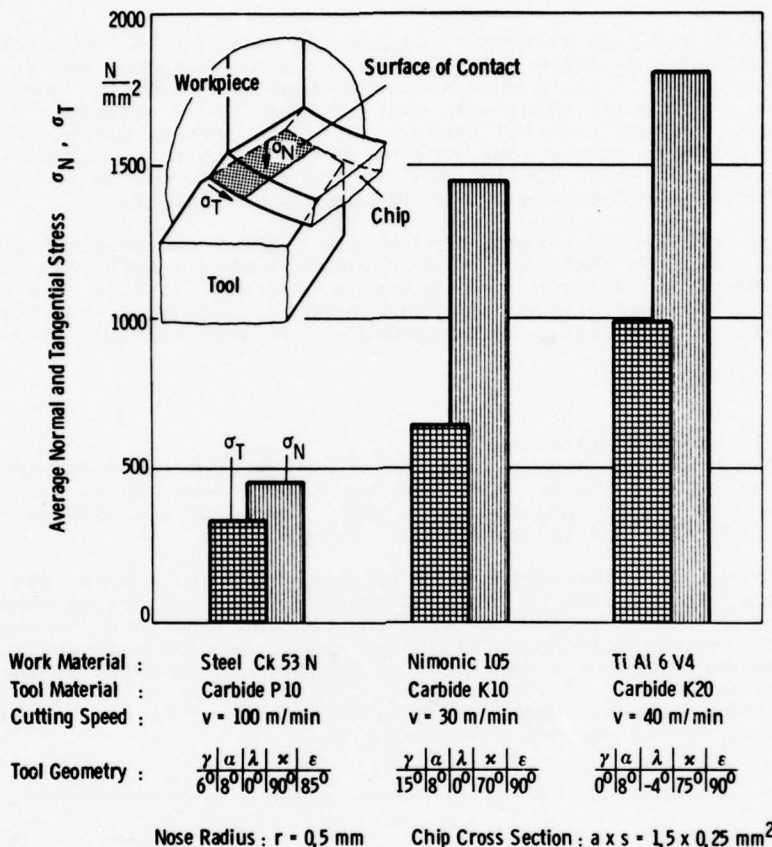


Fig. 2: Stresses on the rake face of turning tools

Through the high cutting forces with at the same time high temperatures on the surface of contact plastic deformations occur to HSS tools and accelerate the wear.

The reason for the failure of carbide tools is, apart from the high mechanical and thermal loads, the occurrence of cracks, which can be ascribed to the mechanism of the formation of lamellar chips. This kind of chip formation suggests an alternation between compression and sliding processes in a limited material volume close to the area where the chips are originated. Together with high dynamic cutting forces which can amount to 30 per cent of the value of the static forces, the formation of lamellar chips is the cause of additional temperature oscillations in the area of the contact zone. The formation of cracks and the chipping of the cutting edge resulting as a consequence of this, are therefore to be finally ascribed to dynamic stresses on the cutting edge.

Since thermal effects as the cause of wear are of decisive significance, when machining titanium materials, special attention must be drawn to the question of cooling.

2. Cutting materials for the machining of titanium

The special characteristics mentioned demand the observance of additional criteria in the choice of the cutting materials. In addition to good thermal conductivity and a high degree of heat capacity, high qualities of dynamic strength are just as essential a condition for adequate tool life as the inertia in reaction of constituents of the cutting material with those of the work material.

Because of the rapid loss of hardness at elevated temperatures above 600°C, high speed steels can be used only at low cutting speeds (fig. 3). They are still used today in nearly all machining operations. The best cutting efficiency is to be obtained with the grades containing high amounts of tungsten and cobalt.

Stellites have proved themselves extremely good in the machining of titanium. Because of the high cobalt content, their thermal conductivity is about double as high as that of the high speed steels. For this reason the generated heat is quickly led away from the contact zone and the temperature gradient in the tool tip is comparatively low. The favourable effect of these qualities can be read from the higher cutting speed that can be used (fig. 3), which lies some 150 per cent above that possible with high speed steel.

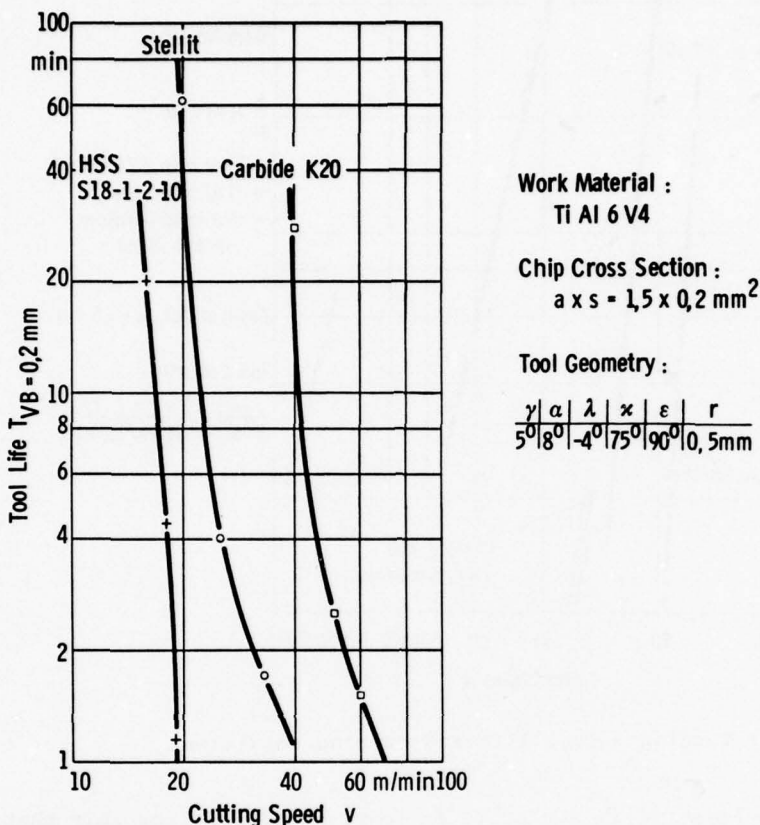


Fig. 3: Performance of different cutting materials in turning

Carbides of the ISO grade P are not suitable for machining titanium. The reason for this is likewise to be found in their thermal properties. Because of stresses due to temperature, chipping on the rake face occurs. With cutting speeds above $v = 63 \text{ m/min}$, the cutting edges break completely down immediately after cutting has begun. Using grades with a high titanium carbide content, increased wear results at lower cutting speeds by reason of chemical reaction between the tool and the work material.

For the reason too that the binding metal cobalt easily dissolves in titanium, carbides containing only little cobalt should be used. A lower cobalt content, however, leads to reduced rigidity of the cutting edge. The most favourable compromise between a limited cobalt content and a still adequate rigidity of the cutting edge for machining titanium is obviously to be found in the carbides of the ISO grades K10 to K20. They have proved their superiority in almost all machining processes [1].

3. Turning

In turning, carbide tools with rake angles $\gamma = -5^\circ$ to $+5^\circ$ and back rake angles $\lambda = 0^\circ$ to -5° have proved to be optimal. The clearance angle α should amount to $\alpha = 8^\circ$, the side cutting edge angle κ should by choice be as large as possible. To avoid instabilities and too high thrust forces, side cutting edge angles $\kappa > 45^\circ$ are, however, not to be recommended.

Within the profitable range small changes in cutting speeds may cause extremely high changes in tool life (fig. 4).

Because of these high tool life-cutting speed-gradients, a loss of tool life of more than 90 per cent is to be expected when the cutting speed is increased by approximately 10 per cent. Only values taken at random are available for the unalloyed titanium as well as for the titanium alloys TiAl6 Sn 2 Zr 4 Mo 2 and TiAl 6 Zr 5 Mo 0.5. However, it can be seen from them that the more temperature resistant alloys are more difficult to machine. The cause of this can be that the dynamic cutting force components measured with these materials are considerably higher than with the Ti Al 6 V 4 alloy. On the other hand the cutting force values ascertained with the unalloyed titanium (DIN 3.70 55) are very much

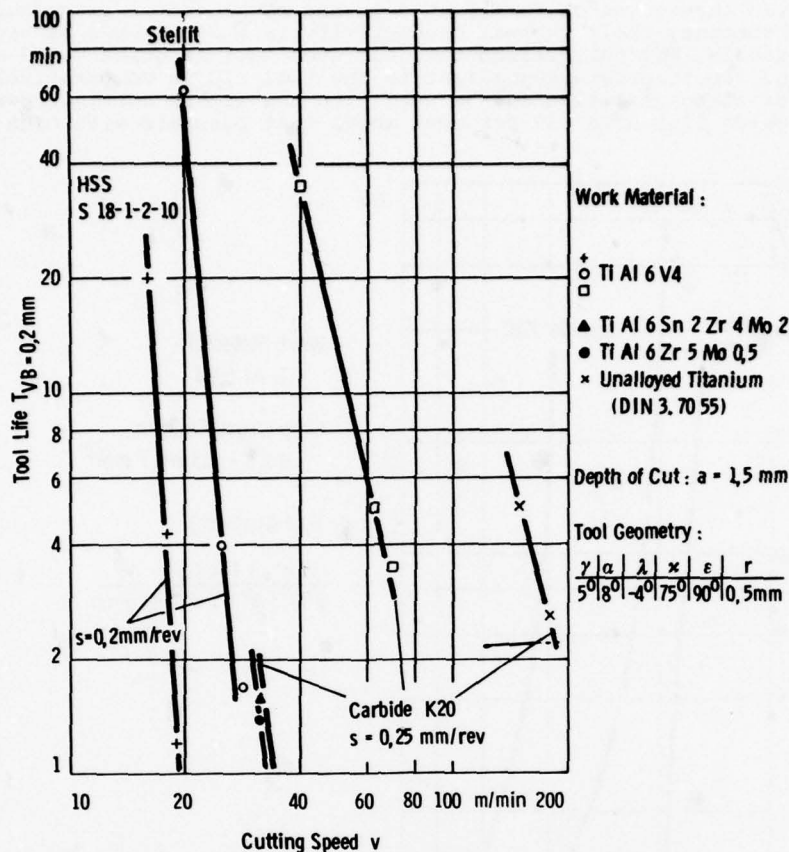


Fig. 4: Turning - tool life and cutting conditions

lower than with the alloy Ti Al 6 V 4. It is to be concluded from this that the tool life is influenced by the value of the dynamic cutting forces and the dynamic stresses caused on the cutting edge [2].

The feed has considerably less influence on tool life. In order to obtain the greatest possible economic use it should be selected as high as possible. Limits for the increase in feed can be based in the geometry of the workpieces and in the stability of the system "tool-machine". Over and above $s = 0.4$ to 0.5 mm/rev ($s = 0.016$ to 0.02 in/rev) one must be prepared to be faced with scatter. Feeds of about $s = 0.2 \text{ mm/rev}$ ($s = 0.008 \text{ in/rev}$) have proved favourable.

In general the surface quality of turned workpieces of titanium alloys is satisfactory. The surface roughness is within the range of the theoretical values that can be calculated from the nose radius of the tool and the feed. With an increase in cutting time the surface quality does not become essentially worse as long as the tool keeps its cutting efficiency. If the flank wear of carbide tools begins to increase rapidly, the surface quality deteriorates even more rapidly.

It has already been mentioned that cooling has a decisive influence on the tool life. This is now to be explained in more detail (fig. 5). The use of coolants does not in every case lead to the expected improvements in tool life. It can even lead to deterioration in tool life if cooling is done with fluids which are unsuitable for the combination of work material and cutting material. Suitable coolants normally give increases in tool life. However, there must always be checks to see whether or not even more favourable results are possible by increasing the amount added. Multiplying the amount of coolant by four leads in the example given to a doubling of the tool life. The fact that the removal of heat is decisive when machining titanium materials, is apparent from the comparison of tool life values for cooling with emulsion or oil. In spite of the repeated doubling of the quantity from 6.8 ltr/min to 11.6 ltr/min , the tools cooled with oil wear out quicker because oil can absorb far less heat than emulsion [3].

The interrelationships shown in the example of turning titanium are also valid in principle for the other methods of machining with geometrically defined cutting edges. For this reason, in the rest of this paper, only the purely technological characteristics of the individual methods are dealt with.

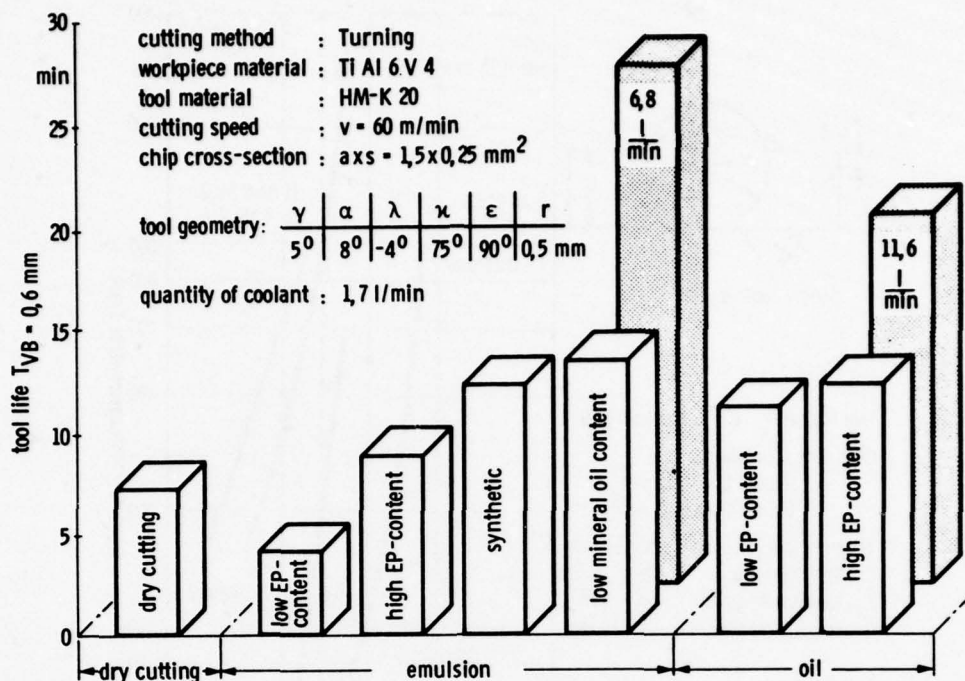


Fig. 5: Cooling - influence of type of coolant and quantity supplied

4. Milling

In Milling, the high thermal and mechanical stresses described have an especially unfavourable effect because of the interrupted cutting. The choice of the type of milling process and the conditions of contact therefore become of great importance.

In face milling, climb milling is to be preferred to conventional milling as far as the stability of the workpiece permits this. For the most part, in conventional milling only those workpieces are processed on which a hard surface layer has to be removed. The tools become worn out because of flank wear and chippings of the cutting edge. The tendency to chip is unfavourably influenced by the sticking together of work material and tool material.

The U-contact has a favourable effect on tool life. In this, the first contact between workpiece and tool takes place at the point of the rake face which is the greatest possible distance away from the cutting edge corner and the cutting edge. In this way the danger of chipping at the cutting edge is considerably lessened.

The best tool life is obtained with tools having the following geometry: rake angle

$\gamma_{ax} = \gamma_{rad} = 0^\circ$ to 5° , clearance angle $\alpha = 12^\circ$ to 15° , back rake angle $\lambda = 0^\circ$ to -5° . The dependence of the work travel that can be attained on the cutting speed and on the feed for the single tooth milling of various titanium alloys, is shown in fig. 6. The curves also show the considerable dependence on the cutting speed, already noticed in turning. The alloy TiAl6 Zr5 Mo 0.5 is much more difficult to machine than the alloy TiAl6 V4. In contrast, the alloy TiAl 6 Sn2 Zr4 Mo2 shows a slightly better machinability. For further information, fig. 6 contains two tool life curves for TiAl6 V4 for two different feed rates. Worthy of notice is that an increase of the feed from $s = 0.15 \text{ mm/tooth}$ ($s = 0.006 \text{ in/tooth}$) to $s = 0.25 \text{ mm/tooth}$ ($s = 0.01 \text{ in/tooth}$) necessitates a reduction in the cutting speed by about half. So, in a certain length of time with a smaller feed, a similar or slightly larger amount of material can be removed. The advantage of small feeds lies in the reduction of the cutting forces, so that the deformation in the system "machine, milling cutter and workpiece" can be kept small.

As tool materials when milling, carbides of the ISO grade K (K10 to K20) and high speed steels are also used. The tendency of the chips to stick to the tool can be considerably reduced by the use of cutting oils containing sulphur.

The slab milling of titanium alloys is usually carried out with tools having a helix angle of 30° to 45° . As well as a smooth running of the milling cutter, a high surface quality is attained [2/].

Because of the increase in the use of integral parts made of titanium in the construction of aircraft, the end milling process has in this field acquired great importance. To manufacture parts as exact as possible in shape and dimension, it is above all of decisive importance to observe certain relations between axial and radial cutting depths depending on the cutting conditions as well as the geometry and the number of cutting edges of the milling cutter.

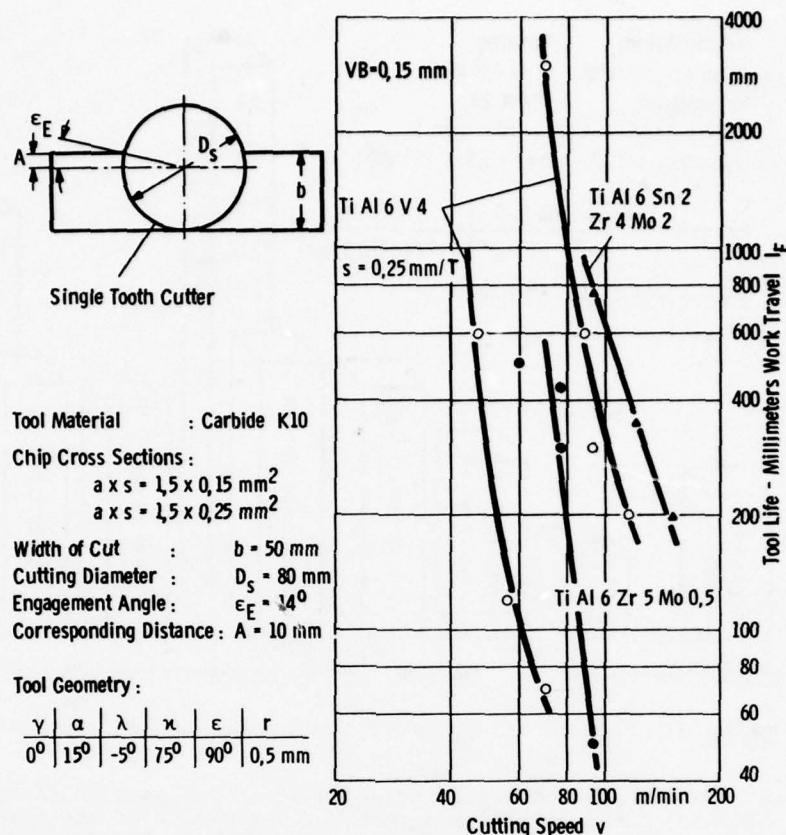


Fig. 6: Face Milling - tool life and cutting conditions

Especially in finishing with end mill cutters, because of the necessary workpiece geometry, often not very rigid tools with a small diameter and a large collar length are used. These bend under the effect of the cutting forces and this leads to wobbling motions (fig. 7). As a consequence inaccuracies result, of which the deviations in shape are the most difficult to correct.

In the right part of the illustration are shown the results of measurements, and these measurements taken from various work examples illustrate such faults. The fact that they were obtained in end mill cutting of an aluminium alloy is here of secondary importance. Basically, faults of this kind also appear in the milling of titanium alloys.

The upper and middle workpieces were milled conventionally. As tools a milling cutter with three cutting edges with 15° helix angle (above) and a non-helixed milling cutter with two cutting edges (in the middle) were used. The third workpiece was produced with a milling cutter with three cutting edges, 30° helix angle, in climb milling.

Without going into closer details attention can be drawn to the fact that in the two examples above the smallest deviations do not occur fully-left on the workpieces that is with the smallest radial depths of cut. That means that with increase of the radial depth of cut the faults become even smaller up to a certain limit. In the third example, on the other hand, practically no shape deviations but only deviations of measurement occur. By corresponding correction of the adjustment of the machine these are more easily controllable than the deviation in shape.

The fact is new that in finishing by means of a higher depth of cut a greater accuracy in shape is to be attained but this can be explained by the kinematic characteristics of this process.

The knowledge obtained up till now must be extended in future by the further development of an already existing model for the mathematical simulation of the end milling process. This is all the more important since in contrast to turning tools end milling tools with various geometries are only to be procured, if at all, with considerable expenditure of time and money [3].

Not only accuracies in shape and dimension of the workpiece are influenced by the uneven running of the milling cutter, but also very substantially the tool life. Great accuracy in true running as well as minimal collar length are therefore always to be striven for. Further, because of the extremely small feeds of each tooth and also because of the corresponding small chip thicknesses, sharp and absolutely notch-free cutting edges are basic requirement to obtain both, adequate tool life and surface quality.

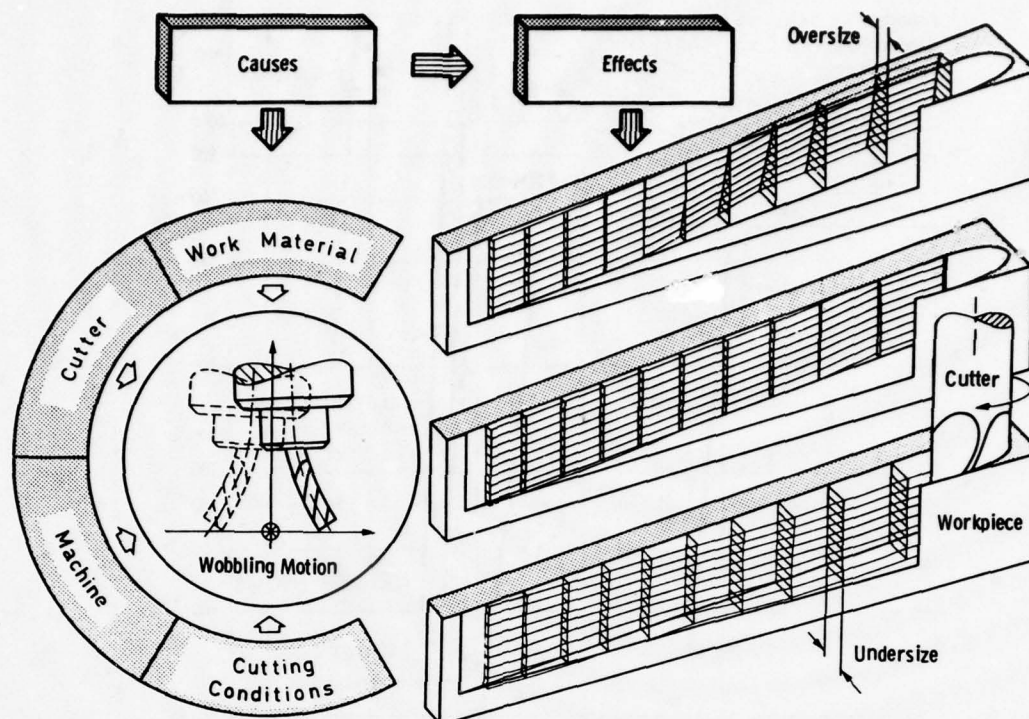


Fig. 7: End Milling - factors affecting accuracy

Tools with four cutting edges are to be preferred to those with two or three for reasons of stability. As cutting materials carbide (K10 to K20) and high speed steel are suitable, as with face milling. The cutting speeds are comparable with those of face milling.

With the use of carbide as cutting material the normal feeds per tooth are about $s_T = 0.04$ to 0.12 mm/tooth ($s_T = 0.0016$ to 0.0047 in/tooth), with high speed steel about a third greater. Rake angles of $\gamma_{ax} = \gamma_{rad} = 0^\circ$ as well as helix angles $\lambda \approx 30^\circ$ have proved to be favourable. As with face milling, the clearance angle to be chosen is about 50 per cent greater than with steel machining.

In respect of exactness of shape conventional milling is to be preferred, in respect of surface quality climb milling should be chosen.

Emulsions with a synthetic base are suitable as coolants. Large quantities should be added in a saturating stream in order to ensure, apart from an adequate cooling, also the removal of the chips.

5. Drilling

The wear of drills is in principal similar to that of turning and milling tools (fig. 8).

The tool life cutting speed gradient is very high, both with twist drills made from HSS and also with twist drills tipped with carbide. Accordingly, despite intensive and ample cooling by a saturating stream in the machining of titanium, the realisable tool life of a drill is very considerably dependent on the cutting speed. The results from the drilling of TiAl6 V 4 with forging skin show that the forging skin hardened by, for example, TiN, TiO₂, considerably reduces the drillability, so that with the same material removal rate the cutting speed must be reduced by more than 30 per cent. The HSS-drills with tool geometry as used for drilling cast iron have a point angle of 90° . This geometry of the drill point as well as the relatively high chisel edge angle of 70° produced a favourable tool life. Experiments with carbide tipped drills showed that even with higher feed the practicable cutting speed can be increased to more than 100 per cent. The attainment of these good results is dependent on an exact observance of the cutting edge geometry, especially of the notched point area with a defined length of chisel edge and the large chisel edge angle already mentioned. In comparison with chisel edge angles of 55° for normal twist drills, this relatively big angle brings with it a shortening of the chisel edge when the web thickness of the drill is the same. An additional notched point area of this chisel edge reduces the axial force and thus reduces to a minimum the pressure on the material in the area of the web. Through this the tool life of the drill and the quality of the holes are increased. As a consequence of the notched point the drill deviates less when starting to cut and the holes have less faults in roundness and are becoming less conical. At the same time the lower axial force brings about a reduced deflection of the drilling machine and deformation of the drill, so that faults resulting from this can be kept small /4/.

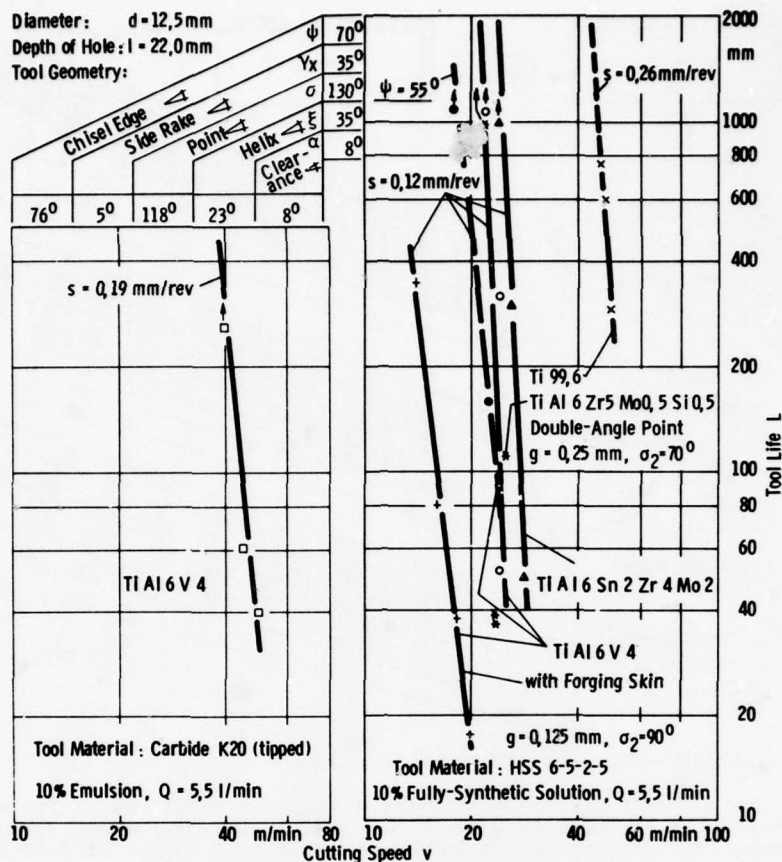


Fig. 8: Drilling - tool life and cutting conditions

An increase in the tool life of twist drills can be attained by cooling them internally (fig. 9). Inside the drills, close to the minor cutting edges, are two supply channels through which the coolant is transported straight to the major cutting edges. By means of this type of cooling, with the same tool life of the drill the cutting speed can be increased by approximately 150 per cent. The wear on the minor edge remains small, so that a better surface quality of the holes is to be expected /5/.

6. Grinding

In grinding, wheel wear is not only an important economic factor, but also in many cases a technological problem, when demands for dimensional accuracy are high. E.g. the quality of profiles in surface or cylindrical plunge grinding is directly dependent from the ability of the grinding wheel to maintain its shape during the operation.

Especially grinding of titanium and its alloys frequently goes along with excessive wheel wear, which is, generally spoken, due to three reasons: Among the mechanical material properties, high tensile strength leads to high grinding forces and corresponding frictional, tensile and shear loads on the abrasive grain and the bonding material. As a consequence of the material toughness a big portion of the input energy is converted to heat by rubbing and ploughing of the grains instead of free cutting. Furthermore, heat which is once generated will not dissipate fast enough for reasons of the low thermal conductivity of titanium. Thus, high temperature will be encountered in the contact zone between wheel and workpiece. With the presence of high temperature and pressure, finally, a precondition for the chemical activity of titanium is given.

Fig. 10 illustrates this in terms of the G-ratio (stock removal/wheel wear volume): In the field of different grinding wheel specifications, the aluminium oxide wheel A 60 R 5 V performs poorly even with the application of oil as coolant. Obviously, the affinity of titanium to oxygen does not permit the use of oxidic abrasives.

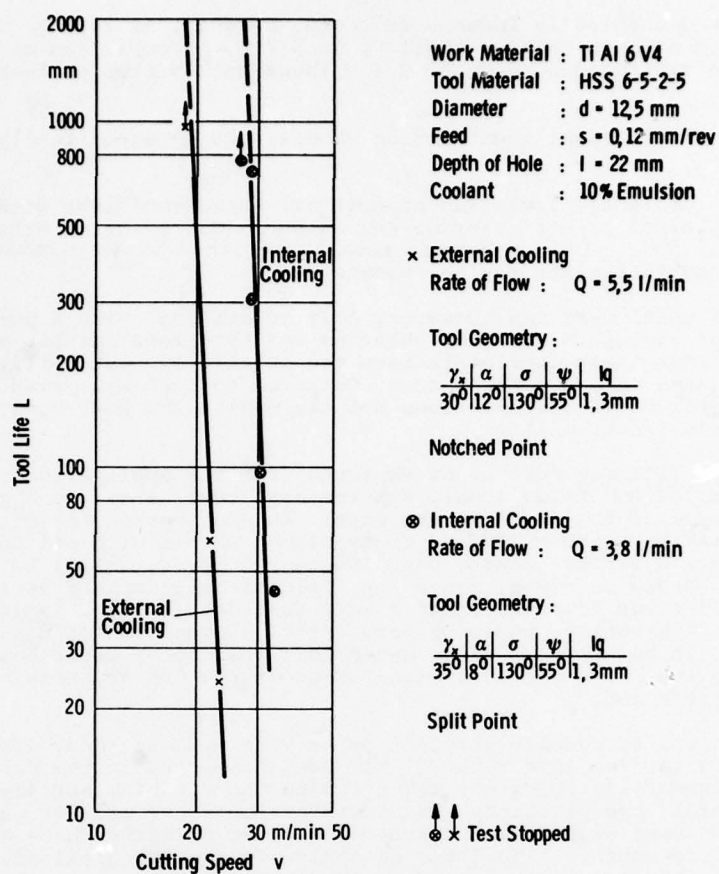


Fig. 9: Drilling - effect of internal and external cooling

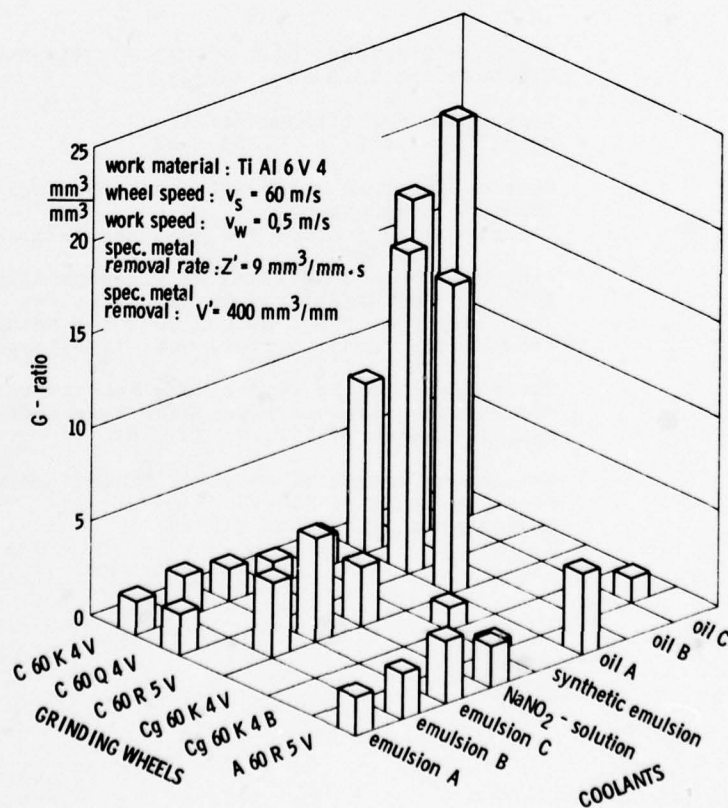


Fig. 10: Cylindrical Grinding - influence of wheel specification and coolant

Combined thermally and chemically induced wear can, however, as well be observed with a resinoid bond green silicon carbide wheel Cg 60 K 4 B. A comparison to the same specification with a vitrified bond Cg 60 K 4 V shows much better performance for the latter.

Within the group of vitrified silicon carbide wheels, the G-ratio finally is a matter of hardness.

Among the variety of coolants, including mineral oil based emulsions without (A) and with E.P.-additives of chlorine (B) or chlorine and sulphur (C), a sodium nitrate solution and a synthetic emulsion, none gives a G-ratio much better than 5. When emulsion has to be applied, sulphur based lubricants may be recommended.

Reasonable values of wheel wear can, however, only be attained with a pure oil coolant. Remarkable advantages are again given by chlorine and even more sulphur based additives. It can be concluded that these lubricants have the relatively best ability to withstand pressure and temperature in the contact zone. Compared to pure oil, even the much better heat transport of water based coolants does not compensate the heat generation which is due to insufficient lubrication /6/.

Improvements of wheel life may further be expected from the application of "super-abrasives" as diamond and cubic boron nitride (CBN). Experimental results are to a great extent dependent from the type of bond used in the wheel. An improper choice of this factor may lead to the same G-ratio as those of good conventional wheels with oil cooling. Under reasonable conditions, G-ratios greater than 100 can, however, easily be reached. Detailed recommendations can hardly be given, since the field of these abrasives themselves as well as the composition of bonds is still under a very fast development. In general, diamond and CBN perform equally. Apparently, superior hardness of diamond cannot make up for greater thermal sensitivity. It has further to be noted that the use of water based coolants may at high temperatures lead to a chemical dissolution of the CBN crystals, so that in this case oil should be preferred.

In grinding of titanium, especially aircraft parts with dynamic load, great care has to be taken with respect to surface integrity. It has been suspected in the past that some coolant additives, especially chlorine, might invade the titanium surface and cause stress corrosion. Very careful investigations have therefore been carried out parallel to these grinding tests. In no case significant traces of coolant additives have been found on or near below the machined surface. Thus, the economic and technological advantages of this wear reducing coolant should be reason enough to consider whether such tests should be initiated once more by interested industrial companies because of alterations in the binding mechanism of the present chlorine containing coolants.

References:

- 1 Kreis, W. Verschleißursachen beim Drehen von Titanwerkstoffen
Dissertation TH Aachen (1973)
- 2 Kreis, W. Zerspanung der Titanwerkstoffe
Schröder, K.-H. Metall 29 (1975) 1, S. 58 - 62
- 3 Autorengruppe Wettbewerbsfähig durch Nutzung technologischer Reserven,
Spanende Bearbeitung
Vortrag anlässlich des 16. AWK, Mai 1975, WZL, TH Aachen
- 4 König, W. Face Milling and Drilling of Titanium Alloys
Schröder, K.-H. Influence of Metallurgy on Machinability
Proc. Nr. 7 in the American Soc. for Metals, Materials/Metalworking, Techn. Series, Oct. 1975, pages 308 - 323
- 5 Autorengruppe Unveröffentlichter Bericht des Arbeitskreises
"Bearbeitung schwerzerspanbarer Werkstoffe"
WZL, TH Aachen (1972), S. 73 - 97
- 6 Hönscheid, W. Abgrenzung werkstoffgerechter Schleifbedingungen für die
Titanlegierung Ti Al6 V4
Dissertation TH Aachen (1975)

RESIDUAL STRESSES IN GRINDING

by

Prof. J. Peters, Prof. R. Snoeys,
 Dr. M. Maris
 Katholieke Universiteit Leuven
 Departement Werktuigkunde
 Afdeling Werkplaatstechniek & Industriëel Beleid
 Celestijnenlaan 300B
 B-3030 Heverlee (Belgium)

SUMMARY

Understanding the mechanism of residual stresses in grinding requires besides a precise knowledge of the thermal, metallographic, mechanical characteristics of the ground material, a measure of Young's modulus of the grinding wheel as grade characteristic, as well as the exponent f relating the equivalent cut thickness to the grinding force.

A theoretically and experimentally confirmed model gives the temperature as a function of the grinding parameters (v , v_w , a , d_e , f) and the thermal characteristics of the material.

Experimental observations will allow to explain the role of thermal expansion, metallographic transformations and mechanical forces with respect to the value of the maximum stresses and the depth of the heat affected zone. A series of hints for practice will be deduced.

SYMBOLS

a	infeed per revolution of the workpiece in plunge cylindrical grinding, depth of cut in plunge grinding
b	wheel width
c	specific heat
d_e	equivalent diameter $\frac{d_w d_s}{d_w + d_s}$ (+ for external grinding, - for internal grinding)
d_s	wheel diameter
d_w	work diameter
$e_{0.1}$	reference specific energy (for $h_{eq} = 0.1 \mu m$)
f	force sensitivity exponent
h_{eq}	equivalent cut thickness $\frac{z'}{v_s} = \frac{av_w}{v_s}$
k	thermal conductivity
	stiffness of the machine-workpiece-tool set-up
l_k	contact length
q	speed ratio $\frac{v_s}{v_w}$
v_f	feed velocity (plunge velocity)
v_s	wheel surface speed
v_w	work surface speed
z	depth under the surface
z_t	decay coefficient $z_t = \left(\frac{\sigma T}{\sigma z}\right) z=0$
z_T	depth at which a temperature T is reached
A	area
F'_t	tangential force per unit wheel width
F_l	force reference coefficient for h_{eq} equal to unity
T_{max}	maximum temperature at a depth z
T_K	maximum temperature at the surface (grinding contact)
T_{cr}	critical temperature
α	thermal diffusivity
λ	linear expansion coefficient

INTRODUCTION

Trying to survey present state of our knowledge concerning residual stresses in grinding is a challenge. For this reason we refer to a joint survey paper written on "Thermally induced surface damage in grinding" (1) as keynote paper at the General Assembly of the International Institution for Production Engineering Research 1978 and to be published in CIRP Annals 1978, Vol. I, which includes a very exhaustive list of the publication of the last 5 years. For more details about the theory of the thermal model we refer to the monography presented at the Royal Academy of Belgium in 1975 (2).

For all technical data and experimental procedures we refer to A. Decneut's (3) and M. Maris' (4) doctoral dissertations.

In the first part of this article we shall recall some notions about the role of Young's modulus as grade indication of a grinding wheel and about grinding charts as they result from our previous studies and appear fundamental for the understanding of grinding stresses.

In a second part we summarize the main findings concerning the thermal model of grinding operations and its practical applications.

We then shall consider the grinding stresses as they are experimentally observed.

We shall claim that grinding stresses are dominated by thermal expansion effects to which structural transformations and mechanically induced deformation are superimposed. Finally some hints for practice will be emphasized.

1. Fundamental parameters

The main difficulty one faces in any research on manufacturing problems is that manufacturing engineers, whose main objective is to deliver economically a product in due time, generally show no interest at all in precisely recording and analysing the manufacturing conditions. Machine tools are poorly equipped in measuring devices, apart from the dimensional ones. Nothing to measure power, forces, speed, temperature, not even hardware to check the quality of the tooling. No request for grinding charts, nor material characteristics!

No wonder that residual stresses, cracks, burning marks are treated with the tricks of medicine men or witches!

In order to master residual stresses following parameters must be carefully recorded and controlled:

a) All speed parameters, as shown in fig. 1.

wheel speed v_s , workspeed v_w , infeed speed v_f , infeed per rev a . Let us not forget that in machining operation the peripheral speed and not the number of revolutions per min is important.

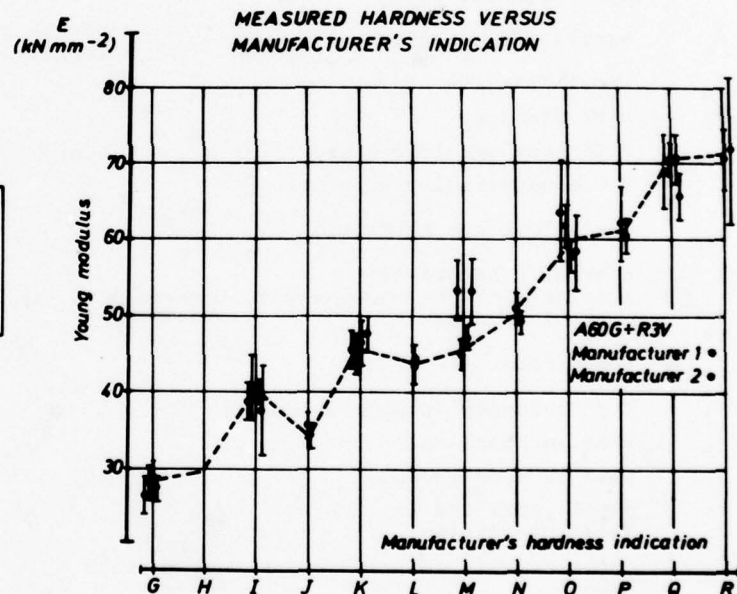
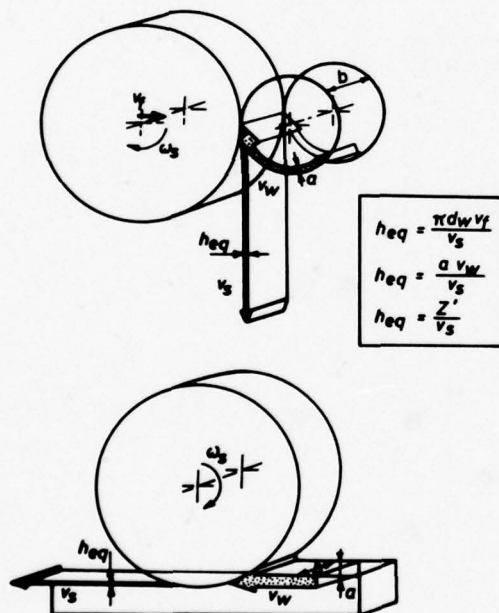


Fig. 1. Visual representation of the main notations as well as of the meaning of h_{eq} .

Fig. 2. Measured hardness versus manufacturer's indication.

b) Grinding wheel parameters and coolant characteristics must be well-known.

In general it can be admitted that the manufacturer can provide accurate information of all characteristics he masters: namely the nature of grain and bond, the grain size, porosity, etc. However previous research has shown how unreliable the commercial grade information is (fig. 2). For this reason at the starting point of this research it was proven that Young's modulus (5) of the wheel bulk material, easily measured by means of a sonic method (Grind-O-Sonic) is a reliable characteristic of the wheel grade, which is significant of its behavior at work.

It will also be shown that the composition of the coolant (oil or water emulsion) as well as the dressing lead on the grinding wheel have a major importance.

c) It can be anticipated that the thermal as well as the mechanical and metallographic properties of the work material are governing the surface integrity; therefore their numerical value should be provided to the manufacturing engineers. For the considered steel types they will be given Table I in appendix.

d) Finally basic machining data are provided by the so called "grinding charts" (fig. 3), which have been developed and now available for 50 steel-grinding wheel combinations(8).

100Cr6 (1C-1.43Cr)	HR _C : 62-63	EK60L7VX	E: 52.2 kN/mm ²
d _s (mm): 665-720	v _s (m/s): 30-45-60	SB-C 3%	
d _w (mm): 83-100	q (v _s /v _w): 20-60-120	Q _p (l/min.mm): 2	s _d (mm/t): 0.2
d _g (mm): 80	V _w (mm ³ /mm): 500	p _f (atm): 2	a _d (μm): 50 3x
b (mm): 30	k _m (N/μm): 12	A (BF/s): 0.093	C (BF): 36.5

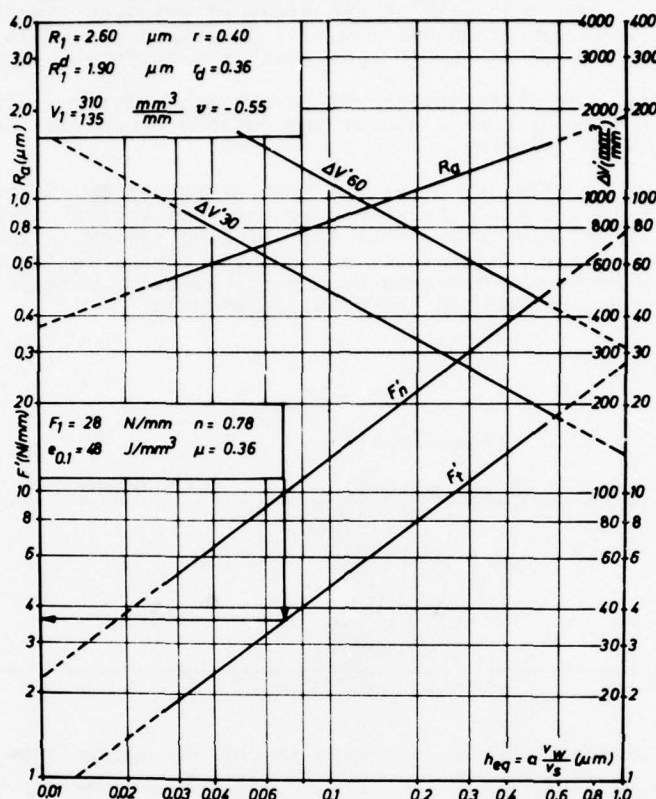


Fig.3. Grinding Chart.

Cooperative research within CIRP has confirmed Woxen's and Colding's findings (16) that surface roughness, grinding forces, grinding ratio and to some extent the tool-life volume can be expressed as power functions of a quantity called the equivalent cut thickness

$$h_{eq} = \frac{Z'}{v_s} = \frac{av_w}{v_s}$$

computed as the ratio of metal removal rate per unit wheel width Z' and wheel velocity (6). The physical meaning of the equivalent cut thickness is the thickness of the material ribbon flowing at the surface speed of the grinding wheel and the volume of which equals the actual metal removal (fig. 1).

In particular the tangential force F'_t per unit wheel width can be expressed as follows $F'_t = F_1 (h_{eq})^f$

f is the force sensitivity exponent

F_1 is the reference force per mm wheel width for $h_{eq} = 1 \mu m$.

On the other hand, it is well-known that the specific energy is proportional to the tangential force, and as such it varies with the equivalent cut thickness h_{eq} . For the sake of comparison, the specific energy is taken for $h_{eq} = 0.1 \mu m$; the symbol used is $e_{0.1}$.

Both quantities, F_1 and $e_{0.1}$, as well as f are characteristic of the workpiece-grinding wheel combination as well as of the coolant. A series of evaluations of coolant and grain quality have been carried out on this base (7). Typical values of F_1 , f and $e_{0.1}$ are given in Table II of the appendix.

Experiments show that a clear relation exists between the specific energy and the surface damage.

2. Thermal model

2.1. General procedure

Literature is unanimous to designate thermal phenomena as major factors in producing residual stresses. The authors are however not so unanimous in assigning either differential expansion or metallographic changes thermally produced as main causes.

Also the link between the temperature and the grinding parameter is not clearly explained.

For that reason a precise thermal model was developed by A. Decneut and M. Maris, the validity of which they experimentally assessed. The study based upon Jaeger's (9) two dimensional model of heat distribution for a moving heat source with infinite length, first applied to grinding by K. Takazawa (10) and N. Des Ruisseaux (11). Jaeger's model gives the temperature fields as well as function of the time and of the distance to the moving heat source. Owing to the fact that in the study of grinding stresses only the maximum temperature is of interest, Takazawa (10, 11) developed a formula giving the maximum temperature as function of the depth underneath the surface as well as of the grinding parameters.

M. Maris developed the model for different shapes of the heat source (rectangular, parabolic, triangular) and considered to main cases: the cut-off operation, the creep grinding, conventional plunge or surface grinding.

The case of cut-off operations (fig. 4) shows the heat distribution. It is seen that the material is heated up just in front of the wheel, so that the largest heat flux is evacuated through the chip. It has been shown that the grinding energy is lower with higher infeed speed, and that the surface damage even at the side flanks is low. This explains why practically no burning marks are observed by cut-off grinding, except at the end of the cut where the heat evacuation through the metal is reduced.

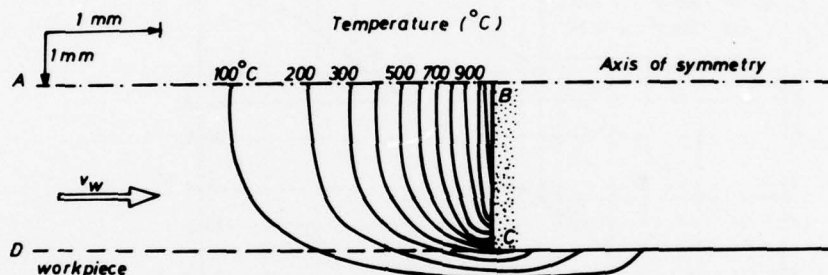


Fig. 4. Representation of isotherms in cut-off operations.

The case of creep grinding lies between the cut-off grinding and the conventional grinding. It shall not be discussed here.

The case of conventional plunge or surface grinding is most important in the mechanical workshop, and can be represented schematically as fig. 5.

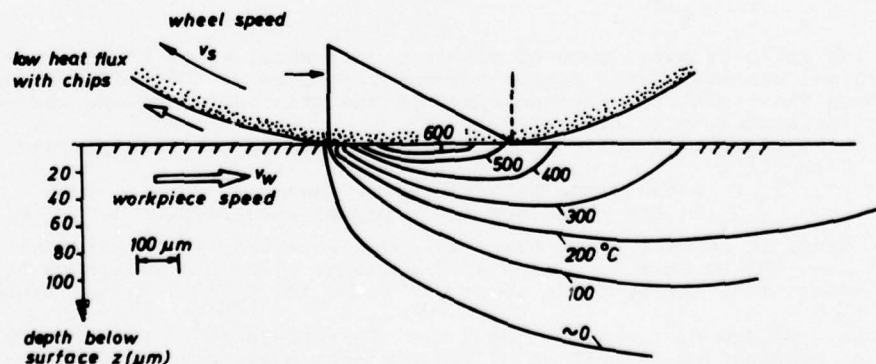


Fig. 5. Schematic representation of isotherms due to the thermal input in conventional plunge or surface grinding.

2.2. Temperature model for conventional grinding

The heat intensity input Q_w in the workpiece in the case of conventional grinding can be written as:

$$Q_w = K \frac{F'_t (v_s + v_w)}{l_k}$$

where l_k is the actual contact length between the wheel and workpiece. A fair agreement between the authors exist to consider the real contact length as twice the theoretical contact length.

$$l_k = 2\sqrt{ad_e}$$

d_e is the equivalent diameter $\frac{d_w d_s}{d_w + d_s}$

K is the amount of energy flowing into the workpiece. A good agreement exists among the authors, also confirmed experimentally by M. Maris: $0.8 < K < 0.85$. In this study $K = 0.85$.

The Takazawa-Maris formula giving the maximum temperature at a depth z , has the form:

$$T_{\max} = T_K \exp(-z/z_t)$$

$$T_{\max} = 0.58 F_1 (\rho c)^{-0.47} k^{-0.53} a^{f-0.235} v_w^{f-0.57} v_s^{1.1-f} d_e^{0.765-f} \exp \left| -0.4459 \left(\frac{\rho c v_w}{k} \right)^{0.63} (ad_e)^{-0.185} z \right|$$

T_K is the maximum contact temperature for $z = 0$.

z_t is a measure of the decay of the temperature into the body of the workpiece; when z_t is large the decay is slow, and the heat affected zone is large, and inversely.

The expression of T_{\max} can also be written as function of the metal removal rate (per unit wheel width) $Z' = av_w$.

$$T_{\max} = 0.58 F_1 (\rho c)^{-0.47} k^{-0.53} (Z')^{f-0.235} v_w^{-0.335} v_s^{1.1-f} d_e^{0.765-f} \exp \left| -0.4459 (Z')^{-0.185} v_w^{0.815} \left(\frac{\rho c}{k} \right)^{0.63} d_e^{-0.185} z \right|$$

2.3. Experimental confirmation

Experimental confirmation of this formula has been given by means of a series of temperature measurements using a method designed by J. Peklenik (12). The results are given fig.6. A confirmation of these measurements and of the calibration is given further when the boundary of the heat affected zone at a critical temperature T_{cr} will be computed and measured (Table III).

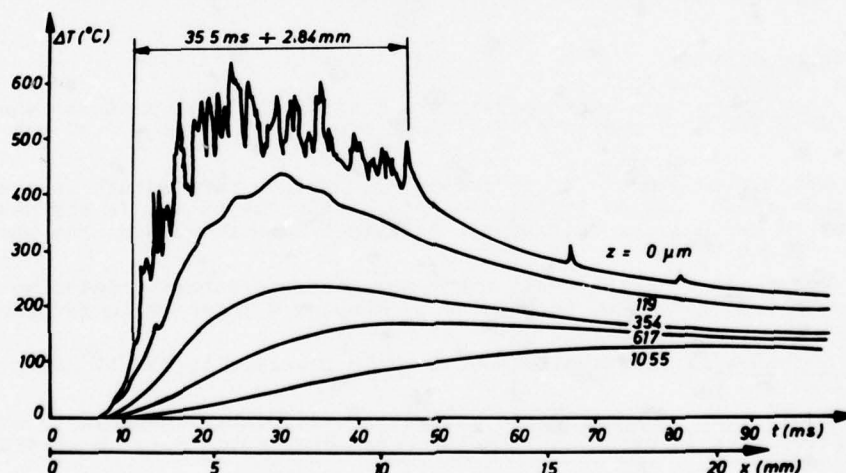


Fig. 6. Temperature distribution at low workspeed $v_w = 0.08$ m/sec and large infeed.

2.4. Interpretation of the thermal model (fig. 7)

2.4.1. The thermal characteristics of the material.

The contact temperature T_K is approximately inversely proportional with the square root of the product of the specific heat ρc and the thermal conductivity k . However the temperature decay gradient increases with the thermal diffusivity $\alpha = \frac{k}{\rho c}$ as anticipated.

2.4.2. The force sensitivity exponent f has a major importance. Practically $0.35 < f < 1$.

a. Grinding with a workpiece - wheel combination characterized by a large f value makes the contact temperature T_K less sensitive to an increase of wheel velocity. Generally high alloy steels have a small f value with most currently used grinding wheels. It is well-known that they are more sensitive to burns and cracks. On the other hand in some examples given later f equals 1, so that the exponent of v_s is 0.1!

- b. f is also governing the influence of the infeed a . An increase of a is always detrimental.
- c. $f = 0.57$ is a discriminating value for the influence of the work speed. For ordinary steels increasing the wheel speed may somewhat increase the contact temperature T_K , but increases very much the decay coefficient, as a factor $v_w^{0.63}$ appears in the exponent (which is negative) and this is independent from f . The consequences of this will be explained in what follows.

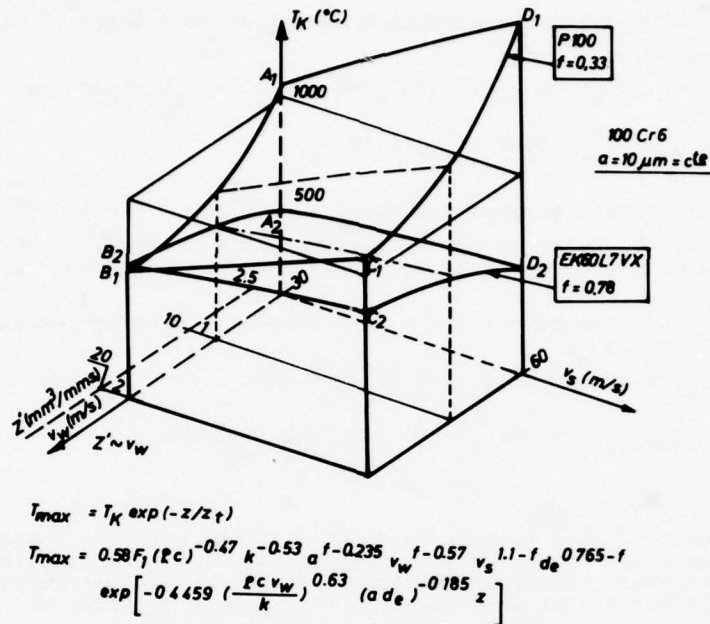


Fig. 7. Tridimensional display of the thermal model of the maximum contact temperature T_K .

2.4.3. The working conditions.

As to the contact temperature T_K :

- An increase of wheelspeed v_s (other parameters constant) always produces when f is smaller: (e.g. when $f = 0.97$ one gets $v_s^{0.13}$ on the contrary for $f = 0.37$ one yields $v_s^{0.73}$!).
- Increasing the metal removal rate Z' increases the surface temperature in most of the cases, except when $f < 0.57$ and an increase of Z' is only due to v_w . In any case by increasing the infeed depth a the detrimental influence is more marked than when increasing v_w (indeed $a^{f-0.235}$ and $v_w^{f-0.57}$).
- Increasing the workspeed v_w keeping all other parameters constant (including Z') is very favorable. To increase Z' by increasing v_w keeping a constant is favorable as long as $f < 0.57$.
- Increasing the infeed a is always detrimental while practically in all cases f is larger than 0.235.
- Increasing the equivalent diameter d_e is generally unfavorable, especially when $f < 0.765$. It explains difficulties in grinding with large diameter Cubic Nitride wheels, and also in internal grinding.

As to the temperature decay coefficient z_t : an increase of the workspeed v_w is always very favorable, while an increase of grinding depth a and of the equivalent diameter d_e are both detrimental.

It must however be noted that the depth of the heat affected zone is a function of the contact temperature as well as of the decay gradient.

A summary of these conclusions is visualized fig. 7 for the case of constant infeed a . A similar graph is provided for the case of constant metal removal rate in (1). The graph of the residual stresses as commented in the last section confirms completely the validity of this thermal model.

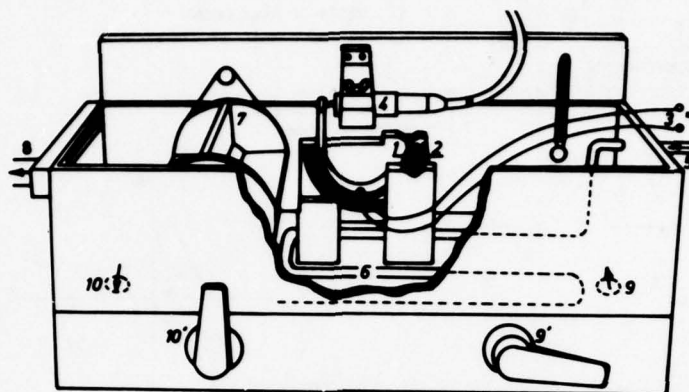
3. The residual stresses

3.1. Experimental method

The method used for measuring the residual stresses is the relaxation method applied on rings of 90mm diameter. The method is fully described by A. Decneut in (13). Fig. 8 represents schematically the apparel used. The deflection is directly measured and fed into a computer which processes the information into stress values by means of a modified E. Thomsen-J. Frisch formula (14).

Verification measurements have been made by X-Ray method. Both methods gave compatible results. X-Ray measurements are local and directional but cumbersome.

The etching method is perfectly valid as long as average stresses are considered. The method is easy and fast. X-Ray data may however be required when trying to correlate local stresses with fatigue resistance.



- 1-2 the ring hinged on one side and frictionless supported on the other side
- 3 electric supply
- 4 displacement pick-up
- 5 cooling water supply
- 7 circulator

Fig. 8. Device used for measuring residual stresses by relaxation.

3.2. Factors affecting residual stresses

In order to explain the observed shape of the residual stress distribution three major components must be taken into account. The first two ones result from the temperature effects, the third one is due to mechanical effects.

3.2.1. The thermal expansion stress component.

The workpiece surface can conveniently be subdivided into three layers (Fig.9):

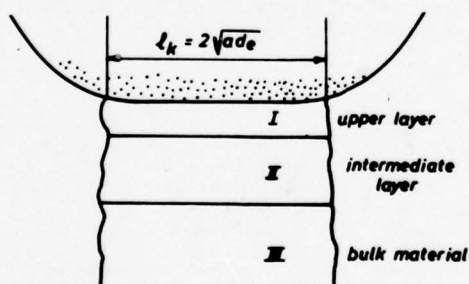


Fig. 9. Real contact length.

I. the upper layer, generally less than 10...15 μm deep has been directly exposed to the surface temperature as described in preceding sections.

II. the intermediate layer thermally affected by conduction and as well as by stresses balancing the previous ones.

I and II are generally referred to as heat affected zone (HAZ).

III. the bulk material, unaffected by grinding operation.

Let us consider the stress-strain diagram of an ideal elastic-plastic material (Fig.10) and assume that initially no stresses exist in the material (point O). If the upper layer is heated up, it tends to expand, but it is held back by the underlaying layers and it behaves as a bar heated up but firmly held by two fixed ends preventing its expansion. Zone I is then submitted to compressive stresses, which often reach the yield point so that plastic deformation occurs.

The stress strain situation of layer I at maximum temperature is represented by point I, while layer II is submitted to tensile stresses but still in the elastic domain as represented by point II₁. During the cooling phase the upper layer I relaxes elastically and ends up at point I₂ subjected to residual tensile stresses; on the other hand layer II reaches a compressive state II₁, so that the overall situation in equilibrium. Taking into account the variation of the mechanical properties due to temperature rise, the yield point is reached earlier and a stress-chain cycling as indicated fig. 10b occurs.

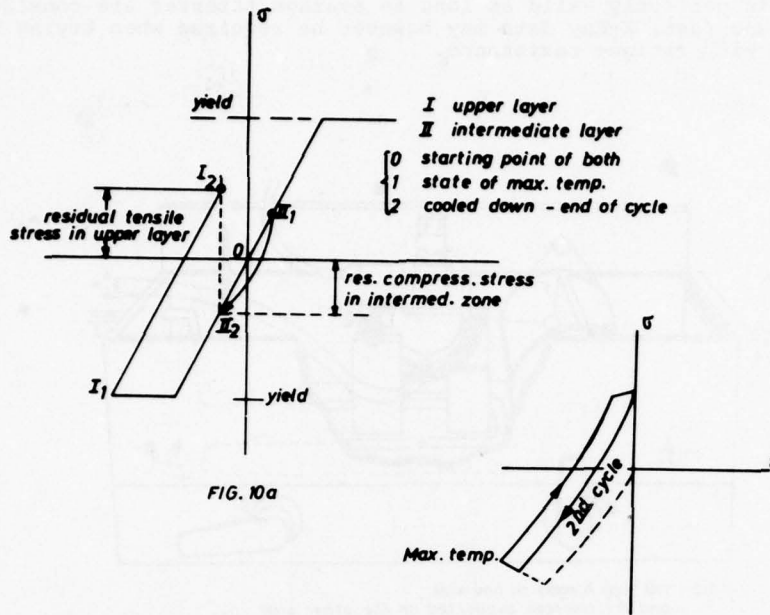


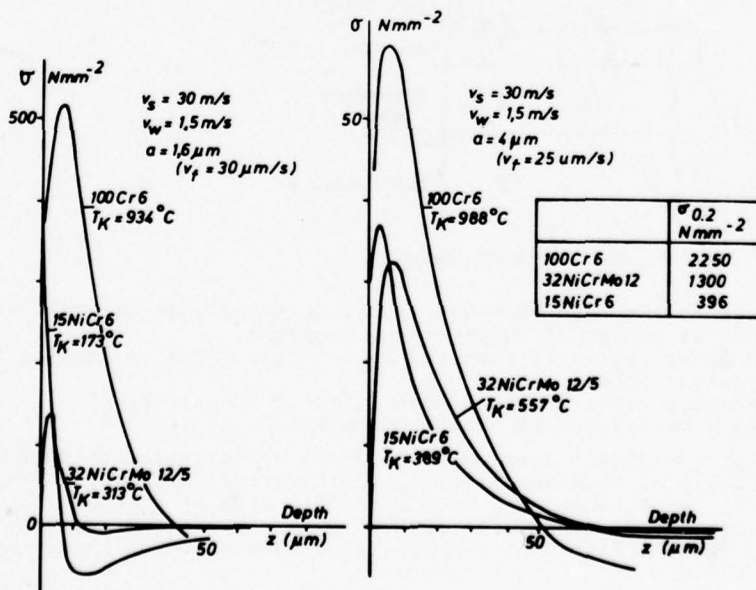
Fig. 10. Thermal origin of the residual stresses.

As a conclusion it can be said that, neglecting pure mechanical effects and structural transformation, tensile stresses remain in the upper layer, while compressive stresses appear in layer II.

It must also be pointed out that residual stresses will be higher when the thermal expansion coefficient is larger, the yield strength of the material at elevated temperature is lower, because in this case the plastic deformation is larger.

Fig. 11 shows that notwithstanding the fact that 15NiCr6 steel reaches a lower surface temperature than 32NiCrMo12, the maximum residual stresses are higher.

On the other hand it must be pointed out that when the temperature reaches a point between AC_1 and AC_3 , the starting point and the end point of the Austenitic transformation, a volume contraction occurs, which explains the unexpected fact that lower residual stresses have been recorded in 100Cr6 for rougher grinding conditions causing higher temperatures. Fig. 12 demonstrates clearly this point. The major importance of the thermal expansion will be confirmed further in correlating the maximum residual stresses with the free expansion at the maximum surface temperature λT_K .

Fig. 11. Comparison of the surface stresses for 3 materials with different yield strength $\sigma_{0.2}$.

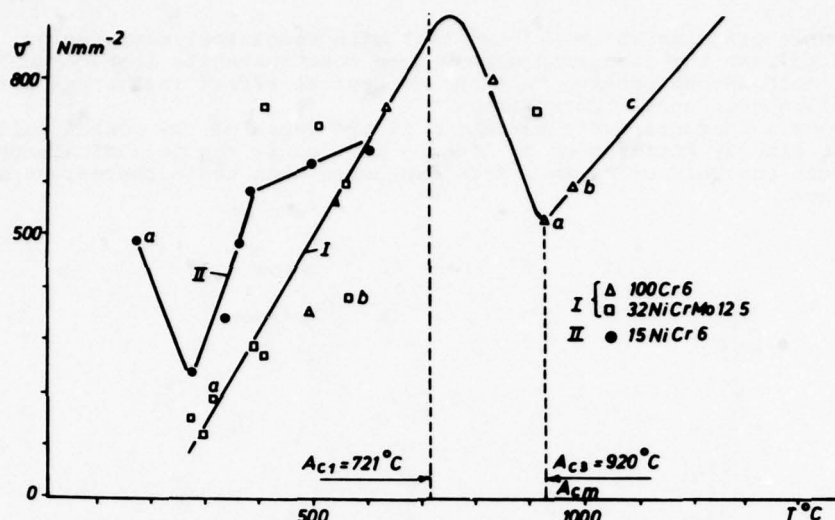


Fig.12. Residual stresses as function of the contact temperature showing the influence of the free expansion.

3.2.2. The stress component due to the metallographic transformations.

Metallographic structural transformation superimposed upon the thermal expansion can modify fundamentally the shape of the residual stresses.

- In preceeding section it has already been mentioned that the transformation from ferrite to austenite results in a volume contraction.
 - On the other hand when this austenite is quenched, untempered martensite is generated which increases the specific volume. While this generally happens at a temperature range where plastic deformation does not occur any more, compressive stresses will appear in the upper layer I and tensile stresses in layer II. This often explains a typical decrease of the thermally induced tensile stresses in the upper layer I, 5 to 10μm wide underneath the surface. This has been confirmed by examining the micrographs. Untempered martensite shows up as the so called "white layer". On the other hand microhardness measurements made on the tapered layers give a final confirmation of this assumption.
 - Finally, when a hardened material is heated up martensite or residual cementite will be annealed to ferritic structure, producing a shrinkage of the upper layer I (volumetric shrinkage 2%, linear 0.67%). Here again tensile stresses are produced, in layer I and compressive ones in layer II.
- The superposition of thermal expansion stresses and this martensite annealing may produce high residual stresses even in gentle grinding as shown fig. 15 test 311(hardened 32NiCrMo 12-5).

3.2.3. The mechanical stress component is due to Herzian compression and shear forces in grinding. It generally result in compressive stresses in the upper layer I, generally 5 to 10μm wide. They increase when the contact pressure is large as due to large infeed values a. This phenomenon explains superficial relaxation of the tensile stresses even in steels where martensitic transformation can hardly occur as in 15NiCr6, fig. 13 and 14. This effect was mainly studied by Nakajima (17).

4. Experimental confirmation

4.1. General comments of the experiments

A series of about 100 experiments has been made by M. Maris and A. Decneut mainly on 3 different steels:

- 100Cr6 a ball bearing steel body hardened and tempered
- 15NiCr6 a typical cementation steel - normalized
- 32NiCrMo 12/5.

All characteristics of these steels are given table I and II. The grinding charts were also established. After grinding in different conditions, stresses as well as micro-hardness measurements were recorded. Only some typical examples can be discussed here. For further study we refer to the thesis of A. Decneut and M. Maris (3) (4). Figs. 13 and 14 are related to 15NiCr6.

- The difference between fig. 13 and 14 may be wrongly interpreted as due to the difference of wheelspeed. This is only partially true because $f=1$ (Table I) so that one gets $v_s^{0.1}$. This steel however is very sensitive to an increase of the infeed depth a and somewhat to v_w . However the heat affected zone is clearly enlarged when v_w decreases and the contact temperature is high. On the other hand the yield strength of this steel drops significantly above 150°C.
- Test 296 : shows high tensile stresses in layer I, due to thermal expansion of a material with low $\sigma_{0.2}$. The infeed is small ($a = 1.5\mu\text{m/rev}$) so that no mechanical compressive stress compensates the tensile stresses.
Test 294 : would normally yield higher thermally induced tensile stresses as expected by the large free expansion ΔT_s . However this is compensated by mechanical compressive stresses due to larger infeed ($a = 4.5\mu\text{m/rev}$).
Test 297 : again thermal tensile stresses more compensated by the mechanical compressive stresses ($a = 7.5\mu\text{m/rev}$).

Test 295 : gentle grinding ($Z' = 0.75 \text{ mm}^3/\text{sec}$) with mechanical compression. It must be noted that the micrographs show some rest austenite transformed to ferrite. On the other hand one can observe that the mechanical effect influences a small region of less than $10 \mu\text{m}$ deep under the surface. Micrographs show a characteristic variation of the depth of the mechanically affected zone (MAZ). As already anticipated by looking at fig. 12 the mechanical compressive stresses disturb the rule of maximum free expansion when these thermal stresses are near the surface.

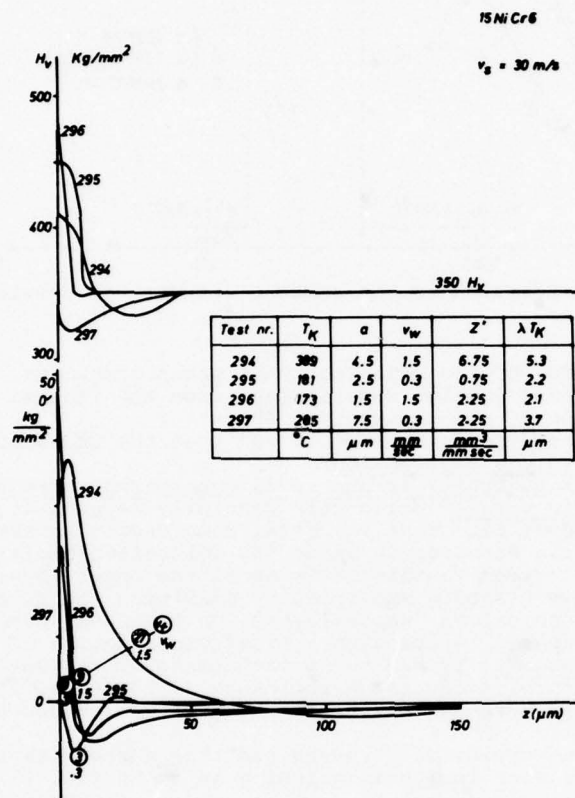


Fig. 13. Hardness and residual stresses in plunge grinding for 0.15% Carbon steel at a wheel speed $v_s = 30 \text{ m/sec}$.

Fig. 14 : again 15NiCr6.

- The major influence of the workpiece speed v_w on the width of the stress affected zone is clearly marked.
- Test 302 shows the largest free expansion - the largest maximum stress, compensated by strong mechanical compression at the surface ($a=7.5 \mu\text{m}$).
- Test 302, 305, 303, 304 give a decreasing maximum stress as a decreasing free expansion λT_K . (λ is the thermal expansion coefficient).
- Test 303 as 305 show the large stress affected zone due to low v_w ($0.3 \mu\text{m/sec}$). Although the stress reversal depth is, as expected larger in test 305 ($z = 180 \mu\text{m}$) than in test 303 ($140 \mu\text{m}$), the stress distribution is somewhat uncommon, but correspond very well to the large martensite layer formed under the surface.
- Test 304 lowest surface temperature and small stress affected zone due to relatively large v_w ($1.5 \mu\text{m/sec}$ against $0.3 \mu\text{m/sec}$).

Fig. 15 : shows similarly the hardness and residual stress distribution for 32NiCrMo 12/5.

- Again the maximum stresses are in the order as the free thermal expansion λT_K .
- Test 313 shows a much deeper stress affected zone as test 310 because v_w is smaller ($v_w = 0.5 \mu\text{m/sec}$ against $1.5 \mu\text{m/sec}$).
- On the other hand 313 and 310 show a marked layer of untempered martensite as well in the micrograph as in the hardness.

In tests 312 and 311 the thermal stresses are compensated in the upper layer by some martensite formation and mechanical effects.

Fig. 16 confirms previous findings for a ball bearing steel 100Cr6. It must be observed that $f = 0.78$, consequently the increase of wheel speed from 30 to $60 \mu\text{m/sec}$ (tests 4 and 14) produces only an increase of the contact temperature (15%). However the increase of a has a major influence (test 10 and 8). On the other hand smaller v_w values increase the depth of the heat affected zone. On fig. 16 some experiments with 15NiCr6 have been recorded for the sake of comparison.

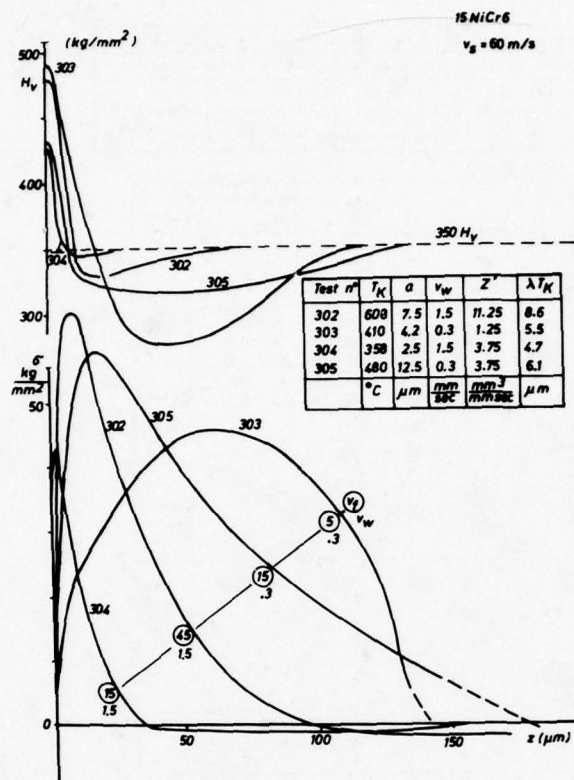


Fig. 14. Hardness and residual stresses in plunge grinding for 0.15% C steel at wheel speed $v_s = 60 \text{ m/sec}$.

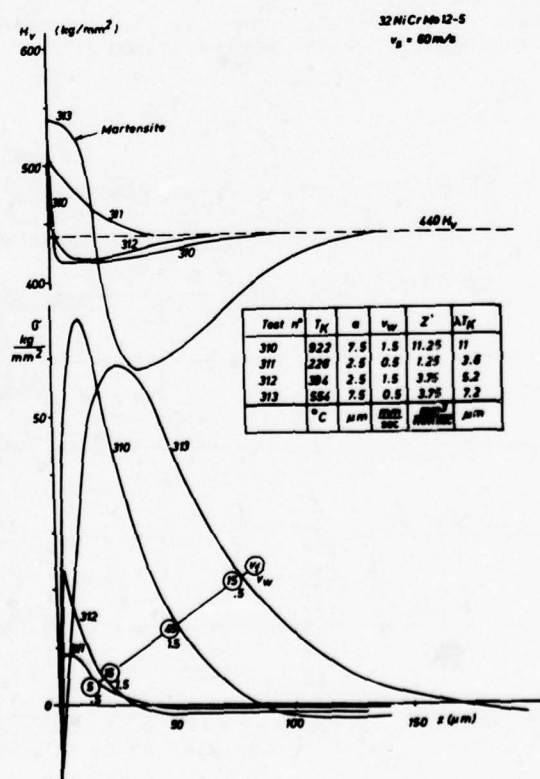


Fig. 15. Hardness and residual stresses of 0.32% C steel for wheel speed $v_s = 60 \text{ m/sec}$.

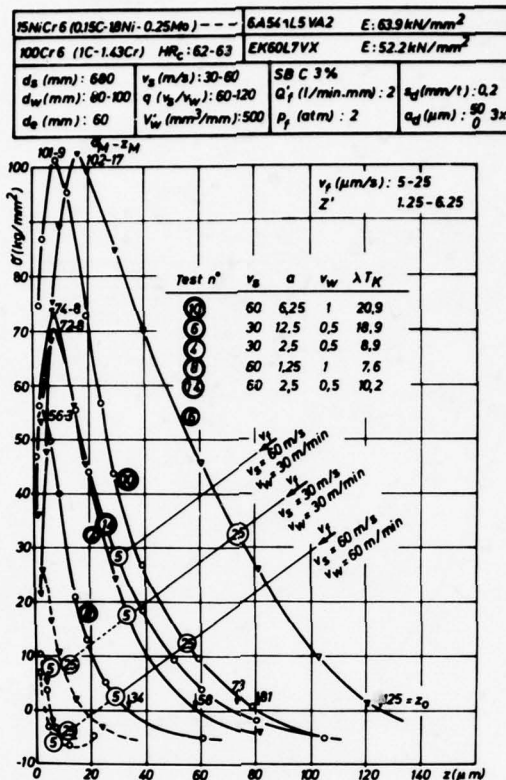


Fig. 16. Influence of the machining parameters upon the residual stresses of 15NiCr6 and 100Cr6.

4.2. Depth of the hardness affected zone.

Another interesting confirmation of the thermal model is yielded when considering the depth z_T where the critical temperature T_{cr} is reached at which the original hardness H of the material is unaffected.

Metallographic data give:

for 100Cr6 $T_{cr} = 150^\circ\text{C}$

for 15NiCr6 $T_{cr} = 250^\circ\text{C}$

for 32NiCr12-5 $T_{cr} = 200^\circ\text{C}$

When the corresponding depth z_T is computed with T respectively equal to 150°C , 250°C and 200°C and compared with the measured value of z_T at which the original depth is found unaffected, following table is yielded and a very satisfactory correspondence is found.

Table III

	Test No.	Computed z_T	Measured z_T
		μm	μm
100Cr6	4	127	125
	6	240	190
	8	90	110
	10	193	190
15NiCr6 30m/sec	294	38	46
	295	0	10
	296	0	5
	297	37	46
60m/sec	302	66	67
	303	116	112
	304	28	32
	305	120	125
32NiCr12-5	310	164	100
	311	47	50
	312	86	75
	313	135	117

It must be noted that whenever $z < 10\mu\text{m}$ the thermal expansion is often compensated by mechanical or metallographical effects, as it is the case in test 295-296.

5. Conclusions for practice

It clearly appears that thermal expansion is a main cause of residual stresses. The thermal characteristics and the yield stress of a material are major factors. A low yield stress at elevated temperature can produce high residual stress. Consequently all factors producing a decrease of surface temperature will be beneficial. Let us consider them individually:

a. Cooling

Oil coolant instead of water emulsion : it is proven that the specific energy of the grinding operation is much lower using oil coolant then using water emulsion. The explanation is that oil decreases the friction coefficient very much. Using a oil coolant prevents the contact temperature to reach high values; however the average temperature of the workpiece may increase which in turn may cause dimensional problems. Water emulsions, on the contrary, do not penetrate the grinding contact. So that high local temperature and thermal damage will be caused. Immediately after heating, the piece will be quenched and its average temperature will be kept low.

Fig. 17 shows how stresses can be reduced to about nothing even become compressive using oil coolant. One should however keep in mind that oil must be detrimental for the health when inhaled. It must be evacuated. Oil may also increase the "ploughing" depth when the contact length is large e.g. in internal grinding.

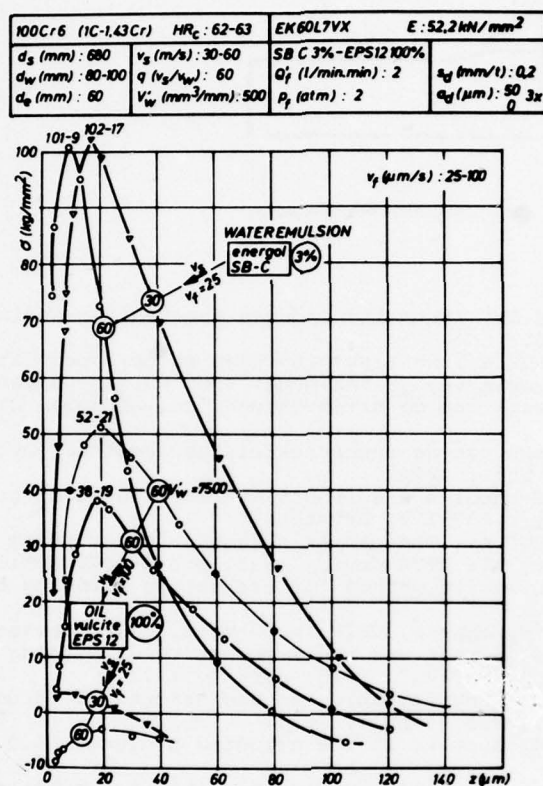


Fig. 17. Influence of the coolant on residual stresses.

Segmented profile(fig.18) or dressing tread (large dressing lead) brings the coolant to the contact place (15), but this technique simultaneously increases the h_{eq} and the roughness. On the other hand it has been proven that even high pressure cooling has a minor influence except as to cleaning the wheel.

b. The grinding conditions:

the thermal model provides the information.

wheel speed v_s has less effect as anticipated except in cases where f is small as
e.g. in the case of exotic steels.

infeed a : has a major influence, not only in producing larger surface temperature, but also in generating compressive compensation in the upper layer, when large infeeds are used.

workspeed v_w : lowering the workspeed is generally detrimental, it increases the surface temperature when $f < 0.57$; but in any case it increases the depth of the heat affected zone in any case.

equivalent diameter d_e : increase of the contact length is detrimental.

c. Thermal and mechanical properties also have a major influence.

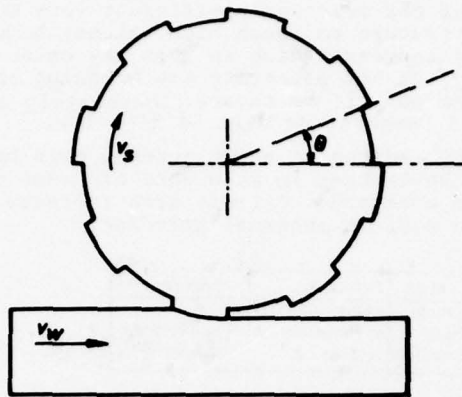


Fig. 18. Segmented wheel.

References

1. SNOEYS R.; MARIS M.; PETERS J., Thermally induced damage in grinding, CIRP Annals, Vol.II, 1978, being printed.
2. PETERS J.; SNOEYS R.; DECNEUT A., De restspanningen en de oppervlakteintegriteit bij de slijpbewerking. Mededelingen van de Kon.Acad. voor Wetenschappen, Brussel, 1975,37p.
3. DECNEUT A., Verantwoorde keuze van de slijpvoorwaarden, Doctoral diss.,K.U.Lv., Heverlee, 1974, 186p.
4. MARIS M., Thermische aspecten van de oppervlakteintegriteit bij het slijpen. Doct. Diss. K.U.Lv., Heverlee, 1978, 2 Vol., 300p.
5. PETERS J., SNOEYS R., The E-modulus a suitable characteristic of grinding wheels, Revue M, Vol.II,no.4, 1965, p.167-177, Brussels.
6. PETERS J.; SNOEYS R.; DECNEUT A., The proper selection of grinding conditions in cylindrical plunge grinding, XVI MTDR Conf., 1975, p.345-352, McMillan.
7. PETERS J.; AERENS R., An objective method for evaluating grinding coolants. CIRP Annals, Vol.25, 1976, I, p.247-250.
8. AERENS R.; SMETS G., Grinding charts, CRIF Tech. Note, CRIF, Brussels, 1978, 70p.
9. JAEGER J.C., Moving sources of heat and the temperature at sliding contacts, Journ. and Proc. of Roy. Soc. of N.S. Wales, Vol. 1976, part 3, 1972.
10. TAKAZAWA K., Effects of grinding variables on the surface of hardened steel. Bull. of Jap. Soc. of Precision Eng., Vol.2, no.1, 1966.
11. DES RUISSEAU N.R., Thermal aspects in the grinding process. Ph.D. Thesis, Univ. of Cincinn. 1968.
12. PEKLENIK J., Ermittlung von geometrischen und physikalischen kenngrößen für die Grundlagen forschung des Schleifens, Doct. Diss. T.H. Aachen, 1957.
13. DECNEUT A., Continuous measurement of residual stresses in thin cylindrical pieces using deflection etching techniques, MC47, CRIF, Brussels, 1973, 23 p.
14. FRISCH J.; THOMSEN E.G., Residual grinding stresses in mild steel. Trans. ASME 1951.
15. VERKERK J., Kinematical approach to the effect of wheel dressing conditions on the grinding process. CIRP Annals, vol. 25/1/1976, p.209-214.
16. COLDING B.N., A wear relationship for turning, milling and grinding. Machining Economics, Stockholm 1959.
17. NAKAJIMA, Chip formation physics in grinding, Thesis Kyoto University, Japan, 1969.

APPENDIX : Table I : Characteristics of investigated steels

	T	ρ Kg m^{-3}	C J (Kg $^{\circ}$ C)	k J (mS $^{\circ}$ C)	α $m^2 s^{-1}$ $\times 10^{-6}$	$\sigma_{0.2}$ Nmm $^{-2}$ (MPa)	Wheel EK60L7VX	
100Cr6	20	7772	459	21.07	5.9	2100	$F_1 = 28 Nmm^{-1}$ $f = 0.78$ $e_{0.1} = 48 Jmm^{-3}$	$Ac_1 = 730^{\circ}C$ Ac_3 $Ac_m = 800^{\circ}C$ $M_s = 250^{\circ}C$ $T_{cr} = 150^{\circ}C$
1.02C	200	7721	522	19.28	4.78			
1.43Cr	400	7653	593	16.71	3.68			
0.29Mn	600	7577	740	13.79	2.46			
0.03Si	800	7507	936	11.24	1.6			
0.01C								
15NiCr6	20	7840	435	51.9	15.22	394	$F_1 = 35 Nmm^{-1}$ $f = 1$ $e_{0.1} = 34 Jmm^{-3}$	$Ac_1 = 735^{\circ}C$ $Ac_3 = 840^{\circ}C$ $M_s = 390^{\circ}C$ $T_{cr} = 250^{\circ}C$
0.15C	200	7788	528	49.0	11.92			
1.55Ni	400	7720	599	42.7	9.23			
0.85Cr	600	7648	754	35.7	6.17			
(NMRI)	800	7646	838	26.0	4.08			
	1000	7540	657	27.2	5.49			
32NiCrMo 12/5	20	7840	490	34.3	8.93	1300	$F_1 = 32 Nmm^{-1}$ $f = 0.8$ $e_{0.1} = 50 Jmm^{-3}$	$Ac_1 = 705^{\circ}C$ $Ac_3 = 760^{\circ}C$ $M_s = 315^{\circ}C$ $T_{cr} = 200^{\circ}C$
0.32C	200	7789	523	36.8	9.03			
3.5Ni	400	7723	599	36.4	7.87			
1.2Cr	600	7652	774	31.8	5.37			
0.45Mo	800	7644	557	26	6.11			
FDMA	1000	7540	550	27.6	6.66			

Table II : Some values of F_1 and f

Material	Grinding wheel	Coolant	$e_{0.1}$ Jmm^{-3}	F_1 Nmm^{-1}	f
100Cr6	EK60L7VX ($E = 52.2 kNmm^{-2}$)	SB-C 3%	48	28	0.78
	EK80J7VX ($E = 45 kNmm^{-2}$)	id	38	15	0.60
	EK60L7VX ($E = 52.2 kNmm^{-2}$)	EPS12 (100%)	28	17	0.78
	P100 ($E = 15.7 kNmm^{-2}$)	SB-C 3%	60	11.5	0.33
15NiCr6	EK60L7VX ($E = 52.2 kNmm^{-2}$)	SB-C 3%	34	35	1
32NiCrMo 12.5	EK60L7VX ($E = 52.2 kNmm^{-2}$)	SB-C 3%	50	32	0.8
X210CrW12	EK60L7VX ($E = 52.2 kNmm^{-2}$)	SB-C 3%	54/85	20	0.35
X5CrNiMo 17.12	EK80J7VX ($E = 45.0 kNmm^{-2}$)	id	100	56	0.74

EXPERIENCE D'UTILISATION DE LA COMMANDE ADAPTATIVE EN FRAISAGE

par

J.Y. Lhommet
Research and Engineering Lab.
Aérospatiale
Direction Industrielle
12 rue Pasteur, 92152 Suresnes, France

1. BUT

La réalisation de pièces aéronautiques en alliages légers ou en métaux durs exige, de par les dimensions et la complexité grandissantes, l'emploi de machines à commande numérique dont le coût est très élevé. Tout système amenant un gain de productivité par réduction des temps technologiques ou des temps d'immobilisations permet de réduire le nombre de machines, donc de réduire l'investissement.

Pour réduire les temps d'immobilisations (montages de pièces, changement d'outils), on a pu proposer les systèmes de palettes, ou les changeurs d'outils automatiques. En ce qui concerne les temps technologiques, donc la coupe, les améliorations sont longtemps venues des fabricants d'outils offrant des matériaux et des géométries d'outils de plus en plus performants. Cependant, la complexité des paramètres à prendre en compte ne permet pas au programmeur pièce d'en tirer tous les bénéfices.

Un système complet de commande adaptative, incluant la génération et la modulation des vitesses d'avances, déjà largement utilisé par l'industrie aéronautique américaine, a paru intéressant à implanter sur une machine FOREST V500 à CN TELEMECANIQUE NUM 353 du Département Production-Recherches de la Société. Ce système est fabriqué par la Société MACOTECH à Seattle (U.S.A.).

2. DESCRIPTION DU SYSTEME

Sur une CN classique, la vitesse d'avance choisie par le programmeur est perforée sur la bande. Elle ne peut être modifiée, généralement minorée, que manuellement, sur les machines possédant une correction d'avance, par l'opérateur suivant son appréciation (vibration, risque de rupture d'outil).

Le système MACOTECH intervient au niveau du programmeur et de l'opérateur, car il comprend une partie "logiciel" et une partie "matériel".

2.1. La partie "logiciel"

C'est un programme ordinateur, écrit en Fortran, travaillant seul (version "STAND ALONE") ou en liaison avec l'APT, qui permet de définir les conditions technologiques optimales d'usinage.

Ce programme, en fonction de paramètres fixés par le programmeur :

- . machine utilisée,
- . matériau à usiner,
- . outil,
- . genre d'opération (ébauche, finition, etc.),
- . précision (déflexion en bout d'outil),
- . état de surface désiré,

détermine à l'aide de modèles mathématiques et de fichiers de données issues du "METCUT" :

- la vitesse d'avance,
- la vitesse de coupe (en T/mn),
- l'effort nécessaire pour casser la fraise,
- l'effort nécessaire pour casser 1 dent de la fraise,
- l'effort nécessaire pour faire fléchir la fraise d'une valeur fixée par le programmeur,
- l'effort nécessaire pour déformer la pièce ou l'outillage hors des limites fixées.

De plus, il sélectionne à partir de ses fichiers, l'effort de sécurité pour la machine considérée.

En prenant comme référence le plus faible de ces efforts, il calcule une vitesse d'avance et une vitesse de rotation broche, et il génère un code Force qui sera transmis à l'armoire MACOTECH par une adresse spécialisée (en général P) de la bande.

2.2. La partie "matériel"

La partie "matériel" se compose essentiellement de :

- . un ensemble de 4 capteurs à induction contrôlant les déplacements de la broche en fonction de l'effort de coupe. Ces capteurs sont logés dans un support annulaire adapté à la machine considérée; il remplace le couvercle de roulement d'origine,
- . l'unité MAC. I qui est un ensemble électronique de conception modulaire comportant les circuits de transformation et de comparaison des signaux provenant des capteurs avec les informations issues de la bande. Il comporte également l'interface permettant l'adaptation au système de commande numérique.

La commande adaptative MAC. I contrôle la force appliquée sur la pièce par l'outil (effort de coupe). La mesure de cette force est effectuée par les capteurs montés sur la broche. Elle compare cette force à une force de référence (force de sécurité sélectionnée par le programme et perforée sur la bande d'usinage).

Elle réduit automatiquement la vitesse d'avance chaque fois que l'effort de coupe tend à dépasser la force de référence.

Les vitesses d'avance perforées sur la bande sont choisies volontairement trop élevées pour une grande partie de la séquence d'usinage considéré, de manière à pouvoir être réduites lorsque cela est rendu nécessaire par un dépassement de la force de référence.

3. MISE EN OEUVRE DU SYSTEME.

3.1. Programmation

En programmation automatique APT, le programmeur doit introduire au début de son programme des instructions spéciales d'appel de sous-programmes lui permettant d'initialiser le modèle mathématique avec les caractéristiques des machines, de la ma-

tière à usiner et des outils. Ensuite, il suffit de remplacer les instructions de vitesse (FEEDRATE) par un appel au sous-programme de calcul en décrivant le travail qui va être effectué : section maximum de matière rencontrée, déformations admissibles, état de surface souhaité. Le logiciel transmet à l'APT, sous forme appropriée, les conditions de coupe (vitesse d'avance et de rotation) et les codes "Force".

En programmation manuelle, à partir des mêmes informations, les résultats sont sortis sur papier et doivent être intégrés sur la bande avec les codes appropriés (F, S, P).

3.2. Implantation du logiciel

Le logiciel, écrit en fortran, a été implanté sans problème sur l'IBM 370/158 du Centre Technique. La version employée était une version INCH, avec conversion en entrée métrique/inch écrite sur place.

3.3. Installation du matériel

L'installation sur la machine a nécessité une semaine d'immobilisation de la machine. Ce travail consiste en :

- . l'étalonnage de la broche,
- . le montage de l'anneau porte-capteurs,
- . la liaison coffret MACOTECH à l'armoire C.N. TELEMECANIQUE (inclusion d'une carte interface et câblage),
- . les câblages entre les capteurs et le coffret MACOTECH.
- . l'étalonnage de l'ensemble et les essais de réception.

4. EXPERIMENTATION

4.1. Domaine d'application de l'expérimentation

L'expérimentation a été faite, pour la Société dans les métaux durs. C'est en effet le cas où :

- . le rapport temps technologiques/temps "main" est le plus élevé,
- . l'optimisation de vitesse d'avance sur la trajectoire est la plus longue, et la plus nécessaire,
- . l'emploi d'ébauches matricées ou forgées amènent des formes :
 - évolutives (variations de section de coupe en cours de passe),
 - peu répétitives d'une pièce à l'autre (usure rapide des matrices),
- . la matière présente des hétérogénéités locales ("points durs") amenant des bris d'outils.

4.2. Choix des pièces

L'expérimentation a été faite sur l'usinage en commande adaptative d'un certain nombre de pièces représentatives des fabrications aéronautiques réalisées en C.N. dans différentes usines de la Société :

- . 16 ferrures de pales principales SA 341 acier 35 NCD 16.
- . 4 + 4 nervures 14 de mât AIRBUS acier 30 NCD 16
- . 2 nervures 8 de mât AIRBUS en TA6V (matricés)
- . 5 balanciers de train de MIRAGE F1 en 35 NCD 16 (forgés)
- . 6 ferrures d'articulation de porte AIRBUS en 30 NCD 16
- . 5 ferrures d'ancrage en 35 CN 6

4.3. Principe

Toutes ces pièces ont été usinées en utilisant la programmation initiale pour ce qui concerne les trajectoires outils. Les fraises utilisées ont été également celles employées en usine. Les conditions de coupe, vitesse et avance ont été définies par le logiciel MACOTECH. La vitesse de rotation de broche a été choisie dans la gamme machine aussi proche que possible de la vitesse calculée par le programme.

Les pièces ont été bridées dans les mêmes conditions qu'en production soit sur des outillages fournis par l'usine soit réalisés par nos soins suivant les mêmes principes.

Le chronométrage des temps a été fait de datum à datum.

4.4. Résultats

(voir à titre d'exemple les fiches d'essais pages 3 et 4).

4.3.1. Temps de coupe

Les temps de coupe enregistrés lors des différents essais sont assez ~~vo~~ ^{vé}ritatifs et cohérents pour qu'on leur accorde crédit. On constate des gains variant de 45 à 70% sur les temps usine. Il est à noter que ces temps usine sont des temps de bande théoriques n'incluant pas les conséquences de l'utilisation de potentiomètre de correction d'avance par l'opérateur.

Dans tous les cas, la commande adaptative est venue moduler les avances affichées par le logiciel. Ces avances étaient pratiquement toujours supérieures, pour les mêmes outils, à celles prévues par les programmeurs.

La qualité et l'efficacité du logiciel ont été étroitement liées à la description la plus exacte possible des conditions réellement rencontrées sur les pièces.

4.3.2. Durée de vie des outils

La limite d'utilisation des outils a été déterminée par un examen visuel en fin de séquences d'usinage ou par le passage du système en "OVERLOAD" (surcharge).

Dans la majorité des cas, la tenue des outils est au moins égale à celle que l'on obtient en usine, en considérant le volume de copeaux entre affûtages.

L'adaptation de l'avance aux efforts de coupe amène d'autre part une réduction des détériorations constatées, donc un affûtage plus aisé des outils avec moins de matière à retirer. En particulier, si l'on a constaté quelques bris d'outils -d'ailleurs identiques à ceux constatés en usine- les bris de dents ou ébréchures d'arêtes sont moins fréquents.

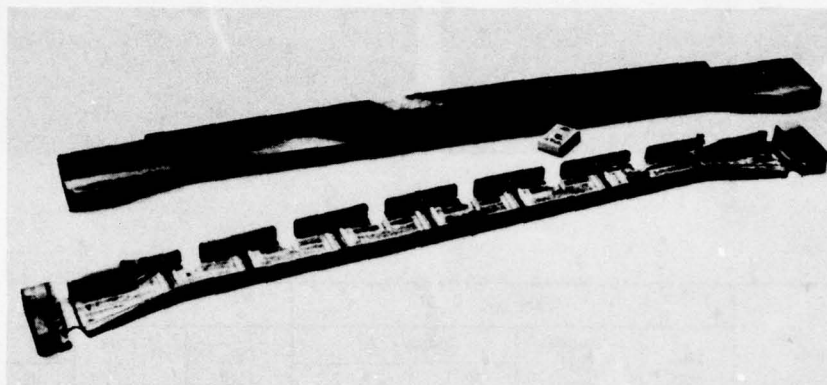
5. CONCLUSION

La commande adaptative de vitesse intéresse plus particulièrement les utilisateurs qui usinent des pièces complexes dans la masse

ou dans des ébauches matricées ou forgées, et dans des matériaux à hautes caractéristiques qui conduisent à des temps de coupe très long et pour lesquels la détermination des conditions de coupe est la plus difficile.

Qualitativement, les avantages que l'on peut en retirer sont :

- . la protection des machines et des outils,
- . la réduction substantielle des temps de coupe,
- . la constance des résultats obtenus,
- . la réduction des temps de mise au point des programmes et des coûts de traitements induits,
- . l'élimination de l'appréciation du programmeur et de l'opérateur dans la détermination des conditions d'usinage, donc de l'expérience et de la compétence de ces personnes par rapport au résultat.



Matière : 30 NCD 16 R = 108 hba

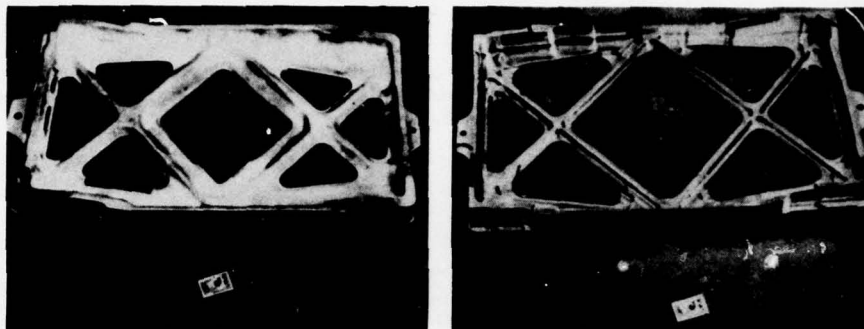
OPÉRATION	ébauche	ébauche	chanf.	ébauches alvéoles	finition	reprise	détourage	reprise	balayage profil	
FRAISE	Ø 50 2 T. Ra	Ø 32 2 T.	Ø 40 con.	Ø 25 2 T.	Ø 16 2 T.	Ø 14 2 T.	Ø 20 2 T.	Ø 16 2 T.	Ø 32 con.	temps total
Temps usine	116	58	6	249	109	19	60	41	260	918
N° pièce										
1	53	23	2	53	80	16	42	*	*	*
2	*	33	2	103	77	6,20	48	16	104	*
3	*	33	2	*	80	6,20	50	16,20	105	*
4	41	31	2	78	71,20	7,20	49	16,20	76	371,60
5	40	31	2	85	71,50	6,20	55	16	68	374,70
6	42	27,20	2	74	69,20	6	41	16	74	351,40
7	37	35	2	78	72	6	36	16	64	346
8	41	31	2	80	78	6,80	37,40	17,20	76	369,40

* Mise au point du programme et incidents MACOTECH.

Tenue des outils : Temps moyen entre 2 affûtages : 1 heure de coupe. Chaque fraise assure au moins son opération pour 1 pièce.

Réduction des temps de coupe : 60%

Nota : Les temps sont donnés en minutes et 1/100.



Matière : TA6V

OPÉRATION	Face AR				Face AV			
	Dia. outil	temps C.N. usine	temps C.A.		Dia. outil	temps C.N. usine	temps C.A.	
			N° 1	N° 2			N 1	N° 2
Usinage intérieur	50	7 h 37	4 h 55	4 h 11	50	4 h 36	2 h 35	1 h 50
Détourage extérieur	50	1 h 12	0 h 32	0 h 35	50	1 h 38	0 h 36	0 h 28
Reprise des rayons	25	1 h 51	1 h 18	1 h 14	25	2 h 00	1 h 18	1 h 18
Total :		10 h 40	6 h 45	6 h 00		8 h 14	4 h 30	3 h 36

* La vitesse de broche passe de 85 à 112 tr/mn.

Tenue des outils : Dans tous les cas les outils ont assuré l'usinage complet d'une face. Le réaffûtage est nécessaire après chaque face.

Réduction des temps de coupe : 45%.

Note : Les temps sont donnés en heures et minutes. La face AR de la place n° 1 a servi à la mise au point du programme.

INNOVATIVE MANUFACTURING FOR AUTOMATED
DRILLING OPERATIONS
Carl Micillo, Manager
John Huber, Group Head
Advanced Materials and Processes Development
Grumman Aerospace Corporation
Bethpage, New York 11714, U.S.A.

SUMMARY

The major cost drivers in airframe fabrication are identified. In the assembly area, drilling for various fastening systems is described both from economic and quality aspects. The Five-Axis Automated Assembly Fixture developed jointly by Grumman and the U. S. Air Force addresses both labor intensity and reliability with minimal capital investment. The system can automatically locate the substructure of a part using a digital scanning process and form a precise map of the location of the parts. The digitized information is used to drill and countersink through skins and substructures without costly templates. The evolution of the system is followed from the development stage into production, and economic analyses and projections for aircraft structures at various learning curves and production rates are given, including the aluminum A-6E wing and A-10 horizontal stabilizer, and advanced composite B-1 horizontal stabilizer.

INTRODUCTION

In the brief history of aviation, a continuous and rapid evolution of new materials and design concepts has occurred. In the quest to fly faster and further with ever-increasing mission requirements, stronger, lighter and more corrosion-resistant materials have been developed, ranging from wood and simple fabrics to aluminum, titanium and advanced composites. Technological advances in airframe structures, however, have increased production costs which must be offset by innovative manufacturing approaches. Some of the major cost drivers identified in the acquisition cost of today's aircraft are:

- Cost of new raw materials
- Design complexity
- High part count
- High fastener-to-weight ratio
- Non-optimum utilization of equipment and facilities

It is interesting to note that assembly and subassembly labor account for as much as 50% of the total manufacturing cost of current airframes. Production labor is almost directly proportional to the number of detail parts, holes for joining, and fasteners. Since a fighter may have 250 000 to 400 000 holes and a bomber or transport 1 000 000 to 2 000 000 holes, drilling has become a major production cost factor.

DESIGN/MATERIAL IMPACT ON PROCESS SELECTION

Automated drilling and riveting can drastically reduce subassembly costs. This approach should be considered whenever design criteria, weight considerations or raw material costs warrant its use. For example, an efficient design concept for a small, high-performance wing structure involves use of a skin-stringer structure that must be subassembled to produce a skin assembly before it can be installed on the wing box substructure (Fig. 1). A five-axis, numerically controlled (N/C) drilling/riveting machine (Fig. 2) is being used to produce titanium wing structures for the F-14A air-superiority fighter. This machine is capable of oversqueezing a rivet or slug at a predetermined stress level to produce a specified amount of fastener-to-hole interference or installing precision attachment hardware in high interference ranges in titanium structures. This approach is also being used to produce large aluminum wing structures for transport and commercial airliners (McDonnell Douglas DC-10, Lockheed 1011 and Boeing 727, 737 and 747) for which the most cost-effective configurations are skins stiffened with riveted stringers with access to both sides of the structures.

For other types of wing structures, such as multi-spar wing box configurations (Fig. 3), however, automated systems are either unavailable or simply have not yet been developed. In this case, attaching hardware must be located and installed on assembly fixtures. As a result, preparation of the proper drilling operation can be the most costly aspect of the total mechanical fastening operation (Fig. 4). Positioning of stringers, beams and ribs beneath a skin can be off by as much as 6.4 mm (0.250 in.). Normally, pilot drilling, back drilling, countersinking and templates are required for such "blind" drilling operations.

As a case in point, let us examine a typical manual fastening operation on an aluminum fighter wing structure for which an average manufacturing tolerance of 0.8 mm (0.032 in.) is required. The procedure would normally involve placement of the substructure without its covers (Fig. 5) in an assembly fixture, followed by manual positioning of a series of templates on the substructure (Fig. 6) and then laboriously moving the templates by hand to obtain the proper edge distance (as measured from the hole to the

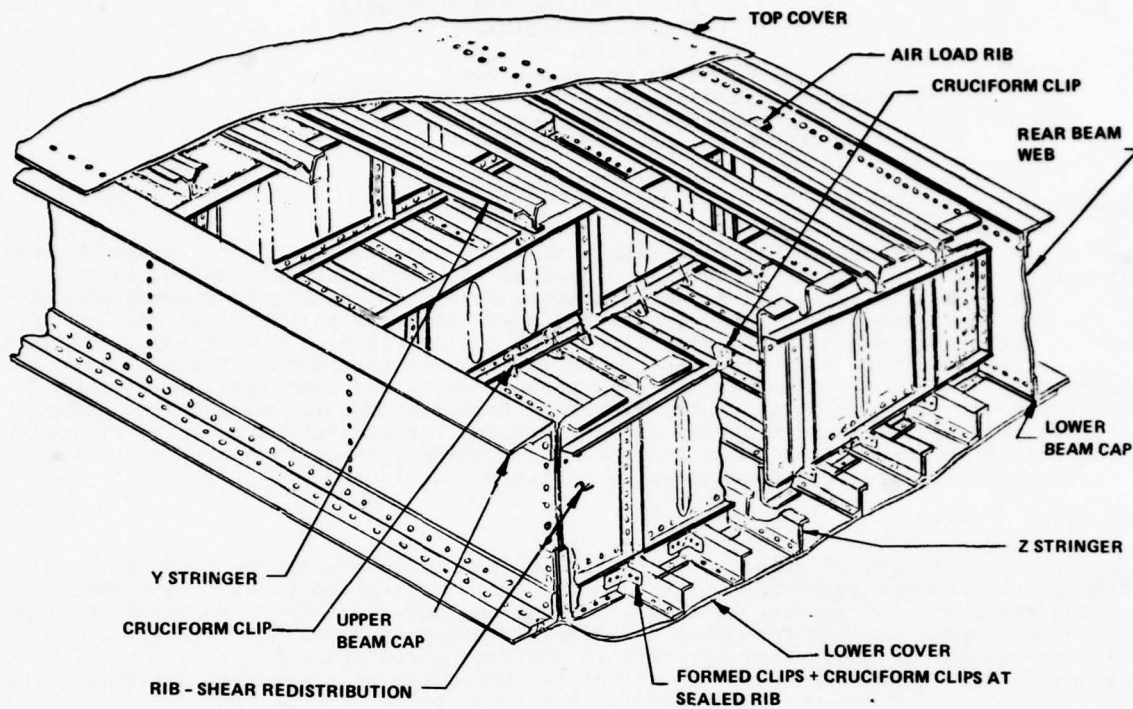


Fig. 1 Multi-Rib Wing Box Configuration

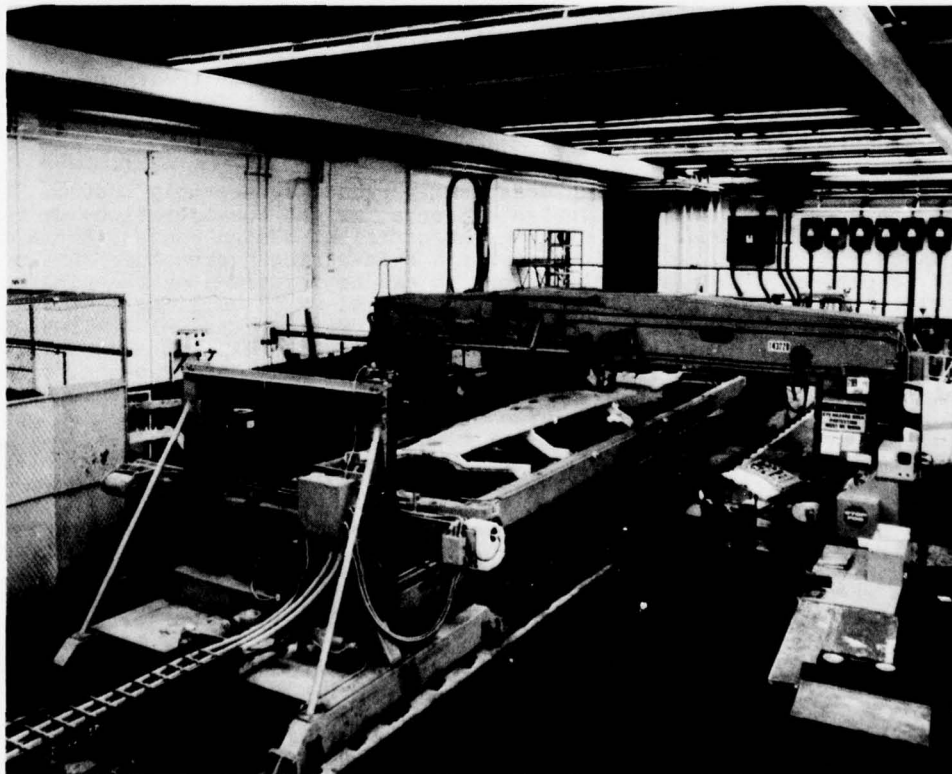


Fig. 2 Five-Axis, Numerically Controlled Drilling/Riveting Machine

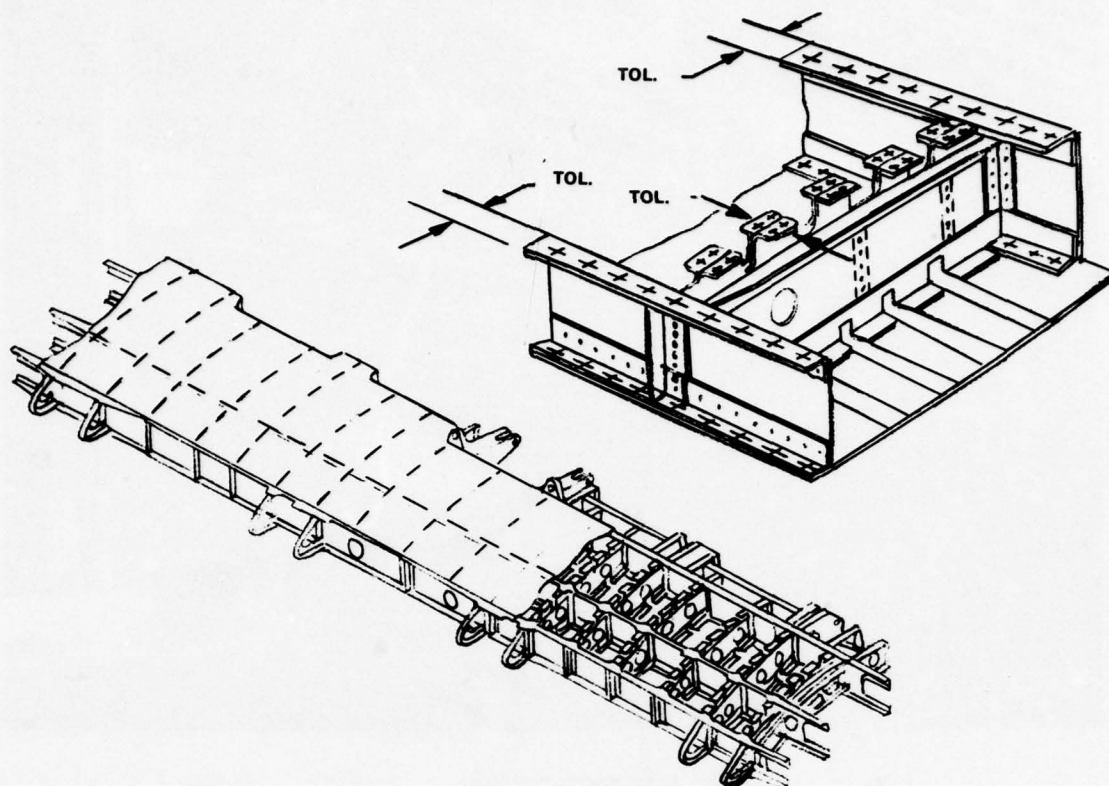


Fig. 3 Multi-Spar Wing Box Configuration

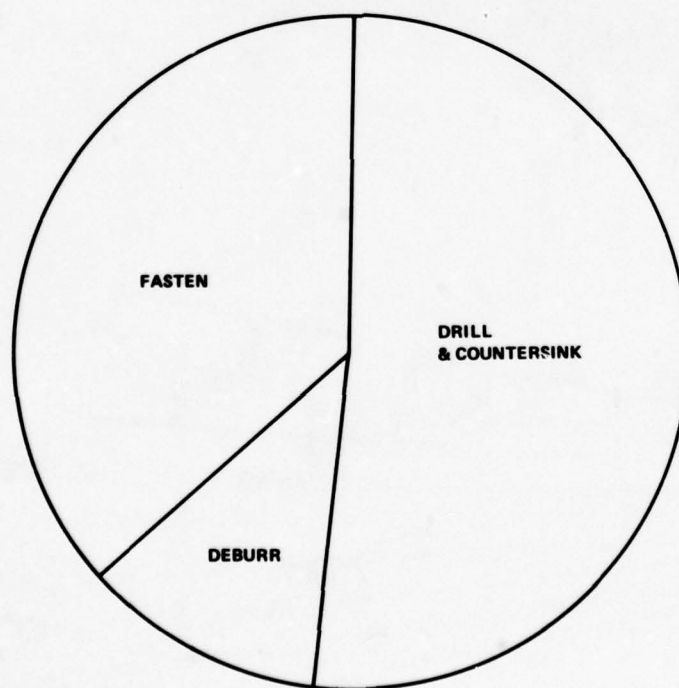


Fig. 4 Breakdown of Mechanical Fastening Operation

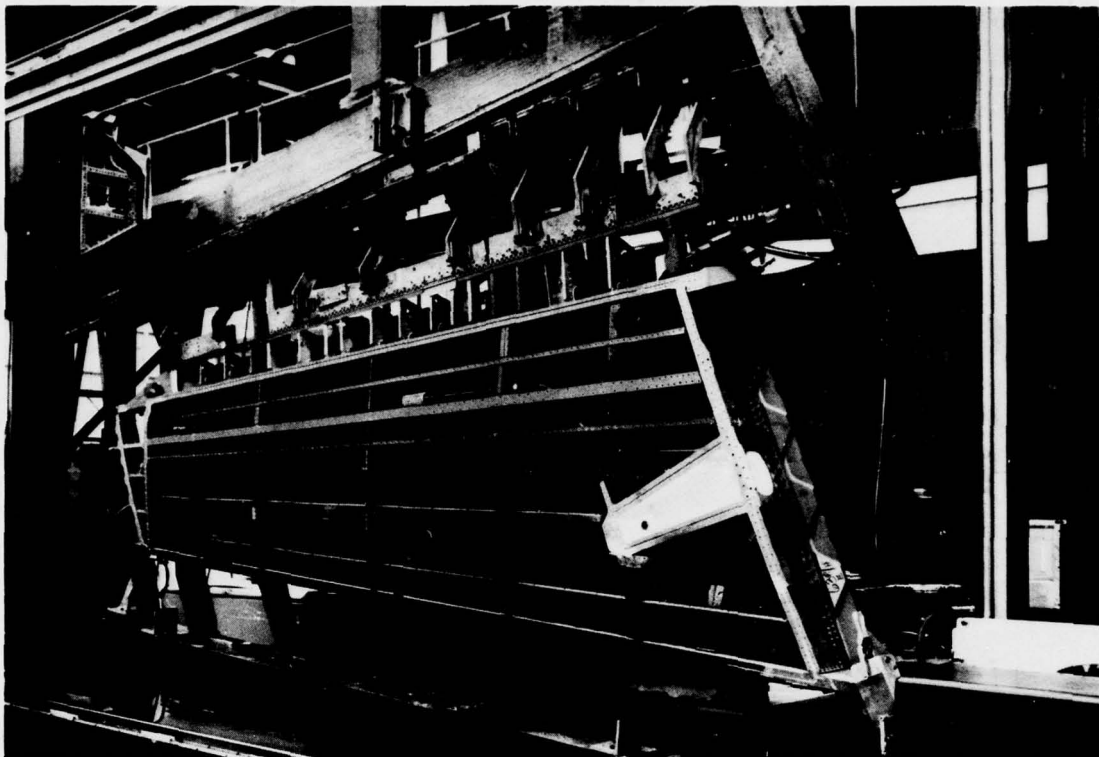


Fig. 5 Aircraft Wing Substructure in Assembly Fixture

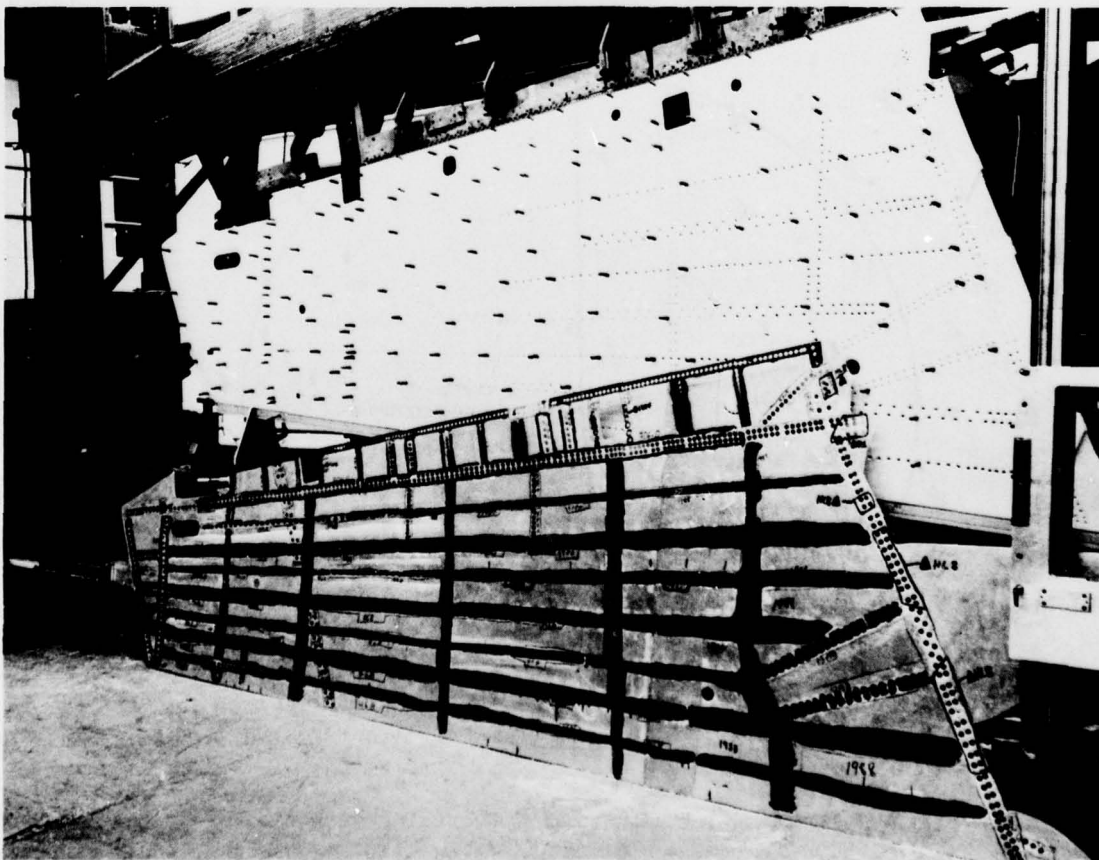


Fig. 6 Aircraft Wing Structure with Cover and Templates

edge of the individual spar, rib or stringer). These time-consuming operations, for which all misalignments and tolerance build-ups must be accounted for and corrected, are unavoidable unless we are fortunate enough to be working with oversized details (at a significant weight penalty) to get the proper edge distances. After all dimensional corrections have been indicated, holes can be drilled through the wing cover and substructure. Since these are manual operations, we are all too painfully aware of the potential for improperly positioned holes.

SELECTIVITY OF AUTOMATION IN AEROSPACE MANUFACTURING

When the purchase and deployment of automated equipment are being considered, the nature of the aerospace manufacturing community must be examined. We are essentially batch-type producers, often manufacturing various details in relatively small quantities. As a result, the advantages of full automation, such as that found in the automotive industry, are not applicable to the aerospace industry. If design and procurement criteria warrant large capital investment and "upfront" money, then full automation is the answer.

In all other cases, the obvious challenge is a system providing production cost savings and reliable hole quality with nominal capital expenditures. The system we have developed, the Five-Axis Automated Assembly Fixture (Fig. 7), is capable of automatically locating and correcting for variations in the positions of the substructure components by means of a digital scanning process, and then automatically positioning and operating a portable drilling device on an assembly fixture. The unique and most attractive feature of this system is the capability to create a precise map of the locations of the various substructure components without the need for costly templates. The digitized information obtained in the scanning process is computerized and subsequently used by the Five-Axis Assembly Fixture to automatically drill and countersink through the cover and substructure in one operation - - rapidly, accurately and economically. This system is being used in production on Grumman A-6E wings and is being evaluated for use with the Fairchild A-10 stabilizers.

FIVE-AXIS AUTOMATED ASSEMBLY FIXTURE

Modular Features

Since the Five-Axis Automated Assembly Fixture is modular in nature, it can be readily adapted to many other applications. The system consists of a horizontal fixture that holds the wing structure, a vertical gantry that holds the drill head which houses either the scanning camera or drill unit, a central controller, a remote interface box, and an operator control pendant. The central controller consists of a DEC PDP-8/E unit with

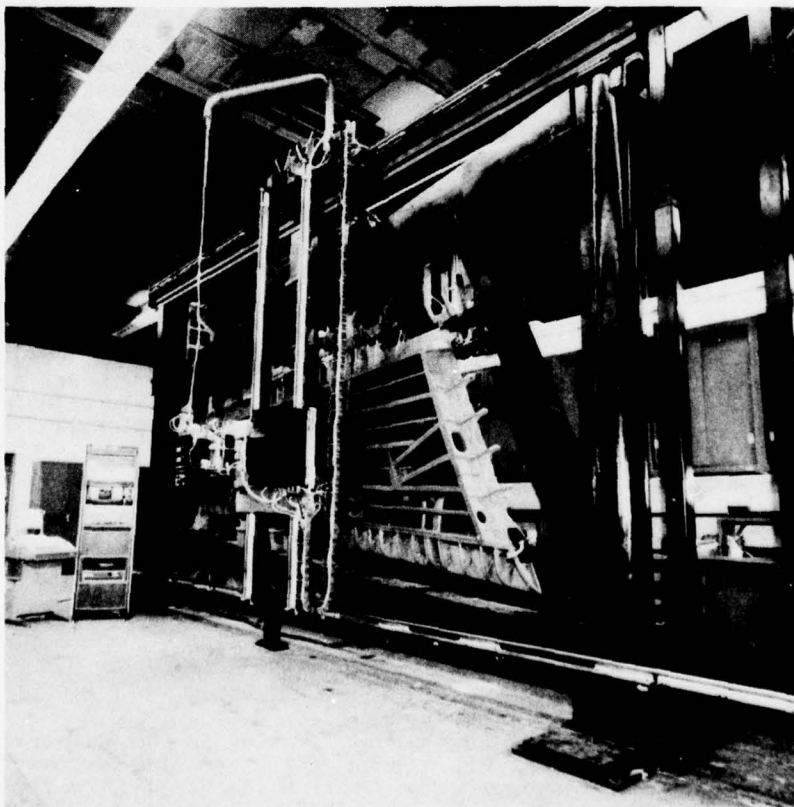


Fig. 7 Grumman Five-Axis Automated Assembly Fixture

disk storage, a real-time clock, power supplies, interface electronics and a teletype. The system has five axes of motion (Fig. 8). Four axes of motion are operated electrically by drive motors. These are:

- X-Axis - horizontal movement (left to right) of the gantry across the wing structure
- Y-Axis - vertical movement (up and down) of the scanning camera/drill head unit on the gantry
- α -Axis - rotation around the X-axis that allows the drill spindle or camera lens to pitch up or down at various angles
- β -Axis - rotation around the Y-axis that allows the drill spindle or camera lens to yaw left or right at various angles.

The fifth axis of motion (Z axis) is operated by a pneumatic cylinder for drill feed and camera focus control.

Hole Position Calculation

Through the control pendant, the operator can direct the computer to issue electrical camera-positioning signals for the drive motors in the four axes to start the scanning operation. The digital scanning camera (Fig. 9), which is housed in the drill head assembly, locates the edge of the structural members. The computer then calculates the offset distance for hole placement from the individual electrical pulses generated through detection of the reflected light by a linear array of photodiodes as a function of light intensity and exposure. Since the scanning camera is positioned so that it is centered at the edge of the substructure, half of the photodiodes respond to the reflected light. The operational range of the camera is 256 pulses (plus 6.5 mm (0.256 in.)) because there are 512 photodiodes in the array. If the scanning camera is more than 6.5 mm (0.256 in.) from the center while seeking the edge of a substructure component, the computer run-time software drives the camera to its computed midpoint so that it can rescan the hole after taking into account any overshoot or undershoot. If the camera finds the edge of the substructure component within its operational range of 6.5 \pm 1.3 mm (0.256 \pm 0.050 in.), it is not moved. Hole position is calculated by the computer based on the camera reading once the reading is within 1.3 mm (0.050 in.).

Scanning

The scanning cycle is the first operation in the sequence, since holes must be scanned before being drilled. In the case of the wing structure assembly (described previously for manual operation), the substructure without the cover is placed in an assembly fixture, the scanning camera is placed in the drill head assembly, and all five axes are at the zero position. Through the control pendant, the operator activates the program for the scanning cycle, which turns on the camera lights and sends back signals to the computer to identify the actual position of the substructure. The computer corrects the nominal hole position to the desired position as a function of the actual substructure position and sends this information to the disk file. The scanning program, based on a file of master coordinates taken from engineering drawings, generates a modified set of hole coordinates to drill holes for temporary fasteners to hold the cover to the substructure and then another set of hole coordinates to drill and countersink all other holes.

Drilling

Upon completion of the scanning program, all axes are returned to the zero position, a drill head replaces the camera in the drill head assembly, and the wing cover is temporarily clamped to the substructure. Drilling and installation of temporary Cleco fasteners precedes the drilling of finished holes in accordance with the modified program. Normality of the drill head to the wing cover surface is maintained by programming. A residual force of 91 kg (200 lb) is maintained at the nosepiece to clamp the cover to the substructure. The minimum-to-maximum diameter differences are within 0.05 mm (0.002 in.). The overall system falls within a true-position hole tolerance of \pm 0.4 mm (\pm 0.016 in.). A typical cycle to drill one hole is as follows:

<u>Operation</u>	<u>Time, seconds</u>
Advance drill to structure	2.0
Drill and countersink hole	5.0
Retract drill assembly	2.0
Advance to next hole	2.5
Total	11.5

The drilling operation is followed by manual riveting of the wing covers to the substructure. The accuracy and time-saving aspects of the scanning operation and the rapidity of the drilling cycle enabled us to transfer the Five-Axis Automated Assembly Fixture from the laboratory to production. An additional bonus, which should not be overlooked in any comprehensive economic analysis, is the repeatable reliability of the holes

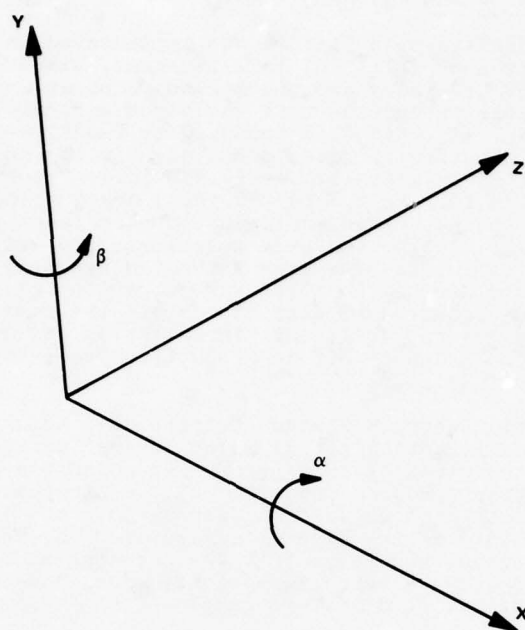


Fig. 8 Five Axes of Motion of Automated Assembly Fixture

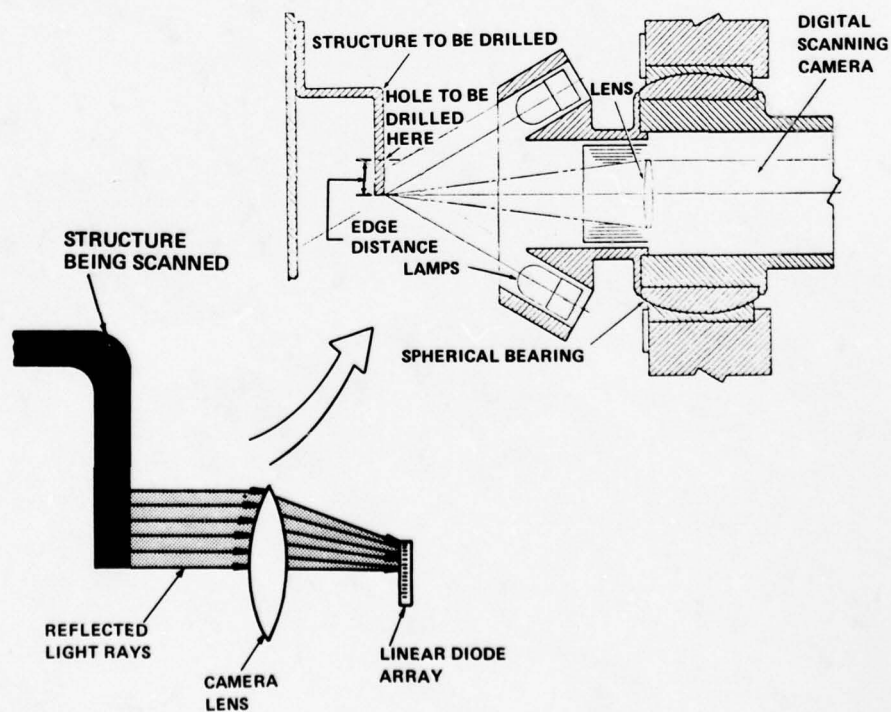


Fig. 9 Operation of Scanning Camera

produced by this system that precludes or effectively minimizes extensive inspection and repairs.

PRODUCTION IMPLEMENTATION - A-6E and A-10

The Five-Axis Automated Assembly Fixture was implemented in production on the Grumman A-6E program. The A-6E (Fig. 10) is a two-seat, all-weather attack aircraft being manufactured for the U.S. Navy and the Marine Corps at a rate of one and one half aircraft per month; the peak production rate was eight aircraft per month. Over 40 outer-wing assemblies (Fig. 11) have been produced by the Five-Axis Automated Assembly Fixture. This structure consists of five beams, eight ribs, and two covers ranging in thickness from 3.2 mm (0.125 in.) to 11.1 mm (0.438 in.). About 2000 holes, ranging in diameter from 3.2 mm (0.125 in.) to 6.4 (0.250 in.), are drilled in this structure. Prior to introduction of the automated equipment, the average production time to set up the hole templates manually, locate the hole positions, and drill an A-6E wing cover was 65 hours at Aircraft No. 600. The Five-Axis Automated Assembly Fixture performed the same task in about 25 hours during the first demonstration run. As shown in Fig. 12, about half of the time was required to scan and drill; the remainder was used in set-up operations such as camera re-use, drill unit installation and drill/countersink changes. This results in a reduction of up to 60% in production labor for the drilling operation at aircraft production unit No. 600.

The Five-Axis Automated Assembly Fixture is currently being evaluated on the Fairchild A-10 close-support aircraft (Fig. 13) which became operational this year with the U.S. Air Force. Production rates of 15 aircraft per month are anticipated. In a joint Grumman-Fairchild development program sponsored by the Air Force Materials Laboratory, aimed at demonstrating additional production cost savings via innovative manufacturing technology, the applicability of the Five-Axis Automated Assembly Fixture to the A-10 horizontal stabilizer is being studied. This 20-foot-long aluminum structure, consisting of upper and lower covers and a substructure with 3 spars and 17 ribs (Fig. 14), requires the drilling of 3750 holes having diameters ranging from 4.4 mm (0.172 in.) to 6.4 mm (0.250 in.).

The manual procedure for drilling the A-10 horizontal stabilizer involves drilling pilot holes in the rib flanges prior to assembly of the flanges in the box substructure. After the box substructure has been installed in the assembly fixture, one cover is placed against the substructure so that pilot holes can be drilled in the cover from the rear through the previously drilled pilot holes in the rib flanges. Full-size holes and



Fig. 10 A-6E Intruder

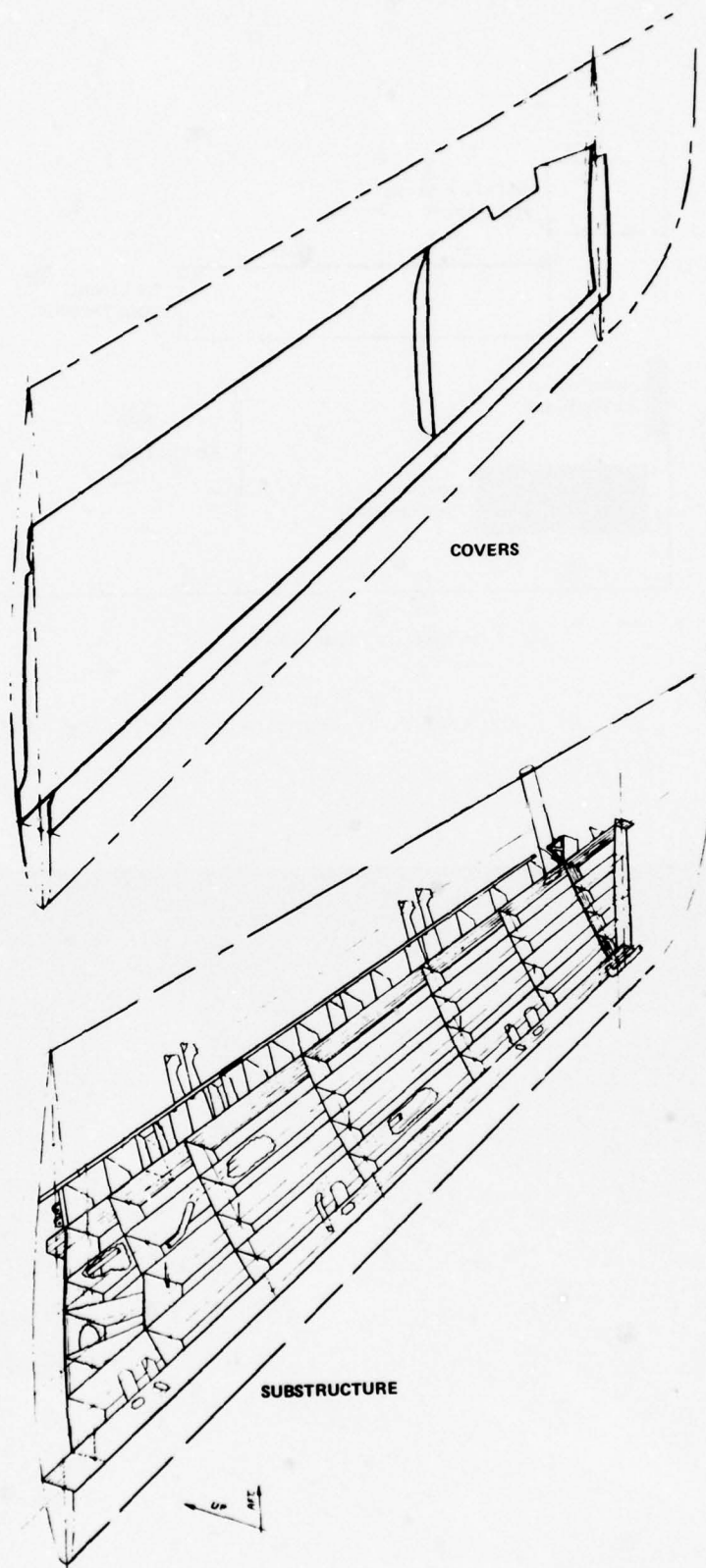


Fig. 11 Exploded View of A-6E Wing

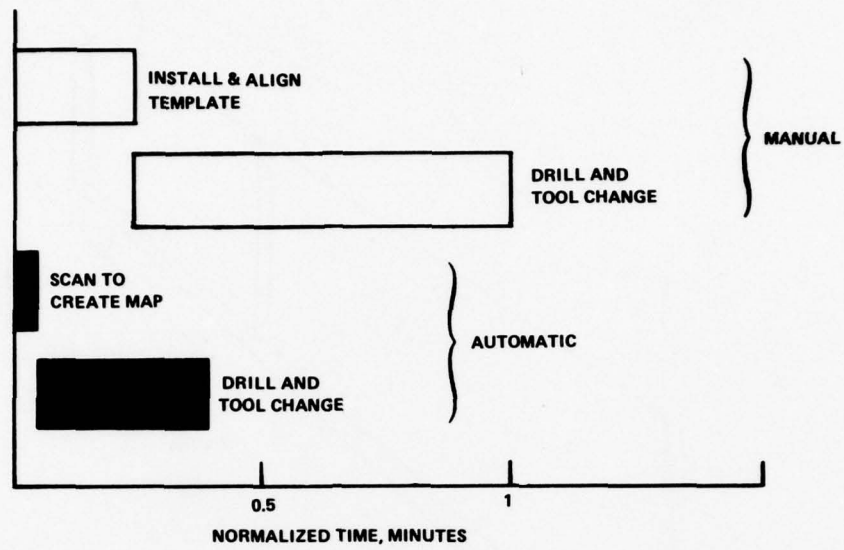


Fig. 12 Comparison of Scanning and Drilling Times

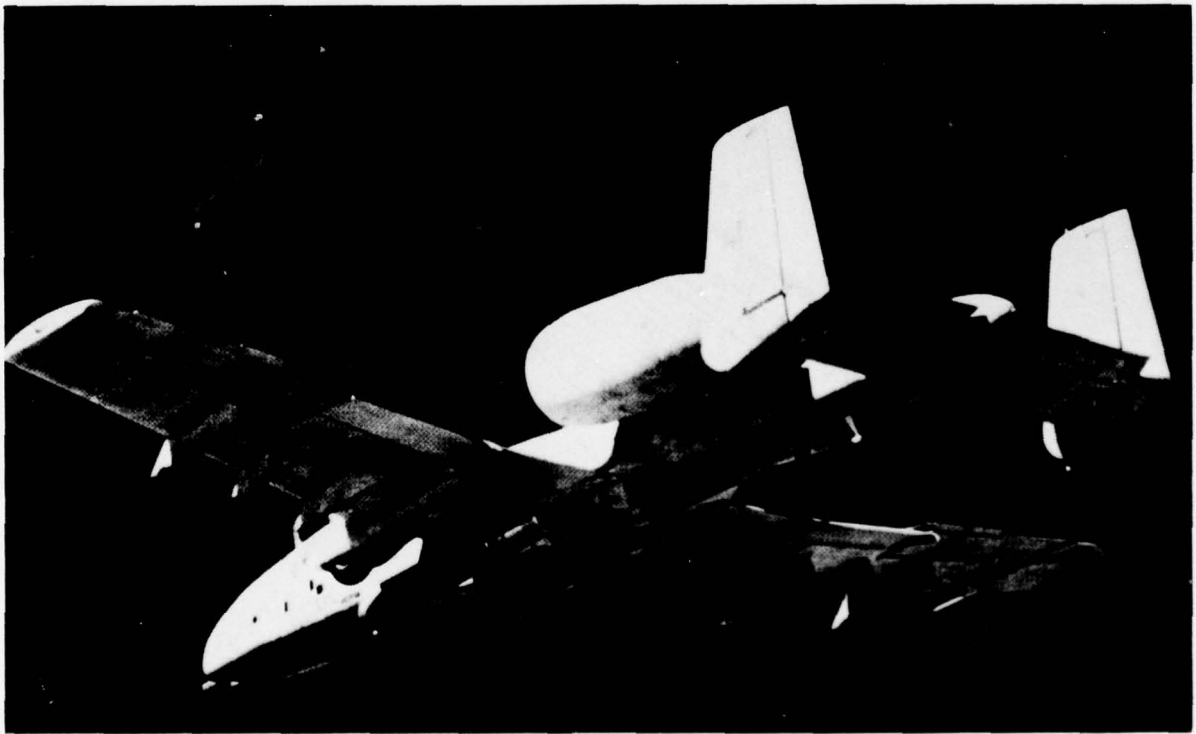


Fig. 13 Fairchild A-10 Close-Support Aircraft

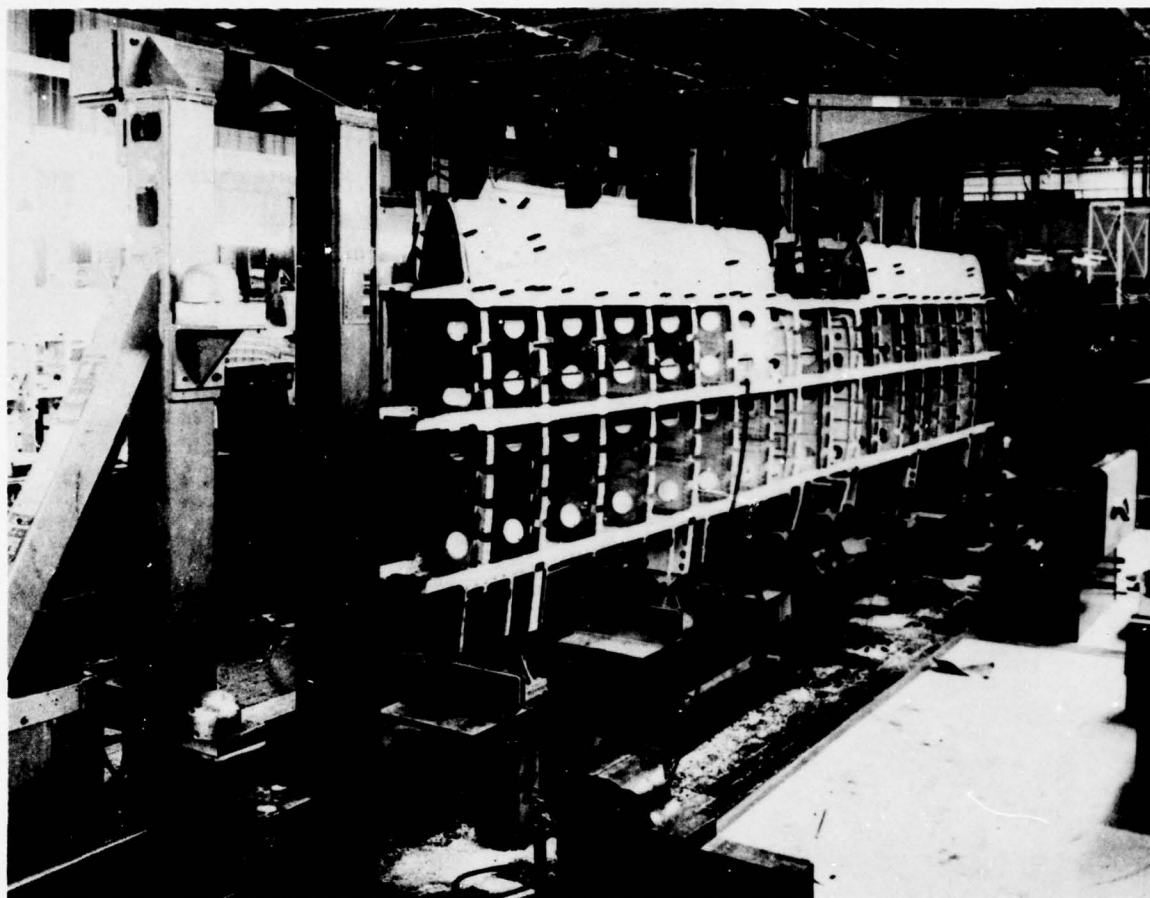


Fig. 14 A-10 Horizontal Stabilizer

countersinks are then drilled from the front of the cover using the pilot holes as guides. When one cover has been drilled, it is removed from the assembly fixture so that the other cover can be similarly drilled. Substantial cost savings are anticipated by using the Five-Axis Automated Assembly Fixture to drill and countersink the A-10 horizontal stabilizer in a manner similar to that for the A-6E wing structure. If the projected cost savings are, in fact, realized when this Air Force-sponsored program is soon completed, the Five-Axis Automated Assembly Fixture will be implemented in production to drill and countersink the A-10 horizontal stabilizer, with subsequent extension to wing boxes and other areas of the aircraft.

IMPACT ON HIGH-MATERIAL-COST STRUCTURES

Another projected application for the Five-Axis Automated Assembly Fixture was the production program for the hybrid boron-graphite/epoxy B-1 horizontal stabilizer (Fig. 15). This swing-wing, intercontinental bomber (Fig. 16) is capable of flying at speeds up to Mach 1.6 at high altitudes and at near-supersonic speed at low altitudes. The implementation of advanced composites in this structure resulted in weight savings of 243 kg (535 lb) per aircraft (16.2%) and the elimination of 10 000 fasteners (41%) compared to the baseline metal structure.

The drilling parameters for the cover-to-substructure attachments must be closely controlled to prevent delamination. Insuring proper hole location is also difficult because of the relatively large thickness tolerance of advanced composite parts. Since the substructure parts cannot be precisely located in the assembly fixture, the drilling operation becomes highly labor-intensive. About 2850 holes per cover (80% of the total number of holes) are drilled and countersunk through graphite/epoxy in one operation using carbide cutters mounted in a Winslow Spacematic Model M-62 drilling unit equipped with a vacuum foot (Fig. 17). Hole location in the interior spar-to-cover joints is controlled by strip templates pinned to the cover through the pilot holes which are drilled from the inside using a contoured bushing that picks up the corrugated web. After the interior has been drilled, additional strip templates are used to locate the attachments to the ribs relative to the flat webs.

The Five-Axis Automated Assembly Fixture is directly applicable for drilling and countersinking all of the holes in the graphite/epoxy regions of the B-1 horizontal stabilizer covers. After assembly of the substructure, the exact location of selected holes would be marked and the substructure scanned automatically to correct the computer program for variations in part thickness and alignment. The cover is then placed in

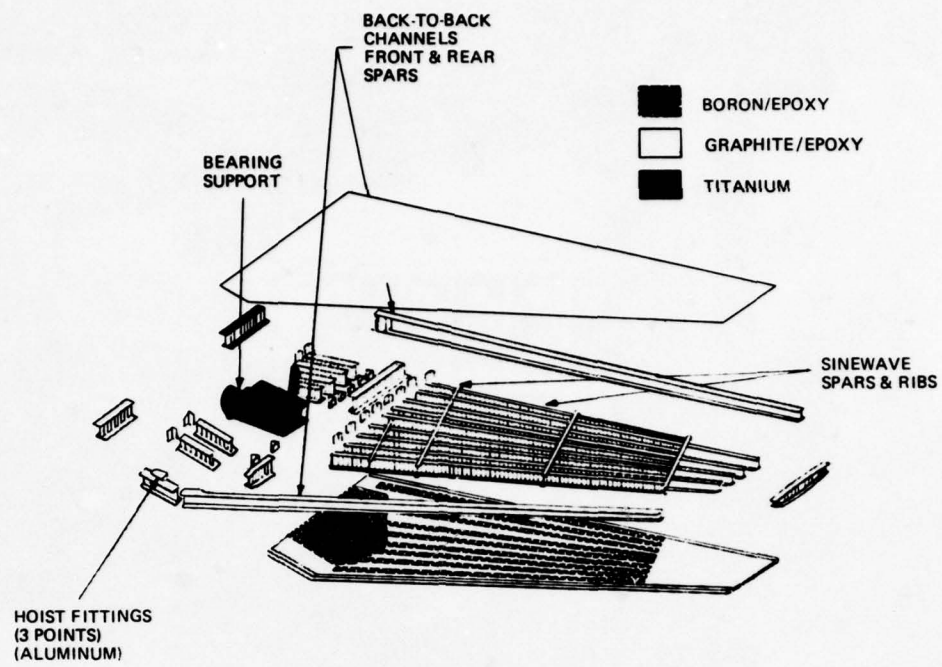


Fig. 15 B-1 Horizontal Stabilizer



Fig. 16 B-1 Bomber

position and the holes are drilled and countersunk in one operation, as described previously. Again, use of the Five-Axis Automated Assembly Fixture would improve the accuracy and perpendicularity of fastener placement, and would also improve hole quality. The automated fixture would also be adaptable for installation of the tip cap and leading/trailing edges to the completely assembled torque box. These operations, including fastener installation, represent 18% of the manufacturing labor cost for the entire stabilizer (Fig. 18). Thus, the anticipated savings in drilling costs, as verified on metal structures, are about 8 to 10% of the total stabilizer cost, which makes the advanced composite B-1 horizontal stabilizer even more cost-effective.



Fig. 17 Winslow Spacematic Drill Unit

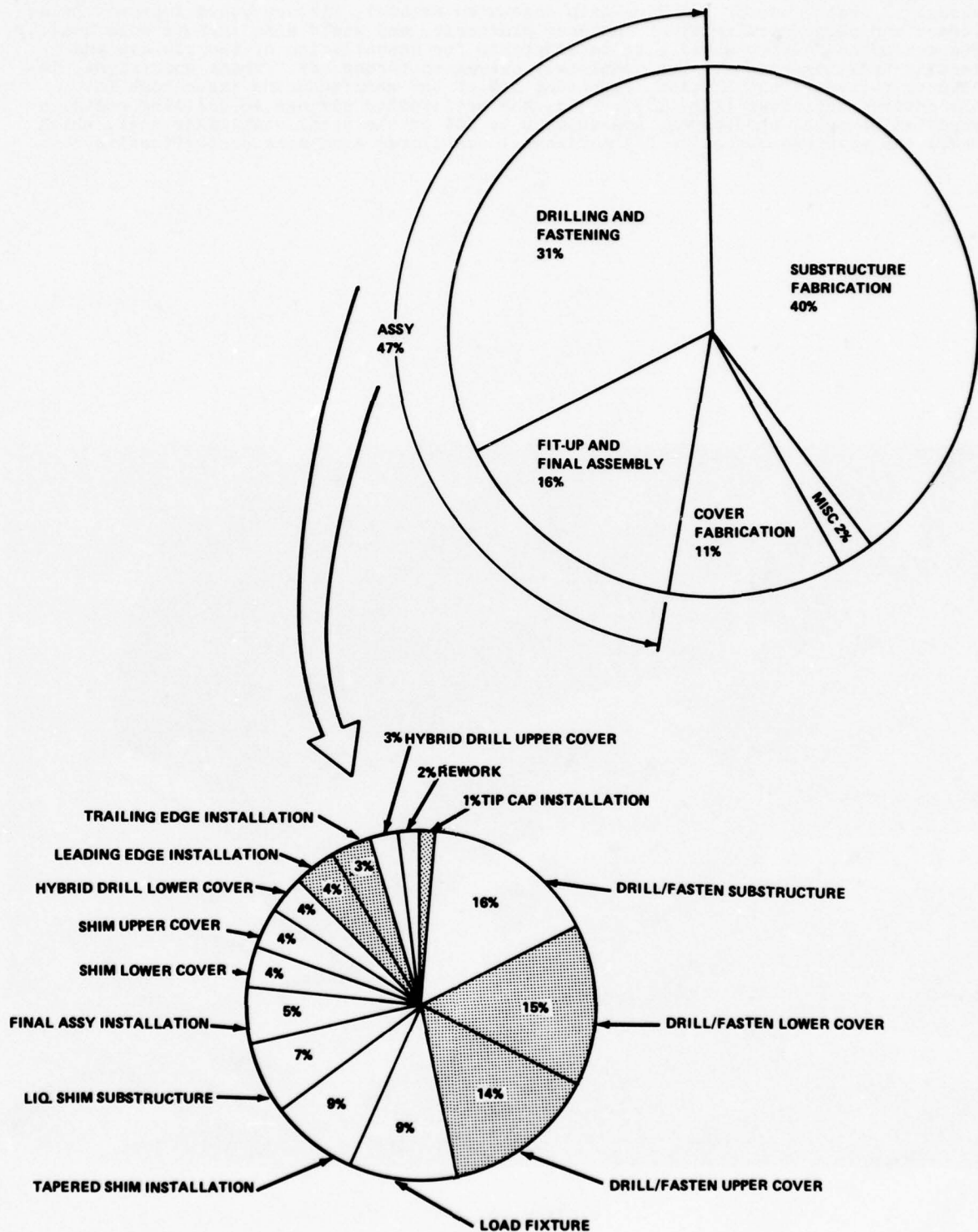


Fig. 18 Manufacturing Breakdown for Advanced Composite B-1 Horizontal Stabilizer

APPLICABILITY, EFFICIENCY AND RAPID PAYBACK

Until the advent of the Five-Axis Automated Assembly Fixture, automation of the manufacturing operations for such aircraft structures as the A-6E wing and A-10 and B-1 horizontal stabilizers was not possible. The Grumman-developed system, as demonstrated under U.S. Air Force auspices, can be applied to most assembly procedures that require multiple manipulations of drilling equipment and templates to locate fasteners precisely at the intersections of underlying substructure components that have been pre-assembled with their own network of locating tolerances.

Assuming a \$100 000 base cost for system hardware and software and considering our experience in this area, it is estimated that the breakeven cost for implementing an automated drilling system would occur at about 250 000 holes (Fig. 19). Automated scanning and drilling operations would have the following advantages:

- 50 to 60% reduction in production labor
- Improved hole quality due to better tool platform
- Elimination of costly templates
- Predictable and consistent flow rates
- No cost penalty due to inexperience (learning curve effect)
- Less dependence on operator skill

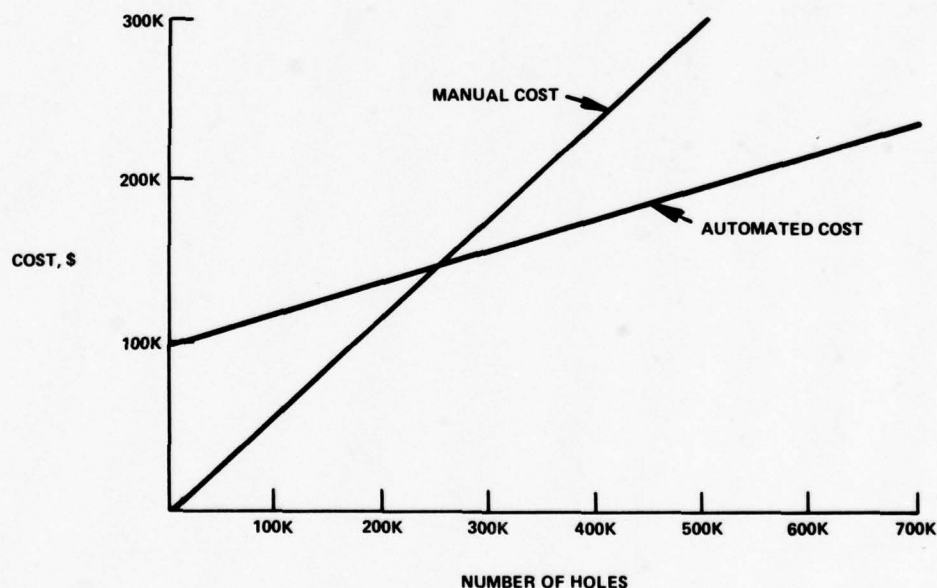


Fig. 19 Breakeven Point for Automated Drilling

The Five-Axis Automated Assembly Fixture, therefore, offers such attractive features as low capital investment, rapid payback, and repeatable and precisely drilled structures. This system is truly representative of those emerging efforts in the aerospace community that offer significant opportunities for lower cost and higher quality components.

ION VAPOR DEPOSITED ALUMINUM COATINGS FOR IMPROVED CORROSION PROTECTION

by

E. R. Fannin

Program Manager - Ivadizer Technology

McDonnell Aircraft Company

St. Louis, Mo. 63166 - USA

SUMMARY

The corrosion resistant properties of metallic aluminum are well documented. However, commercial processes for the application of aluminum coatings, such as electroplating, spray metallizing, hot dipping, cladding, and others have severe limitations. Production equipment has recently been developed for plating with aluminum by ion vapor deposition (IVD) without incurring many of the problems associated with these commercial processes. The coating is called IvadizeTM and provides outstanding corrosion protection. In addition, the coating can be used at temperatures up to 925°F (496°C); and the process does not cause hydrogen embrittlement. The coating and the coating process are non toxic and do not contribute to the pollution of our environment.

Because of its performance advantages, ion vapor deposited aluminum can be used in a wide range of applications, and is particularly effective as a replacement for cadmium coatings.

INTRODUCTION

The aircraft industry, like most industries, is confronted with the challenge of protecting products from corrosion and its deleterious effects. We must meet this challenge in the face of increasingly stringent demands for improved product life and performance. Therefore, new materials and coating systems for protection against corrosion are continuously being sought.

Cadmium electroplating has been the favored method for protecting steel on aircraft structure for many years. Obvious problems with its use were minimal prior to the use of high strength steel and aluminum alloys. Cadmium electroplating on high strength steel often caused hydrogen embrittlement, and cadmium plated fasteners installed in high strength aluminum alloys helped promote exfoliation corrosion in the countersinks. More recently it has received further disfavor because it was found to cause solid metal embrittlement of titanium structure and because of its toxicity and harmful effects on the environment.

However, it was mainly for the first two reasons that McDonnell Aircraft Company (a division of McDonnell Douglas Corporation) started looking for a viable alternate for cadmium in the early 1960's. After extensive paper studies, aluminum coatings were selected as the best substitute. Being the least dissimilar to aluminum alloy structure, it is ideally compatible. Furthermore, aluminum is anodic to steel and provides galvanic protection as does cadmium.

It was quickly found that available processes for applying aluminum coatings such as metal spraying, electroplating, cladding, hot dipping and others had severe limitations such as thickness control, adhesion, size and shape of product that could be coated, and effect on substrate properties.

During this same period we had selected vacuum deposited cadmium as the coating for solving the problem of hydrogen embrittlement of high strength steel. Our production experience with the vacuum coating process was very favorable. For this reason we started looking at vacuum coating processes for aluminum. This included physical vapor deposition, ion vapor deposition, and chemical vapor deposition. Ion vapor deposition provided the best adhesion and most uniform coating thickness and with other considerations was selected for further development.

In the late 1960's the United States Air Force and Navy sponsored in-service testing of several coatings on fasteners installed in operational aircraft. (Reference 1) These tests showed that aluminum coatings provided the best protection against corrosion. These results along with numerous laboratory tests confirmed the performance advantages of ion vapor deposited aluminum.

The production feasibility of the process was demonstrated with a full scale coating system fabricated and delivered to the Naval Air Rework Facility, San Diego, in 1974. Since then a military specification has been issued and coating equipment fabricated for the U.S. Air Force. Additional coating systems for both fasteners and larger structural components have been fabricated and ion vapor deposited aluminum is being used on several production aerospace programs.

DESCRIPTION OF THE EQUIPMENT AND PROCESS

The basic equipment required for ion vapor deposition, called IvadizerTM at McDonnell, is a steel chamber, a pumping system, an evaporation source, and a high voltage power supply. A schematic of a typical Ivadizer is shown in Figure 1.

The process sequence consists of pumping the system down to about 10^{-4} Torr. The chamber is then backfilled with an inert gas to about 10 microns and a high negative potential applied between the parts being coated and the evaporation source. The gas becomes ionized and creates a glow discharge around the parts to be coated. The positively charged gas ions bombard the surface of the parts and perform final cleaning. The clean surfaces resulting are essential for good coating adhesion.

Following glow discharge cleaning, commercially available aluminum wire (1100 alloy) is evaporated by continuously feeding into resistance heated crucibles. As the aluminum vapor passes through the glow discharge, a portion of it becomes ionized. This, in addition to bombardment by the inert gas ions, accelerates the aluminum vapor toward the part surface. This results in denser coatings and also improves the coating adhesion. The ionization also provides better throwing power and allows complex shapes to be more uniformly plated. A typical plating cycle requires about 45 minutes.

After coating, parts are generally chromate treated in accordance with MIL-C-5541 (Reference 2). This provides additional protection against corrosion. It also forms a good base for paint adhesion and is a common treatment for aluminum surfaces.

COATING PERFORMANCE

Ion vapor deposited aluminum is a soft, ductile coating and has properties nearly identical to pure aluminum. We use three classes and two types of coatings. The classes reflect coating thickness and the types are I, as coated, and II, as coated with a supplementary chromate

treatment. Type II is generally used for reasons previously mentioned. The corrosion resistance requirement for type II coatings is shown in Table 1 for the various class coatings.

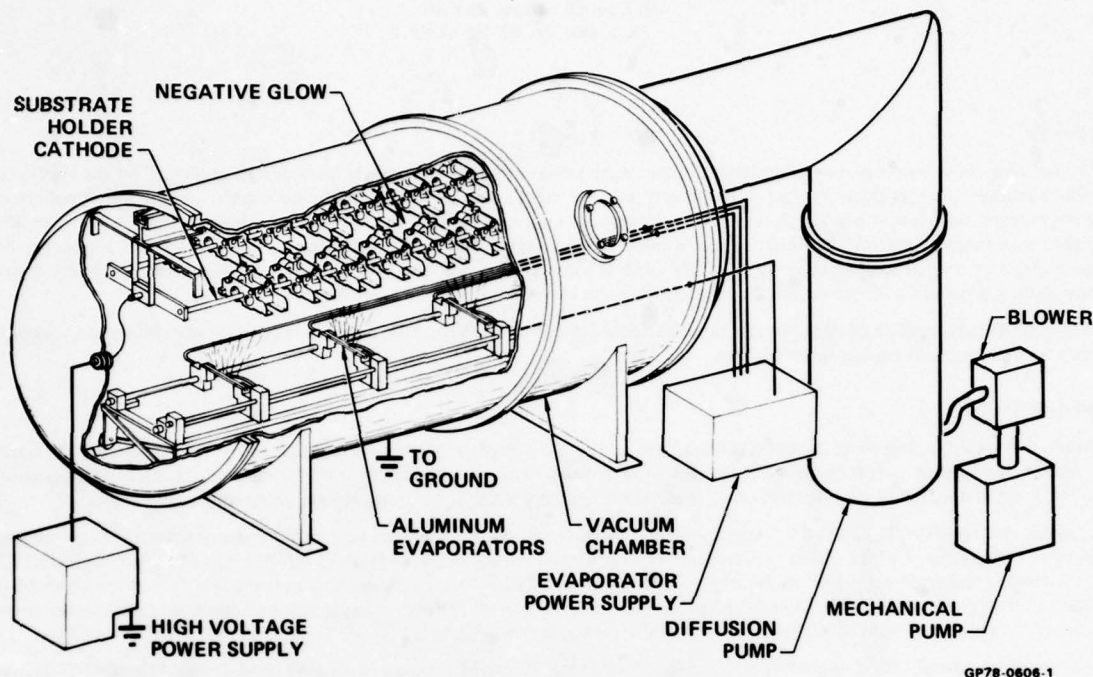


FIGURE 1
SCHEMATIC OF AN ION VAPOR DEPOSITION SYSTEM

TABLE 1
MINIMUM CORROSION RESISTANCE
REQUIREMENTS PER MIL-C-83488 (REFERENCE 3)

CLASS	MINIMUM THICKNESS		CORROSION RESISTANCE (HR)
	(IN.)	(MICRONS)	
1	0.0010	25	672
2	0.0005	13	504
3	0.0003	8	336

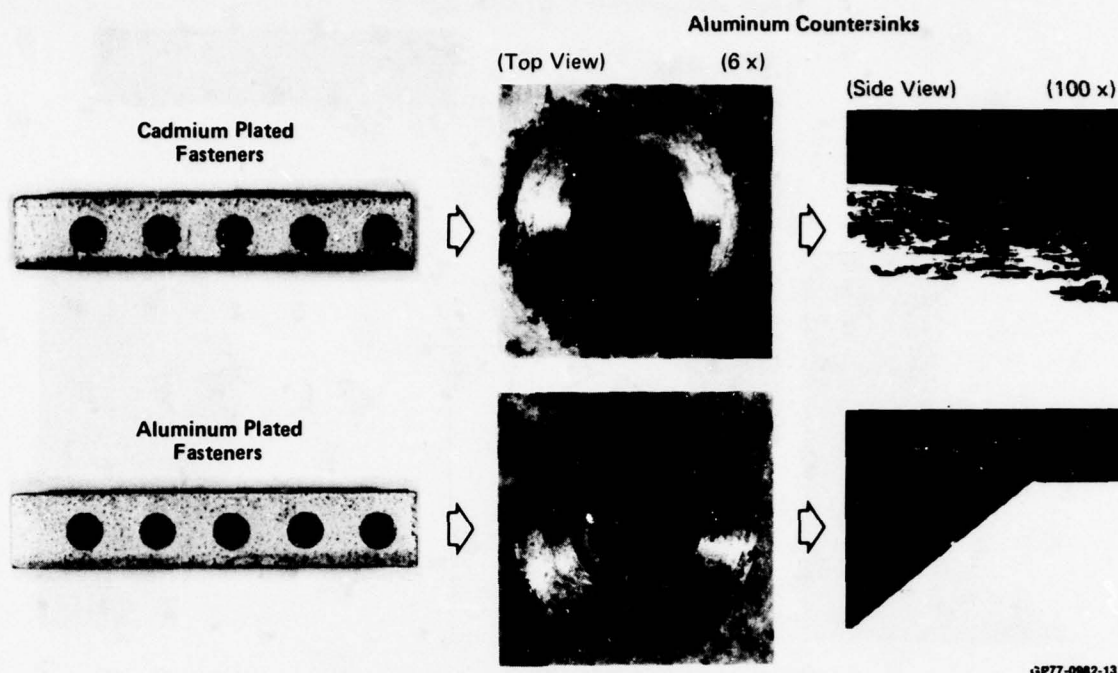
Class 1 coatings are used for high temperature and exterior applications where severe corrosion environments are encountered. Class 2 is recommended for interior parts where less severe environments are encountered, and Class 3 is used only when close tolerances are required such as fine threaded parts.

Corrosion testing of bright, electroplated cadmium on steel panels along with IVD aluminum of comparable thickness in 5% salt spray per ASTM Method B-117 will generally show cadmium to be better. However, if a scratch is made through the coatings to the substrates, the cadmium will generally sacrifice itself more quickly and allow red rust to form before the IVD aluminum.

Results obtained in laboratory tests when cadmium and IVD aluminum coated steel fasteners were installed in 7075-T6 aluminum alloy and exposed to SO_2 - salt spray for 168 hours are shown in Figure 2. The cadmium plated fastener heads are more severely rusted. More important is the condition of the countersinks in the aluminum. The IVD aluminum has provided protection to the countersinks while the cadmium coated fasteners appear to have promoted corrosion of the countersinks.

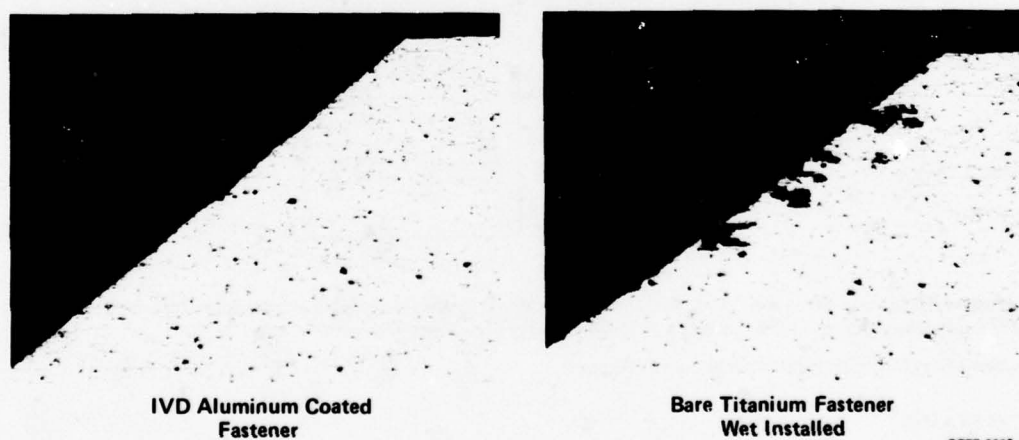
There are also advantages for IVD coating titanium fasteners installed in aluminum structure. A comparison was made between IVD aluminum coated titanium fasteners installed dry, and bare titanium fasteners installed with wet epoxy primer. The latter is a standard procedure used on aircraft. These fasteners were installed in 7075-T6 aluminum alloy that had been MIL-C-5541 treated. After fastener installation the panel was sprayed with one coat of MIL-C-23377 primer and exposed to SO_2 -salt spray for 28 days. Visual examination showed that the blistering of primer around the peripheries of the fasteners installed with wet primer was more severe than around the IVD aluminum coated fasteners. Examination of the countersinks after fastener removal also showed less corrosion resulted where IVD coated fasteners were installed (Figure 3). Studies at McDonnell have also shown a cost advantage of using IVD aluminum coated fasteners in lieu of wet installation.

Coating adhesion and thickness uniformity are comparable to electroplating. The adhesion requirements are the same as those specified in Reference 4 for cadmium electroplating. An example of the coating uniformity on a fastener is illustrated in Figure 4.



GP77-0982-13

FIGURE 2
IVD ALUMINUM AND CADMIUM COATED STEEL FASTENERS
INSTALLED IN 7075-T6 ALUMINUM ALLOY AND EXPOSED
TO 168 HOURS OF SO₂ - SALT SPRAY



GP77-0982-14

FIGURE 3
CORROSION TESTS OF IVD COATED AND WET INSTALLED TITANIUM FASTENERS
IN 7075-T6 ALUMINUM ALLOY COUNTERSINKS

A lot of fastener qualification data has been generated on the use of IVD aluminum (Reference 5). A summary of the tests performed is listed in Table 2. This data is too voluminous to present here, however the conclusions can be summarized as follows:

1. The aluminum coating does not produce any detrimental effects on mechanical properties.
2. The coefficient of friction of aluminum is higher than cadmium, therefore, higher installation forces are required. These higher values, however, are within the working ranges presently used for cadmium in most cases. Interference fit fasteners may require closer attention to the type of lubricants used.

Ion vapor deposited aluminum has also been evaluated on gas turbine components. (Reference 6). In the low temperature sections, less than 850°F (454°C), it is being considered as a replacement for diffused nickel cadmium and aluminum pigmented paints.

It has also been evaluated in the hotter sections. There it also shows promise as a replacement for pack cementation. In this case the aluminum is applied to the nickel base alloy components by ion vapor deposition and then diffused to form the nickel aluminide coating. This approach results in a more uniform coating and does not require the use of noxious chemicals. Only preliminary testing has been completed in the hotter sections.

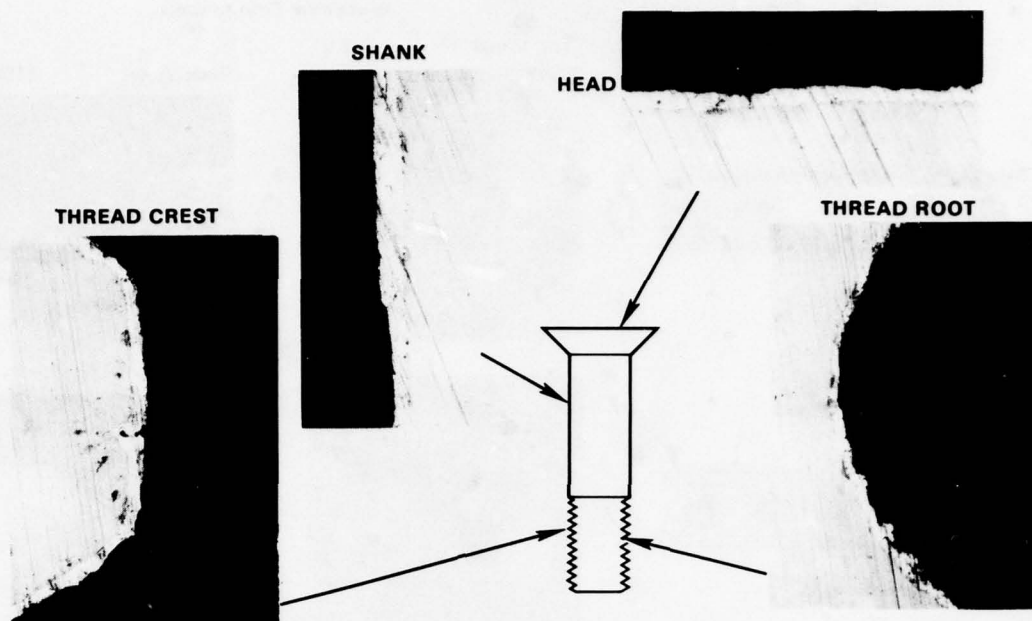


FIGURE 4
IVD ALUMINUM THICKNESS DISTRIBUTION ON A FASTENER

TABLE 2
FASTENER QUALIFICATION TESTS

Mechanical	Installation
Tensile Strength	Torque Tension
Double Shear	Locking Torque
Tension Fatigue	Reuseability
Stress Durability	Interference Fit
Stress Rupture	

Another potential application exists for IVD aluminum on titanium components in gas turbine engines. Tests have shown that the IVD coating significantly improved the resistance of Ti-8-1-1 alloy to ignition (Reference 7).

Test specimens after laser impingement are shown in Figure 5.

PRODUCTION STATUS

The first production size coater was sponsored by the Naval Air System Command and delivered to the Naval Air Rework Facility at North Island, San Diego, in April 1974. During this contract period, a number of our aircraft parts, both steel and aluminum components, were plated and evaluated. Coating uniformity, adhesion and corrosion performance were all very satisfactory. This unit is 4 feet in diameter and 8 feet long and is shown in Figure 6.

At about this same time a new approach was conceived for coating small parts on a more economical basis. The technique is similar to barrel electroplating in that parts are placed in rotating barrels over the aluminum evaporation source. Following conceptual verification in the laboratory, a 4 foot diameter by 6 foot long system was designed and fabricated. The unit has been used to demonstrate the process and as a test bed for design development. The system has evolved from one to two barrels per unit, doubling the output. Production capacity was increased further by placing vacuum locks on the feed and discharge ends of the system (Figure 7). This allows fasteners to be loaded and unloaded without breaking the vacuum and reduces the total coating cycle by about 50 percent. A similar unit installed this year at a fastener manufacturer, The Voi-Shan Corporation, is also shown in Figure 6.

Early in 1976 a large detail parts coater 7 feet in diameter and 12 feet long was installed in our manufacturing facility. (Figure 6) Approval had been obtained from the Air Force to use ion vapor deposited aluminum coatings on the F-15 Eagle. Fatigue improvement and economics were the motivating reasons. Sulfuric acid anodize coatings were replaced on fatigue critical aluminum wing skins. This resulted in a fatigue improvement without a design configuration change. It also eliminated a shot peening operation, resulting in a cost savings. In addition, IVD coated low alloy steel was used to replace higher cost stainless steel components.

IVD aluminum is presently being used on the F-4 Aircraft and is required for use on the Harrier and the F-18 Hornet. It will be the primary corrosion protective plating on the F-18. On this aircraft it will be utilized on all fatigue critical aluminum structure, all high strength steel structure and on titanium and low alloy steel fasteners.

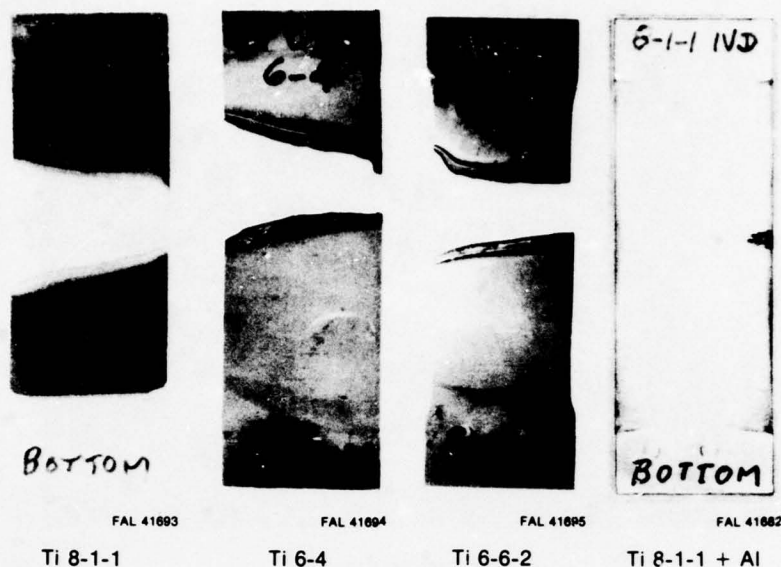


FIGURE 5
APPEARANCE OF TEST SPECIMENS AFTER LASER IMPINGEMENT
 240°C (400°), 0.62 MPa (90 psia), 122 m/Sec (400 Ft/Sec) Airstream

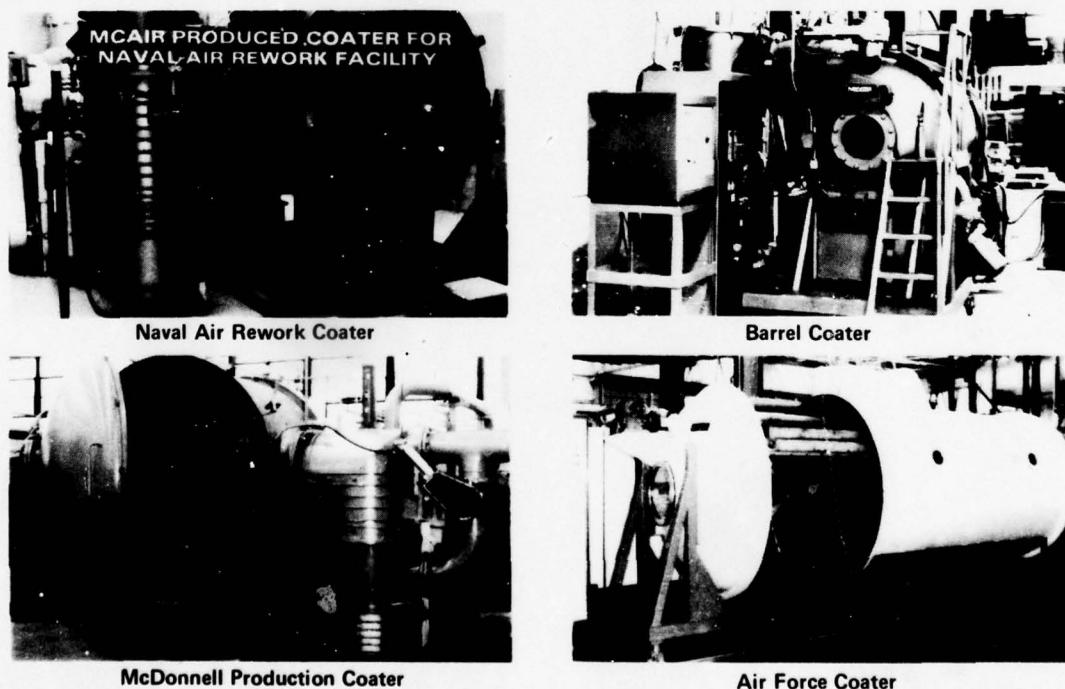
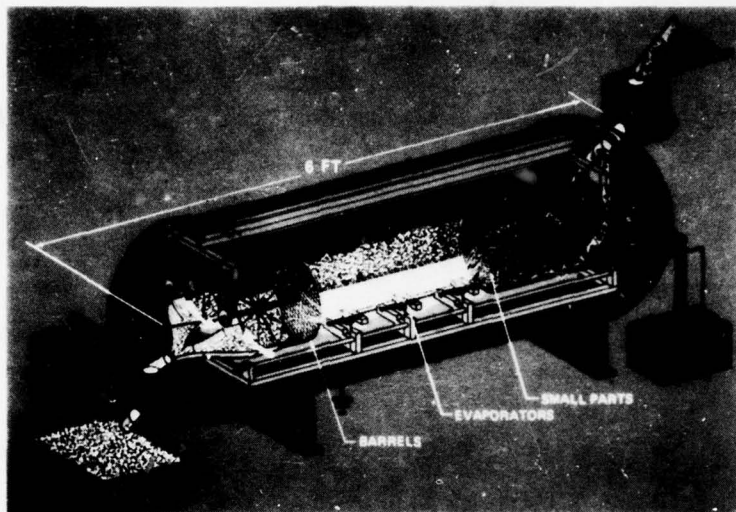


FIGURE 6
PRODUCTION COATERS

GP77-0982-15

A unit has also been fabricated under contract with the Air Force Materials Laboratory, Manufacturing Technology Division. This unit was used to develop optimum parameters and fixturing for coating both aircraft and engine parts. It will be utilized mainly as a replacement for vacuum deposited cadmium on high strength steel parts. This unit is 6 feet in diameter and 10 feet long (Figure 6) and was delivered to Hill Air Force Base in March 1978.

Photographs of a few of the aircraft and engine parts that have been coated at McDonnell are shown in Figure 8. There is also a lot of interest in aluminum coatings outside the aircraft industry. A few examples include computer discs, consumer hardware, automotive parts, space systems, electrical components, appliances, etc. Examples of sample parts coated for evaluation are shown in Figure 9.



GP77-0982-16

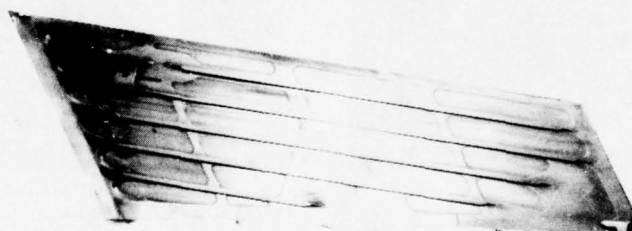
FIGURE 7
SCHEMATIC OF BARREL COATER



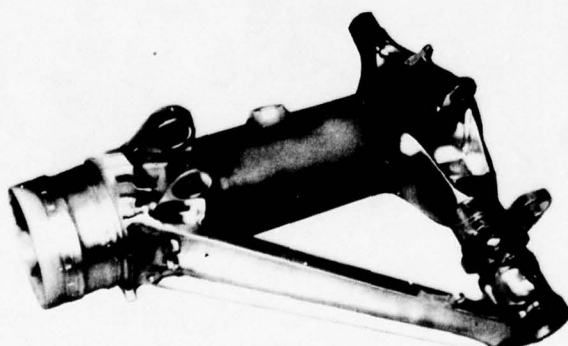
Engine Mount



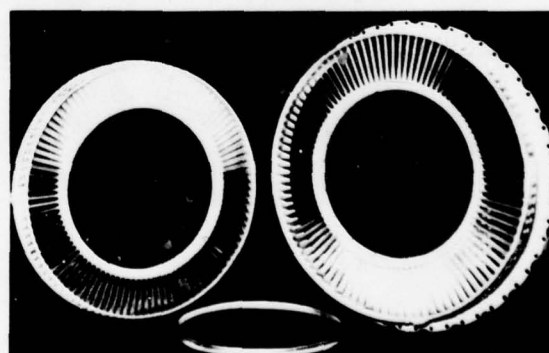
Bellcrank



Wing Skin



Landing Gear



Stator Vane Assemblies

GP77-0982-17

FIGURE 8
IVD ALUMINUM COATED AIRCRAFT AND ENGINE PARTS

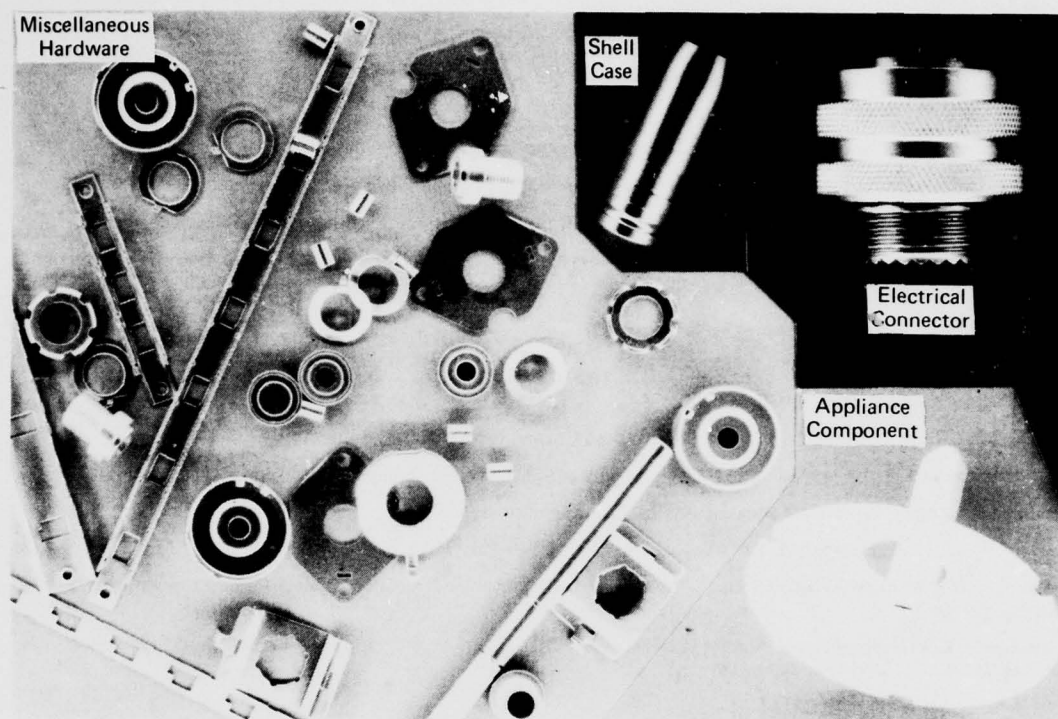


FIGURE 9
MISCELLANEOUS PARTS IVD COATED

CONCLUSIONS

Equipment has been developed and is commercially available for ion vapor deposition of aluminum. The coating, after undergoing extensive laboratory and in-service testing on aircraft, has been verified as an environmentally clean, high performance corrosion protection finish. Specific advantages include:

- (a) It outperforms cadmium and other coatings in actual service tests.
- (b) It has a useful temperature to 925°F (496°C).
- (c) It can protect steels of all strength levels because there is no hydrogen embrittlement.
- (d) It does not cause solid metal embrittlement of titanium.
- (e) It can be used in contact with fuel.
- (f) It provides galvanic protection to aluminum alloys and does not cause fatigue reduction.
- (g) It can be applied thinner than alclad on aluminum alloys resulting in weight savings and is not limited to rolled forms.
- (h) Neither the process nor the coating involve toxic materials, therefore, there is no clean-up or ecology problems.

With these advantages, ion vapor deposited aluminum provides an effective means for meeting many of today's challenges in the fight against corrosion.

REFERENCES

1. F.H. Meyer, Jr. and E. Jankowsky, "Corrosion Performance of New Fastener Coatings on Operational Military Aircraft", International Corrosion Forum, NACE, March 1973.
2. Military Specification, MIL-C-5541, "Chemical Conversion Coating for Aluminum Alloys".
3. Military Specification, MIL-C-83488 (USAF), 23 September 1976, "Coating, Aluminum, Ion Vapor Deposited".
4. Federal Specification, QQ-P-416, "Cadmium Plating (Electrodeposited)".
5. McDonnell Aircraft Company M&PD R&D Report No. 118, 16 February 1975.
6. R. Fishter, Pratt & Whitney Aircraft Group, "IVD Aluminum Coatings for Protection of Steel Turbine Components," 1978, Report No. FR 9865.
7. V.G. Anderson, B.A. Manty, Pratt & Whitney Aircraft Group, "Titanium Alloy Ignition and Combustion", 1978, Report No. NADC-76083-30.

AN EVALUATION OF COATINGS FOR STEEL AND TITANIUM ALLOY FASTENERS FOR AIRCRAFT APPLICATIONS

by

V C R McLoughlin

Materials Department
Royal Aircraft Establishment
Farnborough, Hants
England

SUMMARY

To evaluate their use as alternatives to cadmium on bolts the properties of various coatings are examined. Judged by marine atmosphere exposure the corrosion resistance of the coated bolts varies from excellent (cadmium and zinc plate) to negligible; their galvanic compatibility with aluminium alloy shows similar variations. The results of laboratory tests to evaluate these corrosion characteristics conflict with the marine atmosphere tests. The measurement of the currents generated and weight losses which occur in galvanic cells between the bolts and aluminium alloy electrodes is shown to be a useful and very rapid screening test for galvanic compatibility. The uniformity of the coatings is established metallographically and various properties of the coatings examined include fluid resistance, paint adhesion properties, electrical conductivity and resistance to thermal shock. The effect of the coatings on the fatigue properties and torque-tension characteristics of the bolts are also assessed.

1 INTRODUCTION

Cadmium plated steel and titanium alloy bolts have been used in aircraft structures for many years. The plating cathodically protects the steel bolts and prevents galvanic corrosion at contacts with aluminium alloys. Zinc is the more widely used sacrificial coating for steel but cadmium has been preferred in aircraft structures for various reasons. Thus, cadmium is more galvanically compatible with aluminium alloys, cadmium plated bolts exhibit lower frictional properties and they are far less prone to seizure due to the wedging action of corrosion products. However, cadmium suffers two major draw-backs: it is toxic, the body accumulating the metal from very low dose rates¹; and cadmium can embrittle high strength steels² and titanium alloys³. Several alternatives to cadmium have been championed in the past few years and at RAE a representative selection (see Table 1) is being examined, using 100° countersunk, parallel shank, 6.35 mm diameter bolts produced to aircraft standards. The factors considered are summarized in Table 2.

2 CORROSION TESTS

The corrosion properties of the coated bolts are of prime importance, and much of the present evaluation is concerned with the corrosion resistance of the coatings and their galvanic compatibility with aluminium alloys. As in other corrosion testing and evaluation programmes at RAE both laboratory and natural environment tests are being used. The advantage of laboratory tests is that the conditions used can be reproduced precisely and the tests usually accelerate the corrosion processes being considered; but their relevance must be established by parallel natural environmental tests. For aircraft structures it is generally accepted that the most corrosive atmospheric environment is the marine one, and such an environment is employed in the current evaluation.

TABLE 1 BOLT COATINGS EXAMINED

ON STEEL BOLTS	ON TITANIUM ALLOY BOLTS
Cadmium electroplate	Cadmium electroplate
Zinc electroplate	Zinc electroplate
Aluminium coated	Aluminium coated
Coating A	Coating A
Coating B	Coating B
Coating F	Coating D
	Coating E
	Anodized + resin bonded MoS ₂

(Coatings A, B, D, E and F are all non-metallic matrices containing aluminium particles and are referred to as "composite coatings".)

TABLE 2 ASPECTS CONSIDERED IN THE ASSESSMENT OF BOLT COATINGS

A Corrosion Resistance

Protection of steel bolts, assessed by:

- i exposure to neutral salt fog for 6 weeks, and
 - ii exposure to a marine atmosphere for 12 months
- (Bolts assessed as received and after simulated use.)

Compatibility with aluminium alloy (7075-T6 type) based on:

- i galvanic current measurements,
- ii exposure of bolted assemblies to laboratory tests, and
- iii exposure of bolted assemblies to a marine atmosphere.

B Properties of the Coatings

Thickness and uniformity
Resistance to aircraft fluids
Electrical conductivity
Resistance to thermal shock
Paint adhesion properties

C Effects of Coatings on Bolts

Fatigue properties of coated bolts
Torque-tension relationships of coated bolts

2.1 The Corrosion Resistance of Coated Steel Bolts

The corrosion resistance of the 100° countersunk head bolts is assessed in both a continuous neutral salt fog⁴ and in a marine atmosphere using the Central Dockyard Laboratory Exposure Trials Station at Eastney, on the English south coast. The bolts are supported in Perspex blocks machined with countersunk holes (see Fig 1), the holes being up to 100 µm greater in diameter than the bolt shanks to allow access for moisture and salt solution. Most of the threaded area of the bolts protrudes through the block holes. Tests are done on bolts both as received and after 16 nut runs to simulate the damage caused by normal use.

The results, judged by surface appearance and the time to rusting of the steel bolts, are summarized in Table 3. The marine atmosphere tests indicate that zinc and cadmium plate are equally protective, that coating F and aluminium coated bolts are partially successful in preventing rusting, and that coatings A and B perform very poorly. The salt fog tests suggest that aluminium coated bolts are far more corrosion resistant than zinc plated bolts, at least in the as-received condition, but otherwise the results closely parallel those of marine exposure. Of particular interest is the effect of simulated use on aluminium coated bolts: corrosion resistance is very much worse in both the marine and laboratory tests. After the tests on coating A had been concluded it was found (see 3.1) that the coating was discontinuous. A second batch of bolts was obtained and their corrosion resistance in neutral salt fog is as good as that of cadmium, but results so far from marine tests indicate that, while they are better than the initial batch, the protection afforded to steel is still inferior to that of zinc, cadmium and aluminium, and only as good as that of coating F.

TABLE 3. RESULTS OF CORROSION TESTS ON STEEL BOLTS

Bolt coating	Exposure to a marine atmosphere		Exposure to continuous neutral salt fog (5% NaCl)	
	Time to first rust	Condition after 52 weeks exposure	Time to first rust	Condition after 6 weeks exposure
Bare steel	2 weeks (first inspection)	Totally rusted	3 days (first inspection)	Totally rusted. Wedged into holes.
Cadmium plated	-	No rust. Some pitting of cadmium on the head area only.	-	No rust. Slight pitting of the cadmium.
Zinc plated	-	No rust. Surface dull with some white corrosion product.	8 days	Most of head area rusted. Thick white corrosion product elsewhere.
Aluminium coated	9 weeks	Head rusted in centre. Some spots of rust on threaded area.	-	No rust. Some corrosion at edges of head area, otherwise as new.
i as received				
ii after 16 nut runs	4 weeks	All of head and threaded areas completely rusted.	3 days (first inspection)	Edge of heads rusted. Threaded areas completely rusted.
Coating A	2 weeks (first inspection)	Except for one or two areas on the shank, completely rusted.	5 days	Completely rusted. Wedged into holes.
i initial batch				
ii second batch	(In alloy blocks)	(In alloy blocks) Rust stains on head. Exposed threaded area completely rusted.	-	No rust. Covered in white corrosion product.
Coating B	2 weeks (first inspection)	Except for about 25% of shank area, completely rusted.	21 days	Except for parts of shank area, completely rusted.
Coating F	39 weeks	Rust stains on head and threaded areas.	21 days	One or two spots of rust on head and threaded areas.

2.2 Galvanic Compatibility of Coated Bolts with Aluminium Alloy

2.2.1 Galvanic Current Measurements

A galvanic current is generated when dissimilar metals immersed in an electrolyte are electrically connected. To assess the compatibility of the various bolts with aluminium alloy a plastic rig is used which holds a bolt and a 7075-T6 aluminium alloy electrode a fixed distance (about 40 mm) apart while they are immersed in acidified (pH 3) 5% NaCl solution. Electrical connections are made through the rig from both the bolt and alloy electrode to a zero resistance ammeter. The current generated is continuously recorded for at least 48h and the weight changes of both bolt and alloy electrode (after chemical cleaning) are then determined.

The results of the galvanic current measurements indicate that the metallic coatings cathodically protect the aluminium alloy for most of the exposure period (see Fig 2 and 3). The initial periods when the alloy is the cell anode, and cadmium or aluminium coated bolts form the cathode, is probably related to the chromate passivation treatment normally applied to those coatings: when unchromated aluminium coated bolts are used this initial period is not observed (see Fig 3). With some of the zinc plated bolts the coating is completely consumed in less than 48 hours causing a dramatic change in polarity of the galvanic cell, and the bolt becomes a far more efficient cathode than a bare steel or titanium alloy bolt. A similar change of polarity occurs with cadmium plated bolts but after several days; with aluminium coated bolts no change of polarity occurs in 14 days. All but one of the composite coatings are slightly cathodic to the aluminium alloy suggesting that the coatings act as barrier films with high electrical resistivity. The exception is coating A which on steel is a more efficient cathode than is bare steel and on titanium alloy gives rather erratic results. The behaviour is probably due to some extent to the discontinuous nature of the coating; it is possible that the uncoated steel areas are cathodically protected by the aluminium alloy, and that the adjacent coating in some way acts as a cathode depolarizer. The second batch of bolts with coating A show no change in behaviour in the galvanic current measurements in the case of titanium alloy bolts, but behave quite differently on steel (see Fig 2); the latter result suggests that the discontinuous nature of the coating on the initial batch of bolts prejudiced the coating's performance. The resin-bonded MoS_2 coating on anodized titanium alloy bolts acts as an electrical insulator, slightly reducing the magnitude of the galvanic current compared with uncoated bolts (see Fig 3).

TABLE 4 WEIGHT LOSSES OF BOLTS AND ALUMINIUM ALLOY ELECTRODES USED FOR GALVANIC CURRENT MEASUREMENTS

Coating	Bolt material	Weight loss in mg/day (average values)		
		Bolt	Alloy coupled to bolt	Alloy coupled less (a) wt loss of alloy alone
None	Steel	0	7.7	+3.6
	Titanium	0	6.7	+2.6
Cadmium	Steel	17.3	1.3	-2.8
	Titanium	25.3	1.7	-2.4
Zinc	Steel	29.6	7.8 (0.1) ^(b)	+3.7 (-4.0) ^(b)
	Titanium	30.7	10.9 (0.5)	+6.8 (-3.9)
Aluminium	Steel	3.6	3.1	-1.0
	Titanium	3.3	1.7	-2.3
Coating A (initial batch)	Steel	1.6	9.9	+5.5
	Titanium	1.5	4.6	+0.5
Coating A (second batch)	Steel	2.4	0.8	-3.3
	Titanium	2.4	0.7	-3.4
Coating B	Steel	0	4.8	+0.7
	Titanium	0	2.7	-1.4
Coating D	Titanium	1.0	6.2	+2.1
Coating E	Titanium	0.4	1.0	-3.1
Coating F	Steel	0.5	0.8	-3.3
Resin bonded MoS_2	Anodized titanium	0.3	7.8	+3.3

a. Aluminium alloy electrodes exposed to 5% NaCl solution at pH 3 suffered weight losses of 4.1 mg/day on average. A positive value in this column indicates a greater rate of weight loss, a negative value represents a reduced rate.

b. In galvanic cells between zinc plated bolts and alloy electrodes when sudden reversals of polarity occurred the larger weight losses were suffered by the alloy. Values in parentheses correspond to cases where this polarity reversal did not occur.

The weight losses of bolts and aluminium alloy electrodes used in the galvanic cells (see Table 4) are broadly in line with the galvanic currents generated: when the bolt forms the cell anode and cathodically protects the alloy a relatively large weight loss is suffered by the bolt while the alloy loses less weight than it does when immersed alone in the electrolyte; when the bolt forms the cathode it is protected while the alloy loses more weight than it does alone. It is interesting to compare the average rates of weight loss of the sacrificial metal coatings with the theoretical weight losses calculated from the galvanic currents observed. The actual weight losses are about 3.5 mg/day for aluminium, about 21 mg/day for cadmium and about 30 mg/day for zinc. The corresponding calculated values are about 0.7 mg/day for aluminium and about 6 mg/day for both cadmium and zinc, suggesting that all three coatings are corroding more rapidly because of corrosion processes concerned with the protection of the bolt itself than with cathodic protection of the alloy electrode. There are anomalies in the weight losses of alloy electrodes connected to bolts with coatings B, D, E and F; even though all cause similar galvanic current flows with the alloy electrode apparently forming the anode, alloy electrodes connected to some bolts with coatings B, E and F enjoy a degree of cathodic protection, while the expected result is obtained with coating D and steel bolts with coating B. This is being investigated further.

These galvanic current and weight loss experiments serve to illustrate an inherent danger in relying solely on sacrificial metal coatings on steel and titanium bolts. If a galvanic cell is set up between the alloy of an aircraft structure and a bolt coating it is possible that the eventual consumption of the coating will leave a very efficient cathode, and further galvanic corrosion will lead to very rapid attack of the alloy. This could occur at any time in the life of an aircraft so that an apparently sound bolt/alloy interface could rapidly deteriorate between routine inspections.

2.2.2 Corrosion Tests on Bolted Assemblies

Corrosion tests are performed on assemblies of the various coated bolts fastened into anodized aluminium alloy (7075-T6 type) blocks, using holes up to 100 μ m larger in diameter than the bolts (see Fig 5). To avoid any other galvanic couple anodized 7075-T73 alloy nuts are used to tension the bolts. Four conditions of assembly are used: assembled wet with a chromated, non-setting jointing compound and painted overall with a chromated epoxy polyamide paint primer to simulate normal aircraft practice; assembled wet but unpainted; assembled dry and painted; assembled dry and unpainted. Two test environments are used: exposure for up to 104 weeks to a marine atmosphere, and exposure to the dry salt humidity test⁵. The latter test procedure has been used previously to simulate tropical marine conditions, and involves exposing the assemblies, bolt head upwards, covered with sea salt, to a cycle of 6h at up to 95% relative humidity followed by 6h when the relative humidity is reduced to 20%, all at 35°C. In this way the assemblies are alternately covered by a saturated sea salt solution and by dry sea salt.

None of the painted blocks show significant corrosion in any of the tests, only the isolated case of blistering occurring under the paint film at the bolt/alloy interface. The amount of corrosion of the unpainted assemblies is surprisingly slight and is mainly limited to corrosion of the bolt head and the surface of the alloy blocks; very little corrosion is found in the countersinks of the alloy blocks. The results are summarized in Tables 5 and 6. There are major differences between the results of the laboratory and the marine exposure tests on unpainted assemblies, probably because of the unusual electrochemical conditions existing in the saturated sea salt solutions which leads to most of the bolt heads being covered by a white deposit, consisting mainly of aluminium salts, in the laboratory tests. These deposits prevent rusting of several of the steel bolts which suffered severe rusting in the marine atmosphere tests. The pattern of corrosion of the aluminium alloy blocks is also quite different in the two test media.

TABLE 5 RESULTS OF CORROSION TESTS ON STEEL BOLTS ASSEMBLED IN ANODIZED ALUMINIUM ALLOY BLOCKS

Bolt coating	Exposure to a marine atmosphere for 78 weeks			Exposure to the dry salt humidity test for 40 weeks		
	Bolt head condition	Corrosion of alloy surface around bolt head	Intergranular corrosion inside countersink	Bolt head condition	Corrosion of alloy surface around bolt head	Intergranular corrosion inside countersink
Bare steel	Completely rusted.	5	5	No rust, white deposit.	5 (4)	5
Cadmium	No rust, dull.	2	0	No rust, white deposit.	4	3
Zinc	No rust, dull.	1	0	No rust, thin white deposit.	1	0
Aluminium	Rusted in centre.	2	1	Completely rusted.	2	3 (0)
Coating A (initial batch)	Completely rusted.	3	5	No rust, white deposit.	5 (4)	5 (4)
Coating A (second batch)	Rust stained (52 weeks).	1	-	-	-	-
Coating B	Completely rusted.	5	3	Rust stains, white deposit.	4	3
Coating F	Rust stained (52 weeks).	1	-	As new (20 weeks).	1	-

Corrosion ratings given for dry assembled bolts (wet assembled in parentheses when different) according to the scale:

0 - None 2 - Slight 4 - Moderate to extensive
1 - Very slight 3 - Moderate 5 - Extensive

TABLE 6 RESULTS OF CORROSION TESTS ON TITANIUM BOLTS ASSEMBLED IN ANODIZED ALUMINIUM ALLOY BLOCKS

Bolt coating	Exposure to a marine atmosphere for 78 weeks			Exposure to the dry salt humidity test for 40 weeks		
	Bolt head condition	Corrosion of alloy surface around bolt head	Intergranular corrosion inside countersink	Bolt head condition	Corrosion of alloy surface around bolt head	Intergranular corrosion inside countersink
Bare titanium	As new.	2	2.5 (0)	White deposit.	5	5
Cadmium	Dull.	1	0	Thick white deposit.	4	4
Zinc	Dull.	1	0	White deposit.	2	0
Aluminium	Dull.	1	0	White deposit and some loss of coating.	2.5	2 (0)
Coating A (initial batch)	Dull.	2	5 (3)	Thin white deposit.	5 (3)	5 (1)
Coating A (second batch)	As new (52 weeks).	1	-	-	-	-
Coating B	Some coating lost.	2	3 (2)	Some white deposit, coating blistered.	2.5	2
Coating D	As new.	2	0 (2)	Slight loss of coating in head recess.	2.5	2
Coating E	Some coating lost (52 weeks).	1	-	Dull (20 weeks).	1	-
Resin bonded MoS_2	As new.	2	1	Thick white deposit.	5 (4)	4

See footnotes to Table 5.

The indications after 78 weeks exposure to a marine atmosphere are quite clear. On steel, cadmium and zinc both perform very well, suffering little or no corrosion; aluminium coated bolts rust on the heads but protect the alloy blocks almost as effectively as cadmium; coatings A and B perform almost as badly as bare steel. With titanium alloy bolts the corrosion problem is far less than with steel: uncoated titanium bolts cause only light corrosion of the blocks and that in the countersink is completely suppressed by wet assembly. The metallic coatings overall performed better than the composite coatings on titanium, although this distinction was not apparent after 52 weeks exposure. These marine atmosphere test results are broadly in agreement with the galvanic cell measurements with respect to the protection afforded by the coatings to aluminium alloy: cadmium, zinc and aluminium coatings perform well; coatings A and B on steel perform poorly; steel is more problematic than titanium.

The results of the laboratory tests on the bolted assemblies are disappointing. It had been hoped that they would have paralleled the results obtained by marine exposure, which would have allowed the laboratory test to be used with confidence in assessing the merits of any other bolt coatings. However, it may be valid to use galvanic current measurements, together with weight loss determinations, as a very rapid method of assessing the suitability of other coatings, not only for operations in contact with 7075-T6 type alloys but also with the more cathodic aluminium-copper alloys.

3 PROPERTIES OF THE COATINGS

3.1 Coating Thickness and Uniformity

To examine the bolt coatings three bolts of each type are sectioned and the coating thickness is determined from photomicrographs. The average thickness is determined on the head, shank, thread crest and root; the results are summarized in Table 7. Most specifications for bolts of 6.35 mm diameter require bolt coatings for corrosion prevention purposes to be between 5 and 13 μm thick, although it can be beneficial for the coating on the heads to be thicker. Most of the coatings are fairly uniform and between 7 and 14 μm thick, exceptions being:

- i coating A which on the initial batch of bolts is discontinuous and varies in thickness with a maximum of 27 μm in the thread roots, and on the second batch of bolts is mainly continuous but varies between 15.5 μm and 30 μm thick;
- ii coating D which varies in average thickness at different points between 8 μm (bolt shank) and 77 μm (thread roots);
- iii coating F which is uniform but on the head the thickness (average 17.5 μm) is twice that on other parts;
- iv zinc plated titanium bolts which have thinner coatings on the shank (5.5 μm) and thread root (8.5 μm) than on the thread crest (11.5 μm) and head (15 μm);
- v aluminium on steel which is markedly thicker (15.5 to 20 μm) than the other metal coatings.

TABLE 7 THICKNESS AND UNIFORMITY OF BOLT COATINGS

Coating	Bolt material	Coating uniformity	Average thickness of coating in μm			
			Head	Shank	Thread root	Thread crest
Cadmium	Steel Titanium	uniform uniform	13	13	11.5	14
			12	13	13	14
Zinc	Steel Titanium	uniform uniform	14	14	15.5	13
			15.5	5.5	8.5	11.5
Aluminium	Steel Titanium	variable uniform	20	18.5	15.5	18.5
			13.5	10	10	10
Coating A (initial batch)	Steel Titanium	variable and discontinuous discontinuous	16 0-17	0-18.5 0-17	10.5 27	0-15.5 15.5
Coating A (second batch)	Steel Titanium	variable partly discontinuous	18.5 30.5	15.5 0-23	26.5 17.5	23.5 20
Coating B	Steel Titanium	uniform uniform	14	14	14	14
			10	10	11.5	8.5
Coating D	Titanium	variable	8.5	8	77	11.5
Coating E	Titanium	uniform	10	7	7	7
Coating F	Steel	uniform	17.5	8.5	7	8.5
Resin bonded MoS_2	Anodized titanium	uniform	7	7	7	7

3.2 Resistance to Aircraft Fluids

To assess their resistance to phosphate-based hydraulic fluids and to aviation kerosine, the bolts are immersed in the fluids for 35 weeks before being exposed to neutral salt fog for 6 weeks. To date no differences have been detected in the corrosion resistance of coatings due to exposure to either aircraft fluid, nor have there been any changes in the infrared spectra of the fluids following these exposures.

3.3 Electrical Conductivity

TABLE 8 ELECTRICAL RESISTANCE MEASURED BETWEEN CENTRE COUNTERSINK AND OUTER BOLTS IN ALUMINIUM ALLOY BLOCKS

Coating	Bolt material	Electrical resistance, $\text{m}\Omega$	
		Wet assembled bolts	Dry assembled bolts
None	Steel Titanium	3	8
		10	21
Cadmium	Steel Titanium	13	21
		8	34
Zinc	Steel Titanium	3	18
		3	25
Aluminium	Steel Titanium	8	10
		10	41
Coating A	Steel Titanium	2	25
		21	37
Coating B	Steel Titanium	47	381
		8250	15700
Coating D	Titanium	> 40000	20400
Coating E	Titanium	300	3000
Coating F	Steel	> 60000	> 100000
Resin bonded MoS_2	Anodized titanium	1200	4650

To obtain some measure of the electrical conductivity of the coated bolts when they are incorporated in an aircraft structure, measurements are made when the bolts are fastened into the aluminium alloy blocks for the corrosion tests (see Fig 4). The two outer bolts are installed and the electrical resistance is measured between the centre countersink and the two outer bolts. The coating of the outer bolts is penetrated by a hard probe during the measurements. The mean values obtained from six measurements for each bolt type are given in Table 8, for both wet and dry assembled bolts. With the metallic coatings and with coating A the electrical resistances recorded are similar to those for bare steel and titanium alloy bolts; with coatings B, D, E and resin bonded MoS₂ on anodized titanium, and coating F on steel much higher electrical resistances are obtained; coating B on steel gives intermediate values. Therefore, if electrical continuity through fasteners is a design requirement it appears that most of the composite coatings could cause difficulties. Also, it is interesting that, in general, lower resistance measurements are obtained with wet assembled bolts.

3.4 Resistance to Thermal Shock

The ability of the coatings to withstand severe thermal shock (probably in excess of conditions met even in supersonic aircraft), and to provide corrosion protection in high humidity conditions coupled with such thermal shock, are both assessed by subjecting the bolted assemblies used for corrosion tests to the following cycle:

- i immerse in distilled water at 20°C for 16h;
- ii place, bolt head down, onto a metal block of large thermal mass in a refrigerator at -20°C, for 2h;
- iii transfer rapidly to an oven at 130°C and place, bolt head down, onto a metal block of large thermal mass, for 4h;
- iv transfer rapidly to the refrigerator at -20°C, as in (ii), for 2h.

At the completion of the cycle the blocks are immersed in fresh distilled water again. At week-ends the blocks are left in distilled water. The test is completed after 28 cycles.

At the end of the test period two bolts are extracted and the coating examined for any breaks or losses. The head of the third bolt is cross-hatched at 2 mm intervals⁶ and the coating tested for any deterioration in adhesion by attaching and rapidly detaching a piece of self-adhesive cellulose acetate tape⁷ over the cross-hatched area. Only in the case of the resin-bonded MoS₂ coating was there detectable loss of coating. In all cases the countersink holes were free from corrosion.

3.5 Paint Adhesion Properties

Paint adhesion tests are applied to the heads of fasteners, installed in aluminium alloy blocks and then over-painted with a chromated epoxy polyamide primer paint after the blocks have been exposed to the dry salt humidity test described in 2.2.2 for 78 weeks. The cross-hatch test is again used⁶ followed by the application of cellulose acetate tape⁷, as described in 3.4. Only in the case of bare steel bolts is there any loss of paint from the bolt head. This suggests that all of the coatings should show very adequate paint adhesion properties in service, even after exposure to a corrosive environment.

4 EFFECTS OF THE COATINGS ON BOLT PERFORMANCE

4.1 Fatigue Properties of the Coated Bolts

The minimum requirements for aerospace standard titanium alloy bolts are laid down in BS A101⁸, and all of the bolts being evaluated in the present programme meet these requirements with regard to fatigue properties. There are no British Standard requirements for steel bolts, but the BS A101 test requirements are also met by all of the steel bolts. Table 9 summarizes the results of tension-tension fatigue tests applied at the stress level required by BS A101 (5.43 ± 3.25 kN for 6.35 mm dia bolts), and at two higher stress levels. Comparing the fatigue endurance of the bolts with uncoated steel and titanium alloy bolts it appears that most of the coatings markedly reduce the fatigue endurance of the bolt materials. The notable exceptions are coatings D and E on titanium alloy which appear to have no detrimental effect, and in some instances the fatigue lives of the coated bolts exceed those of uncoated bolts. However, only the aluminium coated bolts were from the same source as the uncoated bolts (while the bolts with zinc, cadmium and coating B were from another single source) so the results must be tempered to allow for variations in fatigue properties of the different bolts prior to coating. Thus, the apparent slight advantages of aluminium on steel and coating A on titanium may not be too significant in practice; but the results with coatings D and E strongly suggest that these coatings should show real advantages over cadmium plate.

4.2 Torque-tension Relationships of the Bolts

It is important that any replacement coating for cadmium should not cause any marked change in the torque values required to achieve a given bolt tension, and that variations in torque-tension relationships from bolt to bolt should be a minimum. Also it is desirable that the torque-tension relationship does not alter if a bolt is re-used. To obtain the torque and tension values five bolts of each type are used and (except in the case of resin bonded MoS₂ on anodized titanium bolts) self-locking anodized aluminium alloy (7075-T73) nuts lubricated with cetyl alcohol are used to tension the bolts held in a load cell. Aluminium alloy nuts are used because they are required in the corrosion tests (see 2.2.2). The values of torque applied to the nut and tension achieved in the bolt shank are recorded at incremental load values at least until 8.5 kN is achieved, equivalent to 30% of the tensile strength of the bolts. To obtain a measure of their re-usability the bolts are also subjected to 16 nut runs before determining their torque-tension relationships.

TABLE 9 ENDURANCE OF BOLTS IN TENSION-TENSION FATIGUE TESTS
AT VARIOUS STRESS LEVELS

Coating	Bolt material	Log mean fatigue endurance in kilocycles		
		5.43 \pm 3.25 kN	5.97 \pm 3.57 kN	6.51 \pm 3.90 kN
None	Steel	10800	494	309
	Titanium	> 5300	257	121
Cadmium	Steel	57	39	26
	Titanium	40	27	28
Zinc	Steel	43	33	22
	Titanium	35	27	12
Aluminium	Steel	928	156	190
	Titanium	88	109	57
Coating A	Steel	58	35	25
	Titanium	367	144	79
Coating B	Steel	49	35	37
	Titanium	43	28	20
Coating D	Titanium	-	1460	156
Coating E	Titanium	1190	762	211
Coating F	Steel	139	84	56
Resin bonded MoS ₂	Anodized titanium	684	58	50

The results are shown graphically for a representative selection of the bolt coatings on steel (Fig 5), on titanium (Fig 6) and, in the case of resin bonded MoS₂ on anodized titanium, the torque-tension relationship using MoS₂ coated cadmium plated steel nuts up to a load of 17 kN are shown in Fig 7. The results of torque-tension determinations on five bolts after 16 nut runs are given as a single point, the average torque required to achieve a load of 8.5 kN, or, in the case of resin bonded MoS₂ on anodized titanium, a load of 17 kN.

It is apparent that there is considerable variation in the determination on any single type of bolt. For example, in the case of cadmium on steel (Fig 5) the load achieved at any given torque is subject to an error in the region of $\pm 50\%$. On steel bolts aluminium coatings give far less scatter, but on titanium aluminium coatings cause greater scatter than does cadmium plating. The only bolt coating to show a marked change after simulated use is the resin bonded MoS₂ on anodized titanium (Fig 7) with which coating the torque required to achieve a load of 17 kN is doubled after 16 nut runs. This one result may derive in part from the higher loading imparted on the bolt.

If the results obtained are realistic then all of the alternative coatings with the exception of the resin bonded MoS₂ appear to be acceptable with regard to their torque-tension characteristics.

5 CONCLUSIONS

In this assessment of bolt coatings the corrosion resistance and galvanic compatibility with aluminium alloy is probably of prime importance. Results to date suggest that cadmium plating will be difficult to replace. If titanium alloy bolts alone are considered it is possible to conclude that uncoated bolts can be safely used provided wet assembly is used for installation into aluminium alloy. However, provision must be made for the accidental omission of wet assembly materials, and aluminium or zinc coatings would be the most acceptable alternatives to cadmium, closely followed by coatings D and E, provided that electrical continuity through the bolts was not a design requirement. In the case of steel a coating must be used, and the only promising alternatives are zinc or aluminium. Coating A may perform almost as well if a good batch is obtained but the risk of obtaining unsatisfactory bolts must weigh heavily against the coating. Coating F shows promise but requires further evaluation.

The choice between zinc and aluminium involves balancing the excellent protection of steel by zinc and the poor performance of aluminium against the dangers of using zinc in contact with aluminium where the large difference in galvanic potential leads to more rapid corrosion of zinc than of an aluminium coating in the same situation. If it were necessary to choose between the two then aluminium coatings should be used because it is more important in most cases to protect the aluminium alloy in contact with the bolt than it is to prevent the more readily visible rusting of the steel.

Secondary conclusions can be made regarding the types of corrosion tests which should be employed to evaluate the various coated bolts. It would seem to be sensible to accept the validity of the marine atmosphere exposure tests and compare the results with those obtained in the laboratory methods. On this basis the continuous neutral salt fog test should not be relied on by itself and the dry salt humidity

test is quite unsuitable. The measurement of galvanic current and ensuing weight losses is a promising very rapid method of assessment, and it may be worthwhile varying the conditions of the test to cover a wider range of environments.

Setting aside the problems associated with corrosion resistance, the present evaluation suggests that the bolt coatings examined are acceptable with only a few reservations. First, if electrical continuity is to be obtained through the bolts then only the metal coated (or uncoated) bolts, or those with coating A would be acceptable. Secondly, the unevenness of coatings A and D could be a problem in some applications, such as on interference fit bolts. Thirdly, the resin bonded MoS₂ on anodized titanium alloy bolts shows relatively poor paint adhesion, thermal shock resistance, and torque-tension characteristics after simulated use.

REFERENCES

- 1 G Braude, in "Cadmium colloquy", Plating and Metal Finishing, 64, pp8-14 (1977)
- 2 D N Fager and W F Spurr, Solid cadmium embrittlement: steel alloys, Corrosion-NACE, 27, pp72-76 (1971)
- 3 D N Fager and W F Spurr, Solid cadmium embrittlement: titanium alloys, Corrosion-NACE, 26, pp409-419 (1970)
- 4 British Standards Institution, Methods for corrosion testing of metallic coatings. Part I: Neutral salt spray test, BS 5466 (1977)
- 5 R Salmon, Factors influencing the performance of corrosion inhibiting systems, DMat Report No 169 (1971)
- 6 British Standards Institution, British standard methods of test for paints. Part E6, Cross-cut test, BS 3900 (1974)
- 7 British Standards Institution, Performance tests for protective schemes, BS 1391 (Appendix C) (1952)
- 8 British Standards Institution, General requirements for titanium bolts, BS A101 (1969)

ACKNOWLEDGEMENTS

Miss J A Gray performed most of the corrosion assessment work described in this paper, and Mr N J F Gunn determined the torque-tension relationships and performed the tension-tension fatigue measurements.

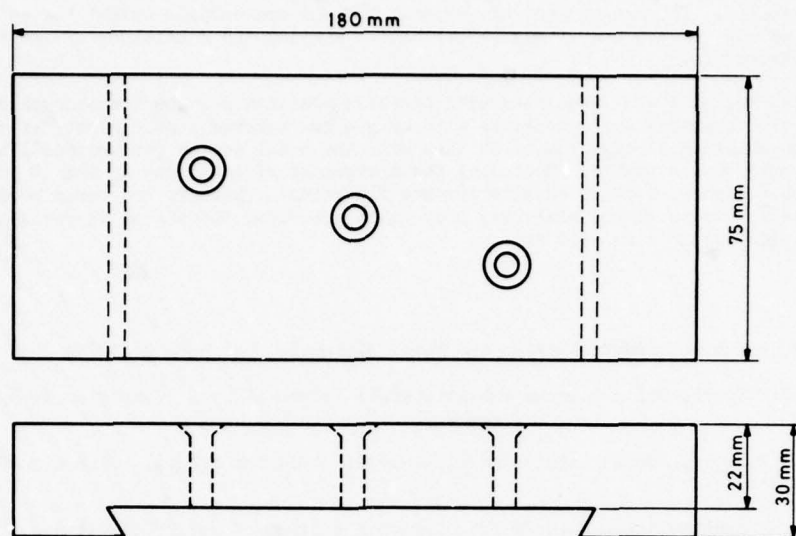


Fig 1 Perspex block for holding bolts in corrosion tests.
Holes up to 100 μ m oversize on bolt shanks

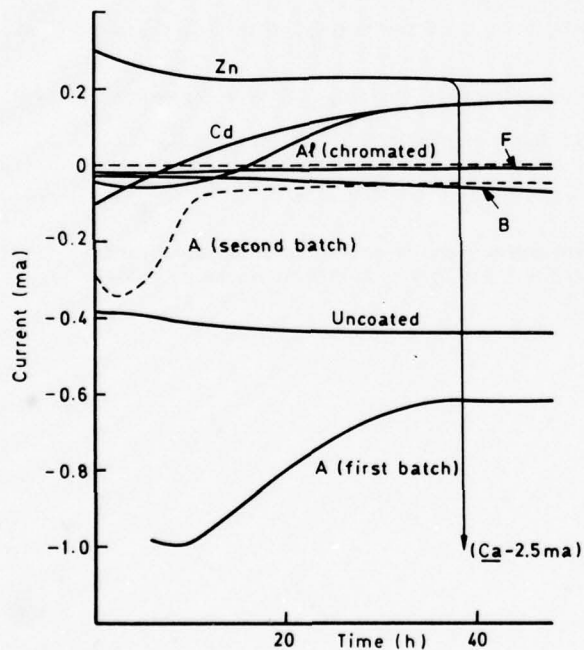


Fig 2 Galvanic current (with respect to aluminium alloy electrode) of steel bolts coupled to 7075-T6 aluminium alloy in 5% NaCl at pH3

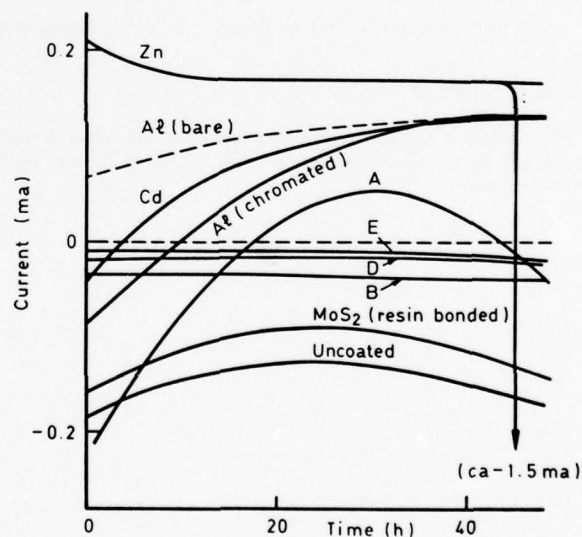


Fig 3 Galvanic current (with respect to aluminium alloy electrode) of titanium alloy bolts coupled to 7075-T6 aluminium alloy in 5% NaCl at pH3

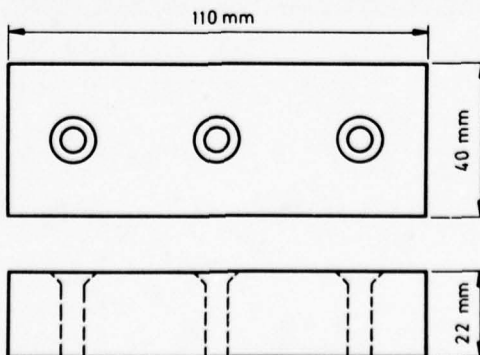


Fig 4 Aluminium alloy blocks for corrosion tests with bolts. Holes up to 100 μ m oversize on bolt shanks

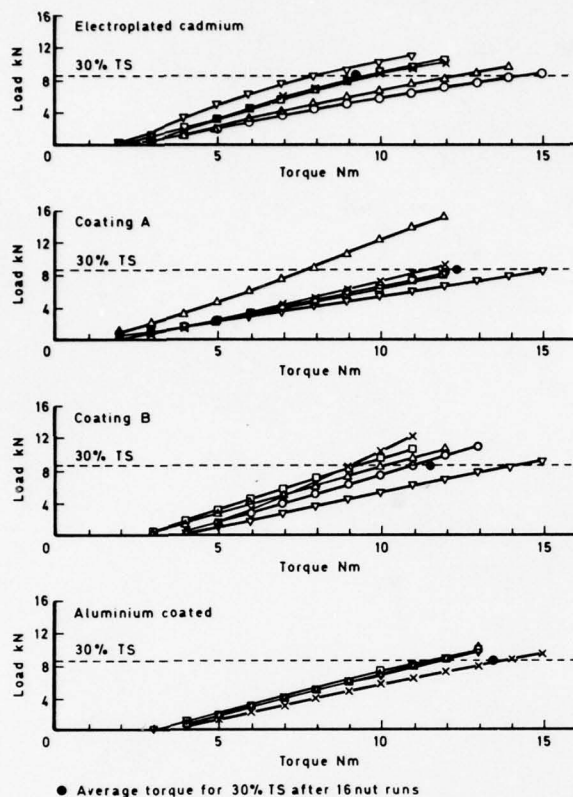


Fig 5 Torque-tension relationships for coated steel bolts, using self-locking anodized aluminium alloy nuts lubricated with cetyl alcohol

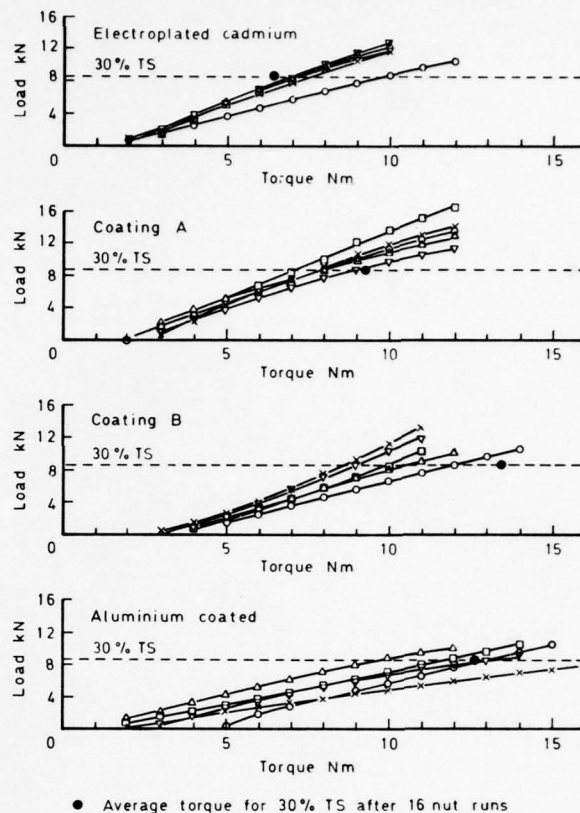


Fig 6 Torque-tension relationships for coated titanium alloy bolts, using self-locking anodized aluminium alloy nuts lubricated with cetyl alcohol

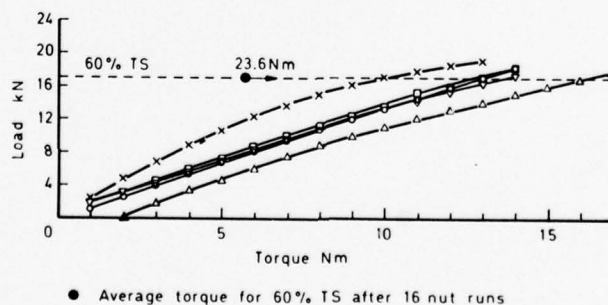


Fig 7 Torque-tension relationships for resin bonded MoS_2 on anodized titanium alloy bolts, using self-locking cadmium plated steel nuts lubricated with MoS_2

PHYSICAL VAPOUR DEPOSITION AND ION BEAM TECHNIQUES FOR SURFACE DURABILITY

J. P. Coad (Materials Development Division) and N. E. W. Hartley (Nuclear Physics Division), A.E.R.E., Harwell, Oxfordshire, OX11 0RA, U.K.

SUMMARY

Two surface treatment processes under development at Harwell are described which make increasing use of the throwing power and versatility of ion beams. At low plasma discharge energies (< 1 keV) ionised atoms cause sputter cleaning of surfaces and enable fully dense and adherent coatings to be built up on complex industrial items. Ion implantation, in which the bombarding atoms are accelerated through typically 30 KV, causes the original surface to become heavily impregnated with ions. The reproducibility and relative ease of scaling up make both processes attractive for large volume automatic surface treatment, although the vacuum requirements for ion implantation are more stringent (10^{-5} mbar). Some examples taken from recent evaluations on components treated for corrosion and wear resistance in the aerospace and other industries are described.

INTRODUCTION

This paper describes two surface treatment processes which significantly increase the range of materials available to the designer. Surface treatment is required whenever the bulk properties of a material are inadequate to cope with the special demands of corrosion, wear, fatigue or oxidation and modern methods of improving surface durability under development within the U.K.A.E.A. include controlled atmosphere oxidation, laser hardening and ion implantation.

A different approach is to coat the surface with another substance so that bulk and surface properties relate to completely different materials. A number of methods of achieving this objective exist, including electro-plating, chemical vapour deposition (CVD), electron beam evaporation and ion plating. One problem with all coating techniques is to achieve sufficient adhesion between the surface film and the substrate material so that the coating remains intact throughout the service life of the component. Nevertheless, coatings have also achieved large increases in resistance to corrosion and wear, and can change the surface nature more completely than modifications to the bulk material. A novel coating technique known as 'sputter ion plating' is described, together with some of its applications to materials technology.

In contrast to conventional deposition methods, ion implantation (the second surface treatment process described in this paper) does not produce a coating in the normal sense of the term because atoms are introduced below the surface of the original material and exert their influence within this matrix. The common features of sputter ion plating and ion implantation treatments for surface durability are that they are versatile vacuum techniques and employ energetic ionised gases. With ion implantation there is no change in the dimensions of the component and no interface is created, which is so often subject to mechanical weakness or interfacial corrosion (a frequent problem with electroplated finishes, for example). Ion implantation is applied to finished components and tools and, because it is a low-temperature process (carried out as a rule below 200°C) there is no risk of distortion. Subsequent treatment or machining is both unnecessary and undesirable.

COATING METHODS

(a) Sputter Ion Plating

Ion plating is a term originally coined by Mattox⁽¹⁾ to describe a method of physical vapour deposition in which the substrate is bombarded with ions during a vacuum coating operation. As conceived by Mattox a vacuum system is employed which contains inert gas, usually argon, at a pressure in the range 10^{-2} to 10^{-1} mbar. Vapour of the material to be deposited is generated from a heated crucible. It diffuses through the inert gas from source to substrate and a useful throwing power is achieved owing to the gas scattering which takes place. The essential feature of ion plating, however, is the application of an appropriate negative voltage between the substrate and another electrode (the anode) within the vacuum system. This causes a glow discharge to take place in which the substrate is the cathode and there is continued bombardment of the substrate by ions of the inert gas. Mattox and many other workers have found that under these conditions of simultaneous bombardment and deposition, particularly well adhered and dense metallic coatings may be formed.

In sputter ion plating (SIP)⁽²⁻⁴⁾ the crucible and its contents are replaced by an electrode fabricated from the source material itself. A negative voltage is applied to it so that a second and more powerful glow discharge is set up with respect to the same anode as before. Under the ion bombardment which occurs the source is sputtered, i.e. eroded by atomic collision processes, and vapour is again formed in atomic and molecular form which ultimately diffuses to the substrate. Unlike the conventional ion plating

process the method is particularly well suited to the deposition of refractory metals, alloys and compounds since the atoms of any of these materials can readily be produced using sputtered ion bombardment.

The source material in the present system is in the form of sputtering cathodes distributed uniformly round the outside of the volume containing the samples to be coated. Consequently excellent throwing power is achieved and components of irregular shape may be uniformly coated with complex alloys and compounds without the need for mechanical manipulation. D.C. sputtering is a low rate coating process (usually up to a few $\mu\text{m/hr}$) but this means that substrate bias power density is also low, e.g. $\sim 0.1 \text{ W/cm}^2$. Dense, pore-free coatings can be put down without overheating the substrates. Although the process is relatively slow it is suited to batch coating of many components at one charge. Owing to the general simplicity of the equipment long coating exposures may be carried out unattended with a minimum of control devices.

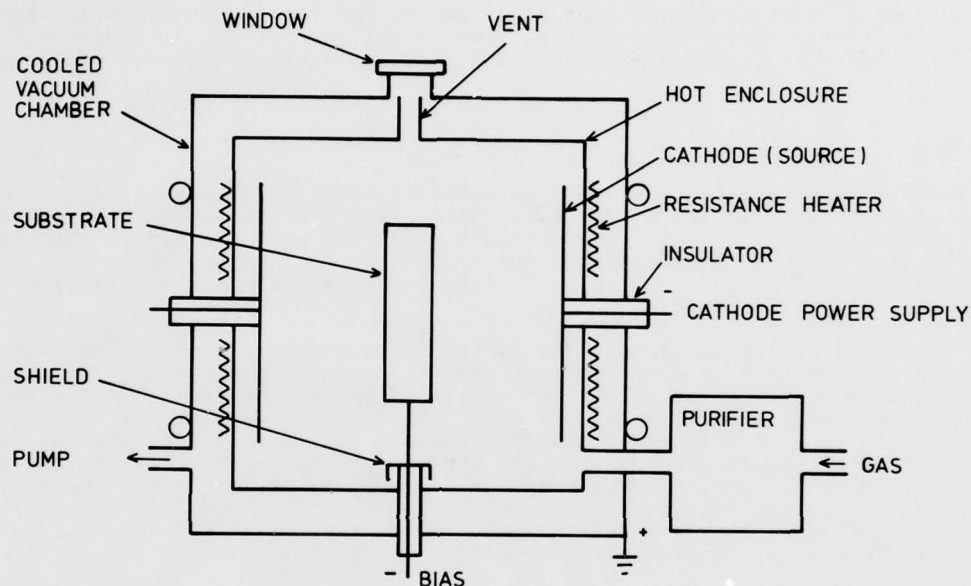


Figure 1 Schematic diagram of sputter ion plating system

A schematic diagram which indicates the main features is shown in Figure 1. The coating operation takes place within a heated enclosure mounted within the vacuum chamber, (though the chamber itself could be heated if this is practical). Heating the sample region to about 200°C and holding this temperature during coating prevents any contamination from the chamber walls being incorporated into the coating. Purified argon is passed continuously through the heated enclosure at a pressure of about $(1/d)$ mbar, where d is the chamber dimension in cm. A mechanical pump is sufficient to maintain the working pressure; no high vacuum pumps or vapour traps are needed.

Before the coating is deposited the surface to be coated must be thoroughly cleaned, and this is done by ion bombarding the sample. The normal purging gas, argon, can be used readily by applying a few hundred volts (negative) to the samples and setting up a discharge between them and the walls of the chamber.

(b) Ion Implantation

Ions, produced by a variety of means in an ion source (of which there are many designs⁽⁵⁾), are accelerated by an electric field towards the workpiece. Energies lie usually between about 10 keV and 200 keV and, since the ions mostly have a single electronic charge, these values correspond to the voltages required. A limit is set to the lowest energy which can be used by the fact that the ions must penetrate the thin oxide films normally present on metallic surfaces. The process is carried out in a moderately good vacuum of 10^{-5} to 10^{-6} mbar, so that undue scattering or neutralisation of the charged particles does not occur. Implantation machines are commercially available which meet most of the needs of the semiconductor device industry⁽⁶⁾. These developments have kept pace with ever increasing silicon wafer sizes and more demanding specifications of implantation uniformity and wafer throughput. The geometry of the application is very simple, universally involving thin flat discs of semiconductor and a limited variety of non-metallic ion species.

In the treatment of advanced engineering components and tools the situation is radically different⁽⁷⁾. In the first place much higher ion doses are usually required, and this calls for powerful ion beams for the process to be economically attractive.

Secondly, the components vary very greatly in size and they are rarely of a simple geometry, particularly in aerospace and allied industries. Special ion source configurations and even multiple ion sources may therefore be needed in order to direct the beam appropriately. Implantation treatments for corrosion protection call for a variety of ion species, for example chromium, molybdenum, rare earths, etc. which are not normally available in high energy intensities in ion sources currently obtainable.

By comparison with the application of ion implantation to semiconductors, some of the constraints can be relaxed in dealing with engineering materials. It is not necessary to employ ion beams of such high purity, and the uniformity and reproducibility of the dose delivered rarely needs to be better than about 20%. A spread in ion energy is usually not detrimental. Reliability and simplicity of operation are much more important.

The net result is that machine designs for ion implantation in the engineering field must be

- (i) versatile, particularly with respect to work handling;
- (ii) efficient, with a throughput matched as far as possible to the batch size desired;
- (iii) compact, so as not to occupy valuable floor space;
- (iv) simple to operate, and automated so far as possible;
- (v) reliable in service, with long-life ion source and high voltage supplies and easy maintenance;
- (vi) completely safe, from the point of view of electrical safety and from X-ray emission.

These requirements have now largely been met in prototype equipment based upon work carried out at Harwell over some five years. Figure 2 shows the schematic arrangement of ion implantation equipment which resembles electron beam welding apparatus as regards cost, complexity and general design principles. A high voltage supply, vacuum equipment and workpiece manipulation gear is required in each case, an ion gun being substituted for the electron gun in this case. Figure 3 shows a photograph of the prototype unit built at Harwell, incorporating a 50 cm cubical work chamber, a compact 100 kV power supply, automatic vacuum system and thoroughly tested safety features.

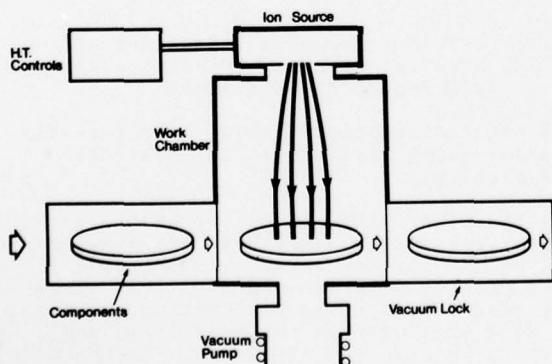


Figure 2 Schematic arrangement of ion source and work chamber suited to the ion implantation of engineering components

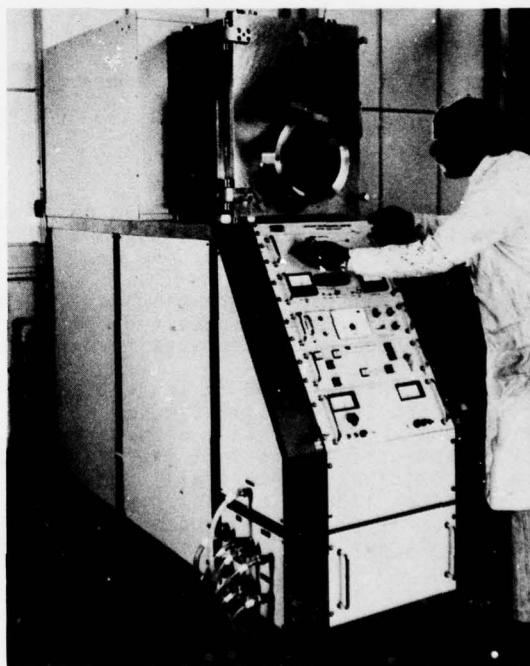


Figure 3 Photograph of a prototype ion implantation machine at Harwell for treating small batches of tools and components

APPLICATIONS

The fields of application of these two surface treatments methods are shown in the following figure (Figure 4), which divides the potential areas for exploitation into physical, chemical and physico-chemical regimes. Sputter ion plating and ion implantation have been applied to a variety of surfaces for wear reduction, both on laboratory test samples and on small scale industrial trials.

Wear Resistance

There is industrial interest in surfaces with improved wear resistance either for increased lifetime of tools and dies, or reduced wear rate of surfaces in sliding contact with other components or erosive and fretting wear in turbines. One area of particular interest is the application of surface coating technology to tools, both of the cemented carbide and high speed steel types. Over the last ten years chemical vapour deposition, CVD⁽⁸⁾, had been used to deposit TiC and T-C-N coatings which strengthen cemented carbide tools and can increase the lifetime of the tools by a factor of 2 to 10; this has also been achieved using ion plating. CVD cannot be used to coat steel components unless the components are subsequently heat treated, because the temperatures reached by the substrate during coating, typically 1000 to 1100°C, would soften the steel. Sputter ion plating has been applied experimentally to coat tools and other components with TiC and TiN and with each of these materials dense, smooth, well-adhered coatings of Vickers hardness in excess of 2,000 have been deposited. Coatings of WC, CrC and a mixed Ta/Ti carbide have also been successfully deposited, and a section through the last mentioned is seen in Figure 5.

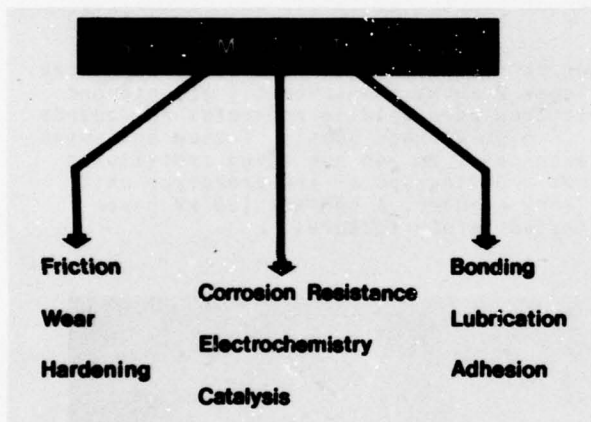


Figure 4 Material properties which can be altered by sputter ion plating and ion implantation

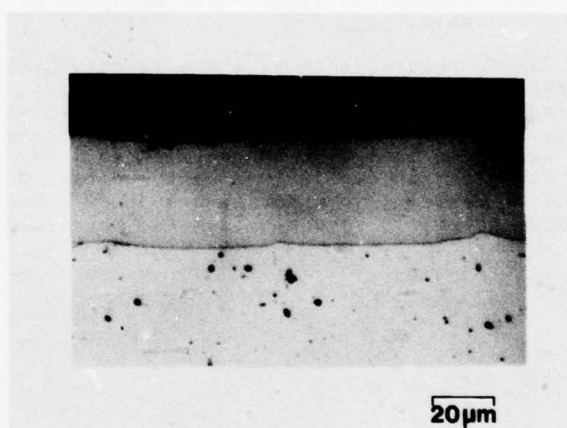


Figure 5 Section through a titanium-tantalum carbide coating deposited by sputter ion plating on to mild steel

Another application for which some of the SIP coatings mentioned above have recently been tested is resistance to erosion by high speed air-borne particles; the coatings have proved to be very effective in combating this problem.

The principle adopted in ion implantation, on the other hand, is to introduce into a metal surface those atomic species which will form very strong bonds with the original material, and which will have a hardening effect upon the surface layer. This chemical effect is enhanced by the fact that ion bombardment creates disorder and displaces atoms within the original polycrystalline metal⁽⁹⁾. The result is a dense dislocation network, not unlike that induced by shot peening, although much shallower in depth ($< 1 \mu\text{m}$) and fortunately free from the changes in surface finish which peening introduces. Furthermore, the surface is put into a state of high compressive stress at the ion doses usually employed.

It was observed during the early stage of this work at Harwell that the effectiveness of nitrogen or carbon ion implantation upon wear resistance of steel is much longer lasting than might be expected on the basis of the shallow ion penetration. Measurements of the amount of nitrogen still present in a surface after wear tests combined with profilometry of wear tracks indicate that a significant fraction of implanted material is still present after wear to a depth of 10 microns. It seems likely that some mechanism is serving to carry forward the nitrogen or carbon as wear progresses.

The examples of ion implantation studies listed in Table 1 represent a selection of manufacturing trials on ion implanted components⁽¹⁰⁾. It must be stressed that ion implantation is still at the exploratory stage. No equipment yet exists outside Harwell which has been specifically designed to treat metallurgical items on a production basis. Some of the examples listed in the Table have reached relatively large pre-production assessments (i.e. over 100 components) and the trials are continuing.

Table 1
Evaluations of Ion Implanted Components in Production Engineering

Ref	Application	Material	Treatment	Result
A	Paper slitters	1C 1.6 Cr steel	8.10^{17} N/cm ²	Cutting life X2
B	Acetate punches	Cr-plate	4.10^{17} N/cm ²	Improved product
C	Taps for drilling plastic	HSS	8.10^{17} N/cm ²	Life X5
D	Slitters for synthetic rubber	WC-6% Co	"	Life X12
E	Dies for copper rod	"	5.10^{17} C/cm ²	Throughput X5
F	Drawing dies	"	2.10^{17} CO/cm ²	Improved life
G	Dies for steel wire	"	3.10^{17} C/cm ²	Wear rate X 1/3
H	Tool inserts	4 Ni 1 Cr steel	4.10^{17} CO/cm ²	Contamination X 1/3
I	Forming tools	12Cr 2C	4.10^{17} N/cm ²	Much reduced adhesive wear

The applications are grouped into three main areas: A to D - cutting and slitting operations; E, F, and G, extrusion operations and applications where large surface forces occur; H,I - corrosive applications.

In the first group of applications ion implantation was chosen for evaluation because sharp surfaces are intrinsically difficult to surface treat without becoming embrittled. In addition cutting processes in industry usually involve very large volumes of material and thus it becomes important to maintain a steady throughput and minimise shut-down of plant. In example A two 20 cm diameter slitter discs were ion implanted with nitrogen round the cutting edges. The steel was a high carbon with chromium heat treatable cutting steel. These steels form chromium carbides which induce hardness and good wear resistance but surface treatment by induction or flame hardening is not advised because grain growth occurs. Cold working causes severe embrittlement and although it is possible to furnace heat treat the steel, local decarburisation can occur if a slightly oxidising atmosphere is present.

In this example, the wear took place by an abrasive process, caused by small particles of silicates contained within the paper. Abrasive wear occurs in all the applications within the first group of examples. In Case B the punching process has to be precise within a very high degree of accuracy ($< 1 \mu\text{m}$) and abrasive wear by the plastic-based material can rapidly lead to an unacceptable product.

The third application (C) concerns a high volume market in which the treated tool is inexpensive. High speed steel taps are used to provide threaded holes in injection moulded thermosetting resin components. The taps are found to wear out, largely by an abrasive mechanism, in about 1500-2000 operations. A set of implanted taps tested alongside controls showed no measurable signs of deterioration after 7500 tapping operations. One tap achieved 19,000 operations.

The fourth application for ion implantation in Table 1 concerns the abrasive wear of cobalt-based cemented tungsten carbide slitters for cutting synthetic rubber. This is another high volume market where penalties occur if plant is unable to be kept running for any length of time. Normally slitter blades are refurbished before a single shift is ended. This halts production and is therefore a costly operation. High dose nitrogen implantation extended the cutting life of these slitters by a factor 12 which allowed the machine operators to run large batches of material through without interruption.

Considerable increases (by factors of 5 to even 100) in the life of cemented tungsten carbide tools used for certain wire-drawings and metal-forming operations on copper, steel and other materials have also been achieved by carbon and nitrogen implantations (E, F and G in Table 1). Both adhesive and abrasive wear have been reduced in this material as well as in Stellite⁽¹¹⁾. Once again the effectiveness is prolonged and a die may still show the benefits of ion implantation after wear to a depth 1000 times the implanted layer thickness. The mechanisms are less well understood in inhomogeneous materials than they are in steels, but probably involve migration and strong bond formation at grain boundaries since it is only here that diffusion can occur within the times and temperatures experienced.

The relatively high value of a tungsten carbide tool means that implantation is likely to add only a fraction to its cost yet the service life can be much increased. Plant utilisation is increased, and the quality of the machined produce is improved. Figure 6 shows a (sectioned) die of a type which has been improved by ion implantation.

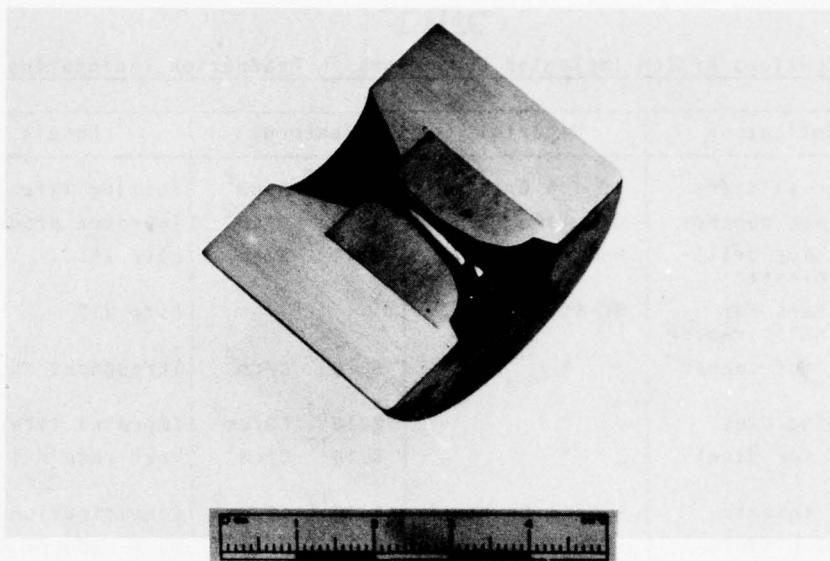


Figure 6 Photograph of a sectioned wire-drawing die with a tungsten carbide insert which can be ion implanted for improved performance

Corrosion and Adhesive Wear

Cases H and I in Table 1 demonstrate the application of ion implantation for combating corrosion and adhesive wear in manufacturing industry. With the development of more powerful ion sources which can deliver milliamp beams of rare earth elements and other suitable corrosion inhibitors, it is envisaged that ion implantation will have a significant contribution to make towards improving the surface durability of turbine blades and other high temperature components. Many industrial corrosion problems are, however, centred on relatively inaccessible regions of stress concentration or internal surfaces and it is here that the particular advantages of sputter ion plating become important. We look first at ion implantation.

An early example of the use of ion implantation for oxidation protection was the case of yttrium implanted 20 Cr/25 Ni/Nb stainless steel⁽¹²⁾, see Figure 7.

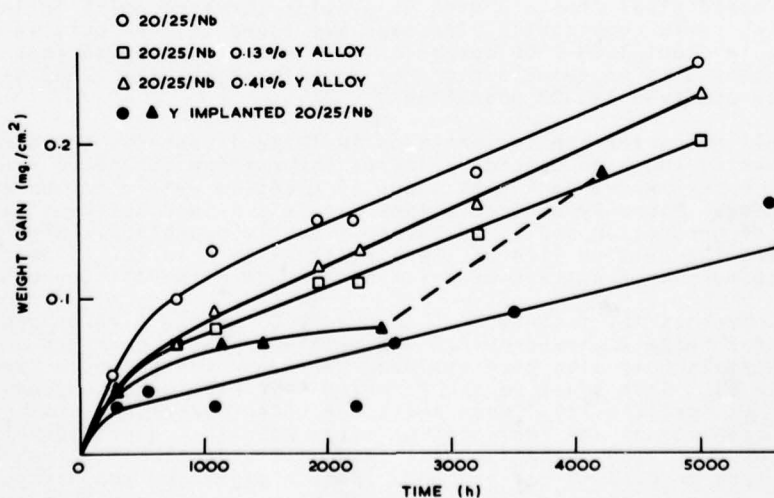


Figure 7 Effect of yttrium ion implantation on the oxidation of austenitic stainless steel in CO_2 at 800°C compared with the behaviour of alloyed yttrium

In pack-aluminized nimonic alloys used in turbine blades, however, ion implanted Y^+ or Ce^+ were observed to convey no benefit because the atomic transport mechanisms are different to those occurring in steels to which rare earth additions have been made(12). The implanted atoms remain at the outer surface of an alumina-rich scale and they are soon lost due to spalling. In this case, the obvious method of protection is to ion implant additional aluminium and this has proved to be the case for Fe-Cr-Al-Y. The parabolic rate constant for oxidation in O_2 at $1100^\circ C$ was reduced by a factor of 140 by implanting $10^{17} Al^+$ ions per cm^2 into an alloy containing 1.42% Al(13).

An alternative to increasing deliberately the aluminium content to improve the high temperature oxidation resistance of this material is to substitute ion implanted yttrium for the bulk addition of this element, in an analogous way to the 20 Cr/25 Ni/Nb austenitic stainless steel application discussed earlier. Recent work at Harwell(14) has shown that Y implanted into Fe-Cr-4.8% Al brings about a very large reduction in thermal oxidation at temperatures in excess of $1000^\circ C$. It appears that the ability of Y to stimulate the formation of an effective layer against an outwardly migrating cation flux depends on the presence of other elements within the bulk material, such as chromium.

Ion-implanted Cr^+ , Al^+ , and Ti^+ have each reduced thermal oxidation and atmospheric tarnishing in copper by leading to the formation of a more protective oxide.

Correlated changes in corrosion and oxide electronic properties were observed in the case of titanium, in which the favourable species (e.g. Sr^+ , Ba^+ , Eu^+) share a low electronegativity and a large ionic radius. It is believed that in this case these implants act by providing traps for migrating O^{2-} ions, forming in the process a bulky compound comprising the implanted impurity together with titanium and oxygen, which form the perovskite structure. This appears to block certain fast diffusion paths through the oxide and into the metal.

There are therefore an increasing number of instances where ion implantation can improve corrosion performance. The amounts of material required can be two orders of magnitude lower than for friction and wear reduction, although the ion species are less easily produced than carbon or nitrogen as discussed in the earlier examples included in Table 1. With the development of efficient ion sources capable of treating large surface areas, ion implantation seems likely to make a valuable contribution to high temperature oxidation both for materials improvement and as an aid to understanding oxidation mechanisms.

An alternative method of providing corrosion protection is to exclude the environment completely by coating external surfaces with a fully dense protective layer. To be effective, prevention from corrosive attack must be total. The microstructure of a deposited coating must therefore be well controlled.

Figure 8 shows a section through a coating deposited by Sputter Ion Plating of CoCrAlY alloy on nickel: no structure is visible in the deposit. Although this coating is typical of sputter ion plating it contrasts markedly with the dendritic structures prevalent in electron beam evaporation, for example. Dendritic structures not only give a high density of points where the coverage of the substrate is far thinner than the normal film thickness, but also give a much higher specific surface area for absorption of gases etc. than does the denser smooth coating obtained by sputter ion plating. A more uniform coating might also be expected to give improved life to cathodic protection layers which are in widespread use following deposition by other plating techniques. At Harwell, coatings of Fecralloy(15), which is also of the general form MCrAlY, have been tested and have good properties. Fecralloy coatings on 20 Cr/25 Ni/Nb have been heated to $1000^\circ C$ in CO_2 for over 400 hours, and the coatings gave total protection to the flat areas of the substrates, though there was localised attack at the hole used for mounting the samples, where the coating was incomplete and internal stresses during oxidation were greatest. There was no detectable spread of the attacked area, showing that no decohesion was caused by attack along the interface.

CoCrAlY, together with NiCrAlY, are finding increasing applications as coatings in the aerospace industry. In particular, the operating temperatures for gas turbines are steadily increasing so that the life of the Inconel blades is becoming too short for economic use. CoCrAlY and/or NiCrAlY coatings have been shown to increase the operating life of the blades. Sputter ion platings has achieved dense enough deposits of this material to alleviate the need for subsequent shot peening and heat treatment. The process is being scaled up to improve the deposition rate so that these coatings can be built up more rapidly.

Practical applications of sputter ion plating and ion implantation to the physico-chemical areas of surface technology shown in Figure 4 (bonding, lubrication, adhesion) have so far been limited to a study using SIP for soldering and brazing(4,16). Sputter ion plating has been used to coat a range of materials with nickel or copper, so that they can be soldered to copper. In Figure 9 a section is shown through an aluminium base, nickel coating, solder and copper. Other materials coated by SIP include: titanium, titanium alloy, molybdenum, Fecralloy, cast iron and tantalum. The sections have been etched lightly in nitric acid to improve the visibility of some of the layers, and the arrowheads indicate the position of the nickel coating, which is a few microns thick. Such coatings can also be applied to ceramics or glasses, and allow these items to be soldered or brazed conventionally in the same way as the metals.

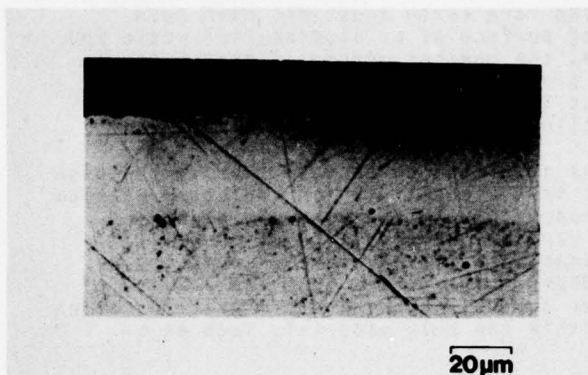


Figure 8 Section through Co-Cr-Al-Y on nickel deposited by Sputter Ion Plating

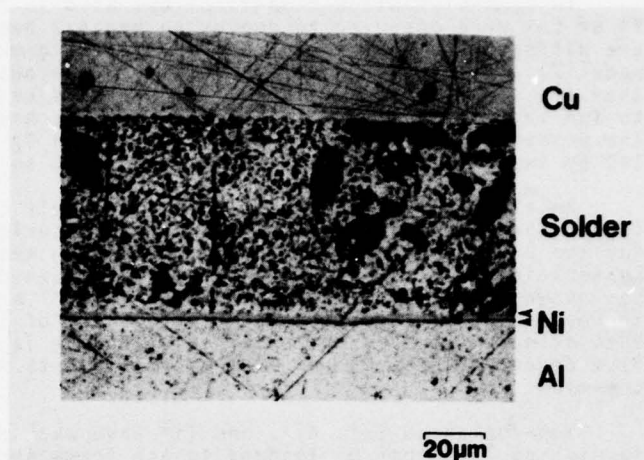


Figure 9 Section through a nickel film deposited by SIP onto aluminium to form a soldered joint with copper

CONCLUSIONS

The two surface treatment techniques described in this paper, Ion Implantation and Sputter Ion Plating, have each been shown to have a wide range of industrial applications. Ion implantation can provide considerable protection from low temperature abrasive wear, whilst SIP coatings can improve a wide variety of abrasive or erosive wear situations. Implanted surface layers and sputtered coatings can each be used as corrosion inhibitors, and this is an area where work is being expanded. Ion implantation has the advantage of minimising problems of pinholes and galvanic attack, though both sputtered coatings and implanted surfaces have been effective in reducing various types of high temperature oxidation. At present ion implantation is the more industrially oriented of these surface treatment methods and is now being evaluated in manufacturing applications and in advanced materials applications. It is anticipated that the more recent emergence of sputter ion plating as a coating technique will also lead to full scale evaluations in the near future.

ACKNOWLEDGEMENT

The research project which is evaluating ion implantation as a potential treatment method for machine tools is supported by the U.K. Department of Industry under a Requirements Board scheme.

REFERENCES

1. D. M. Mattox, J. Appl. Phys. 34 (1963), 2493.
2. R. A. Dugdale, Thin Solid Films 45 (1977), 541.
3. R. A. Dugdale, International Conference on "Ion Plating and Allied Techniques" Edinburgh, June 1977, Publ. by CEP Consultants Ltd.
4. J. P. Coad and R. A. Dugdale, Wire Industry 44 (1977), 771.
5. L. Vályi, "Atom and Ion Sources", Wiley (1977).
6. G. Dearnaley, J. H. Freeman, R. S. Nelson and J. Stephen, "Ion Implantation" NHPC(1973), 255.
7. G. Dearnaley and N. E. W. Hartley, International Conference on "Scientific and Industrial Applications of Small Accelerators", Denton, USA, IEEE (1976), 20.
8. See for example K. K. Yee, Internat. Metall. Rev. 23 (1978), 19.
9. Ref. 6, p.154.
10. N. E. W. Hartley, "Ion Implantation Case Studies - Manufacturing Applications", AERE Report (1978) R 9065 (U/C).
11. Cobalt based alloys containing Cr, W, Mo and Fe.
12. J. E. Antill, M. J. Bennett, R. F. A. Carney, G. Dearnaley, F. H. Fern, P. D. Goode, B. L. Myatt, J. F. Turner and J. B. Warburton, Corrosion Sci. 16 (1976), 729.

13. U. Bernabai and G. Dearnaley, To be published.
14. M. J. Bennett, priv. comm.
15. Fecralloy - Registered Trade Mark of U.K.A.E.A.
16. M. Page, Metals and Materials, Oct. 1977, 27.

METAL BONDED CARBIDES FOR WEAR RESISTANT SURFACES

L. F. Norris, V. Silins, M. Adamovic and M. A. Clegg
 Sherritt Research Centre
 Sherritt Gordon Mines Limited
 Fort Saskatchewan, Alberta T8L 2P2, Canada

ABSTRACT

Experiments were conducted to relate the wear resistance and matrix hardness of metal-refractory metal carbide coatings to the extent of dissolution of the refractory metal in the coating matrix during plasma spraying. Powders prepared by coating TiC, Cr_3C_2 , TaC and WC with nickel or cobalt by hydrometallurgical processes were plasma sprayed in tests in which the heat input to the powder particles during spraying was varied. Increasing the heat input generally increased the amount of refractory metal in solution in the coating matrix as determined by microprobe analysis. The matrix microhardness generally increased with refractory metal content but the wear resistance of the coatings varied widely for the eight systems evaluated. It was concluded that the superior wear resistance of plasma sprayed coatings based on WC and Cr_3C_2 is not simply a consequence of extensive dissolution of the refractory metal in the coating matrix and must be related to a more complex interrelationship of hardness, toughness, density and metal-carbide bond strength.

1. INTRODUCTION

Several commercial wear resistant coatings consist of a dispersion of refractory metal carbide particles in a metal matrix. One family of such coatings is obtained by plasma spraying powders which contain both a metallic phase and a carbide phase. These powders may be produced by either solid state or liquid phase sintering, by hydrometallurgical processes in which the carbides are coated with a metallic phase or by agglomerating metallic and carbide phases with an organic binder. In all cases, however, there is little, if any, of the refractory metal from the carbide in solution in the matrix of the powder. During thermal spraying, however, there is sufficient heating to dissolve some of the carbide and the coating then contains both undissolved carbide particles and an alloy phase with some of the refractory metal in solution.

The objective of the present study was to determine whether coating performance, as measured by wear resistance and the hardness of the matrix phase, is influenced by the dissolution of the carbide phase into the matrix during thermal spraying. By plasma spraying several nickel- and cobalt-refractory metal carbide powders under conditions of varying heat input to the powder particles, variable dissolution of the carbide phase was expected. This variable dissolution was defined and monitored by the presence of the refractory metal in the matrix.

It is well known that the solubility of carbides in nickel and cobalt vary widely. According to Edwards and Raine⁽¹⁾ the solubilities of WC in nickel and cobalt at 1250°C are 12% and 22% respectively, for TiC, 5% and 1% respectively and for Cr_3C_2 , 12% and 12% respectively. Knowing that both WC and Cr_3C_2 composites have been more successful commercially than TiC composites, it was decided to test the hypothesis that this is, at least in part, a result of the greater dissolution of these carbides during spraying. Tantalum carbide was also included in the study as previous tests had indicated that satisfactory wear resistance might be achievable.

The four carbide powders (Macro Division of Kennametal, Inc., Port Coquitlam, British Columbia) were coated with nickel and cobalt using Sherritt's hydrometallurgical processes⁽²⁾. For nickel coatings the carbide particles were suspended in a nickel ammonium sulphate solution in an autoclave and the nickel was reduced from solution with hydrogen at elevated temperature and pressure. Cobalt ammonium ammonium sulphate solutions were used to prepare the cobalt-coated carbide powder after a thin nickel precoat had been applied. The nickel precoat amounted to 1 - 3% of the final composite powder composition but has been omitted from the powder designation, e.g., 18Co/2Ni/WC80 is reported as 20Co/WC80. Composite powders produced in this fashion have a uniform coating, the thickness of which is generally constant irrespective of particle size.

The test program began with a series of screening experiments to define compositions of interest for the plasma spraying experiments which followed. The latter were designed to explore the effect of carbide dissolution on the hardness and wear characteristics of the coatings.

2. COMPOSITION SCREENING EXPERIMENTS

The purpose of these experiments was to establish metal-refractory metal carbide compositions in the eight systems under study which would yield plasma sprayed coatings with hardness and wear resistance generally comparable to commercial hardfacing coatings. With one exception, four compositions of each carbide-metal combination were prepared; only three Ni/WC composite powders were made. The particle size distribution of the products was not controlled. All powders were plasma sprayed with an Avco PG 100 torch using a spray parameter of intermediate enthalpy:

nozzle	- 901345-1
current	- 700 A
voltage	- 38 V
plasma gas	- argon
plasma gas flow	- 49 l/min at 280kPa (40 psig)
powder feed	- 200 rpm
spray distance	- 10 cm

The composition of the powders and the matrix hardness and wear resistance of the coatings are summarized in Table 1 along with comments from metallographic examination of the coatings. As groups, both the WC- and Cr_3C_2 -containing coatings had the best combinations of structure and properties. The TiC coatings had an extremely wide range of wear resistance and microhardness; both the Ni/TaC and Co/TaC coatings had lower hardnesses and densities.

From the above data and prior experience at Sheritt with some of these composites the compositions listed in Table 2 were selected for the plasma spraying experiments to be described in the next section. The actual compositions were close to the target values with the exception of the Co/ Cr_3C_2 where the cobalt content was about 10% higher than planned; none of the deviations were expected to affect the plasma spraying experiments significantly. During preparation of the powders, significant differences in particle size distribution occurred among the eight compositions as indicated in Table 3. Most powders had a tight distribution centered within the range 30-60 μm while both Co/WC and Co/ Cr_3C_2 had wider distributions (10-75 μm). The composite powders were sprayed in the as-received condition. Careful control of the particle size distribution would be an important aspect of any further work with regard to both composition (the composition varies with particle size) and response to plasma spraying conditions (particle size affects both the trajectory and final temperature of the impinging particles).

3. PLASMA SPRAYING EXPERIMENTS

The eight carbide composite powders described in the concluding paragraph of Section 2 were plasma sprayed with an Avco PG 100 system to coatings approximately 0.25 mm thick. Three sets of spray parameters, selected to vary the dwell time of the powder particles in the plasma, were employed. Increasing the dwell time was expected to increase the heating effect (which was not measured directly) and thereby intensify the reaction between the carbides and their Ni or Co coating. For the three sets of spray parameters, denoted A, B and C in Table 4, the size of the plasma nozzle exit port opening was the principal variable, while the plasma arc power, plasma gas flow, powder feed setting and spray distance were held constant. The sprayed coatings were subsequently characterized by matrix microhardness, wear resistance, chemical analysis (by electron microprobe as described in Appendix A) and metallography.

4. RESULTS

Results of the above experiments are shown in Table 5 which contains the data on matrix hardness (kg/mm^2), coating wear (mm^3) and matrix composition of each coating as established by microprobe examination (\bar{X}). The final column in Table 5 indicates the amount of refractory metal in solution after spraying, expressed as percent of the total refractory metal present in the powder before spraying (M). These figures indicate how much of the available refractory metal has dissolved and are thought to be a good basis for studying the effects of different enthalpies.

The degree of dissolution (M) and \bar{X} are correlated with the heat input (enthalpy) employed during spraying in Figure 1. The enthalpy values (abscissa) were quantified by arbitrarily assigning a value of unity to spray parameter A and assuming that the enthalpy provided by the parameters B and C increased linearly with the increase of the nozzle exit port cross-section. (For equal flow of plasma gas an increase in the exit port results in lower velocity of the plasma gas which means longer powder dwell time, i.e., longer time period in which plasma-to-powder heat transfer takes place.) Figure 1 demonstrates that

- increased plasma enthalpy results in increased dissolution of the refractory metal in the Ni or Co matrix.
- dissolution is generally higher for Ni than for Co matrices.
- for the spray parameters employed, the solubility in Ni matrices approaches a limit in all cases, whereas the solubility in Co matrices approaches a limit only in combination with WC.
- largest dissolution (M) for the enthalpies employed was observed for (in decreasing order): Ni/ Cr_3C_2 , Ni/WC, Ni/TiC, Co/WC.

Figure 2 is a plot of sprayed coating properties as a function of degree of dissolution of the refractory metal M in the matrix. As expected, the matrix hardness data correlate generally well with the extent of refractory metal dissolution. Major deviations from the expected relationship of increasing matrix hardness with increasing dissolution can be observed with TiC composites. Much more variability, however, can be seen in the relationship between wear resistance and the amount of refractory metal in solution. The largest changes in wear volume are not associated with the largest changes in dissolved refractory metal. Since, unlike matrix hardness, the wear characteristics

of sprayed coatings are influenced directly by the remaining undissolved carbide, the data on wear are also plotted as a function of retained carbide content (Figure 3). No pronounced general correlation can be observed in this case either. All Co/WC coatings have excellent wear characteristics irrespective of the amount of dissolved refractory metal. The two materials which exhibit the largest dissolution (Ni/Cr₃C₂ and Ni/WC) also show satisfactory behaviour in wear tests (Coating Wear <0.05 mm³) and more so with increasing degree of dissolution.

Metallographic examination indicated a decrease in carbide content in all coatings with increasing particle dwell time in the plasma. With greater dissolution the remaining carbide particles were smaller and more rounded, see Figure 4. Exceptions to the latter were the two TiC-containing composites where the acicular shape of the carbide was retained at all particle sizes, see Figure 5. Particle "pull-out" during metallographic preparation precluded accurate comparison of the densities of the coatings, especially with both TiC composites. The extent of particle "pull-out" during metallographic preparation was interpreted as a measure of the bond strength between the carbide particles and the matrix.

5. DISCUSSION

The expected trend of increasing dissolution of the carbides in the matrix with increasing heat input during spraying which results in increased matrix hardness was confirmed. A correlation between carbide dissolution and the particle size distribution (i.e., less dissolution for coarser powders) was expected but not established, which suggests that other factors such as plasma spraying conditions, diffusion rates, etc. had stronger influences.

The relationship between the dissolution and the wear resistance of the 24 coatings tested cannot be generalized as wear resistance is a complex function of the carbide and matrix hardness and toughness, the carbide-matrix bond strength and the coating density. Indirectly, the melting temperature of the coating matrix and the particle velocity at the moment of impact against the substrate are also variables determining coating properties. It is believed that the wide variations in wear resistance that occurred with increasing carbide dissolution relate to undocumented changes in these above properties. These changes appear to be specific to the metal-carbide combinations under consideration. For example, the wear resistance of the Co/WC coatings was excellent for all spray parameters investigated and substantially independent of the amount of tungsten dissolved in the matrix. This composite has all the attributes of a successful wear resistant plasma sprayed coating: the carbide is very hard (DPH 2200-2000 kg/mm²), is not unduly brittle, and also bonds extremely well to the cobalt matrices. Titanium carbide is also very hard (DPH >3000 kg/mm²), but is brittle and, from metallographic evidence, is more weakly bonded to cobalt and nickel alloy matrices; the wear resistance of the Ni/TiC and Co/TiC coatings was lower. Tantalum carbide is the softest of the carbides tested (DPH 1200-1400 kg/mm²) and exhibited quite different responses to spray parameter changes depending on whether it was bonded with cobalt or nickel.

It was shown that the three metal-refractory carbide systems with the best wear characteristics also manifest extensive dissolution of the refractory metal (Ni/Cr₃C₂, Ni/WC, Co/WC). However, fuller analysis of the data shows that extensive dissolution is neither necessary nor sufficient for good wear resistance (Coating Wear <0.05 mm³). The data also suggest that poor carbide properties (inadequate hardness and/or brittleness) will result in commercially unacceptable sprayed coatings regardless of the degree of the refractory metal dissolution in the matrix (TaC and TiC composites). One exception in this category is Co/TaC where, due to refractory metal dissolution, the hardness of the matrix increases and seems to compensate for the inadequate hardness of the TaC so that the wear characteristics of the sprayed coating improve with increased dissolution. For less critical applications this composite may have commercial utility. When good carbide properties and also adequate carbide-matrix bonding are present, such as in Co/WC, the increase in refractory metal dissolution seems unimportant in terms of sprayed coating properties, at least after initial dissolution takes place (37.3% W in Co for spray parameter A). There seems to be an intermediate case, however, where carbide properties are satisfactory but carbide-matrix bonding is relatively weak such as in Ni/WC and Ni/Cr₃C₂. In this case, the increase in the refractory metal dissolution improves the wear characteristics, possibly by improving carbide-matrix bonding.

The study has shown that the commercial success of WC and Cr₃C₂ plasma sprayed coatings is not due simply to the extensive dissolution of the carbide in the alloy matrix. However, an improvement in the wear characteristics has been correlated with increased refractory metal diffusion into the matrix in some cases where the carbide properties are satisfactory (Ni/WC, Ni/Cr₃C₂). In addition to the commercially established Co/WC and Ni/Cr₃C₂ systems, the potential commercial utility of Ni/WC has been demonstrated. For less critical applications, the technical merit of Co/TaC has also been shown.

6. ACKNOWLEDGEMENTS

The authors express their appreciation to David D. Thomas, President and Chief Executive Officer, Sherritt Gordon Mines Limited, and Vladimir N. Mackiw, Executive Vice President, Sherritt Gordon Mines Limited, for permission to publish this paper. The authors also thank Kenneth G. Reid for developing a method for chemical analysis of the plasma sprayed coating matrices. Financial assistance for this study in the form of Department of Supply and Services Contract No. 8SS5-2146 on behalf of the Defence Research Establishment Pacific (DREP) of the Department of National Defence is gratefully acknowledged.

7. REFERENCES

1. Edwards, R. and Raine, T., Proceedings of the First Plansee Seminar, 1952, Reutte/Tyrol, Edited by F. Benovsky, Metallwerk Plansee Ges.M.B.H., 1953, p. 232-240.
2. Evans, D. J. I., Advances in Extractive Metallurgy, Symposium of the Institution of Mining and Metallurgy, London, 17-20 April, 1967.

APPENDIX ACHEMICAL ANALYSIS OF PLASMA SPRAYED COATING MATRICES

Obtaining the chemical analyses of the plasma sprayed coating matrices was a challenging part of the experimental program. From the metallographic evidence that the carbide particles in the coatings were smaller than those in the powder before spraying it was recognized that the carbide must be "dissolving" in the matrix. The analytical problem, then, was defined as the identification and measurement of the refractory metal (from the carbide) added to the matrix. The initial experiments were conducted with Co/WC coatings.

One approach was to use the selective dissolution technique customarily employed to analyze liquid phase sintered carbides (A-1). The sprayed coating was stripped from its substrate, ground with a mortar and pestle and digested in 40% citric acid at ambient temperatures for at least seven days. The solution plus the filtrate from washing the undissolved residue were then analyzed for tungsten. A mass balance on the results indicated incomplete extraction of both tungsten and cobalt. There was only partial extraction when Co/WC composite powder was similarly analyzed. The cobalt extraction for Co/WC composite powder reached 100% when boiling 5M HCl was used rather than citric acid (A-2) but, again, very low values were obtained from the plasma sprayed coatings. Moreover, the cobalt extractions varied with the plasma spraying conditions (lowest extractions with hottest plasma conditions). This, coupled with the fact that the selective dissolution methods worked with commercial liquid phase sintered Co/WC powder but not with plasma sprayed coatings from this powder, showed that these methods were inappropriate for the present experiments.

X-ray diffraction methods were next explored. Ground portions of plasma sprayed coatings and Co/WC composite powder and liquid phase sintered Co/WC powder were analyzed. Both Co and WC were detected in both powders but unambiguous identification of Co or WC was impossible in the sprayed coatings where the patterns contained only a few, weak lines. The intensity of the WC pattern decreased further with hotter plasma conditions while at the cooler plasma conditions new, very weak lines appeared. Thus it was not possible to measure the lattice dilation of the matrix associated with the presence of tungsten and it was concluded that x-ray diffraction was not a suitable method for these analyses.

The electron microprobe was then used for quantitative analysis. Because of the chemical non-uniformity of the sprayed coating matrices, statistical treatment of the data was required. It was found that the mean concentration and the standard deviation, computed for each element, could be used to characterize the coating chemistry and were sufficiently sensitive to permit a correlation of the coating chemistry with the plasma spraying conditions.

To carry out the microprobe analyses the coating on a steel block substrate was ground using a 320 grit diamond grinding wheel and then polished using 1 μ m diamond paste on a rotating nylon-covered polishing wheel. In most cases the unreacted carbide in the polished sprayed deposit surface could be discerned at a magnification of x300. When the particles were difficult to see, contrast between the matrix and the particles was enhanced by lightly etching the matrix or by vacuum depositing interference coatings onto the prepared surface. A special polished copper-filled plastic sample holder was prepared which contained all the necessary pure element reference standards for the microprobe analyses. The central portion of the holder was drilled and shaped to accept the steel blocks which were carefully positioned after insertion so that the polished sprayed surface was coincident with the holder surface.

Both wavelength and energy dispersive x-ray detection systems were used in the microprobe analyses of the cobalt-containing deposits while only the latter could be used for the nickel composites. Each sample was analyzed at twenty randomly selected areas of the matrix using x-ray data acquisition times of at least 60 s. The sample data were bracketed by reference standard data so that microprobe drift could be corrected as a linear function of time. All the x-ray data were corrected for background and deadtime effects and then converted to percent concentration using a time-sharing version of FRAME-3 from the U.S. National Bureau of Standards.

No attempt was made to monitor carbon losses during spraying nor to analyze for carbon in the coatings.

REFERENCES

- A-1 Private communication, W. J. Huppmann, Max Planck Institute, Powder Metallurgy Laboratory, Stuttgart, W. Germany.
- A-2 Jonsson, H., Scand. J. of Metals, 4, 220 (1975).

Table 1. Results from Composition Screening Experiments

Coating Composition		Wear ¹ (mm ³)	Microhardness ² (kg/mm ²)	Metallographic Observations ³
Ni (%)	Co Carbide (Bal) (%)			
-	22 78 TiC	0.06	1400	Particle pullout, poor density
-	32 68 TiC	0.40	940	Extremely poor density
-	45 55 TiC	0.084	640	Extremely poor density
-	60 40 TiC	0.091	610	Poor density
19	-	wore through	too loose	Extremely poor density
29	81 TiC	3.0	320	Extremely poor density
44	56 TiC	2.2	340	Extremely poor density
62	38 TiC	0.17	540	Poor density
-	20 80 Cr ₃ C ₂	0.11	500	Some pullout, fair density
-	32 68 Cr ₃ C ₂	0.064	850	Good density
-	41 59 Cr ₃ C ₂	0.094	700	Good density
-	59 41 Cr ₃ C ₂	0.056	660	Good density
21	-	0.047	620	Some pullout, fair density
34	66 Cr ₃ C ₂	0.095	590	Good density
49	51 Cr ₃ C ₂	0.074	730	Good density
63	37 Cr ₃ C ₂	0.074	800	Good density
-	11 89 TaC	5.8	too loose	Particle pullout, extremely poor density
-	22 78 TaC	1.9	650	Poor density
-	34 66 TaC	0.098	660	Fair density
-	41 59 TaC	0.07	660	Fair density
12	-	4.5	too loose	Particle pullout, extremely poor density
26	88 TaC	0.10	690	Particle pullout, fair density
36	64 TaC	0.09	690	Fair density
50	50 TaC	0.14	470	Fair density
-	10 90 WC	0.11	1630	Particle pullout, poor density
-	16 84 WC	0.067	1470	Good density
-	28 72 WC	0.092	1460	Good density
-	38 62 WC	0.056	1150	Good density
10	-	0.16	1200	Particle pullout, poor density
17	83 WC	0.037	1400	Good density
20	80 WC	0.054	700	Good density

1. LFW-1 Wear Test - Wear Volume in 110 m sliding distance under 27 kg load against hardened steel ring.

2. DPH, 100 g load; average of 10 measurements.

3. Good density = ASTM B-6 or better (ASTM porosity standard B 276-54 for sintered carbides).

AD-A068 980

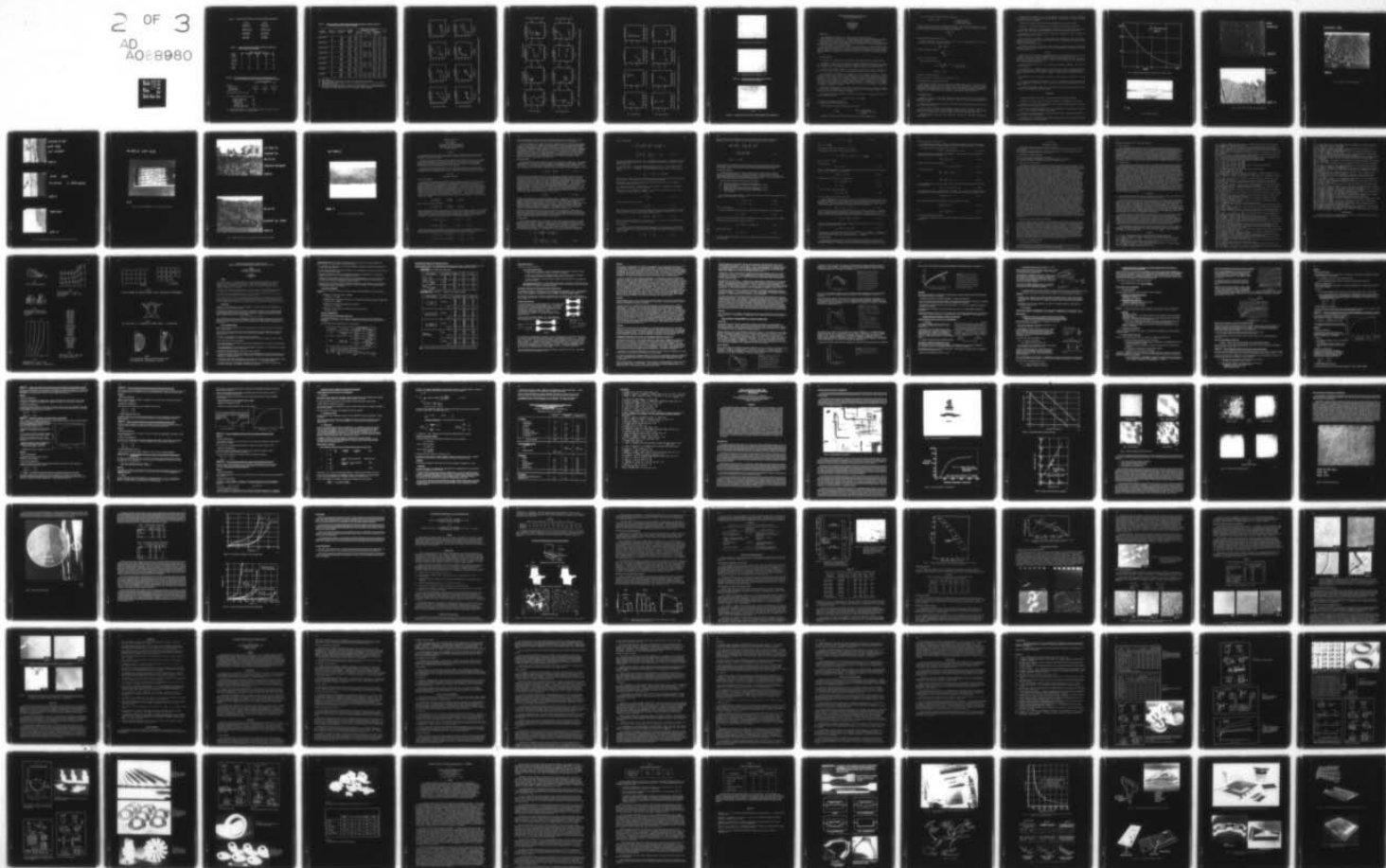
ADVISORY GROUP FOR AEROSPACE RESEARCH AND DEVELOPMENT--ETC F/G 11/6
ADVANCED FABRICATION PROCESSES. (U)
MAR 79

UNCLASSIFIED

AGARD-CP-256

NL

2 OF 3
AD
A068980



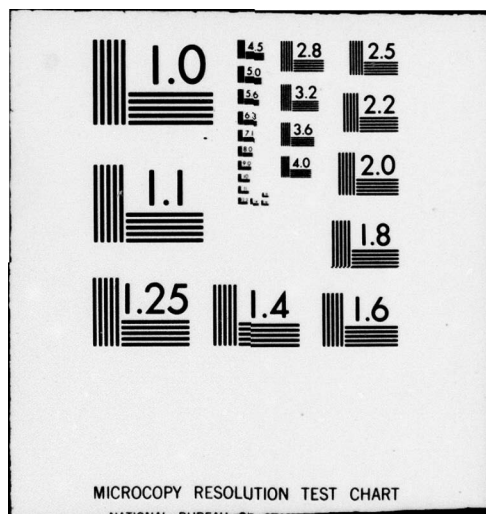


Table 2. Compositions Selected for Plasma Spraying Experiments

<u>Target</u>	<u>Actual</u>
60Ni/TiC40	60Ni/TiC40
21Co/TiC79	19Co/TiC81
49Ni/Cr ₃ C ₂ 51	48Ni/Cr ₃ C ₂ 52
49Co/Cr ₃ C ₂ 51	54Co/Cr ₃ C ₂ 46
40Ni/TaC60	40Ni/TaC60
40Co/TaC60	42Co/TaC58
20Ni/WC80	20Ni/WC80
20Co/WC80	21Co/WC79

Table 3. Screen Analyses of the Eight Powders Prepared for Plasma Spraying Experiments

<u>Powder</u>	<u>Screen Fraction (μm)</u>				
	<u>-10</u>	<u>+10/-20</u>	<u>+20/-30</u>	<u>+30/-44</u>	<u>+44</u>
Ni/TiC	0	0	32	54	14
Co/TiC	0	20	56	24	0
Ni/Cr ₃ C ₂	0	0	21	39	40
Co/Cr ₃ C ₂	3	11	9	6	71
Ni/TaC	0	2	42	48	8
Co/TaC	1	2	2	10	85
Ni/WC	0	40	56	4	0
Co/WC	0	12	26	28	34

Table 4. Spray Parameters for Plasma Spraying Experiments with Ni- and Co-Coated TiC, Cr₃C₂, TaC and WC Composite Powders

	<u>Spray Parameter (1)</u>		
	<u>A</u>	<u>B</u>	<u>C</u>
Nozzle designation	SG #1	SG #2	SG #3 (2)
cross-section opening (mm ²)	circular 16	circular 28	circular 45
Argon Plasma Gas Flow (l/min)	50	50	50

(1) Other parameters held constant:

Plasma voltage (V)	38
Plasma current (A)	700
Powder feed	
Screw (rpm)	100
Vibrator (%)	25
Carrier gas (l/min)	3.5
Spray distance (cm)	10

(2) Powder feed tube 5 mm inside nozzle opening; all other nozzles have feed tube 2 mm outside nozzle.

Table 5. Matrix Hardness, Coating Wear Resistance and Matrix Chemical Analysis of Plasma Sprayed Metal-Carbide Coatings

Powder Composition	Spray (1) Parameter	Hardness (2) (kg/mm ²)	Coating Wear (3) (mm ³)	Coating Matrix Chemical Analysis (4) (Wt %)						M (5) (%)
				Nickel		Cobalt		Refractory Metal		
				\bar{x}	σ	\bar{x}	σ	\bar{x}	σ	
60Ni/TiC40	A	430	0.10	88.0	5.7	-	-	9.7	4.6	20.1
	B	720	0.11	77.5	5.7	-	-	17.8	4.8	40.6
	C	490	0.08	71.9	7.3	-	-	22.1	5.4	53.2
19Co/TiC81	A	1000	0.10	6.4	3.5	46.5	12.1	33.9	11.0	15.0
	B	990	0.09	4.7	2.4	44.2	18.2	40.2	14.1	19.7
	C	940	0.17	5.1	3.4	33.8	11.0	49.1	9.7	28.3
48Ni/Cr ₃ C ₂ 52	A	850	0.06	71.2	5.6	-	-	22.2	4.7	30.4
	B	910	0.03	54.7	7.4	-	-	39.6	6.6	69.9
	C	1130	0.04	48.2	7.4	-	-	44.2	6.4	84.4
54Co/Cr ₃ C ₂ 46	A	710	0.10	3.6	1.2	76.4	6.9	16.1	5.6	26.0
	B	720	0.04	3.1	1.3	75.2	11.4	17.8	10.0	29.3
	C	720	0.22	3.2	1.3	68.8	3.2	23.5	3.2	30.7
40Ni/TaC60	A	500	0.07	75.6	6.4	-	-	21.0	5.9	18.8
	B	660	0.07	64.5	6.7	-	-	29.8	6.0	30.2
	C	750	0.13	64.4	7.8	-	-	32.1	7.6	33.6
42Co/TaC58	A	390	0.09	5.5	5.4	79.5	2.0	7.6	8.1	6.3
	B	620	0.06	3.7	0.7	69.1	5.9	23.4	6.2	23.6
	C	720	0.05	3.2	0.6	59.6	6.3	33.5	6.7	38.9
20Ni/WC80	A	1020	0.05	41.3	10.3	-	-	58.6	10.1	37.7
	B	1040	0.05	21.9	5.0	-	-	74.0	4.5	75.8
	C	1040	0.03	22.1	5.0	-	-	73.9	5.0	75.8
21Co/WC79	A	910	0.03	5.1	1.5	53.7	17.8	37.3	18.6	16.8
	B	1260	0.03	3.3	0.8	31.6	10.7	60.9	11.2	44.1
	C	1120	0.03	3.1	0.9	31.7	12.7	60.0	12.0	42.5

(1) See Table 4.

(2) DPH microhardness of matrix; average of 10 tests with 100 g load.

(3) LFW-1 Wear Test - Wear volume in 110 m sliding distance under 27 kg load against hardened steel ring.

(4) Electron Microprobe Analyses \bar{x} = Mean of 20 determinations; σ = standard deviation.

(5) The amount of refractory metal in solution after spraying expressed as percent of the total refractory metal present in the powder before spraying.

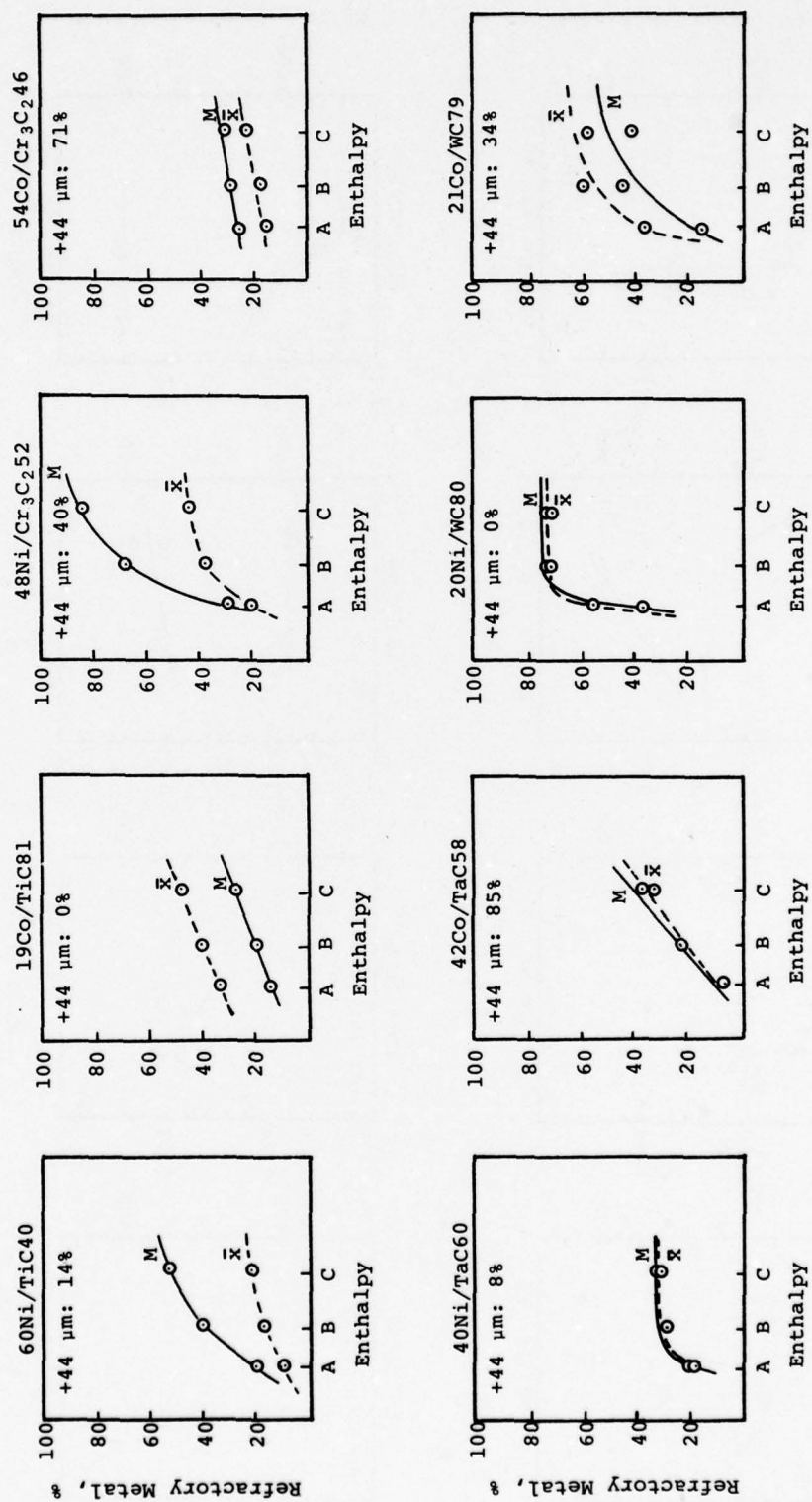


Figure 1. Dissolution of Refractory Metal (M, \bar{x}) as a Function of Enthalpy (A<B<C)

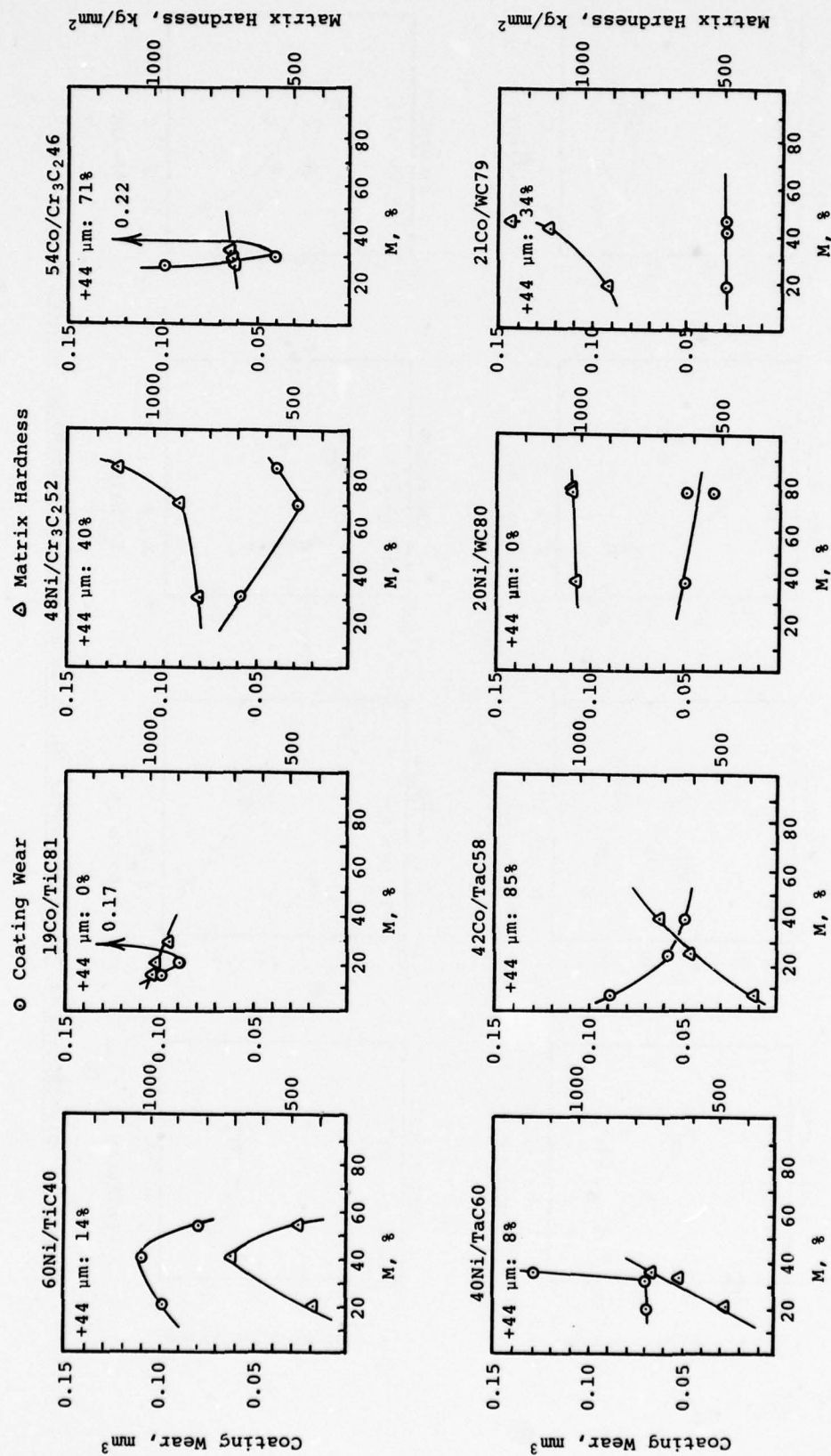


Figure 2. Matrix Hardness and Coating Wear as a Function of Percent Refractory Metal in Matrix (M)

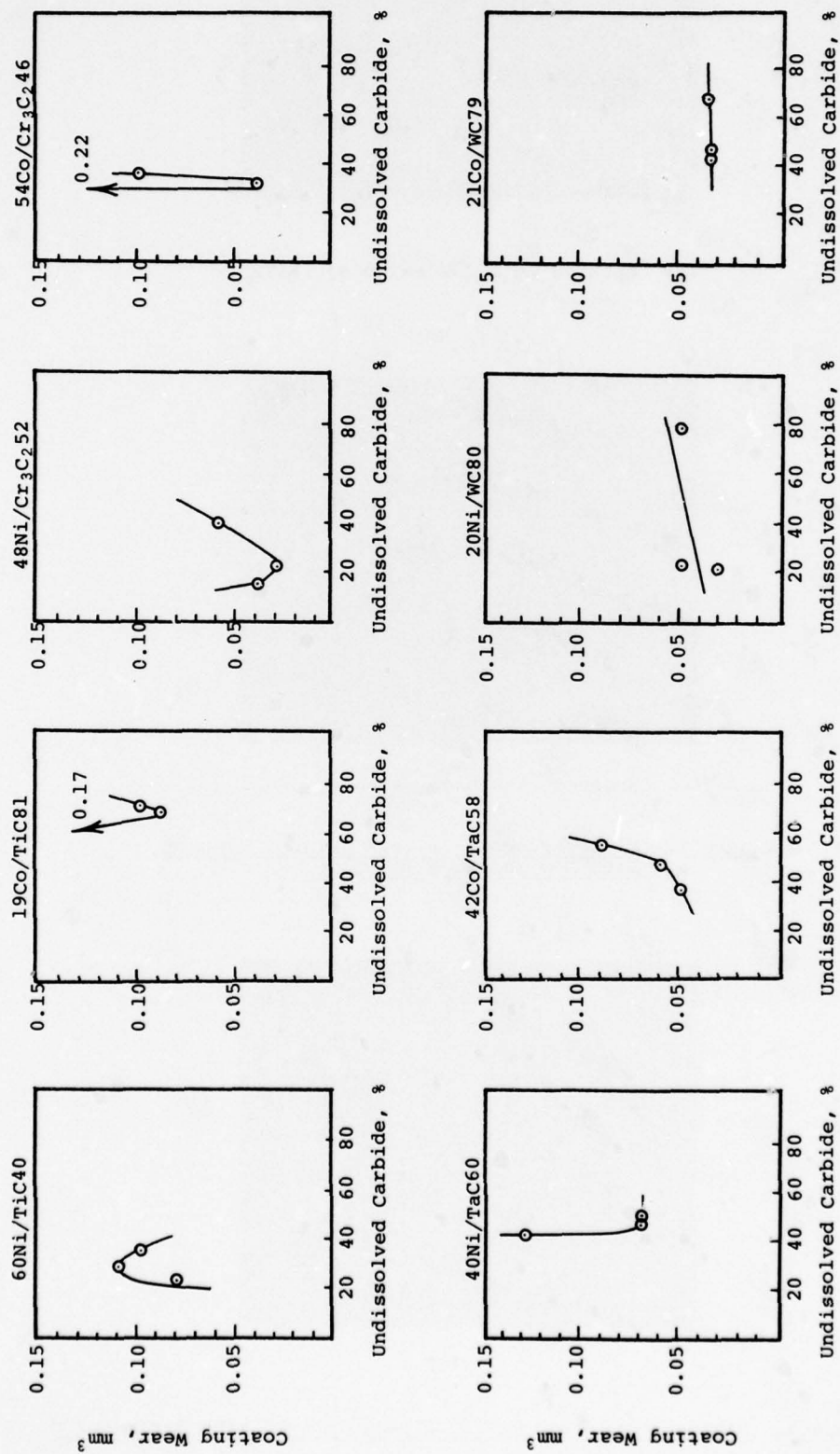


Figure 3. Wear as a Function of Percent Undissolved Carbide (vol %)

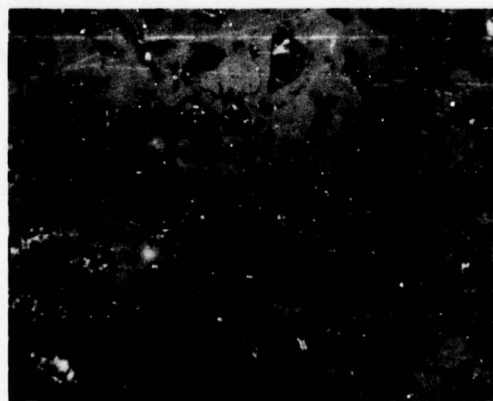


4a. Sprayed with low enthalpy, X472



4b. Sprayed with high enthalpy, X472

Figure 4. Microstructure of Co/WC Plasma Sprayed with Low and High Enthalpy



X472

Figure 5. Microstructure of Ni/TiC Plasma Sprayed with Parameter B

SURFACE TREATMENTS BY HIGH POWER LASER ON NICKEL BASE SUPERALLOYS

by

D.Bacci and S.Tosto
FIAT-Centro Ricerche
Strada Torino 50
10043 Orbassano
Italy

1. INTRODUCTION

Laser treatments are a powerful tool to perform surface treatments on materials.

These treatments allow to modify the surface structure of the sample, by changing some properties, to cladding or alloying, to make coatings or to treat coatings already performed by other methods.

The goodness of the results depends on many parameters, among them we mention: the specific power, the interaction time and the shape of the treating spot for what concerns the Laser; the thermal conductivity, the surface state and the nature of the material.

The laser treatment can be localized on the surface (for thickness up to some millimeters) without affecting the bulk. This characteristic, together with the reproducibility and rapidity of the treatments, make this technique an unique tool to confer new properties to the materials. In this paper we want to show some examples of applications of the high power laser (15 kw, 10.6 μm) to the problem of the super-alloys.

2. THE LASER TREATMENT

It is possible to show many cases in which the Laser can be employed, without competitive methods.

For example, in the case of ceramic coating (e.g. Al_2O_3) plasma-sprayed on super-alloys, the reported layer presents porosity typical of this kind of deposition, that cannot be removed by conventional heat treatments because of the higher melting point of ceramics with respect to the metallic phases.

By controlling the treating parameters it is possible to restrict the effect of the laser radiation just on the ceramic layer so that it can locally melt and compact without problems for the metal.

Also the interface can be improved in consequence of a correct treatment. Moreover, it is possible to obtain oriented surface structure with elongated grains in some preferential direction without changing the isotropy of the bulk. This could be helpful to enhance surface mechanical properties in that direction (i.e. fatigue). It is necessary to avoid laser energy loss by radiation reflection on the surface in order to reach correctly the planned working conditions. Blackening (i.e. by a graphite thin cover) and sand blasting are two commonly employed techniques. To determine the correct parameters of treatment it is necessary to know what happens when a wave train of electromagnetic energy reaches the surface of the sample to be treated.

Thermal effects on metals due to a laser beam can be theoretically treated by using Maxwell's equations for what concerns electromagnetic-waves and metals interaction and by applying the equation of heat diffusion for what concerns the temperature distributions.

As well known, a solution of Maxwell's equations at the surface of a semi-infinite solid for a normal impinging plane wave is =

$$E = E_0 \exp i\omega \left(\frac{nz}{c} - t \right) \exp \left(-\frac{K\omega z}{c} \right)$$

n = real part of complex refractive index

N = imaginary part of complex refractive index

From this equation one defines the skin depth δ for a metal

$$\delta = \frac{c}{\sqrt{2\pi\sigma\omega}}$$

where c = light velocity

σ = electrical conductivity

ω = frequency

The damping of the wave causes heating by Joule effect in the surface absorbing layer.

We can account for this heating by applying the equation

$$\frac{\partial^2 T}{\partial z^2} - \frac{1}{\alpha} = - \frac{A(z)}{K}$$

α = thermal diffusivity
 K = thermal conductivity
 z = depth inside the sample

in which we neglect variations in thermophysical properties of the material with temperature (e.g., the model doesn't take into account phase changes or melting). $A(z)$ is the heat produced for unit volume and unit time. The boundary condition to describe heat diffusion is

$$K = \frac{\partial T}{\partial z} \Big|_{z=0} = 0$$

neglecting radiative and convective losses.

It can be shown that in the case of metals, due to the fact that absorption occurs in a very narrow layer, we can handle the problem by writing

$$\frac{\partial^2 T}{\partial z^2} - \frac{1}{\alpha} \frac{\partial T}{\partial z} = 0$$

with the new boundary condition =

$$-K \frac{\partial T}{\partial z} \Big|_{z=0} = F_0$$

where F_0 is the entering power.

The well-known solution then is

$$T(z,t) = \frac{2F_0}{K} \sqrt{\frac{\alpha t}{\pi}} \cdot e^{-z^2/4\alpha t} - \frac{z}{2} \operatorname{erfc} \left[\frac{z}{2\sqrt{\alpha t}} \right]$$

$$\operatorname{erfc}(x) = 1 - \operatorname{erf}(x)$$

An example is reported in picture 1.

With $F_0 = 12.6 \text{ Kw/cm}^2$ $\alpha = 0.22 \text{ cm}^2/\text{S}$ | $K = 0.8 \text{ W/cm}^2 \text{ K/t}$ $t = 0.03 \text{ S}$

which corresponds to the case of a Nickel alloy.

Actually the laser source is not so clean as here supposed; infact because of the finite size of the beam, boundary effects around the affected zone are present; moreover, the interaction time is obtained by moving the sample during laser treatment and the rectangular shape of the beam is obtained by a fast waving of the gaussian spot with a frequency of 120 Hz in one direction and 60Hz in the other one. By moving too fast the sample under the spot one can see this sinusoidal oscillation (Fig. 2).

3. EXPERIMENTAL RESULTS

Samples of Inconel X - 750 have been submitted to laser treatments to check the possibility of performing grain refinement on the surface. This is made possible by the fast cooling of the material after laser treatment.

The grain sizes and the depth of the treated layer depend upon the power and the time of interaction between laser beam and surface.

In Fig. 3 is shown the surface structure (highly dendritic) obtained by setting a power of 22 Kw/cm^2 with interaction time of 0.2 seconds. The depth of the melted zone is about 300μ . As one can see, the dendrites are oriented toward the surface, following to the direction along which heat is lost.

Hardness measurement carried out on this sample give an increase of 10% between treated and not treated material.

Another example is shown in Fig. 4, in which refinement was obtained by different parameters = $P_w = 15 \text{ Kw/cm}^2$ $\tau = 0.570 \text{ s}$. The depth of melting was about 250μ ; Sand-blasting was always performed on the sample before laser treatment.

The same alloy (Inconel X-750) was coated by plasma sprayed Al_2O_3 and then laser treated.

Purpose of it was to improve the structure of the coating which as well-known is quite porous.

This treatment requires very different powers and interaction times; that's due to the dielectric behaviour of Al_2O_3 , whose absorption and thermophysical properties are quite different from metals.

The best results, for what concerns porosity content, were obtained with power of 4.8 Kw/cm^2 and interaction times of 0.300 s . (Fig. 5).

Also the goodness of the interface structure (between metal and Al_2O_3) was checked; cracks were not observed as in the case of not treated coating. Moreover, the effect of overlapping of contiguous scanning traces was taken into account: long cracks were detected in this zone.

With power density similar to that used in the case of metal surfaces we have got an uncontrolled melting of Al_2O_3 , with droplets formation due to surface tension phenomena and the result is an increase in porosity content. (Fig. 6).

Ni-Cr-Al

Samples of In 738 LC were coated by plasma-sprayed Ni-Cr-Al. The structure of the coating is shown in figure 7, where one can easily observe oxides and pores as well as droplets splatted by plasma-spray. As previously done, by applying the equation of heat diffusion, the laser parameters to be used were fixed: $P_w \approx 20 \text{ Kw/cm}^2$ $\tau \approx 30 \text{ ms}$. In this way only the coating is drawn to the melting point, without affecting the base material.

The results are shown in Fig. 7: it can be seen how the morphology is modified, with a very fine dendritic structure.

The treatment is not homogeneous because of the short time of interaction employed that reveals the oscillating structure of the beam, and more treatments are required to get a homogeneous treatment. In the observed coating there is no evidence of porosity or large inclusions and the interface is quite good.

Unfortunately, it must be underlined the presence of surface cracks, to be referred to thermal stresses.

The same kind of treatment was performed on In 738 LC uncoated, but only sand-blasted. Melted zones are obtained at the surface with a very fine structure, quite similar to these obtained in coated samples. (Fig. 8).

Microhardness measurements carried out in the surface zone show a slight decrease in hardness as compared to the base material (from 440 to 480HV).

CONCLUSIONS

The examples presented are sufficient to show the possibilities of the laser treatments.

As concerns the coatings of Al_2O_3 , their corrosion resistance at room temperature is well known.

The reduction of porosities avoids the diffusion of the aggressive agents through the coating and the protective action of the Al_2O_3 is enhanced.

Also in the case of metallic coatings, e.g. Ni-Cr-Al, an improvement of the performances is expected in view of the better homogeneity consequent to the treatment.

In any case it is necessary to carry out experimental tests in order to evaluate quantitatively how much the surface properties are modified.

In particular, it is interesting to study the grain boundary corrosion on laser treated surfaces and the fatigue properties of the oriented grains.

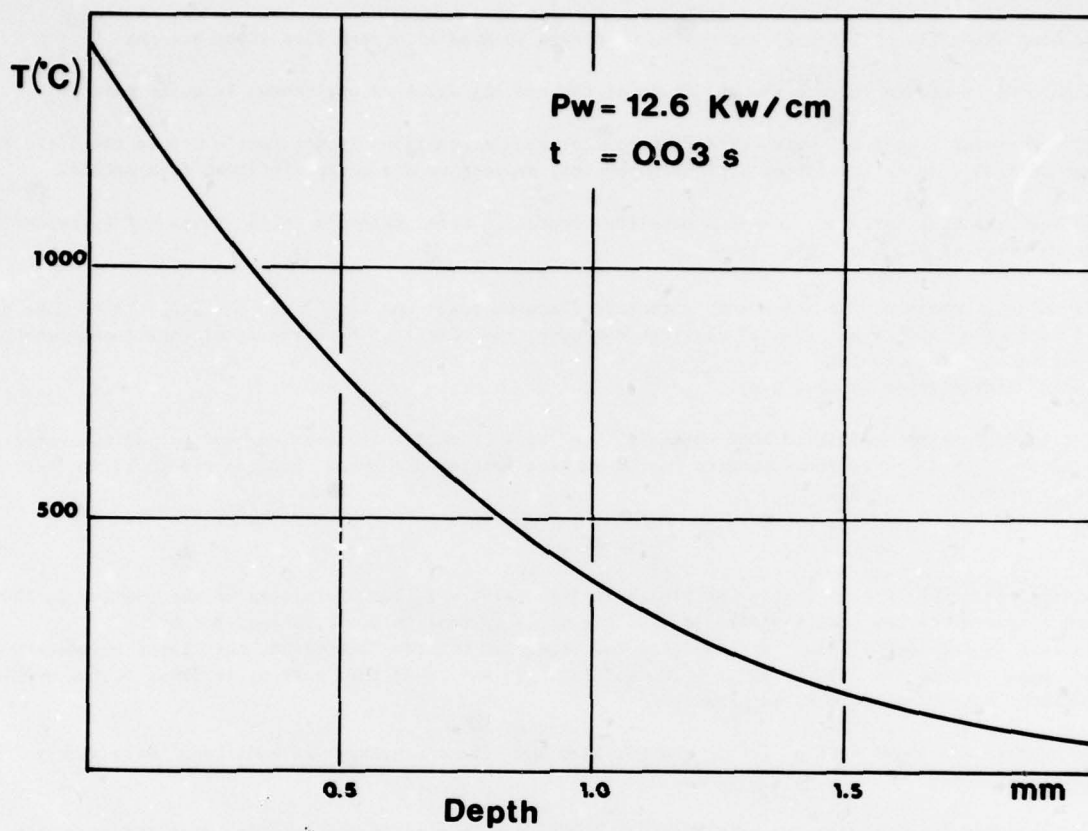
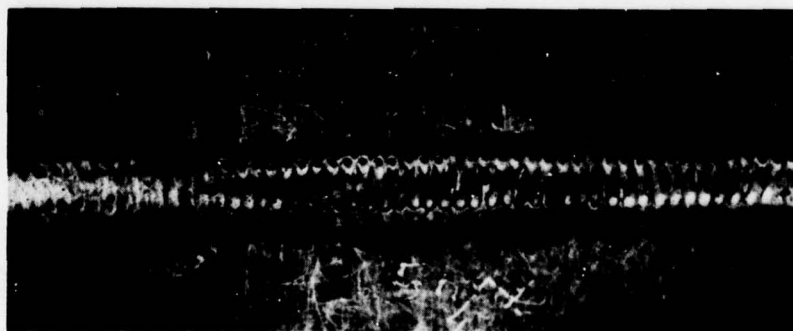
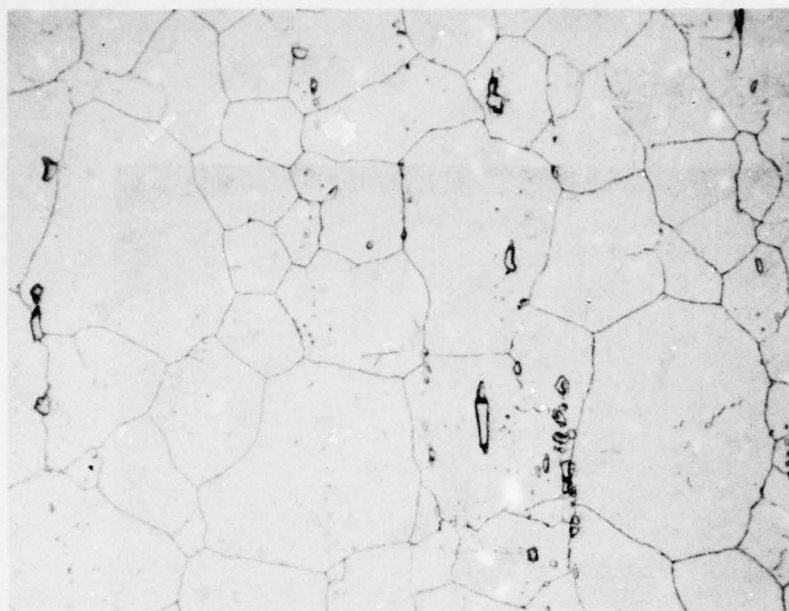


Fig. 1: Temperature distribution on the surface of a metallic sample.



1 X

Fig. 2: Laser scanning.



**base
material**

300 X



**laser
treated**

300 X

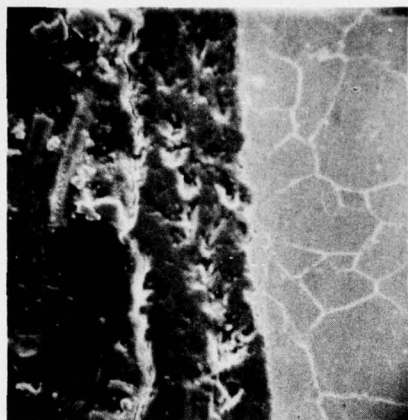
Fig. 3: Inconel X750 before and after Laser treatment.

Inconel X - 750



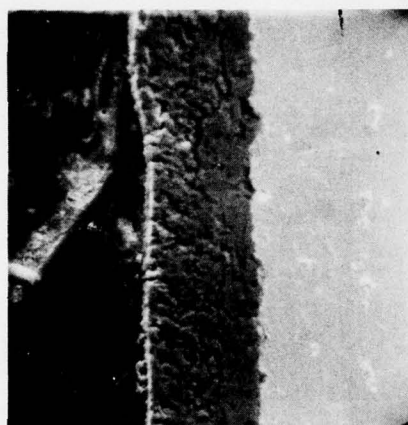
300 X

Fig. 4: Inconel X750 after Laser treatment.



**Inconel X-750
with Al₂O₃
not treated**

250 X



after laser

P=1.75 Kw v = 100 cm/min

250 X

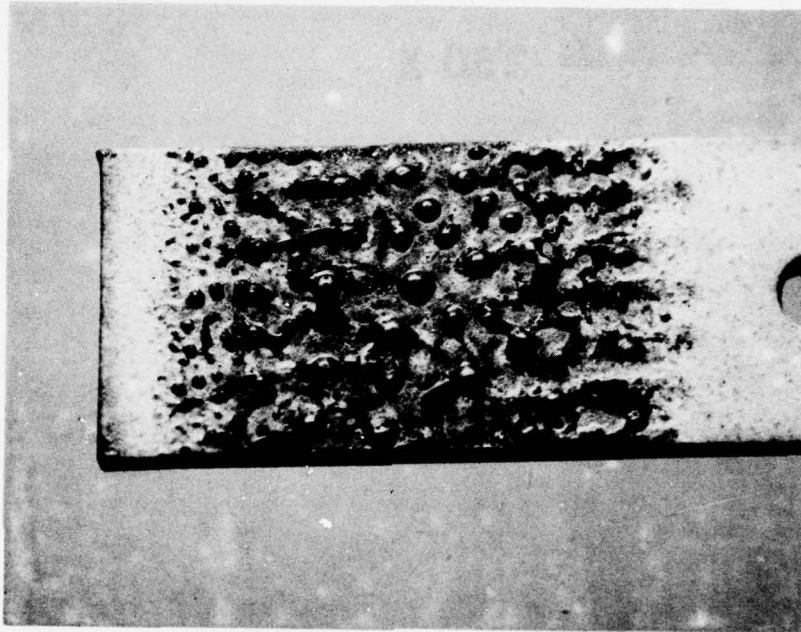


Interface

250 X

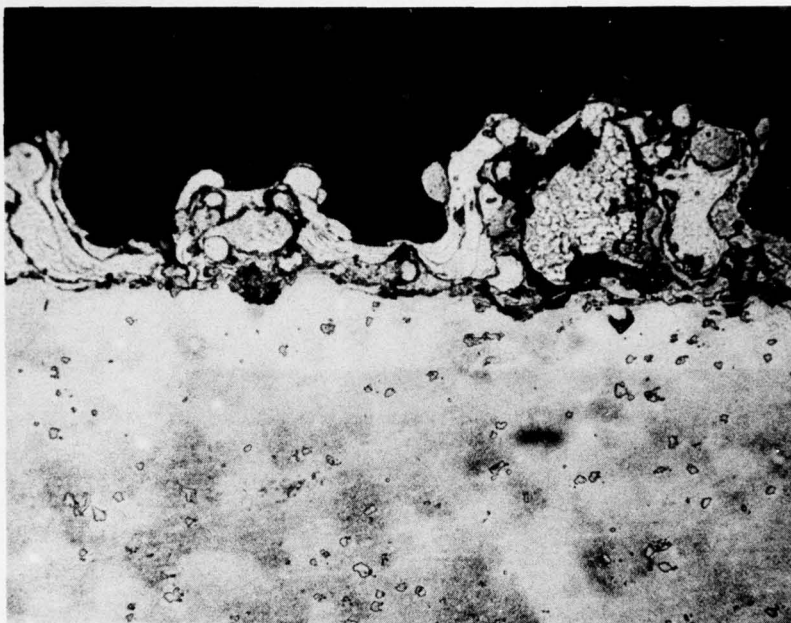
Fig. 5: Plasma sprayed Al₂O₃ coating before and after Laser treatment.

IN 738 LC with Al_2O_3



5 X

Fig. 6: Al_2O_3 coating melted on IN 738 LC after Laser treatment.



**In 738 LC
coated by
Ni-Cr-Al
plasma-sprayed**

300 X

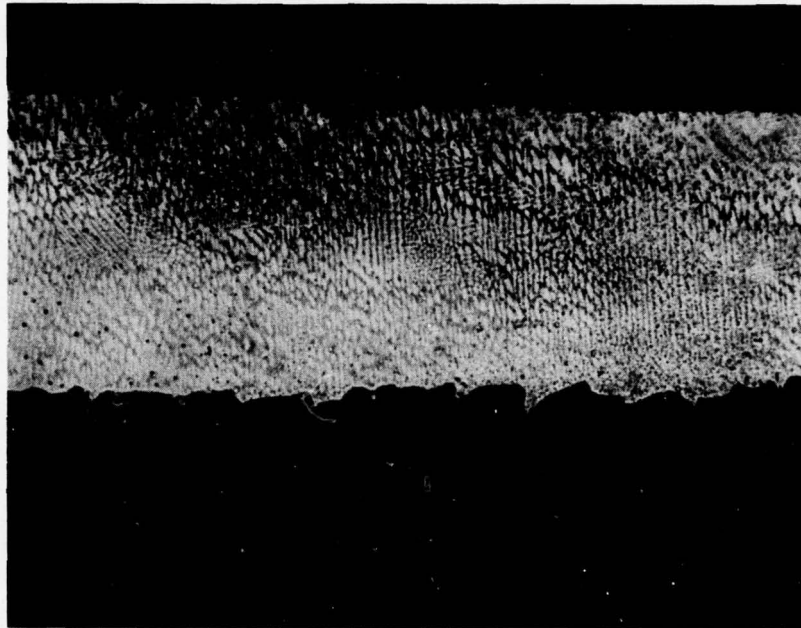


**Ni-Cr-Al
treated by laser**

500 X

Fig. 7: Plasma sprayed Ni-Cr-Al coating before and after Laser treatment.

IN 738LC



300 X

Fig. 8: In 738 LC after Laser treatment.

PLASTICITY MODELLING

Prof.G.W. Rowe
Mr. P. Hartley
Department of Mechanical Engineering,
South West Campus, The University of
Birmingham, P.O. Box 363, Birmingham,
B15 2TT, England.

SUMMARY

This paper will present a brief review of some of the more common theoretical and experimental techniques used today for the analysis of plasticity problems, with particular reference to their application in metalworking processes.

Part One deals with the well-known Slip Line Field and Upper-Bound techniques, but also discusses the more recent developments of these methods involving the use of computers. Visioplasticity, Flow Function Theory and Variational Methods are also mentioned. Recent improvements in the digital computer and the available facilities have led to the widespread use of the Finite Element Method. Its application to metal-forming problems will also be discussed.

Part Two deals with experimental work which has largely been dominated by the Visioplasticity technique and simple experiments involving the use of model materials such as plasticine and soft metals. A new technique, that of using photoelastic models to predict plastic deformation, is also discussed.

PART ONE

THEORETICAL TECHNIQUES

SLIP-LINE FIELD THEORY

The slip line field method has become one of the most popular techniques for the analysis of metal-working problems. A number of authors discuss in depth its theory and extensive applications (1-5). Although the assumptions of a rigid plastic, non-hardening material may be considered unrealistic, accurate predictions of forces and metal flow can be obtained. The first step in the slip-line field approach is to identify the deforming areas of the specimen. This is done by constructing a network of orthogonal lines. The path of the lines is indicated from the directions of the maximum shear stress, (assumed to coincide with the directions of maximum shear strain rate). The limits of the network or field are determined from the surface boundary conditions, (friction or shear stress), and the geometry of the process. The extent of the field defines the plastic zones. If the lines whose clockwise rotation is towards the areas of highest pressure are referred to as α -lines and the orthogonal ones β -lines, the following well-known relationships between local hydrostatic pressures p and the rotation of the lines ϕ apply.

$$\begin{aligned} dp + 2k.d\phi &= 0 & \text{---}\alpha\text{-line} & \text{----- (1)} \\ dp - 2k.d\phi &= 0 & \text{---}\beta\text{-line} & \text{----- (2)} \end{aligned}$$

Similarly for the velocity distribution,

$$\begin{aligned} du - v.d\phi &= 0 & \text{---}\alpha\text{-line} & \text{----- (3)} \\ dv - u.d\phi &= 0 & \text{---}\beta\text{-line} & \text{----- (4)} \end{aligned}$$

With the simple relationships in Eq.(3) and Eq.(4) the slip-line field method is powerful for the analysis of metal flow problems. The velocity distribution is however, more commonly assessed by a much quicker graphical method. Figure 1 illustrates a typical slip-line field. Slip-line fields have been found to be of use in the study of metal cutting, an area in which strain-hardening is of some importance. The influence of this phenomenon has been included in the following relationships (6),

$$dp + 2k.d\phi - \frac{\partial k}{\partial s_\beta} \partial s_\alpha = 0 \quad \text{---}\alpha\text{-line} \quad \text{----- (5)}$$

$$dp - 2k.d\phi - \frac{\partial k}{\partial s_\alpha} \partial s_\beta = 0 \quad \text{---}\beta\text{-line} \quad \text{----- (6)}$$

The preceding formulae, Eqs.(1-6) apply to plane-strain only, but since axi-symmetric conditions are common in practice attempts have been made to incorporate the slip-line approach into these areas. The resulting relationships, given below, are somewhat complex and have not found common use.

$$dp + 2k.d\phi + (\sigma + p - k.Cot\phi) \frac{dr}{r} = 0 \quad \text{---}\alpha\text{-line} \quad \text{----- (7)}$$

$$dp - 2k.d\phi + (\sigma + p - k.Tan\phi) \frac{dr}{r} = 0 \quad \text{---}\beta\text{-line} \quad \text{----- (8)}$$

To avoid this complexity Thomsen and Frisch (7) and Rowe and Hartley (8) used plane-strain slip-line fields to approximate to the working loads and flow patterns respectively in axial-symmetry.

The rapid development of the computer has been the stimulus for much of the more recent developments in the use of slip-line fields. Dewhurst and Collins (9) formulated a matrix technique which required a computer to perform the large number of calculations required. Dodd and Osakada (10) presented an analysis of wedge indentation, using a computer to determine and draw the slip-line fields for wedges at various angles. Computers have also been used to draw slip-line fields at various stages of deformation in backward extrusion (11). Work by Rowe and Li (12, 13) shows slip-line field solutions prepared by computer for constant friction and constant interface shear. It is important to note that slip-line field solutions are unique only to an instantaneous step in the deformation, since even small changes of shape may result in a change in the boundary conditions. This may be overcome, with the aid of a computer, by reassessing the slip-line field after each small increment of deformation in order to develop a solution for a large range of deformation (8).

UPPER BOUND THEORY:

The upper-bound method (14) has primarily been used for the analysis of forming loads. The inherent assumption is that the work done in forming is equal to the dissipation of internal energy together with frictional work. If the stress system is thus deduced from an assumed mode of deformation the forces will be equal to or greater than those actually required; the solution is thus an upper-bound. If the rate of dissipation of internal energy is denoted by \dot{E} , then the internal energy can be expressed as, (2),

$$\dot{E} = \int_V \bar{\sigma} \dot{\epsilon} dv + \int_S \tau u ds \quad \text{----- (9)}$$

The first term in the expression represents the work done within a homogeneously deforming zone and the second term represents the work rate along a velocity discontinuity or along a surface. Since the external work is a function of the applied load, equating Eq.(9) with an expression for the work done will enable the load to be evaluated. In order to ascertain the internal energy with reasonable accuracy the billet is divided into a number of sections, each being analysed separately. Kudo (15) established a method where the billet is divided into a number of rigid triangles, Fig.(2). The arrangement of these which resulted in a minimum internal energy dissipation was considered as the most accurate. The velocity field must, of course, be self consistent and satisfy the velocity boundary conditions. The assumption of rigid zones within which there is no deformation must result in the first term of Eq.(9) being equal to zero. In the second term, τ is equal to zero for a frictionless interface or k for an internal shear line or sticking surface. This results in the simplification of Eq.(9) for velocity discontinuities under plane strain conditions to the following,

$$\dot{E} = \sum_{i=1}^n k u_i \quad \text{----- (10)}$$

The upper bound technique has been adapted for axially symmetric problems (16). In this case the rigid triangles or other shapes are constructed on diametral sections. Kobayashi (17,18), improved the axisymmetric technique by considering rigid triangles with curved rather than straight boundaries. McDermott and Brawley (19) have proposed a similar approach. Chen and Ling (20), in their examination of axisymmetric problems, extended the method to look at cosine, elliptic and hyperbolic shaped dies. Another extension of the method has been proposed by Johnson and Kudo (21) who used the upper bound approach to evaluate the temperature distributions in axis-symmetric extrusion. This was done by considering a relationship between the temperature changes and the internal energy.

Although the upper-bound method has been used very successfully in the analysis of forming loads, its application to study metal flow has been somewhat limited. This is mainly because the division of the billet into relatively large rigid zones does not allow any detailed analysis and the resulting solutions are not necessarily unique. Adie and Alexander (22) improved this situation a little by introducing a graphical method for determining the velocities in each rigid unit.

VISIOPLASTICITY:

The visioelasticity method (23) is a technique for evaluating the stress distributions in forming problems from the experimental observations of the metal flow. The experimental work, which will be discussed in detail in part 2, consists of determining the nodal displacements of a square grid etched onto the billet in the plane of interest. The theoretical part of the analysis proceeds once the nodal point displacements have been established; From these results the velocity and strain-rate distributions can be evaluated. The following formulae, derived from the equilibrium equations and the Levy-Mises plasticity equations, can be applied (2), for rigid-plastic material in plane-strain,

$$\sigma_x = \frac{2}{3} \int_{y_1}^y \left[\frac{\partial}{\partial y} \left(\frac{\dot{\epsilon}_x}{\dot{\epsilon}/\bar{\sigma}} \right) - \frac{1}{2} \frac{\partial}{\partial x} \left(\frac{\dot{\gamma}_{xy}}{\dot{\epsilon}/\bar{\sigma}} \right) \right] dy - \frac{1}{3} \int_{x_0}^x \left[\frac{\partial}{\partial y} \left(\frac{\dot{\gamma}_{xy}}{\dot{\epsilon}/\bar{\sigma}} \right) \right]_{y=y_1}^{y=y_0} dx + (\sigma_x)_{y=y_1}^{y=y_0} \quad \text{----- (11)}$$

and for axial-symmetry;

$$\sigma_z = \frac{2}{3} \int_{r_1}^r \left[\frac{\partial}{\partial r} \left(\frac{\dot{\epsilon}_z - \dot{\epsilon}_r}{\dot{\epsilon}/\sigma} \right) - \frac{\dot{\epsilon}_r - \dot{\epsilon}_\theta}{\dot{\epsilon}/\sigma} - \frac{1}{2} \frac{\partial}{\partial z} \left(\frac{\dot{\gamma}_{zr}}{r\dot{\epsilon}/\sigma} \right) \right] dr$$

$$- \frac{1}{3} \int_{z_0}^z \left[\frac{\partial}{\partial r} \left(\frac{\dot{\gamma}_{zr}}{\dot{\epsilon}/\sigma} \right) + \frac{\dot{\gamma}_{zr}}{r\dot{\epsilon}/\sigma} \right] dr + (\sigma_z)_0 \quad \text{----- (12)}$$

Thus the stress distribution for plane strain axial-symmetry can be evaluated. Two methods of solution of equations (11) and (12) may be used; (a) a graphical method (23) and (b) a mathematical approximation technique (24).

(a) Graphical method: If the axial and radial velocities are U and V , and the axial and radial distances are z and r respectively, then four graphs can be drawn. (i) $u - r$ (ii) $u - z$ (iii) $v - r$ (iv) $v - z$. The slopes of these curves may then be used to evaluate the various strain rates, i.e.

$$\dot{\epsilon}_z = \frac{\partial u}{\partial z}; \quad \dot{\epsilon}_r = \frac{\partial v}{\partial r}; \quad \dot{\gamma}_{zr} = \frac{\partial v}{\partial z} + \frac{\partial u}{\partial r}$$

Further graphs of strain rate against radial position may then be plotted and the generalised strain and stress evaluated. The formulae in Eq.(11) and Eq.(12) may then be solved.

This somewhat tedious and lengthy operation has been greatly improved by the use of a computer to determine the various solutions (25, 26).

(b) Mathematical approach: The initial step in this technique is to approximate the experimental flow lines with a sixth order polynomial expression.

Taking the case of axial symmetry as an example; if a function ψ , is defined as the rate of volume flow through a circular cross-section of radius r , then;

$$\psi = 2\pi \int_0^r r u dr \quad \text{----- (13)}$$

the axial velocity may then be written

$$u = \frac{1}{2\pi r} \cdot \frac{\partial \psi}{\partial r} \quad \text{----- (14)}$$

Since there is no volume change in plastic deformation the flow function must be constant at any interface or free surface. If it is assumed that in steady flow the total volume passing between any two stream lines will be constant for all positions along the axis then:

$$d\psi = \left(\frac{\partial \psi}{\partial r} \right) dr + \left(\frac{\partial \psi}{\partial z} \right) dz = 0 \quad \text{----- (15)}$$

Since it is possible to determine ψ as a function of r and z , the axial and radial velocities and hence the strain and stress distributions can be evaluated.

FLOW FUNCTIONS:

A drawback of the viscoplasticity method is the need for an initial experiment to be performed. Shabaik (27, 28) attempted to avoid this problem by developing a purely theoretical approach. If the velocity components u, v , are expressed in terms of a function ϕ , referred to as the flow function, this will yield,

$$u = \frac{\partial \phi}{\partial y}, \quad v = - \frac{\partial \phi}{\partial x} \quad \text{----- (16)}$$

The strain rates and stress components can also be expressed in terms of the flow function and substitution of the various terms into the equilibrium and plasticity formulae will yield,

$$\frac{\partial^2}{\partial x \partial y} \left(\frac{2}{\lambda} \frac{\partial^2 \phi}{\partial x \partial y} \right) + \frac{\partial^2}{\partial y^2} \left[\frac{1}{2\lambda} \left(\frac{\partial^2 \phi}{\partial y^2} - \frac{\partial^2 \phi}{\partial x^2} \right) \right] - \frac{\partial^2}{\partial x^2} \left[\frac{1}{2\lambda} \left(\frac{\partial^2 \phi}{\partial y^2} - \frac{\partial^2 \phi}{\partial x^2} \right) \right] = 0 \quad \text{----- (17)}$$

$$\text{where } \dot{\lambda} = \frac{3}{2} \cdot \frac{\dot{\epsilon}}{\bar{\sigma}}$$

Thus evaluating the flow function at any position will yield the velocity, strain rate and stress distributions. Although the results of this method show very good agreement with those revealed by experiment (Fig.3) it has found very little use except in analyses of forward extrusion.

FINITE ELEMENT ANALYSIS:

The finite element method (29) is the most recent theoretical approach to be used for the solution of metalforming problems. Originally developed for the solution of elastic problems, particularly in the aircraft industry, its use has now spread to many other fields. The diversity of finite element applications has closely accompanied the rapid development of the digital computer and a number of authors have applied the technique to metalforming (30 - 43).

The finite element method basically consists of four steps:

- (i) the model is divided into a number of discrete elements
- (ii) the stiffness matrix for each element and subsequently the complete model is established.
- (iii) applied forces and boundary conditions are imposed and the resultant displacements of each element nodal point is determined
- (iv) further information such as the stress and strain distributions may then be evaluated.

The strain within a simple triangular element can be related to the nodal point displacements by first assuming a linear relationship of the form,

$$u = \alpha_1 + \alpha_2 x + \alpha_3 y \quad \text{----- (18)}$$

$$v = \alpha_4 + \alpha_5 x + \alpha_6 y \quad \text{----- (19)}$$

where α_{1-6} are constants.

The strain components can thus be related to the nodal point displacements in the following form,

$$\{\epsilon\} = [B]\{q\} \quad \text{----- (20)}$$

Where $[B]$ is a matrix whose coefficients are determined from the local co-ordinate system of the element.

The stress-strain relationship for elasticity is given by,

$$\sigma_{ij} = \frac{E}{1+\nu} (\epsilon_{ij} + \delta_{ij} \frac{\nu}{1-2\nu} \epsilon_{kk}) \quad \text{----- (21)}$$

Which in matrix form is,

$$\{\sigma\} = [D]\{\epsilon\} \quad \text{----- (22)}$$

For plastic deformation incremental stress strain is needed which necessitates the inclusion of the plastic component,

$$d\epsilon'_{ij} = \sigma'_{ij} d\lambda + \frac{d\sigma'_{ij}}{2G} \quad \text{----- (23)}$$

where $d\lambda = \frac{3}{2} \cdot \frac{d\bar{\sigma}}{\bar{\sigma}H}$

Incorporating the Mises yield criterion, $\sigma'_{ij} \sigma'_{ij} = \frac{2}{3} \bar{\sigma}^2$

The incremental stress-strain relationship can be written as,

$$d\sigma_{ij} = \frac{E}{1+\nu} (d\epsilon_{ij} - \delta_{ij} \frac{\nu}{1-2\nu} d\epsilon_{kk} - \sigma'_{ij} \frac{\sigma'_{KL} d\epsilon_{KL}}{S}) \quad \text{----- (24)}$$

where, $S = \frac{2}{3} \bar{\sigma}^2 \{1 + \frac{H'}{3G}\}$

or in matrix form,

$$\{\Delta\sigma\} = [D] \{\Delta\epsilon\} \quad \text{----- (25)}$$

Now, if a virtual displacement $\{\delta q\}$ is applied to the nodes then the external work done by the applied forces $\{Q\}$ can be equated to the internal work,

$$\{Q\}\{\delta q\} = \int \{\sigma\}\{\delta\epsilon\}^T dv \quad \text{----- (26)}$$

Substitution of Eqs.(20) and (22) in (26) will yield,

$$\{Q\} = [B]^T [D] [B] V_e \cdot \{q\} \quad \text{----- (27)}$$

or

$$\{Q\} = [K] \{q\} \quad \text{----- (28)}$$

for a linear elastic process, and similarly,

$$\{\Delta Q\}_i = [K]_{i-1} \{\Delta q\}_i \quad \text{----- (29)}$$

for the incremental elastic-plastic relationship.

The above method has been used in the analysis of extrusion-forging (34), Fig.(4), plane strain and axi-symmetric compression (35, 36), hydrostatic extrusion (37), and flat punch indentation (38). Various details such as internal flow, change of shape, stress and strain distributions and working loads have been considered. Gordon and Weinstein (39) adopted a slightly different approach in their analysis of plane-strain drawing by developing the force-displacement relation in the form,

$$[\Delta F] + [\Delta T] = [K] \{\Delta U\} \quad \text{----- (30)}$$

where $[\Delta F]$ and $[\Delta T]$ are defined as the applied forces and surface tractions respectively. Kobayashi et al. (40 - 42) have introduced a rigid-plastic analysis in the form of a matrix method which was used to analyse axi-symmetric compression of cylinders, cold heading (Fig. 5), and ring compression. The method required an iterative-incremental approach which involved the minimisation of a function ϕ , where,

$$\phi = \int_V \bar{\sigma} \dot{\epsilon} dv + \int_V \lambda C^T \dot{\epsilon} dv - \int_S T^T u ds \quad \text{----- (31)}$$

Sharman (43) used an approach whereby plastic deformation was approximated by use of the elasticity relations, assuming Poissons ratio ≈ 0.5 :

i.e. $\epsilon_{ij} = \frac{3}{2E} \{ \sigma_{ij} - \delta_{ij} \cdot \frac{\sigma_{KK}}{3} \} \quad \text{----- (32)}$

However with $\nu = 0.5$, the formulation could not be solved because $(1 - 2\nu)$ appears in a denominator, ν was therefore approximated close to, but not equal to 0.5. A reasonable analysis of the stress and strain distributions in forward extrusion was presented with $\nu = 0.49999$.

VARIATIONAL METHODS

The calculus of variations can be applied to metal-working in various ways, one of which is the upper-bound technique described earlier. A promising method recently applied in engineering (44, 45) uses weighted residuals. An approximate solution is postulated and progressively improved by finding

functions that minimise residual errors.

The problem is set up in terms of integral or differential equations and a solution is postulated that should be consistent with boundary conditions and the stress-strain relationship for the material.

For example, the differential equations may be given as

$$D_1 [f(x)] = f_1(x) \text{ and } D_2 [f(x)] = f_2(x) \quad \text{-----}(34), (35)$$

respectively in the body continuum and at the boundaries. A trial function $f^*(x)$ is postulated in terms of discrete position co-ordinates x .

$$f^*(x) = \sum_{i=1}^n A_i \phi_i(x) \quad \text{-----}(36)$$

This must satisfy the continuity equations,

$$\dot{\epsilon}_r + \dot{\epsilon}_\theta + \epsilon_z = \frac{\partial \dot{u}}{\partial r} + \frac{\dot{u}}{r} + \frac{\partial \dot{v}}{\partial z} = 0 \quad \text{-----}(37)$$

and the stress equations,

$$\frac{\partial \sigma_r}{\partial r} + \frac{\partial \tau_{rz}}{\partial z} + \frac{\sigma_r - \sigma_\theta}{r} = 0 \quad \text{-----}(38)$$

and,

$$\frac{\partial \tau_{rz}}{\partial r} + \frac{\partial \sigma_z}{\partial z} + \frac{\tau_{rz}}{r} = 0 \quad \text{-----}(39)$$

for the deforming body, but it will in general differ from the time continuous function $f(x)$, the error or residual being,

$$E(x) = \sum A_i D_1 [\phi_i(x)] - f(x) \quad \text{-----}(40)$$

which depends on the function ϕ and the choice of parameters A_i . The function of discrete variables is then modified by selecting weighting factors w_i to reduce the error as nearly as possible to zero.

$$\int_V w_i(x) \cdot E(x) \cdot dv = 0 \quad \text{-----}(41)$$

Using a least squares method, with variables A_i , this is equivalent to finding

$$\frac{\partial}{\partial A_i} \int_V E^2(x) \cdot dv = 0 \quad \text{-----}(42)$$

so,

$$w_i(x) = \frac{\partial}{\partial A_i} [E(x)] \quad \text{-----}(43)$$

giving the individual weighting factors.

The process is lengthy and requires considerable computation, but complete solutions have been obtained (46).

PART TWO

EXPERIMENTAL TECHNIQUES

Metallforming experiments may be divided into two categories,

- (i) Observation of internal deformation, from which stress and strain distributions and other details may be obtained.
- (ii) Simulation of metallforming processes by the use of cheaper and softer model materials in order to predict deformation characteristics in the actual process.

(i) OBSERVATION OF INTERNAL DEFORMATION

This area of experimental work may again be subdivided,

- (a) observation by means of grids marked on relevant sections prior to deformation;
- (b) observation subsequent to deformation by etching the deformed surfaces.

(a) Observation by preformed grids.

This approach basically consists of preparing specimens in two halves with a grid marked on one of the mating surfaces. Examination of the grid after a small increment of deformation illustrates how the material has moved, which leads to an analysis of the stress, strain and velocity distributions. Methods adopting this type of approach are normally referred to as viscoplasticity techniques. One of the earliest developments of this method was that of Thomsen and Lapsley (47). In their examination of axisymmetric forward extrusion, a lead billet was cut in half along its axis. A regular square grid was then scribed onto one of the mating meridian surfaces. The two halves of the billet were then replaced in the die and a small increment of deformation applied. When the billet was removed, and the halves separated, the internal flow was clearly revealed. The displacements of the grid intersection points from their initial positions were then used to determine the stress, strain-rate and velocity distribution through the specimen. The procedure for determining the various values is that given in section one of this paper. Processes such as extrusion-forging (48), (Fig. 2), rolling (49), drawing (50), forging (51) and even machining (52) have been examined by the use of square grids. In each case the grids were prepared by cutting or scribing the complete grid onto one surface. In order to reduce the surface deformation caused by this type of preparation, Hamed (53) prepared his specimens for backward extrusion with horizontal grid lines on one half and vertical grid lines on the other. When the two halves were reassembled a complete square grid was formed. A much improved technique, called the photo-resist method (54, 55), has recently been developed. This involves the preparation of a grid on the mating surface using a photographic technique which almost completely removes any surface deformation. The mating surface of each half of the billet must be carefully ground flat and highly polished, normally finishing with 1µm diamond powder on the hard plate to avoid rounding of the edges. One of the specimen halves is then prepared for the photographic process by degreasing in 5% NaOH followed by immersion in 35% HNO₃. The polished surface is then washed, allowed to dry and, under red or yellow light, coated with a 2:1 mixture of a commercial 'metal etching reagent' and thinners. The thickness of the film must be kept as uniform as possible, usually helped by spinning the specimen when the solution is applied. When dry a negative of the required grid is held in tight contact against the surface and exposed under ultra violet light. The emulsion is then developed in a commercial developer followed by washing and drying. When the specimen has cooled the surface is etched with a 10% NaOH solution. The final grid of hardened emulsion is thus clearly revealed. When a small increment of deformation is then applied to the reassembled specimen, the half without the grid reveals the highly deformed plastic regions, while detail can be measured from the grid. A similar approach has been used by Rowe and Shin (2, 56) to determine slip-line fields experimentally. This uses a circular rather than a square grid (Fig. 6), also prepared by the photo-resist techniques. During a small increment of deformation the circles will deform into ellipses whose major axes are assumed to coincide with the direction of principal strain. Using a large magnification, small lines are drawn at the centre of each ellipse at 45° to the direction of principal strain. The lines drawn give the direction of maximum shear strain assumed to coincide with the directions of maximum shear strain rate and maximum shear stress. By following the direction indicated at each ellipse centre, a complete experimental slip line field may be drawn. Slip-line fields prepared in this manner on work-hardened aluminium show extremely close correlation the those predicted theoretically.

(b) Observation by etching subsequent to deformation

Etching a section of a billet subsequent to the deformation will obviously not provide the detail evident in the previous technique. However, etching to reveal the grain or fibre structure can delineate areas of high deformation, the homogeneity of the specimen and the approximate strain distribution. This method of studying the billet after deformation is very common. Hopson et al. (54) studied metal flow in forward extrusion by etching their aluminium specimens by immersion in a solution of 10-20% HNO₃ and 2-5% HF for 10-20 seconds. This clearly revealed the deformed fibre structure. Shah and Kobayashi (41) also examined the fibre structure in their steel specimens for cold heading. The solution used was one of 50% HCL, hot-etching for about 30 minutes. Li (13) and Shin (58) examined areas of high deformation in aluminium specimens by observing the grain structure revealed by etching for 2 hours at 550°C. 'Frys' Reagent, (180 ml. HCL, 100 ml. H₂O, 45 gm. Cupric Oxide), has been used frequently to etch high nitrogen steel specimens, which reveals any yielded areas as well as the localised yielding on these areas. The yielding areas occur in bands referred to as Lüders lines; close correlation can be demonstrated between the Lüders lines and slip line field solutions (58), (Fig. 7).

(ii) SIMULATION OF METALLFORMING PROCESSES

Two approaches may be used here;

- (a) consideration of an actual metallforming process, but using a replacement material which is much softer and cheaper while displaying similar deformation characteristics.
- (b) use of a simulative model process, as in the photoelastic technique, in an attempt to predict

deformation characteristics by a simplified experiment.

(a) Model Materials

Many different model materials have been used to simulate actual metalforming processes. Soft metals such as aluminium (59), lead (60), copper and copper-nickel alloys (61), have found common use. Non metallic materials such as plasticine (62, 63), paraffin wax (64), and some thermoplastic materials such as polyethylene and polypropylene (65), have been used. The thermoplastic materials however were not very successful, while the plasticine and paraffin wax are very good closely representing non-hardening metals. Some authors (66) have shown that the paraffin wax can be etched, showing a close resemblance to the grain deformation in steel. Danckert and Wanheim (67) have recently developed a new type of wax, referred to as 'slipline wax'. Their wax specimens were prepared and then left for a period of time during which the wax developed a surface coating. Upon subsequent deformation the coating displayed a series of cracks which followed paths very closely resembling theoretical slip-lines.

(b) Photoelasticity

Photoelasticity has for many years been used for the analysis of stress distributions in components or structures suffering elastic deformation. Recently, fairly successful attempts have been made to predict stress distributions in dies and billets for a metalforming process, which obviously involves plastic deformation. The photoelastic models were prepared to the same geometry as the billet at the required deformation and then given a small elastic deformation (68, 69). An interesting development in this field is the use of the technique to predict experimental slip-linefields (55, 58). The model is prepared as before, but instead of plotting the stress distribution from the isochromatics, a plot of the isoclinic pattern is drawn. The complete distribution of the isoclinic lines across the specimen is obtained by rotating the plane of polarisation through a small angle and plotting the new positions of the isoclinics at each angular movement. The loci of constant inclination of the principal strain directions can thus be found, and hence the maximum shear strain direction. An experimental 'slip-line field' showing maximum shear stress directions can thus be drawn. Although there is an implicit assumption that the directions of maximum shear do not change in the transition to plastic deformation, very good correlation is found with the results from viscoplasticity experiments (56), (Fig. 8). Recent work by Tan (70) supports this view. Tests were conducted with gelatine specimens with up to 30% deformation with no significant variations in the isoclinic patterns. Ohashi et. al. (71, 72), examined the stress distribution in strip drawing by making use of the different properties of different photoelastic materials. In their experiments, celluloid was used for the workpiece and araldite for the die. At certain temperatures the celluloid would become plastic while the araldite remained elastic. This had the advantage of allowing a stress analysis in both the die and workpiece where the conditions more accurately simulate real conditions.

CONCLUSION

The most important theoretical techniques available have been briefly reviewed and though each would seem to have much to offer, they also have their own inherent restrictions.

The slip-line field method can be used to determine accurately the working forces and the internal deformation under plane-strain conditions. However assumptions such as a rigid-plastic, non-hardening material must be made. The technique can be used for axial-symmetry in only an approximate manner, and hardly at all for general three-dimensional problems. The Upper Bound method, whilst providing a quick and easy method for evaluating forces in plane-strain and axial-symmetry, can only provide a very rough approximation to the flow mechanism. The viscoplasticity method is one which can only be applied subsequent to performing an experiment and hence cannot be of a predictive nature. One advantage however, is that the influence of various boundary conditions can easily be assessed without the need to introduce any modifications to the theory. The flow-function approach has yet to be developed to consider non-steady problems, which are obviously predominant in metalforming.

Variational methods are in principle detailed and powerful, but like all matrix analyses, require extensive computer time and capacity. The finite element method seems to hold much promise at the moment, with its facilities for including the effects of variations in the material properties, temperature and boundary conditions. It can be used to predict, in detail, the internal deformation, working loads, and the homogeneity and distribution of properties of the final product. The main disadvantage at the present time is the need for computer programs with large storage and running time. It would appear that, until commercial packages are available, users would need to co-operate with academic institutions who have the expertise and access to a sufficiently large computer.

Current experimental techniques have also been briefly reviewed. There are clearly a number of reasonably simple methods available from which detailed information relating to the actual process can be obtained. The photoelastic method is a novel development which can be used to predict deformation characteristics from a very simple test.

be

REFERENCES

- (1) R. HILL: "The Mathematical Theory of Plasticity" Oxford University Press (1964)
- (2) G.W. ROWE: "Principles of Industrial Metalworking Processes" Edward Arnold (1977)
- (3) W. JOHNSON, R. SOWERBY, J.B. HADDOW: "Plane Strain Slip-line Fields: Theory and Bibliography" Edward Arnold (1970)
- (4) W. JOHNSON, H. KUDO: "The Mechanics of Metal Extrusion" Manchester University Press (1962)
- (5) H. FORD: "Advanced Mechanics of Materials" Longmans (1963)
- (6) L.E. FARMER, P.L.B. OXLEY: "A Slip-line Field for Plane Strain Extrusion of a Strain Hardening Material" J. Mech. Phys. Sol., 19, pp 369 - 388, (1971).
- (7) E.G. THOMSEN, J. FRISCH: Trans. ASME, 80, p117, (1958)

- (8) G.W. ROWE, P. HARTLEY: "A Computer Analysis of Progressive Deformation in Extrusion-Forging" Proc. 5th NAMRC Conf., Massachusetts, (1977).
- (9) P. DEWHURST, I.F. COLLINS: "A Matrix Technique for Constructing Slip-line Field Solutions to a class of Plane Strain Plasticity problems" Int. J. Num. Meth. Engg., 7, pp 357 - 378, (1973).
- (10) B. DODD, K. OSAKADA: "A Note on the type of Slip-line Field for Wedge Indentation determined by Computer" Int. J. Mech. Sci., 16 pp 931 - 938, (1973).
- (11) P. HARTLEY: "Metal Flow and Homogeneity in Extrusion-Forging" M.Sc. Thesis (Qual.), University of Birmingham, (1977).
- (12) G.W. ROWE, T.F. LI, L.E. FARMER: "A Study of Deformation in Simple Forging with Variable Finite Friction" Proc. 3rd NAMRC Conf., Carnegie-Mellon University, (1975)
- (13) T.F. LI: "Metal Flow in Cold Forging Operations" M.Sc. Thesis, University of Birmingham, (1975)
- (14) B. AVITZUR: "Metal Forming: Processes and Analysis" McGraw-Hill (1968)
- (15) H. KUDO: "An Upper-Bound Approach to Plane Strain Forging and Extrusion"
1; Int. J. Mech. Sci., 1, pp 57 - 83, (1960)
2; Int. J. Mech. Sci., 1, pp 229 - 252, (1960)
3; Int. J. Mech. Sci., 1, pp 366 - 368, (1960)
- (16) H. KUDO: "Some Analytical and Experimental Studies of Cold Forging and Extrusion"
1; Int. J. Mech. Sci., 2, pp 102 - 127, (1960)
2; Int. J. Mech. Sci., 2, pp 91 - 117, (1960)
- (17) S. KOBAYASHI: "Upper Bound Solutions of Axisymmetric Forming Problems"
1; J. Eng. Ind., 86B, pp 122 - 126, (1964)
2; J. Eng. Ind., 86B, pp 326 - 332, (1964)
- (18) S. KOBAYASHI, E.G. THOMSEN: "Upper and Lower Bound Solutions to Axisymmetric Compression and Extrusion Problems" Int. J. Mech. Sci., 7, pp 127 - 143, (1965)
- (19) R.D. McDERMOTT, A.N. BRAMLEY: "Forging Analysis - A New Approach" Proc. 2nd NAMRC Conf., Madison (1974)
- (20) C.T. CHEN, F.F. LING: "Upper Bound Solutions to Axisymmetric Extrusion Problems" Int. J. Mech. Sci., 10, pp 863 - 879 (1968)
- (21) W. JOHNSON, H. KUDO: "The Use of Upper Bound Solutions for the determination of Temperature Distributions in Fast Hot Rolling and Axi-Symmetric Extrusion Processes" Int. J. Mech. Sci., 1, pp 175 - 191, (1960)
- (22) J.M. ADIE, J.M. ALEXANDER: "A Graphical Method of Observing Hodographs for Upper Bound Solutions to Axi-Symmetric Problems" Int. J. Mech. Sci., 9, pp 349 - 357, (1967)
- (23) E.G. THOMSEN, C.T. YANG, S. KOBAYASHI: "Mechanics of Plastic Deformation in Metal Processing" MacMillan, New York, (1965)
- (24) R.E. MEDRANO, P.P. GILLIES: "Visioplasticity Techniques Axisymmetric Extrusion" J. Strain Anal., 7, pp 170 - 177, (1972)
- (25) A. SHABAIK, S. KOBAYASHI: "Computer Application to the Visioplasticity Method" J. Eng. Ind., 89B, pp 339 - 346, (1967)
- (26) A. SHABAIK: "Computer Aided Visioplasticity Solution to Axisymmetric Extrusion through Curved Boundaries" J. Eng. Ind., 94B, pp 1225 - 1231 (1972)
- (27) A. SHABAIK: "Theoretical Methods for Analysis of Metal Deformation Problems" Ph.D. Thesis, University of California, Berkeley, (1966)
- (28) A. SHABAIK, E.G. THOMSEN: "A Theoretical Method for the Analysis of Metal-Working Problems" J. Eng. Ind., 90B, pp 343 - 352, (1968)
- (29) O.C. ZIENKIEWICZ: "The Finite Element Method" McGraw-Hill (1977)
- (30) C.S. DESAI, J.F. ABEL: "Introduction to the Finite Element Method" Van Nostrand Reinhold, (1972)
- (31) P. HARTLEY: Ibid.
- (32) G.W. ROWE: "Recent Developments in the Theory and Practice of Metalforming" Proc. 3rd NAMRC Conf., Carnegie-Mellon University, (1975)
- (33) Y. YAMADA, N. YOSHIMURA, T. SAKURAI: "Plastic Stress-Strain Matrix and its application to the solution of Elastic Plastic Problems by the Finite Element Method" Int. J. Mech. Sci., 10, pp 343 - 354, (1968)
- (34) P. HARTLEY, C.E.N. STURGES, G.W. ROWE: "A Finite Element Analysis of Extrusion Forging" Proc. 6th NAMRC Conf., University of Florida, (1978)
- (35) A. NAGAMATSU, T. MUROTA, T. JIMMA: "On the Non-Uniform Deformation of a Block in Plane-Strain Compression caused by Friction" Bulletin JSME, 14, No 70, pp 314 - 321, (1971)
- (36) A. NAGAMATSU, T. MUROTA, T. JIMMA: "On the Non-Uniform Deformation of Material in Axially Symmetric Compression caused by Friction" Bulletin JSME, 14, No 70, pp 339 - 347, (1971)
- (37) K. IWATA, K. OSAKADA, S. FUJINO: "Analysis of Hydrostatic Extrusion by the Finite Element Method" J. Eng. Ind., pp 697 - 703, May, (1972)
- (38) C.H. LEE, S. KOBAYASHI: "Elastoplastic Analysis of Plane-Strain and Axisymmetric Flat Punch Indentation by the Finite Element Method" Int. J. Mech. Sci., 12, pp 349 - 370, (1970)
- (39) J.L. GORDON, A.S. WEINSTEIN: "Finite Element Analysis of the Plane Strain Drawing Problem" Proc. 2nd NAMRC Conf., University of Wisconsin, (1974)
- (40) C.H. LEE, S. KOBAYASHI: "New Solutions to Rigid-Plastic Deformation Problems Using a Matrix Method" J. Eng. Ind., ASME, 95, p. 865, (1973)
- (41) S.N. SHAH, S. KOBAYASHI: "Rigid Plastic Analysis of Cold Heading by the Matrix Method" Proc. 15th Int. MTDR Conf., University of Birmingham, (1974)
- (42) H. MATSUMOTO, S.I. OH, S. KOBAYASHI: "A Note on the Matrix Method for Rigid-Plastic Analysis of Ring Compression" Proc. 18th Int. MTDR Conf., Imperial College London, (1977)
- (43) F.W. SHARMAN: "Hot Bar Extrusion and the Effect of Radial Temperature Profiles in the Billet" Electricity Council Research Centre, Report R851, (1975)
- (44) B.A. FINLAYSON, L.E. SCRIVEN: "The Method of weighted residuals - a review" App. Mech. Rev. 19, pp 735 - 748 (1966)
- (45) S.H. CRANDAL: "Engineering Analysis", McGraw Hill, (1956)
- (46) E. STECH: "Numerische Behandlung von Verfahren der Umformtechnik" Ber 22 Inst. Umf. Univ. Stuttgart, (1971)
- (47) E.G. THOMSEN, J.T. LAPSLEY, JR.: "Experimental Stress Determination within a Metal During Plastic Flow." Proc. Soc. Exp. Stress Anal., 11, No. 2, pp 59 - 68, (1954)

- (48) H. KUDO: "Some Analytical and Experimental Studies of Axisymmetric Cold Forging and Extrusion" 1; Int. J. Mech. Sci., 2, pp 102 - 127, (1960)
 2; Int. J. Mech. Sci., 3, pp 91 - 117, (1960)
- (49) N.R. CHITKARA, W. JOHNSON: "Some Results for Rolling with Circular and Polygonal tools" Proc. 5th Int. Conf., University of Birmingham, (1964)
- (50) B. AVITZUR, J. FUEYO, J. THOMPSON: "Analysis of Plastic Flow through Inclined Planes in Plane Strain" J. Eng. Ind., 89B, pp 361 - 375, (1967)
- (51) S.C. JAIN, S. KOBAYASHI: "Deformation and Fracture of an Aluminium Alloy in Plan-Strain Side Pressing" Proc. 11th Int. MTDR Conf., University of Birmingham, (1970)
- (52) M. HAMED: "Parameters Affecting Impact Extrusion" M.Sc. Thesis, University of Alexandria, (1973)
- (53) W.B. PALMER, P.L.B. OXLEY: "Mechanics of Orthogonal Machining" Proc. Inst. Mech. Engrs., 24, pp 623 - 638, (1959)
- (54) P.V. VAIDYANATHAN, T.Z. BLAZYNSKI: "A Theoretical Method of Efficient Die-Design" J. Inst. Metals, 101, pp 79 - 84, (1973)
- (55) H.S. SHIN: "Flow and Deformation of Metals in Forging" Ph.D. Thesis, University of Birmingham, (1974)
- (56) G.W. ROWE, I.M. DESAI, H.S. SHIN: "Transverse Deformation in Section Rolling and Forging" Proc. 15th Int. MTDR Conf., University of Birmingham, (1975)
- (57) M.W. HOPSON, K.J. WEINMANN, A.A. HENDRICKSON, G.W. ROWE: "The use of Fibre Structure of High Purity Aluminium for the Study of Metal Flow in Plastic Deformation" Proc. 2nd NAMRC Conf., University of Wisconsin, (1974)
- (58) R. SOWERBY, W. JOHNSON, S.K. SAMATA: "The Diametral Compression of Circular Rings by 'point' Loads" Int. J. Mech. Sci., 10, pp 369 - 383, (1968)
- (59) P.F. THOMASON: "The use of Pure Aluminium as an Analogue for the History of Plastic Flow in Studies of Ductile Fracture Criteria in Steel Compression Specimens" Int. J. Mech. Sci., 10, pp 501 - 518, (1968)
- (60) R.A.C. SLATER, W. JOHNSON, S.Y. AKU: "Experiments in Fast Upsetting of Pure Load Cylinders and a Tentative Analysis" Int. J. Mech. Sci., 10, pp 169 - 189, (1968)
- (61) C. BLAZEY, L. BROAD, W.S. GUMMER, D.R. THOMPSON: "The flow of Metal in Tube Extrusion" J. Inst. Metals, 75, pp 163 - 184, (1948)
- (62) A.P. GREEN: "The Use of Plasticine Models to Simulate the Plastic Flow of Metals" Phil. Mag., 42, pp 365 - 373, (1951)
- (63) S.Y. AKU, R.A.C. SLATER, W. JOHNSON: "The Use of Plasticine to Stimulate the Dynamic Compression of Prismatic Blocks of Hot Metals" Int. J. Mech. Sci., 9, pp 495 - 525, (1967)
- (64) J.W. BARTON, C. BODSWORTH, J. HALLING: "The Use of Paraffin Wax as a Model Material to Simulate the Plastic Deformation of Metals" J. Iron Steel Inst., 188, pp 321 - 331, (1958)
- (65) K.T. CHANG, T.M. BRITAIN: "An Investigation of Analog Materials for the Study of Deformations in Metal Processing Simulations" J. Eng. Ind., 90B, pp 381 - 386, (1968)
- (66) C. BODSWORTH, J. HALLING, J.W. BARTON: "The Use of Paraffin Wax as a Model Material to simulate the Plastic Deformation of Metals" J. Iron Steel Inst., 185, pp 375 - 383, (1957)
- (67) J. DANCKERT, T. WANHEIM: "Slip-line Wax", Exp. Mech., Aug. pp 318 - 320, (1976)
- (68) E.P. UNKSOV, Y.S. SAFAROV: "Photoelastic Investigation and Initial Plastic Straining" Int. J. Mech. Sci., 17, pp 545 - 549, (1975)
- (69) E.P. UNKSOV, Y.S. SAFAROV: "A Photoelastic Investigation of Contact Stresses in The Backward Extrusion Process" Int. J. Mech. Sci., 17, pp 597 - 602, (1975)
- (70) L.C. TAN: "Use of Photoelastic Models for Metal Deformation Problems" Undergraduate Thesis, Mechanical Engineering, University of Birmingham, (1977)
- (71) Y. OHASHI, T. NISHITANI: "On a Method for Analysing the Effect of Back Tension in Strip Drawing through Wedge Shaped Die" J.S.M.E., Semi - Int. Symp., Tokyo, Sept., (1967)
- (72) Y. OHASHI, T. NISHITANI: "Photo-Rheological Stress Analysis on Strip Drawing through Roller Dies" Int. J. Mech. Sci., 9, pp 359 - 372, (1967)

ACKNOWLEDGEMENTS

The authors would like to acknowledge the support of the Science Research Council for their on-going project in the analysis of extrusion-forging.

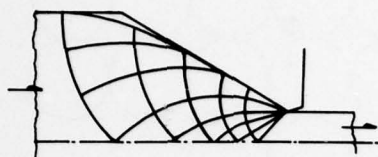


Fig. 1
SLIP LINE FIELD (Rowe²)

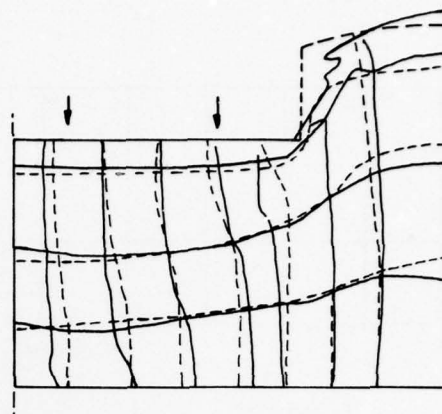


Fig. 4
FINITE ELEMENT (—) AND
EXPERIMENTAL (---) GRID LINES
(Hartley³⁴)

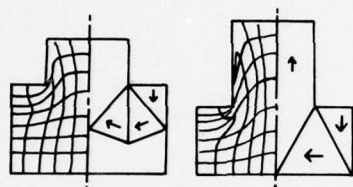


Fig. 2
UPPER BOUND DIAGRAM AND
EXPERIMENTAL FLOW PATTERN
(Kudo¹⁵)

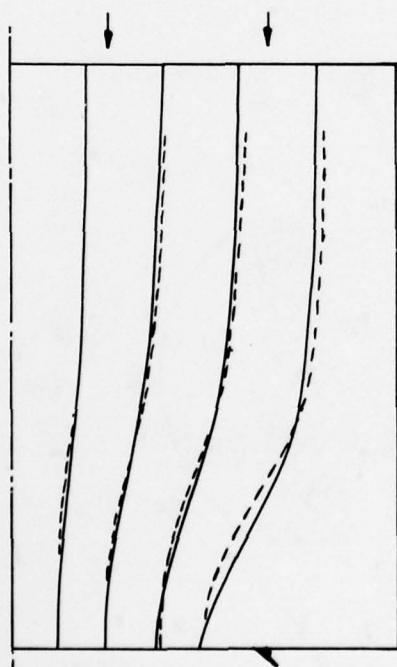


Fig. 3
EXPERIMENTAL (---) FLOW LINES
COMPARED WITH THEORY (—). (Shabaik²⁷)



FIG. 5
THEORETICAL FLOW LINES FOR
COLD HEADING (Shah⁴¹)

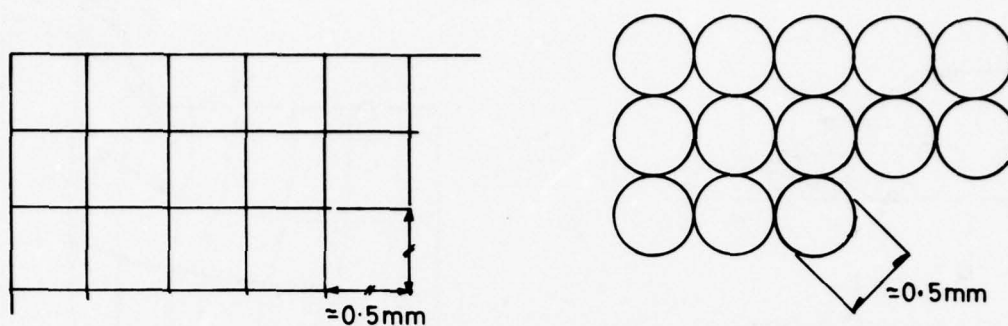


FIG. 6
TYPICAL SQUARE AND CIRCULAR GRIDS USED IN VISIOPLASTICITY EXPERIMENTS

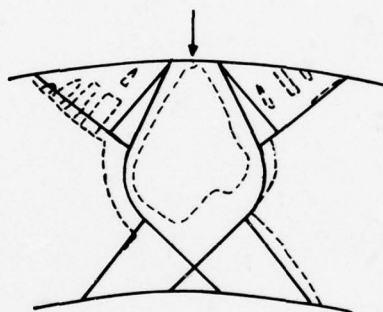


FIG. 7
SLIP LINE FIELD (—) COMPARED TO LÜDERS LINES (----), (Sowerby⁵⁸)

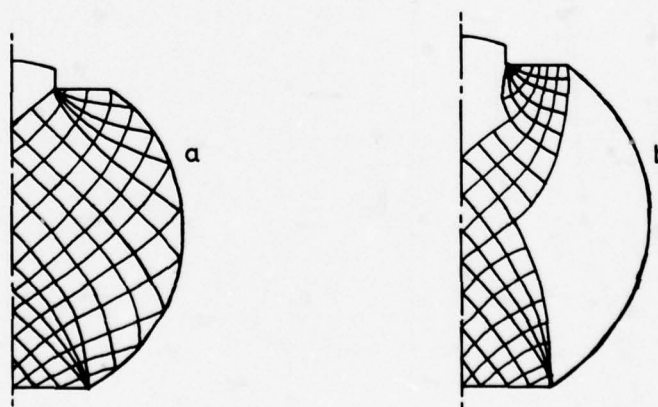


FIG. 8
SLIP LINE FIELDS FROM (a) PHOTOELASTICITY AND
(b) VISIOPLASTICITY EXPERIMENTS (Rowe⁵⁶)

ASPECTS FONDAMENTAUX DE LA SUPERPLASTICITE EXEMPLES DE REALISATION INDUSTRIELLE EN ALLIAGE DE TITANE Ti-6 Al-4V

par

E. Budillon
Aérospatiale - Laboratoire Central
12 rue Pasteur, 92152 Suresnes, France

et

J.P. Lechten
Université de Metz
France

RESUME

Pour qu'un métal ou un alliage présente un comportement superplastique, dans des conditions précises de température et de vitesse de déformation, il faut que sa structure soit à grains fins et équiaxes. C'est le cas, notamment, des tôles industrielles en alliage de titane Ti-6 Al-4V dont la taille des grains est, en général, inférieure à 10 microns.

Le domaine de déformation superplastique de cet alliage a été déterminé par l'étude du coefficient m , de sensibilité de la contrainte à la vitesse de déformation.

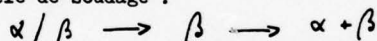
Des pièces, de formes hémisphérique et torique, ont été thermoformées par gonflage à partir de tôles non soudées ou soudées par procédé TIG.

Sous réserve de tenir compte des amincissements causés par les déformations atteintes au cours du formage, il est envisageable de thermoformer des pièces en optimisant au mieux la gamme de fabrication et la conception de l'outillage en fonction des applications industrielles souhaitées, en particulier dans le domaine aéronautique et spatial.

INTRODUCTION

Lorsqu'on veut réaliser des pièces de formes complexes, le formage à chaud devient indispensable pour pratiquement tous les alliages de titane

La réalisation de ces pièces à partir de tôles peut se faire en utilisant, soit une ébauche découpée, soit une ébauche présoudée. Dans ce dernier cas, la question est de savoir si les cordons de soudure possèdent eux aussi des propriétés superplastiques malgré leur structure aciculaire qui résulte de la double transformation au cours du cycle de soudage :



Cette influence de la structure sur la superplasticité peut être envisagée également pour d'autres demi-produits de départ, tels que des ébauches forgées, matricées ou extrudées : la connaissance de leurs propriétés superplastiques permettrait de choisir le demi-produit le mieux adapté à la réalisation d'une pièce donnée.

CHOIX DU THEME DE TRAVAIL

Ainsi, la réalisation de capacités toriques et sphériques pour le stockage d'Azote peut être envisagée dans le domaine spatial.

Pour thème de travail, nous avons donc choisi le thermoforgeage de pièces élémentaires en alliage de titane T-A6V qui, assemblées par soudure, pourront constituer une capacité. Ces pièces se prêtent en effet assez bien :

- au calcul des déformations et au contrôle de leurs trajectoires,
- à l'étude du comportement d'un cordon de soudure sollicité en traction bi-axiale au cours du formage.

L'étude comporte deux objectifs principaux :

- Sur le plan théorique, la détermination des propriétés superplastiques de l'alliage T-A6V (demi-produit forgé, cordon de soudure)
- Sur le plan industriel, la réalisation par thermoforgeage de demi-tôres, à très faible rayon de cintrage, et de demi-sphères en alliage de titane T-A6V.

La réalisation du premier objectif a nécessité les études suivantes :

- des essais de traction sur éprouvettes soudées en T-A6V déformées dans le domaine de comportement superplastique de l'alliage de base (étude de l'évolution de la structure de la zone soudée et de la tenue mécanique des cordons de soudure).
- une analyse du comportement superplastique de demi-produit en T-A6V forgé dans le domaine α/β et traité thermiquement dans le domaine β (détermination du coefficient m , étude métallographique).
- une analyse théorique du thermoformage superplastique afin de mettre en évidence l'influence des conditions opératoires sur la géométrie des pièces ainsi réalisées.

Le deuxième objectif était d'assurer le thermoformage en milieu industriel de pièces élémentaires à partir de flans circulaires, soudés ou non, en T-A6V, afin :

- de concrétiser les possibilités et les conditions opératoires de déformation déterminées en laboratoire pour des températures $\geq 900^{\circ}\text{C}$,
- de vérifier le comportement d'un cordon de soudure T.I.G. en déformation bi-axiale pour le cas d'utilisation des préformes mécano-soudées,
- d'optimiser la géométrie du plan de joint réalisable sur des pièces élémentaires qui seront ensuite assemblées par soudure T.I.G. ou par bombardement d'électrons,
- de démontrer les possibilités de mise en oeuvre d'un outillage économique, conçu pour une faible série et construit avec des éléments modulaires qui peuvent être aisément modifiés et à moindre frais, au cours de la mise au point du thermoformage en phase prototype,
- de vérifier qu'il est possible d'assurer l'étanchéité nécessaire à la bonne conduite du thermoformage en s'affranchissant de toute force extérieure exercée au niveau du serre-flan sur l'outillage qui peut alors être utilisé dans un four industriel.

CONDUITE DE LA RECHERCHE

L'ensemble de cette étude a été effectué en plusieurs étapes, citées précédemment, par les laboratoires suivants :

- AEROSPATIALE - Laboratoire Central - SURESNES
dirigé par M. G. HILAIRE
- UNIVERSITE DE METZ - Laboratoire de Physique et de Technologie des Matériaux (associé au CNRS n°155)
dirigé par M. B. BAUDELET
- AEROSPATIALE - Laboratoire de Recherches de la Production
dirigé par M. JP. BRUSSON
- AEROSPATIALE - Centre Industriel des MUREAUX, département production
dirigé par M. BIGAY.

ANALYSE ET INTERPRETATION

Etude métallurgique de demi-produits industriels

Deux types de demi-produits, tôle et forgé, en alliage de titane T-A6V, ont été approvisionnés pour apprécier leur qualité et leur aptitude à la déformation superplastique dans différents états thermiques.

Ces deux échantillons se répartissent de la façon suivante :

Fournisseur	Demi-produit	Etat thermique	
		d'origine	d'essai
RMI	Tôle d'épaisseur 2 mm *	recuit	recuit
		recuit	soudé **
		recuit	recuit
UGINE	Forgé ϕ 60 x 120 mm ²	recuit	traité *** α/β STOA
		recuit	traité *** β STOA

* Tôle pour étude du soudage et thermoformage des demi-tôres

** Soudage TIG automatique sans métal d'apport

*** Traité STOA : mise en solution à 960°C trempe eau + recuit à 730°C

STOA : " " " 1025°C " " + " à 730°C

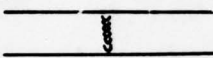
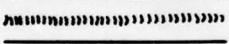
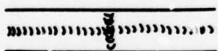
Caractéristiques mécaniques à température ambiante

Dans les tableaux suivants sont consignées les caractéristiques obtenues, à température ambiante, sur les différents demi-produits. Ces caractéristiques sont conformes aux spécifications en vigueur.

BARRE FORGÉE T-A6V UGINE (sens travers long)

Etat thermique	R 0,2 (MPa)	R (MPa)	A%	Z%
Recuit à 730°C	929	965	14,0	35,1
	918	949	14,0	34,8
Traité α/β T.E. 960°C + recuit à 730°C	1020	1055	13,5	25,9
	1006	1032	13,0	42,6
Traité β T.E. 1020°C + recuit à 730°C	1009	1044	3,5	8,0
	1015	1056	7,5	17,4

TOLE SOUDEE T.I.G. T-A6V R.M.I. - épaisseur 2 mm (cordon non arasé)

Type de soudage	Sens	R 0,2 (MPa)	R (MPa)	A%(5,65 S)
	Travers	1015	1123	4,7
		1016	1123	4,3
		978	1128	5,0
		1010	1114	6,0
		1048	1121	6,0
	M	1013	1121	5,2
	Travers	963	1101	6,7
		939	1103	8,7
		971	1109	9,3
		991	1102	9,3
		1006	1091	8,3
	M	974	1101	8,5
	Travers	987	1056	12,0
		983	1058	10,7
		993	1058	12,0
		1005	1060	11,7
		991	1046	11,7
	M	992	1055	11,6
Non soudé (tôle de base)	Long	931	1009	12,1
		948	1006	15,8
		940	1005	15,4
	M	940	1007	14,4
	Travers	1018	1058	14,1
		996	1044	14,5
		1008	1050	13,0
	M	1007	1051	13,8

Nota - Toutes les ruptures se sont produites en dehors de la zone soudée (tôle de base)

Examen métallographique

L'analyse de la structure montre :

- pour la barre forgée en T-A6V
 - . à l'état recuit, les grains α sont de forme allongée, dont la taille moyenne est d'environ $6 \times 32 \mu\text{m}$ avec un pourcentage de phase α supérieur à la phase β .
 - . à l'état traité α/β STOA, le pourcentage de phase α est inférieur à celui de la phase β , la taille moyenne des grains est la même qu'à l'état recuit ($6 \times 32 \mu\text{m}$).
 - . à l'état traité β STOA, la structure devient aciculaire à fines aiguilles avec la présence de grains bêta primaire.
- pour la tôle de T-A6V servant au thermoformage des demi-tôres, les grains α à l'état initial sont approximativement équiaxes et leur taille moyenne est d'environ $5 \mu\text{m}$ tandis que dans la zone soudée la structure est aciculaire à fines aiguilles alpha.

Comportement superplastique d'éprouvettes soudées en alliage T-A6V

La superplasticité permet la réalisation de pièces métalliques par thermoformage [1]. Pour des pièces particulièrement complexes, il est nécessaire, soit d'assembler par soudage des éléments préalablement formés, soit de thermoformer directement une structure composée de tôles initialement soudées.

Cette dernière technique pose le problème du comportement de la zone soudée au cours d'une déformation dans le domaine superplastique. Nous nous proposons d'étudier le cas de l'alliage de titane superplastique T - A6V [2].

Techniques expérimentales

Le matériau de départ est un alliage commercial de titane Ti 6% Al 4%V qui se présente sous forme de tôle d'épaisseur 2 mm. Cet alliage est biphasé, la phase α étant approximativement équiaxe et de taille $5 \mu\text{m}$ environ. Des observations plus fines ont montré que la phase est bordée par la phase β et la phase α' , laquelle résulte de la transformation martensitique de la phase β [3]. Les éprouvettes sont découpées dans le sens travers de la tôle puis assemblées par soudage T.I.G. sans apport de matière et sans arasage du cordon.

Afin d'étudier le comportement plastique de la zone soudée dans différentes conditions de sollicitation, trois types d'éprouvettes ont été préparés (fig. 1).

Eprouvettes soudées après essai

- a) soudure transversale
- b) " longitudinale

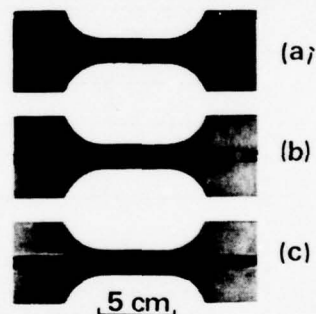
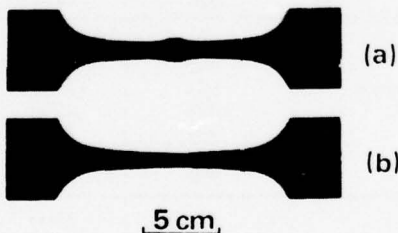


Fig. 1 - Eprouvettes soudées avant essai.

- a) soudure transversale
- b) " longitudinale
- c) soudures croisées

La zone soudée est principalement constituée par la phase α' martensitique, laquelle est caractéristique de l'alliage de titane T-A6V obtenu par solidification et refroidissement rapide [3, 4]. On notera qu'au cours du temps de maintien en température avant les essais mécaniques, la phase α' se transforme en phase α et β [3, 5]. Les éprouvettes ont été sollicitées en traction à l'air et à vitesse de déformation constante. Un revêtement à base de graphite est appliqué avant essai sur les éprouvettes pour limiter les effets de l'oxydation à haute température. Les conditions d'essai correspondent à celles où le comportement superplastique de cet alliage se manifeste [2]. Chaque type d'éprouvettes a été sollicité à trois températures (850°C , 900°C et 950°C) et selon trois vitesses de déformation : ($2,7 \times 10^{-3} \text{ mm}^{-1}$; $2,7 \times 10^{-2} \text{ mm}^{-1}$ et $2,7 \times 10^{-1} \text{ mm}^{-1}$).

L'allongement maximum des éprouvettes a été limité à 150% par la longueur utile du four. Après chaque essai, les éprouvettes sont refroidies à l'air.

Résultats

Tous les essais réalisés mettent en évidence le bon comportement de la soudure, quels que soient le type de l'éprouvette, la température et la vitesse de déformation : absence de décohésions à l'interface soudure-matériau de base et de rupture dans la partie soudée. Pour les éprouvettes à soudure transversale, on observe que la zone de soudure se déforme moins que l'alliage de base; pour les éprouvettes à soudure longitudinale, la contrainte d'écoulement est de l'ordre de trois fois supérieure à la contrainte nécessaire pour déformer dans les mêmes conditions une éprouvette non soudée. Ceci est en accord avec l'observation précédente qui montre la faible déformation de la zone soudée dans le cas d'une éprouvette à soudure transversale. Des résultats identiques sont observés avec les éprouvettes à soudures croisées.

Au cours de la déformation dans le domaine superplastique, un grossissement de la phase α apparaît dans le matériau de base; la vitesse de grossissement dépend des conditions expérimentales, comme il a été montré dans de nombreux alliages superplastiques [6,7]. Dans la zone soudée, l'évolution de la structure dépend du taux de déformation : lorsque la soudure se déforme très peu, la structure aciculaire n'est pas modifiée et seul un grossissement des aiguilles se manifeste, dont l'amplitude dépend encore des conditions expérimentales; lorsque la soudure se déforme comme le matériau de base, la structure aciculaire évolue vers un état composé de petits grains approximativement équiaxes, cette évolution de structure étant fonction de la température et de la vitesse de déformation. Une analyse plus fine de la structure, observée le long d'une éprouvette à déformation non uniforme, permet de préciser comment évolue cette structure aciculaire au cours de la déformation. Pour un taux d'allongement très faible, les aiguilles de la phase α sont orientées de façon aléatoire par rapport à l'axe de traction; pour un taux d'allongement local de 90%, les aiguilles sont inclinées sur l'axe de traction et une faible densité de petits grains équiaxes apparaît; après un allongement local de 370%, on retrouve la structure à petits grains déjà discutée. Les résultats énoncés ci-dessus se vérifient avec les éprouvettes à soudures croisées.

Discussion

L'étude précédente montre, d'une part que la zone soudée tend à adopter une structure caractéristique des matériaux superplastiques au cours de la déformation, et d'autre part, que cette évolution de structure nécessite une contrainte d'écoulement plus élevée.

Le premier résultat est en désaccord avec des études réalisées sur des alliages eutectiques [8] ou eutectoïdes [9], qui ont montré qu'une structure dendritique n'est pas favorable à un comportement superplastique. En revanche, il est en accord avec des travaux qui ont mis en évidence le passage à l'état équiaxe d'une structure brute de coulée dans l'alliage eutectique Al-Cu [10] avec une augmentation du coefficient de sensibilité à la vitesse de déformation [11]. Dans le cas de l'alliage de titane T-A6V, la présente étude permet, de plus, de proposer un mécanisme de transformation depuis la structure aciculaire initiale jusqu'à une structure de type superplastique: au cours de la déformation, un glissement se manifeste au niveau de l'interface entre la phase α et la phase β plus ductile; ce glissement conduit à une réorientation suivant l'axe de traction des aiguilles; celles-ci se scindent ensuite au niveau des joints de grains de la phase α en petits grains approximativement équiaxes, comme cela a été montré par ailleurs [12, 13]. La contrainte d'écoulement plus élevée qui accompagne ce passage à une structure compatible avec un comportement superplastique, est en parfait agrément avec les études menées sur le laiton 60/40 superplastique qui a montré que le passage à l'état équiaxe nécessite bien une contrainte d'écoulement plus élevée [14].

Conclusion

Cette étude montre qu'au cours de la déformation, la structure aciculaire initiale de la zone soudée évolue vers une structure à grains fins, caractéristique du comportement superplastique. Cette évolution s'effectue sous une contrainte d'écoulement plus élevée que celle nécessaire pour déformer dans les mêmes conditions le matériau de base. Ces résultats permettent d'envisager la mise en forme par thermoformage de tôles préalablement soudées; il explique également que des sphères en alliage de titane T-A6V aient pu être obtenues par thermoformage à partir de deux flans soudés selon une circonférence.

COMPORTEMENT SUPERPLASTIQUE DE L'ALLIAGE T-A6V INITIALEMENT FORGE DANS LE DOMAINE α/β

L'ensemble des travaux menés sur les matériaux présentant un comportement superplastique a montré qu'une telle propriété est obtenue avec des structures fines et équiaxes lorsque la valeur du coefficient m est élevée (m représentant la sensibilité de la contrainte à la vitesse de déformation) [16, 18]. Dans ces conditions, la déformation procède sans striction localisée et, par conséquent, les allongements à rupture sont importants. Des modèles métallurgiques ont tenté d'établir une corrélation entre la structure et les valeurs du coefficient m et les allongements à rupture [19]. Dans ce chapitre, nous nous proposons de montrer que de grandes valeurs du coefficient m associées à des déformations importantes sans striction peuvent apparaître dans des matériaux ayant une structure non équiaxe.

La connaissance des propriétés superplastiques de ces matériaux devrait permettre ultérieurement de choisir le demi-produit le mieux adapté à la réalisation d'une pièce donnée.

Cette étude a été effectuée sur l'alliage industriel de titane T-A6V préalablement forgé dans le domaine α/β et traité thermiquement dans le domaine β (mise en solution à 1020°C puis trempe eau suivie d'un recuit à 730°C); cet alliage présente une structure composée d'aiguilles de phase α soulignées d'un liseré de phase β [20].

Dans la phase β apparaît, en fonction de la vitesse de trempe, une proportion de phase α' issue de la transformation martensitique de cette phase β [20]. Les éprouvettes ont été déformées par traction à des températures égales à 850°C et 900°C et des vitesses de déformation constantes comprises entre $2,7 \times 10^{-3}$ et $2,7 \times 10^{-1} \text{ mn}^{-1}$. Les essais sont suivis d'une trempe à l'air.

Les observations, sur une éprouvette dans une zone non déformée et déformée de 30% à 900°C avec une vitesse de déformation égale à $2,7 \times 10^{-2} \text{ mp}^{-1}$, montrent une structure en vannerie caractéristique d'un traitement thermique dans le domaine β [20]. Dans la zone non déformée, les aiguilles de phase α ont environ $3 \mu\text{m}$ de diamètre et $50 \mu\text{m}$ de longueur tandis, qu'après déformation, leurs dimensions sont égales respectivement à 5 et $30 \mu\text{m}$. Des résultats semblables ont été observés au cours des essais effectués aux températures et vitesses de déformation citées ci-dessus.

L'analyse de la courbe de relaxation [21] obtenue avec l'éprouvette précédente conduit à une valeur du coefficient m égale à 0,45. Dans les mêmes conditions, la méthode des sauts de vitesse révèle une valeur plus élevée égale à 0,6. Cette différence est bien connue, elle est imputable au fait que la structure varie au cours d'un saut de vitesse alors qu'elle reste approximativement constante durant l'essai de relaxation [21].

D'autres mesures du coefficient m , effectuées dans le même domaine de températures et de vitesses de déformation que celui de l'étude de l'évolution de structure ont conduit à des valeurs de même ordre de grandeur. Des allongements uniformes de 150%, limités par la longueur de la zone isotherme du four, confirment les valeurs élevées du coefficient m . Il est à noter que des études ont montré que l'alliage de titane T-A6V à phase équiaxe, de quatre à cinq microns de diamètre, présente, dans ce même domaine de températures et de vitesses de déformation des valeurs comparables du coefficient m [22 - 24].

Ces résultats mettent en évidence la possibilité d'observer un comportement superplastique à partir de structures non équiaxes. Il a été montré que de telles structures évoluent, après quelques dizaines de pourcents de déformation, vers un état équiaxe [14]. Mais, contrairement à nos résultats, les valeurs du coefficient m restent faibles tant que la structure reste allongée [11].

Cette étude semble montrer qu'une structure équiaxe n'est pas une conditions nécessaire pour obtenir un comportement superplastique. Nous suggérons qu'un tel comportement peut être observé dans les matériaux biphasés lorsque la phase la moins ductile à la température de l'essai n'est pas continue et qu'elle limite à quelques microns la taille de l'autre phase. Une analogie hydrodynamique permet de penser que la loi de comportement globale d'un tel matériau est fortement influencée par celle de la phase la plus ductile. Or, la loi de comportement, sous faibles contraintes, d'un matériau ayant un libre parcours moyen de quelques microns, doit être très différente de celle du même matériau non limité par des îlots de phases peu ductiles. En effet, pour ce dernier, des cellules à parois de dislocations peuvent être générées au cours d'un essai de déformation à chaud [20] alors qu'elles ne peuvent pas se former lorsque la taille des cellules, fonction de la valeur de la contrainte [26] devrait être supérieure au libre parcours moyen.

Conclusion

Cette étude montre qu'il est possible d'envisager la mise en forme par thermoformage superplastique d'un produit en alliage de titane T-A6V dont la transformation dans le domaine β est obtenue par traitement thermique.

ANALYSE THEORIQUE DU THERMOFORMAGE DANS LE DOMAINE DE SUPERPLASTICITE

Introduction

Le gonflement d'une tôle encastrée circulairement et soumise à une pression est un essai simple de thermoformage [27,28]. Dans ce chapitre, nous analysons théoriquement et expérimentalement un tel essai avec deux matériaux présentant un comportement superplastique. Nous mettons en évidence l'influence d'un paramètre rhéologique sur la géométrie des pièces et nous déterminons les cinétiques de la déformation en fonction de la loi de variation de la pression appliquée.

Plusieurs auteurs ont réalisé des gonflements de tôles dans le domaine où elles présentent un comportement superplastique [29 - 31] et certains ont proposé une analyse théorique de cette opération de mise en forme [32 - 35]. JOVANE [33] et BELK [35] supposent que la répartition des épaisseurs est uniforme au cours du thermoformage, cette hypothèse n'est admissible que dans le cas de gonflement de sphère complète. HOLT [34] adopte l'égalité en chaque point des déformations principales; cette hypothèse est incompatible avec les conditions aux limites imposées par l'encastrement. Nous avons adopté les mêmes hypothèses que celles retenues par CORNFIELD et JOHNSON [36]. L'intérêt du présent travail réside dans le fait qu'une loi de pression mieux adaptée à la mise en forme par gonflement de matériaux superplastiques a été établie et les cinétiques de gonflement ont été déterminées avec cette loi de pression.

Analyse théorique

Dans un premier temps sont présentés les résultats indépendants de la loi de pression et uniquement fonction du paramètre rhéologique m , supposé constant en tout point de la calotte et à chaque instant de la déformation. La répartition des épaisseurs est d'autant plus uniforme que la valeur du coefficient m est plus élevée: l'écart entre l'épaisseur au sommet et à la base s'accroît au cours de la déformation d'autant plus que la valeur du coefficient m est plus faible (fig. 2)

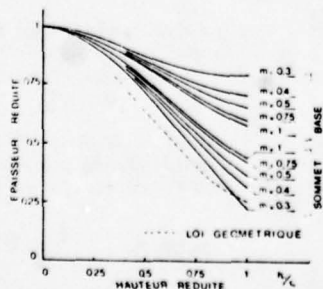


Figure 2 - Evolutions théoriques de l'épaisseur au sommet et la base rapportée à l'épaisseur initiale, en fonction de la hauteur h_0 de la calotte rapportée au rayon d'encastrement r_0 , pour différentes valeurs du coefficient m .

La répartition finale des épaisseurs de long d'un méridien est d'autant plus uniforme que la valeur du coefficient m est plus grande. La connaissance de l'évolution de l'épaisseur au sommet au cours du thermoformage permet de déterminer une loi de variation de la pression appliquée qui maintient constante la valeur du coefficient m au sommet de la déformée (fig. 3).

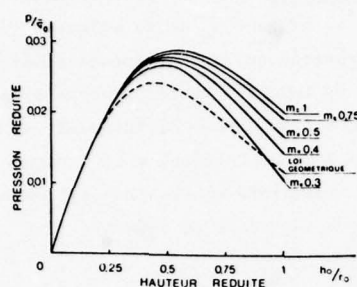


Figure 3 - Evolutions théoriques de la pression de formage p rapportée à la contrainte équivalente initiale $\bar{\sigma}_0$ en fonction de la hauteur de la calotte h_0 rapportée au rayon d'encastrement r_0 , telle que la contrainte équivalente au sommet soit maintenue constante et pour différentes valeurs du coefficient m .

Une autre loi est également proposée à partir d'une analyse purement géométrique de la déformation [36]. Cette loi de variation de la pression appliquée coïncide avec les lois précédentes au début de la déformation.

Nous considérons maintenant les résultats qui sont fonction à la fois du coefficient rhéologique m et de la loi de pression retenue. On constate que la vitesse de déformation aréolaire en chaque point de la déformée et au cours du temps varie (fig. 4) : en chaque point, le rapport des vitesses est au maximum dans un rapport trois entre le début et la fin de l'essai et, à un instant donné, ce rapport en deux points différents est au maximum égal à cinq.

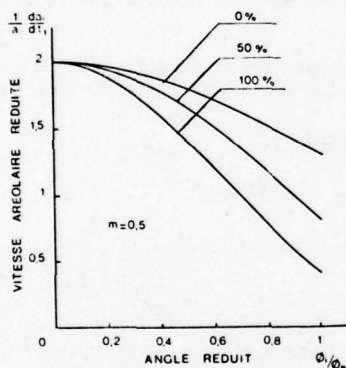


Figure 4 - Courbes théoriques donnant la vitesse d'accroissement de la surface de l'élément i repéré par son angle i rapporté à l'angle N pour trois étapes de gonflement :
- 0 % au début du gonflement
- 50 % lorsque la surface de la calotte a augmenté de 50 %
- 100 % lorsque la surface de la calotte a augmenté de 100 % c'est à dire lorsque la demi-sphère est atteinte.

Des variations de cet ordre ont peu d'influence sur la valeur du coefficient m et d'autant moins que cette valeur est plus élevée. Ce résultat justifie, d'une part, l'hypothèse qui a été faite de supposer constant le coefficient m en chaque point et à chaque instant, et d'autre part, le choix de la loi de pression retenue. Certaines opérations de thermoformage, généralement à températures élevées, ne permettent pas le contrôle de la déformation; il est alors intéressant de déterminer, par le calcul, les temps de formage ainsi que les cinétiques de déformation. Des temps réduits de formage ont été déterminés en fonction du coefficient m pour la loi de pression précédente (fig. 5).

Le temps réel de mise en forme est calculé en associant au temps réduit un temps caractéristique du matériau.

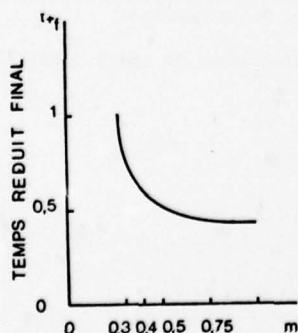


Figure 5 - Evolution théorique du temps réduit final en fonction de la valeur du coefficient rhéologique m .

Sur la figure 6 sont reportées les cinétiques déterminées pour différentes valeurs du coefficient m .

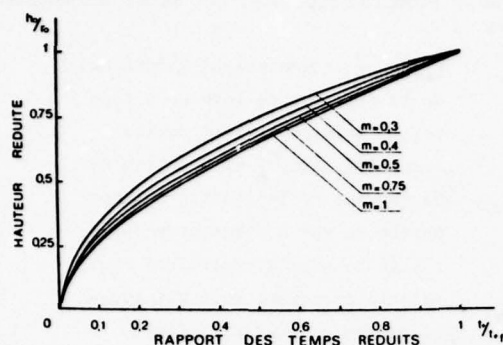


Figure 5 - Evolutions théoriques de la hauteur h_0 de la calotte rapportée au rayon d'encastrement r_0 en fonction du temps caractéristique final, pour différentes valeurs du coefficient m et lorsque la contrainte équivalente est maintenue constante au sommet.

Conclusion

Dans la partie théorique de cette étude du gonflement dans le domaine superplastique de tôles encastrées, les résultats suivants ont été obtenus :

- la géométrie des pièces est fortement dépendante du coefficient rhéologique m .
- une loi de variation de la pression appliquée a été déterminée afin de rendre le coefficient m constant dans la zone qui se déforme le plus, c'est-à-dire au sommet de la déformée.
- la cinétique de la déformation en fonction du coefficient m et de la loi de variation de la pression appliquée a été établie.

Ces résultats sont à considérer lors de la conception des pièces et de l'établissement des gammes de fabrication.

L'analyse expérimentale montre un bon accord, compte tenu des hypothèses simplificatives qui ont été faites lors du calcul, à savoir coefficient m supposé constant et loi de comportement du type superplastique

RESULTATS DES ESSAIS INDUSTRIELS DE FORMAGE DES DEMI-TORES

Moyens industriels de mise en oeuvre pour le thermoformage

1°/ Outillage

L'outillage de formage conçu pour une série de 10 à 20 pièces est réalisé en acier XC 38. Il est constitué par :

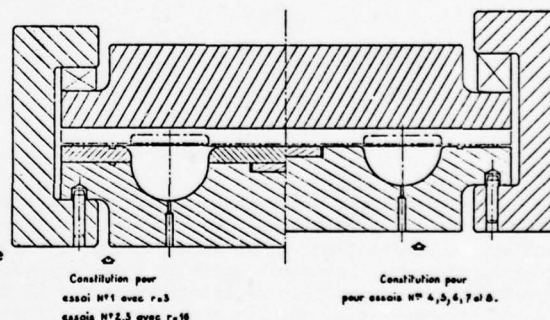
- Une matrice inférieure usinée à la forme extérieure du demi-tore. Elle possède deux trous d'évent $\phi 2$ mm diamétralement opposés et est équipée d'un thermocouple pour le contrôle de la température sur l'outil et de deux pions utilisés pour le centrage de la bride rendue solidaire du flan T-A6V par soudure étanche.

- Une rondelle extérieure plus une rondelle intérieure.

Ces éléments intermédiaires démontables ont été utilisés pour l'étude de la géométrie du plan de joint réalisable sur les demi-coquilles toriques et l'optimisation des rayons d'entrée minimaux qu'il est nécessaire de prévoir sur les diamètres extérieur et intérieur de la matrice.

- Une plaque supérieure qui joue le rôle de serre-flan et est maintenue sur la matrice par l'intermédiaire de 8 étriers avec serrage par coins.

- Masse de l'outillage ainsi constitué : 550 kg.



Outillage pour formage des $\frac{1}{2}$ coquilles.

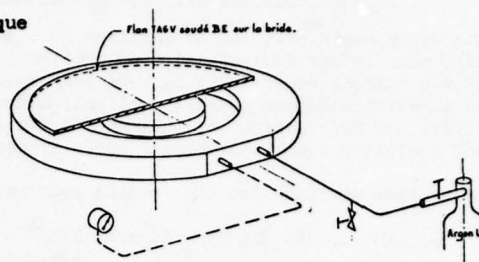
Fig. 7

2°/ Bride support étanche du flan T-A6V (cf. fig. 8)

Quatre brides rigoureusement identiques, usinées dans une plaque T-A6V épaisseur 20 mm, ont été utilisées à tour de rôle pour les essais réalisés par AEROSPATIALE.

Après soudage par bombardement d'électrons du flan sur leur face supérieure, ces éléments constituent une chambre étanche par laquelle se fait l'admission d'argon sous pression et, pour ce faire, ils sont équipés des embouts qui seront reliés aux circuits métalliques annexes pour la mise en pression et la mise à air libre de l'enceinte.

A noter que le soudage mentionné ci-dessus a été effectué avec la machine "SCIARY" opérationnelle au Laboratoire de recherches productions (AEROSPATIALE SURESNES).



Bride support étanche et circuit de mise en pression du flan.

Fig. 8

3°/ Equipement annexe pour la mise en pression et détente de la bride support étanche du flan (cf. fig. 8)

Dans cet équipement, deux tuyauteries métalliques raccordées à la bride support étanche du flan sont à considérer.

- Le premier circuit constitué pour la mise sous pression contrôlée du flan est relié à une bouteille d'argon qualité U, comprimé puis détendu et possède, monté en dérivation, un robinet qui est utilisé pour la mise à air libre du réseau et le réglage de la pression dans l'éventualité d'une surpression constatée.
- Le deuxième circuit est relié au manomètre de contrôle de la pression exercée à l'intérieur de la bride support étanche du flan.

4°/ Four Ripoché

La totalité des essais de thermoformage sur demi-tôres a été effectuée dans le four "Ripoché" à sole mobile qui est installé à l'AEROSPATIALE, usine des MUREAUX. - Température maxi d'utilisation : 1000°C.

Essais réalisés

1°/ Programme de travail pour les essais industriels de thermoformage

a) Etude du plan de joint réalisable sur des demi-coquilles toriques

Deux types de joints, qui conditionnent la conception de la matrice, ont été retenus pour cette étude :

- joint à bords relevés pour assemblage par soudure T.I.G. des demi-coquilles minces (cf. fig. 9).

Le thermoformage d'un plan de joint de ce type a été décidé en vue d'optimiser le rayon mini admissible sous le bord relevé de demi-coquilles destinées à être assemblées par soudure T.I.G. pour constituer des coudes ou autres éléments des circuits "basse pression" réalisés en tôles T-A6V d'épaisseur $\leq 1,5$ mm.

Pour cette étude, nous avons adopté $R = 1,5 \epsilon_0$

avec : r = rayon sous bord relevé

ϵ_0 = épaisseur nominale du flan T-A6V.

- Joint auto-centreur pour assemblage soudé des demi-coquilles par bombardement d'électrons (cf. fig. 10).

Ce mode de soudage est prévu pour l'assemblage des demi-coquilles en T-A6V d'épaisseur $> 1,5$ mm. Il nécessite un usinage du joint auto-centreur à chicane pratiqué dans chacune des ébauches qui, dans ce cas, doivent avoir une légère surlongueur.

Pour le thermoformage de ces ébauches, il est préférable de concevoir une matrice avec de grands rayons d'entrée qui doivent permettre d'obtenir une répartition plus homogène des épaisseurs sur la préforme.

Pour cette étude, nous avons adopté $r = 8 \epsilon_0$

avec : r = rayon d'entrée sur la matrice

ϵ_0 = épaisseur nominale du flan T-A6V

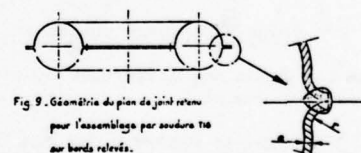


Fig. 9. Géométrie du plan de joint relevé pour l'assemblage par soudure TIG aux bords relevés.

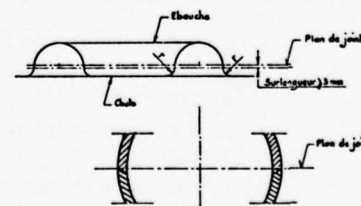


Fig. 10. Principe de jonctionnement des 1/2 coquilles par bombardement d'électrons.

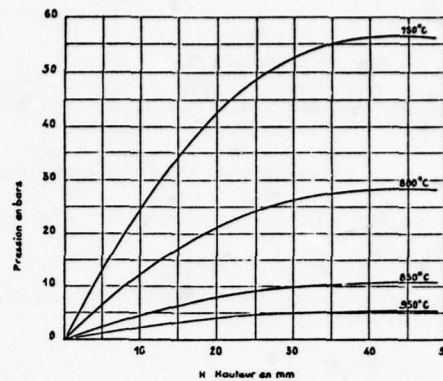
Choix de la température de travail pour les essais industriels

Suite à son étude expérimentale, le Laboratoire de Physique de l'Université de METZ nous a fourni les courbes théoriques de modulation de la pression de formage du demi-tore en fonction de la hauteur de la déformée et ce pour les températures d'essais 750°C - 800°C - 850°C et 950°C. (cf. fig. 11).

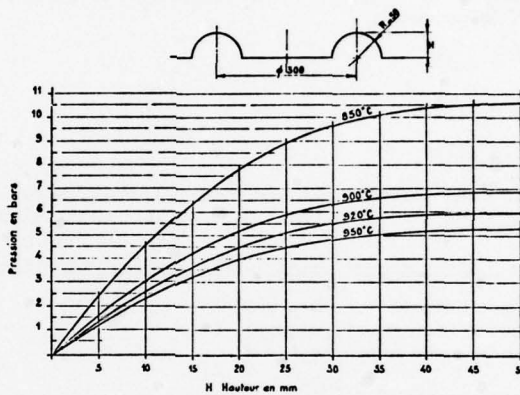
Ces courbes montrent que l'ultime pression ≈ 56 bars est nécessaire pour former le demi-tore à 750°C, alors que $\approx 5,5$ bars suffisent pour former cette même pièce à 950°C.

Compte tenu des très fortes pressions à exercer, jugées excessives pour le formage du demi-tore à faible température, et des possibilités de travail aux températures

$\geq 900^\circ\text{C}$ offertes par le four installé à AEROSPATIALE LES MUREAUX, nous avons adopté la plage de 900 - 920°C pour le déroulement des essais et, pour ce faire, nous avons extrapolé les courbes de modulation des pressions qui devaient nous permettre de travailler dans ce domaine. (cf fig. 12)



Modulation de la pression en fonction de H.
de 750°C à 950°C Fig. 11



Modulation de la pression en fonction de H.
de 850°C à 950°C Fig. 12

Modulation de la pression en fonction de la durée du formage

L'exploitation directe des courbes ci-dessus, pour nos essais, nécessitait le suivi, en continu ou par étapes, de l'évolution des déformations au cours du formage. Nous nous sommes affranchis de cette contrainte en adoptant une loi de modulation de la pression, non plus en fonction des déformations, mais en fonction de la durée du formage et ce, dans l'hypothèse :

- que le flan reste bloqué à la naissance des rayons d'entrée sur la matrice,
- que les vitesses de déformation sont inférieures à 2% par minute.

Ces courbes apparaissent pour chaque essai ou série d'essais effectués avec la même configuration d'outillage.

Essais de thermoformage des demi-tores

1° Phase 1 - Etude du plan de joint réalisable sur des demi-coquilles toriques

Quatre flans T-A6V, épaisseur 2mm, sans soudure TIG, préparés dans les conditions décrites précédemment, ont été utilisés pour cette étude.

ESSAI n° 1 - Essai de formage d'un demi-tore avec plan de joint à bords relevés

Cet essai préfigure la réalisation du plan de joint désigné ci-dessus et, pour ce faire, nous avons équipé la matrice avec les rondelles intérieure et extérieure, d'épaisseurs respectives 19,5 et 20 mm - $r = 3$ mm.

A noter que les conditions de formage sont les plus difficiles dans cette configuration qui conduit à la déformation maximum prévue pour ces essais. Dans l'hypothèse :

- a/ du flan bloqué dès la naissance des rayons d'entrée sur la matrice :
A% moyen sur le méridien de la pièce $\approx 90\%$
- b/ du flan seulement bloqué sur les rayons extérieurs de la matrice :
A% moyen sur le méridien de la pièce $\approx 46,3\%$
- température d'essai : $910^\circ\text{C} + 10^\circ\text{C}$
- mise en pression du flan + 0

Résultats- Mesure des déformations

Les déformations mesurées sur la pièce, dans le sens long et le sens travers du laminage, sont sensiblement identiques et l'on constate :

a/ un glissement du flan sur la zone interne de la pièce

b/ que l'allongement maximum $\approx 79\%$ est localisé sur le rayon interne du demi-tore.

- Répartition des épaisseurs

La pièce thermoformée a été découpée, pour le contrôle des épaisseurs, sur les méridiens sens long et sens travers du laminage.

On observe :

a/ une certaine homogénéité dans la distribution des épaisseurs "sens long" et "sens travers"

b/ que les épaisseurs maxima sont localisées près de l'encastrement du flan, alors que les épaisseurs minima apparaissent sur le rayon interne de la demi-coquille où nous avions relevé l'allongement maximum. Les rapports respectifs de ces épaisseurs sur l'épaisseur initiale du flan apparaissent comme suit :

$$e_{\min} / e_0 = 0,34$$

$$e_{\max} / e_0 = 0,70$$

- Contrôle géométrique de la pièce

Le profil extérieur de la demi-coquille est une réplique conforme de la matrice et les rayons $r = 3$ mm projetés pour le plan de joint à bords relevés sont parfaitement calibrés.

/ESSAI n° 2/ - Formage d'une ébauche demi-torique pour capacités assemblées par bombardement d'électrons

Pour ce faire, la matrice est équipée avec les rondelles extérieure et intérieure $r = 16$ mm et, compte tenu des résultats précédents, nous avons décidé :

- de travailler à la température $900^\circ\text{C} \pm 10^\circ\text{C}$
 $\pm 0^\circ\text{C}$

- de conserver la modulation de la mise en pression appliquée au cours de l'essai (cf fig.13).

Résultats- Mesure des déformations

Une nouvelle fois, nous observons que les déformations mesurées dans le sens long et le sens travers du laminage sont très homogènes.

On constate :

a/ un allongement important sur la zone intérieure de la pièce

b/ que l'allongement maximum $\approx 67,5\%$ est à nouveau localisé sur le rayon interne du demi-tore.

- Répartition des épaisseurs

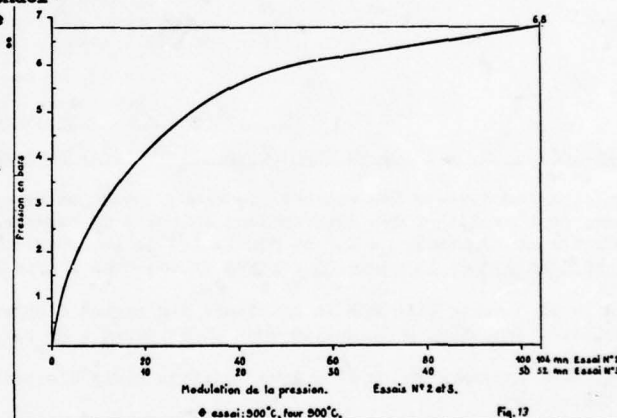
Les valeurs enregistrées sont sensiblement identiques pour le sens long et le sens travers du laminage et, une nouvelle fois, les épaisseurs mini et maxi sont localisées sur les rayons interne et externe du tore avec :

$$e_{\min} / e_0 = 0,48$$

$$e_{\max} / e_0 = 0,71$$

- Contrôle géométrique de la pièce

Les résultats enregistrés sont rigoureusement identiques à ceux de l'essai précédent.



/ESSAI n° 5/ - Etude du formage d'un demi-tore à partir d'un flan soudé TIG "sens long"

Pour cet essai, bien qu'aucune anomalie n'ait été constatée au cours de la mise en pression du flan, la pièce formée présente une rupture du cordon de soudure localisée sur le rayon de bord tombé interne.

Résultats- Mesure des déformations

Malgré la rupture observée ci-dessus, la dispersion est très faible pour les mesures "sens long" et "sens travers" du laminage.

- Répartition des épaisseurs

Même remarque que ci-dessus (écart maxi enregistré 0,06 mm), avec :

$$e_{\min} / e_0 = 0,53$$

$$e_{\max} / e_0 = 0,68$$

- Contrôle géométrique de la pièce

Au sommet du demi-tore et sur le méridien matérialisé par le cordon de soudure, le flan n'est pas parvenu au fond de la matrice alors que partout ailleurs la pièce est parfaitement calibrée au profil extérieur.

/ESSAI n° 6/ - Etude du formage d'un demi-tore à partir d'un flan soudé TIG "sens travers"

Là encore, malgré l'absence d'un signal de "crevaisin" au cours de la mise en pression du flan, une rupture du cordon de soudure s'est produite sur le rayon du bord tombé interne.

Résultats- Mesure des déformations

Aucune dispersion marquante n'est apparue au cours de la mesure des déformations "sens long" et "sens travers" du laminage.

- Répartition des épaisseurs

Sur cette pièce, la répartition des épaisseurs mesurées "sens long" et "sens travers" est homogène, mais, cette fois, l'écart maxi = 0,04 mm est enregistré sur le rayon interne du demi-tore.

$$e_{\min} / e_0 = 0,45$$

$$e_{\max} / e_0 = 0,75$$

- Contrôle géométrique de la pièce

L'état de la pièce est rigoureusement comparable à celui de la pièce formée précédemment.

/ESSAIS n° 7 et 8/ - Etude du formage d'un demi-tore à partir d'un flan soudé TIG "sens long" ou "sens travers"

Ces essais ont été réalisés dans le but de vérifier une nouvelle fois les possibilités de formage d'un flan soudé TIG et, pour ce faire, nous avons reconduit intégralement les conditions de travail des essais n° 5 et 6 en utilisant :

- 1 flan T-A6V soudé sens long pour l'essai n° 7
- 1 flan T-A6V soudé sens travers pour l'essai n° 8.

Résultats

Pour chacun de ces essais, les résultats ont été identiques à ceux des essais n° 5 et 6 et la rupture systématique du cordon de soudure TIG sur le rayon du bord tombé interne a pu être décelée à la pression $\approx 5,5$ bars.

3°/ Phase 3

Suite aux ruptures systématiques observées sur les flans soudés TIG n° 5 à 8, il a été décidé de modifier l'outillage, dans le but d'améliorer le glissement du flan sur la partie centrale de la matrice et d'obtenir ainsi une meilleure répartition des épaisseurs.

Pour ce faire, nous avons à nouveau équipé la matrice avec les rondelles extérieure et intérieure profilées selon la figure 15.

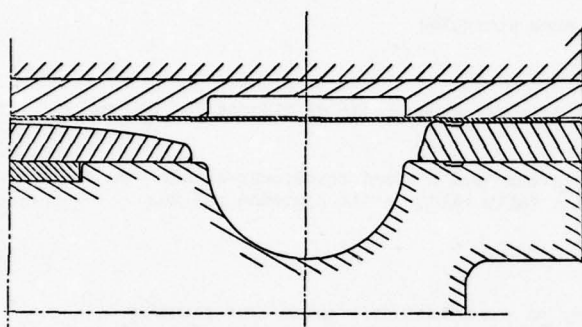
A noter que, dans cette configuration qui a été établie dans le souci de limiter le coût et le cycle de cette modification, nous avons :

A% moyen sur le méridien de la pièce = 32,2 %, alors que nous avions A% = 27 pour les essais cités ci-dessus.

- Conditions générales de travail adoptées pour les essais

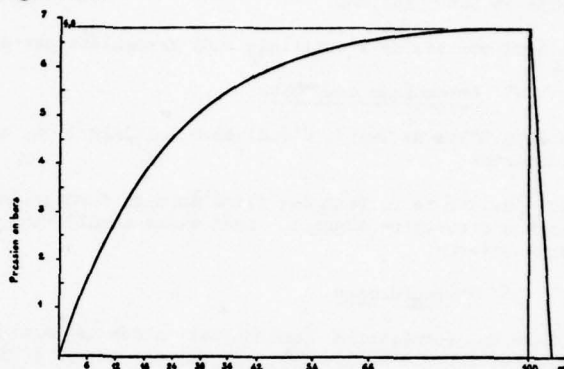
Température de formage $900^{\circ}\text{C} + 10^{\circ}\text{C}$
 $+ 0^{\circ}\text{C}$

Modulation de la mise en pression du flan suivant figure 16.



Modification de l'outillage pour essais N° 9 et 10

Fig. 15



Modulation de la pression.

Essais N° 9 et 10.

Fig. 16

/ESSAI n° 9/ - Etude du formage d'un demi-tore à partir d'un flan de référence non soudé

Résultats

- Mesure des déformations

Aucune dispersion importante n'a été relevée au cours de la mesure des déformations "sens long" et "sens travers" du laminage.

Une nouvelle fois, l'allongement maximum $\approx 60\%$ est localisé sur le rayon interne du tore.

- Répartition des épaisseurs

Au cours de la mesure des épaisseurs "sens long" et "sens travers" du laminage, l'écart maxi = 0,04 mm est localisé au sommet du demi-tore.

La répartition des épaisseurs est meilleure que dans les essais de la phase 2 :

$$e_{\min} / e_0 = 0,53$$

$$e_{\max} / e_0 = 0,71$$

/ESSAI n° 10/ - Etude du formage d'un demi-tore à partir d'un flan soudé TIG "sens long"

Les conditions de travail appliquées pour cet essai sont rigoureusement identiques à celles de l'essai précédent et les résultats obtenus sont satisfaisants car le demi-tore a été formé avec succès, sans rupture du cordon de soudure TIG.

Résultats

- Mesure des déformations

Les déformations constatées au cours de ce contrôle sont très peu différentes des valeurs enregistrées pour l'essai n° 9.

- Répartition des épaisseurs

Par rapport à l'essai précédent, la dispersion est plus importante dans la mesure des épaisseurs "sens long" et "sens travers" et l'écart maxi = 0,08 mm est enregistré sur le rayon interne du demi-tore.

Pour ce cas : $e_{\min} / e_0 = 0,44$

$$e_{\max} / e_0 = 0,65$$

- Contrôle géométrique de la pièce

Le profil extérieur de la demi-coquille est une réplique conforme de la matrice et le "bourrelet" que nous craignons voir subsister sur la pièce, au droit du cordon de soudure TIG, est inexistant.

RÉSULTATS DES ESSAIS INDUSTRIELS DE FORMAGE DES DEMI-SPHÈRES

Moyens industriels mis en œuvre pour le thermoformage

1°/ Outillage

Dans un four à 920°C, est placé un outillage composé de 2 demi-sphères entre lesquelles sont glissées deux tôles de T-A6V soudées à leur périphérie, sur un diamètre de 740 mm.

Les deux demi-sphères de ϕ 560 mm ont été fabriquées en fonte réfractaire au nickel chrome.

La masse totale de l'ensemble est 1120 kg.

Après coulage, la pièce a été réusinée pour obtenir le profil interne exact de la sphère, les plans de joints et les fixations.

Les deux moitiés de l'outillage sont assemblées par des axes clavettés.

2°/ Assemblage des tôles

Les deux tôles de T-A6V, d'épaisseur initiale 3 mm, sont détournées sous forme de disques de 740 mm de diamètre.

Afin d'éviter le retrait des flans lors du formage, nous avons tout d'abord soudé ceux-ci sur une couronne circulaire support. Ceci étant insuffisant, il a fallu raidir cette couronne par une plaque interne.

3°/ Thermoformage

Le flan est formé, après homogénéisation des températures, en insufflant de l'argon sous pression entre les deux tôles soudées. Le gaz est envoyé à débit constant par bouffées dans la cavité (1,11 dm³ toutes les 2 minutes, à 0°C et 1 bar de pression). La surpression ΔP créée dans la cavité provoque une déformation des tôles et donc, fait redescendre la pression à $P + \Delta P$ ($\Delta P < \Delta P$) par accroissement du volume offert. Le calibrage fait, la pression croît linéairement. Donc, après deux heures environ à 920°C, les flans auront pris leur forme demi-sphérique, avec une épaisseur légèrement décroissante entre l'extérieur et le centre.

Le montage et les tôles T-A6V sont protégés de l'oxydation par du produit Kal-gard. Le système de maintien des deux demi-sphères par axe claveté est efficace et facile à employer. Le blocage des flans par la couronne de maintien est efficace, mais les efforts sont tels que la plaque interne se déforme malgré tout.

Essais réalisés - Résultats

- Quatre essais de formage de sphères de diamètre 580 mm à partir de tôle de 3 mm

1°	(1A	1A1	1° chauffe	h = 120 mm incomplète	850°C
	(1A2	2° chauffe		
	("		
	(1B		"		
2°	(2A		formées, usinées chimiquement	soudure BE finale	850°C
	(2B		850°C		
	(3A		épreuves (R, A%, épaisseur)		
	(3B		usinage FMG		
4°	(4A			920°C	
	(
	(4B				
	(

Chaque essai a fait l'objet de relevés dimensionnels sur 8 méridiens divisés chacun en 8 points.

On note ainsi une dispersion sur les épaisseurs obtenues de 8% en moyenne sur un même parallèle. Il est à noter que la dispersion sur l'épaisseur initiale de la tôle est de 3%.

Pour les deux températures retenues, les paramètres de formage ont été les suivants :

(850°C : t = 1 h 25, p = 2 bars
(920°C : t = 1 h 17, p = 0,8 bar

On peut dire, en première approximation, que la pression de formage est proportionnelle à l'épaisseur à former et inversement proportionnelle au diamètre de la sphère à obtenir.

$$P = k \frac{e}{D}$$

et

$$P_0 = k \frac{e_0}{D_0} \quad \text{essai de référence} \quad \left(\begin{array}{l} P_0 = 0,8 \text{ bar} \\ D_0 = 580 \text{ mm} \\ e_0 = 3 \text{ mm} \end{array} \right. \quad t_0 = 1 \text{ h } 17$$

donc :

$$P = P_0 \frac{D_0}{D} \frac{e}{e_0}$$

L'influence de la température, compte tenu du fait que nous n'ayons que deux valeurs est approchée par une loi linéaire sur l'intervalle 850°C, 920°C.

$$P \quad = \quad 16,57 \quad - \quad 0,01714 \quad T$$

(bars) (°C)

Variation des épaisseurs : pour les essais les plus corrects

920°C t = 1 h 17	($\frac{e_{\text{sommet}}}{e_0} = 0,37$	($\frac{e_s}{e_0} = 0,36$
		$\frac{e_{\text{base}}}{e_0} = 0,63$		$\frac{e_b}{e_0} = 0,65$
				850°C t = 1 h 25

Un formage plus long à température plus basse donne les mêmes résultats qu'à 920°C.

- Tenue de l'outillage de formage

L'outillage en fonte grise nickel-chrome a été usiné à la cote ϕ_0 ci-dessous :

$$\phi_0 = 580,10 \text{ mm}$$

Après 3 cycles de formage :

$$\phi_0 = 581,45 \text{ mm}$$

Après 5 cycles de formage :

$$\phi_0 = 581,80 \text{ mm}$$

L'ovalisation du profil reste de l'ordre de $\pm 0,1 \text{ mm}$.

La solution qui devra pallier ce défaut consistera à changer le matériau pour un acier fortement allié ayant une tenue meilleure à haute température, mais aussi un prix plus élevé.

- Démoulage

La différence de dilatation titane T-A6V et fonte oblige à démouler l'ensemble à $\approx 300^\circ\text{C}$.

CONCLUSIONS

Les études théoriques et les applications industrielles de la superplasticité de l'alliage T-A6V permettent de dégager les points suivants :

- L'étude métallurgique montre qu'au cours de la déformation, la structure aciculaire résultant du soudage ou d'un traitement dans le domaine β évolue vers une structure à grains fins caractéristique du comportement superplastique. Cette évolution s'effectue sous une contrainte d'écoulement plus élevée dans la zone soudée que dans le matériau de base, à déformation identique. Ces résultats ont été confirmés lors des essais de thermoformage de demi-torcs.

- Par la mise en œuvre d'un outillage économique, les essais industriels ont permis de vérifier les possibilités de fabrication de pièces par thermoformage à partir de flans T-A6V soudés ou non. Ces essais ont pu être effectués dans les conditions proches de celles envisagées par l'étude théorique préalable.

- L'examen des pièces ainsi formées - répartition des épaisseurs, structure métallurgique - conduit à poser certaines conditions à l'utilisation de ce procédé de fabrication.

- Pour les besoins aéronautiques, toujours sévèrement tolérancés, ces pièces ne seront que des ébauches calibrées qui seront nécessairement reprises par un usinage intérieur conventionnel.

- Une comparaison des coûts de fabrication, par trois méthodes : matriçage, emboutissage et superplasticité, montre l'intérêt économique de cette dernière. (cf. tableau ci-après)

**COMPARAISON DES PRIX RELATIFS DE REALISATION DE SPHERES EN T-A6V
DE DIAMETRE 600 mm ET D'EPAISSEUR 0.6 mm**

PAR TROIS METHODES :

matriçage, emboutissage à chaud et superplasticité

(calculés pour une série de 10 sphères)

	Matriçage	Emboutissage à chaud	Superplasticité
Outillages			
. de matriçage	2,53
. d'emboutissage	0,45
. de formage	0,80
. de tour	0,93	0,93	0,50
. de contrôle	0,16	0,16	0,16
. d'usinage chimique	0,25
. de traitement thermique	0,30	0,30
. de soudure BE	0,96	0,96	0,96
Totaux outillages	4,88	2,80	2,68
Approvisionnements matière (1 sphère)			
. tôle	0,28 (e = 7 mm)	0,12 (e = 3 mm)
. ébauche matriçée	0,91 (e = 14 mm)
Fabrication			
. Formage	0,13	0,10
. Tour	0,45	0,30	0,15
. Contrôle	0,10	0,10	0,08
. Usinage chimique	0,10
. Soudure BE	0,14	0,14	0,14
. Contrôle radio	0,04	0,04	0,04
	0,73	0,71	0,61
Conclusions			
Coût unitaire d'une sphère pour un lancement de 10	2,13	1,27	1

BIBLIOGRAPHIE

- 1 B. BAUDELET, Mém. Sci. Rev. Mét., Février 1975, p. 101
- 2 B. BAUDELET, A. BOURGEOIS, JP. BRUSSON et G. SERTOUR, Rapport D.G.R.S.T. n° 7371757, Juillet 1975
- 3 B. HOCHÉID, R. KLIMA, C. BEAUVAIS, M. RAPIN et C. ROUX, Mém. Sci. Rev. Mét., LXVII, n° 9, 1970
p. 583
- 4 H.P. LIEBIG und K.W. NAGEL METALL, n° 6, 1975, p. 608
- 5 R. MOLINIER, L. SERAPHIN, R. TRICOT et R. CASTRO, Revue de Métallurgie, Janvier 1974, p. 37
- 6 B.M. WATTS and M.J. STOWELL, M. Mater. Sci., 6, 1971, p. 228
- 7 M.A. CLARK and T.H. ALDEN, Acta Met., 21, 1973, p. 1195
- 8 H.E. CLINE and T.H. ALDEN, A.I.M.E., 239, 1967, p. 710
- 9 K. NUTTALL, Ph. D. Thesis, Univ. Manchester, 1969
- 10 D.L. HOLT and W.A. BACKOFEN, Trans. A.S.M., 59, 1966, p. 755
- 11 S. HORI, N. FURUSHIRO and S. KAWAGUCHI, "Structural Changes during Superplastic Deformation of Al-Cu Alloys", Reprint from Proceeding of the 19th Japan Congress on Materials Research, March 1976, p. 1.
- 12 G. HERRIOT, M. SUERY and B. BAUDELET, Scripta Met., 6, 1972, p. 657
- 13 M. SUERY, B. BAUDELET, B. LABULLE et C. PETIPAS, Scripta Met., 8, 1974, p. 703
- 14 M. SUERY and B. BAUDELET, J. Mater. Sci., 8, 1973, p. 363
- 15 J.W. EDINGTON, Metals Technology, March 1976, p. 138
- 16 R.H. JOHNSON, Metal Rev., 1970, p. 115
- 17 B. BAUDELET, Mem. Sci. Rev. Mét., 1971, LXVIII, p. 479
- 18 J.W. EDINGTON, K.N. MELTON, C.P. CUTLER, Progress in Materials Science, 1976, 21, p. 61
- 19 D.A. WOODFORD, Trans. Quart A.S.M., 1969, 62, p. 291
- 20 R.F. MEHL, Metal Hand Book American Society for Metals, 1972, p. 327
- 21 J. HEDWORD, M.J. STOWELL, J. Mat. Sc., 1971, 6, p. 1061
- 22 J.E. LYTLE, G. FISCHER, A.R. MARDER, J. Metals, 1965, 17, p. 1055
- 23 D.LEE, W.A. BACKOFEN, Trans. A.I.M.E., 1967, 239, p. 1034
- 24 J.P. LECHTEN, Thesis, METZ, 1976
- 25 J.J. JONAS, H.J. McQUEEN, Mise en Forme des Métaux et Alliages, Editions du C.N.R.S., 1976,
VII, p. 99
- 26 J.J. JONAS, C.M. SELLARS, W.J. Mc G. TEGART, Metals and Materials Review, 1969, 130, p. 1
- 27 D.M. WOO, Int. J. Mech. Sci. 1964, 6, p. 303
- 28 B. STORAKERS, In. J. Mech. Sci. 1966, 8, p. 619
- 29 J. HESTERER, E.W. LANGER, A. ROSEN, Journal of the Institute of Metal, 1971, 99, p. 306
- 30 T.Y.M. AL-NAIB, J.L. DUNCAN, Int. J. Mech. Sci. 1970, 12, p. 463
- 31 T.H. THOMSEN, D.L. HOLT, W.A. BACKOFEN, Metals Engineering Quaterly, May 1970, 11, p. 1
- 32 D.L. HOLT, Int. J. Mech. Sci. 1970, 12, p. 491
- 33 F. JOVANE, Int. J. Mech. Sci. 1964, 6, p. 303
- 34 G.C. CORNFIELD, R.H. JOHSON, Int. J. Mech. Sci. 1970, 12, p. 479
- 35 J.A. BELK, Int. J. Mech. Sci. 1975, 17, p. 505
- 36 R. HILL, Phil. Mag. 1950, 41, p. 1113
- 37 AVERY W.A. BACKOFEN, Trans. A.S.M., 1965, 58, p. 551.

RAPIDLY SOLIDIFIED POWDERS, THEIR PRODUCTION, PROPERTIES, AND POTENTIAL APPLICATIONS

A. R. Cox*, J. B. Moore*, E. C. van Reuth**

*Pratt & Whitney Aircraft Group, West Palm Beach, Florida, USA

**U. S. Defense Advanced Research Projects Agency,
Arlington, Virginia, USA

SUMMARY

Forced convective cooling of superalloy powders generated by rotary atomization is a method (designated RSR) to produce bulk quantities of metal solidified at rates near 10^4 to 10^6 K/sec. The basic design concepts for the RSR process center about a high speed turbine driving a rotary disk which disintegrates a molten stream of metal into fine particles and accelerates them into an environment of high velocity, high mass flow helium quench gas. The process has achieved throughput rates which are favorably comparable to those of conventional industrial powder processes. More than 150 superalloy compositions have been processed by the RSR process. Typically, these alloy microstructures can be characterized as supersaturated solid solutions, of high incipient melt point, and near perfect chemical homogeneity. The boundary limits within which alloying can be effectively achieved are beyond those defined for conventional processes. Consolidation of particles and subsequent working operation, such as extrusion and forging, can be accomplished satisfactorily under parametric conditions normally used for superalloy processing. Metallurgical and mechanical tests of superalloy compositions produced in the RSR manner indicate that the process offers advantages relative to alloy strengthening, microstructure stability at high temperatures, and resistance to environmental degradation. Immediate application of the process is directed toward producing turbine blades for high performance gas turbine engines. Results to date show that a 110K increase in material temperature capability can be achieved with RSR alloys over presently used directionally solidified superalloys. Further beyond the blade application, concurrent studies show that the RSR process can have a major near term impact on components such as turbine disks and inlet guide vanes and can lead to major improvements in operating efficiencies and performance of tomorrow's turbomachinery.

INTRODUCTION

The strongest superalloy turbine airfoil used in today's most advanced production jet engine is cast from a composition developed more than 15 years ago. This composition is the alloy Mar M 200 and the application is in the Pratt & Whitney Aircraft F100 engine, which powers the USAF F-15 and F-16 aircraft. Better component design and better materials processing have enabled significant gains in jet engine performance since the alloy was introduced; however, it is apparent now that turbomachinery cannot be improved further until better superalloys become available.

The greatest contributing factor to this 15-year leveling-off period has not been the lack of development interest; every major aerospace organization has performed extensive efforts to further upgrade turbine blade superalloy capability. Rather, it is that the boundary conditions imposed by exclusive use of vacuum induction melting-vacuum arc (or electroslag) remelting have been reached and cannot be extended without a change to this mode of processing. These boundary conditions exist in the form of chemical segregation of ingot or casting, which subsequent solid state operations cannot eliminate.

Rapid solidification of powder metals, i.e., in the range of 10^4 K/sec and faster, has been shown in the laboratory to provide unique and distinct characteristics which circumvent these alloying constraints. Massive phase reactions, eutectic formations, and abnormally low incipient melt temperatures are eliminated with this approach, all of which are common to conventional casting processes. Additionally, alloying boundaries are expanded such that more effective utilization of refractory alloying additions, interstitials, and precipitation hardening elements is achieved.

Finally, the homogeneity resulting from such a process enhances the metallurgists' capability to work the material into a desired form and subsequently to heat-treat for maximum strength.

As a result of these findings, the U.S. Defense Advanced Research Projects Agency (ARPA) initiated a program with Pratt & Whitney Aircraft to develop the technology for gas turbine airfoil application. Two objectives were established. The first was to demonstrate that rapid solidification of superalloy powder could be achieved under circumstances of realism relative to jet engine requirements for volume production of material. The second, and most important, was to apply the technology in order to develop a superalloy composition which could increase the turbine airfoil metal operating temperatures in the F100 engine. Specifically, the goal was set at an improvement of 55K operating capability over the best turbine airfoil material now in production.

RAPID SOLIDIFICATION RATE ATOMIZATION

A device for producing rapidly solidified alloy powders was constructed by Pratt & Whitney Aircraft which uses the principle of forced convective cooling of molten particles accelerated from a central source into a high conductivity gas quench medium.

The actual rig is shown in Figure 1 and uses helium as the quench gas. The atomizer is a spinning disk driven by a radial impulse turbine. The present melt capability is 45 kg. The unit is equipped with high speed recorders and cameras, and real time video, for data acquisition. The operating parameters can be varied independently for individual study. Maximum capability now is (1) turbine speed, 25,000 rpm; (2) He mass flowrate, 0.91 kg/sec; and (3) He velocity, 0.7 Mach; (4) metal flowrate, 0.23 kg/sec.

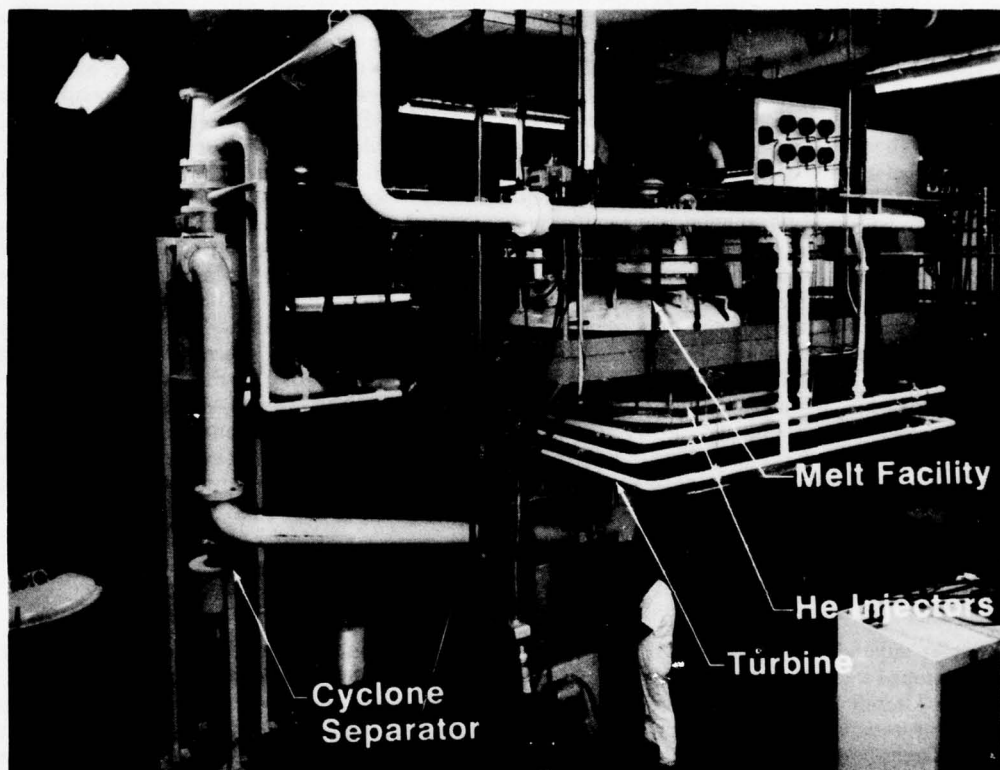


Figure 1. Rapid Solidification Powder Rig

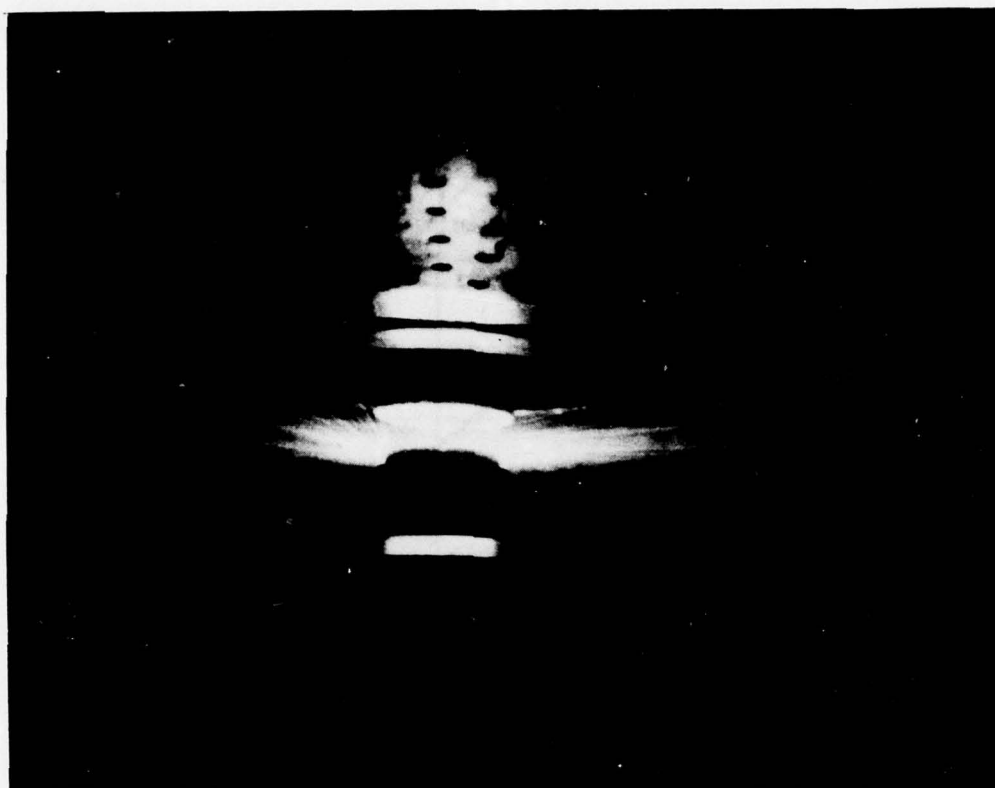
PC 33756

The sequence of events for operation is, in order, (1) vacuum induction melting, (2) He back filling, (3) turbine activation, (4) liquid metal pouring, (5) gas injection, (6) atomization, and (7) collection. The operation is shown in Figure 2. Steady-state atomization occurs within a fraction of a second after startup. Total system equilibration, as measured by cooling water temperature stabilization, occurs after about 12 to 14 sec into the run.

Operation in the mode described results in a high yield of powder of the size fractions desired. Figure 3 shows the statistical distribution of powder particles generated at a turbine speed of 24,000 rpm and a metal mass flowrate of 0.18 kg/sec. The total powder yield approaches 98% of the poured metal charge, with about 70% of this amount in the size range commensurate with greater than 10^4 K/sec cooling. The distribution for most (95% of total) of the particle sizes appears statistically as a normal distribution, which is highly desirable since it typifies a narrow particle size range. The upper deviation is attributed to transients on startup and shutdown.

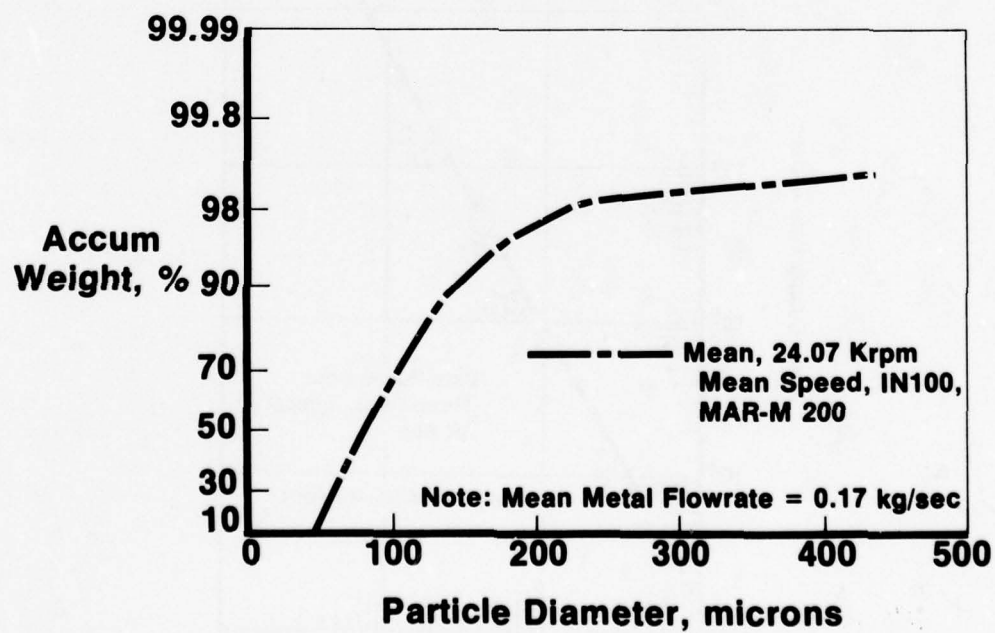
Cooling rates analytically predicted for this device, as a function of particle size, are shown in Figure 4. They are compared in this figure to rates possible with infinitely fast heat transfer. It is interesting to note that only about 2-3 orders of magnitude separate the rates possible with forced convection with He (the quench medium used in the rig) from those obtained when resistance to heat extraction is nil. Dendrite arm spacing (DAS) is a widely used measurement of cooling rate. In relating measurements of DAS from powders produced by this method to actual cooling rate and to the analytical predictions, it is evident that expectations have been achieved. Figure 5 shows the relationship of the analytical prediction to experimental results.

The powder produced by this process is spherical and free from the aggregate buildup common to conventional gas atomization. This is important for efficient heat transfer and is the result of all particles attaining the same initial velocity and proceeding on trajectories common only to the same particle sizes. The tap density of the material is about 63% of theoretical. Experiments which were run to determine whether settling of the fines would occur in a containerized situation, resulting in local density variations, proved negative. Even after extensive vibration in a confined stack, no variation in starting density was evident. The typical appearance of the powder is shown in Figure 6.



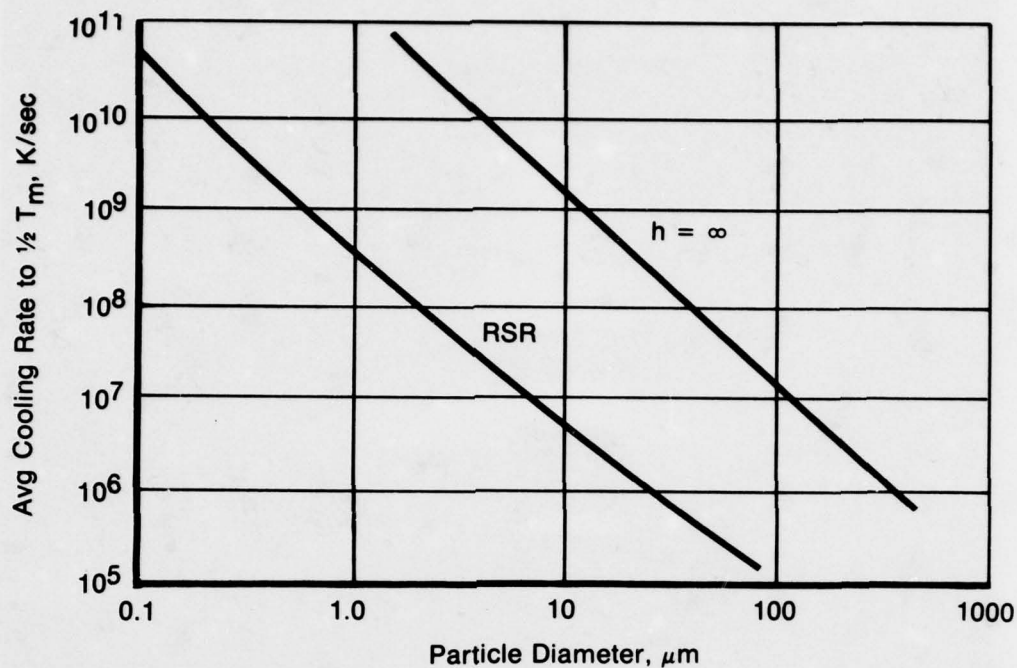
PC 38053

Figure 2. Appearance of RSR Atomization



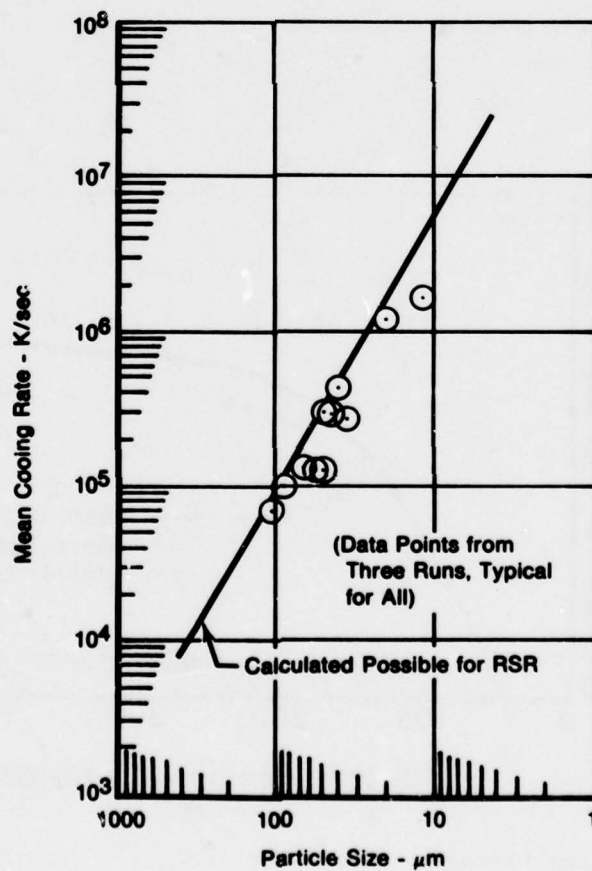
AV 118859

Figure 3. Accumulated Weight % vs Particle Size



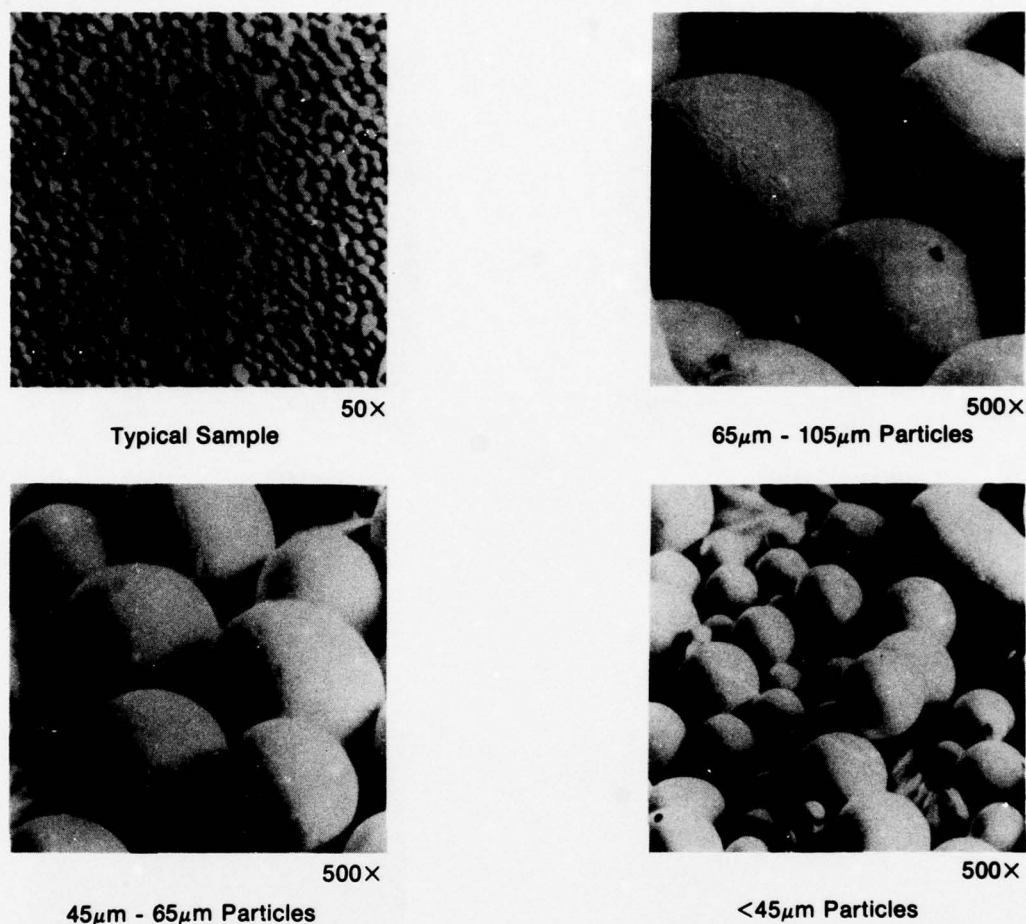
AV 116706

Figure 4. Cooling Rates Possible in Superalloy Powder



FD 98342

Figure 5. Experimentally Determined Cooling Rates



FD 98339

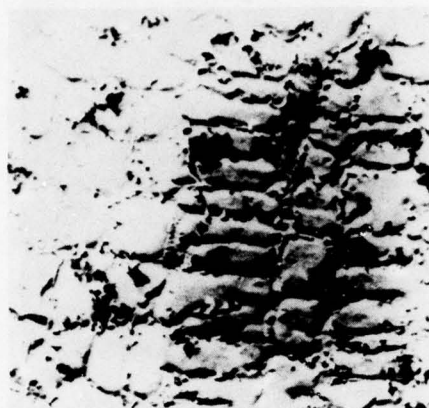
Figure 6. Surface Appearance of IN100 Alloy Powder

More than 150 experimental superalloy compositions have been atomized and evaluated to date. All fall within the general class of precipitation hardening nickel-base alloys but can be categorized further according to the following particulars:

1. Conventional precipitation hardening superalloys
2. Alloys normally referred to as DS eutectics
3. Alloys with high γ concentrations (>60 a/o)
4. Alloys based on the Ni-Al-Mo ternary.

Photomicrographs of alloy powder microstructures are shown in Figure 7 and point out in dramatic terms how rapid solidification improves chemical homogeneity and suppresses phase reaction. The coarse particles (150 μm) exhibit a typical dendritic structure with fairly extensive reaction in the interdendritic regions. As the powder becomes finer (100 μm), a refinement in structure and suppression of secondary reaction is very evident. These two conditions represent cooling of about 10^4K/sec and about 10^6K/sec , respectively. When even finer particles are produced, such as those shown in the lower photos, almost complete homogeneity is obtained. Secondary reactions in these cases are minimal and the structure can be viewed as essentially a single phase, supersaturated solid solution. The solidification rates which produced these structures were about 10^6K/sec . These photos are of the alloy IN100 and are considered typical for all alloys evaluated to date.

The classically dendritic solidification form has been observed in all runs and was the only form anticipated. As is also shown in Figure 7 in the lower left photograph, a microcrystalline form of powder developed. This form of structure was observed to be predominant in the finer powders produced by the atomization. The crystallites have a mean diameter of about $2\mu\text{m}$ and are free of any dendrite appearance. Microprobe traces across both forms show that the microcrystalline form is more homogeneous. The standard deviation of Ti (the most sensitive element to our probe analysis) in the dendritic material was about 18%; in the microcrystalline material it was about 5%. Both are a magnitude or more better than the alloy homogeneity which can be obtained by other process techniques.



~150 μ m Particle



~100 μ m Particles

10 μ m



1 μ m

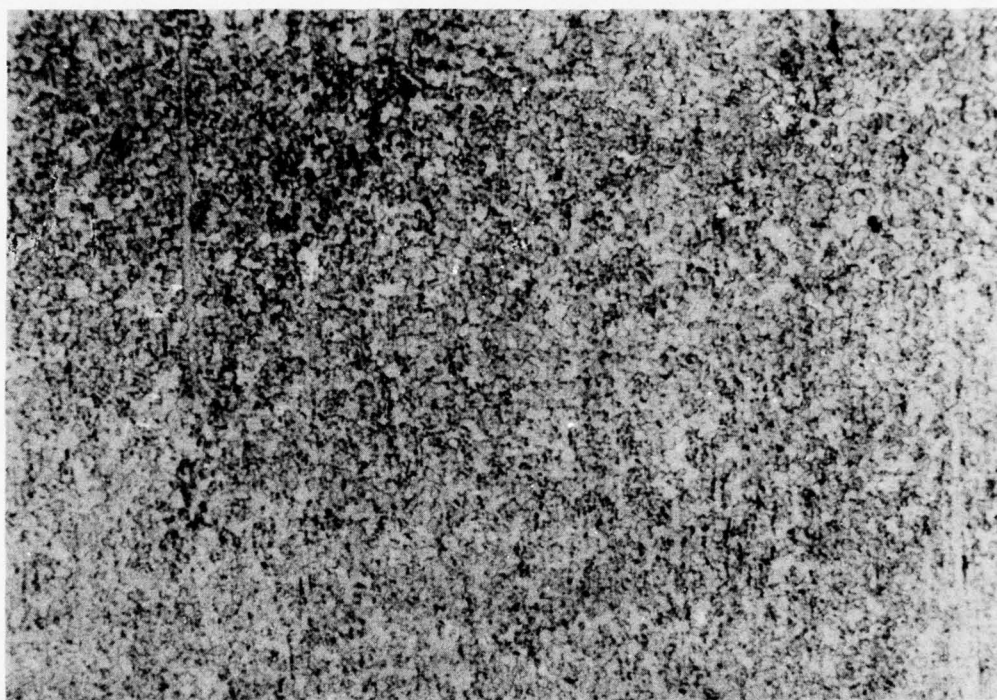
Particle Sizes \leq 65 μ m

Figure 7. IN100 Alloy Powder Microstructures

METALWORKING AND MECHANICAL PROPERTIES

Not surprisingly, the parameters for consolidation and metalworking were different for those rapidly solidified materials than for the conventionally processed alloy. It was found that, typically, recrystallization temperatures were higher and kinetics of reaction slower.

HIP and HIP + isothermal forging were satisfactory methods for powder consolidation and forming, and were best accomplished in the temperature range of 0.8-1.0 of the principle secondary phase solvus. Recrystallization was not effectively controlled by so doing, however. Apparently, those particles referred to as microcrystalline would undergo superplastic deformation during HIP consolidation and result in little, if any, deformation of the dendritic particles. During isothermal forging, the same result occurred. Subsequent annealing at very high temperature ($\sim 0.9 T_m$) was effective in eliminating the residual cast structure, but at the expense of grain coarsening, a condition we were trying to avoid. HIP consolidation followed by extrusion or direct extrusion of the loose powders did, however, lead to consolidated product with a uniform recrystallization pattern. The extrusion conditions we judged best included temperatures again in the range of 0.8-1.0 of the principle secondary phase solvus and reduction ratios in excess of 8 to 1. Typical examples of alloy microstructure after extrusion are shown in Figure 8. The structural uniformity is striking. No massive phases exist, the precipitation hardening reaction has proceeded with almost total uniformity, recrystallization is complete, and the grain size is uniform throughout. The incipient melt temperature for this material was measured to be more than 90K higher than that of a conventionally processed alloy. For high temperature operation such as this program addresses, this could be one of the major factors contributing to the overall success.

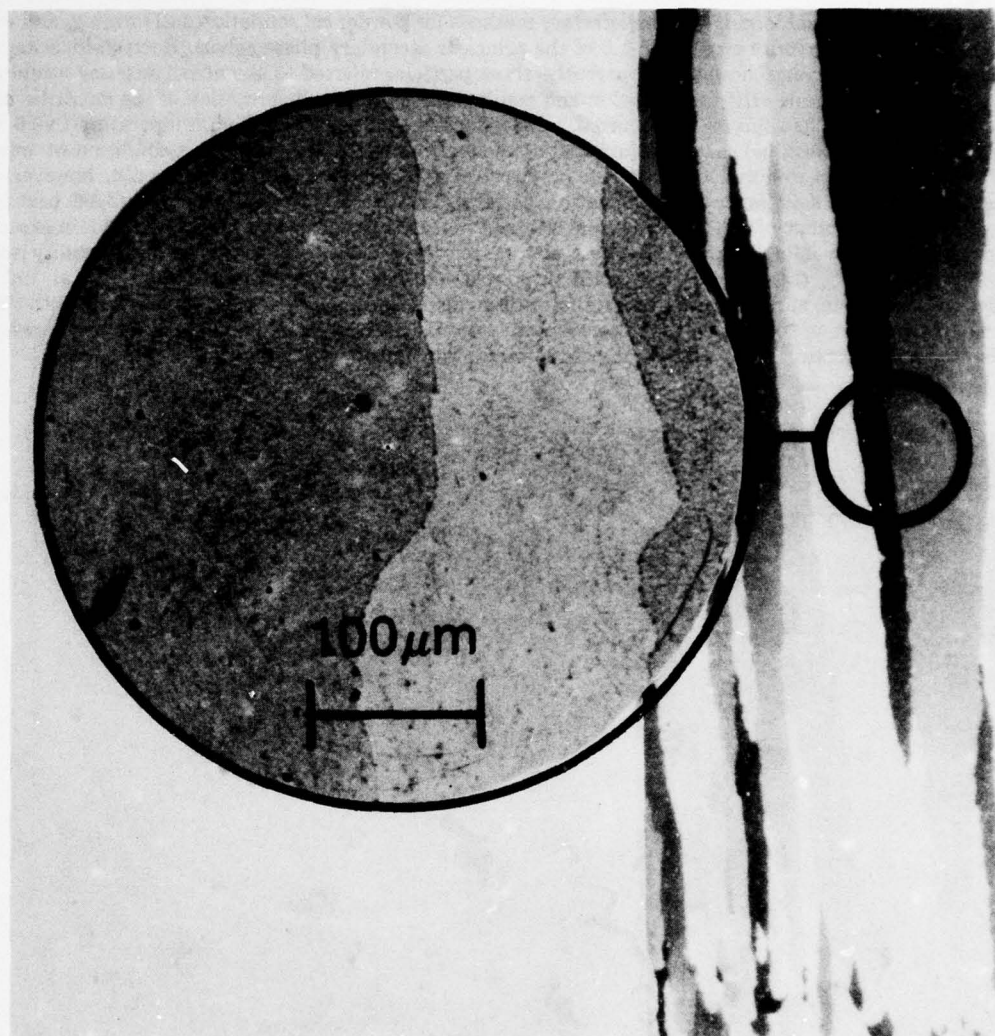


MAR M 200 Alloy
RSR 108
Mag: 100X

AV 118570

Figure 8. As Extruded Microstructure

For those alloys in which secondary phase dissolution could be achieved prior to melting, it was possible to affect abnormal grain growth, or secondary recrystallization, by annealing slightly above the phase solvus. Further, it was possible to control the grain growth by zone annealing, such that aligned grain structures of the type shown in Figure 9 could be produced. This condition was established for alloys in all classes but the eutectics.



1X

AV 116716

Figure 9. Aligned Grain Microstructure

In early tests, IN100 alloy was heat treated in accordance with specifications for standard IN100 material (PWA 1073) and repetitively tested in tensile and creep-rupture to the specification conditions. The data in Table 1 showed that tensile properties were about the same for the rapidly solidified material as for the conventional alloy. However, for the case of creep-rupture, as shown in Table 2, the rapidly solidified material showed a distinct and significant improvement over the standard alloy. Both the minimum and average test results for the fast quenched alloy were above the 4 σ upper bound of the PWA 1073 alloy. Stated in other terms, this says that in testing the PWA 1073 alloy, the chance for the conventional alloy to achieve this life is less than one in a million.

Table 1. Tensile Properties of RSR IN100

Temperature K	0.2% YS MPa $\times 10^3$	UTS MPa $\times 10^3$	EI %
Ambient	1.119	1.580	25.0
Goal at Ambient	1.124	1.586	22.0
978	1.100	1.255	14.0
Goal at 978	1.089	1.269	17.0

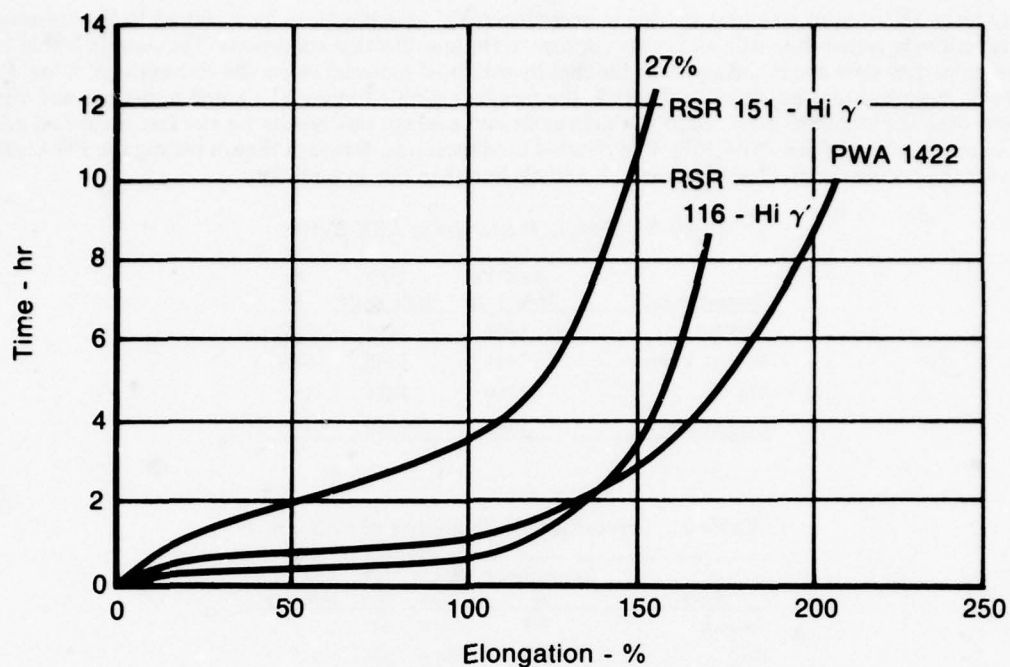
Table 2. Creep-Rupture Properties of RSR IN100

Sample	Temperature K	Stress Mpa	0.2% (hr)	Life (hr)	EI %
Smooth	978	551.6	272	-	-
Goal	978	551.6	195	-	-
Smooth	1005	637.8	-	78	7.7
Goal	1005	637.8	-	34	-
Notch, $K_T=3.2$	1005	637.8	-	96	-
Notch Goal	1005	637.8	-	>34	-

Subsequent to abnormal grain growth, the conventional series of modified Mar M 200 and AF2-1DA alloys was heat treated to re-solution the γ phase ($\sim 1488K/4$ hr/air cool), followed by somewhat arbitrarily selected 1353K/4 hr/AC + 1148K/12 hr/AC age cycles. Generally, all test results fell in line with those of directionally solidified castings of similar compositions. Enough evidence was gathered to show that increasing the concentrations of carbon, or refractory elements of γ forming elements, increased alloy strength, but no indications were detected which would suggest that major alterations to this series, relative to strength, could be achieved by powder metallurgy alloying methods. Grain orientation in these powder alloys was [110] in the aligned direction, which did result in a substantial increase in modulus of elasticity over that of directionally solidified alloys (approximately double) which, in turn, leads to favorable benefits for turbine blades relative to engine vibration characteristics.

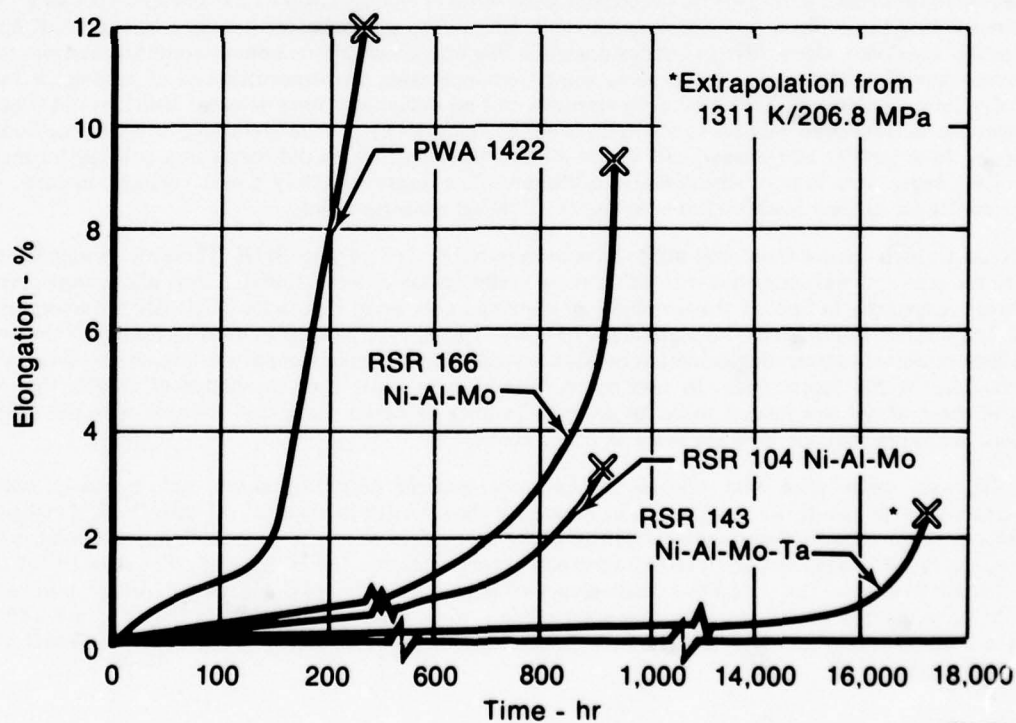
The Ni-Al-Cr high volume fraction γ alloys have been tested to date only at 1311K. These alloys were heat treated similarly to the conventional series but with solutioning cycles on the order of 1598K. These alloys were surprisingly creep resistant, especially in light of the simplicity of alloying as shown in Figure 10. Obviously refractory additions, such as W, Hf, and Nb, improved the strength of the base Ni-Al-Cr alloy. The most interesting feature of this series was that the alloys exhibited outstanding oxidation resistance while simultaneously imparting strength levels approaching those of the Mar M 200 composition. In concurrent dynamic and static tests conducted at 1423K, the oxidation resistance of these alloys was judged to be an order of magnitude better than that possible with the Mar M 200 composition. Grain orientations were the same as noted above.

The Ni-Al-Mo series were heat treated in the same manner described above and, typically, solutioning temperatures were near 1588K. As can be seen in Figure 11, the strength levels attained with these compositions far surpassed those achieved with directionally solidified alloys and can be shown to be a 110K improvement in the high temperature regime, which is twice the level of improvement set as the objective of this work. The strength is attributed to a high Mo partitioning to the γ and to a finely dispersed α Mo phase in the Ni-Mo matrix. Alloy modifications are presently being evaluated and it appears that substitution of elements, such as W or Ta or minor additions of interstitial elements, further increase strength through a series of dispersion strengthening reactions. Grain orientation with these alloys was [111].



FD 134761

Figure 10. Creep Deformation of High γ' Alloys 1311K/97.9 Mpa



FD 134762

Figure 11. Creep Deformation of Ni-Al-Mo (+Ta) 1311K/97.9 MPa

CONCLUSION

Granted, the testing has only started and the amount of data contributing to this comparison is limited with respect to the rapidly solidified material. However, it gives every suggestion that better materials are possible using this process mode. This is especially true when one stops to consider that no effort was made to develop an optimum heat treat for this material, which is known to react differently to the precipitation hardening mechanisms.

It is now accepted that the technology being developed under this present program is indeed new and offers many benefits beyond the one gained through turbine blade application. For other components in the jet engine alone, the list of possible uses becomes astounding. Better turbine disks become imminently possible, and new alloys for combustors and vanes do not seem unrealistic.

Beyond the jet engine, the implications of rapid solidification excite one's imagination to levels rarely offered. Magnetic materials, glassy alloys, superconductors, higher strength aluminum, more corrosion resistant alloys, and totally new alloys all seem possible.

The technology is only emerging. It is in its infancy, but already results show that a new era of metals is fast approaching. This ARPA program has provided the necessary stimulus. As time will tell, not only will the better turbine blade for the F100 engine evolve, so too, will many many other applications benefiting DoD and society in general.

ACKNOWLEDGMENTS

This work is being sponsored by the U. S. Defense Advanced Research Projects Agency under ARPA Order 3152. The monitoring agency is the U. S. Air Force Materials Laboratories, Wright-Patterson Air Force Base, Ohio.

The views and conclusions contained in this document are those of the authors and should not be interpreted as necessarily representing the official policies, either expressed or implied, of the Advanced Research Projects Agency or the U. S. Government.

HOT ISOSTATIC PROCESSING OF IN-738 TURBINE BLADES

by

G. Van Drunen and J. Liburd1,
Turbine and Generator Division, Westinghouse Canada,
Hamilton, Ontario, L8N 3K2

and

W. Wallace and T. Terada,
National Aeronautical Establishment, National Research Council of Canada,
Ottawa, Ontario, K1A 0R6

SUMMARY

The removal of casting defects by hot isostatic processing (HIP) benefits turbine designers with improved alloy utilization and turbine users with increased reliability. The present paper describes work performed with an investment cast nickel-base turbine blade alloy, IN-738. The effects of different HIP parameters on microstructures and mechanical properties were examined. It was found that properly HIP processed blades exhibit improved stress rupture, fatigue and tensile properties compared to conventionally cast and heat treated material.

INTRODUCTION

One of the earliest and most important technologies in net-shape processing was precision investment casting. The benefits resulting from this process are well known and need not be elaborated on here. Notwithstanding the merits of investment casting the process is not without its many problems. Random casting defects such as shrinkage cavities, hot tears, microporosity and inhomogeneity can lead to high scrap rates, high fabrication costs, and can limit application of castings in favour of more predictable but more expensive wrought materials. Where cast parts are used, variations in product quality and properties can severely limit their allowable design stresses.

Many of the defects mentioned above can be eliminated by hot isostatic pressing, involving simultaneous application of heat and pressure to the part in an autoclave. HIP densification has been demonstrated on a wide range of aerospace materials, including superalloys (1-5), ferrous alloys (2), aluminum (2) and titanium (1,2,6) alloy castings. These studies have indicated that HIP processing can provide benefits from:

- (a) Reduced scrap rates and hence lower cost.
- (b) Use of higher strength alloys which previously were unusable due to poor castability.
- (c) Wider application of large complex castings otherwise prone to excessively high porosity.
- (d) Improved weldability and hence lower fabrication costs.
- (e) Replacement of expensive wrought components by premium castings.

These benefits indicate that HIP processing itself warrants special consideration in discussions of net shape processing.

In the case of superalloys, numerous empirical studies have established the time, temperature and pressure parameters required to close internal voids and achieve full density. However there has been relatively little attention given to the detailed effects of HIP processing on microstructure, and therefore to the optimization of HIP or post-HIP thermal cycles for specific applications. Also very little has yet appeared on the improvements that might be expected by HIP processing of production lot quantities of parts.

This paper describes a study of HIP processing carried out on a production set of IN-738 turbine blades for a Westinghouse industrial gas turbine engine (7). The effects of the HIP thermal cycle on microstructure and mechanical properties are examined critically, and the need for modified thermal cycles to counteract deleterious side effects of HIP is demonstrated. While the study relates to land based turbine hardware the information presented is equally applicable to similar aero engine components.

MATERIALS AND PROCEDURES

Initial work was carried out with cast-to-size (CTS) test bars (6 mm diameter). Since CTS bars are not machined after HIP processing and heat treatment they provide information on surface effects resulting from exposure to high gas pressures at elevated

temperature. In addition, test bars machined from blades (MFB) are used to verify internal blade properties. CTS test bars of both the standard and the low carbon, low zirconium (LC) alloy modification of IN-738 were evaluated. The nominal alloy compositions are given in Table I.

TABLE I

Nominal Alloy Composition for IN-738, Composition in Weight %

Element	Cr	Co	Ti	Al	W	Mo	Ta	Nb	C	Zr	B	Ni
LOW carbon mod.	16	8.5	4.4	3.4	2.6	1.75	1.75	0.9	0.11	0.04	0.01	Bal
STANDARD	"	"	"	"	"	"	"	"	0.17	0.11	"	"

Following the feasibility study with the CTS bars and sample blades, a full engine set of compressor turbine blades cast in the LC alloy modification were HIP processed. These blades can exhibit significant (X-ray undetectable) microporosity particularly in the heavier sections of the casting such as the airfoil/root transition shown in Figure 1.

HEALING OF CASTING DEFECTS BY HOT ISOSTATIC PRESSING

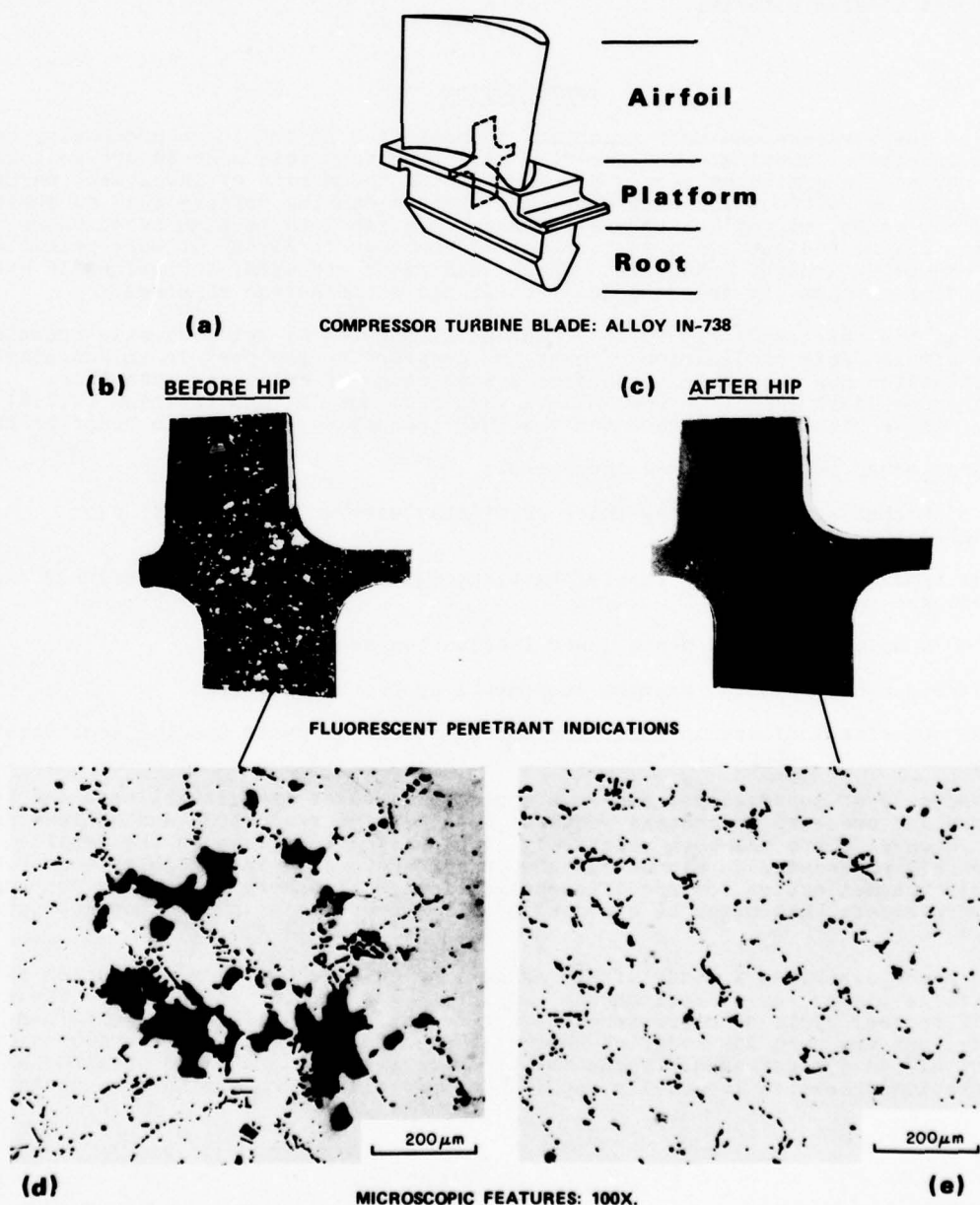


Figure 1 Effect of HIP processing on microporosity in an investment cast turbine blade.

HIP processing was carried out at Westinghouse Canada using a top loading autoclave fitted with a Kanthal wound furnace. The furnace work zone is 300 mm in diameter by 900 mm high and has a temperature capability of 1230°C. The system can be pressurized to 140 MPa with argon.

No unusual measures were taken to minimize surface contamination during processing of the CTS test bars. Subsequent mechanical testing and metallography revealed that oxidation and nitriding had occurred with deleterious effects. To minimize this problem with blade castings care was taken to suppress surface attack. This was accomplished by argon shrouding and purging during loading and unloading and the use of several evacuate/backfill cycles prior to increasing temperature and pressure to process levels.

HIP and Post-HIP Thermal Cycles

Previous work on superalloys (2,3) has shown that HIP temperatures should be above the gamma prime (γ') solvus of the alloy so that the material can flow readily under the external pressures imposed to close internal voids. For IN-738, temperatures in the range 1180°C to 1200°C and pressures of 100 MPa applied for about two hours lead to complete densification (3).

While observing these general requirements two distinct HIP + post-HIP thermal cycles were examined. The first (HIP-A), shown schematically in Figure 2(b), was similar to that employed by Wasielewski and Lindblad (3). After hot loading at the furnace idle temperature of 900°C, the vessel was closed and evacuated and then heated and pressurized simultaneously to 1200°C and 100 MPa. After two hours the temperature and pressure were lowered simultaneously until the temperature reached 900°C. The charge was then removed and air cooled. Post-HIP treatment consisted of a full γ' solution treatment for two hours at 1200°C (FST in Figure 2(b)), followed by a partial γ' solution treatment for two hours at 1120°C (PST) and ageing for 24 hours at 845°C. This post-HIP treatment is essentially the optimum heat treatment developed by Bleber and Mihalisin (8) for cast IN-738, with the addition of the FST stage which is used to refine the γ' precipitate which otherwise would be over-aged due to the initial slow autoclave cool. The standard heat treatment (SHT), shown schematically in Figure 2(a), was applied to as-cast material for reference purposes.

As observed by Wasielewski and Lindblad (3) the HIP-A procedure resulted in acceptable 980°C stress rupture properties, however, as will be shown later, it can cause considerable loss of intermediate temperature stress rupture life and ductility, particularly in CTS bars. Accordingly a modified cycle (HIP-B) was developed. This is illustrated in Figure 2(c). The cycle was similar to HIP-A except that the full solution treatment was eliminated, and the autoclave was depressurized and cooled directly, under controlled conditions, to the partial solution temperature. In the HIP-B cycle therefore material is slowly cooled through the γ' precipitation range, compared to the rapid air cool experienced following the full solution stage (FST) of the HIP-A cycle.

Mechanical Testing and Metallography

Cast to size bars were tested in the processed condition without further machining. Additional test bars were machined from fully processed blades selected at random from the full blade set. These MFB samples were identified according to their original locations in the blades, (airfoil, platform, or root samples) as indicated in Figure 1. Tensile and stress rupture samples had gauge sections 3.75 mm in diameter by 20 mm long, while fatigue samples had gauge diameters of 5 mm. Fatigue tests were carried out under uniaxial loading at 650°C on samples machined from blade roots only.

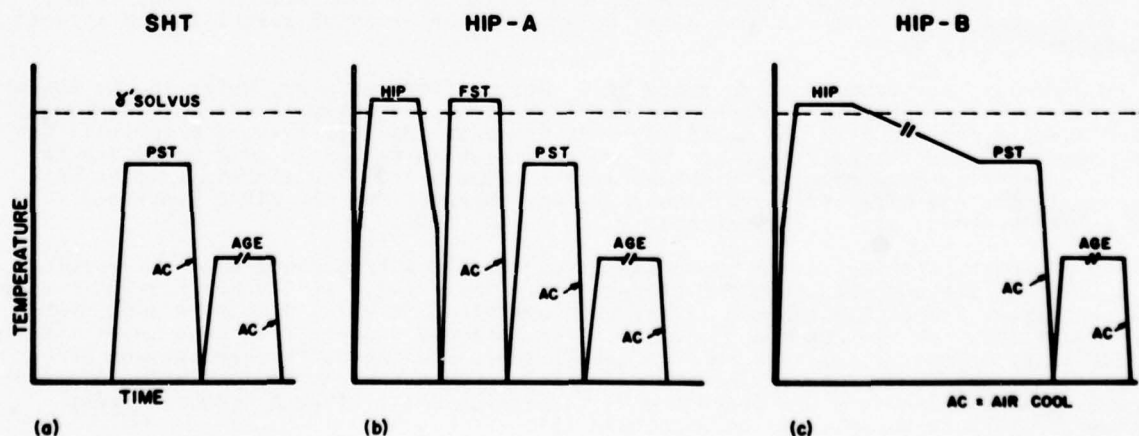


Figure 2 Heat treatments and HIP thermal cycles applied to IN-738 compressor turbine blades.

As-cast and HIP processed samples were examined metallographically before and after mechanical testing. Various etchants, as listed in Table II, were used to reveal the γ' precipitates, carbides and grain boundary structures. Carbides were also extracted electrolytically (9) after the various treatments and identified by X-ray diffraction.

TABLE II

Etchants Used in the Preparation of Metallographic Samples

Etchant	Method of Application	Used to reveal
50ml. HCl+25ml. HNO ₃ + 2g. CuCl ₂ +200ml. H ₂ O	Immersion	Chemical etch to reveal general grain and precipitate structures.
1 part - 4% aqueous NaOH + 1 part saturated solution of KMnO ₄	Swab	Stain etch to reveal carbides.
2% or 5% Bromine in methanol	Immersion	Vigorous chemical etch to reveal grain boundary structures.
10% HCl in methanol	Electrolytic	For carbide extraction and grain boundary networks

MECHANICAL PROPERTY RESULTS

Major attention in this work was paid to intermediate temperature properties since the average blade metal temperature for the part in question was expected to be under 800°C.

Stress Rupture Properties of CTS Bars

Initial stress rupture tests were carried out at 760°C and 586 MPa on the CTS bars of the low carbon and standard carbon alloys. The results are shown in Figure 3. For both heats the HIP-A cycle resulted in decreased life and ductility, compared to cast and conventionally heat treated material. In contrast the HIP-B cycle resulted in increased life and ductility for the standard carbon heat, and slightly decreased life but greater ductility for the low carbon heat. Since as-cast porosity in the gauge lengths of both types of test bars was generally low, these variations in properties are due primarily to the effects of HIP and post-HIP thermal cycles.

Minor variations in the HIP-A thermal cycle did not significantly affect the results shown in Figure 3. Material which was rapidly cooled from temperatures between 1175°C and 1200°C exhibited low life and ductility at 760°C relative to cast + SHT properties. However, HIP-A material tested at higher temperatures had properties similar to those reported by Wasielewski and Lindblad (3), that is, approximately 200 hours at 870°C and 275 MPa, or 50 hours at 980°C and 152 MPa.

Stress Rupture Properties of MFB Test Bars

Having shown that HIP-B could yield acceptable properties, further testing was confined to samples machined from blades in the IN-738 (LC) composition. These tests were to determine the benefits that might be achieved by removing porosity from actual production quality parts.

The results are summarized in Table III. For platform samples, which in the as-cast condition contain appreciable porosity, the HIP-B processed material showed slightly higher average rupture life and ductility than the cast and heat treated material. The cast properties were largely degraded by one sample which failed in 13.4 hours due to high microporosity occurring in the gauge length (Figure 4). For airfoil samples an increase in average life of approximately 30% was observed for the HIP-B processed material compared to cast + SHT material.

As a matter of interest one blade was given the HIP-A treatment; the test results for this blade are compared to HIP-B properties in Table III. At 586 MPa and 760°C both treatments gave comparable rupture lives, although HIP-A material displayed appreciably lower ductility. At 345 MPa and 830°C the HIP-A material suffers from both lower life and ductility. However, as test temperature is increased the difference between HIP-A and HIP-B appears to diminish. This is shown by the last two entries in Table III which compare HIP-B results from the present work to slab material given a treatment very similar to HIP-A by Wasielewski and Lindblad (3).

Comparison of the Table III MFB results with the CTS data of Figure 3 reveals several notable differences. First, the HIP-B MFB bars have considerably lower lives than comparable CTS test bars. This is attributed to differences in grain structure and test bar size. Similar behaviour has been reported previously for cast nickel-base

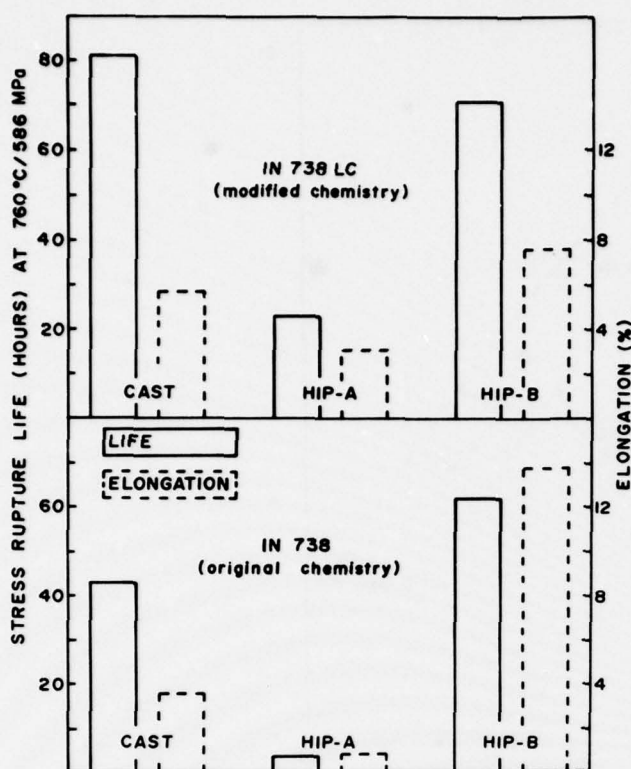


Figure 3 Comparison of the average 760°C stress rupture properties of IN-738LC and IN-738 CTS bars in the as-cast and HIP conditions.

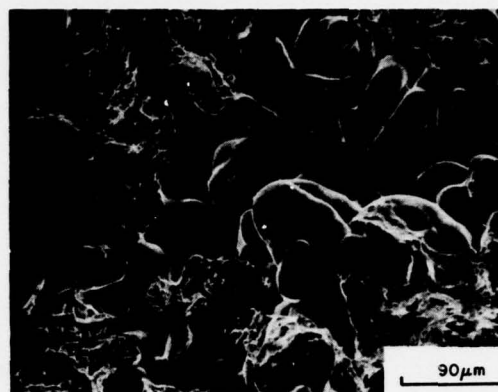


Figure 4 Porosity revealed by scanning electron microscopy on the fracture surface of an as-cast MFB test bar which failed in 13.4 hours at 760°C/586 MPa. 220 X

TABLE III

Comparison of Average Stress Rupture Properties of MFB Test Bars

Material Condition	Test Bar Location	No. of Tests	Stress (MPa)	Temp. (°C)	Life (Hrs)	Elong. %
Cast blade	Platform	5	586	760	31.8	6.5
HIP-B blade	Platform	4	586	760	38.7	7.5
Cast blade	Airfoil	5	586	760	42.6	9.4
HIP-B blade	Airfoil	8	586	760	56.3	9.6
HIP-A blade	Various	5	586	760	48.0	5.9
HIP-B blade	Various	12	586	760	50.4	8.9
HIP-A blade	Various	3	345	830	182.6	3.8
HIP-B blade	Various	10	345	830	245	9.0
HIP-B blade	Various	4	152	980	51.2	12.5
HIP slab (Ref.3)	-	-	152	980	42-60	10-18

superalloys (10,11). A second point of interest is that HIP-A MFB bars have much better stress rupture properties than similarly treated CTS bars. This is believed to be due to surface contamination effects during high temperature processing as will be discussed in a subsequent section.

Finally, in addition to the results of Table III, stress rupture testing was extended to ensure that HIP-B processed material retained its favourable rupture properties over wider ranges of stress and temperature. These results are shown in Figure 5 where they are compared to CTS bar data for cast and conventionally heat treated material. In general it was observed that test bars from blade roots had the shortest lives, while the longest lives were observed in bars from the blade airfoils.

The results of Figure 5 are comparable to properties reported elsewhere for HIP processed IN-738 (3). With the exception of one test at 760°C, all the HIP-B processed 3.75 mm diameter MFB tests fell inside the scatter band for 6.25 mm heat treated (SHT) CTS bars.

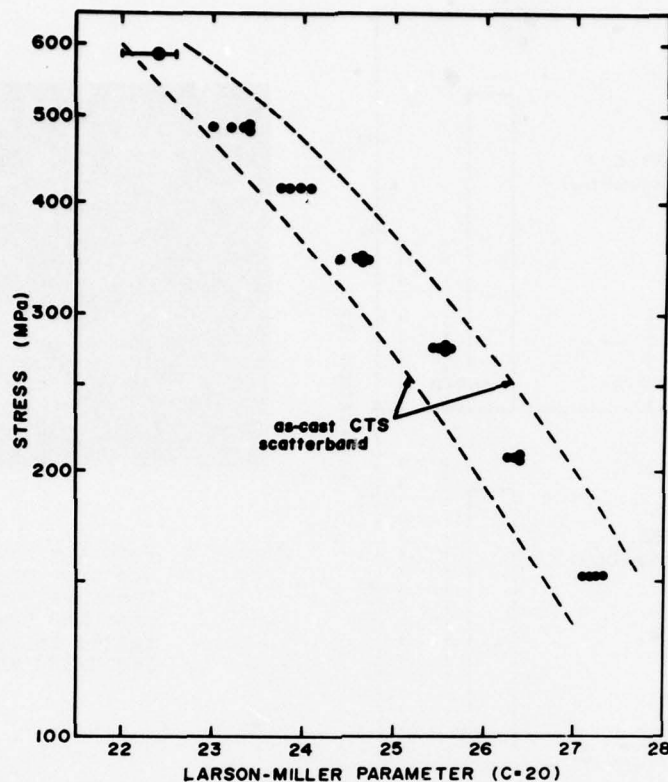


Figure 5 Larson-Miller plot for HIP-B treated MFB test bars compared to the scatterband for as-cast CTS test bars.

Tensile Properties

The results of tension tests at 25°C and 650°C on MFB test bars are given in Table IV. With the exception of room temperature elongation, the HIP-B processed material exhibited higher strength and ductility than the cast and heat treated material.

TABLE IV

Comparison of Tensile Properties in Cast and HIP Processed IN-738 (LC), Samples Machined from Blades

Material Condition	Test Temp. °C	UTS MPa	0.2% YS MPa	Elong. %	R.A. %
Cast + SHT	25	917	779	6.9	8.5
HIP-B treat.	25	952	841	5.7	13.0
Cast + SHT	650	938	662	8.3	10.6
HIP-B treat.	650	986	710	8.9	13.3

Fatigue Properties

High cycle fatigue properties of HIP-B material are compared to cast material in Figure 6 in the form of a stress range diagram, where each point represents the combined mean stress and stress amplitude required to produce failure in 10^8 cycles. The data for the HIP processed material shows a 10% to 20% improvement over normal cast and heat treated material.

Mechanical Property Summary

The mechanical property study has confirmed the important practical benefits that can be achieved by HIP processing. Tensile and fatigue strengths were increased, and stress rupture properties in thick section components were improved to match typical properties of sound cast to size material.

At the same time the study has shown that HIP processing can cause deleterious side effects. Material processed by the HIP-A cycle exhibited inferior rupture properties at 760°C and 830°C, indicating a pronounced sensitivity to the ductility trough problem (12-14), while material processed by the slightly modified HIP-B cycle was less prone to this problem. Metallographic examinations were conducted to explore the reasons for these differences.

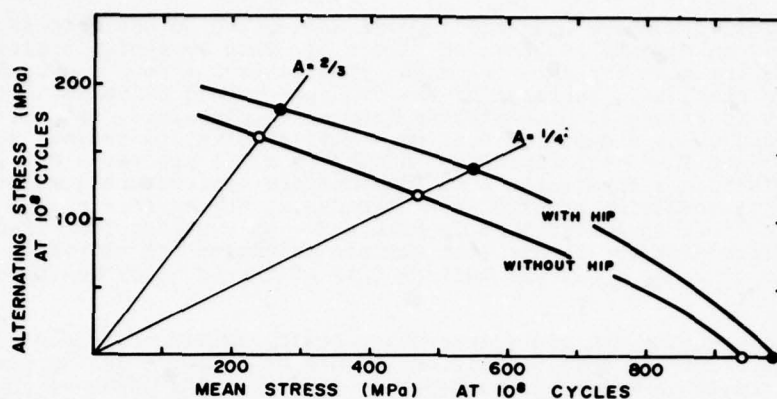
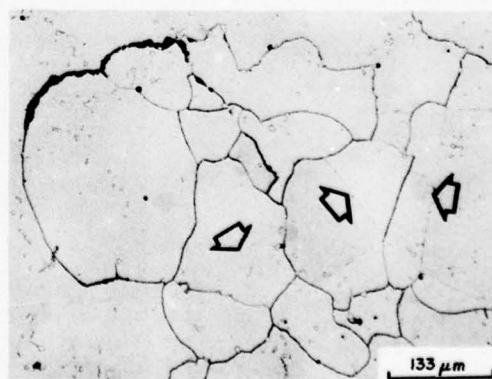
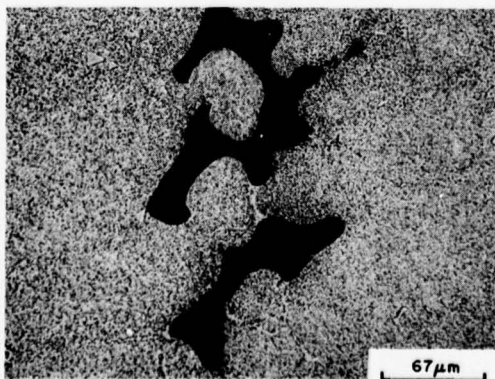
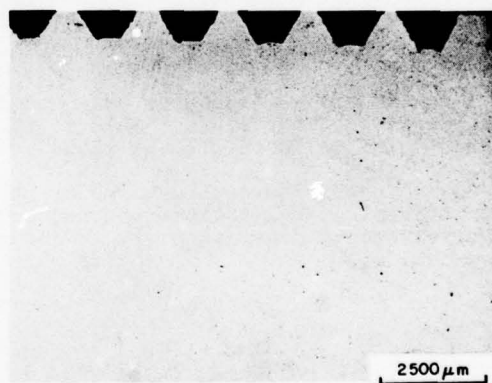
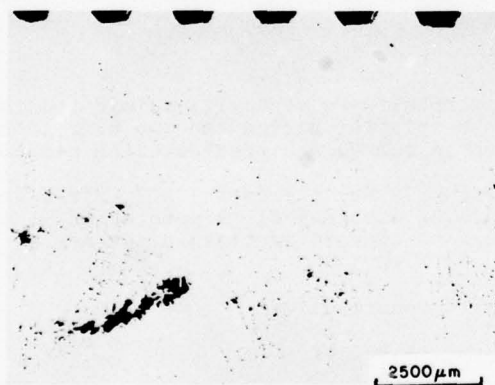


Figure 6 A stress range diagram comparing the high cycle fatigue properties of HIP and cast IN-738LC at 650°C.

METALLOGRAPHIC RESULTS

Porosity Closure and Surface Effects

The CTS bars generally had X-ray detectable porosity in the grip sections as shown in Figures 7(a) and 7(c). Both of the HIP cycles examined were successful in closing internal (non-surface connected) porosity, as indicated in Figure 7(b). During HIP processing extensive flow of material occurs to fill these large voids, often resulting in regions containing recrystallization twins as shown in Figure 7(d). Also, precipitate structures developed in these regions differ slightly from those developed elsewhere in the structure. In stress rupture samples secondary cracks are occasionally observed at grain boundaries in such twinned regions. The full significance of these observations is not yet known and further work is in progress. However, the results suggest that the salvaging of castings containing gross porosity (X-ray detectable) by HIP processing may not result in as strong a product as would be obtained from a sound casting.



Occasionally unclosed (surface connected) pores were found in the grip sections of HIP processed CTS bars, an example is shown in Figure 8. This type of porosity fails to close during HIP since the high pressure argon gas penetrates the pore and counteracts the external isostatic pressure. Surfaces of the CTS bars showed evidence of oxidation and nitriding as shown in Figure 8. The nitride needles or platelets, oxidation and alloy depletion extended up to a depth of 0.05 mm. This observation can be used to rationalize the difference in stress rupture behaviour in HIP-A processed CTS and MFB bars. The HIP-A condition has inherently less intermediate temperature ductility as shown in Table III, this condition coupled with nitrides at the surface results in the notch sensitive type of behaviour displayed in Figure 3. By contrast the HIP-B condition possesses ample ductility with the result that surface oxidation and nitriding may only account for the slight decrease in stress rupture life of the LC alloy modification evident in Figure 3.

Surface connected porosity and gross internal porosity should not occur in the turbine blade castings. Both of these conditions should be detected during normal non-destructive testing procedures which all blades have to pass. The depth of the surface affected zone in HIP processed blades was less than 0.02 mm and consisted solely of oxidation and alloy depletion, no nitride formation was found. This indicates that the surface protection measures employed were effective. Recent improvements in this area have shown that depth of surface attack can be kept to about 0.002 mm.

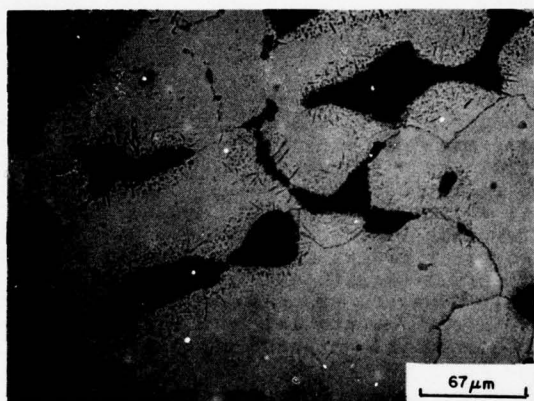


Figure 8 Surface connected porosity in the grip section of a CTS bar after HIP-A processing. Note the internal oxidation and nitride formation.

Precipitate Structures

The eutectic γ - γ' nodules observed in cast material were virtually eliminated in the HIP processed materials. This γ' is taken into solution during the two hour 1200°C treatments and is therefore available to take part in subsequent precipitation reactions.

The γ' precipitate structures are shown in Figure 9 for the cast + SHT, HIP-A and HIP-B materials. All treatments produced a mixture of cuboidal first generation γ' and spheroidal second generation γ' , as shown in Figure 9. The γ' particle sizes are as follows:

Treatment	Cuboidal γ'	Spheroidal γ'
Cast + SHT	0.45 μm	0.1 μm
HIP-A	0.38 μm	0.1 μm
HIP-B	0.6 μm	0.1 μm

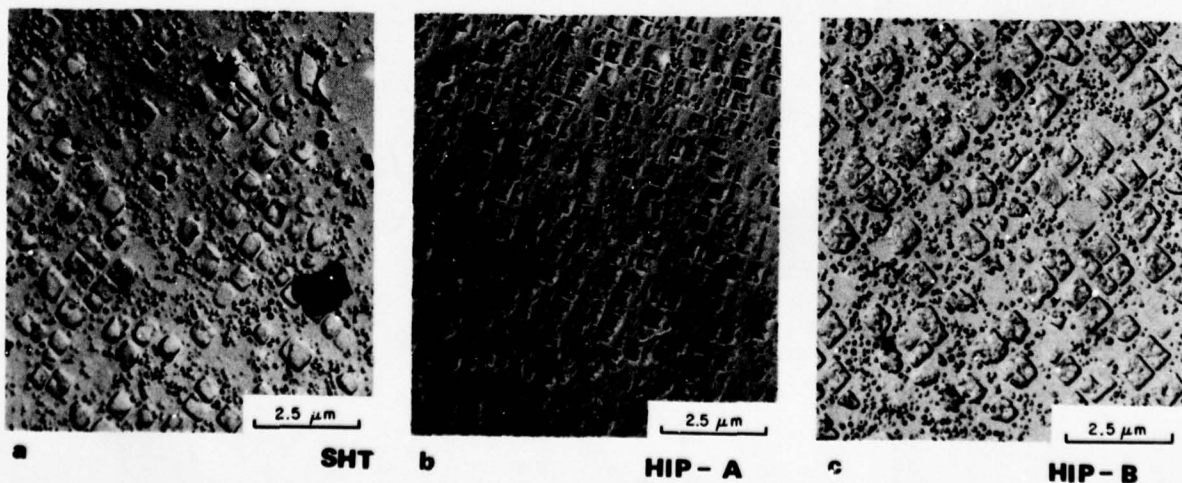


Figure 9 Electron micrographs showing the gamma-prime precipitate structures in cast and heat treated IN-738LC.

The rapid air cool through the γ' solvus in HIP-A causes a more homogenous nucleation of γ' and the subsequent competitive growth of these nuclei at 1120°C leads to smaller particle size and interparticle spacing than in cast or HIP-B processed material. The spheroidal γ' size was similar in all conditions examined.

Carbide Structures and Grain Boundaries

The carbide contents were virtually identical in all materials with respect to type and amount, as indicated in Figure 10 and Table V. The dominant carbide was MC ($a=4.38\text{\AA}$) which occurred as blocky primary particles at grain boundaries and in grain interiors. The grain boundaries also contained films of fine secondary MC which formed at high temperatures prior to ageing at 845°C. The HIP processed materials contained larger amounts of precipitated carbide (see Table V) than the cast + SHT material, but there were no significant differences between HIP-A and HIP-B conditions, and only faint traces of $M_{23}C_6$ were found in each sample both before and after stress rupture testing.

While carbide contents were similar, there were consistent differences in grain boundary structure. The cast + SHT and HIP-B processed materials showed boundaries having a finely serrated or zig-zag structure, while HIP-A material showed very smooth grain boundaries as illustrated in Figure 11(a) and 11(b). The scanning electron micrograph of Figure 11(c) was obtained using a 5% Br in methanol chemical etch which attacks the γ phase preferentially, while Figure 11(d) was obtained using an electrolytic etch which attacks γ' preferentially. Both etching techniques revealed similar carbide films in all material conditions, thus confirming that the films are carbides and not undissolved γ' . The carbide films sometimes appeared thicker in HIP-B material because of the zig-zag nature of the boundary, as indicated in Figure 11(d).

Apparently the serrated grain boundary structure is an inherent feature of as-cast material, and is one which tends to be destroyed during high temperature (1200°C) processing. Controlled HIP processing, as in HIP-B allows these serrations to reform during the later stages of the thermal cycle.

TABLE V

Carbide Contents in Cast and HIP Processed IN-738.

Material Condition	Carbide Type and Content.	
	Lattice Param.	Wt%
Cast + SHT	MC* 4.38 $\overset{\circ}{\text{A}}$	1.58
HIP-A	MC* 4.38 $\overset{\circ}{\text{A}}$	1.89
HIP-B	MC* 4.38 $\overset{\circ}{\text{A}}$	1.92
Cast + SHT + 41 hours at 760°C and 586 MPa.	MC* 4.38 $\overset{\circ}{\text{A}}$	1.65
HIP-A + 4.5 hours at 760°C and 586 MPa.	MC* 4.38 $\overset{\circ}{\text{A}}$	1.73
HIP-B + 71 hours at 760°C and 586 MPa.	MC* 4.38 $\overset{\circ}{\text{A}}$	1.83

*Traces of $M_{23}C_6$ present in all cases.

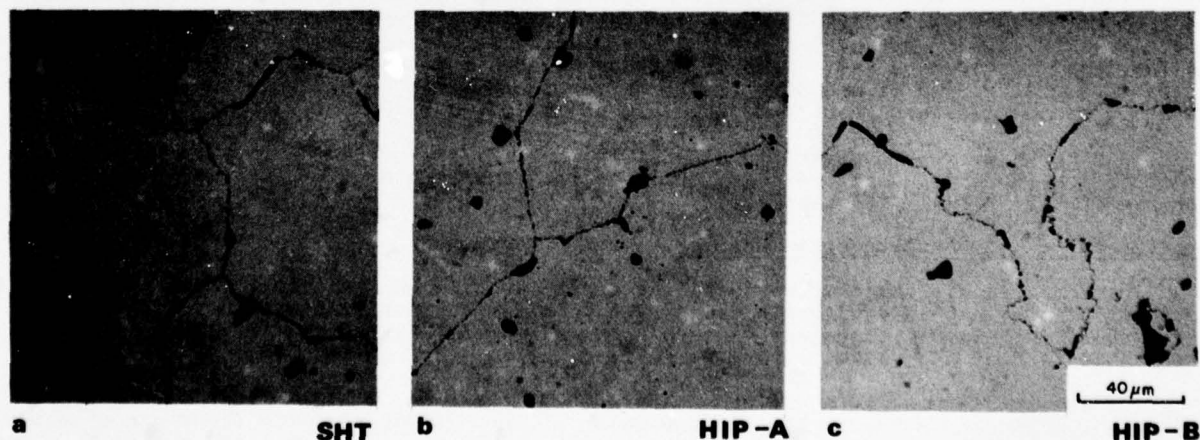


Figure 10 Carbide phases (MC) in cast and heat treated IN-738.

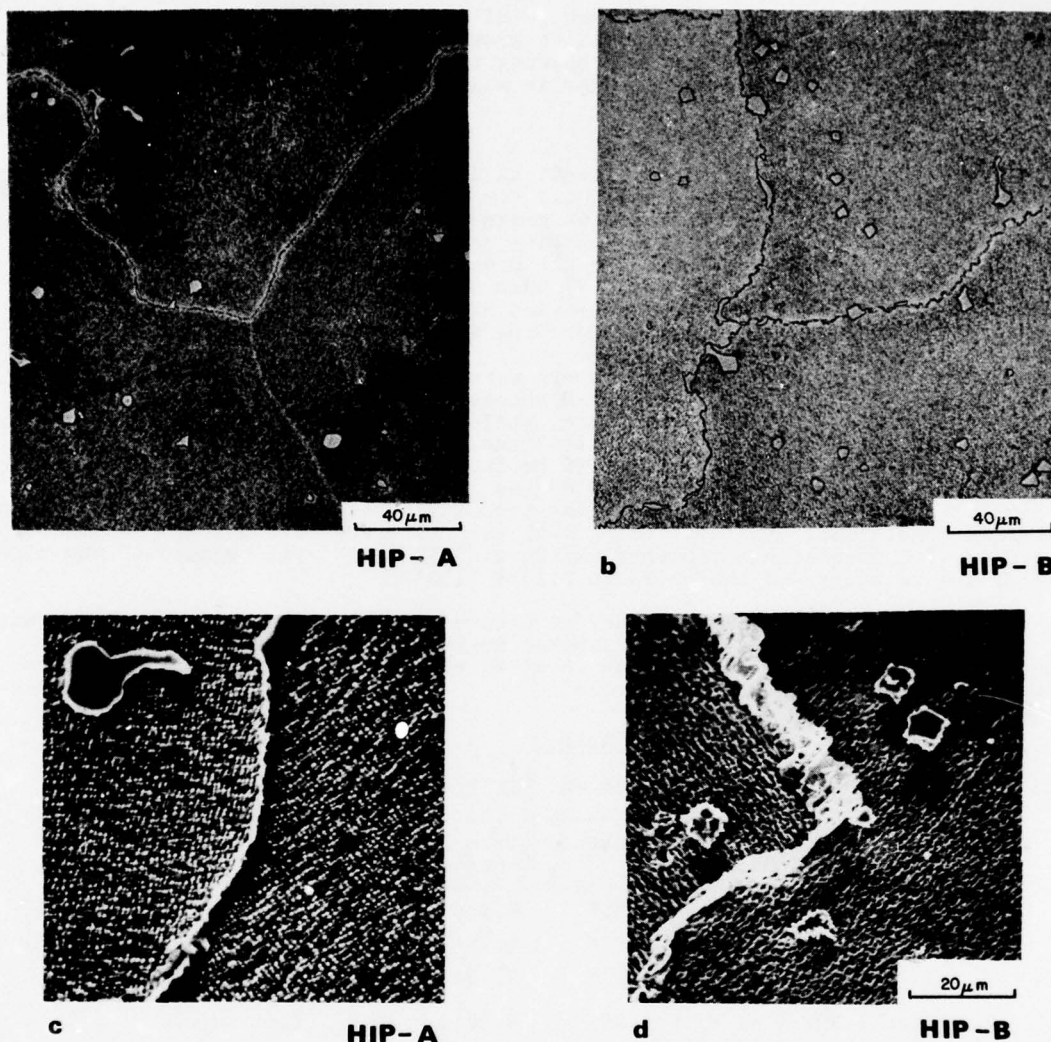


Figure 11 Grain boundary structures in cast and HIP processed IN-738. (a) and (b) are optical micrographs of samples etched in 2% bromine in methanol. (c) and (d) are scanning electron micrographs, sample in (c) etched in 5% bromine in methanol, sample in (d) electrolytically etched in 10% HCl in methanol. Note the finely serrated grain boundary structure in HIP-B processed material, figs. (b) and (d).

Deformation and Fracture Behaviour

Examination of rupture samples after testing showed some differences in deformation and fracture behaviour. HIP-A samples generally failed by cracks which nucleated at the specimen surface, and propagated along grain boundaries towards the centre of the sample, as indicated in Figure 12(a). Cast or HIP-B processed samples tended to fail by the growth and coalescence of discrete crack segments and voids which nucleated randomly at grain boundaries throughout the material, as indicated in Figure 12(b).

Slip markings were observed in HIP-B (CTS) materials after 760°C rupture testing, as shown in Figure 13, thus providing evidence of intragranular flow, whereas none were observed in the HIP-A (CTS) material.

Interpretation of Metallographic Results

The intermediate temperature ductility trough problem has previously been explained in terms of the inability of grain boundaries to accommodate strain without cracking (13). The problem is believed to be exaggerated when intragranular strength is high and deformation and crack nucleation are localized to grain boundaries (14).

The intermediate temperature ductility problem observed in HIP-A material can be explained in a similar manner. The intragranular γ' in this material was finer and probably more effective as a strengthening agent than that in HIP-B or in cast + SHT material. This would tend to force deformation to occur in grain boundaries which would have little ductility due to the carbide films. Moreover, crack propagation would tend to occur more easily and rapidly along the smooth grain boundaries of HIP-A material than along the zig-zag grain boundaries of the cast or HIP-B processed materials. These explanations are also consistent with the observations of slip and grain boundary fracture behaviour.

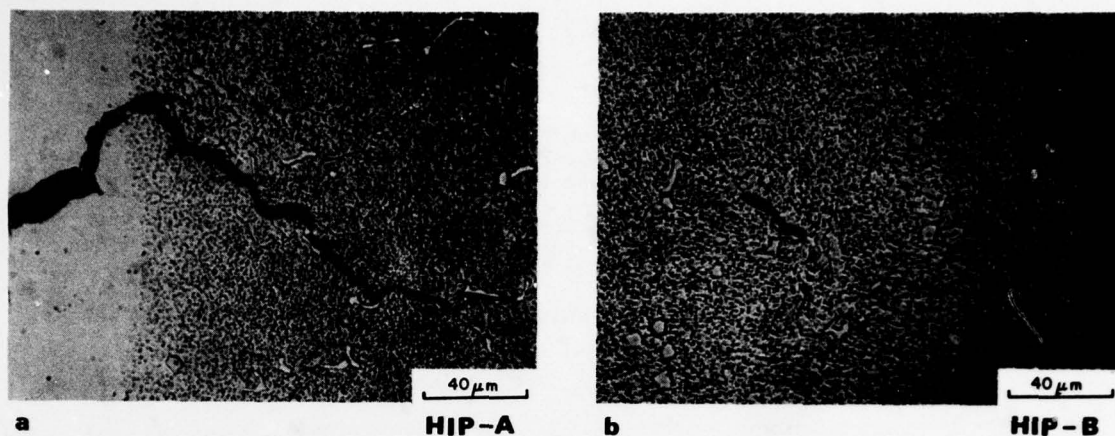


Figure 12 Secondary cracking along grain boundaries in cast and HIP processed IN-738 as a result of stress rupture testing at 760°C and 586 MPa.

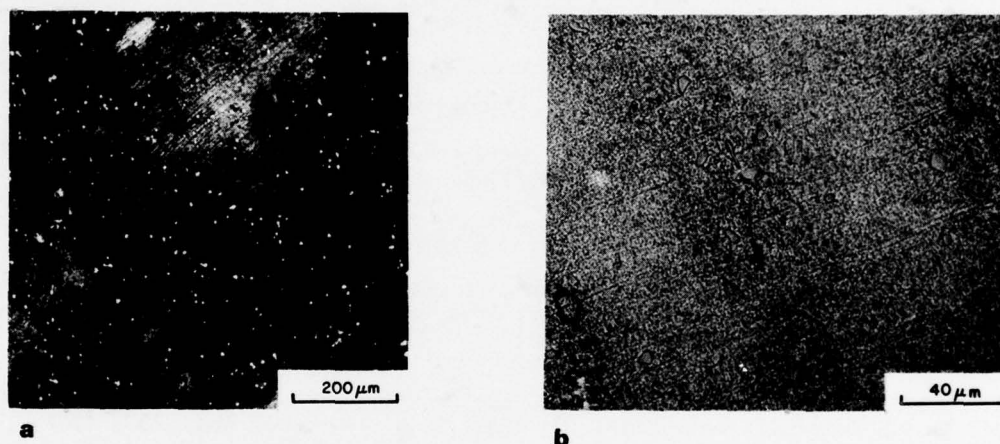


Figure 13 Slip markings observed in IN-738 HIP-B after stress rupture testing to failure in 71 hours at 760°C and 586 MPa. (a) Sample etched in 5% bromine in methanol, (b) sample etched in 2% bromine in methanol.

DISCUSSION

HIP processing has been shown to yield significant improvements in the mechanical properties of critical rotating turbine hardware. However, the process should not be regarded as a solution for all problems. Measures must be taken to minimize undesirable surface effects such as oxidation and nitriding. HIP processing can also destroy desirable microstructural features in cast material. Each application must therefore be considered as a special case and the necessary processing conditions established to develop the optimum response.

On the applied side, there is need for a continuation of the work of Wasielewski and Lindblad on the development of low cost, effective surface sealing and protection systems that can be applied and removed easily, and which are harmless to the autoclave, its atmosphere and the component. On the academic side, work is needed to confirm the beneficial effects of serrated grain boundaries and to explain their mechanism of formation in coarse grained investment cast alloys.

Serrated grain boundaries are known to form, with beneficial effects, in fine grained wrought or powder fabricated alloys when they are slow cooled through the γ' precipitation range. The serrations form when migrating grain boundaries are pinned by γ' particles or carbides (15-18). These fine serrations are an inherent feature of investment cast alloys, and one which is destroyed by the high HIP processing temperatures. The HIP thermal cycle must therefore be adjusted such that γ' is allowed to precipitate heterogeneously on grain boundaries during cooling while the boundaries are migrating, thus allowing the serrations to reform. This is believed to be the first report of the formation of serrated grain boundaries in coarse grained investment cast material where grain boundary migration would be minimal.

REFERENCES

1. P.G. Bailey and D.H. Lowe, "Process for High-Integrity Castings", Air Force Technical Report, AFML-TR-152, July 1974.
2. P.G. Bailey and W.H. Schweikert, "HIP Densification of Castings", Superalloys: Metallurgy and Manufacture, Proc. 3rd Int. Symp., ed. by B.H. Kear, D.R. Muzyka, J.K. Tien and S.T. Wlodek, Claitors, Baton Rouge, La., 1976, pp 451-462.
3. G.E. Wasielewski and N.R. Lindblad, "Elimination of Casting Defects using HIP", Superalloys: Processing, Proc. 2nd Int. Conf., Metals and Ceramics Information Center, Battelle, Columbus, Ohio, 1972, pp D1-D24.
4. Anon. "Hipping Improves Properties in Castings and PM Parts", Iron Age, August 23, 1976, pp 37-38.
5. W.R. Freeman, Jr., "HIP'ing Raises Casting Performance Levels", Metal Progress, August 1977, pp 32-38.
6. J. Magnuson, "Repair of Titanium Airframe Castings by Hot Isostatic Pressing", Metallography, Vol. 10, 1977, pp 223-232.
7. A.W.J. Upton, "Design and Development of a New 30,000 HP Class Two Shaft Type Gas Turbine", Proc. 4th Turbomachinery Symposium, Gas Turbine Laboratories, Texas A&M University, October 1975, ed. by M.P. Boyce, pp 71-81.
8. C.G. Bieber and J.R. Mihalisin, "Structural Studies and Properties of a New Cast High Strength Corrosion Resistant Superalloy", Proc. 2nd Int. Conf. on Strength of Metals and Alloys, ASM, Metals Park, Ohio, Vol. 3, 1970, pp 1031-1036.
9. M.J. Donachie, Jr., and O.H. Kriege, "Phase Extraction and Analysis in Superalloys", Journal of Materials, Vol. 7, No. 3, 1972, pp 269-278.
10. C.H. Lund and J. Hockin, "Investment Casting", The Superalloys, ed. by C.T. Sims & W.C. Hagel, John Wiley, New York, 1972 pp 403-425.
11. R.G. Dunn, D.L. Sponseller and J.M. Dahl, "Ductility Improvements in Superalloys", Toward Improved Ductility and Toughness, Proc. of a Conference Sponsored by Iron and Steel Inst. Japan, Japan Inst. Metals and Climax Molybdenum Development Co. (Japan) in Kyoto, Oct. 25, 26 (1971), pp 319-340.
12. S.M. Copley and B.H. Kear, "Temperature and Orientation Dependence of the Flow Stress in Off-Stoichiometric Ni₃Al (γ' Phase)", Trans. AIME, Vol. 239, 1967, pp 977-984.
13. D.H. Maxwell, J.F. Baldwin and J.F. Radavich, "New Concept in Superalloy Ductility", Metall. Met. Form, Vol. 42, No. 10, October 1975, pp 332-339.
14. N.F. Fiore, "Mid-Range Ductility Minimum in Ni-Base Superalloys", Reviews on High-Temperature Materials, ed. by J.B. Newkirk, Freund, Tel-Aviv, Vol. II, No. 4, 1975, pp 373-408.
15. J.M. Larson, "Carbide Morphology in P/M IN-792", Met. Trans. Vol. 7A, 1976, pp 1497-1502.
16. J.M. Larson and S. Floreen, "Metallurgical Factors Affecting the Crack Growth Resistance of a Superalloy", Met. Trans., Vol. 8A, 1977, pp 51-55.
17. O. Miyagawa, M. Yamamoto and M. Kobayashi, "Zig-Zag Grain Boundaries and Strength of Heat Resisting Alloys", Superalloys: Metallurgy and Manufacture, Proc. 3rd Int. Symp., ed. by B.H. Kear, D.R. Muzyka, J.K. Tien, and S.T. Wlodek, Claitors, Baton Rouge, La., 1976, pp 245-254.
18. Anon, "Structures of NIMONIC Alloys", Publication 3563A, Henry Wiggin & Company Limited, Hereford, England, 1973, pp 10-11.

ACKNOWLEDGEMENTS

This paper is published by permission of Westinghouse Canada Limited and the National Research Council of Canada, and the support of these organizations is gratefully acknowledged.

NET-SHAPE PROCESSING OF NON-OXIDE CERAMICS

by

Prof. Dr. Ernst Gugel
Annawerk Keramische Betriebe GmbH
Ceranox Division
D-8633 Rödental

SUMMARY

Ceramic materials are being widely considered for use in advanced engines because their densities are much lower than those of metals. Only non-oxide ceramics will be considered here because of their superior thermal stability and mechanical strength. Of these, silicon carbide and silicon nitride are most attractive since they can be used in oxidizing atmospheres. The raw materials needed are relatively cheap; thus the cost of a component is determined by the pressing and sintering operations. It is important to avoid mechanical working since this increases costs greatly. Special attention must therefore be given to the shaping operation so that the unsintered preform is close to the final shape of the product. The available fabrication methods are examined with particular attention to their ability to produce structural components.

INTRODUCTION

Traditionally, the technology of ceramics has differed from that of metals in that shaping was carried out before any heat was ever applied. This order of processing was rather unusual in metallurgy until powder processing was developed, and consequently these powder products have been referred to as metal-ceramic (1).

The important question in shaping ceramics is how closely can the final dimensions of a part be achieved using a preform which must undergo thermal treatments. With traditional ceramic products such as bricks, tiles or dinnerware this problem was not so important since dimensional tolerances were less critical. But where ceramics are required for high technology applications, the ability to process accurately to final dimensions becomes an important consideration.

Of course, there is always the possibility of machining to final shape. However since ceramics are among the hardest materials known, diamond tools are required and the costs are prohibitive. Some products, such as complicated profiled sealing rings, might need finishing operations which would account for 50% or more of the total costs.

In principle complex shapes can be produced by grinding, but the costs would still need to be kept to a minimum. There are numerous ceramic products made by grinding to final shape after sintering. For example, ceramic sealing rings made of aluminum oxide or silicon carbide, ceramic pumps or pump parts for the chemical industry, cutting tools, and many others are produced in this way. In contrast other products, such as spark plugs, in which high dimensional accuracy is not required, need not be mechanically finished.

The dimensional changes during thermal treatment depend on the material. A material which does not shrink during the firing process can be fabricated more closely to the required dimensions than a sintered product, where linear shrinkage up to 18% might occur. However in spite of this, sintered aluminum oxide ceramics can be produced to tolerances of about 1%. Although aluminum oxide has many attractive properties and was one of the first ceramic materials used, now non-oxide ceramics are preferred because of their high temperature strength. This paper will examine the possible fabrication methods for ceramic products, which are now seen as competitors to metals in many mechanical engineering applications.

MATERIALS

Here mainly materials based on silicon nitride and silicon carbide are concerned. Compared to other materials considered for high temperature use (2), these compounds possess exceptional thermal stability due to their covalent bonds, and this leads to good high temperature mechanical strength. However the problem is how to produce components from these materials when their melting points are much higher than those of metals, and when sintering operations are severely impeded because of their thermal stability. The fabrication processes which are being considered for non-oxide ceramics are examined briefly below:

SILICON NITRIDE

Silicon nitride can be produced either by reaction sintering or hot pressing. Serious efforts have been made to achieve normal sintering, but only larger amounts of additive such as Ceroxid will allow this to be achieved and then only at the expense of thermal stability. However, much remains to be done in this area. The solid solution of silicon nitride and aluminum oxide (3), known as Sialon, should also be mentioned.

This can be produced either by hot-pressing or, under special conditions, by normal sintering. However the problem of making homogenous components reproducibly has not been solved yet, and therefore products are not available commercially.

REACTION BONDED SILICON NITRIDE

The fact that nitrogen will react with silicon to form silicon nitride allows reaction sintering of green pressed silicon powder parts to be carried out in a nitrogen atmosphere (4). Although an increase in volume of 22% takes place during this reaction the dimensions of the molded part remain practically unchanged. This occurs since the volume increase counteracts the usual shrinkage associated with the elimination of pores (5). This provides the unique possibility of producing accurately sized parts without grinding. When suitable organic binders are used as plasticizers, almost all of the standard methods used for shaping ceramics can be applied.

The important properties which can be achieved in this material are given in table 1, together with those of other materials of interest here.

HOT-PRESSED SILICON NITRIDE

In many cases hot-pressing or pressure sintering are the only ways of producing fully dense products from powders which do not respond to sintering (6). But even here, additives must be introduced to the powder, which act as lubricants during the densification process under pressure. With axial hot-pressing in graphite dies the pressure is limited by the strength of the graphite. In the case of hot isostatic pressing (7), less flux is necessary, and it may be eliminated entirely when the highest available pressures are used. However equipment is still being developed to achieve the highest temperatures required.

Of course fluxing agents strongly affect the properties of the material, particularly the high temperature mechanical properties, as table 1 shows. Nevertheless, the highest mechanical strengths achieved in ceramic materials have been obtained with silicon nitride powder using this process (table 1).

SILICON CARBIDE

The range of silicon carbide products available is broader than that for silicon nitride, since this compound is also amenable to processes such as recrystallization and even normal sintering. This is due to its higher melting or decomposition temperature

RECRYSTALLIZED SILICON CARBIDE

Silicon carbide can be strengthened at temperatures above 2100°C by a process which involves vaporization and condensation occurring at the surface of the particles. The porous product exhibits only moderate strength at room temperature (table 1), but since it consists of 100% silicon carbide its strength remains constant at temperatures up to 1600°C. Also, this material does not show any shrinkage or expansion during thermal treatment. Its density is solely dependent on how the preform was compacted. The principal methods used to form this material are dry-pressing and slip casting. Methods which require plasticizers are of little use since the residual carbon in the material influences the recrystallization process.

REACTION BONDED SILICON CARBIDE

Silicon carbide can also be reaction bonded. However the process is not as simple as that used for silicon nitride since one of the reactants is not necessarily gaseous. However the method offers particular advantages when organic binders are used, since the carbon remaining after the removal of volatile components can be used as the reacting agent.

The carbon is usually added in solid form, and the silicon can also be introduced in this way, but a high porosity and very low strength would be achieved. Therefore it is beneficial to introduce silicon as a gas or fluid (infiltration) during the firing process. Also since this reaction involves a volume increase, the green compact must possess sufficient porosity to accommodate this and maintain a constant shape. Also the product may contain primary silicon carbide.

The passage of silicon through the full cross-section of a structural component is only possible when free paths are maintained during the reaction process. This means that a reaction bonded silicon carbide product must also retain some porosity. However, good strength is achieved by a fine grained microstructure (table 1).

A reaction can also be made to occur between the silicon carbide and any free silicon remaining in the pores, to produce a complex material showing excellent strength values. However these properties are only maintained up to 1300°C, when the silicon softens and the strength declines. This product is dense, and yet since the overall volume remains constant during firing the shape and dimensions of the green body can be preserved through to the end product.

SINTERED SILICON CARBIDE

Only a few years ago it was discovered that silicon carbide is sinterable in spite of its highly covalent bonding (8). For sintering to occur an extremely fine powder with a high surface area is required and small amounts of additives of boron and carbon are needed. However it is extremely difficult, if not impossible, to achieve exact dimensional control, since sintering is accompanied by large shrinkage associated with the decrease of porosity (9). Table 1 again gives typical properties that may be obtained.

It must be mentioned that silicon carbide is easier to grind than silicon nitride, and thus the expense of mechanical finishing is not so high. But on the other hand the material is far more brittle, so that silicon nitride has far better chance of being used in engineering components.

HOT-PRESSED SILICON CARBIDE

In general the processing of this material is similar to that of silicon nitride. Additives are needed to promote sintering, but these are only needed in small amounts because of the higher hot-pressing temperatures used, typically above 2200°C, and so better high temperature properties are achieved.

BORON CARBIDE

Boron carbide (10) also belongs to the non-oxide class of ceramics, although it is of very little interest for high temperature use. It oxidizes readily at relatively low temperatures, and the oxide films are not protective as in the case of silicon carbide and silicon nitride. At the present time boron carbide can only be densified satisfactorily by hot-pressing.

BORON NITRIDE

Basically, hexagonal boron nitride is much the same as boron carbide; it too can only be densified by hot-pressing. Boron nitride is an extremely refractory material, but it is totally unresistant to oxidation. Unlike the other materials it is soft. However in the cubic form it is the hardest material known after diamond, and this is significant in the grinding field.

Hot-pressed hexagonal boron nitride is easy to machine. Its density is usually rather low and one must try to keep the material free of boron oxide; or to stabilize the boron oxide by CaO- containing additives, so that the material is not destroyed by hydration during heating.

SHAPING AT ROOM TEMPERATURE

In the following section methods that are used for producing non-oxide ceramic shapes are described in detail, while those which are not considered as net-shape forming methods are mentioned only briefly for completeness.

The methods are listed in table II, together with the materials with which they have been used so far. (Hot-pressing is treated separately in Shaping at Hot Temperatures.) There are a number of forming methods available, the selection of which depends on the type and quantity of parts required. It also depends on the properties required since the forming method influences the density and hence the properties of the final component - especially with reaction bonded silicon nitride - as shown in table 1.

DRY PRESSING

Dry pressing (fig. 1) is a frequently used process for shaping ceramics. Without doubt it contributes to net-shape processing, particularly if no cutting is required before or after sintering. Usually it is used for simple shapes, such as gas turbine shrouds, which can be produced by axial pressing between two dies. The process can only be used when the quality of the material produced is adequate for the intended application.

The isostatic process leads to better density and thus better mechanical properties, but normally it does not lead to final shape. Semi-isostatic presses are used for pressing grinding balls or spark plugs out of oxide ceramics.

On the other hand, isostatic dry-pressing provides the opportunity to produce almost any complex shape (an example is shown in fig. 2) by mechanically machining a pressed, or if necessary a pre-sintered green part. This is a costly method, but it is justified for the manufacture of prototypes and other small quantity products.

INJECTION MOLDING

This is probably the most interesting method for mass producing small and medium sized parts having complex geometries. This method, which is well known for producing plastic parts, was adopted for oxide ceramics in the mid-thirties (12). The first patents date from the year 1936. However the large scale use of this process did not occur until 20 years later, and it is now a standard technology for producing thread guides and wire guide nipples from oxide ceramics.

In this process (fig. 3) the ceramic powder is mixed with a thermoplastic organic binder in heated mixers. The mixture is granulated and fed into an extruder where it is pressed by a piston or screw system through the injection chamber and into a cooled mold. Here it hardens, and after a very short time the green part can be removed. The parts are then heated in an oxidizing atmosphere to drive off the organic binder, and then finally fired.

In the following sections the processing parameters and different steps are discussed.

POWDER

In all cases the characteristics of the powder are most important, since they influence both densification and reactivity. This is particularly true with non-oxide ceramics since the final product is obtained by reaction sintering without shrinkage, rather than by conventional sintering and shrinkage. The density of the final product is therefore critically dependant on the initial powder densification. The optimum result is achieved by a correct blend of very fine powder which promotes reaction, and a somewhat coarser powder which promotes good density.

Furthermore, good wetting of the powder by the organic plasticizer is essential and this can be improved by the addition of surface activating agents.

ORGANIC BINDER

The success of injection molding depends on the flow characteristics of the heated mass. Composition and quantity of the plastic components play an essential part. The chemical industry offers a large number of usable organic materials, the selection of which is done in an empirical manner. In order to improve plasticity and separation from the mold, and also to avoid softening during burnout, the plastic mixtures can also have a certain portion of thermally irreversible waxes.

Since the volume ratio of pressed powder does not amount to more than 60%, an organic content of above 40% is necessary to fill the pores. Lower percentages of the plastic constituent might be possible if a good grain size distribution is used and if the plastic constituent is able to flow properly. This is an important point since the quantity of the solid matter needs to be as high as possible in order to get the best possible density in the end product. On the other hand of course, the powder/plastic ratio influences the flow behaviour markedly, such that an increase in the powder content of only a few percent may raise the viscosity by an order of magnitude. Use of higher temperatures can only affect this in a limited way.

Figure 4 shows the major effects of adding excessive plastic (A), or insufficient plastic (C) to a ceramic powder mixture. Overcharging leads to a thick organic layer between powder particles, which result in good flow characteristics, but the plastic component is difficult to remove, shrinkage is large, and shape stability is poor. The required stability in shape can only be achieved by grain to grain contact, and this can only be obtained by a degree of under charging together with well controlled pressure conditions. This means that certain pores between the grains may remain free of plasticizer and flow behaviour may deteriorate.

In order to hold the injection pressures within normal limits (up to 200 N/mm²), and to achieve complete filling of the mold, a viscosity of 2000 poise is necessary. To ensure uniform filling of the mold, without local stiffening, precise control of temperature is required. The optimum temperature must be determined beforehand by empirical tests because of the complex relationships between heat capacity and thermal transfer.

The flow behaviour of the injection molding mass deviates from Newtonian flow; it is pseudoplastic, which means that flow begins after yielding and the flow rate increases disproportionately with forming pressure. Injection molding masses which expand should be avoided.

Attention must also be paid to abrasion which occurs in the injection molding channels, and this increases with increasing pressure and with decreasing content of the plastic constituent. But since high density is required, abrasion caused by the hard ceramic powder cannot be avoided, and it can only be reduced by proper design of the extruder.

TOOLS

The injection molder is no problem; there are enough good brands on the market in all the required sizes. Either pistons or screw injection devices can be used to move the heated mass through the extruder, and there are numerous variations of both types of machine available. The screw extruder supplies a more evenly plasticized mass, while the piston extruder offers higher pressures. Therefore combination machines are becoming popular, in which the mixture is transported by a screw and then injected into the mold with the help of a piston. For medium sized parts at least an injection pressure up to 200 N/mm² is required.

The heart of the machine is the tool or mold and this must be designed to allow homogenous filling without premature hardening, and easy - if possible automatic - removal of the part. The more complex is the part, the more complicated and expensive is the tool, and the process may only be profitable if a large number of parts is required.

In such cases the process may become especially economical since a short cycle-time of only a few seconds is involved.

The tool design must also take into account the best feed of the ceramic mixture so that textures are avoided. Positioning of supply ports is important, as are the number of ports used, whether tangential or radial flow is achieved, and at which cross-section the feed enters. The development of a tool for a new component is based on experience. Problems, such as insufficient mixing which result from poor tool design, may appear as warpage only after the ceramic has been fired.

REMOVAL OF ORGANIC BINDER

The removal of the binder from larger components is a process that can take several days. This is therefore an important economical factor. The duration is a consequence of slow heating rates that must be used to prevent deformation during the time that the binder softens and the time that it is destroyed. It is also due to the fact that non-oxide ceramics cannot be heated higher than about 400 to 500°C in an oxidizing atmosphere without oxidation occurring, but at temperatures below this the rate of removal of carbon is very slow.

Reaction bonded silicon carbide offers a fundamental advantage in this respect since it already contains carbon as a basic ingredient. This means that the residual carbon from the binder can be determined, and then used as a constituent in the reaction bonding process.

Figure 5 shows the results of a thermo-gravimetric examination of the reaction sintering process used to convert silicon powder in air, to silicon nitride. It can be seen that marked oxidation occurs at temperatures of 400°C and above, and therefore these should be avoided. During removal of the binder no dimensional changes should occur, and this is only possible when the ceramic particles are in solid-solid contact, and the organic constituent is confined to the cavities between grains (fig. 4).

COMPONENTS

Some components of the gas turbine section (13) are shown in fig. 6 and 7. These parts were made at Degussa Metal Development. Figure 6 shows small single blades of reaction bonded silicon nitride and fig. 7 rotor blade rings in a simplified form made in one piece out of the same material. The weight of these parts is constantly within $\pm 0.3\%$. The change in dimensions of simple single blades does not exceed $\pm 0.04\text{mm}$ with an allowed tolerance of $\pm 0.15\text{mm}$ (table III).

For the control of dimensions the distance between the blades was measured (on the rotor blade rings) with the result shown in fig. 8. With a reference value of 12.75mm this distance differed by about $\pm 0.12\text{mm}$ after nitriding. This was within the allowable tolerances for this part.

WARM MOLDING

This is also a plastic forming method (fig. 9), but in contrast to injection molding a duroplastic binder or plasticizer is used (14). The process is similar to dry-pressing in that the cold mixture is fed into a pre-heated mold. The mixture may also be squeezed into the mold by a piston. In this case the process is similar to injection molding. There are many variants of the two basic processes, in terms of the method of feeding the material, tooling, and the combination of duro- and thermo-plastic material used. When duroplastics are used one must consider not only the change of viscosity with temperature, as with thermoplastics, but also the hardening reaction which affects viscosity as shown in fig. 10.

Warm molding offers some advantages compared to injection molding. The appearance of flow textures is strongly reduced, and since very high pressures up to 500 N/mm² can be used, good densities can be achieved. This avoids shrinkage and ensures good strength in the product.

Furthermore burnout, that is the removal of the plastic constituent, is easier and more rapid since danger of deformation due to softening of the plastic is avoided.

A disadvantage is the long duration of the hardening process, which may take several minutes depending on the wall thickness of the green part. Figure 11 shows some turbine blades of reaction bonded silicon nitride, which are typical examples.

This method will probably be used only in special cases where the complexity of the components, and/or the required properties do not permit dry-pressing, and when injection molding is precluded due to inadequate dimensional control or other processing problems. An example of this process is shown in fig. 12 and is a preform of a silicon nitride duodensity rotor (15) (See Shaping at Hot Temperatures). The hub is produced from silicon powder in an initial pressing to produce a part which can be hot pressed after nitriding. A second pressing is then carried out to form the rotor from further silicon powder, and after nitriding and further hot pressing a stable, high temperature resistant, reaction bonded silicon nitride part is obtained.

EXTRUDING

Extruding is also a plastic forming method and is shown in fig. 13. It is limited to elongated shapes having uniform cross-sections along their lengths, and to parts which can tolerate dimensional variations of several percent along their length.

The body is plasticized with an organic binder, which is partially hardened by drying at low temperature, so that it can be squeezed through a nozzle in an extruder. This requires a relatively high organic content. Because of this the green part has a low ceramic content and the resulting product a relatively low strength (see table 1). Dimensional changes are due to shrinkage, which occurs because of the high organic content and because of softening and flow which occurs in the green part under its own mass during drying and removal of binder.

As with other plastic forming methods the organic constituent is removed by burnout which might take 4 to 8 days. The burned parts have a high porosity and thus little strength, which makes transfer to the sintering furnace rather difficult.

Typical components for extruding are tubes and rods (fig. 14); for example thermo-couple tubes made of reaction bonded silicon nitride, and of silicon nitride bonded silicon carbide (which has not been discussed here) have been used for a long time. Also rings or cylindrical components of reaction bonded silicon nitride and silicon carbide have been made for some time by extruding and cutting to the required length.

SLIP CASTING

Slip casting has been known for producing clay based products for more than two centuries. It is based on the fact that when electrically charged particles are held in suspension in a liquid of suitable composition, an unusually low volume of liquid is required to make the solid powder mass fluid. Since this method is also suitable for ceramic powders other than clay, it is of interest for producing complicated components from non-oxide ceramics, and has been successful with relatively low mold costs (16).

The slip is poured into a porous mold (fig. 15), which absorbs the liquid—mostly water—and the ceramic body is allowed to set. After removal from the split mold the component is dried and then usually forwarded to the sintering process.

Good properties of the slip itself do not guarantee a good casting process. It must be possible to cast the slip without streaks or bubbles, but also the mold must allow the water to be withdrawn evenly through its porous walls thus allowing the part to set uniformly. The mold must be designed such that the shrinkage, which occurs because of the removal of liquid, is allowed to take place freely. Finally the part must have sufficient strength that it can be handled, and can be removed from the mold without sticking.

Some further aspects of the casting methods are discussed in the following sections.

DISPERSION LIQUID

The liquid dispersant is expected to wet the powder mixture and yet its volume fraction should remain as low as possible in the mixture to ensure a high solid content. This can be achieved by using a favourable particle structure, and by adding dispersing agents which are added to the slip. In addition binding agents might be added to the slip to develop strength in the product.

A basic requirement of course is that the liquid dispersant does not react with the ceramic powder at any stage of processing and also that it does not contain any contaminants that might influence the characteristics of the final product. Obviously an aqueous slip is relatively simple to handle, and poses few problems with silicon carbide. To use water with silicon is more difficult since reactions might lead to the formation of gas bubbles. An outgassing treatment in a vacuum system may help. However due to their spherical nature the bubbles do not cause a great loss of strength in the material. Nevertheless they may create weaknesses by reducing the load bearing cross section at critical points in a component.

GRAIN

The dispersion effect and the concentration of the solid that can be achieved are also dependent on the properties of the powder. A relatively coarse particle size can be kept in suspension quite well provided there is a certain portion of extremely fine particles below 2mm. A high solid content is necessary to keep shrinkage as low as possible during setting in the mold. Shrinkage obviously complicates the molding process by causing changes in shape and lower dimensional accuracy. Shrinkage can be considerably reduced by using a mixture containing 80-85% by weight of solid, and with particles having a very specific shape and particle size distribution.

It is difficult to produce the most favourable grain size distribution reproducibly since this depends on many milling parameters that are not easy to control. Strict control of grain structure, specific surface area, viscosity, and specific gravity of the slip are most important.

CASTING MOLD

When complicated components are cast the design of the mold is of great importance. The method will not be used for complicated components if excessive shrinkage occurs in the slip during setting. Shrinkage cannot be completely avoided and values up to about 1% must be expected depending on the material.

In order to make the mold a pattern of the final component is needed, and this must be enlarged to allow for shrinkage. Because of this the mold must be made of an absorbent material which is usually plaster of Paris. The mold is made in several parts to allow the cast component to be removed easily after setting. The hardening of the slip in the mold is a slow process which may take several hours. Therefore if many parts are required an adequate number of these rather cheap molds are needed.

COMPONENTS

After the green part has been removed from the mold it is set out for drying to remove the remaining liquid. If any further work is required, such as smoothing surfaces or removing small defects, this is best done in the dry condition, or, with reaction bonded silicon nitride, in a presintered condition. No further work is done after the final nitriding has been carried out.

Figure 16 shows a gas turbine stator produced as a single component by casting using reaction bonded silicon nitride. Figure 17 shows radial rotors for the turbocharger made from reaction bonded silicon carbide. The dimensional accuracy on these parts is better than 0.5 to 1% depending on the part. The surface finish depends on the mold surface, which is reproduced in detail by the slip cast body.

SHAPING AT HIGH TEMPERATURE

Apart from fusion casting of a few oxide ceramic products, hot pressing or pressure sintering is the only method available for shaping ceramics at high temperatures. Usually this does not lead to the final shape of a part, and therefore this should not be considered as a method of net-shape processing. However the process involves plastic flow and often reasonably close shape can be achieved.

The need to hot-press is due to an ability to sinter non-oxide ceramic powders in the usual way. However with pressures that are technically feasible it is not possible to produce fully dense compacts without introducing additives or contaminants. Therefore it is the aim of hot pressing to produce materials that are free of pores, since there are already several methods available for producing porous parts.

With traditional hot pressing (17) the powder is mixed with densification aids and pressed axially in graphite dies as shown in the flow sheet for silicon carbide in fig. 18. The pressure that can be used is limited by the strength of the graphite material to 30-50 N/mm². The required temperature for silicon nitride is about 1700°C, and for silicon carbide above 2100°C.

The flow properties of the powder even at these high temperatures are only marginal, so the production of complex shaped parts by pressing in shaped dies is limited. Alternatively powders with a higher flux content can be used, but this degrades the desired properties, particularly at high temperatures.

Further work might promote the use of pseudoisostatic methods (17) where non-sinterable powder is used as the pressure transmitting medium, the so-called powder vehicle process. Figure 19 shows a gas turbine rotor hub in an as-pressed condition, which is within 0.5mm of the final shape. The surface is relatively smooth, but not even. It is anticipated that eventually, surfaces may be used in the as-pressed condition and without further finishing. But in no case will this happen with surfaces which are highly stressed in service, such as those in the bore and the neck. A precise surface finish is needed to achieve an optimum strength (fig. 20), and this can only be obtained by using diamond tools. The ceramic ball bearings in fig. 21 show what can be obtained by careful surface treatment. Here the balls have a sphericity of better than 0.2μ (19).

Pseudoisostatic methods are particularly suitable for producing hot pressed silicon nitride from reaction bonded starting material (14). This method is used particularly when the component has widely differing section thicknesses, as is the case with gas turbine rotor hubs.

Hot pressing of reaction bonded silicon nitride was developed as a process because it produces a fully dense material. The advantage of this process is the shorter densification time compared to direct hot pressing of powder. This method established the feasibility of producing particularly homogenous components, which is a very severe problem with large components.

Another possibility with hot pressing is the production of duodensity rotors from silicon nitride using a reaction bonded blade ring and hot pressed hub. This concept is part of the development of the ceramic gas turbine, and as it is planned, it should provide a gradual transition from one material to the other. The working scheme is shown in fig. 12.

Without doubt the hot isostatic pressing process (7) is an important development which will find widespread use for final densification of metallic materials (20). A clear advantage is the possibility of using higher pressures than are feasible with axial hot pressing in graphite dies, and the opportunity of using powder mixes with lower flux contents. Also facilities have been developed with higher temperature capabilities than were previously available. However final densification of already dense non-oxide ceramic components is not a viable process since the starting preforms cannot be produced by normal sintering. The only interest is in pressing green powder compacts directly in the HIP system. This process requires a gas tight protective container for the powder. There are certain advantages in using quartz-glass containers for protection, but the forming of complicated components to final shape requires much more development time if it is ever to be successful. However the development of this process is certainly worth watching.

CONCLUSIONS

In producing ceramic components for high temperature engineering great attention must be given to processing as closely as possible to the final shape, since this determines the economics of the process. Therefore those fabrication methods which provide the most direct route, and which lower fabrication costs and loss of material without sacrificing product quality, are of special interest.

If a fully dense material is required with high strength, this can only be produced by hot pressing and will involve a final grinding operation using diamond tools. Rather complicated parts can be produced with excellent surface finish, and this is necessary in order to achieve high strength. But the effort required is considerable and the costs are enormous.

For materials with less stringent strength requirements a variety of forming methods are available and have been described in this report. Table IV provides a qualitative comparison of the important features of these methods.

When a large number of parts is required then dry pressing and injection molding may be considered since the high costs of tooling become less significant. Dry pressing is preferred provided the part is not too complicated and the strength requirements are not too severe. With reaction bonded silicon nitride this process is only capable of achieving moderate density.

For larger components which are also required in large numbers, the tool design for injection molding and hot pressing is rather difficult, and therefore slip casting must be considered. In any case slip casting is also useful when small numbers of parts are required which may be the case during the development of an optimum design.

Warm molding will be limited, on the one hand to less complicated shapes, and on the other hand to specialty products such as duodensity components.

All of the methods mentioned are relatively well developed. But this does not preclude the need to adjust and optimize processes for special components. The main problem is the reproducible production of homogenous components, and this is a pre-requisite for safe processing of large quantities of parts. Processes which involve flow of ceramic powder, for example injection molding, may be troubled by defects such as streaks or sections of reduced porosity which of course make a part absolutely useless. Further work on forming methods and development of specific materials is therefore required.

Also, as expected, a high success with development work does not preclude the need for non-destructive inspection tests, and this is particularly so with ceramic components. Promising starts have already been made in this area, but unfortunately this is beyond the scope of this paper.

ACKNOWLEDGEMENT

The research work, as far as it is concerned with the development of ceramic gas turbine components, is supported by the Ministry of Research and Technology, Federal Government of Germany, which is gratefully acknowledged.

The author thanks his co-workers in the Ceranox Division of Annawerk, who are essentially engaged in the success of this project.

REFERENCES

- (1) F. Skaupy: Metallkeramik; Verlag Chemie, Weinheim 1929 (1.Ed.), 1950 (3. Ed.)
- (2) E. Gugel: Die hochschmelzenden Stoffe und ihre Verwendung für feuerfeste Zwecke, Ber. Deut.Keram.Ges. 40 (1963) p. 533-543.
- (3) W. Wruß, E. Gugel, R. Kieffer, B. Willer: Technologische Untersuchungen im System $\text{Si}_3\text{N}_4\text{-Al}_2\text{O}_3$, Sprechsaal 108 (1975) p. 378-383.
- (4) A. Fickel: Herstellungs- und Anwendungsmöglichkeiten von Siliziumnitridwerkstoffen, CZ-Chemie Technik (1973) p. 155-159.
- (5) E. Gugel, O.W. Flörke, N. Hauck: Zum Nitridieren von Silizium-Preßlingen, Ber. Deut.Keram.Ges., in prep.
- (6) E. Gugel, A. Fickel, H. Kessel: Development in the Production of Hot Pressed Silicon Nitride, Powder Metallurgy International 6 (1974) p. 136 -140.
- (7) Kompaktes Siliziumnitrid, VDI-Nachr. 31 (1977) No. 12, p.13.
- (8) S. Prochaska: Sintering of Silicon Carbide, General Electr. Techn. Inf. Series, Report No 73, CRD 325 (1973).
- (9) G. Leimer, E. Gugel, H. Hausner, W. Böcker: Sintern von Siliziumcarbid, BMFT Status-Seminar Bad Neuenahr April 1978 in print.
- (10) E. Gugel: Nichtoxidkeramik, Handbuch der Keramik, Verlag Schmid, Gruppe II, K2, p. 1-8 (1975).
- (11) E. Gugel: Nichtoxidkeramik (2. Teil), Handbuch der Keramik, Verlag Schmid, Freiburg, Gruppe II, K2, p. 9-14.
- (12) H.W. Hennicke, K. Neuenfeld: Spritzgußtechnik als Formgebungsverfahren in der Keramik, Ber. Deut.Keram. Ges., 45 (1968), p. 469 - 473.
- (13) E. Lange, N. Müller, K. Olapinski, L. Stanneck: Turbinenbauteile aus spritzgegossenen reaktionsgebundenem Siliziumnitrid, BMFT Status Seminar Bad Neuenahr April 1978, in print.
- (14) E. Gugel, H. Kessel: Post Hot Pressing of Reaction Bonded Silicon Nitride, AMMRC-2nd Material Conference "Ceramics for High Performance Application", Newport, R.I./USA - in print.
- (15) E. Gugel, H. Kessel, N. Müller, E. Lange: Herstellung von Siliziumnitrid-Verbundbauteilen für die Gasturbine, BMFT Status-Seminar Bad Neuenahr, April 1978 - in print.
- (16) A. Novotny, E. Gugel, G. Leimer: Schlickergegossene Gasturbinen-Bauteile aus Siliziumnitrid und Siliziumcarbid, BMFT Status-Seminar Bad Neuenahr, April 1978 - in print.
- (17) H. Kessel, E. Gugel: Die Herstellung von Gasturbinenrotoren aus heißgepreßtem Siliziumnitrid, BMFT Status-Seminar Bad Neuenahr, April 1978 - in print.
- (18) H. Kessel, E. Ryser: Spanende Bearbeitung von heißgepreßtem Siliziumnitrid, Industrie-Diamanten-Rundschau (1977) p. 377-380.
- (19) H. Kessel, E. Gugel: Wälzlager aus heißgepreßtem Siliziumnitrid, Antriebstechnik 16 (1977), p.130-135.
- (20) G. Vandruen, I. Laburdi, W. Wallace, I. Terada: Hot Isostatic Pressing of Investment Cast IN-738 Turbine Blades. This conference.

Product N - Silicon Nitride C - Silicon Carbide	Bulk Density	Porosity	Flexural Strength			Young's Modulus	Thermal Expansion
			20 °C	1000 °C	1400 °C		
	g/cm ³	%	MN/m ²	MN/m ²	MN/m ²	10 ³ MN/m ²	10 ⁻⁶ K ⁻¹
N - Reaction Bonded(1)	1,9 - 2,2		150	150	150	120	3,0
N - Reaction Bonded(2)	2,4 - 2,6		250	250	300	160	3,0
N - Hot Pressed	3,2	0	700	700	400	320	3,2
C - Reaction Bonded	2,7	16	250	250	250	280	4,5
C - Silicon Impregnated	3,1	0	400	500	250	380	4,3
C - Recrystallized	2,6	20	100	100	100	200	4,5
C - Sintered	3,0	5	500	450	400	400	4,6
C - Hot Pressed	3,2	0	550	550	450	420	4,6

(1) - Axial dry pressed, extruded
(2) - Isopressed, slip cast, injection and warm molded

Table I:

Main properties of non-oxide (silicon nitride and silicon carbide based) high temperature structural ceramic materials.

Product N - Silicon Nitride C - Silicon Carbide	Shaping Method						
	Dry pressing		Injection molding	Warm molding	Extruding	Slipcasting	Hot pressing
	axial	isostatic					
N - Reaction Bonded	x	x	x	x	x	x	
N - Hot Pressed							x
C - Reaction Bonded	x	x	x	x	x	x	
C - Silicon Infiltrated	x	x	x	x	x	x	
C - Recrystallized	x	x				x	
C - Sintered	x	x				x	
C - Hot Pressed							x

Table II:

Shaping methods for non-oxide ceramics.

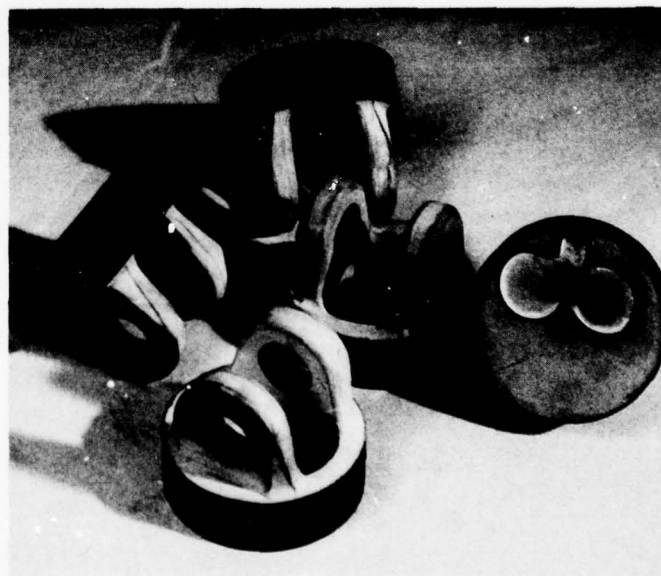
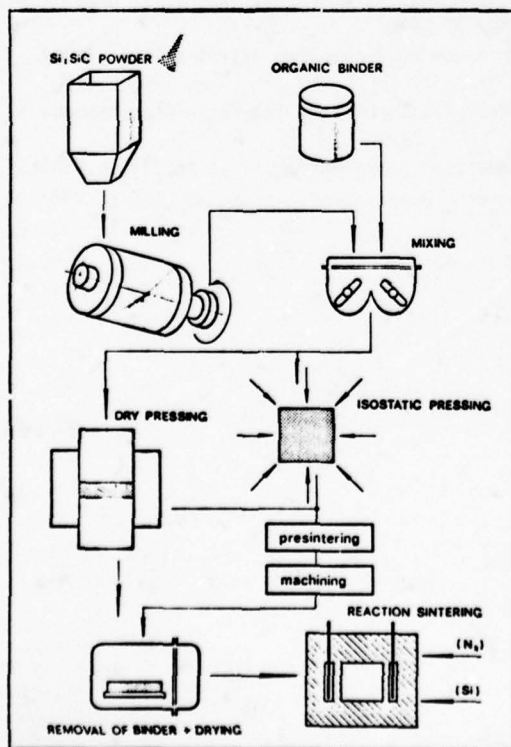


Fig. 2: Reaction bonded silicon nitride test pistons for diesel engines fabricated by machining of isostatically dry pressed silicon prior to nitriding.

Fig. 1 (left):
The axial and isostatic dry pressing process.

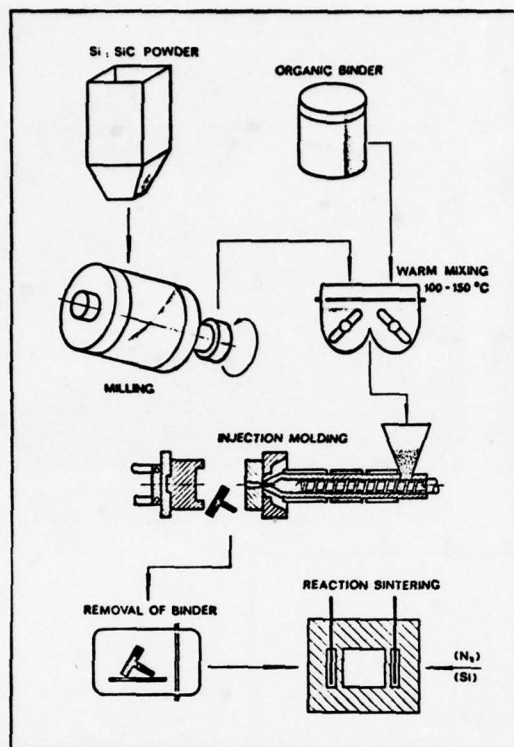


Fig. 3:
The injection molding process.

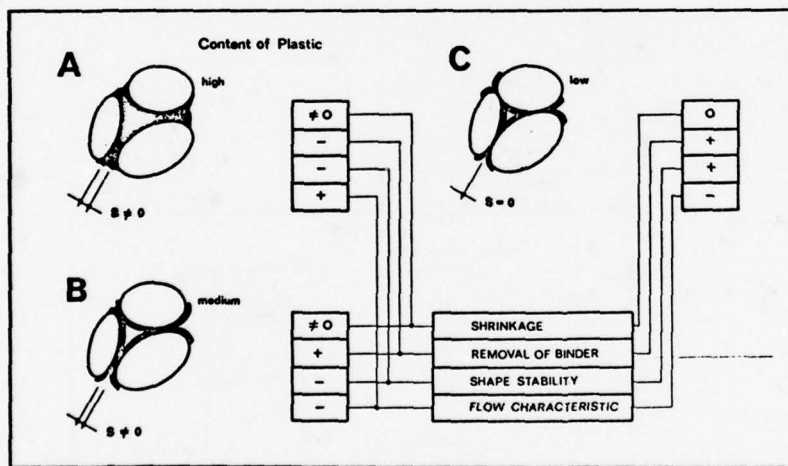


Fig. 4:
Influence of plastic
content upon injection
molding behavior.

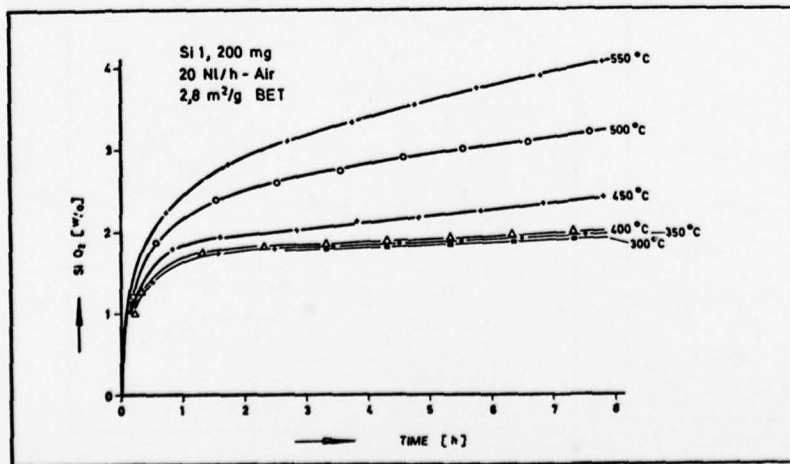


Fig. 5:
Oxidation characteristics
of silicon at burnout tem-
peratures: Thermogravi-
metrical determination of
 SiO_2 -development.

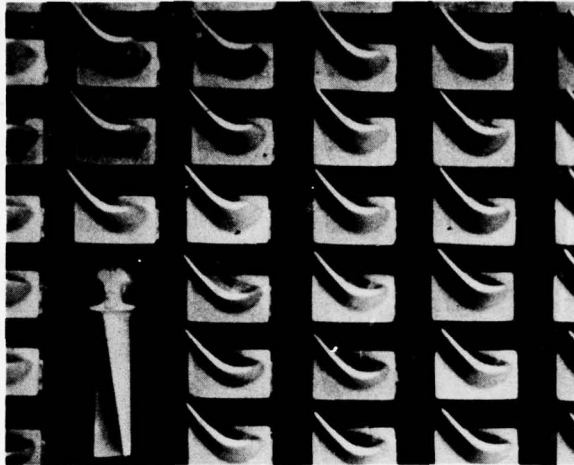


Fig. 6: Reaction bonded silicon nitride single gas turbine blades made by injection molding (Degussa)

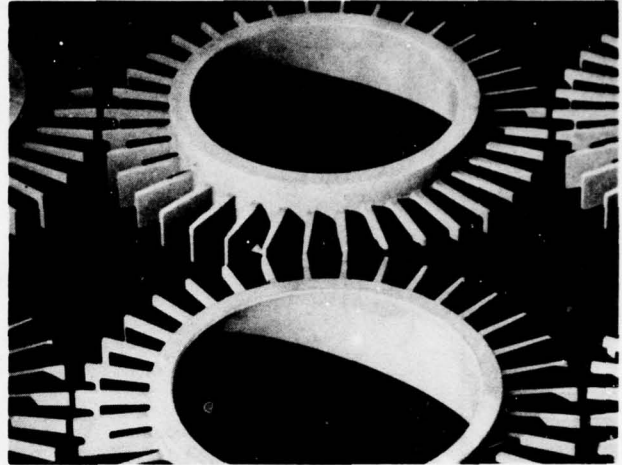


Fig. 7: Reaction bonded silicon nitride gas turbine blade rings shaped by injection molding (Degussa).

Difference from nominal dimensions in 0,01 mm								
Serie 101-120			Serie 161-180			Serie 281-300		
a	b	c	a	b	c	a	b	c
+1	0	+3	+1	-2	-2	+2	-2	+2
0	-1	+4	0	-1	0	+2	0	+4
+1	-2	0	0	-1	+1	+2	-1	+3
+1	-3	+2	+2	0	-1	+2	-1	+4
0	-1	0	0	-2	-4	+2	-1	0
+1	-2	+1	+1	-2	+2	+2	-2	+1
0	-2	-2	+1	-1	+4	+2	-1	+4
-2	-4	-2	+1	-2	+1	+2	+2	+1
+1	-1	+2	+2	-2	-1	+2	0	-1
0	-3	+1	0	-1	-1	+2	-1	0



Nominal dimensions:
a = 5,48 mm
b = 8,4 mm
c = 12,0 mm

Permissible Tolerance: $\pm 0,15$ mm

Table III:

Differences from nominal dimensions of injection molded turbine blades (Degussa)

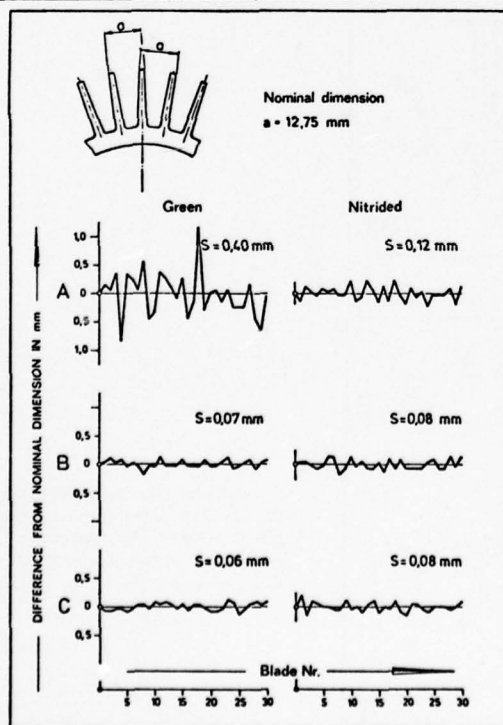


Fig. 8: Differences of blade distances of injection molded rotor blade rings (Degussa).

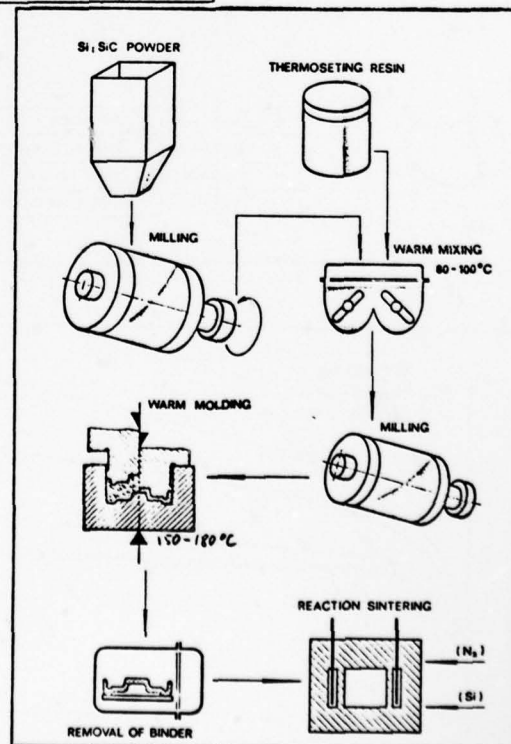


Fig. 9: The warm molding process

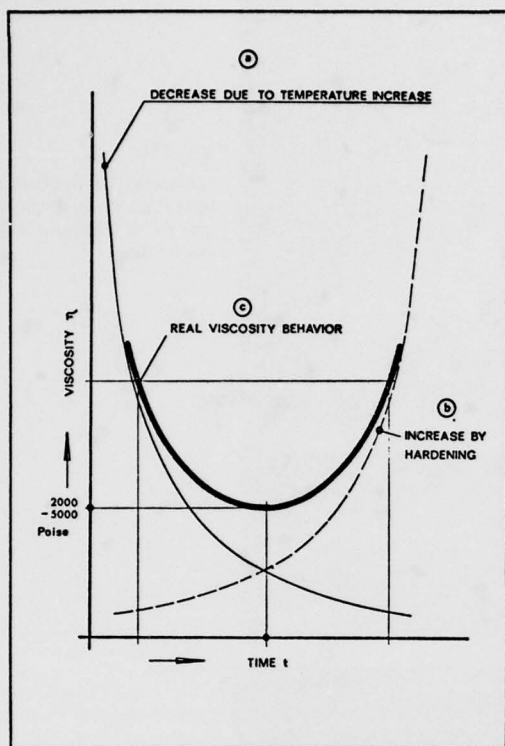


Fig. 10: Change of viscosity during hardening of duroplastics.

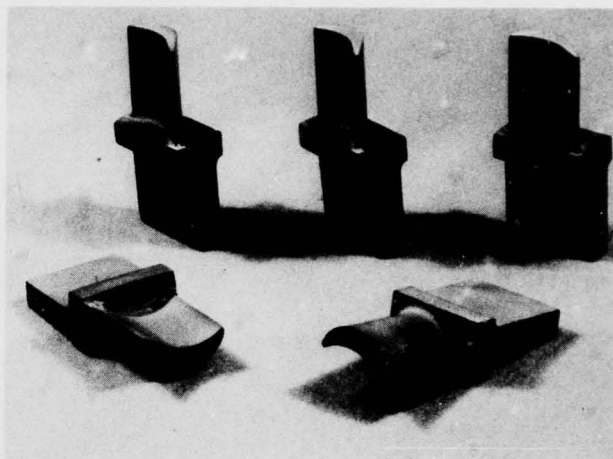


Fig. 11:
Warm molded reaction bonded silicon nitride gas turbine blade preshapes.

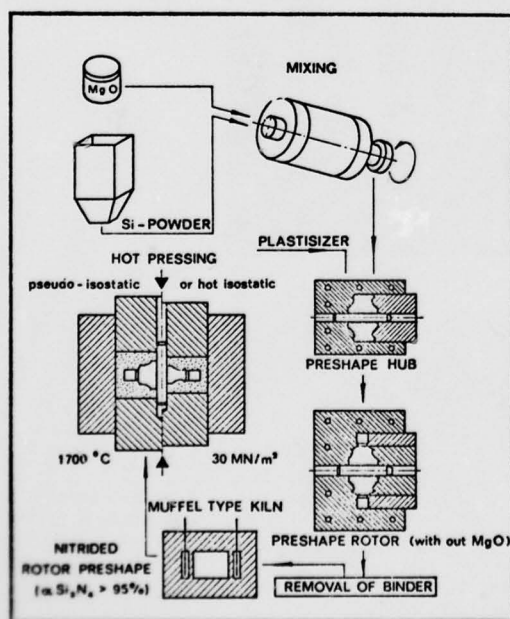


Fig. 12: The production of duodensity silicon nitride gas turbine rotors by warm molding and post hot pressing.

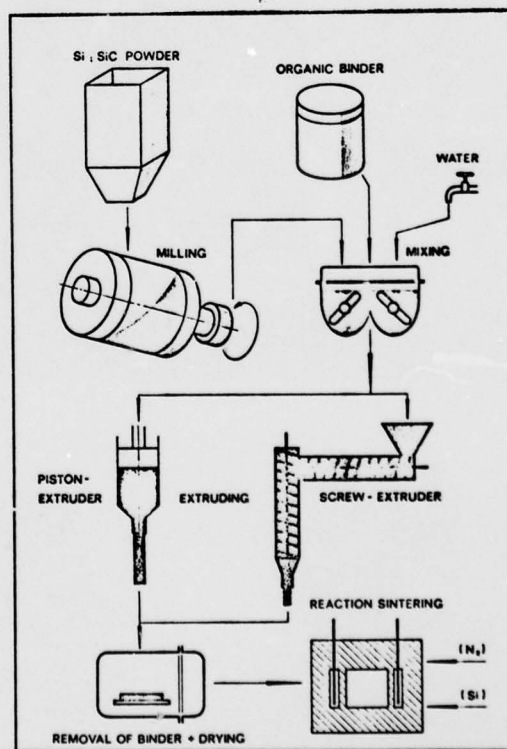


Fig.: The extrusion process

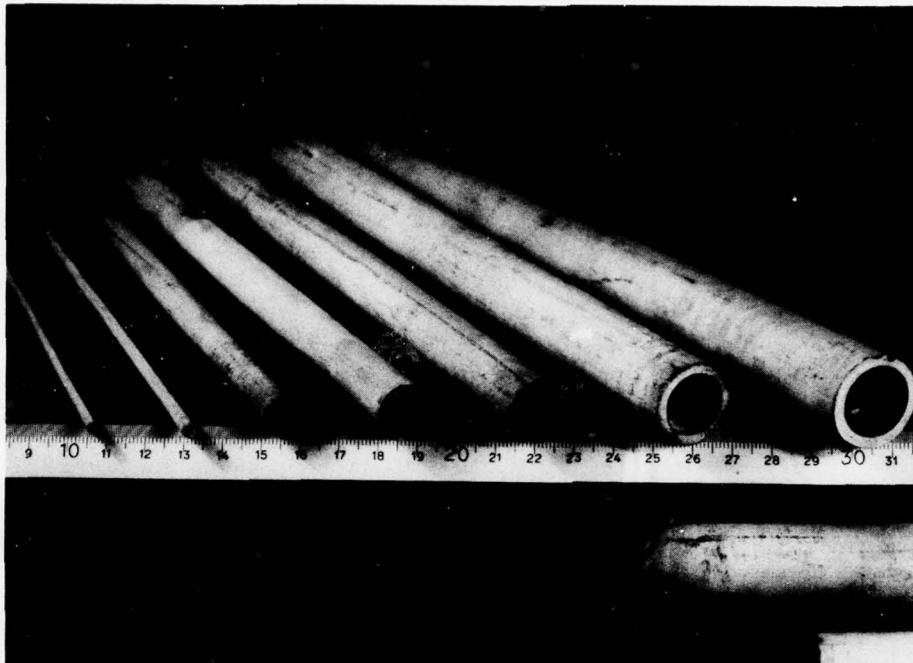


Fig. 14:
Thermocouple protection
sheets made by extru-
sion of a plastic si-
licon mix.

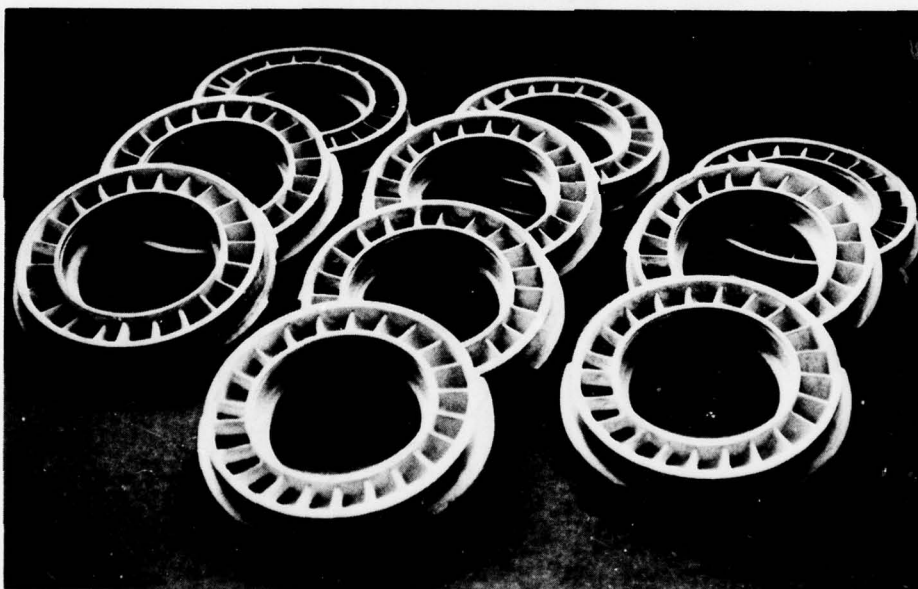


Fig. 16:
Reaction bonded sili-
con nitride and sili-
con carbide gas tur-
bine stators made by
slip casting

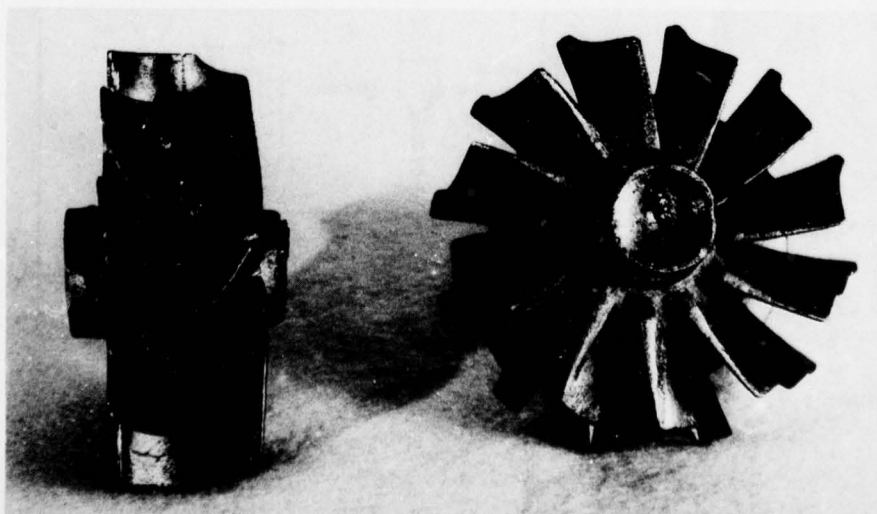


Fig. 17:
Reaction bonded sili-
con carbide turbo-
charger radial rotor
made by slip casting.

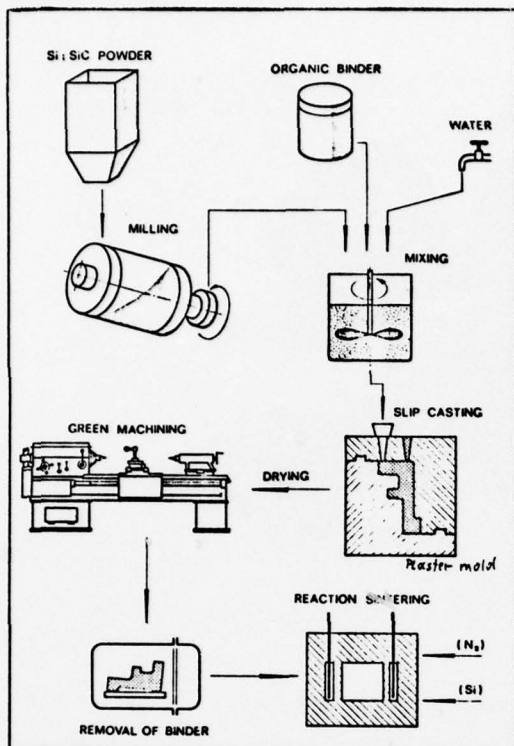


Fig. 15:
The slip casting process

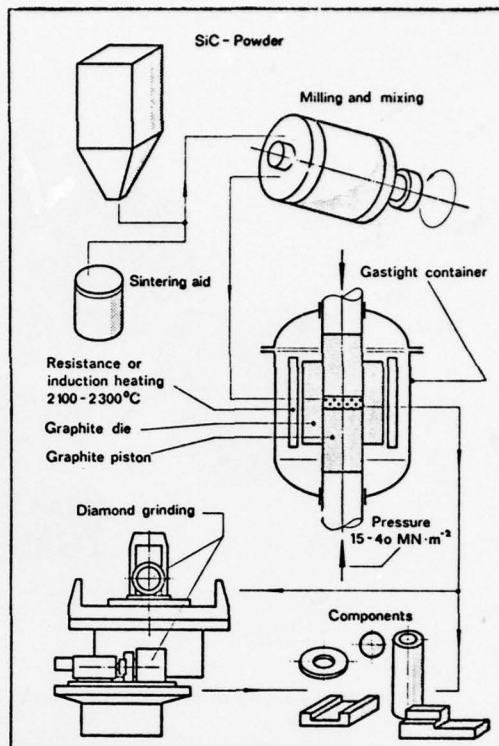


Fig. 18:
The hot pressing process (silicon carbide)

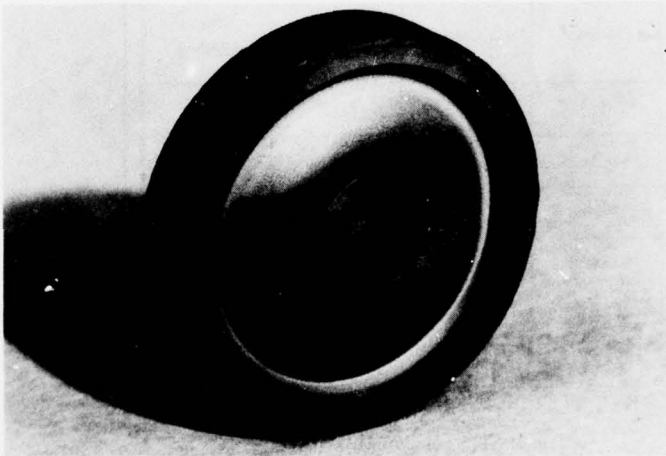


Fig. 19:
Hot pressed silicon nitride gas turbine rotor hub aspressed.

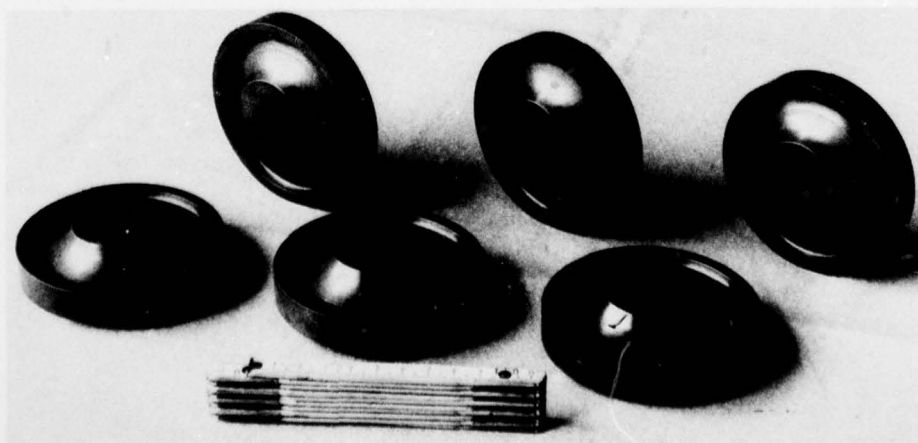


Fig. 20:
Hot pressed silicon nitride gas turbine rotor hubs diamond ground, ready for spin testing.

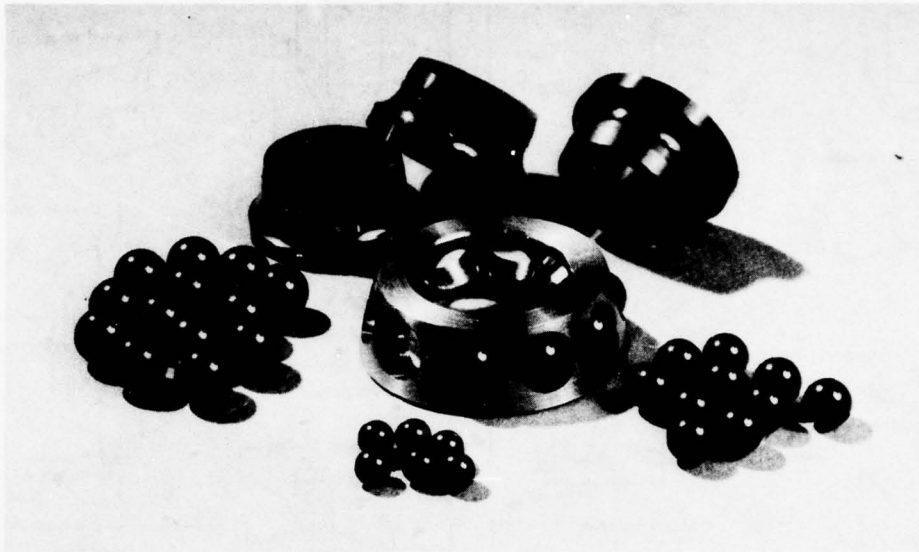


Fig. 21:
Ball bearing parts, diamond ground from hot pressed silicon nitride.

	Axial Dry Pressing	Extrusion	Slip Casting	Injection Molding	Warm Molding
Pieces	$\geq 10^4$	10^3	10^3	$\geq 10^4$	10^3
Time	seconds	sec.-min.	hours	seconds	minutes
Complexity	medium	limited	high	high	medium
Accuracy	very good	bad	good	good	good
Cost of Tools	high	medium	low	very high	high

Table IV:
Characteristics of net shape forming methods.

CONCURRENT SUPERPLASTIC FORMING/DIFFUSION BONDING OF B-1 COMPONENTS

by

George W. Stacher and Edward D. Weisert
 Advanced Titanium Technology
 Los Angeles Division
 Rockwell International Corporation
 P. O. Box 92098
 Los Angeles, Calif., U.S.A. 90009

SUMMARY

Rockwell International's (Rockwell) concurrent superplastic forming/diffusion bonding (SPF/DB) titanium fabrication process for direct application to advanced aircraft structure has resulted in significant cost and weight savings when compared to conventional titanium manufacturing methods. The phenomenon of superplasticity in conjunction with diffusion bonding has enabled the manufacture of B-1 aircraft parts that could not otherwise be produced. Applications include single-sheet formed parts, selectively formed and bonded hollow sections, and complex sandwich structure replacing multiple-piece assemblies and machined parts. A total of 26 different titanium configurations has been produced and installed on the B-1. Cost reductions and weight savings in all cases have averaged between 30 and 50% when compared to previous construction. This versatile fabrication process for titanium offers a real potential for revolutionizing aircraft design.

A process that combines both SPF and DB of titanium has been developed at Rockwell. Trade studies using this technology in actual applications have shown that this combined process results in cost savings up to 60% when compared to conventional titanium construction methods, while also saving weight. The evolution of these titanium fabrication methods came about because of the necessity to improve aircraft performance and reduce cost of ownership. Titanium aircraft structure is expensive primarily because of the high cost of fabrication and assembly. To take advantage of the structural efficiency and low-ownership-cost benefits of titanium airframe structure, new and innovative concepts of design and manufacturing were required; hence, the introduction of the SPF and SPF/DB fabrication methods. Because these new processes allow severe forming and intricate joining, many structural forms are possible that could not be produced with conventional methods. It has been shown that savings accrue primarily from the reduction of assembly costs, since the processes produce monolithic structure and eliminate details and mechanical fasteners. The specific factors contributing to reductions in cost and weight are reduced tooling requirements, less machining with sheet metal formed to very large elongations, overall reduction in part count by combining details, and a decrease in the use of expensive fasteners. The capability to produce large, complex, inexpensive, monolithic structure of titanium sheet metal is due to the ability of the material to superplastically form, an ability not present in all metals.

The process of press diffusion bonding of titanium is a current production method, having been developed jointly with the Air Force Materials Laboratory. At elevated temperatures (925°C, 1,700°F) and under high pressure, atomic diffusion between the metal interfaces takes place and a single titanium part is created with joint strengths equal to the parent metal. The titanium details are placed in steel tooling and pressed under vacuum using a hydraulic press capable of loading in horizontal directions as well as in the vertical direction. Because the titanium details are precut and placed in the position required to achieve final part configuration, little metal flow is required, and deep pocketed parts are accomplished more efficiently than by other processes. Typically, plan area pressures in the range of 12,060 to 24,120 Kpa (1,500 to 3,000 psi) are applied for a specified period of time to obtain the required metal flow. This process for thick plate bonding is significantly affected by material plastic flow properties at elevated temperature. Observation and interest in this phenomenon at Rockwell led to the study of superplasticity in titanium alloys.

Under specified conditions of temperature and strain rate, several titanium alloys exhibit superplasticity; i.e., elongation significantly greater than normal tensile elongation while localized deformation (necking) tendency is inhibited (figure 1). For superplastic deformation, an alloy requires a fine, equiaxed, stable grain size which is typically found in sheet metal structure. An elevated-temperature tensile test with a range of strain rates imposed is used to establish sheet metal superplastic behavior. The slope of the resultant log flow stress/log strain rate plot is defined as the strain rate sensitivity, m , of the material; i.e., the propensity to deform superplastically. It was found that 6Al-4V titanium alloy, nominally limited to forming operations involving less than 30 percent elongation, can be superplastically formed by more than 10 times that amount. Flow stresses are low in the superplastic condition; thus, metal stock may be formed into a complex die cavity by the application of gas pressure much as non-metallic plastic sheets are vacuum formed. The forming process is shown in figure 2. Formed configurations having structural efficiency previously unachievable in titanium hardware may now be designed and readily fabricated. The feasibility of this method of forming titanium was demonstrated at Rockwell in 1973. The patented technique is described in reference 1.

Under a contract to the Air Force Materials Laboratory (reference 2), the capability to superplastically form complex titanium sheet metal parts has been successfully demonstrated. One of the parts fabricated was the B-1 nacelle forward center beam frame. This component (figure 3) has a plan area of about 1,612 cm² (250 in.²). The conventional multiple-piece assembly combined eight individual parts, three of which were machined, while five were cold preformed and hot sized in closed dies. The assembly required 96 mechanical fasteners. This frame was redesigned into a single SPF part at cost and weight reductions of 55% and 33%, respectively. The SPF was accomplished as a single operation at 925°C (1,700°F).

Development of the SPF process occurred concurrently with the design of the B-1. With A/C-4, a total of 174 SPF parts had been designed and built for the aircraft, including corner clips, sine wave shear webs, bead-stiffened skins, stiffened skin panels, door panels, and shrouds. Examples of these parts are shown in figures 4 and 5. These figures indicate the feasibility of fabricating large complex titanium sheet metal parts in one thermal cycle as opposed to the conventional methods of multiple room temperature preforms followed in separate stages by hot-sizing. The number of steps in the manufacturing sequence was greatly reduced by exploiting superplasticity of titanium.

The optimum temperature for superplastically forming the Ti-6Al-4V alloy is 925°C (1,700°F). This is the same temperature used for the previously described press diffusion bonding process for titanium. It was conceived that unique, highly efficient structure could be produced if SPF and DB could be combined in the same fabrication cycle.

In order to effect DB of sheet metal as opposed to heavy plate and accomplish the bonding using lower pressure, an analysis of the creep deformation required to obtain the necessary intimate surface contact of the 6-4 alloy was conducted. The analysis resulted in the theoretical pressure-time curve shown as a solid line in figure 6. Time-pressure combinations predicted for low-pressure DB were verified by lap shear testing.

Test specimens were fabricated using bonding times and pressures above and below the optimum values indicated by the theoretical curve. The resultant diffusion bonds were evaluated by nondestructive testing, metallography, and by shear testing. The experimental data, also shown in figure 6, verified the analytical prediction, indicating that complete bonding could be obtained at low pressures. Lap-shear strengths for the low-pressure diffusion bonded parts, for example, averaged 580 MPa (84,000 psi) as compared to typical Ti-6Al-4V sheet metal shear strength of 600 MPa (87,000 psi). The diffusion bonds were of essentially the same strength as the parent material.

A wide variety of structural configurations has been fabricated by SPF/DB. Continuing efforts have established three generic types of SPF/DB structures for the Rockwell patented SPF/DB process (reference 3), as shown in figure 7. In each case, titanium sheet is superplastically formed and diffusion bonded to separate details during a single heating cycle. The sequence of operation (i.e., SPF/DB or DB/SPF) is varied, and reinforced sheet, integrally stiffened, and expanded sandwich structures are produced.

Under an Air Force Materials Laboratory contract (reference 4), Rockwell is demonstrating the application of SPF/DB to three full-scale advanced titanium structures, one of each generic configuration. The first is a B-1 nacelle beam frame which is conventionally fabricated using 12 titanium hot-sized sheet and machined plate details assembled with 81 fasteners. Redesign of the frame to use SPF/DB resulted in a beaded monolithic configuration with details preplated for bonding (figure 8). The part incorporates a center cap and a 180-degree reverse flange which are bonded in place. The initial SPF/DB part was sectioned and evaluated to verify bond integrity and metallurgical characteristics; the part showed complete diffusion bonding. Cost and weight trade studies showed that the monolithic SPF/DB design weighs 39% less and costs 43% less than the conventionally fabricated assembly.

The second type of SPF/DB structure, two-sheet-integrally stiffened, is made by simultaneous bonding and forming of two Ti-6Al-4V sheets. A stopoff compound applied selectively to one of the sheets of the mating surfaces prevents bonding in discrete areas which correspond to the tooling cavities. At 925°C (1,700°F), gas pressure is applied externally to the sheets and selective bonding occurs. Immediately following bonding, gas pressure is introduced between the sheets to superplastically form the unbonded areas into the die cavities.

An integrally stiffened SPF/DB version of an auxiliary power unit (APU) door was demonstrated for B-1 application. The SPF/DB version measures approximately 560 by 610 mm (22 by 28 in.) with 20 mm (0.75 inch) deep hat sections. The SPF/DB door would replace a single T-section-stiffened door currently machined from plate (figure 9).

A cost/weight trade-off study indicated that the SPF/DB APU door would provide cost and weight savings of 55% and 31%, respectively, over the conventionally machined version. The SPF/DB door represents typical aircraft part complexity, in that the periphery includes a 2.8 mm (0.109 inch) thick "picture frame" doubler bonded in place and the central area, which accommodates an access door, has an additional 1.5 mm (0.060 inch) thick sheet bonded in place to carry the load. The deep, expanded section is also thickened by bonding, and subsequently formed.

Location of the APU door on the lower side of the B-1 engine nacelle dictated structural qualification by acoustic testing. One APU door was successfully tested under the conditions shown in table I, thus fully qualifying the part for this design application.

Table I

APU DOOR ACOUSTIC FATIGUE TESTS

Energy level (db)	159	163	167
Frequencies (Hz)	0-1,000	0-1,000	0-1,000
Test time (hr)	5	5	5

The third generic SPF/DB form involves three or more sheets and results in sandwich structure. It is fabricated by another Rockwell patented process (reference 5). Three important advantages of the SPF/DB sandwich shown can be cited:

1. The external configuration of the fabricated sandwich part is determined by the tool cavity, which can be variable either in depth or in configuration.
2. The core configuration is determined by the stopoff pattern; it can vary greatly and can be modified without tooling change.
3. The process inherently provides complete flexibility in edge closure design. This avoids what is frequently a significant cost factor in the fabrication of conventional honeycomb sandwich panels. In addition, the truss members of the SPF/DB core become integral with the edge member through the DB pattern, providing reduced cost and improved structural efficiency through simplified shear ties.

Many small and large sandwich parts have been fabricated to date incorporating a myriad of core designs. The capability to vary core configurations without extensive tool modification has resulted in the fabrication of straight truss, dimpled truss (circular diffusion bond areas), sine wave patterns (variations of parallel sine waves and hourglass or nodal sine waves), and hexagonal and pyramidal configurations using four-sheet SPF/DB technology. These sandwich variations are shown in figure 10 which also indicates the capability to fabricate parts having single or compound curvatures.

The first application of SPF/DB on the B-1 is the A/C-4 windshield hot-airblast nozzle assembly. This wide, shallow nozzle, with internal guide vanes and transitions to inlet tubing, posed a fabrication challenge that was met only with great difficulty on the first three aircraft, when conventional fabrication methods were used. Figure 11 shows one previous fabrication method and the SPF/DB approach. As can be seen, each of the two SPF/DB parts of the windshield nozzle incorporates thin, integral internal vanes set at differing angles for preferential airflow. The two parts comprise one-half of a windshield nozzle assembly. Four SPF/DB titanium parts welded together provided a direct replacement for the previous three-piece welded steel assembly which was made up of 32 machined parts. The SPF/DB part resulted in cost and weight savings of 50 percent, and was fully qualified for use on the B-1.

Additional examples are shown of the SPF/DB two- and three-sheet technology which have direct application to advanced aircraft. A typical skin-frame-stringer mechanically fastened design (figure 12) shows the many details of a multiple-piece assembly. A monolithic titanium part, also shown in figure 12, was fabricated by selective DB of two flat sheets, followed by superplastic expansion into a specially configured die. The resulting part incorporated differing heights of hat sections with multiple intersections, vertical stiffening beads, tapered hat sections, and joggles, all of which were accomplished in one processing cycle. A multiple-piece assembly of individually fabricated parts and a large number of mechanical fasteners were eliminated.

A large sandwich structure measuring 1142 mm (45 in.) long, 91 mm (36 in.) wide, and 40 mm (1.4 in.) deep has also been fabricated (figure 13). The part represents an SPF/DB sandwich design for the B-1 engine access doors to replace the existing aluminum honeycomb design. Core configuration is a parallel sine wave pattern. Selective diffusion bonding of the flat sheets was accomplished initially followed by superplastic expansion of the bottom sheet. Capability to include integral door hinges was demonstrated by expanding the bottom sheet against titanium details preplaced in the lower die causing bonding to occur. Projected improvements include substantial cost and weight savings even though the titanium SPF/DB part would replace an aluminum component.

The hardware shown and the cost studies conducted indicate very clearly the benefits offered by the SPF/DB titanium process.

Table II summarizes the several SPF and SPF/DB applications studied on the B-1 aircraft and the cost and weight reductions projected over the life of the program, compared to conventionally fabricated titanium structure.

Table II
SPF/DB COST REDUCTION POTENTIAL

Part Description	Percent	
	Cost Savings	Weight Savings
Nacelle center beam frame	55	33
Nacelle frame	43	40
APU door	55	31
Windshield blast nozzle	40	50
Precooler door	60	46

The SPF/DB process for titanium fabrication, in its relatively short time of development, has resulted in many actual and potential aircraft and industrial applications. The process has proved to be versatile, has opened a broad vista of potential cost and weight reduction applications, and is expected to have a profound influence on aircraft design. The developments described provide designers with an opportunity to take advantage of more efficient and affordable titanium structure for future aircraft designs.

REFERENCES

1. Hamilton, C. H., et al, "Controlled Environment Superplastic Forming of Metals," U. S. Patent 3934411, 27 January 1976
2. Hamilton, C. H., Stacher, G. W., Mills, J. A., and Li, H. W., "Superplastic Forming of Titanium Structures," AFML-TR-75-62, April 1975
3. Hamilton, C. H., and Ascani, L. A., "Method for Superplastic Forming of Metals With Concurrent Diffusion Bonding," U. S. Patent 3920175, 18 November 1975
4. Weisert, E. D., and Stacher, G. W., "Manufacturing Methods for Superplastic Forming/Diffusion Bonding Process," IR798-5 (I-XIII), May 1, 1975 - April 15, 1978
5. Hamilton, C. H., et al, "Method for Making Metallic Sandwich Structures," Patent 3927817, 23 December 1975

**DEFINITION: CAPABILITY OF TITANIUM ALLOYS TO DEVELOP
EXTREMELY HIGH TENSILE ELONGATIONS AT
ELEVATED TEMPERATURES AND CONTROLLED
STRAIN RATES**

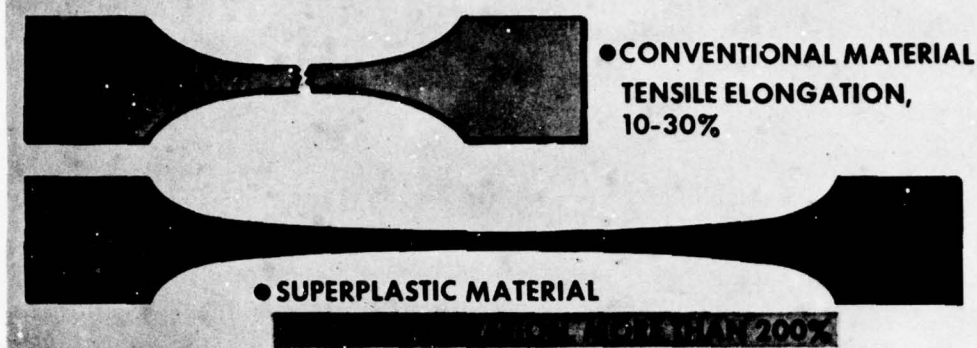


Figure 1. Large Tensile Elongations Possible With Superplastic Materials

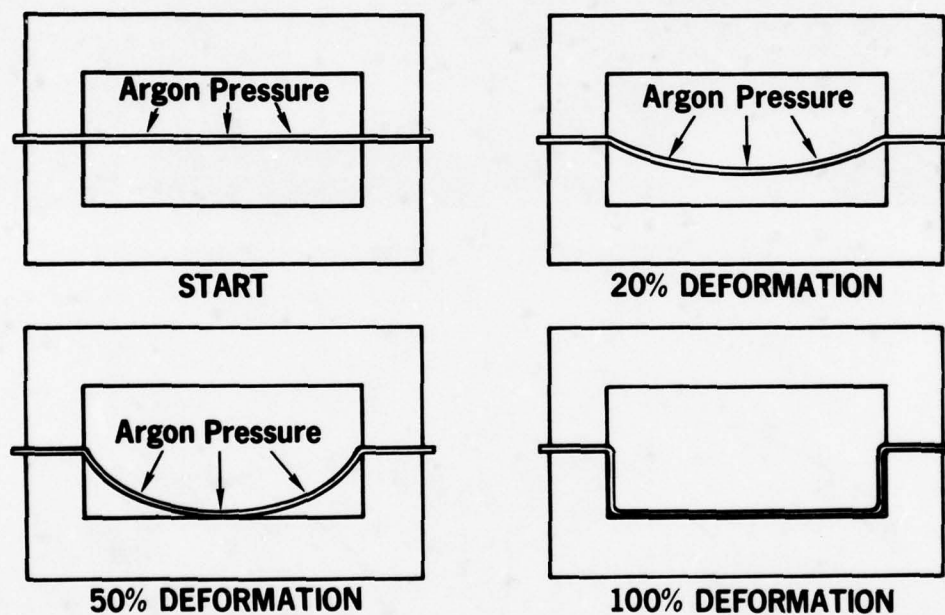


Figure 2. Schematic Description of Superplastic Forming Process

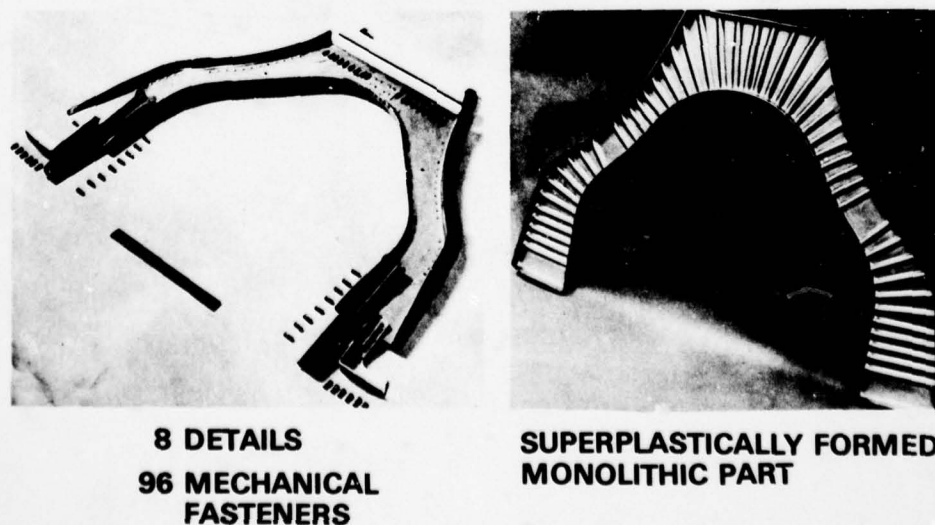


Figure 3. Nacelle Frame Redesign Comparison

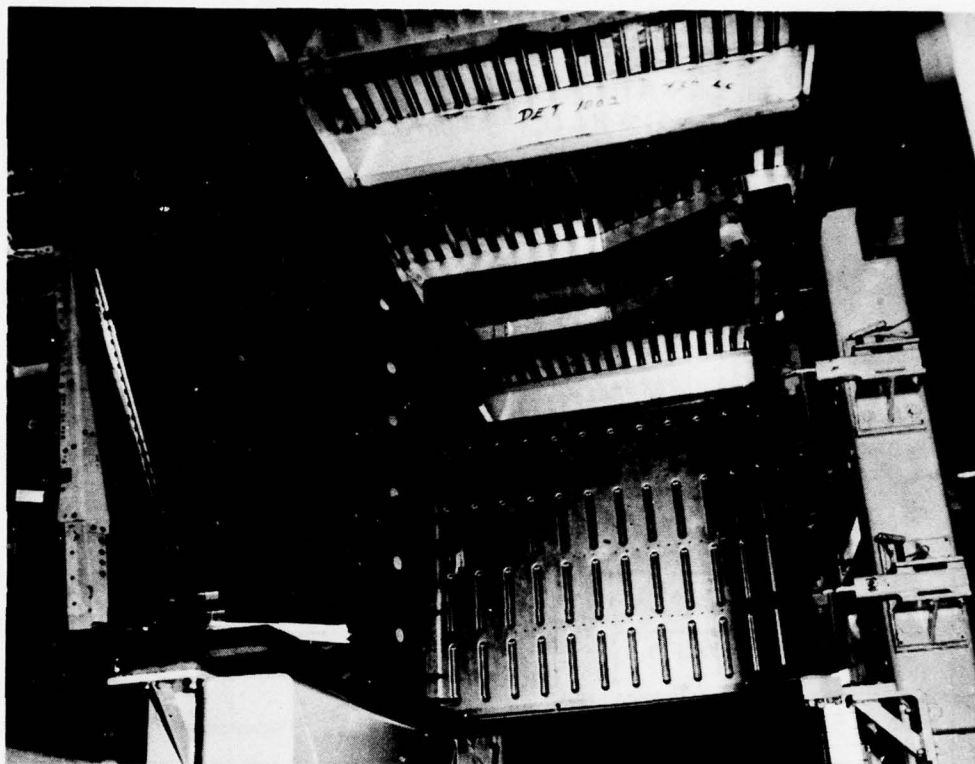


Figure 4. Typical Applications of SPF Titanium Sheet Metal Parts in B-1 Aircraft Nacelle

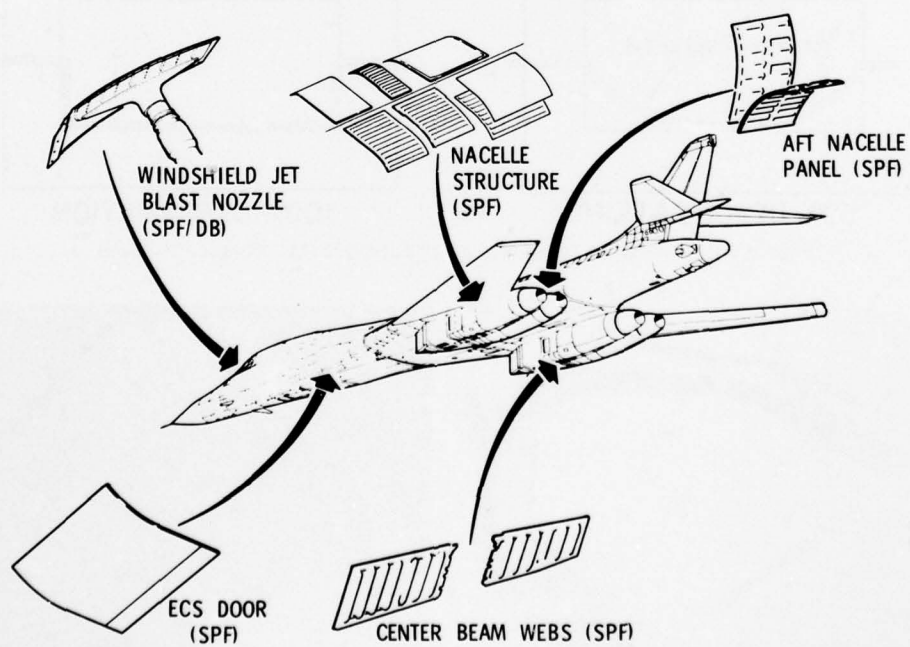


Figure 5. B-1 Usage

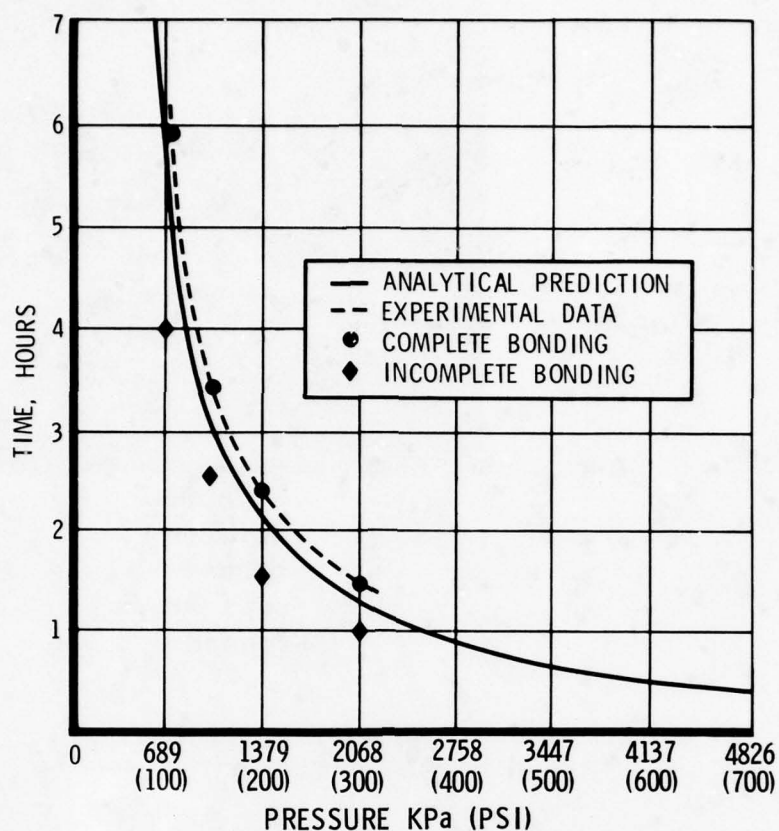


Figure 6. Theoretical and Experimental Pressure-Time Curves for Diffusion Bonding of Ti-6Al-4V Alloy Sheets

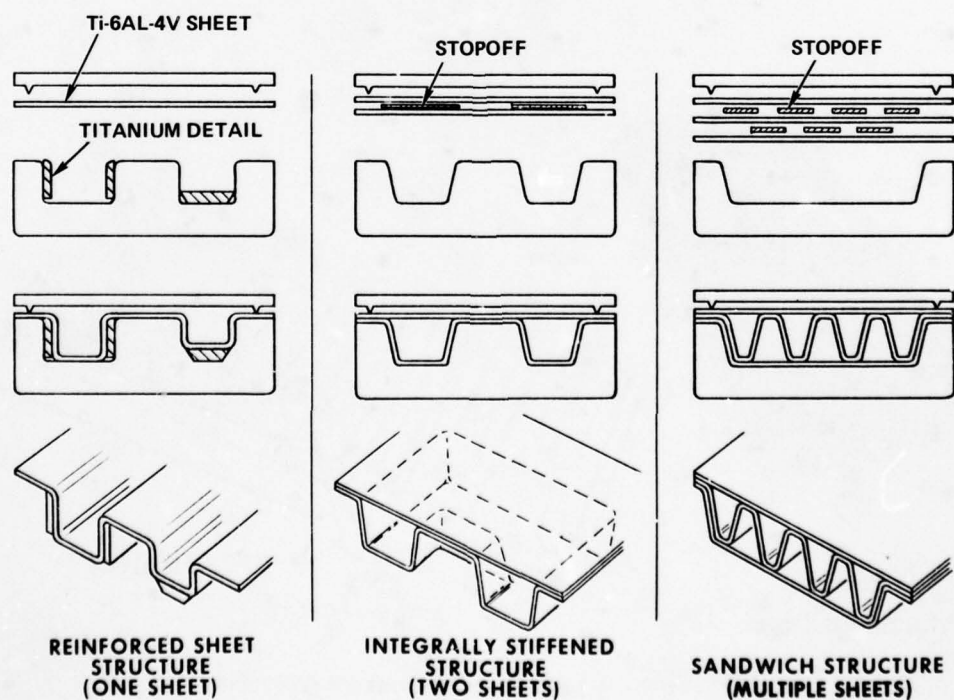


Figure 7. Three Basic Types of Titanium SPF/DB Structures

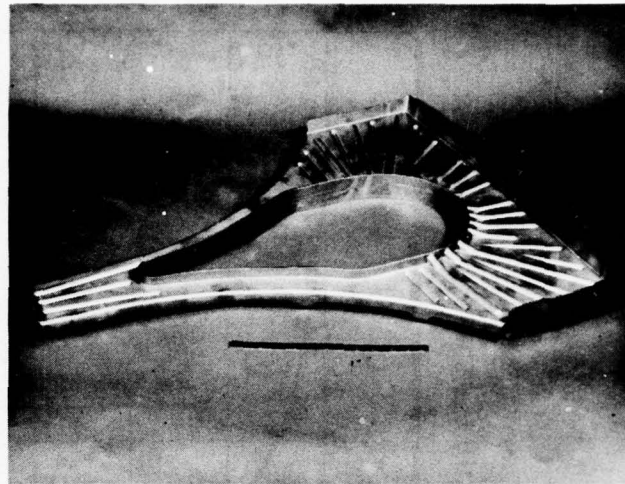
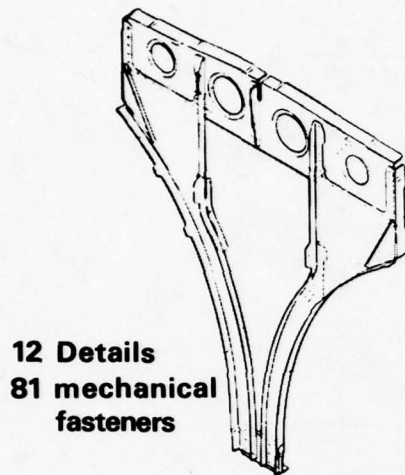


Figure 8. B-1 Nacelle Center Beam Frame Construction Comparison

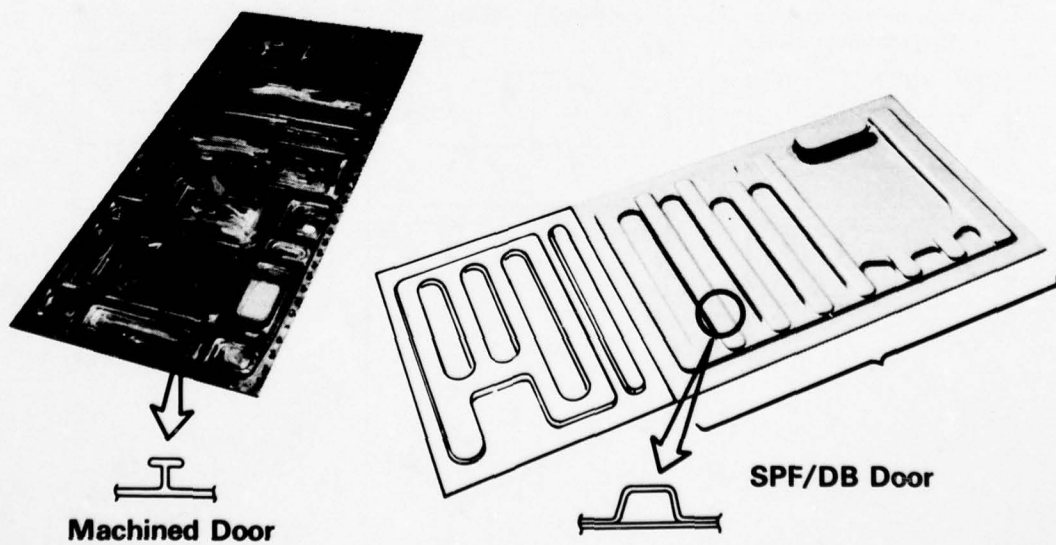


Figure 9. B-1 APU Door Construction Comparison

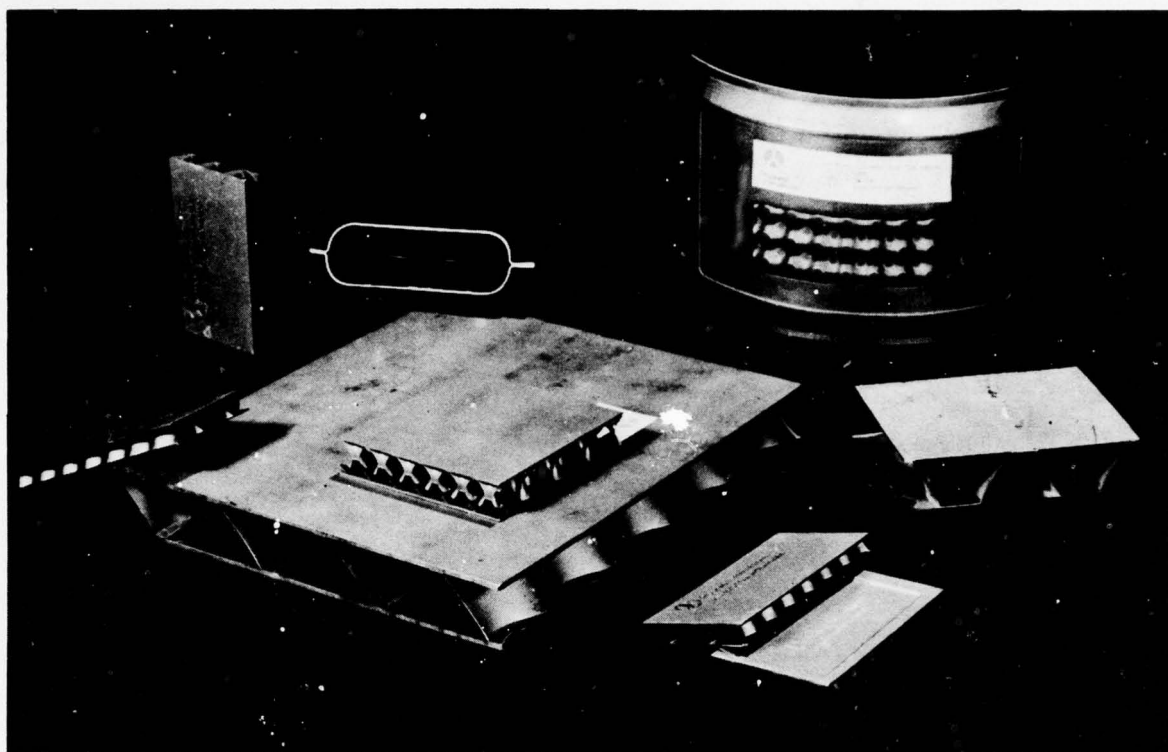
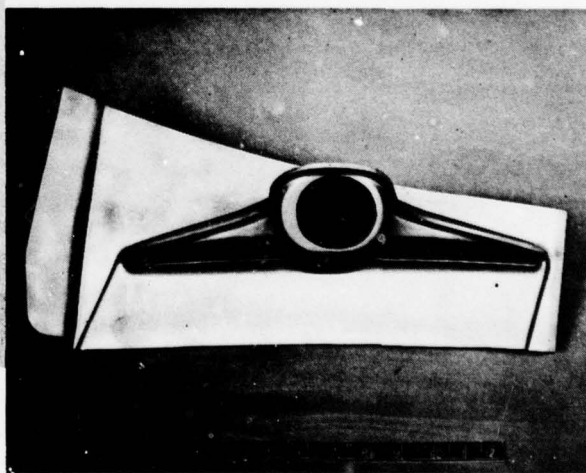


Figure 10. Variety of Sandwich Configurations Demonstrated At Rockwell



**32 PIECE
WELDED ASSEMBLY**



SPF/DB REDESIGN

Figure 11. Comparison of B-1 Windshield Hot-Air Blast Nozzle Fabrication Methods

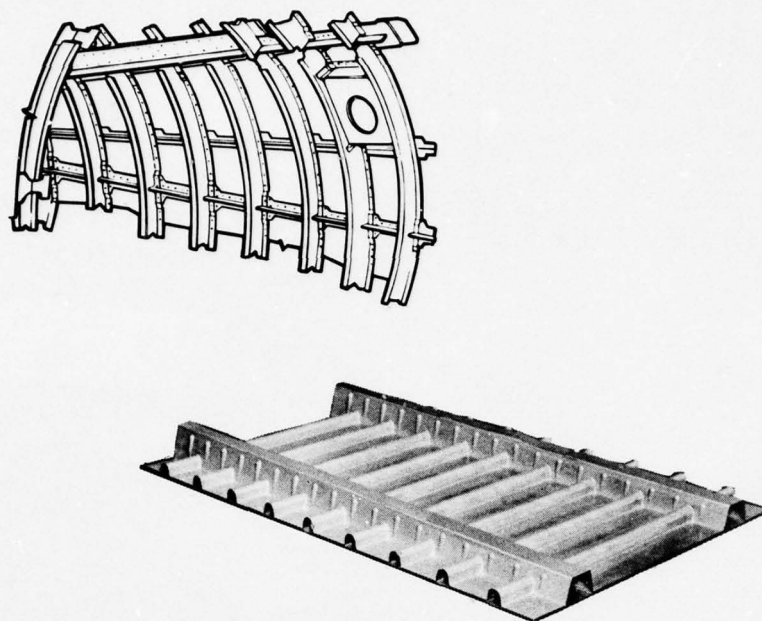


Figure 12. Skin/Frame/Stringer Monolithic Structure, Design, and Fabrication

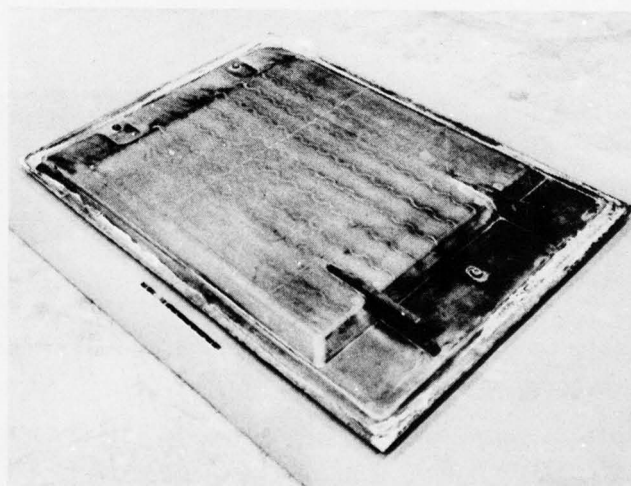


Figure 13. Large Titanium SPF/DB Sandwich With Integrally Bonded Hinge Fittings

AD-A068 980

ADVISORY GROUP FOR AEROSPACE RESEARCH AND DEVELOPMENT--ETC F/6 11/6
ADVANCED FABRICATION PROCESSES. (U)
MAR 79

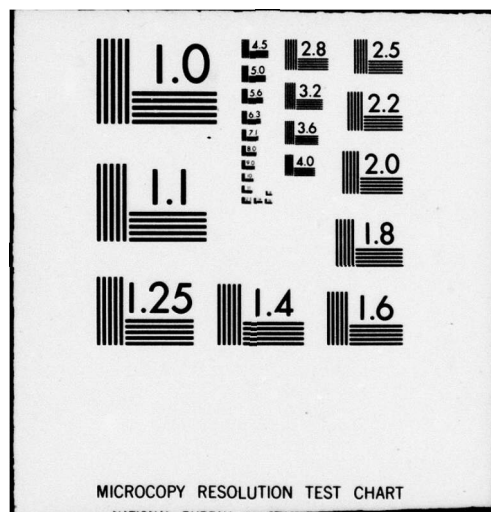
UNCLASSIFIED

AGARD-CP-256

NL

3 OF 3
AD
AO=8980





FABRICATION OF TITANIUM AT HIGH TEMPERATURES

by: S.J. Swadling,
Divisional Research Co-Ordinator (Manufacturing),
British Aerospace,
Aircraft Group,
Weybridge-Bristol Division,
Filton, Bristol,
England.

Investigations, at what is now the Bristol site of British Aerospace, began into the fabrication of titanium in the early post war period. Various applications were studied and in common with many aircraft of that period, a number of components were manufactured from commercially pure titanium particularly around engine installations where the good fire resistance coupled with relatively light weight of titanium could be exploited. These components were, in general, fabricated using conventional cold working processes.

Subsequently the development of high strength alloys such as Titanium 6Al.4V. opened up the potential usage of titanium permitting efficient light-weight structures to be made. However due to the high strength and toughness of the material, conventional cold forming techniques were found to be inadequate for many components so that hot forming at temperatures around 650°C was used. On Concorde, a number of applications of the 6Al.4V. Alloy were successfully developed particularly in the engine installation area, notably the Rear Engine Bay Doors illustrated in Figure 1.

An interesting feature of the Rear Engine Bay Doors was the development of a low cost technique to produce the close pitched I-section transverse frames. Initially these were machined from forged bar stock with a material utilisation of less than 10%. Subsequent components were fabricated by the automatic fusion welding of sheet metal elements to provide the required I-section. The fabricated components are identical in performance to the original machined items, but are approximately 1/7 of the cost.

During the late 1960's a general research and development activity was undertaken on a range of superplastic materials, including a zinc alloy that was being used as a low cost route to simulate the type of structures envisaged for structurally more useful materials.

In particular, at about this time, the Capenhurst Laboratories of the Electricity Generating Authority, had been experimenting with processes requiring the use of electrical energy as a means of promoting increased sales of electricity. During their work they had established that the 6Al.4V. Alloy of Titanium was superplastic at around 950°C, and it was anticipated that this would provide a very adaptable route to manufacture aircraft components of complex shape in this material.

Concurrently the Design Office at Bristol had obtained a Government contract to examine the use of titanium alloys for light-weight aircraft fuselage structures. The structural configuration proposed comprised hot pressed top hat section stringers, electron beam welded to thin external skins with the resulting skin stringer panels supported on hot press formed frames.

However at this time, early experiments at Bristol utilising the superplastic forming characteristic of the Titanium 6Al.4V. Alloy had shown that satisfactory frame components could be made by this route with the added advantage that complex shapes such as corrugated webs could be produced easily, resulting in a more efficient structural component. The results of this work enabled British Aerospace to obtain a subsidiary contract to manufacture, by the superplastic method, and test three structural elements that could be utilised in a titanium fuselage structure. The three elements chosen were:-

- a) a fuselage frame element that could be used in conjunction with the welded fuselage panel mentioned previously, see Figure 2,
- b) a passenger cabin floor beam, see Figure 3,

and c) a passenger cabin floor support strut, see Figure 4.

The first two components were produced utilising the basic tool concept shown in Figures 5 and 6. In this concept the tool is recessed to form a female die of the shape that is required. The superplastic forming is carried out by heating the tool and a sealed envelope of titanium alloy to 950°C, and then inflating the envelope using gas pressure to blow form the component against the tool profile. In a production situation double sided tooling would be utilised thus minimising material wastage and producing two components from a single forming cycle. For this early work the tools were designed to contain the forming pressures utilised and heating was achieved with conventional electric furnaces.

Tool machining complexity and hence cost was reduced by the use of separate tool elements to that each element was produced by simple machining operations. This is illustrated in Figure 6.

For the floor strut, partial tooling concept was used in order to reduce costs, although in a production situation it is probable that full form tooling would be utilised.

During this work it became clear that there were a number of fundamental problems relating to forming of titanium at 950°C that required resolution before a satisfactory production technique could be demonstrated. In particular at 950°C, titanium is highly reactive to both metallic and gaseous contaminants and suitable safeguards to prevent or limit such contamination had to be developed.

Additionally, formed components in intimate contact with tool faces tend to form a joint with the tool material and therefore suitable releasing coatings had to be devised. As part of the work on the Government contract the necessary process disciplines and material treatments were developed to provide practical production processes.

One fundamental point that was established during this work is that only the material in the plan area of the shape part to be produced is used unlike conventional pressing techniques where some additional material is drawn in from surrounding areas. This results in increased thickness reduction for superplastic forming compared with conventional techniques. This has to be allowed for in the design of the component, or alternatively, countered by the utilisation of a pre-form to reduce local thinning.

As a result of the experience gained during this work a potential application to Concorde was examined, this being a local dish required on the Rear Engine Bay Doors to provide clearance with certain engine dressing items, see Figure 7. The existing component was a welded fabrication utilising a number of components produced by the hot pressing route. A one-piece superplastic forming version was produced for evaluation purposes and a value engineering analysis showed potential cost saving in production over the original planned number of aircraft of some 40% coupled with a weight saving of 15%.

By the early 1970's it was considered that sufficient basic knowledge had been gathered to permit production applications to be sought for the superplastic process. A number of miscellaneous applications both within Aerospace and for other industries were found and satisfactory components produced.

For the European Nuclear Research Organisation CERN, in Geneva, sections of a titanium alloy chamber were manufactured. Each section was formed from a number of modules welded together to form a bellows assembly. Each module was some 280 mm long by 275 mm wide by 80 mm depth, and is shown in Figure 8. The module is produced by the superplastic forming of a pre-form envelope of 0.5 mm thick titanium alloy into a multi-part female tool. The superplastic forming was carried out in an electric furnace and to provide the necessary safeguards against contamination, high purity argon was used to provide both an inert atmosphere for the tool and component, and also to provide the necessary gas pressures for the forming cycle. As mentioned earlier, the tooling was designed to react all gas pressure loads and the whole assembly of tool and component is contained in a welded stainless steel muffle box to ease the problem of ensuring a high purity argon atmosphere.

In order to control the necessary cycle of purging the assembly within the muffle box and then heating and forming the component, a semi-automatic electro-pneumatic control system was utilised. The whole system permits preparation of blanks and tools away from the heating facility including the necessary purging sequences, thus reducing time of occupancy of the heating facility.

Figure 9 shows a sample of an aircraft hot air duct currently undergoing tests. In this instance the duct is formed by inflating a sealed titanium envelope produced by edge welding two flat sheets of material together. The weld remains as part of the final component.

As a variation of this technique, it is also possible to produce components which are formed without the use of tooling or with only partial tooling to control the shape. Typical of such components are spherical tanks and circular ducting, i.e. shapes which are formed naturally under pressure loading.

Typical of the "free blown", i.e. with no tooling, component is the bifurcated duct shown in Figure 10 where the component is produced by edge welding two profiled flat sheets to provide a sealed envelope which is then heated in a controlled atmosphere and inflated with argon gas once the superplastic forming temperature has been reached.

A component produced with partial tooling is illustrated in Figure 11, the component being a Positive Expulsion Tank for Space use. For this component hemispheres are produced by free blowing through a ring tool restraint. The ring tool controls the basic diameter of the hemisphere and the height of the hemisphere is controlled by a gas flow proximity switching device. Two such hemispheres are subsequently welded to an equatorial diaphragm ring by electron beam welding to produce a 387 mm diameter tank.

Further development of the facilities at Bristol has enabled British Aerospace to introduce hot platen presses. In such presses one combines the heating function and the reaction of forming loads. This results in considerable reduction in mass and complexity of the tools.

In addition to the superplastic characteristics of titanium alloy diffusion bonding between titanium elements occurs at temperatures, pressures and times which are close to those required for the superplastic forming. It was therefore obvious that the combination of these two processes was attractive in that one could, during a single manufacturing cycle, carry out both the component forming operation and also the assembly processes such as addition of reinforcing elements, local load input fittings, etc. A number of components have been fabricated utilising the combined process.

Typical of these is a development panel intended to provide an alternative replacement structure for part of the Concorde propelling nozzle, see Figure 12. This panel which is approximately 760 mm by 500 mm is made from two flat sheets edge welded to provide a sealed envelope and which are diffusion bonded together in discrete strips by mechanical pressure from the tool faces. In the same thermal cycle the stiffening shapes are superplastically formed utilising gas pressure between the sheets, the stiffener shapes being controlled by tool recesses. For this particular application, it was chosen to follow a route of producing the panels flat and subsequently providing the range of required contours by separate hot pressing operations. However, normally, any required contours would be produced as part of the basic forming and diffusion bonding cycle.

The sub-structure required to mount the panel on the nozzle structure was also produced by superplastic forming, and is shown in Figure 13. Currently the panel and sub-structure are installed in

an engine ground test facility for qualification testing prior to possible manufacture and fitment to service aircraft.

The combination of diffusion bonding and superplastic forming presents the designer with considerable flexibility in the form of structure that he can use. This is exemplified by the wide variation of core configurations that can be provided for sandwich panels. Typical of such sandwich panels is the truss core panel shown in Figure 14. This is formed by utilising a stop-off material applied to the inner faces of the external sheet material so that during the first part of the furnace cycle, under external pressure, diffusion bonding to a third sheet of material takes place in narrow strips only, and then during the latter part of the cycle where pressure is applied between the sheets, the external skins are moved apart to dimensions and shapes controlled by tooling cavities whilst the third sheet is formed to provide the core structure. The geometry of the core that can be produced is controlled essentially by the pattern of the stop-off coating applied to the sheets prior to processing, and therefore is extremely flexible and many different geometries can be produced.

Compared to the Concorde panel described earlier, it is clear that such sandwich panel structures result in much simpler tooling as well as potentially more efficient structures. Tooling is simplified because of the uninterrupted external profiles and the ability to form and diffusion bond from the same gas pressure source. As all the forming and bonding takes place in the controlled atmosphere within the titanium envelope, no contamination from tool contact occurs internally to the panel.

A wide range of actual and potential applications of these processes to current and future British Aerospace projects both Civil and Military has been studied. It is clear that a wide range of components currently manufactured by conventional methods can be replaced by components manufactured by these new techniques with resulting benefits in both cost and weight. Typically, British Aerospace's work suggests that a weight saving of 20% and cost saving of 40% can be achieved by adoption of these techniques to replace titanium components manufactured by conventional processes.

The reduced weight results from the design flexibility the techniques give allowing stiffening patterns to be introduced to permit higher stresses and a generally more efficient use of this material to be made. Cost savings result from the better material utilisation achieved and the significant reduction in man hour content particularly where complex assemblies are produced in a single thermal cycle.

Acknowledgements

In thanking British Aerospace for permission to publish this Paper the Author emphasises that, although it is based on his professional work on the Company's behalf, any views expressed are his own and do not necessarily represent those of the Company.

Funding by the British Government of some of the elements mentioned has been of great benefit and is gratefully acknowledged.

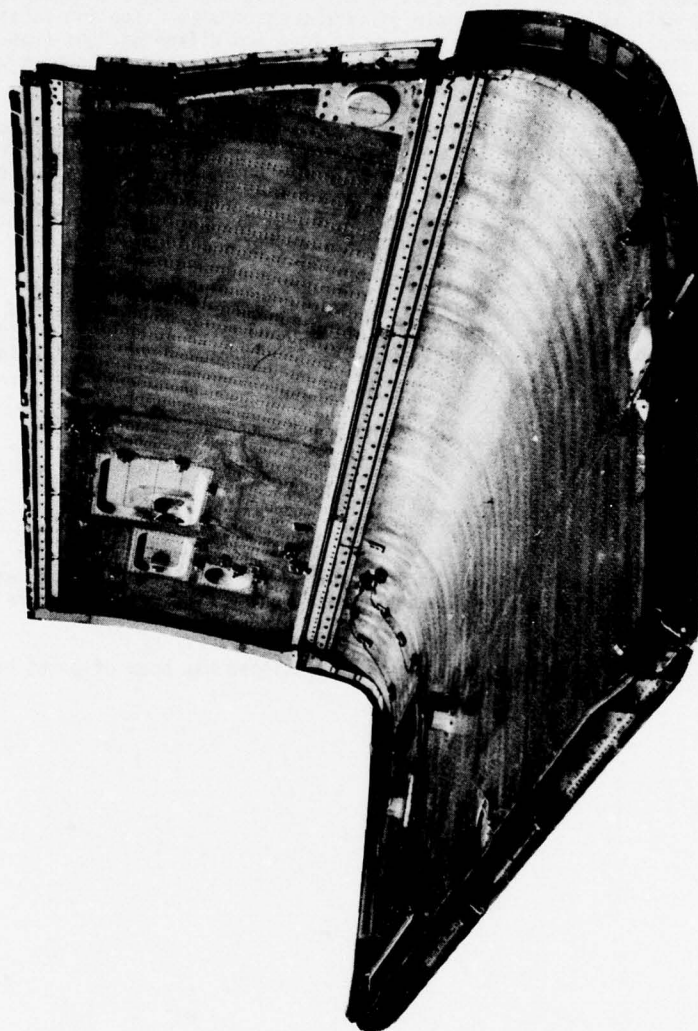


Fig.1. "Concorde" Titanium Rear Engine Bay Doors

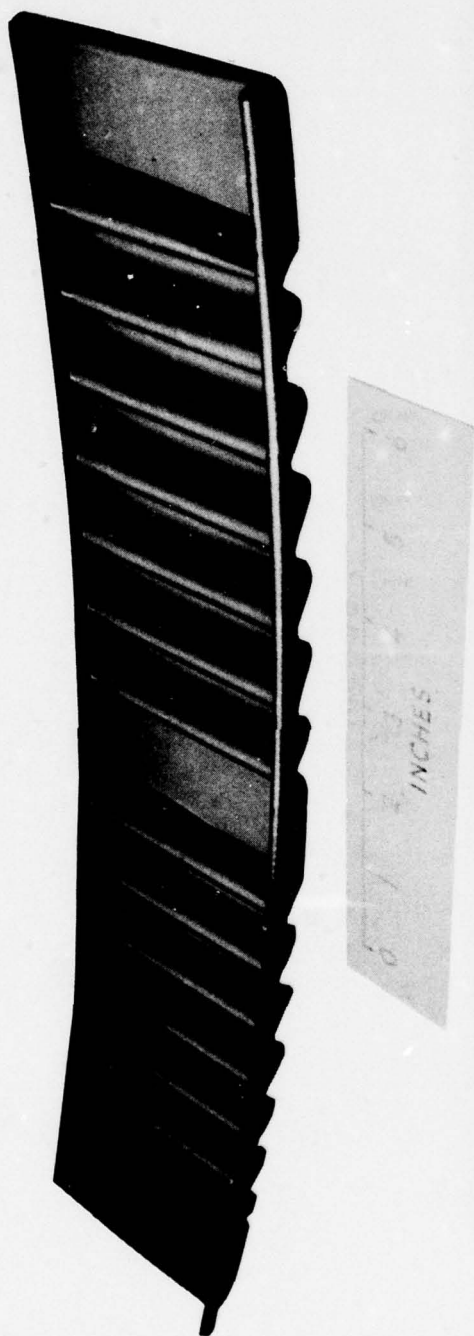


Fig.2. Superplastically Formed Titanium Alloy Experimental Fuselage Frame

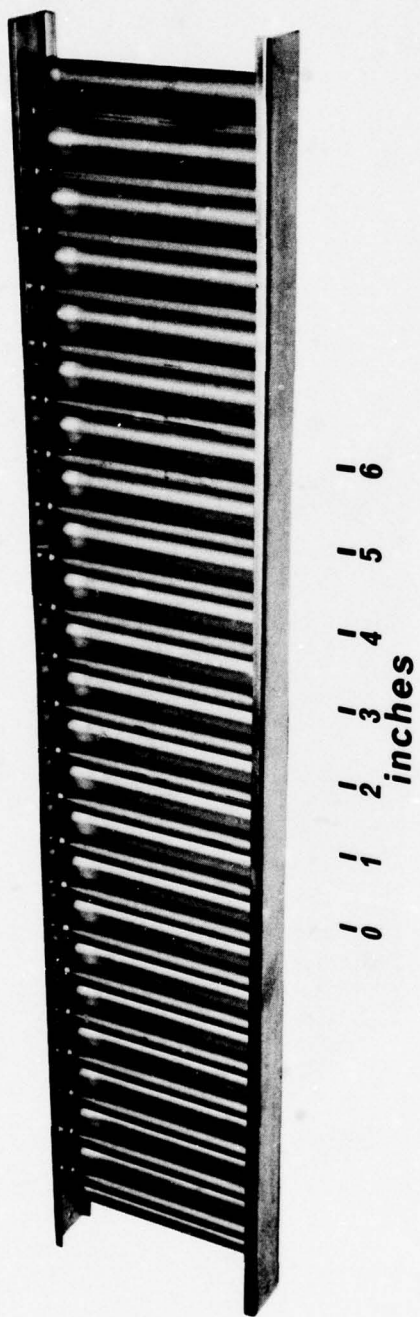


Fig.3. Superplastically Formed Titanium Alloy Passenger Cabin Floor Beam

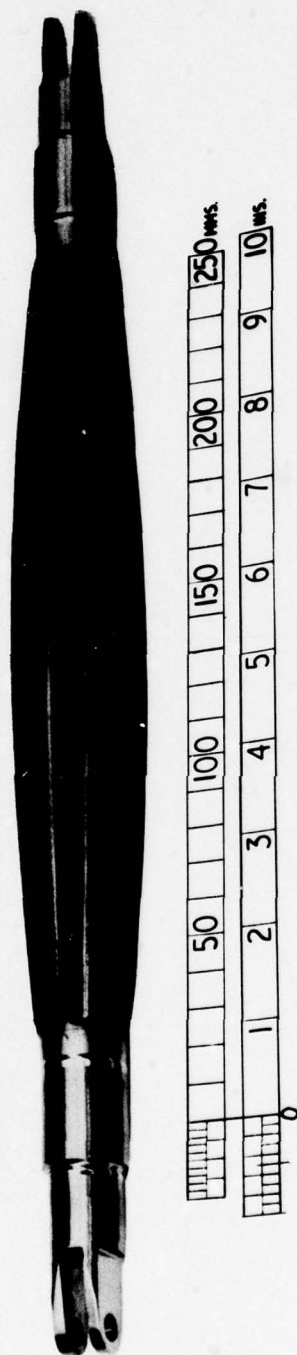


Fig. 4. Welded and Superplastically Formed Passenger Cabin Floor Support Strut

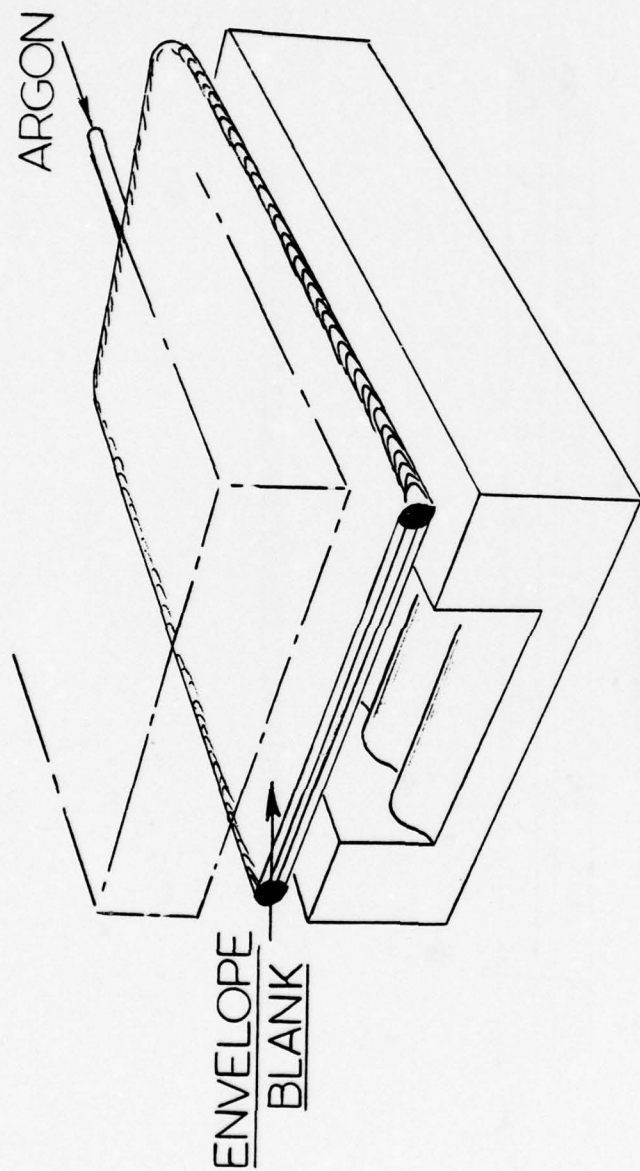


Fig.5. Basic Tool Concept for Superplastic Forming of Titanium Alloy Components

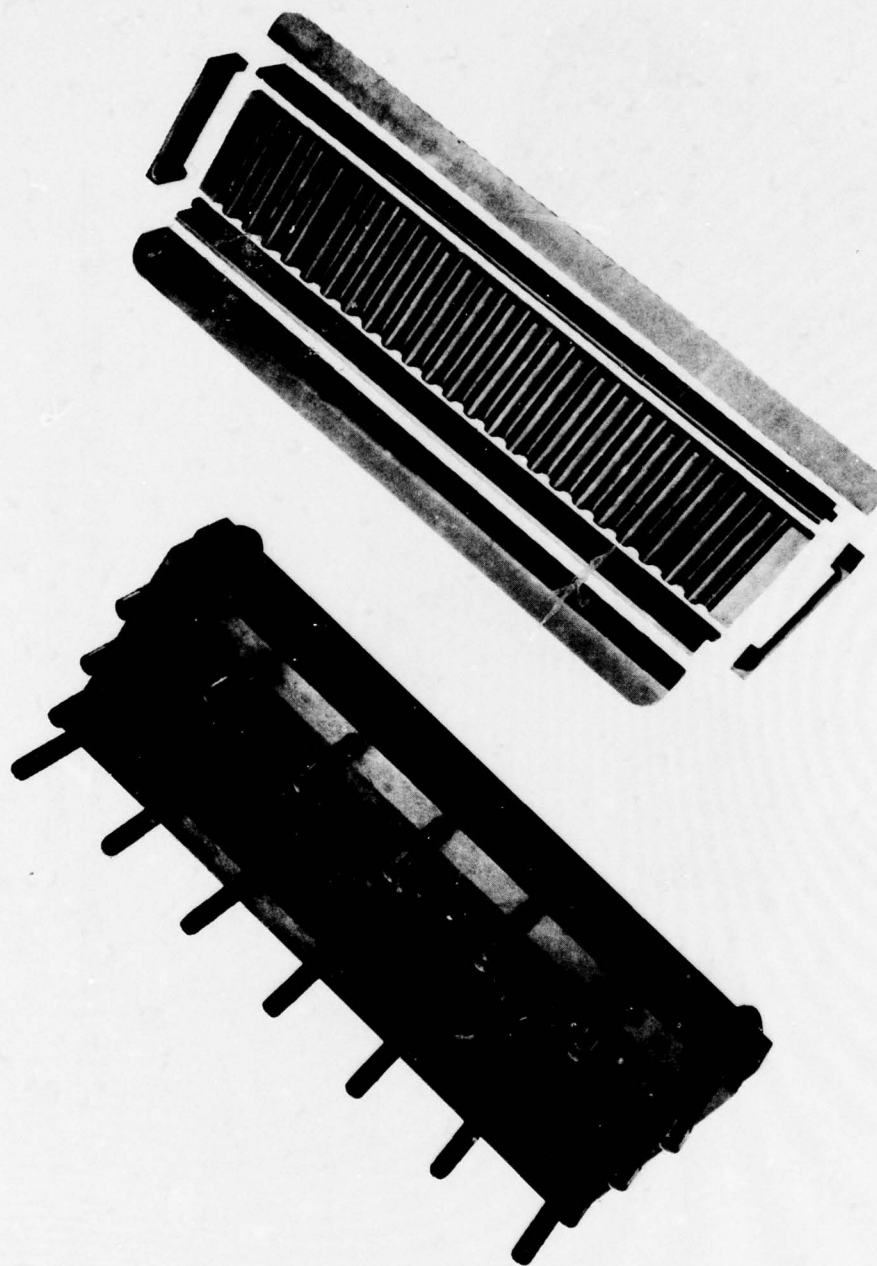


Fig.6. Tooling for Superplastically Formed Floor Beam Component

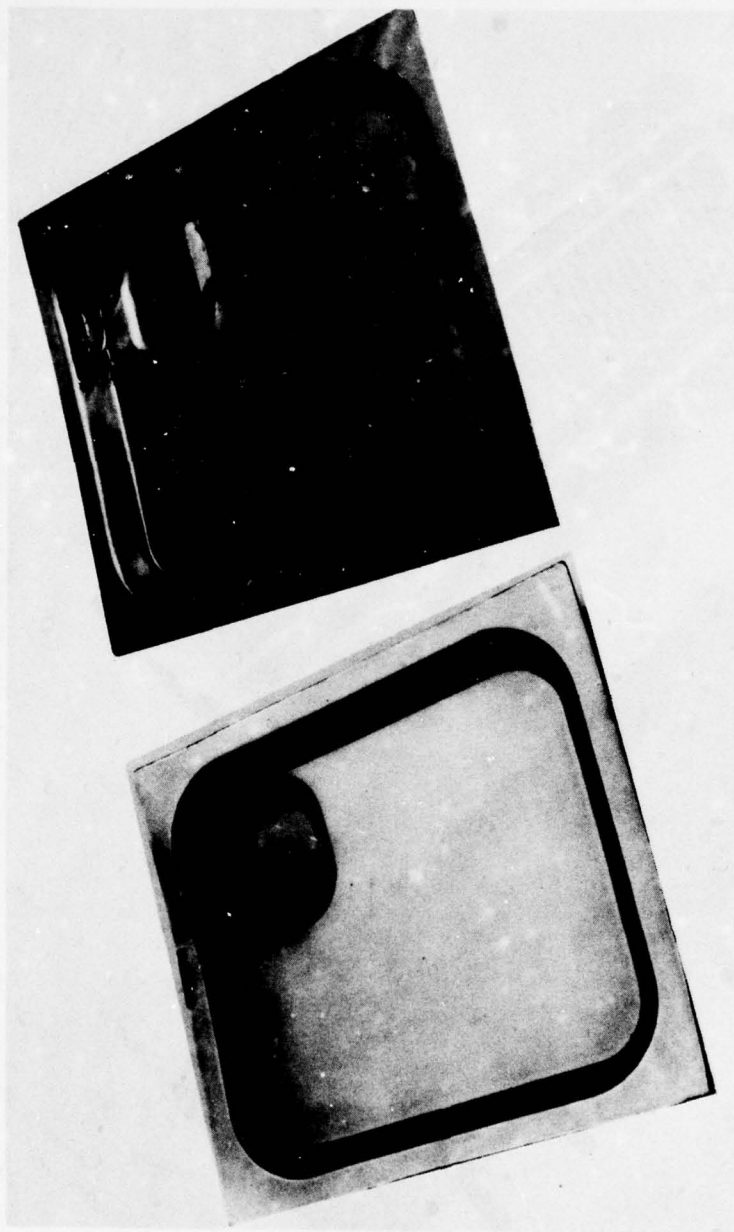


Fig.7. "Concorde" Rear Engine Bay Door Superplastically Formed Titanium Dish
Compared with Hot Pressed and Welded Version

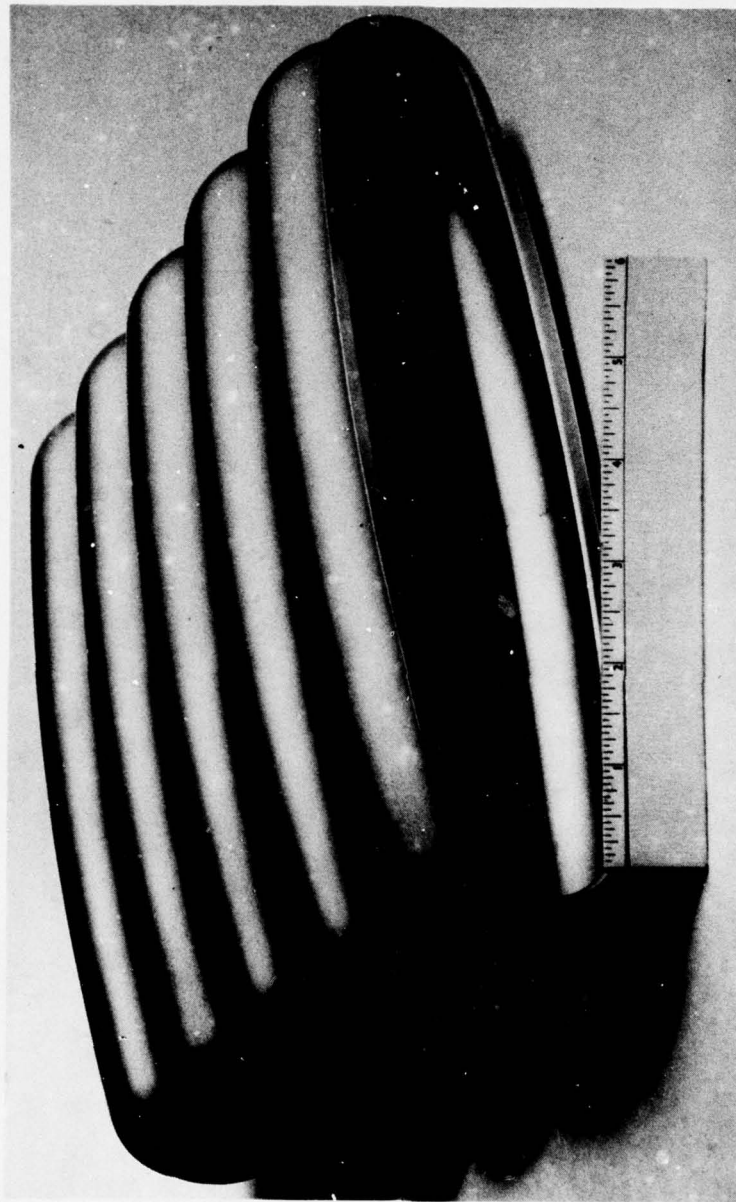


Fig.8. Superplastically Formed Titanium Vacuum Chamber Produced for C.E.R.N. Geneva

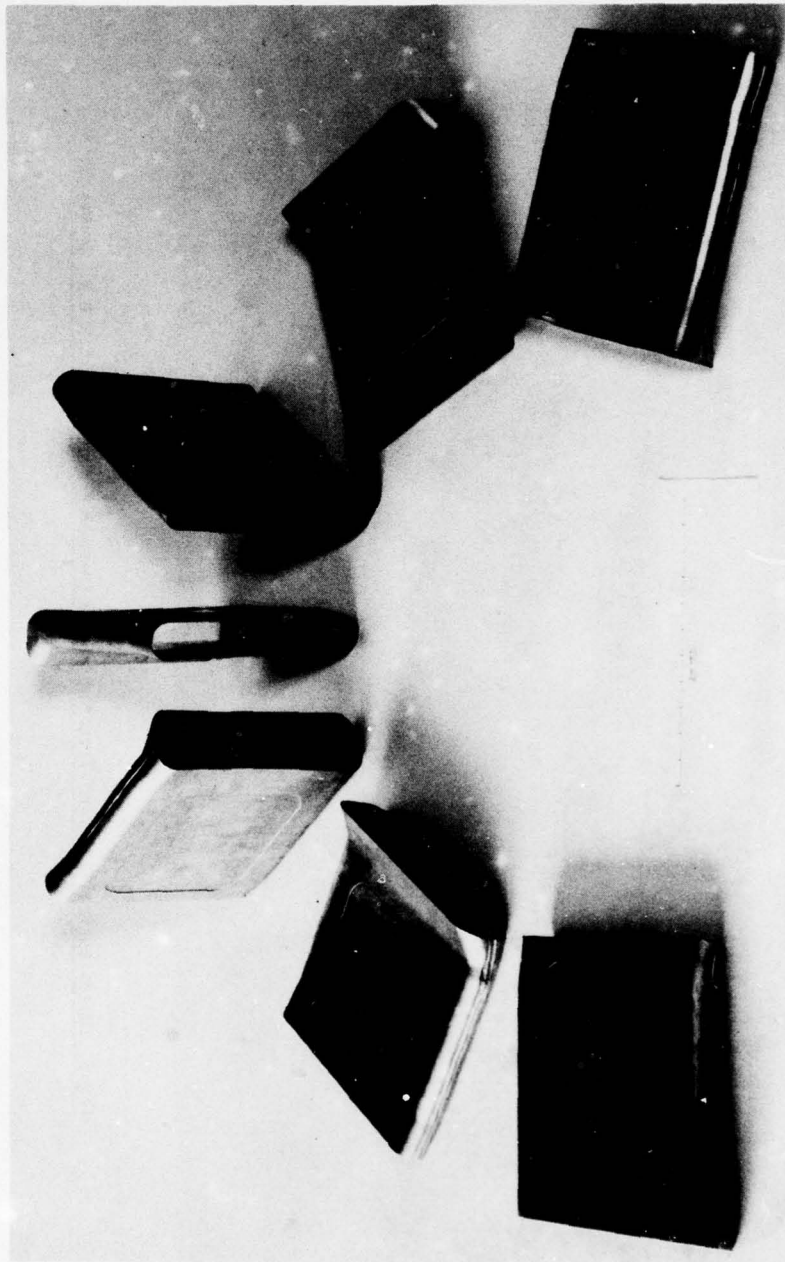


Fig.9. Superplastic Titanium Alloy Development Hot Air Ducts
for Aircraft Systems

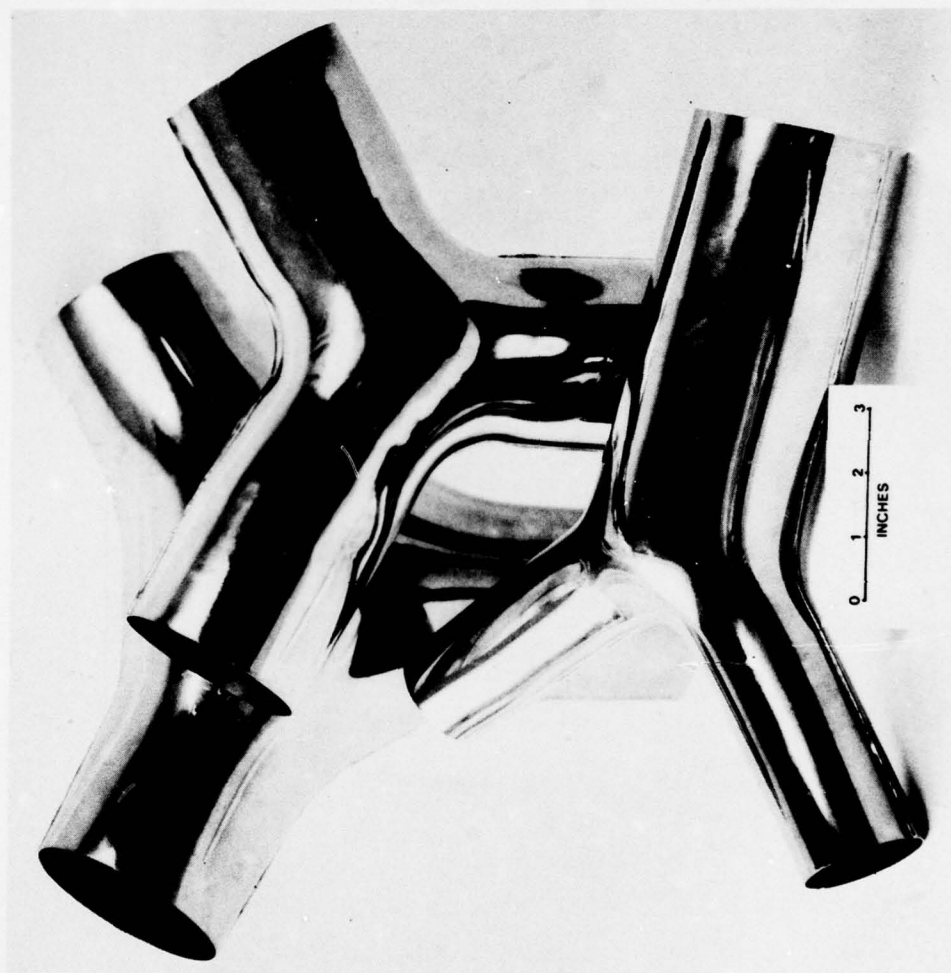


Fig.10. Two-Way Titanium Ducts Produced By Superplastic Forming Without Tools

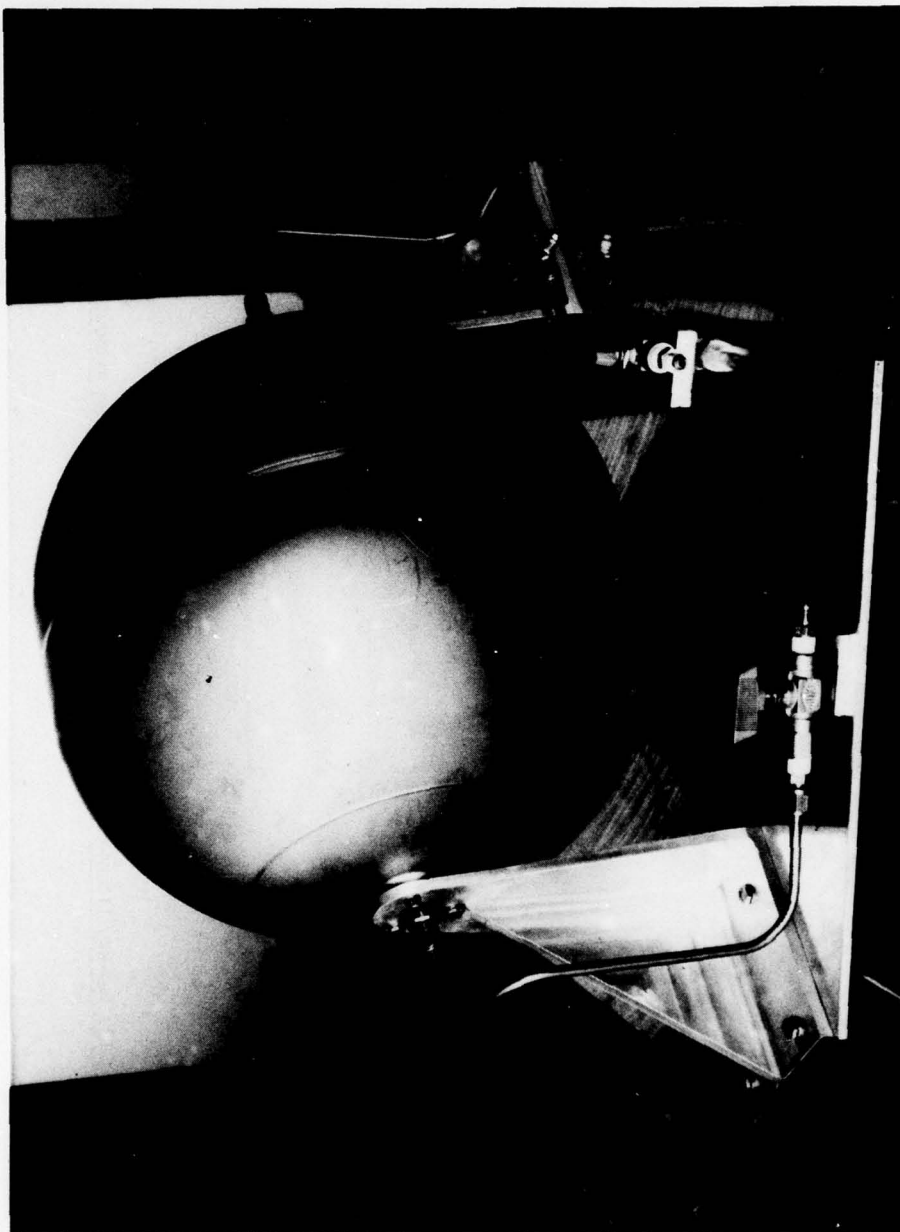


Fig.11. Positive Expulsion Propellant Space Tank Produced
by Superplastic Forming from Flat Sheet

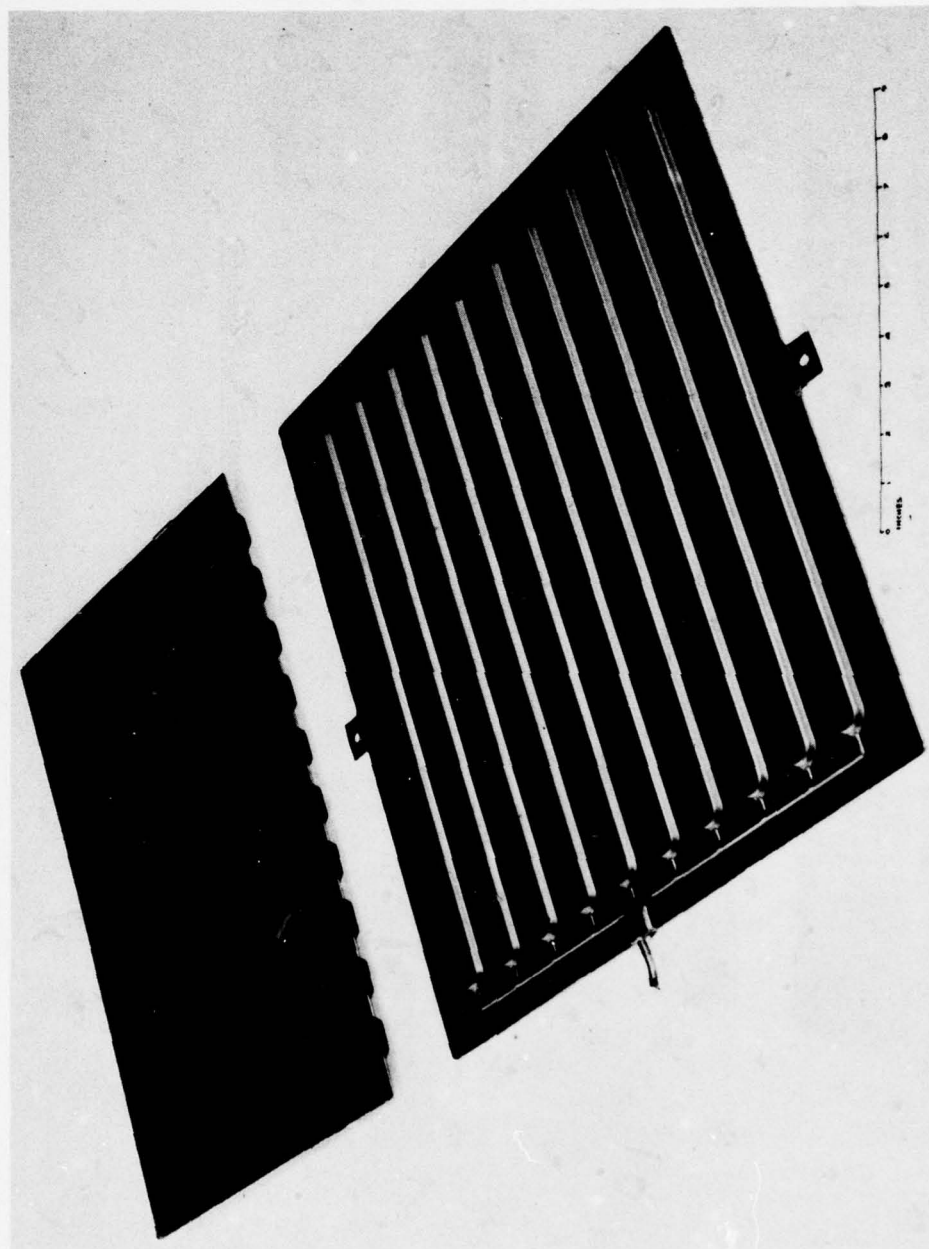


Fig.12. Experimental "Concorde" Panel Superplastically Formed and Diffusion Bonded
in Titanium Alloy

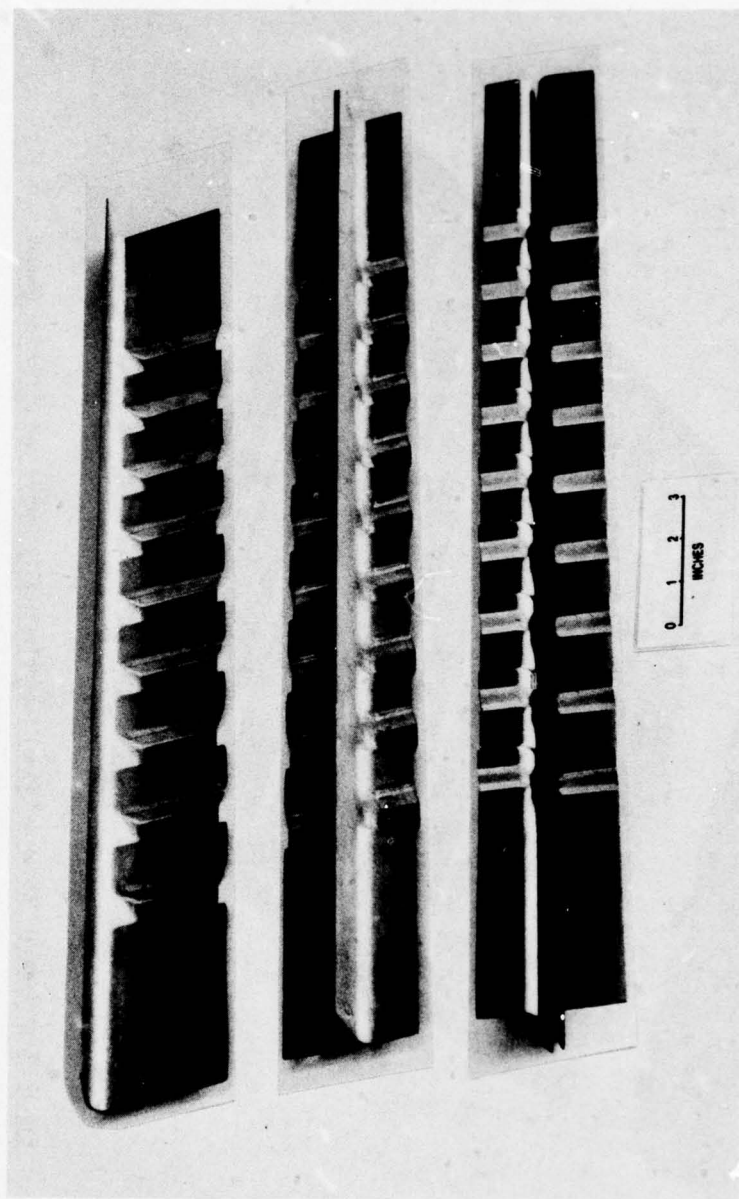


Fig.13. Superplastic Titanium Alloy Corrugated Sub-Frames for
Experimental "Concorde" Panel

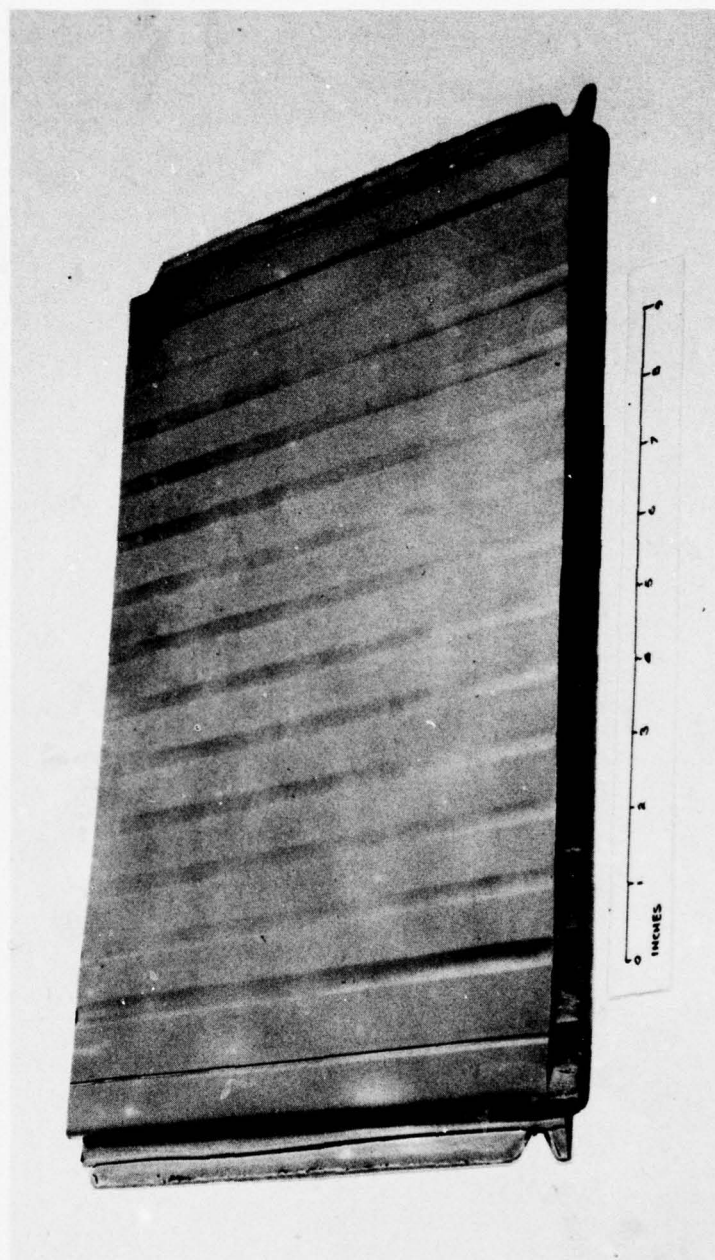


Fig.14. Superplastic/Diffusion Bonded Truss Core
Panel in Titanium Alloy

PRODUCTION OF HIGH PURITY METAL POWDERS BY ELECTRON BEAM TECHNIQUES

by
H. Stephan
H. Schmitt
R. Ruthardt
Leybold-Heraeus GMBH
6450 Hanau/Main

SUMMARY

The paper will report about the progress which has been made during the period of the development and improvement of the EBRD process and equipment. Special attention will be paid to the demands of quality and productivity, the problems which should be and have been solved. Furthermore it should be discussed where the limits of process and equipment will be and which futural aspects command us to go still ahead to meet our goal.

INTRODUCTION

The necessity and the economical advantages of the powder metallurgy for the manufacturing of aircraft and jetengine parts has been proven and has been demonstrated in several investigations, conferences and publications. There are also enough summaries of commercially used powder manufacturing and densification processes. If we concentrate on processes for production of spherical titanium and nickelbase-super-alloys powders, applicable for the net shape HIP - process, then we can say that for titanium the REP process is applied (5) and for the nickel-alloys mainly the vacuum-argon gas atomizing and the vacuum atomizing process are used for industrial production. It must be mentioned that new processes have been developed and are in certain stages of development now.

1. PRODUCT QUALITY

The table in fig. 1 shows the essential advantages and disadvantages regarding the product quality such that a comparison with the EBRD Process developed from Leybold-Heraeus, at the moment sponsored by the AFMRL, can be made. The scope of the Electron Beam Rotating Disc atomizing process is to produce a metalpowder of highest possible purity, applying low cost material with a minimum of running costs and a maximum of material utilization.

Commercial used processes				Laborat. scale and R+D proc.		
Process	Argon atomizing AA	Vacuum atomizing VA	Rotating electrode pr. REP	Centrifug. shot casting CSC	Pulverisat. sous vide PSV	EB rotating disc EBRD
Heat source	Induct.+ ceram. cruc.	Induct.+ ceram. cruc.	Non cons. arc	Consum. arc	Electron beam	Electron beam
Atomizing system	Nozzle + argon beam	Therm. expansion	Rotating consumable electrode	Rotating crucible	Rotating ingot	Rotating disc
Enviroment	Argon	Vac.+A+H ₂	Vac.+A+He	Vac.+A+He	Vac. 0.1mic.	Vac. 0.1mic.
Atom. metals	Ni	Ni	Ni Ti	Ni Ti	Ni Ti	Ni Ti
Contaminations	Heat source	Ceramics of melt. cruc.	Tungsten of diss. elect.	No	No	No
	Atomizing system	Ceramics of nozzle O ₂ and A in small + large partic.	No	No	Carbon fr. bouncing sheet coat.	No
	Enviroment	O ₂ from wall degas.	No	No	No	No

Fig. 1 Comparison of Ti and Ni alloy spherical powder production processes for manufacturing of net-shape HIP-parts and their contaminations in the powder. The RSR process was not considered, since net-shape HIPing of that powder, maintaining its small crystalline grain size seems not reliable (see paper of A.R. Cox, J.B. Moore and E.C. van Reuth, Rapidly Solidified Powders, their Production, Properties and Potential Applications, in this book).

The essential facts regarding product quality are:

- a) No pick up of contamination by the material because of
 - the electron beam and its gun
 - the watercooled rotating copper crucible applied for atomizing the metal and
 - the vacuum of less than 0.3 micron in the environment of the melting and the atomizing process.
- b) Negligible contamination pick-up by degassing of the chamberwalls and by reflection from the deflection sheets.
- c) No hollow vacuum or gasfilled spherical particles which are smaller than 800 microns.

As all the other atomizing methods the EBRD Process at the moment has two disadvantages:

- a) Contaminations in the starting material will be transferred to the powder, without any remarkable reduction in size and amount
- b) Contamination of the powder by foreign particles, e.g. small cotton fibres from tank cleaning agents, peeled off condensed material from the tankwall or the reflection sheets, dirt and dust particles from the environment of the atomizing unit, which enter the atomizing chamber during loading of melting material and cleaning of the tank. This may effect the powder quality especially in the development phase, when very often small quantities of powder will be produced, separately.

But due to the fact that the EBRD offers the possibility to run a production unit for several days, contamination by foreign particles can be reduced and will then be of minor importance in production scale.

The most decisive advantage of the EBRD process is the possibility to produce spherical powder, which can directly be fed hot in a HIP-canning, which can be closed vacuum tight, ready for HIP-ing. The requirements are only that the atomizing tank must be right in shape and size and the atomizing conditions must be in the well tuned relations. The direct way from the clean melting ingot to the high quality net shape HIP part can be achieved. The produced powder must not be screened and exposed to atmosphere or inertgas where chances exist to contaminate the powder. Also the sensitive degassing process can be avoided.

Related to the quality the possibility is given to manufacture spherical powder of a narrow diameter range, if the diameter of the round tank is large enough to avoid a secondary atomizing at the deflection sheets and therefore creation of small spherical particles and flakes can be avoided.

The diameter of the atomizing crucible, its rotating speed, density, surface-tension of the metal to be atomized are decisive for the diameter of the particles. Crucible diameter, its rotating speed, distance between the crucible and the deflection sheets, the heat of fusion and the melting point are decisive for the amount of spherical and splashed material in the powder.

1.2 Productivity

The table in fig. 2 a shows the essential process and production data of comparable powder manufacturing processes.

1.21 Starting material

Regarding the useable material, the EBRD process requires clean, homogenous and straight castings or melting ingots or scrap compacts of reasonable strength. Ti-electrodes should be at least single melted VAR ingots or nonconsumable arc ingots with a clean surface. Ni-base alloys can be VIM cast ingots or bar sticks. At the moment electrodes of 80 - 150 mm diameter and 750 mm length can be applied in the existing machine.

Comparison of Ti and Ni Powder Production Processes and Their Process and Production Data

Process		Commercial used processes			Pilot and R+D processes		
		A-Atomiz.	Vac. Atomiz.	Rot. electr.	Cent. Sh. Cast.	Pulv. s. vide	EBRD
Load. material		Cast. ingot	Cast. ingot	Forged bar bar stick	Forged bar bar stick	Forged bar bar stick	Casting or scrap compact
		Now	Now	Now	Fut.	Now	Fut.
Diameter	mm	430	280	89 63,5	75	50	150 250
Length	mm	1000	400	254 1500	1000	200	750 4500
Ni-Weight	kg	1000	180	11 33,2	30	2,7	93 1600
Surface treatm.		sand blast	sand blast	grinded	sand blast	grinded	sand blast
Melting time	min	30-40	~20	3-4 ~12	20	4	180 480
Atomiz. time	min	15	2				
Down time between loads	min	15	~60	60 20	80	~2	120 30
Length of prod. h campaign		~24	~24	(96?) (96?)	(96?)	~20	96? 200?
Limits for prod. campaign		Replacement of melt cruc. funnel, nozzle	Replacement of melt cruc. atom. cruc. tube	General maintain.	General maintain.	Replacement of coating at bound. sheets	Tank wall cleaning from con- densed material

Fig. 2 a Comparison of Ti and Ni powder manufacturing processes and their process and production data. For the centrifugal atomizing processes data are given for the existing pilot production units and as far as published the data of new developments, enlarged or planned production units.

The surface must be clean and the cross section area be round or multi-edged, e.g. six or eight. The demands are similar as for the argon atomizing processes and much less as for the REP or the PSV process, which reduces the cost for the starting material.

1.22 Process- and production speed

Compared to the existing atomizing processes the atomizing speed in the EBRD Process is lower. But due to the fact, that atomizing is possible with large electrode quantities and nearly continuously possible over several days or weeks the production speed of the EBRD process is comparable with the argon-atomisation process and much higher than the PSV, REP or CSC process.

1.23 Length of a production period

What are or may be the reasons to interrupt a production campaign? Assuming the reliability of the atomizing furnace is of the normal standard, the facts which will limit the production period are peeling off of tank wall coating, composed of condensed material, evaporated from the melting electrode, the crucible and the atomized metal beam and from spraying material from the bouncing plates and the interaction of the liquid and partial solidified metal particles. Up to now we have no experience about the amount of peeled off tank wall material which can be tolerated in the powder and how long we can atomize before cleaning of the tank walls should be necessary. It is evident, that cleaning of the tank walls is absolutely necessary when the alloys to be atomized have to be changed.

1.24 Material - utilisation

The table in fig. 2 b shows the material balance of the comparable processes. From the theoretical point of view the EBRD process carried out in a large enough tank should allow to gain 95 % of spherical material, but a certain amount of material agglomerated to clusters must be considered, therefore, only the 87 % value is written. The expectable 62 % value for the existing pilot unit may be a bit optimistic and should be a challenge. In spite of this low rate of material efficiency, separation of the nonspherical material within the hot metal powder should, if really necessary, be possible inside of the tank, with a minimum of equipment.

Process	Argon	Vacuum	Rotating		Centrif.	Pulveris.	EB rotating	
	Atomiz.	Atomiz.	Electrode Proc.	Short bar	Long bar	Shot Cast	Sous vide	Disc. Process
Atomized metal	Ni-Sup.	Ni-Sup.	Ti6Al4V	Ti6Al4V	Ti6Al4V	Ti6Al4V	Ti6Al4V	Ti6Al4V
Spherical powder	> 97%		> 92%	> 85%	~ 31%	~ 78%	50-60%	70-85%
O ₂ > 100 ppm for Ni-super	~ 10%		< 0.5%	< 1%				
A > 5 ppm alloys	~ 15%		< 0.5%	< 1%				
Nonspherical powder								
(flakes and clusters)	< 2%		< 2%	< 2%	~ 33%	7%	28-38%	5-20%
Evaporation	< 0.1%		< 0.1%	< 0.1%	< 0.1%		~ 5%	~ 5%
Wallspray	< 1%		< 1%	< 1%	< 1%	~ 6%	~ 1%	~ 1%
Fringe			0	0	31%	0%	~ 1%	~ 1%
Stub			75%	~ 10%	5%	9%	~ 1%	~ 1%
Qualified powder	~ 69%		~ 92%	~ 85%	~ 31%	~ 78%	50-60%	70-85%
(flow rate > 0, tap density > 60%)								

Fig. 2 b Material balance of the comparable atomisation processes

1.25 Investment and running costs

Comparison of the investment and running cost can be only of theoretical nature and could be based on a Ni-base-super-alloy production of approx. 6000 t powder applicable for production of net shape HIP-PM-parts.

It is evident that the EBRD furnace is more expensive as an argon atomizing tower. But when considering all the additional costs for the powder screening and cleaning equipment, the consumption of argon, crucibles, nozzles e.g. and the costs for recycling of the unqualified powder with a too high oxygen or argon content then the costs are equal.

2. THE INDIVIDUAL PHASES OF THE PROCESS

Basically the EBRD Process, shown in Fig. 3 is as each other atomizing process a three step process: Melting - Atomizing - Solidification with the following cooling down and collecting into a container.

For better understanding of the process we must look at the details.

- Heating of the electrode tip to a temperature required during drip - melting.
- Drip melting and shaping of the electrode to a pensil-tip such that all melted material can drip into a small crucible even if the electrode diameter is some inches larger than the crucible diameter.
- Splitting of the electrode droplet at the bottom of the crucible such that a thin liquid metal film will be created at the inner walls of the crucible.
- Transportation of the slowly and controllable growing film within the crucible to the crucible rim. Adequate e.b. bombardment is necessary to control this process.
- Atomisation of the liquid metal film at the crucible rim, controlled by the location, size and power density of the beam spot at the crucible edge.

The size of the particle produced there is given by the formula:

$$d = \frac{33.1}{n} \sqrt{\frac{\gamma}{\rho \cdot D}}$$

d = particle diam (cm)
 n = disc rotation (rpm)
 γ = surface tension (dyn cm⁻¹)
 ρ = density (g.cm⁻³)
 D = disc diameter (cm)

Due to the different conditions in size, shape and power density at the electrode tip, crucible interior and crucible rim three guns of different power and design are installed, as shown in Fig. 4.

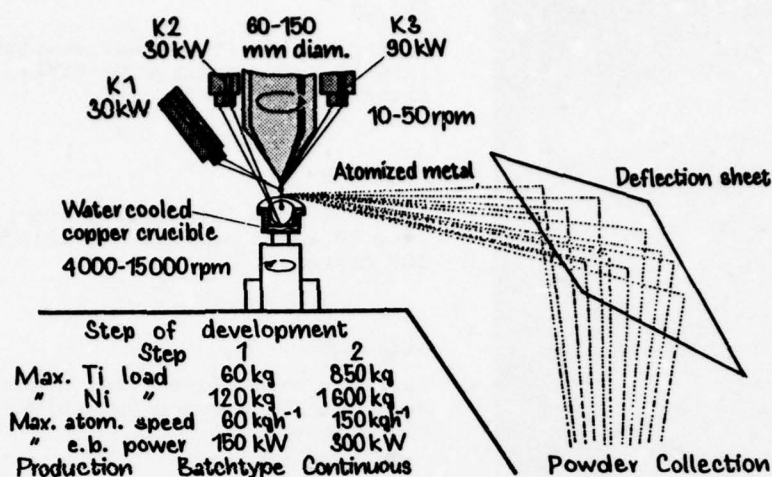


Fig. 3 The EBRD Process (schematic drawing)

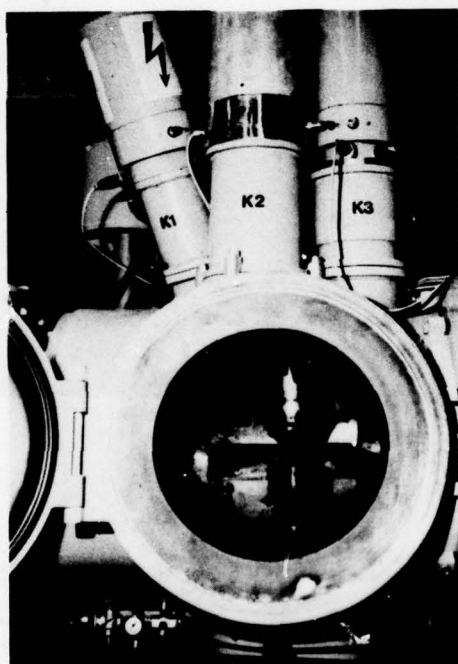


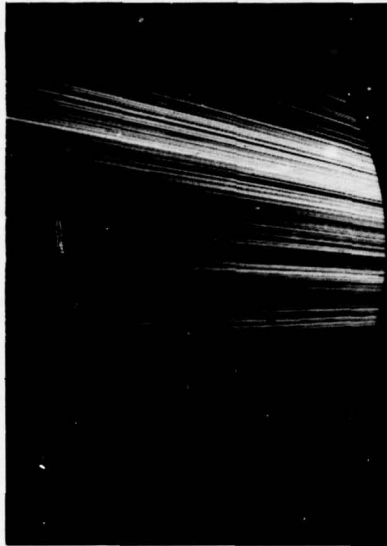
Fig. 4

Meltchamber and gun arrangement of the EBRD Powder Production Furnace ESPM 24/240.

Gun K 1 takes care for atomizing of the metal from the rotating crucible rim, Gun K 2 distributes the metal inside the crucible and helps to move it as a film to the crucible edge. Gun K 3 dripmelts the 150 mm diameter vertical fed electrode.

For a production unit the functions of gun 2 and 3 can be united, such that one gun will melt the electrode and heat the crucible by spreading the electron beam at two locations.

Controlled atomisation is the atomisation in mainly one single direction. A metal particle beam club of 60 - 80° in the width and approx. $\pm 5^\circ$ in the height leaves the crucible. The controlled EBRD atomisation Fig. 5, 6 a, 6 b, is thus a directional atomisation.

Fig. 5

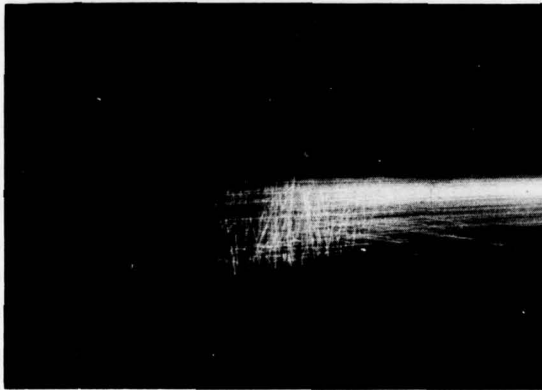
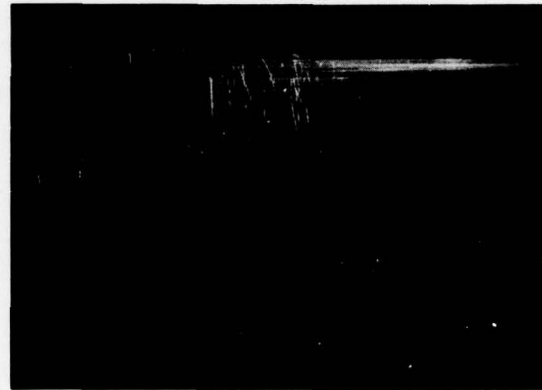
Particle beam (top view), atomizing rate 10 kg/h, average particle diameter 380 micron.

Fig. 6 a

Particle beam (side view) atomizing rate 10 kg/h, average particle diameter 380 micron.

Fig. 6 b

Particle beam (side view) atomizing rate 3 kg/h, average particle diameter 450 micron.

Fig. 6 aFig. 6 b

All around atomizing takes place:

- when the electrode droplet can not be distributed to a film in the crucible and
- when the drip melting speed is higher than the controlled atomizing speed.

On the way from the crucible to the deflection sheets solidification of the metal droplets starts. Flighttime, heat of solidification, melting point and radiation emissivity are decisive for the degree of solidification. Thus strength of the metal skin of the droplet, speed of the droplet at the deflection sheet and the angle of the sheet to the direction of the flying droplet are influencing kind and amount of the secondary atomisation. Flakes and small size spherical particles in the powder show whether secondary atomisation has taken place or not. The bouncing conditions at the water cooled copper reflection sheet are decisive also for the size and shape of the flake material.

Condensed and sprayed material at the copper-wall will in some cases be absorbed from the partially liquid metal droplets or will be loosened or be peeled off by the metal particles.

After reflection the powder cools down to less than 500° C and will therefore not bake together.

3. RESULTS GAINED

3.1 Quality

The main point of interest in our investigations was to maintain the high quality of the material (Ti6Al4V), avoiding the pick up of any contamination and the separation of the oversized particles which influence the flow-rate and the tap density.

3.1.1 Chemical composition

From e.b. melting of Ti6Al4V we know that intolerable aluminium losses can not be avoided when the melting rate is not larger than 60 kg/h. Therefore we have with respect to aluminium concentration specially evaluated 25 out of 100 atomisation tests covering the range of atomisation rate from 3 kg/h to 50 kg/h. The result is given in fig. 7 a.

Melting rate kg·h ⁻¹		Al %	V %	C ppm	O ₂ ppm	N ₂ ppm	H ₂ ppm	Fe %	Cu %
3,6	Elect.	6.15	4.10	95	1520	60	75	0.20	0.002
	Powd.	6.06	4.01	95	1350	40	5	0.19	0.002
4.3	E	6.30	4.05	95	1730	70	35	0.25	0.003
	P	6.03	4.06	95	1330	45	7	0.21	0.003
4.8	E	6.25	4.10	95	1680	70	90	0.20	0.002
	P	6.00	4.01	95	1300	50	6	0.165	0.002
9.6	E	6.15	4.05	95	1750	-	40	0.18	0.002
	P	6.04	4.06	95	1400	-	7	0.14	0.002
15	E	6.15	4.05	96	1750	-	40	0.18	-
	P	6.12	4.06	95	1450	-	8	0.16	-
45	E	6.15	4.06	95	1750	-	40	0.18	-
	P	6.15	4.06	96	1400	-	6	0.14	-

Fig. 7 a Analytical values of EBRD atomized Ti6Al4V

At the low rate of 3 kg/h the reduction of Al is only from 6.25 to 6.05 %. At medium ranges of 15 kg/h aluminium losses are negligible and do not exist at higher rates. Oxygen, nitrogen and hydrogen contents are in the powder somewhat smaller than in the electrode, but this small reduction is for oxygen and nitrogen certainly not an effect of the e.b. melting process in high vacuum. The different analytical values are mainly due to contamination of the sample taken from the electrode, compared to the contamination free powder sample. Reduction of hydrogen has certainly taken place during the process, but not in that amount as it is shown by the analytical values.

The long flight-time of the liquid particle in high vacuum may create some inhomogeneities in the powder particle, e.g. a smaller Al content at the surface area than in the center. Measurements on particles of 100 and 400 microns diameter, produced in a tank modification where the whole possible flying-way was utilized has shown the micro-analysis evaluation given in fig. 7 b. The analogous values of particles, produced in a modified tank are given in fig. 7 c.

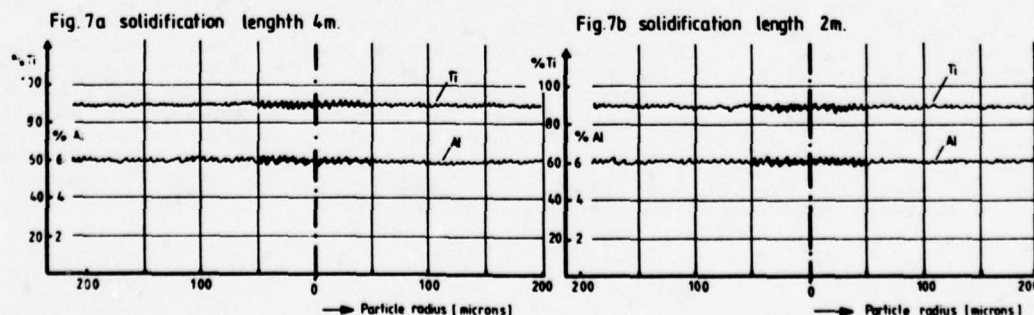


Fig. 7 a/b Al and Ti content of single untreated spherical particles of 100 and 400 micron diameter after 2 and 4 m solidification length

3.12 Metallic impurities and contamination

They have been checked very carefully. The first powder quantities, produced in the new furnace, had contained some magnetical particles. They mainly were smaller than 40 microns, black and of the flake shape. Some small titanium balls (<40 micron) have had very small magnetic properties. Careful screening of the air used for venting the tank and keeping the tank closed have reduced the amount of magnetical particles but not avoided. Splitting up the process in a pre-run, main-run and run after, and collecting the powder in different cans has shown that only the powder of the pre-run did contain magnetical particles. Conclusion:

Iron containing dust from the furnace environment enters the tank and causes contamination problems.

Analyses of the powder for copper, iron and silicon shows only slight changes within the range of accuracy of the analysis. So the increase of copper by water cooled copper crucible and the water cooled reflection sheets can be neglected and must not be considered in the future.

The critical point "Crosscontamination" could not be investigated since only Ti6Al4V was atomized up to now.

Contamination of the powder by tank cleansing agents or dust will certainly exist, the investigations in this regard are not completed.

3.13 Particle size and distribution

Applying certain process parameter, especially small crucible diameter and low rotating speeds, the existing atomizing furnace allows production of spherical powder without secondary atomization at the reflection sheets. In a small range of process parameters it could be confirmed, that manufactured Ti-particles between 300 and 600 micron diameter follow the given rules. When manufacturing smaller particles with larger crucibles and larger rotating speeds secondary atomization at the bouncing sheets can not be avoided. The particle size distribution is given in fig. 8.

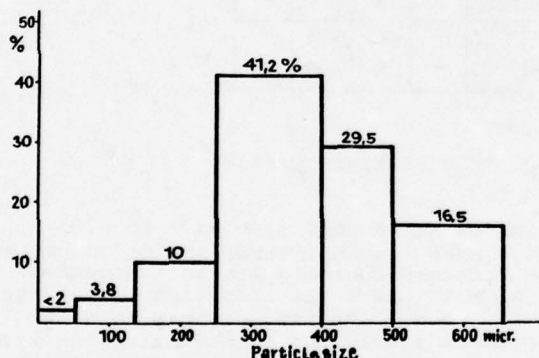


Fig. 8

Particle size distribution of Ti6Al4V powder atomized with a disc rotating speed of 3800 rpm.

3.2 Productivity

Unfortunately the existing tank, shown in fig. 10 a and 10 b is not large enough for the production of 100 % spherical Ti-alloy powder. The reason is the high solidification heat of 120 cal g^{-1} instead of 100 cal g^{-1} . The powder produced in the existing unit consists of 15 - 30 % flake powder, mainly spearhead shaped and the rest of mainly single spherical powder. The mixture of the powder, as produced, can be cold densified with a pressure of 8 t/cm^2 . The achieved density is 63 % and the strength 15 kg/cm^2 . Under the existing circumstances it could be shown that atomisation into a sector is possible. See fig. 9. Under optimum conditions of crucible and electrode diameter and crucible rotation and beam power distribution at the electrode tip, as well as crucible wall and rim 75 percent of the melted material could be specified as qualified since its tap density was larger than 60 %. The rest of the material was flake material and was sprayed off material at the chamber walls. Another test has shown that more than 80 % of the melted material could be collected in the can of the sector tank. The rest was sprayed off material at the tank walls, caused by uncontrolled all around atomization.

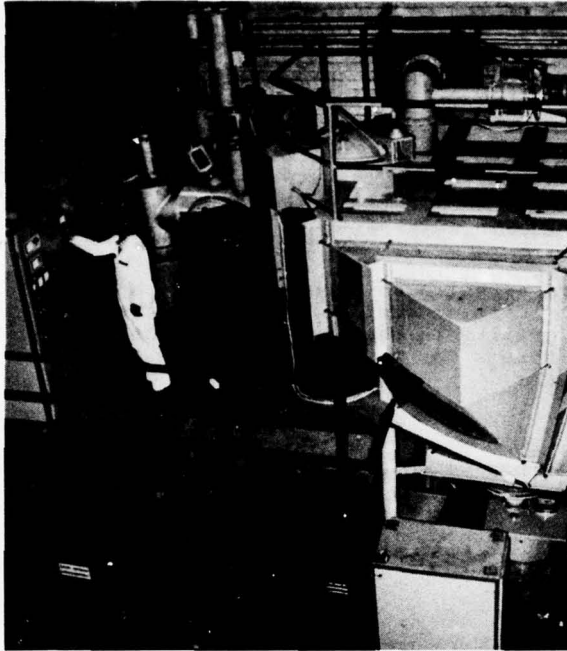


Fig. 10 a

EBRD-Atomizing Furnace ESPM 24/150 for pilot production of flaked and spherical Ti and Ni-alloy-powder.

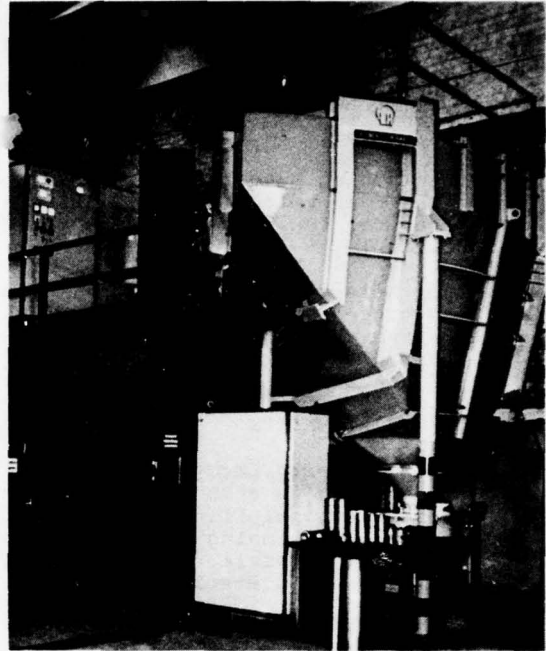


Fig. 10 b

ESPM 24/150 with 150 kW installed e.b. power and 24.000 ls⁻¹ pumping capacity.

Electr. diam.	Rotat. speed	Melt. speed	Melt. power	Vac. press.	Relation Flake/Spheric.	Perc. powd. sector	Spherical Powder Density		Max. diam. part.
mm	rpm	kg·h ⁻¹	kW	mbar		%	Apar %	Jap. %	wicron
80	3900	4.3	67.5	2·10 ⁻⁴	15/85	29.1	50	57	710
80	3900	4.8	67.5	2·10 ⁻⁴	30/70	22.8	52	58	710
80	3000	11.0	95.0	2·10 ⁻⁴	75/25	67.3	55	60	600
80	3500	16.4	88.7	2·10 ⁻⁴	50/50	39	55	60	710
80	3200	45.2	88.7	2·10 ⁻⁴	94/6	54	55	60	500
90	4000	16	53.5	2·10 ⁻⁴	47/53	44.5	55	60	600
100	5400	25	75.0	2·10 ⁻⁴	45/55	40	55	60	600
100	8000	47.7	102.5	2·10 ⁻⁴	42/58	26	-	-	-
120	4000	24	86.7	2·10 ⁻⁴	35/65	28	-	-	-
150	4500	15.1	76.5	2·10 ⁻⁴	40/65	25	-	-	-

Fig. 9 Process and production values for pilot production of Ti6Al4V-powder.

Even if we have seen that the tank is too small for production of 100 % spherical titanium powder we have developed some means and improved some e.b. parameters, that the amount of splashed material could be reduced to such a small amount that flake material could be separated in the vacuum tank and nearly 100 % spherical powder with a tap density of approx. 60 % could be gained. After further improvements of the atomizing process data and the cooling system, we believe that with the existing unit titanium powder production with an atomizing speed of 30 - 45 kg/h, using an electrode of 100 - 125 mm diameter with a material utilization of 50 - 60 % should be feasible.

To improve the material efficiency some tests have been made to recycle the splashed powder and the material splashed to the tank walls of the melting chamber. This material was compacted to an electrode, drip-melted and atomized.

The processes have been running as when using cast electrodes. The oxygen - content of the compacts and the produced powder is approx. 300 ppm. larger than the O_2 content of the powder produced from virgin electrodes.

There is no doubt, that atomizing in vacuum has the problem of solidifying the particles. Only radiation serves for heatlosses. If in case of titanium the heat of solidification is high (120 cal g^{-1}) large flighing times are necessary. Much easier is EBRD atomisation of zirconium, hafnium, niobium, molybdenum, tantalum and tungsten, where heat of solidification is between 30 and 70 cal g^{-1} . As the energy losses by radiation at higher temperatures are by some factors higher for the high melting point metals much shorter tank dimensions are applicable.

Nevertheless atomisation of titanium and nickel-base-super-alloys with the EBRD process can be achieved and will be more economical than with other existing processes, when a high powder quality is required and the annual amount of powder will be more than 100 tonnes for Ti-powder and more than 2000 tonnes for Ni-base-super-alloy powder.

4. FUTURE ASPECTS

If we look for further aspects in the future we should look at fig. 11. This process, a combination between continuous flow melting and EBRD process, offers the possibility of refining the Ni-base-super-alloy from ceramic imourities, swimming on the pool surface of the melting trough and be removed from a barrier. It offers also evaporating of toxic trace elements and reduction of interstitials.

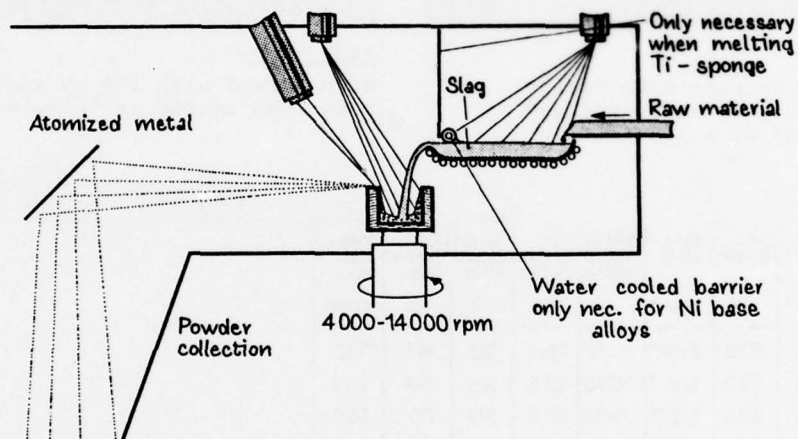


Fig. 11 Advanced powder production starting from heavily contaminated raw material

When applying this combined technology, mixtures of titanium sponge, master alloy and clean scrap can be fed and Ti-powder be produced in an one chamber furnace. Provisions must only be made to keep the magnesium and chlorine of the sponge away from the solidifying powder. These future auspices favour the EBRD process as powder production process of the future and therefore it is worthwhile evaluating further equipment past and process parameters.

REFERENCES:

1. G.P. Peterson - Trends in the application of advanced powder metallurgy in the aerospace industry - AGARD CP 200
2. D.J. Hodkin, P.W. Sutcliffe, P.G. Mardon, L.E. Russell - Centrifugal shot casting: A new atomization process for the preparation of high-purity alloy powders. Powder Metallurgy, 1973, Vol.16, No. 32
3. P. W. Sutcliffe and P. Morton - Titanium powder production by the harwell centrifugal shot casting process - AGARD C.P. 200 SC 3
4. J. M. Wenzell - Metal powder production by vacuum atomization. J.Vac. Sci. Technol. Vol. 11, 1974
5. G. Friedman - Production of titanium powder by the rotating electrode process - AGARD CP SC 1
6. J. Decours, J. Devillard, G. Saintfort - Production de poudres d'alliages de titane par fusion - centrifugation sous-vide - AGARD CP 200 P 1
7. J. Devillard, Ch. Clozet - High purity powder elaboration by electron bombardement of an electrode - 2nd. International Colloquium electron beam welding and melting

HEAT TREATMENT OF P/M NICKEL-BASE SUPERALLOYS FOR TURBINE DISKS

by

P.L. Antona and A. Bennani
 FIAT-Centro Ricerche
 Strada Torino 50
 10043 Orbassano
 Italy

Abstract

Hot isostatic pressing of nickel-base superalloy powder is probably the most important phase in the manufacture of complex-shaped aircraft parts (e.g. turbine disks).

From the microstructure point of view, a preliminary evaluation can be made of as-hip materials produced according to a number of characteristic cycles.

Choice of the most appropriate HIP process to use would appear to depend, to some extent, on subsequent heat treatment which tends to heighten certain aspects of the metallographic structure, such as thermal induced porosity or even distribution of alloying elements and certain intermetallic phases insoluble in the matrix.

One of the main results of the work covered in this paper has been the confirmation of an important basic assumption: the microstructure of a superalloy produced from pre-alloyed powder using the HIP process is such that, besides making subsequent heat treatment much simpler, it also enables mechanical characteristics to be obtained which are comparable with superalloys produced using conventional technologies.

Introduction

Low-carbon Astroloy is a variation of standard Astroloy in which the carbon content is reduced from 0.16% to less than 0.05%.

The reason for this is to minimize the precipitation of stable carbides (e.g. TiC) on the surface of the powder grains during atomization of the powder in argon or molten alloy.

The presence of precipitated carbides hinders densification during the HIP process because of segregation at prior grain boundaries, thus preventing their diffusion.

If carried out under the right conditions, the HIP process provides the material with a more suitable starting structure for subsequent heat treatments.

In comparison with conventional systems, heat treatment of HIP processed parts is much less complex, especially as regards ageing. The homogeneous nature of the material is such that no special heat treatment is required for even distribution of the intermetallic phases (initial powder is prealloyed that is, each grain of powder has the average chemical composition of the alloy as a whole).

This assumption was born out by the final mechanical characteristics of the material.

1) Materials used

The raw material used is L.C. Astroloy powder: the chemical composition and grain distribution are shown in Table 1 and Fig. 1 respectively.

Before being pressed, the powder was put through the following heat treating process: 500°C for 24 h under vacuum at 10^{-3} atm. This process removed the atmospheric water absorbed on the surface of the powder during storage. Two types of HIP process are used to densify the powder:

- 1) Cycle A : T_{max} 1100°C
 P_{max} 1000°C atm
 Dwell time : 1 h
- 2) Cycle B : T_{max} 1200°C
 P_{max} 1000 atm
 Dwell time : 1 h

The superalloys compacted using these two cycles were identified with the letters A and B respectively (Figs. 2 and 3).

2) Microstructure of starting material

2a Residual porosity

To check that material were fully compacted, residual porosity was measured on both material types.

Keep in mind that the initial metal powder did not contain practically any porosity : this means that defects can be attributed entirely to the HIP process.

Table 2 shows the average volume percentage of residual porosity in the two types of Astroloy produced (A and B).

As far as hole size is concerned (these are taken to be spherical and expressed as the surface area in μm of the section), percentage distribution was found to differ according to the HIP cycle used (Figs. 4 and 5).

On both the as-hip superalloys, concentration and average porosity size were very low even though they differed slightly.

To clear up this point, research is currently being carried out into the effect of time and temperature on diffusion at the contact points of powder particles subjected to hot plastic distortion by outside isostatic pressure which may vary during the process.

2b Grain morphology - Intermetallic phases

The granulometry of Astroloy A is characteristic in that the powder grains are clearly visible containing part of the original dendrites and an incipient secondary austenitic structure not fully stabilized. The austenitic structure of Astroloy B, on the other hand, is already partially aged. There is absolutely no trace of dendrites whereas the stable precipitates - oxycarbonitrides and Ti nitrides - not yet diffused on the surface of the dust grains clearly "recall" the primary structure (Figs. 6 and 7).

Table 3 shows the hot static mechanical properties (650°C) of the two materials in the as-hip state without any further heat treatment. These tests show the importance of the primary grain edge, that is, that one coinciding with the spherical dust surface. Fig. 8 shows the microstructure of the fracture surface of Astroloy A. Large breakaways can be seen round the spherical surfaces together with ductile microzones where welding of the particles after the HIP process is better.

Material B, on the other hand, which has the best mechanical characteristics, shows that breakaway is of the intergranular type with ductile microzones (Fig. 9).

No secondary effects were observed produced by the "recollection" of the primary edge such as fractures inside the austenite grain. As-hip superalloys A and B also differ in shape, size and intermetallic phase γ' distribution. This is shown in Figs. 10 and 11 and Table 4.

Two conclusions can be drawn before subjecting these two materials to heat treatment:

1. It is important to overcome the primary structure. This can be done using a suitable HIP process or (as we shall see later on) appropriate heat treatment. As we already know, a number of important final mechanical characteristics depends on grain shape and size.
2. P/M superalloys show very even intermetallic phase distribution. This depends on the use of prealloyed powder in which the chemical composition of each grain is identical with the average composition of the alloy as a whole. The dimensions of phase γ' , however, are fairly high, enough to make plasticity of the hot material excessive.

The aim of heat treatment should be to reduce the average dimension of γ' (increasing the weight ratio of secondary smaller sized γ' phase) without affecting even distribution.

3) Heat treatments

Owing to the need of overcoming the primary structure of superalloy A, solution heat treatment was performed at 1200°C for more and more long times.

Figs. 12a-b-c show the austenitic substructure develops gradually, first eliminating residual dendrites to arrive (Fig. 12c) at an austenitic structure similar to that of Astroloy B (Fig. 7). In the primary structure however, remaining inside the austenite grain, porosity can be seen, particularly in certain triple points, which, by way of its origin, we shall refer to as "heat induced" and which is larger than the porosity detected in the as-hip material. As this jeopardises the quality of the material from the outset, Astroloy A was rejected and attention centered on Astroloy B which constitutes a far superior starting material.

According to ASTM standards, the average austenitic grain size of Astroloy B falls between 7-8 ASTM.

The target size is 4-5 ASTM. Two different heat treatment processes were used to reach this objective:

1. 1200°C for 4 h - salt quenched
2. 1200°C for 12 h - salt quenched

Grain growth was observed in both cases, particularly the second one where ~ 4 ASTM was reached. No no-

ticeable improvement was observed however (all other conditions remaining unchanged) in the creep resistance of the material.

Salt bath quenching was used to get a better check of cooling speed and enable repetition of heat treatment.

Only two ageing processes were adopted in view of the material's "good initial homogeneity".

1. 840°C for 24 h + 700°C for 100 h - A.C.
2. 840°C for 24 h + 750°C for 50 h - A.C.

The carbide stabilizing phase was ignored for two reasons: (i) - the material used was low-carbon content; (ii) - the small amount of carbide present at the outset (on the powder surface) was already present in its most stable chemical form (TiC).

The material thus treated was subjected to hot static testing (650°C), creep testing, in order to evaluate the time necessary to reach 0.2% elongation and the final average size of the austenite grain and γ' phase checked. The results are given in Table 5 which shows four types of P/M Astroloy - B1, B2, B3, B4 - subjected to different heat treating processes. The microstructures and fracture surfaces of the four materials subjected to hot static tensile testing are shown in Figs. 13 a-b, 14 a-b, 15 a-b and 16 a-b respectively. No signs of complete fragile fracture were found in any sample.

Conclusions

The HIP process gives to materials to be produced a top quality from every point of view. HIP processes are decisive starting points as regards nickel-base superalloys and subsequent heat treatment of the material. In particular, it was noted (and this bore out further studies) that the maximum HIP temperature must be way over the solution heat treatment temperature of phase γ' . Only in this way it is possible to overcome structural defects (e.g. thermal induced porosity) and obtain materials with optimum mechanical properties.

Heat treatments of these materials can be furtherly simplified. Metallographic structures and final mechanical properties are fully comparable with materials produced using conventional systems or heat treated using longer and much more complicated processes.

Table 1 - Chemical composition of L.C. Astroloy powder

	%
C	0.022
Cr	14.55
Co	17.50
Mo	5.00
Al	4.08
Ti	3.55
Mn	0.010
Fe	0.09
W	0.03
B	0.022
Cu	0.05
Si	0.019
Zr	0.002
P	0.004
S	0.005
N ₂	20 ppm
O ₂	20-50 ppm
Ni	bal.

	A - ASTROLOY (LOW - TEMPERATURE HIPPED)	B - ASTROLOY (HIGH - TEMPERATURE HIPPED)
VOLUME PERCENTAGE OF POROSITY	0.28	0.08

TABLE 2 - AVERAGE POROSITY IN P/M L.C. ASTROLOY
HIPPED BY TWO HIP - CYCLES

	UTS (N · mm ⁻²)	YS _{0.2} (N · mm ⁻²)	E _l (%)	R.A. (%)
A - ASTROLOY	510.9	492.5	n.d.	3.73
B - ASTROLOY	1105.5	684.3	30.7	33.3

TABLE 3 - MECHANICAL PROPERTIES (650°C) OF P/M
L.C. ASTROLOY AS - HIP IN TWO CONDITIONS:
LOW AND HIGH TEMPERATURE

	A - ASTROLOY (LOW - TEMPERATURE HIPPED)	B - ASTROLOY (HIGH - TEMPERATURE HIPPED)
WEIGH %	43.5	42.8
AVERAGE LINEAR SIZE OF Y'	0.2 ÷ 1.2	1.5
TOPOLOGICAL DISTRIBUTION	UNIFORM INSIDE PRIOR GRAINS	UNIFORM INSIDE AUSTENITIC GRAINS

TABLE 4 - AMOUNT, SIZE AND TOPOLOGICAL DISTRIBUTION
OF Y' - PHASE IN P/M ASTROLOY AS - HIP

		SOLUTION HEAT TREATMENTS			
		1200 °C x 4h - S.Q.		1200 °C x 12h - S.Q.	
AGEING HEAT TREATMENTS	840 °C x 24 h + 700 °C x 100 h A.C.	UTS (N · mm ⁻²)	1035.6	UTS (N · mm ⁻²)	1140.1
		YS _{0.2} (N · mm ⁻²)	828.5	YS _{0.2} (N · mm ⁻²)	1001.1
		El (%)	25	El (%)	19.5
		R.A. (%)	29	R.A. (%)	24.3
		*CREEP (h)	97	*CREEP (h)	105
		GRAIN SIZE (ASTM)	6 - 7	GRAIN SIZE (ASTM)	3 - 4
		γ' SIZE (μm)	1.5	γ' SIZE (μm)	1.2
	840 °C x 24 h + 750 °C x 50 h A.C.	UTS (N · mm ⁻²)	1139.2	UTS (N · mm ⁻²)	1173.7
		YS _{0.2} (N · mm ⁻²)	1034.3	YS _{0.2} (N · mm ⁻²)	1035.6
		El (%)	20	El (%)	16
		R.A. (%)	19.7	R.A. (%)	17
		*CREEP (h)	120	*CREEP (h)	125
		GRAIN SIZE (ASTM)	6 - 7	GRAIN SIZE (ASTM)	3 - 4
		γ' SIZE (μm)	1.0	γ' SIZE (μm)	0.8

* 650 °C/600 N · mm⁻² CREEP - TIME TO 0,2% ELONGATION

TABLE 5 - MECHANICAL PROPERTIES OF P/M L.C. ASTROLOY AFTER HEAT TREATMENTS (650 °C)

L.C. ASTROLOY - GRAIN SIZE DISTRIBUTION OF POWDER

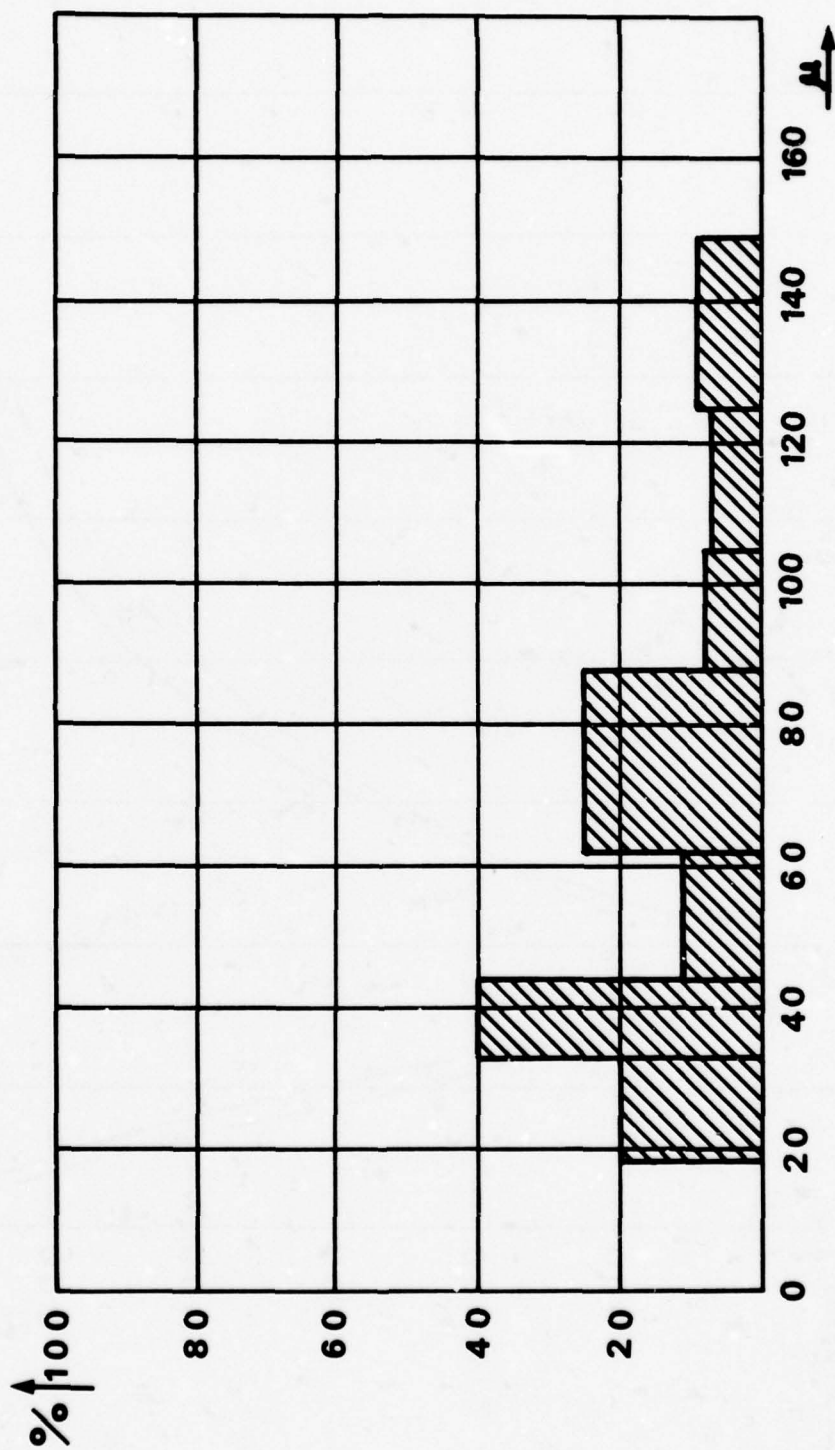


FIG. 1

LOW TEMPERATURE HIP CYCLE

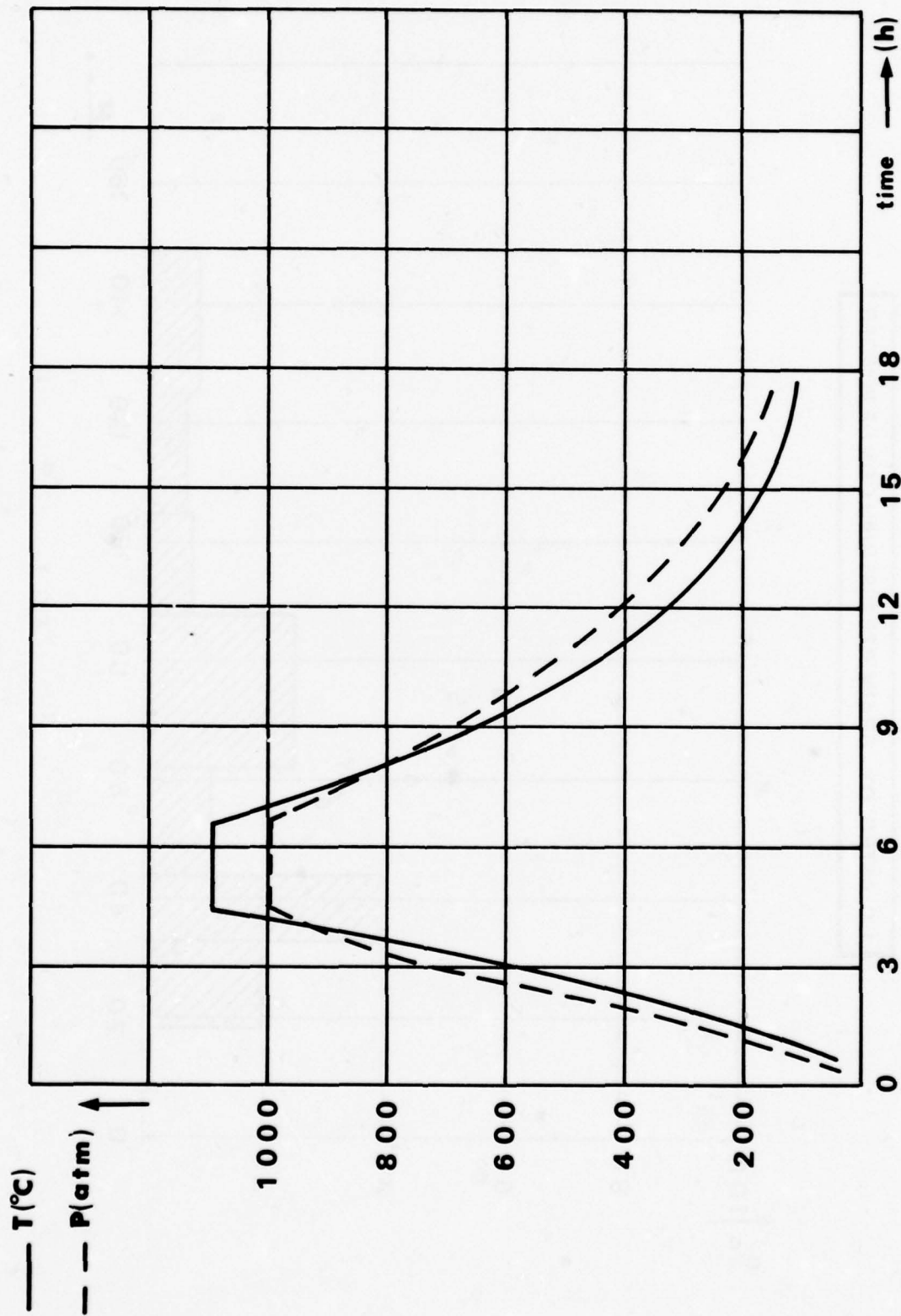


FIG. 2

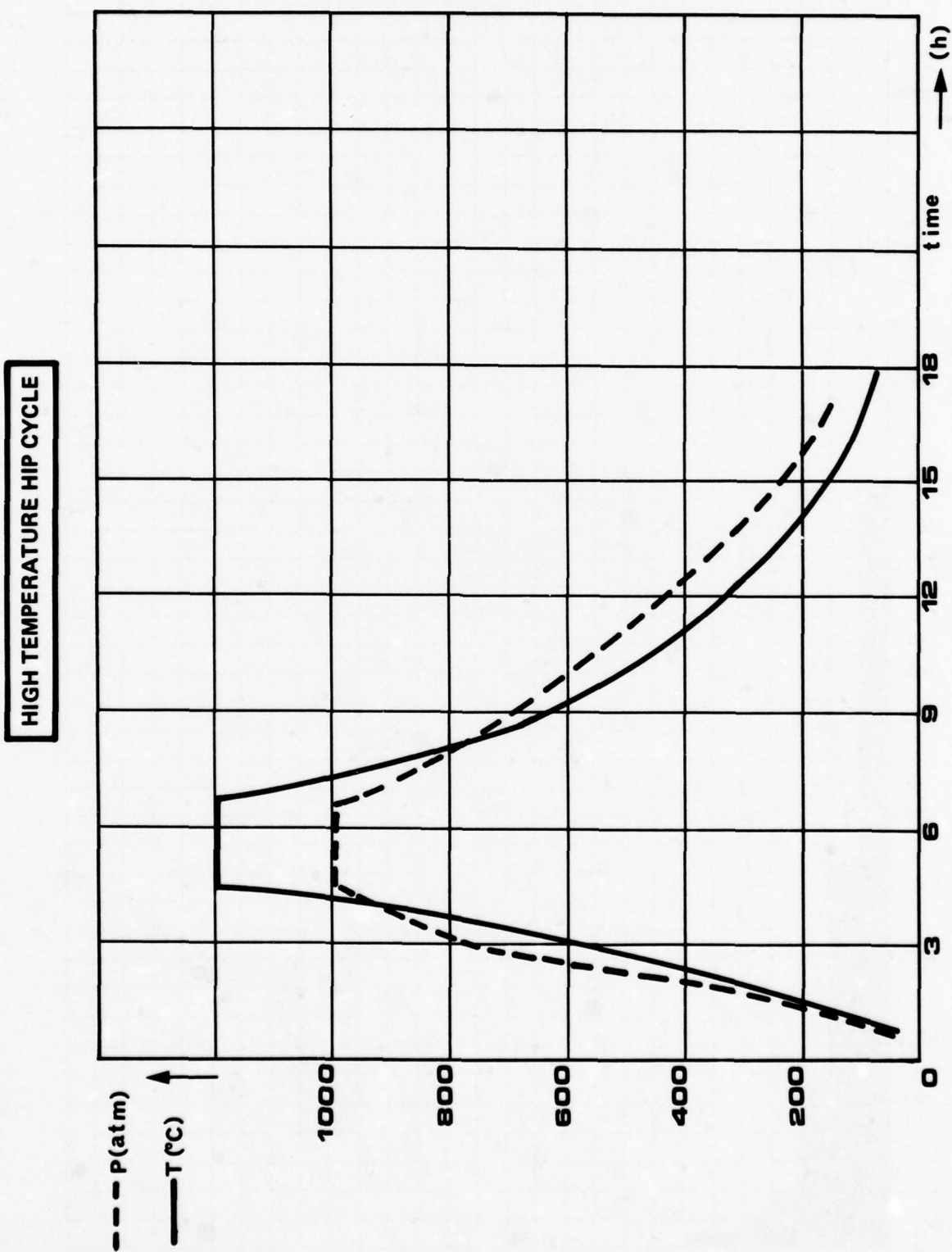


FIG. 3

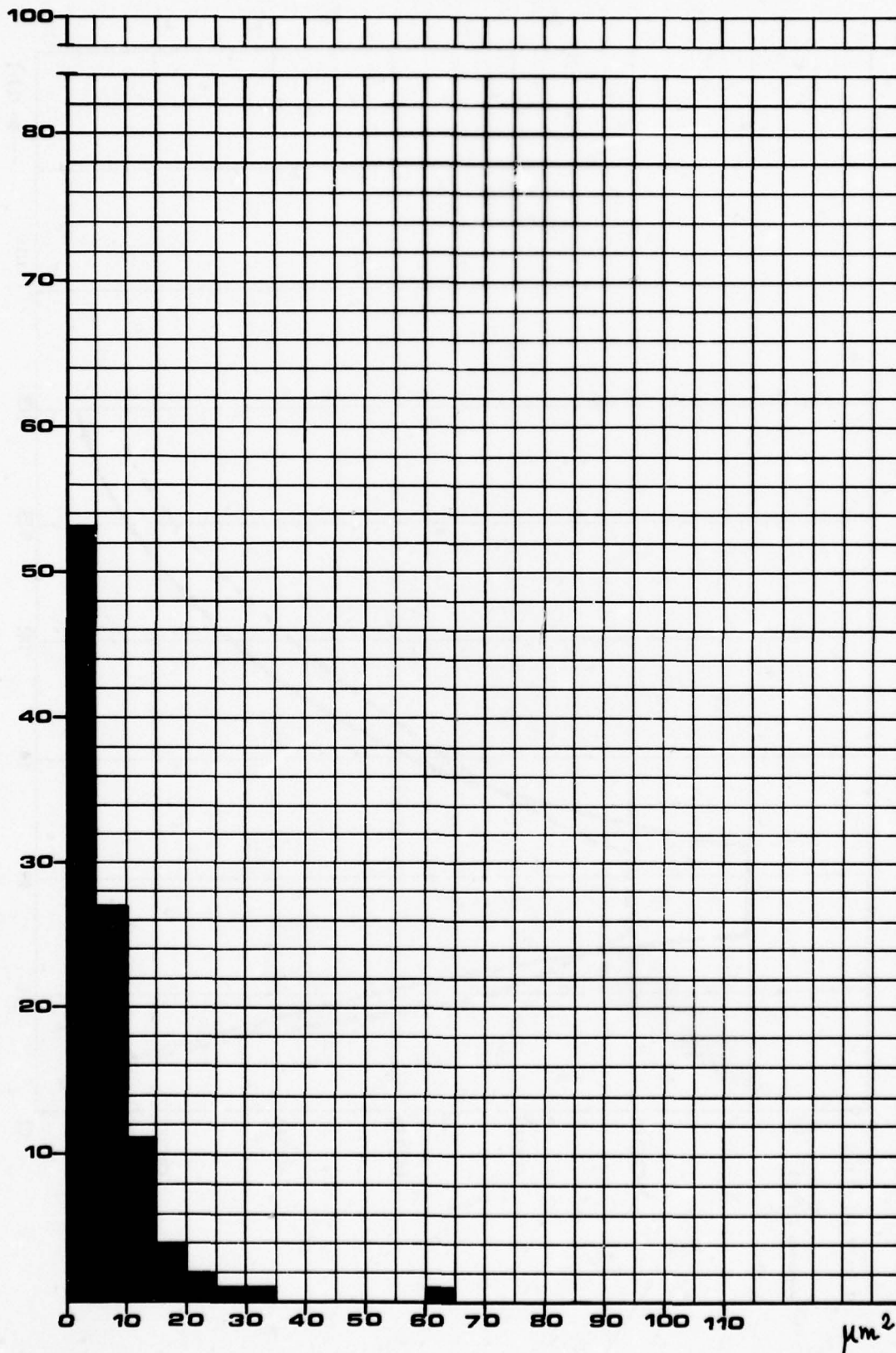
SIZE DISTRIBUTION OF POROSITY
OF A-ASTROLOY AS-HIP

FIG. 4

SIZE DISTRIBUTION OF POROSITY
OF B-ASTROLOY AS-HIP

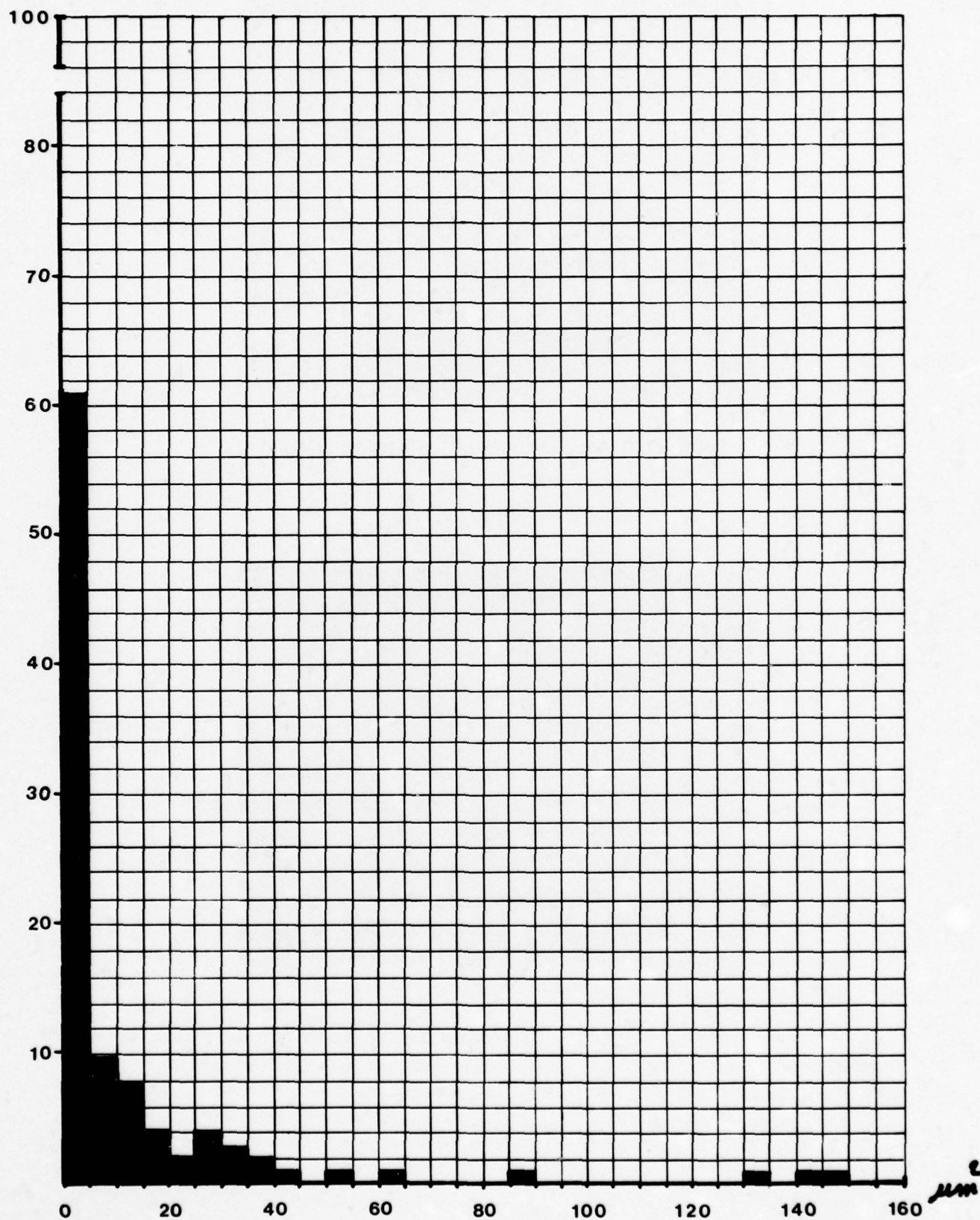


FIG. 5

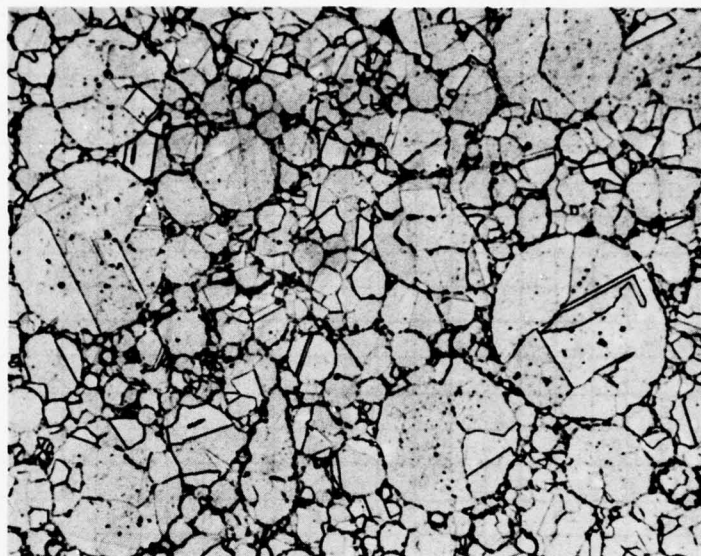


Fig. 6 — L.C. Astroloy as—hip T_{max} 1100°C (200 x)

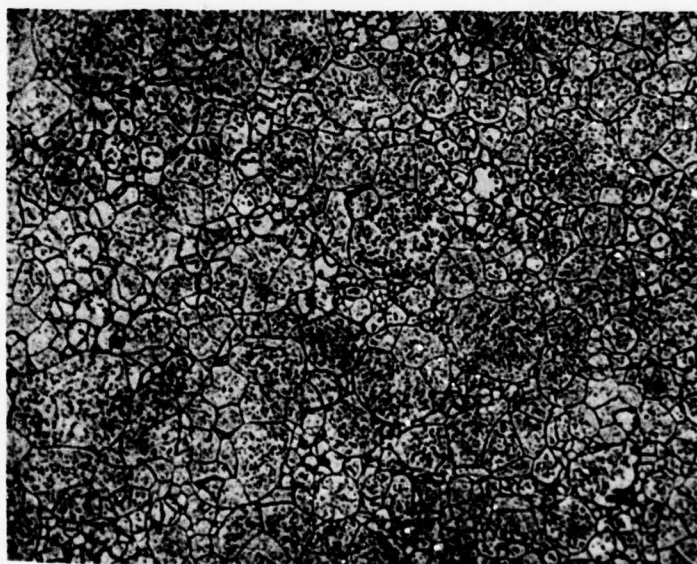


Fig. 7 — L.C. Astroloy as—hip T_{max} 1200°C (200 x)

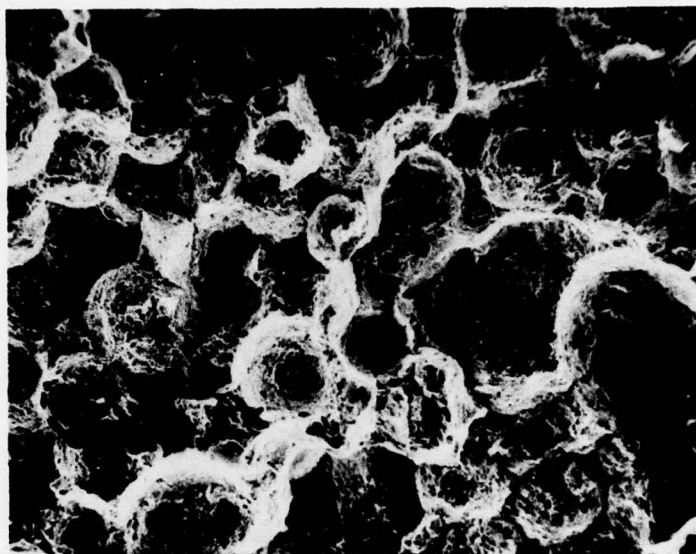


Fig.8 — Fractographs of ruptured smooth Astroloy-A (650°C) (100x)

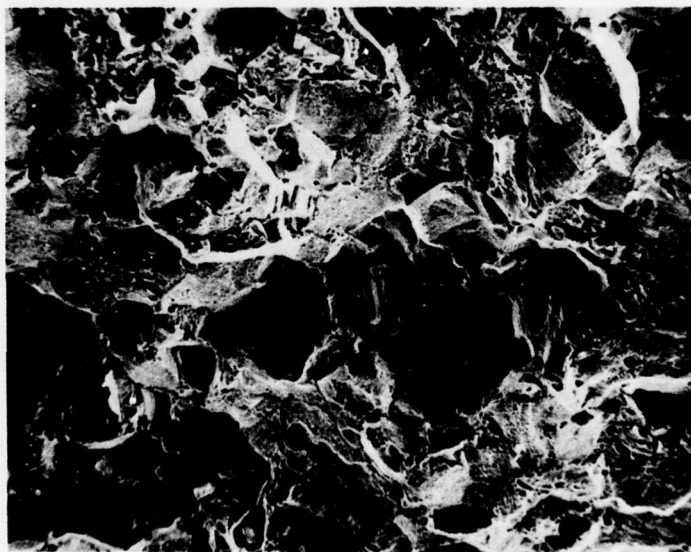


Fig. 9 — Fractographs of ruptured smooth Astroloy—B (650°C) 100 x

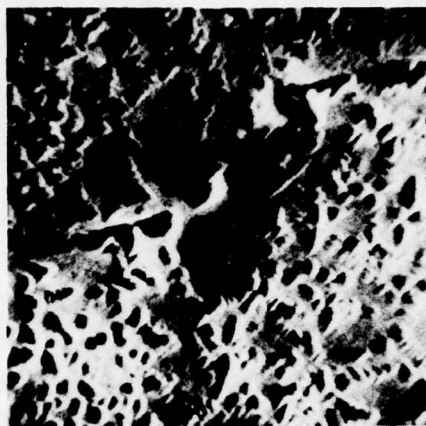


Fig. 10 — γ' phase in Astroloy-A (5000 x)

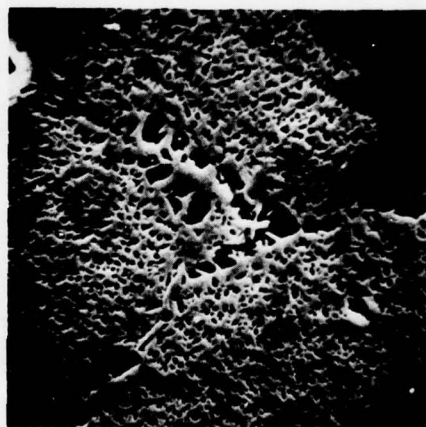
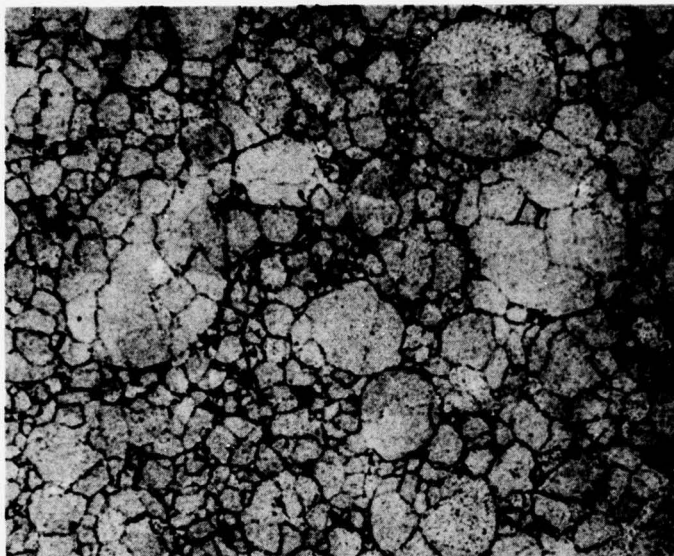
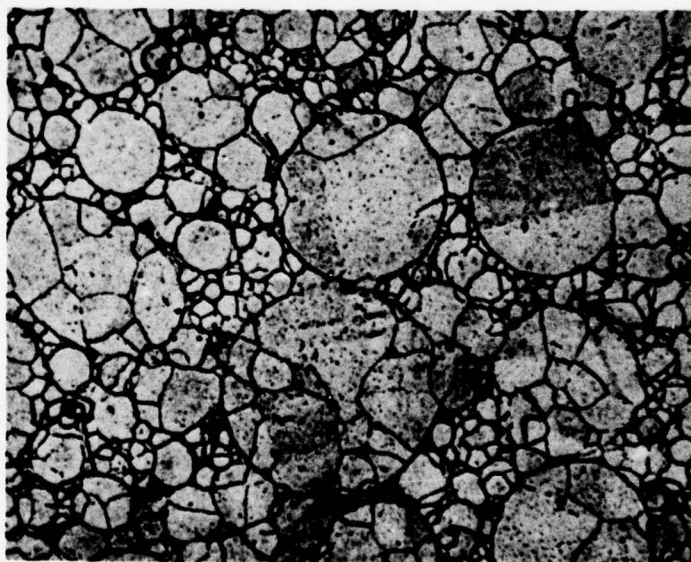


Fig. 11 — γ' phase in Astroloy-B (5000 x)



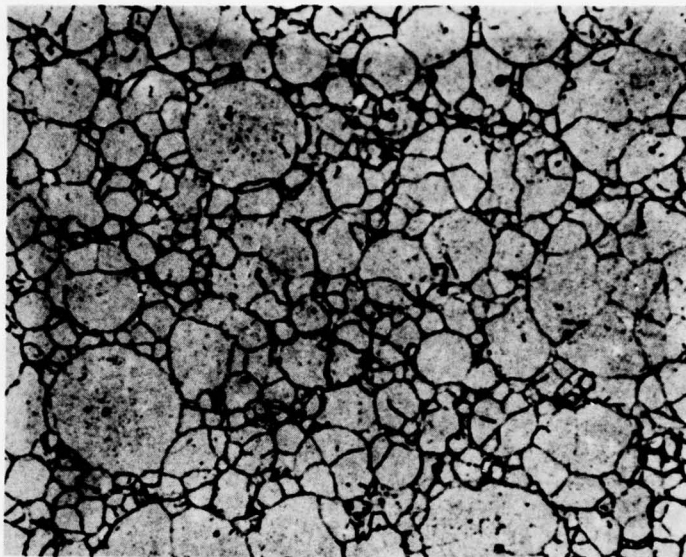
**Fig. 12 a — Astroloy—A structure after solution heat treatment:
1200 C x 4 h (200 x)**



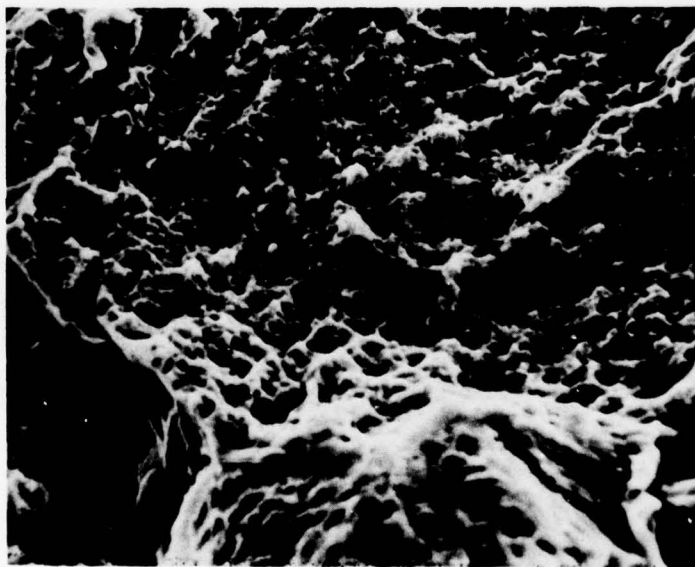
**Fig. 12 b — Astroloy—A structure after solution heat treatment:
1200 C x 10 h (200 x)**



Fig. 12 c — Astroloy-A structure after solution heat treatment
1200°C x 12 h (200x)



**Fig.13 a — Astroloy-B after heat treatment $1200^{\circ}\text{C} \times 4 \text{ h}$ —
SQ + $840^{\circ}\text{C} \times 24 \text{ h}$ + $700^{\circ}\text{C} \times 100 \text{ h}$ — A.C. (200x)**



**Fig. 13 b — Fractograph of ruptured smooth of Astroloy—B after heat
treatment as in fig. 13 a (100 x)**

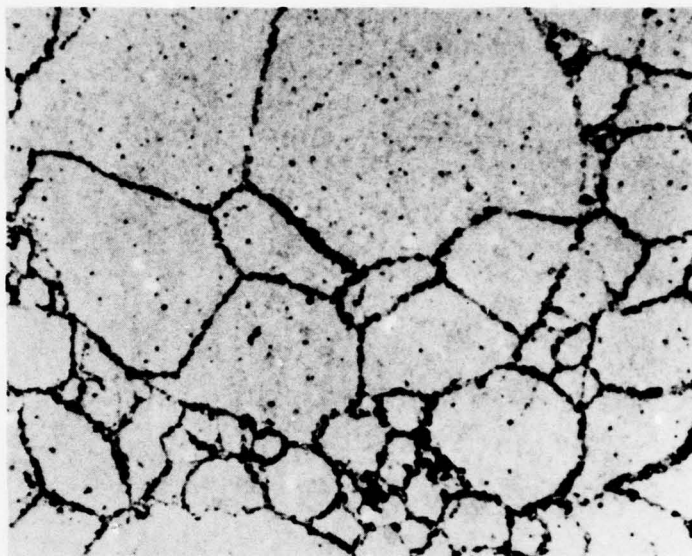


Fig. 14 a — Astroloy—B after heat treatment 1200 C x 4 h S.Q. + 840°C x 24 h + 750°C x 50 h — A.C. (200 x)



Fig. 14 b — Fractograph of ruptured smooth of Astroloy—B after heat treatment as in Fig. 14 a (100 x)

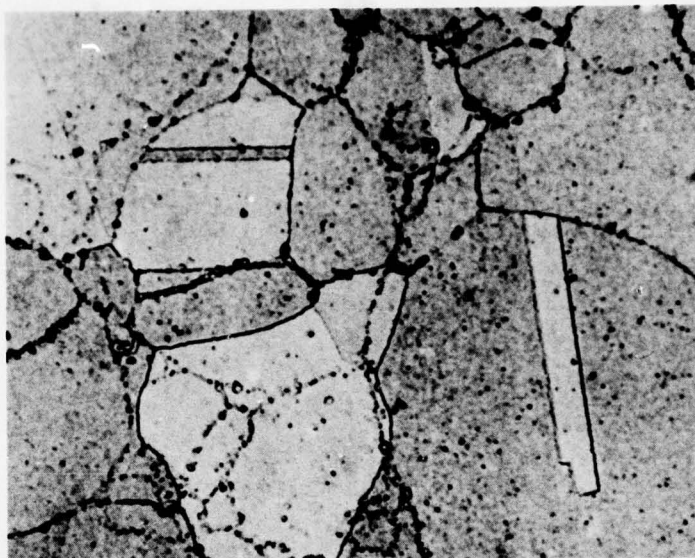


Fig. 15 a — Astroloy—B after heat treatment $1200^{\circ}\text{C} \times 12 \text{ h S.Q.} + 840^{\circ}\text{C} \times 24 \text{ h} + 700^{\circ}\text{C} \times 100 \text{ h A. C.}$ (200 x)

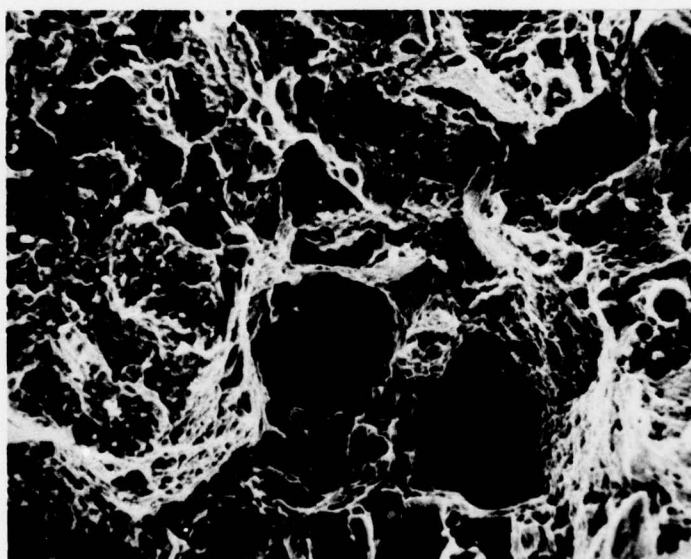


Fig. 15 b — Fractograph of ruptured smooth of Astroloy—B after heat treatment as in fig. 15—a (100 x)



Fig. 16 a – Astroloy–B after heat treatment 1200 C x 12 h S.Q. + 840°C x 24 h + 750°C x 50 h A. C. (200 x)

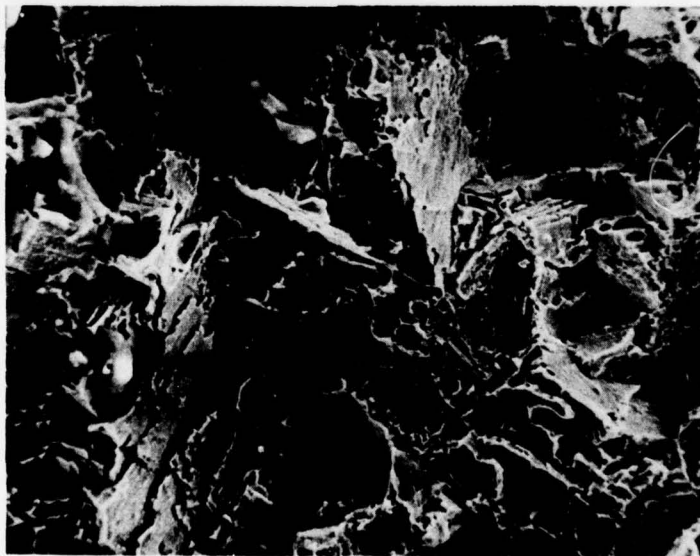


Fig. 16 b – Fractograph of ruptured smooth of Astroloy–B after heat treatment as in fig. 16 – a (100 x)

FORMING METALS BY RAPID SOLIDIFICATION

Professor A.R.E. Singer B.Sc., Ph.D., F.I.M.,
Department of Metallurgy & Materials Technology,
University College of Swansea,
Singleton Park,
Swansea, S. Wales
U.K.

SUMMARY

Three main techniques for forming useful products which benefit from rapid solidification are reviewed. They consist of:

- i. extruding, forging, rolling or pressing rapidly solidified powder or splats.
- ii. solidifying molten metals by contact with a moving cold surface to produce tape or wire.
- iii. spray forming on a cooled substrate or mould.

Spray deposition is selected as the procedure which has the greatest potential in terms of industrial application because of its versatility and relatively low cost. Some of the important factors affecting the integrity of spray deposits and the properties of the subsequent spray formed products are discussed. Particular attention is directed to the effect of spray density in relation to substrate cooling on structure and mechanical properties, and the effect of residual oxygen. Information is given on the process variables involved in, and the properties produced by, spray casting, spray rolling, centrifugal spray forming and spray forging.

BENEFITS OF RAPID SOLIDIFICATION

Rapid solidification is now a band-wagon in the metallurgical field. It is therefore useful to analyse the reasons for its popularity and attractiveness in the area of fabrication together with its weaknesses and limitations. In 1959 it was found that by allowing small atomised drops of molten metal to impinge at high velocity on a cold metal surface thin solid splats were formed which had cooled at rates up to 10^6 Ks^{-1} . Later it was found that by solidifying drops of molten metal between two impacting surfaces using a hammer and anvil technique, thin splats up to 3cms diameter could be produced having similar rates of cooling. Such large splats enabled the tensile properties to be determined accurately. An examination of the structure and properties of these rapidly solidified splats showed several important features the most important being:

- i. with most metals ultra fine grain sizes were produced.
- ii. cooling was so rapid that new phases were formed. Frequently regions of solid solubility were extended enormously giving entirely new meta-stable structures. These metal stable structures could decompose to give pronounced precipitation hardening effects hitherto unknown.
- iii. in many cases enhanced mechanical properties were achieved by the use of rapid solidification.
- iv. with certain special alloys it was possible to cool so rapidly that the materials remained in the amorphous state. Such metal glasses were found to have valuable electrical and magnetic properties in addition to enhanced tensile properties.

Clearly such rapidly solidified materials are of great interest and much endeavour is towards obtaining higher and higher cooling rates. Unfortunately the quest for cooling rates beyond 10^6 Ks^{-1} inevitably leads to many practical problems including materials being produced in thinner sections or layers than hitherto or by means of more exotic equipment and processes. This trend makes it more difficult for the research and development to be applied successfully to the manufacture of useful products endowed with the enhanced properties brought about by rapid solidification.

One of the objects of this paper is to show that there are presently immense possibilities for greatly improving the performance of "conventional" metals and alloys using cooling rates between 10^4 and 10^6 Ks^{-1} . In the view of the author the most valuable approach in this area is to exploit to the full the possibilities of rapid solidification to produce massive and useful metal products of direct interest to industry.

WAYS OF ACHIEVING RAPID SOLIDIFICATION

To obtain rapid solidification it is necessary to cool a molten metal rapidly by conduction of heat away from an exterior surface. The only exception is the case where substantial super-cooling is possible, but even in this case it is generally necessary to cool a small volume of liquid very rapidly.

Metals in the form of ions or metal vapour can be condensed on a cool metal substrate to give effects similar to rapid solidification but the rate of deposition is low so that such methods are mainly used as a means for obtaining strongly adherent thin surface coatings rather than for building up major components.

Molten metals in the form of small drops or thin films are the most convenient and satisfactory ways of obtaining high rates of cooling. Provided the drops are small enough or the films thin enough they both allow very high cooling rates to be achieved. The cooling means can be a cold fluid, either gaseous or liquid, or a cold solid surface. By combining these factors in various ways all the present methods of rapid solidification can be obtained. Liquid metals can be atomised to form small liquid particles which cool rapidly when in contact with a high velocity stream of cold gas. Conventional atomising procedures using air or inert gas give particles of 100-200 μm diameter with cooling rates $\sim 10^4 \text{ Ks}^{-1}$. These rates are not particularly interesting because they are not sufficiently high for the development of superior properties. Water atomising tends to produce slightly more rapid freezing and gives irregular powders. The rate of cooling is lower than might be expected because layers of water vapour formed around the molten particles have an insulating effect.

The most rapid rates of cooling are given by contact of a molten metal with a cold solid surface. This is especially true of integral methods where the highest quenching rates are brought about by rapidly melting a very thin surface layer of a massive piece of cold solid metal. The most startling results are obtained by using the well known technique of laser glazing in which a powerful laser beam passes rapidly over the workpiece melting a thin film which subsequently freezes as the beam passes to other parts of the workpiece. Because the molten film is an integral part of the workpiece and the heat transfer is effectively perfect it is chilled extremely rapidly by conduction of heat to the base. In this way cooling rates up to 10^8 Ks^{-1} have been obtained enabling surface hardening treatments to be carried out or in some cases allowing an amorphous layer to be formed on the surface having mechanical and chemical properties entirely different from the base. Laser glazing does not change the geometric form of the workpiece and cannot therefore be regarded as a means of forming metals. For this reason it will not be dealt with further in this paper.

Other methods of rapidly solidifying films of liquid metal consist of either spreading a drop or stream of molten metal thinly over a cold metal surface or by squeezing a stream of molten metal between two cold metal surfaces. The earliest experiments were

carried out with small droplets of molten metal impacting a cold metal surface at high speed to form very thin splats or flakes. While individual splats may have intrinsically high and interesting mechanical properties they are of no practical value unless a multiplicity of splats can be formed into useful shapes without deterioration of their properties.

RAPIDLY SOLIDIFIED POWDER AND SPLATS

As mentioned above conventional metal powders made by gas or water atomising come within the regime of rapid solidification but at the lower end, cooling rates being generally of the order of 10^4 Ks^{-1} , with water atomising rates slightly higher than gas atomising. The cooling rates depend greatly on the particle size, smaller particles of the order of $50\mu\text{m}$ cooling much more rapidly than larger ones of $150\text{--}200\mu\text{m}$ size. There seems to be a limited future in trying to increase cooling rates by decreasing powder particle size. While it is true that small particles cool far more rapidly than large ones the yield of very fine powder tends to be low and processing difficulties may be increased. The yield of very fine powder, say $1\text{--}10\mu\text{m}$ in size produced from the liquid is increased by the use of high gas pressures and gas/metal ratios and by the use of the recently developed ultrasonic atomising procedure. Such fine powders have the advantage of rapid sintering and acquiring full density more easily but they add greatly to the cost of operations, as a consequence of difficulties of handling, dusting, surface oxidation and pyrophoricity. As a consequence of the lower cooling rates larger sized conventional powders are not specially interesting although clearly they have an important role in more ordinary P/M processes.

A different approach has been taken by Pratt and Whitney who are atomising to reasonably small particle sizes ($60\mu\text{m}$) by centrifugal means and then quenching the liquid particles by high velocity curtains of helium. This gives cooling rates up to 10^6 Ks^{-1} and enables the special characteristics of rapid solidification to be retained. The procedure is detailed in another paper given at the present conference and no further comment will be made here.

Splat powder can be produced by directing an atomised spray onto a rotating water-cooled copper drum from which the splats are scraped. The splats in the form of small flakes each possess the intrinsic benefits of rapid solidification.

The main problem with all such rapidly solidified powder or splat particle routes is that the powder has to be consolidated and fabricated into a useful product without detriment to the potentially high mechanical properties of the particles. This is not an easy objective to attain.

The use of conventional powder metallurgy compacting and subsequent sintering procedures generally causes deterioration of the properties of the product as a consequence of the high sintering temperatures required. Such high temperatures cause reversion to the equilibrium state with substantial loss of the enhanced mechanical properties it is hoped to preserve. Other methods of consolidation are more successful because of the lower temperatures involved and the shorter times required to attain full density. Hot isostatic pressing of the canned powder or splat particles can be used with some measure of success. Extrusion is the most effective because of the large amount of working and consolidation achieved at relatively low temperatures while hot rolling or hot forging remain other possibilities.

The fact remains, however, that the procedure of producing powder or splat particles followed by hot consolidation is an expensive affair. It involves the handling of fine particles and the inevitable oxidation of the surfaces of the particles prior to consolidation. Clearly the process can only be contemplated where the additional cost can be carried by the product and where the small amount of incorporated oxide is not detrimental.

THIN METAL TAPE AND WIRE PRODUCED BY RAPID SOLIDIFICATION

There is now an extensive literature on methods of producing thin rapidly solidified metal tapes and an even more extensive one on the properties of the products, particularly the amorphous materials. It is not the purpose of this paper to review progress so far, but the salient features and special difficulties facing the procedures will be outlined.

All the methods involve allowing a source of molten metal to impinge on a rapidly moving cold metal surface. The high speed of the metal surface drags a thin layer of the molten metal out of the pool formed at the point of impingement and the layer rapidly freezes to form a continuous, or semi-continuous, solid metal tape which can be separated from the surface. Typical processes developed by Battelle are melt spinning (1) and melt extraction (2) each of which can be carried out in an inert atmosphere if necessary. The tape is formed rapidly and cooling rates are commonly between 10^4 and 10^6 Ks^{-1} . Limiting factors are product thickness and width. Tape thickness lies between $25\mu\text{m}$ and $100\mu\text{m}$, and widths are generally between 1 and 5mm. Wider tape can be produced by the use of multiple or slot nozzles and up to 50mm using a special melt extraction procedure. The technique is simple and cheap and several potential uses have been found for the micro-crystalline products such as thin aluminium tape for radar decoys and wire reinforcing for rubber tyres and for cement.

A twin roller process employing high speeds of operation up to 6000rpm is currently being used at several centres for the manufacture of tape and narrow strip (Fig. 1).

The molten metal is fed vertically into the nip of twin rollers which operate like a high speed rolling mill. Wider strip can be produced than is possible with the processes mentioned above and at Swansea, aluminium alloy strip 100 μ m thickness and 70mm wide has been obtained. It has been shown that depending on the process variables and the heat transfer coefficient at the interface between the rollers and the molten metal the equipment can be operated in three modes (i) with low heat transfer, atomisation of the metal stream occurs (3), ii. with fairly high heat transfer twin tapes can be produced each showing one chilled surface (next to the roller) and one "liquid" surface (at the centreline). iii. with high heat transfer a single tape is produced. The twin roller process is not so tolerant of changes in process variables as melt spinning or melt extraction but has several benefits including the possibility of operating at a higher speed for a given tape thickness. One problem of the twin roller equipment is that the length of contact of the tape with the roller is much shorter than with the other processes. For instance, experience at Swansea showed that an alloy steel 100 μ m thickness and 1cm wide issued from the twin roller equipment at 900-1000°C when operating at 3000rpm. The temperature was so high that many of the benefits of rapid solidification were annealed out of the strip. A steel belt system operated satisfactorily as shown in Fig. 2. giving issuing temperature of approximately 700°C with markedly better final properties.

Despite all the interesting structures and properties that can be realised in thin tape and wire and the high speed with which it can be manufactured, the processes producing tape direct from molten metal all suffer from the same constraint. None of them is capable of producing thicker strip than $\sim 150\mu$ m, and width seems to be limited, although major advances in this area are reported by Allied Chemicals including weaving tape into cloth.

FORMING BY SPRAY DEPOSITION

Forming metals by spray deposition can be divided into two categories. In the first category metal is supplied in the form of a wire or a powder to a flame, an arc or a plasma. The metal is melted and propelled by the hot gases towards the surface onto which it is deposited. The second category consists of those processes in which molten metal from a melt is atomised and deposited without the use of an independent heat source.

The processes in the first category are of considerable age and are well known in industry especially for coating other metal. Flame spraying suffers from a major disadvantage of causing substantial oxidation of the deposit - a disadvantage shared to some extent by arc spraying. Plasma spraying has the edge on flame spraying in the sense that deposition can readily be conducted in an inert or reducing atmosphere, the particle size is smaller and velocity greater. Even so, all these processes suffer from the disadvantage of relatively low throughput and the need for the material to be supplied in the form of powder or wire. For the purpose of this paper they will not be discussed further.

The general principle of spraying from the melt is that the metal or alloy is fed into an atomising device operating in an inert atmosphere which forms and directs the spray of liquid metal particles on to a cold surface or mould. The liquid particles flatten as they impinge on the surface to form a multitude of small splats which adhere tightly to the surface and to one another to form a substantial deposit.

Various means of atomising and propelling the molten metal of the melt have been devised, but only gas atomising and centrifugal atomising have yet been developed to the stage where large plant can be designed. For this reason the present paper will deal only with these two main methods and their adaption for spray deposition.

In all spray forming processes from the melt the first objective is to atomise the liquid metal into small liquid particles generally having a mean diameter between 100 and 200 μ m. The liquid particles are propelled rapidly towards the depositing surface either by a high speed stream of gas or by centrifugal force. As the particles move towards the surface they become spherical in form and they also cool in flight by radiation and convection. But it is important that they reach the surface whilst still fully liquid or at least mostly liquid. The liquid particles flatten on the surface to form adherent splats which deposit on one another, thus building-up a substantial layer.

In practice a wide range of particle sizes is produced by any atomising process and generally speaking the larger particles remain hotter longer, and arrive at the depositing surface at higher speeds than the smaller ones. For this reason alone particles tend to arrive at various stages of their thermal history.

Fully liquid particles form large splats which cool rapidly at speeds from 10^4 to 10^6 Ks⁻¹ because of the thinness of the splat and the excellent contact with the cool depositing surface. In these circumstances heat flow occurs uni-directionally perpendicular to the surface, fine columnar crystals are formed having their long axes in the direction of heat flow. Typical splats are 10-20 μ m thick and 500-1000 μ m in length. The width of the columnar crystals may be only a few microns. Many such particles will be undercooled in flight, i.e. still fully liquid although their temperature may be below the liquidus. This is a general phenomenon with small rapidly cooled liquid drops, but can be encouraged by the use of high gas/metal ratios leading to finer particle size and even more rapid cooling in flight. Such under cooled particles will quench even more rapidly on reaching the depositing surface.

Particles in flight which cool to temperatures between the liquidus and solidus will

usually nucleate to form dendrites. Provided that the proportion of liquid is still high, such partially solid particles will also splat on arrival. However, in the act of splatting the dendrites will be fragmented and distributed throughout the splat. The fragmented dendrites will then act as independent nuclei and on cooling an equi-axed structure will be evident in the splat. Very small atomised particles lose heat rapidly in flight partly because their surface area/volume ratio is higher and partly because their flight is of longer duration. Many such particles which are solid on arrival will not splat and will show themselves as rounded particles buried in a mass of splats when a metallographic cross section is examined.

Of the various forms of spray deposition spray casting is the newest and the least well known. The spray casting of billets and slabs of various sections is now being developed at several centres. It shows promise because segregation free castings can be produced having a very fine grain size. In addition there is freedom from coarse inter-metallic aggregates commonly found in conventional ingot and billet castings. The problems are mainly those of obtaining sufficient cooling of the particles by gas prior to deposition and extracting sufficient heat from the spray cast billets or slabs to enable economic casting rates to be achieved.

Hot isostatic pressing has been used with good effect on spray cast products especially where they have appreciable porosity in the "as sprayed" condition. But the cost of hot isostatic pressing is high and more attention to the conditions of deposition might have an equally beneficial effect at a fraction of the cost.

Integrity of Deposit

The integrity of a spray deposit is most easily discussed in terms of deposition on a flat surface or substrate or one which has a large radius of curvature.

An important feature is the spray density. By this is meant the weight of particles arriving at the depositing surface per unit area of surface. Clearly spray densities can vary enormously according to the metal feed rate and the spray distance etc.. Moreover, any one spray varies in density from higher density near the centre to near zero at the edge of the spray cone although this is of less significance with continuous operation. Even so the concept of spray density is important as is shown below.

A low spray density will allow each splat to solidify completely before the next droplet arrives at the same place. Consequently the new substrate i.e. the previous splat, will be at a relatively low temperature so that the following droplet will splat on the earlier one in just the same way as if it were a cold substrate. Rapid cooling will take place and the second splat will crystallize independently of the first. If there is no oxygen present no perceptible oxide films will form on the top of the first splat but the splat boundaries will subsequently be distinguishable under the microscope. Small voids may be present where the second splat has failed to infill at the edges of the first and this will be repeated with subsequent splats. The outcome is that a low spray density will tend to give rapid quenching effects throughout the deposit but will result in some porosity. A typical porosity for a low density spray is 10%.

High density sprays produce different results. Most splats arrive before the preceding ones are completely solid. This enables the two splats to accommodate one another geometrically. Consequently there is complete filling at the edges of preceding splats leading to a very low porosity. Typical porosities with high density sprays are 1% or less. A further feature of high density sprays is that the rate of cooling is lower and the crystallization of a following splat is linked to that of the earlier one. The preceding splat can nucleate the following one giving rise to an epitaxial effect. It is then very difficult to distinguish the original splat boundaries under the microscope and, typically, columnar grains may grow through several splat boundaries. Integrity is high but the cooling rate is lower.

The effect of spray density is also clearly related to the degree of substrate cooling possible in any system. Thus higher spray densities can be tolerated with a high degree of substrate cooling than would otherwise be the case. In all cases however the principles enunciated in the previous paragraph apply.

An important cause of porosity, low mechanical properties and general lower integrity is the presence of oxide in the deposits. Molten metal supplied to the atomiser is usually very free from oxide. Similarly any gas used can generally be provided at very high purity at relatively low cost. The difficulties therefore arise because of leakage residuals, and entrained or adsorbed oxygen in the form of air or oxygen containing compounds such as water. Although all commercially used metals can form undesirable oxides in these circumstances it is particularly difficult when the molten metal contains aluminium, chromium or titanium. In practice therefore, the problems related to oxygen are very important for most commercial applications.

Immediately after atomising the liquid metal is in the form of small high temperature particles in flight having a very large surface area/volume ratios. Even in the few milliseconds of flight time oxide skins form on the surface of the particles if the atmosphere contains oxygen. However, the skins formed in flight are not the most serious problem because during splatting on the substrate, or on preceding particles, the surface area is increased on average approximately 10 times. The oxide skins burst and the pure metal from the interior flows rapidly over the substrate and freezes. The oxide skins

formed in flight are incorporated in the deposit, but in itself this accounts for only a small part of the loss of integrity.

A more important factor is that the surfaces of those splats already deposited become oxidised while they are still at a relatively high temperature. The next molten particle to arrive is then presented with a thin oxide film on to which it must splat. Generally speaking the contact angles that metals make with Al_2O_3 , Cr_2O_3 and TiO_2 are high and constitute non-wetting systems. In contrast the contact angle with a non-oxidised surface of the same metal is very low and constitutes a wetting system.

The presence of oxides give rise to surface tension effects which prevent the newly arrived liquid particles infilling the crevices and interstices of the solidified splats on to which they are deposited. In this way a porous deposit of relatively low integrity having poor mechanical properties is formed.

Quite small amounts of oxygen in the system can cause the above effects. It should be emphasised however, that the total amount of metal oxide formed may also be very small and is significant merely because it prevents the effective welding of one splat to the next during deposition. If the deposit is subsequently hot worked to reduce porosity and disrupt the oxide films the full properties of the metal or alloy return. Nevertheless it is generally beneficial to attain the highest integrity possible in the deposit and with this in view it is important to minimise oxygen in the deposition chamber.

A further matter for note is that the practical difficulties of excluding oxygen are not as great as might at first be supposed. Oxygen derived from residual air and adsorbed oxygen compounds are rapidly scavenged at the commencement of atomising. This "cleaning-up" effect is very noticeable in a continuous or semi-continuous spray forming process where the early deposits are invariably more porous than the later ones. The important feature is to avoid the continuous entry of entrained air or adsorbed oxygen containing films.

Subsequent Treatment of Deposit

The top surface of a spray deposit is invariably rippled because of the random distribution of splats in the last layers. To produce an acceptable product it is therefore essential to carry out some subsequent treatment such as rolling, pressing, forging or machining.

The hot rolling or forging of spray deposits is a favoured method of further treatment. It has the advantage of closing any residual porosity and modifying the internal structure as well as giving a more acceptable external surface. In addition it can be used to correct shape deficiencies that often occur during deposition. The combination of spray deposition with hot rolling or forging is particularly beneficial and can lead to the generation of high mechanical properties. Hot rolling has the additional advantage that it can be operated continuously or semi-continuously. It can therefore be attached conveniently to a continuous spray deposition process and use its sensible heat.

Cold forming immediately following deposition is equally a possibility, but the beneficial effects on porosity and structure are less pronounced. Its most significant advantage is its ease and convenience.

SPRAY FORMING PROCESSES

Spray Rolling

This was the first of the spray forming processes to be developed. In a paper by the author (4) the principles of the process were outlined in relation to inert gas atomising and the original process in many of its aspects is described in patents (5). Several developments are taking place in industry, but as the results of such work are commercially sensitive there is a limit to the detailed technical and commercial information that is divulged. However, the important basic information is freely available and indicates the scope, benefits and drawbacks of spray rolling.

The principle of spray rolling is that a stream of molten metal is atomised by jets of an inert gas at high pressure. The resulting spray of liquid metal particles is directed on to a moving substrate where they quickly build up to form a strong coherent layer which can subsequently be peeled off as a strip. The strip is hot rolled about 50% reduction in thickness to give fully dense ductile strip which has similarities to conventional hot band.

Fig. 3. shows the general concept for producing strip continuously using a rotating wheel as a substrate. Further processing can then be carried out as with normal materials.

A wide range of metals and alloys has been made in this way including aluminium and its alloys, copper and copper base alloys, some superplastic zinc base alloys and various steels. In most cases high purity nitrogen was used as the atomising gas although argon has also been used for certain materials.

A simpler operation in industry involving spray deposition and rolling in separate operations showed the possibility of producing large sheets of spray deposited materials. Fig. 4. shows the general arrangement of a multiple nozzle deposition plant and Fig. 5.

an example of the strip produced at 5mm thickness.

The advantages shown by spray rolling are that relatively thin strip can be made in one operation from the melt. The product after hot rolling is of fine grain size and generally shows a much finer structure in terms of unadsorbed or insoluble constituents. Segregation is zero and many alloys that can not readily be fabricated by conventional means are relatively easily processed by spray-rolling. Finally, the mechanical properties of the product produced by "normal" spray rolling techniques are at least equal and often superior to conventional materials.

The disadvantages are the need for a low oxygen content in the atmosphere to ensure that the top surface of the deposited strip is free from porosity so avoiding spill on the final product. It is necessary to control internal stress, and most important of all, it is essential to produce a deposit which shows only a small variation of thickness across the width of the strip. The latter will be dealt with in greater detail below.

The economy of the process for the manufacture of tonnage materials has not yet been determined. However, the cost of nitrogen at say 700KNm^{-2} used at the rate of $0.4\text{m}^3\text{Kg}^{-1}$ is not prohibitive. The value of the process for the manufacture of certain premium products is now established.

Scanning Spray

The most serious difficulty encountered in spray rolling was that of obtaining uniform deposition over the width of the substrate. Several methods were investigated including the multiple nozzle arrangement shown in Fig. 4. Reciprocating nozzles or substrates, swinging nozzles and modification of the spray pattern were all investigated with marginal success.

The most successful arrangement finally developed turned out to be very effective yet simple in both principle and operation. It consisted of deflecting the spray of metal particles by means of secondary jets of inert gas. The secondary jets were supplied from a rotary valve operating at approximately 500rpm and were capable of swinging the spray of particles across the width of the substrate in a scanning fashion without using any moving parts in the spray chamber. With a scanning rate of six cycles per second, thickness variations of less than 5% were obtained. Some data regarding the operation of the scanning nozzle has been published (6).

Enhanced Mechanical Properties

If relatively thin deposits are used or if care is taken to ensure that the previously deposited layer of particles has reached a temperature below, say, $0.6T_m$ when the next layer is deposited i.e. using a low spray density, heavily quenched structures may be developed in some alloys. Such alloys may show greatly extended solid solubility in the as-deposited state compared with conventionally produced structures. If such structures can be preserved, or very fine precipitation can be induced by careful subsequent hot working, then enhanced mechanical properties will result.

At University College Swansea, alloys based on Al-4%Fe have been produced by depositing on a rapidly rotating drum so that each layer of particles was chilled before the next one was deposited. Subsequent hot rolling at temperatures above 350°C was found to cause coarsening of the precipitate leading to relatively poor mechanical properties whereas hot rolling in the range 300°C - 350°C enabled high mechanical properties to be retained leading to a doubling of strength.

Some interesting experimental results were recently published by Latimer, Read and Reynolds (7) of Alcan International Limited, in which an aluminium base alloy containing iron and nickel was prepared in strip form using a spray rolling technique to ensure that rapid quenching took place which is now known to have used a low spray density. The meta-stable phases were retained by careful control of the hot rolling required to consolidate the deposited strip. The results on this alloy E are shown in Fig. 6. where it is compared with its counterpart, the conventional alloy RR58 which is generally regarded as the best wrought aluminium alloy as regards thermal stability. The spray rolled alloy E was designed to have stability at temperatures such as might be encountered in supersonic aircraft where skin heating poses a structural problem. A guide to the thermal stability of such alloys is given by the deterioration of mechanical properties at room temperatures, after being exposed for a week at temperatures up to 300°C . Even before thermal treatment the spray rolled alloy E showed a 20% advantage over RR58 yet both had similar elongations. After one week at 200°C alloy E had increased in strength whereas RR58 had deteriorated. After treatment at 300°C , the difference was most marked with alloy E having twice the strength of RR58. These results were achieved with relatively undeveloped alloys and it seems certain that many other aluminium alloys could be developed which would show positive advantages conferred by the rapid quenching procedure possible in spray rolling.

More recently doubts have been expressed by Alcan about the impact properties of these particular high strength spray rolled aluminium alloys. It seems likely that the cause was the low integrity of the original deposit and the intrusion of oxygen into the equipment. Improvement in the integrity of the original deposit would bring about a pronounced improvement in the impact properties. Most of the work on enhanced mechanical properties produced by spray rolling have been concerned with aluminium alloys. However the same principle applies to many other metals and alloys where similar benefits are obtainable.

Spray Forging

The procedure in spray forging is first to make a preform by atomising molten metal with an inert gas spray depositing into an open mould. The deposit fills the mould replicating exactly the mould surface. The operation is continued until the mould is sufficiently filled when the atomisation is transferred to another mould. The mould cavity is shaped in such a way that the preform can readily be separated from it in just the same way as with a casting. After separation, the preform is reheated to the forging temperature, transferred to a press and forged hot, usually in a single operation. Spray forging is being carried out by Osprey Limited and information regarding the process has been reported in the literature (8). The structure and mechanical properties of several alloys are shown to be at least equal to those of conventional forgings with the additional advantage of being more isotropic and having a finer structure.

The advantages of spray forging compared with conventional processing may be summarised as:- (i) operating directly from the melt, (ii) a single forging operation from a sprayed preform, (iii) zero segregation and a very fine structure leading to good ductility and toughness.

As with all other processes there are inherent disadvantages, which in this case are mostly of an operational nature. The economy of the process depends on controlling waste "overspray" and the changing of moulds. The shaping of the spray to suit the mould is not an easy operation and in particular the shape of the top of the deposited surface is not conducive to good material economy or minimum flash.

Centrifugal Spray Forming

The main emphasis up to this point has been on gas atomising as a preliminary to spray deposition. The alternative method of centrifugal atomising is equally applicable provided the product can be matched to the geometry involved. Experimental work on the centrifugal spray forming of small sheets of aluminium and its alloys has been reported in the literature (9). The procedure is to pour molten metal onto the centre of a rapidly spinning disc or dish which is usually lined with refractory to avoid erosion by the melt. The liquid metal is accelerated rapidly by the dish and flung out tangentially in the form of small drops. High peripheral speeds of say 30-50m. sec⁻¹ and low thermal conductivity of the dish lining ensure that the particles remain liquid or partially liquid during flight.

With the dish spinning in a horizontal plane it is surrounded by a substrate in the form of a large diameter tube which can be reciprocated in a vertical direction. The liquid particles have an almost horizontal trajectory and splat on the substrate surface provided by the inner wall of the tube. By suitable reciprocating movements of the substrate, rings or tubular spray forms can be produced. By slitting large diameter tubular spray forms a considerable sized sheet can be obtained when required.

The benefits of centrifugal spray forming are that very little inert gas is used. Only sufficient inert gas is required to flush and fill the chamber at the commencement. Because of the scavenging action of the first small quantity of atomised melt and the fact that effectively the equipment can be sealed, the control over atmosphere, and therefore over porosity, is very good. In addition the process is clearly well suited to produce large rings and tubular shapes in either thin or thick section.

The disadvantages of the process are equally clear. It is only suited to batch operation and is not applicable to products required in continuous form. Geometrical considerations are also important. Clearly axisymmetric shapes are readily made provided they have an annular arrangement. Circular products having an external diameter up to 2m are feasible and sheet having a long dimension up to 6m can therefore be produced. However, for many products the geometry is a bar to utilisation.

The structure of products made by centrifugal spray forming is very similar to those produced by inert gas atomising and spray forming. Fig. 7 shows the typical splat structure in which particles having an average diameter of approximately 200µm have formed parallel layers of splats in the presence of small quantities of oxygen which helps to define the splat boundaries. In the absence of oxygen in the form of air or oxygen containing compounds, porosity is very low and mechanical properties are high. An example of a centrifugally spray cast product (10) is a short 400m diameter tube of 6mm wall thickness Nimonic 80A which in the "as spray cast" condition showed a U.T.S. of 800MNm⁻² with 28% elongation. The tubes have a high integrity with fine grains growing through the original splat boundaries which are themselves extremely difficult to distinguish metallographically.

CONCLUSIONS

- i. Amongst the many rapid solidification processes spray forming has the greatest potential in terms of industrial application because of its versatility and relatively low cost.
- ii. It is possible to obtain cooling rates between 10⁴ and 10⁶ Ks⁻¹ using spray deposition techniques. This enables many of the benefits of rapid solidification to be incorporated in spray formed products.
- iii. In addition to enhanced mechanical properties spray forming can give very fine grain sizes, freedom from massive intermetallics, ease of fabrication of otherwise difficult materials and zero segregation.
- iv. Four processes are being developed involving spray forming. These are spray rolling, centrifugal spray forming, spray forging and spray casting. Each process has its

benefits, problems and limitations and has therefore to be selected carefully with these factors in mind.

REFERENCES

1. R.B. Pond, U.S. Patent (1958) No. 2825108.
2. R.E. Maringer, C.E. Mobley and E.W. Collings, Proc. 2nd Int. Conf. on Rapidly Quenched Metals, M.I.T. press. p.29.
3. A.R.E. Singer and R.K. Dube, Modern Developments in Powder Metallurgy, 1977, 9, 127.
4. A.R.E. Singer, Metals and Materials, 1970, 4, 246.
5. A.R.E. Singer, British Patent (1972) No. 1262471.
6. A.R.E. Singer, British Patent (1976) No. 1455862.
7. K.G. Latimer, P.J. Read and T.D.W. Reynolds, Inst. of Metals Conf on Modern Metallurgy, Sept. 1973, Oxford, England.
8. W.C. Keung, T.A. Dean, R. Davies and A.G. Leatham, Proceedings of 18th International Machine Tool Design and Research Conference, Sept. 1977.
9. A.R.E. Singer and S.E. Kisakurek, Metals Technology, 1976, 12, 565.
10. A.R.E. Singer, British Patent (1978) No. 1517283.

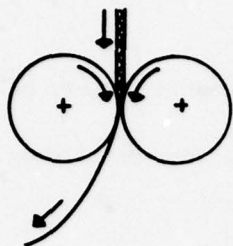


FIG. 1. Twin Roller Equipment

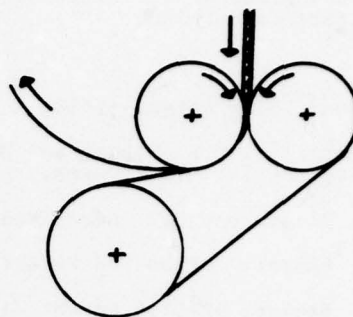


FIG. 2. Twin Roller with Cooling Band

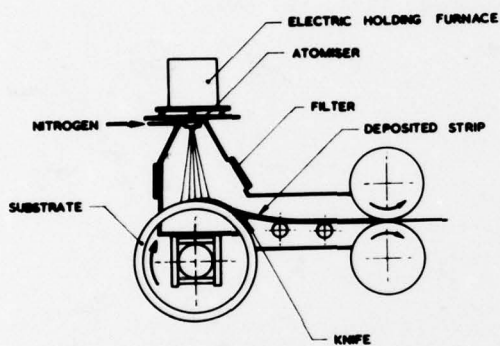


FIG. 3. Equipment for Spray Rolling with a Rotating Substrate

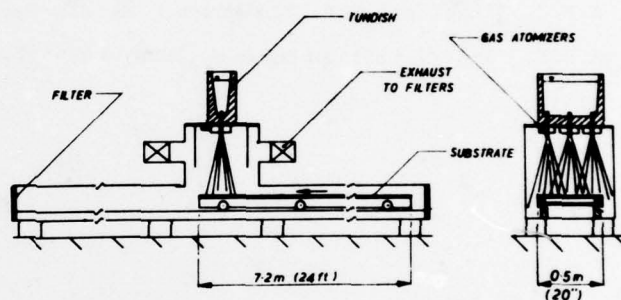
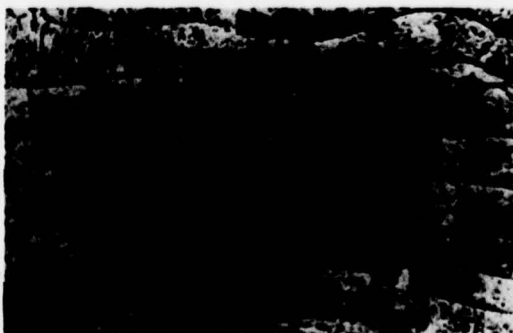
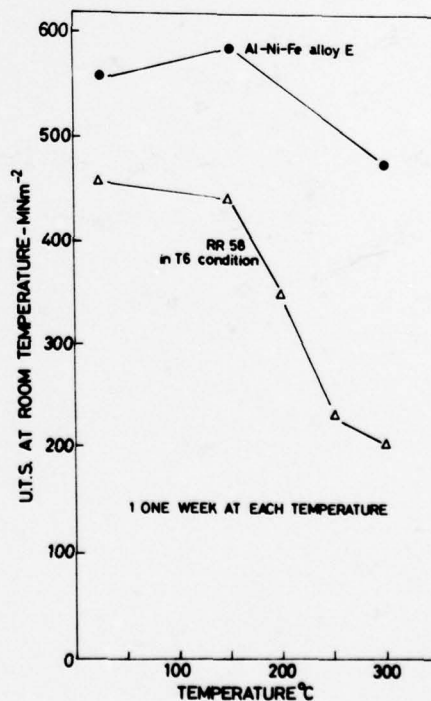


FIG. 4. Schematic Diagram of Experimental Multi-nozzle Plant for Spray Deposition

FIG. 5. Spray Deposited Strip
2.4m x 500mm x 5mmFIG. 7. Cross-section of
Centrifugally Deposited
Strip x 200FIG. 6. Spray Rolled and Conventional
Aluminium Alloys for use at High
Temperatures

DISCUSSION SUMMARY

Session I – Research and Production Aspects of Machining Processes – by Dr Ing. B.Hirsch VFW-Fokker GmbH, Germany

The German work on "Applied Research in Machinability of Titanium and its Alloys" compared steel machining to titanium machining where 50% of heat generated goes into the tool for steel while 80% of the heat for titanium goes into the tool. Therefore, HSS with high tungsten and cobalt contents and carbides, grade K20 (C2), shall be used as cutting materials. Tool failures are caused by very high alternating thermal and mechanical stresses, i.e., fatigue using carbide tools. Synthetic and high EP-containing cutting fluids are most suitable to improve tool life. Considerable additional gains are achieved by increasing the flow rates up to total flooding. In drilling, internal cooling gives best tool life.

Belgian work on "Residual Stress in Grinding" concludes that thermal expansion is a main cause for residual stresses. The thermal characteristics and yield stress of a material are major factors. A low yield stress at elevated temperature can produce high residual stress, consequently all factors producing a decrease of surface temperature will be beneficial. These factors include cooling, grinding conditions and the thermal and mechanical properties of the material.

The French work on "Experience d'Utilisation de la Commande Adaptive en Fraisage" was concerned with modeling end milling operations and the use of adaptive controls. The French effort substantiates our finds of increased tool life productivity achieved through the use of a Macotech adaptive control. The control of cutting forces is the main feature of the French system. The knowledge obtained thus far must be extended from current models of the end milling operation by enlarging adaptive control models.

The USA work on an "Automated Fixture Hole Drilling" production process was well received since the process can substantially reduce costs. Automated fixture drilling can provide benefits like:

- (1) 50–60% reduction in production labor
- (2) Improved hole quality
- (3) Elimination of costly templates
- (4) Predictable and consistent flow rates
- (5) Less dependence on operator skill.

As a number of the holes required exceeds about 250,000 the automated system has a decided advantage.

Session II – Surface Treatments and Processes – by Mr A.R.G.Brown, ADR Mat 2 Directorate of Materials, MOD (PE), United Kingdom

The work discussed in this session falls into two groups. The first consisted of two programmes dealing with corrosion resistance of titanium and/or steel components coated with aluminum using various processes. The second consisted of three programmes dealing with processes for laying down coatings of various types or modifying the surface properties of materials to give desired performance.

Dealing with the work on aluminum coating first, it was clear that there is considerable interest in the development of coatings that can be used to replace the cadmium plating extensively used in the aerospace field. There is wide agreement about the drawbacks of cadmium plating which can be summarized as:

- Hydrogen embrittlement problems.
- Corrosion in aluminum alloy plate.
- Solid metal embrittlement of Ti, and to a lesser extent high strength steels.
- Reduction of fatigue life by cadmium plating.
- Ecological problems

It is probably true to say that of these the solid metal embrittlement and the ecological problems are the major project drivers.

In the search for a substitute for Cd there is also a large measure of agreement that the practical alternatives are very limited, and can, in fact be reduced to two – zinc and aluminum. Of these zinc is by far the more easy to apply and its

properties as far as the protection of components is concerned are undoubtedly very good. However, the work reported from the RAE does show that with zinc plated fasteners, although the initial protection of the fasteners is excellent, once it breaks down the corrosion of the base material into which the fasteners is inserted can be accelerated due to some electro-chemical effects which have not been fully elucidated.

The ion vapor deposited coating developed by the McDonnell Aircraft Company is clearly very advanced and now a practical production process. The method has been developed to cover both large components and fasteners and is capable of putting down coatings from 8 micrometers thick for applications in which close tolerances are required, to 25 micrometers thick for cases where maximum corrosion resistance is required. However, all of these coatings require chromate treatments before they can be used. This is partly to improve the surface condition for paint adhesion, but the indications are that without such chromate treatments the aluminum coatings are not really satisfactory from the corrosion protection point of view.

In the work from the RAE — a number of aluminum coatings were compared for their effectiveness in protecting fasteners and in preventing intergranular corrosion in the countersink of the blocks into which they were fitted. Without going through the results in detail it would appear that aluminum plating is an effective protection, while the coatings consisting of aluminum powder or flakes in an inorganic binder are much less so.

A point clearly raised by these two efforts is the validity of the accelerated corrosion test work. The American work relies on a SO_2 — salt spray test, the RAE used a continuous neutral salt fog test for fasteners, the so-called dry salt humidity test for fasteners assembled in an aluminum alloy test block and natural exposure to a marine environment. The latter is regarded as the most reliable indicator with the dry salt humidity test showing best correlation with natural exposure results. Work has also been undertaken on using electro-chemical measurements (corrosion current measurements with a zero resistance ammeter) to indicate the ranking of various treatments as far as protection is concerned. It would appear that there is a real task to compare various methods of accelerated tests with behaviour in service conditions and this could well form the basis of a combined program of work.

The major discrepancy between the two efforts is probably the assertion by McDonnell that IVD plating with up to 25 micrometers of aluminum does not affect the fatigue behavior of fasteners, whereas the RAE report quotes substantial reductions in fatigue endurance for both steel and titanium bolts plated with cadmium, zinc or aluminum. This is a feature which should receive further attention in view of the interest expressed from the floor.

The AERE Harwell work on sputter ion plating and ion implantation outlined two new processes for modifying surfaces. Both have been the subject of extensive experimental investigation though neither has gone into full scale production. Much interest was shown in the processes, and an assessment of their economic viability when applied to real components is clearly desirable. The applications for which these processes have been used have been largely outside the aircraft structural field, but in view of the obvious ease of application of the sputter ion plating technique, the feasibility of using this process for production of high quality aluminum coatings should be studied. Negotiations for such work are believed presently to be in hand. Ion implantation may well have applications in specialized areas, but the nature of the process, entailing very high voltage applications in hard vacuum conditions suggests that this will never be a widely applied commercial process, though it could well have application in specific areas.

The Canadian work from Sheritt Gordon represents an elegant piece of scientific work originating from detailed observation of the structure of commercial products. The observations suggested a method for improvement of the wear characteristics of some carbide (nickel or cobalt matrix) alloys and the research reported shows great ingenuity in both varying production conditions as desired and carrying out the sophisticated analyses required. It is unfortunate that the results of the work do not indicate any very clear way forward in the development of wear resistant coatings although some interesting compositions were developed. However, wear remains a great problem, especially wear at elevated temperatures, and it is unfortunate that no measurements of wear at elevated temperatures were made. A possible general subject for consideration would be the problem of wear and whether it would be useful to conduct a more detailed review of wear processes and other means of producing wear resistant coatings by other methods such as "dirty" plating in an electroplating process for incorporating hard metal particles in a nickel or cobalt alloy matrix as has been developed in the UK.

The laser beam processing of metal surfaces is a topic which is of great interest to a very great number of people in all of the countries represented. In view of the great variety of treatments that can be applied to metals using the laser, ranging from cutting to welding, so-called "laser glazing", and the development of surface alloying, a full session could be devoted to a discussion of these processes and the properties which can be developed in metals. Experience in the UK supports Professor Torto in his findings that control of the process is not as simple as appears at first sight. The suggestion by Prof. Storer that there could be significant differences between the behavior of wetting and non-wetting surface coatings on laser treatment deserves to be followed up.

Clearly the treatment of surfaces and their behavior and deterioration under service conditions does create considerable interest. The selection of specific topics for discussion is, however, difficult though suitable topics for detailed discussion could include:

- (1) Standardization of accelerated corrosion tests and their correlation with service behavior.

- (2) Detailed study of wear processes and the production of wear resistant coatings.
- (3) Laser processing of materials.

**Session III – Fundamental Aspects of Net Shape Processing – by Mr J.P.A. Immariageon,
National Aeronautical Establishment, National Research Council of Canada**

In the third session of the meeting, five papers were presented dealing with quite different aspects of net shape processing. First, Professor Rowe described the modern analytical techniques that can be used to model deformation processes. It can be seen how these techniques might be used in the future, for example, in specifying the shape of forging preforms prepared by powder processing, and also die shapes, such that the forging will receive the appropriate amounts of strain and strain rate in order to develop the optimum grain structures in specific locations of the finished product.

Prof. Rowe explained that slip line field theory had reached its limit of usefulness, but suggested that finite element techniques might offer further opportunities to introduce more realistic material properties to develop more accurate predictions. In particular, it should be realized that microstructures change dynamically during a working operation and therefore properties also change continuously at any point. It is hoped that these facts could be accommodated analytically.

Clearly there is great interest in producing parts with minimum of effort and minimum material wastage and these methods should be developed to allow these objectives to be achieved in a rational way, thus avoiding the waste of effort and material involved in empirical solutions.

In his work, Mr Boudillon examined superplastic forming of the titanium-base alloy Ti 6-4, from fundamental considerations to practical applications. The purpose of this work was to examine the applicability of isothermal forming operations to welded plates of the alloy.

In this material, the hot-worked and annealed α - β micro-structure is expected to exhibit superplasticity. In his work, Mr Boudillon examined the potential for superplastic forming of forged material which has been solution treated, quenched and annealed. It was also demonstrated that the heat affected zones in welded Ti 6-4 plates exhibit sufficient ductility to allow superplastic pressure molding. This processing opportunity was shown to be limited however, by the need for subsequent conventional finish machining in order to meet the close dimensional tolerances required in aerospace applications. With regard to this material, it was claimed that superplastic forming is more cost effective than other candidate forming operations.

Pratt & Whitney Aircraft of Florida described their Rapid Solidification Rate process, and its application to super-alloy powders. Clearly the process is quite new and had not been fully evaluated. Questions arise whether the finest particle sizes produced might not be more easily produced by techniques such as splat quenching, and whether the textures produced in zone annealed products of these powders are acceptable for all applications.

Several of the audience felt that $\langle 100 \rangle$ textures would be desirable, but $\langle 111 \rangle$ appears to be the dominant zone annealed recrystallization texture. Nevertheless the speaker felt that these afforded certain advantages in terms of vibratory considerations. These points obviously require further attention.

Also, while some advantages may be offered in terms of homogeneity and higher incipient melting points, the conventional limits to alloying, imposed by precipitation of embrittling intermetallic compounds, such as sigma, during consolidation or service at high temperatures, may still exist.

And finally, the powder processing equipment involved is expensive, and in order to minimize running costs, it would be desirable to recycle the inert gas used.

The work discussed by Canadian Westinghouse showed how properties in investment cast parts could be improved by hot isostatic processing. The work showed that while HIP is beneficial in closing porosity, it cannot be considered a remedy for all ills. Parts containing gross defects will involve dimensional changes which may be unacceptable, and in the sample shown, a nickel-base superalloy, the void closure left pockets of material having a microstructure atypical of the rest of the material. Most important, the work showed that simple elimination of porosity is not a guarantee of improved properties, but that specific thermal cycles are needed to counteract deleterious side effects of HIP. These may not be the same for each alloy and therefore they will have to be established to match the particular material and the intended service application of the part. And possibly a far wider range of materials might be processed in this way to good advantage.

The above process might be considered a useful by-product of a technology originally developed for powder processing. There are many other applications of HIP such as the closure of creep or fatigue induced voids or internal

cracks, and the regeneration of properties in used parts. Possibly even surface initiated cracks, such as fatigue cracks might be closed if suitable sealants can be found which could be applied and removed at reasonable cost. HIP processing might also play an important role in the development of ceramic materials, as suggested later by Professor Gugel, and possibly also in the development of artificial composite materials.

Finally, it should be realized that all of these processes involve high capital cost, and additional cost on the price of a finished part, and obviously these have to be examined very carefully.

Finally, Dr Bunk provided a highly comprehensive overview of Professor Gugel's work on non-oxide ceramics. Candidate materials and the most suitable fabrication processes were described in as far as opportunities for continued progress in high temperature engineering are concerned.

It was made clear, however, that before these advanced materials make their way into aerospace applications, the designers of power plants will need to modify their design criteria in order to accommodate the inherently brittle characteristics of these materials. In particular, thermal shock resistance and damage containment may need to take precedence over traditional criteria possibly even at the expense of aerodynamic efficiency.

Of the fabrication processes discussed for ceramics, HIP appears to have the most promising potential. However, at the moment, the temperature capabilities of state-of-the-art autoclaves are rather limited. Higher temperature systems may have to be developed or alternatively, means found to promote densification and bonding at lower temperatures. Also, the canning technology for ceramic materials will need to be developed further.

Session IV – Production Aspects of Net Shape Processing – by Mr E.J.Dulis, Colt Industries, Crucible Materials Research Center, USA

Two excellent efforts on superplastic forming and diffusion bonding of titanium alloy sheet were presented. G.Stacher described the work at Rockwell International (RI) on making titanium alloy B-1 bomber parts by superplastic forming plus diffusion bonding. It involved different types of structures – straight SPF and SPF/DB. Examples of impressive complex production parts were shown and described. Mr Stacher gave information on the final component cost and weight savings involved in applying the process – these were of the order of 40 to 50% cost saving and 50% weight saving.

Mr Rosser described the work on SPF and DB of titanium alloy components for the Concorde and other parts. Impressive examples of complex Ti alloy parts were shown.

Basically both efforts showed close agreement on the applicability and cost and weight savings. Some questions were raised on the applicability of SPF and DB that were pertinent, including how to avoid bonding of titanium to the metal die container. Mr Stacher explained that Yttria (YO_2) is coated on the die prior to heating and SPF. Mr Rosser indicated that B.A. has proprietary coatings used before each forming. On NDT of DB joints, Mr Rosser explained that B.A. uses C-scan ultrasonic inspection.

The applicability of SPF and DB to other alloys was discussed. Work on aluminum alloys is being pursued as well as steel. However there exists some question on cost effectiveness in these materials.

Dr Stephan described the production of high-purity metal powder by EB techniques. The L.H. process was covered in detail. In addition, an overview of the current different processes to make high purity powder of superalloy and titanium alloys was presented. The capacity of the different types of available facilities showed substantial capacity for superalloy powder. The capacity for good titanium alloy powder is lacking. Problems with the various titanium powder processes were reviewed such as tungsten inclusions from the REP powder.

Session V – Panel Discussion of Highlighted Areas and Future Directions for AGARD Advanced Fabrication Activities – by Henry A.Johnson, Air Force Materials Laboratory, USA

The panel session opened with a short summary of the previous Sessions I through IV on Advanced Fabrication Processes. The panel session chairman reviewed the following suggested topics for future activities, and each major topical area was discussed as shown in the outline below:

Suggested Topics**Advanced Fabrication Processes****I *Surface Treatment and Protection***

- IVD/CVD
- Sputtering
- EB
- Plasma
- Electroplate
- Flame
- Ion
- High Temperature/Thermal Barrier
- Oxidation
- Erosion
- Corrosion
- Wear/Tribology
- Test/Standards
- Fatigue Enhancement

II *Advanced Casting Technology*

- Aluminum
- Titanium
- Steel
- Superalloy
- Advanced Melting Methods
 - Rheo Casting
 - Squeeze Casting
 - Die Casting
 - Lost Wax Forming
 - HIP Densification

III *Laser Metalworking*

- Machining
- Drilling
- Cutting
- Coating
- Welding
- Heat Treatment

IV *Advanced Machining Processes*

- High Speed Machining
- Advanced Cutting Tools
- New Lubricants/Coolants
- Controls/Automation
- Modeling

V *Joining Processes*

- Laser
- Diffusion
- Electron Beam
- Inertia Welding
- Plasma
- TIG/MIG
- Brazing

VI *Advanced Powder Processing*

- Alloys/Powder Production
- Alloy Behavior
- Consolidation
 - HIP (Hot Isostatic Pressing)
 - VHP (Vacuum Hot Pressing)
- Properties/Defects

VII *High Temperature Processing*

- Isothermal Forging/Forming, Rolling
- Superplastic Forming
- Diffusion Bonding
- HIP – Thermal Spray

VIII *Non-Destructive Evaluation*

- Ultrasonics
- Acoustic Emission

- X-Ray
- Metrology
- Neutron Radiography
- Fluorescent Penetrant
- Automation

IX *Energy Related Processes*

- Explosive
- Laser
- Plasma
- Electro Magnetic
- High Pressure

X *Energy Conservation in Manufacturing*

- Heat Conservation
- Thermal Recycling

XI *Repair Process*

- Cleaning
- Weld Repair
- Coating
- Surface Buildup

XII *Heat Treatment*

- Thermo Mechanical Treatment

Comment was made that the area of "Surface Treatment" has many ramifications, including pollution problems from cadmium plating as well as various new methods of deposition such as ion implantation and ion sputtering, etc. From these many methods a cooperative test program might be a possibility to compare qualities of the different proprietary coating methods for surface protection.

A comment was also received on the fact that there is very little evidence of detailed work on the microstructure, particularly at the fine grain size amorphous interfaces. This area would be of prime importance in developing the effect of long term exposure of basically meta-stable surfaces.

Another area of common interest is the effect of electric field on fine particle displacement. There is work in this area in the USA and some effort in the UK on electric field acceleration fine particle production.

The area of "Advanced Casting Technology" received favorable comment and it was suggested that this area is of real concern to AGARD and should be given priority as a topic of consideration. It was stated that Italy is interested in new casting processes such as rheo casting for composites with metallic matrix formation.

"Laser Metalworking" was discussed and during the discussion it was pointed out that laser metalworking should be considered as laser "assisted" metalworking. There was Italian interest, especially in high power lasers since there are many low power applications and high power (10 KW or more) lasers are still experimental.

Machining as a topic was of interest to Italy, particularly in the areas of:

- automation
- flexible automation
- material handling and delivery of stock at the right moment.

Another comment made, however, pointed out that there were already sufficient activities in Europe on machining which would tend to make an additional AGARD activity redundant.

The topic of "joining" was reviewed and EB welding second order problems was surfaced as an area of interest in the UK. Undercutting, weld defects, and spattering should be examined. The joining of advanced materials was also covered as a topic and it was suggested that consideration be given to the topic of joining dispersion strengthened alloys and ceramics. In addition, the effects of small defects in welds and rejections due to these defects should be investigated. There appeared to be very little interest in the topics of "Advanced Powder Processing", "High Temperature Processing", and "Heat Treatment of Metals".

There was a suggestion from the UK that, in the NDI area, automation is the topic to concentrate on. It was also pointed out that in-service monitoring of material degradation ought to be considered as a topic.

The topic of "Energy Related Processes" received little comment and apparently was of little interest. Repair and maintenance was of interest particularly with respect to routine repair and maintenance as well as consideration of removal of material from the surface. In addition to the suggested list of topics the following areas were suggested as potential topics for consideration.

- Repair and maintenance
- Fabrication of organic materials, composites and ceramics
- Materials conservation by new processes
- Alloy substitution and scrap reclamation
- Assembly operations in aircraft geared to cost reduction
- Metal bonding cleaning procedures
- Bonding NDT and long term exposure effects

The topics discussed and areas suggested by the attendees will be considered in the Spring meeting of AGARD at Williamsburg, Virginia to determine the future course of Structures and Materials Panel activities on Advanced Fabrication Processes.

REPORT DOCUMENTATION PAGE			
1. Recipient's Reference	2. Originator's Reference	3. Further Reference	4. Security Classification of Document
	AGARD-CP-256	ISBN 92-835-0227-2	UNCLASSIFIED
5. Originator	Advisory Group for Aerospace Research and Development North Atlantic Treaty Organization 7 rue Ancelle, 92200 Neuilly sur Seine, France		
6. Title	ADVANCED FABRICATION PROCESSES		
7. Presented at	the 47th Meeting of the AGARD Structures and Materials Panel held in Florence, Italy on 26-28 September 1978.		
8. Author(s)/Editor(s)	Various		9. Date March 1979
10. Author's/Editor's Address	Various		11. Pages 266
12. Distribution Statement	This document is distributed in accordance with AGARD policies and regulations, which are outlined on the Outside Back Covers of all AGARD publications		
13. Keywords/Descriptors			
Maintenance Aircraft Fabrication		Aerospace engineering Materials Research projects	
14. Abstract			
<p>Interest in advanced fabrication processes stems from the increasing acquisition and maintenance costs of current aerospace systems. This has led to greatly increased emphasis on means of reducing processing costs and improving the quality of manufacturers' components through improved material/process selection and control. Similarly, new processes are emerging both within the aerospace processing community and within the more general commercial area, that offer, significant opportunities for lower cost, higher quality aerospace components.</p> <p>The purpose of the Specialists' Meeting was threefold. Most importantly it was to elucidate on some specific high payoff new processing concepts selected from a cross-section of NATO nations. This broad base of coverage was invaluable in itself but also was intended to aid in steering the Structures and Materials Panel toward selection of specific new areas where data and information interchange in much greater depth would be beneficial. The third purpose was to promote a coupling of the fundamental research activities to more applied efforts.</p> <p>The meeting was highlighted by the Panel Session at which, based on the work presented as well as other work not presented, a significant spectrum of extremely interesting, high payoff, new processing areas was discussed. Advantages for each new area were elucidated.</p>			

<p>AGARD Conference Proceedings No.256 Advisory Group for Aerospace Research and Development, NATO ADVANCED FABRICATION PROCESSES Published March 1979 266 pages</p> <p>Interest in advanced fabrication processes stems from the increasing acquisition and maintenance costs of current aerospace systems. This has led to greatly increased emphasis on means of reducing processing costs and improving the quality of manufacturers' components through improved material/process selection and control. Similarly, new processes are emerging both within the aerospace processing community and within the more general commercial area, that offer,</p> <p>P.T.O.</p>	<p>AGARD-CP-256</p> <p>Maintenance Aircraft Fabrication Aerospace engineering Materials Research projects</p>	<p>AGARD Conference Proceedings No.256 Advisory Group for Aerospace Research and Development, NATO ADVANCED FABRICATION PROCESSES Published March 1979 266 pages</p> <p>Interest in advanced fabrication processes stems from the increasing acquisition and maintenance costs of current aerospace systems. This has led to greatly increased emphasis on means of reducing processing costs and improving the quality of manufacturers' components through improved material/process selection and control. Similarly, new processes are emerging both within the aerospace processing community and within the more general commercial area, that offer,</p> <p>P.T.O.</p>	<p>AGARD-CP-256</p> <p>Maintenance Aircraft Fabrication Aerospace engineering Materials Research projects</p>
<p>AGARD Conference Proceedings No.256 Advisory Group for Aerospace Research and Development, NATO ADVANCED FABRICATION PROCESSES Published March 1979 266 pages</p> <p>Interest in advanced fabrication processes stems from the increasing acquisition and maintenance costs of current aerospace systems. This has led to greatly increased emphasis on means of reducing processing costs and improving the quality of manufacturers' components through improved material/process selection and control. Similarly, new processes are emerging both within the aerospace processing community and within the more general commercial area, that offer,</p> <p>P.T.O.</p>	<p>AGARD-CP-256</p> <p>Maintenance Aircraft Fabrication Aerospace engineering Materials Research projects</p>	<p>AGARD Conference Proceedings No.256 Advisory Group for Aerospace Research and Development, NATO ADVANCED FABRICATION PROCESSES Published March 1979 266 pages</p> <p>Interest in advanced fabrication processes stems from the increasing acquisition and maintenance costs of current aerospace systems. This has led to greatly increased emphasis on means of reducing processing costs and improving the quality of manufacturers' components through improved material/process selection and control. Similarly, new processes are emerging both within the aerospace processing community and within the more general commercial area, that offer,</p> <p>P.T.O.</p>	<p>AGARD-CP-256</p> <p>Maintenance Aircraft Fabrication Aerospace engineering Materials Research projects</p>

<p>significant opportunities for lower cost, higher quality aerospace components.</p> <p>The purpose of the Specialists' Meeting was threefold. Most importantly it was to elucidate on some specific high payoff new processing concepts selected from a cross-section of NATO nations. This broad base of coverage was invaluable in itself but also was intended to aid in steering the Structures and Materials Panel toward selection of specific new areas where data and information interchange in much greater depth would be beneficial. The third purpose was to promote a coupling of the fundamental research activities to more applied efforts.</p> <p>The meeting was highlighted by the Panel Session at which, based on the work presented as well as other work not presented, a significant spectrum of extremely interesting, high payoff, new processing areas was discussed. Advantages for each new area were elucidated.</p> <p>Papers presented at the 47th Meeting of the AGARD Structures and Materials Panel held in Florence, Italy on 26-28 September 1978.</p> <p>ISBN 92-835-0227-2</p>	<p>significant opportunities for lower cost, higher quality aerospace components.</p> <p>The purpose of the Specialists' Meeting was threefold. Most importantly it was to elucidate on some specific high payoff new processing concepts selected from a cross-section of NATO nations. This broad base of coverage was invaluable in itself but also was intended to aid in steering the Structures and Materials Panel toward selection of specific new areas where data and information interchange in much greater depth would be beneficial. The third purpose was to promote a coupling of the fundamental research activities to more applied efforts.</p> <p>The meeting was highlighted by the Panel Session at which, based on the work presented as well as other work not presented, a significant spectrum of extremely interesting, high payoff, new processing areas was discussed. Advantages for each new area were elucidated.</p> <p>Papers presented at the 47th Meeting of the AGARD Structures and Materials Panel held in Florence, Italy on 26-28 September 1978.</p> <p>ISBN 92-835-0227-2</p>
<p>significant opportunities for lower cost, higher quality aerospace components.</p> <p>The purpose of the Specialists' Meeting was threefold. Most importantly it was to elucidate on some specific high payoff new processing concepts selected from a cross-section of NATO nations. This broad base of coverage was invaluable in itself but also was intended to aid in steering the Structures and Materials Panel toward selection of specific new areas where data and information interchange in much greater depth would be beneficial. The third purpose was to promote a coupling of the fundamental research activities to more applied efforts.</p> <p>The meeting was highlighted by the Panel Session at which, based on the work presented as well as other work not presented, a significant spectrum of extremely interesting, high payoff, new processing areas was discussed. Advantages for each new area were elucidated.</p> <p>Papers presented at the 47th Meeting of the AGARD Structures and Materials Panel held in Florence, Italy on 26-28 September 1978.</p> <p>ISBN 92-835-0227-2</p>	<p>significant opportunities for lower cost, higher quality aerospace components.</p> <p>The purpose of the Specialists' Meeting was threefold. Most importantly it was to elucidate on some specific high payoff new processing concepts selected from a cross-section of NATO nations. This broad base of coverage was invaluable in itself but also was intended to aid in steering the Structures and Materials Panel toward selection of specific new areas where data and information interchange in much greater depth would be beneficial. The third purpose was to promote a coupling of the fundamental research activities to more applied efforts.</p> <p>The meeting was highlighted by the Panel Session at which, based on the work presented as well as other work not presented, a significant spectrum of extremely interesting, high payoff, new processing areas was discussed. Advantages for each new area were elucidated.</p> <p>Papers presented at the 47th Meeting of the AGARD Structures and Materials Panel held in Florence, Italy on 26-28 September 1978.</p> <p>ISBN 92-835-0227-2</p>

AGARD

NATO  OTAN

7 RUE ANCELLE · 92200 NEUILLY-SUR-SEINE
FRANCE

Telephone 745.08.10 · Telex 610176

**DISTRIBUTION OF UNCLASSIFIED
AGARD PUBLICATIONS**

AGARD does NOT hold stocks of AGARD publications at the above address for general distribution. Initial distribution of AGARD publications is made to AGARD Member Nations through the following National Distribution Centres. Further copies are sometimes available from these Centres, but if not may be purchased in Microfiche or Photocopy form from the Purchase Agencies listed below.

NATIONAL DISTRIBUTION CENTRES

BELGIUM

Coordonnateur AGARD - VSL
Etat-Major de la Force Aérienne
Quartier Reine Elisabeth
Rue d'Evere, 1140 Bruxelles

CANADA

Defence Scientific Information Service
Department of National Defence
Ottawa, Ontario K1A 0Z2

DENMARK

Danish Defence Research Board
Østerbrogades Kaserne
Copenhagen Ø

FRANCE

O.N.E.R.A. (Direction)
29 Avenue de la Division Leclerc
92 Châtillon sous Bagneux

GERMANY

Zentralstelle für Luft- und Raumfahrt-
dokumentation und -information
c/o Fachinformationszentrum Energie,
Physik, Mathematik GmbH
Kernforschungszentrum
7514 Eggenstein-Leopoldshafen 2

GREECE

Hellenic Air Force General Staff
Research and Development Directorate
Holargos, Athens, Greece

ICELAND

Director of Aviation
c/o Flugrad
Reykjavik

UNITED STATES

National Aeronautics and Space Administration (NASA)
Langley Field, Virginia 23365
Attn: Report Distribution and Storage Unit

THE UNITED STATES NATIONAL DISTRIBUTION CENTRE (NASA) DOES NOT HOLD
STOCKS OF AGARD PUBLICATIONS, AND APPLICATIONS FOR COPIES SHOULD BE MADE
DIRECT TO THE NATIONAL TECHNICAL INFORMATION SERVICE (NTIS) AT THE ADDRESS BELOW.

ITALY

Aeronautica Militare
Ufficio del Delegato Nazionale all'AGARD
3, Piazzale Adenauer
Roma/EUR

LUXEMBOURG

See Belgium

NETHERLANDS

Netherlands Delegation to AGARD
National Aerospace Laboratory, NLR
P.O. Box 126
Delft

NORWAY

Norwegian Defence Research Establishment
Main Library
P.O. Box 25
N-2007 Kjeller

PORTUGAL

Direcção do Serviço de Material
da Força Aérea
Rua da Escola Politécnica 42
Lisboa
Attn: AGARD National Delegate

TURKEY

Department of Research and Development (ARGE)
Ministry of National Defence, Ankara

UNITED KINGDOM

Defence Research Information Centre
Station Square House
St. Mary Cray
Orpington, Kent BR5 3RE

PURCHASE AGENCIES

Microfiche or Photocopy

National Technical
Information Service (NTIS)
5285 Port Royal Road
Springfield
Virginia 22161, USA

Microfiche

Space Documentation Service
European Space Agency
10, rue Mario Nikis
75015 Paris, France

Microfiche

Technology Reports
Centre (DTI)
Station Square House
St. Mary Cray
Orpington, Kent BR5 3RF
England

Requests for microfiche or photocopies of AGARD documents should include the AGARD serial number, title, author or editor, and publication date. Requests to NTIS should include the NASA accession report number. Full bibliographical references and abstracts of AGARD publications are given in the following journals:

Scientific and Technical Aerospace Reports (STAR)
published by NASA Scientific and Technical
Information Facility
Post Office Box 8757
Baltimore/Washington International Airport
Maryland 21240, USA

Government Reports Announcements (GRA)
published by the National Technical
Information Services, Springfield
Virginia 22161, USA

